universität wien

DISSERTATION

Titel der Dissertation

„Variable Flavor Scheme for Final State Jets“

Verfasser

Piotr Pietrulewicz

angestrebter akademischer Grad

Doktor der Naturwissenschaften (Dr. rer. nat.)

Wien, 2014

Studienkennzahl lt. Studienblatt:	A 796 605 411
Dissertationsgebiet lt. Studienblatt:	Physik
Betreuer:	Univ.-Prof. Dr. André H. Hoang

Abstract

In this thesis I describe a setup to treat mass effects from secondary radiation of heavy quark pairs in inclusive hard scattering processes with various dynamical scales. The resulting variable flavor number scheme (VFNS) generalizes a well-known scheme for massive initial state quarks which has been developed for deep inelastic scattering (DIS) in the classical region $1 - x \sim \mathcal{O}(1)$ and which will be also discussed here. The setup incorporated in the formalism of Soft-Collinear Effective Theory (SCET) consistently takes into account the effects of massive quark loops and allows to deal with all hierarchies between the mass scale and the involved kinematic scales corresponding to collinear and soft radiation. It resums all large logarithms due to flavor number dependent evolution, achieves both decoupling for very large masses and the correct massless behavior for very small masses, and provides a continuous description in between.

In the bulk of this work I will concentrate on DIS in the endpoint region $x \to 1$ serving mainly as a showcase for the concepts and on the thrust distribution for e^+e^--collisions in the dijet limit as a phenomenologically relevant example for an event shape. The computations of the corrections to the structures in the factorization theorems are described explicitly for the singular terms at $\mathcal{O}(\alpha_s^2 C_F T_F)$ arising from secondary radiation of massive quarks through gluon splitting. Apart from the soft function for thrust, which requires a dedicated calculation, these results are directly obtained from the corresponding results for the radiation of a massive gauge boson with vector coupling at $\mathcal{O}(\alpha_s)$ with the help of dispersion relations, and most of the relevant conceptual and technical issues can be dealt with already at this level. Finally, to estimate the impact of the corrections I carry out a numerical analysis for secondary massive bottom and top quarks on thrust distributions at different center-of-mass energies.

Zusammenfassung

In dieser Arbeit beschreibe ich eine Vorgehensweise, um Masseneffekte schwerer Quarks aus sekundärer Strahlung in inklusiven harten Streuprozessen mit mehreren dynamische Skalen zu behandeln. Das dabei resultierende Setup verallgemeinert ein bekanntes und auch hier beschriebenes Schema für massive Quarks im Anfangszustand, das für tiefinelastische Streuung (DIS) in der klassischen Region $1 - x \sim \mathcal{O}(1)$ entwickelt wurde. Die Methode, die in den Formalismus von Soft-Collinear Effective Theory (SCET) eingebaut wird, berücksichtigt auf konsistente Weise die Effekte von Schleifen mit massiven Quarks und ermöglicht eine Behandlung aller Hierarchien zwischen der Massenskala und den auftretenden kinematischen Skalen für kollineare und softe Strahlung. Das Schema summiert alle großen Logarithmen durch Renormalisierungsgruppen-Evolution mit einer veränderlichen Anzahl aktiver Quarks, sorgt automatisch sowohl für das Entkoppeln von massiven Quarkeffekten bei großen Massen als auch für den masselosen Limes bei kleinen Massen und liefert ein stetiges Verhalten dazwischen.

Im Hauptteil der Arbeit werde ich einerseits auf das Beispiel von DIS in der Endpunktregion $x \to 1$ eingehen, das hauptsächlich als Demonstration der eingehenden Konzepte dient. Andererseits behandle ich auch die Thrustverteilung bei e^+e^--Kollisionen im Dijetlimes, wo sekundäre massive Quarks auch eine wichtige phänomenologische Auswirkung haben können. Die Berechnungen der Korrekturen durch sekundäre massive Quarks in den Bestandteilen der Faktorisierungstheoreme werden für die singulären Terme auf der Ordnung $\mathcal{O}(\alpha_s^2 C_F T_F)$ explizit beschrieben. Mit Ausnahme der soften Funktion für Thrust können die Resultate direkt aus den entsprechenden Ergebnissen für die Strahlung von massiven Eichbosonen mit Vektorkopplung auf $\mathcal{O}(\alpha_s)$ erhalten werden, was mit der Hilfe von Dispersionsrelationen erzielt wird. Der Großteil der relevanten konzeptionellen und technischen Probleme kann bereits in diesem Schritt behandelt werden. Schließlich führe ich eine numerische Analyse durch, um die Auswirkung der Korrekturen von massiven sekundären Bottom- und Top-Quarks auf die Thrustverteilung bei verschiedenen Schwerpunktsenergien zu bestimmen.

Acknowledgements

Here I would briefly like to thank all of the people who supported me during the time of my PhD. At first place I am indebted to my supervisor Andre Hoang for his time, patience and efforts. We spent a lot of time discussing about physics and his door was open for any questions I had. Moreover, I am also thankful to Andre that he encouraged me to present our work on different occasions and helped me to get introduced into the scientific community.

Furthermore, I am grateful to my collaborators and colleagues, among them in particular my friends Bahman Dehnadi, Ilaria Jemos, Patrick Ludl, Vicent Mateu, Peter Poier, Moritz Preißer, Daniel Samitz and Maximilian Stahlhofen, for the great working atmosphere with many fruitful discussions, but also for the social interactions with legendary coffee breaks.

I want to thank my parents for their unrestricted support and encouragement to pursue my interests during my whole lifetime. Finally, I am also obliged to my girlfriend Zoi who was never tired of cheering me up especially during times when my work was progressing slowly.

Contents

1 Introduction **1**

2 SCET: An EFT for jet physics **5**
2.1 Effective Field Theories . . . 5
2.2 Momenta and modes in SCET I . . . 6
2.3 The Lagrangian in SCET I . . . 9
2.4 Wilson lines and gauge symmetries . . . 11
2.4.1 Collinear Wilson lines . . . 11
2.4.2 Ultrasoft Wilson lines . . . 13
2.5 SCET II . . . 14
2.6 Factorization and resummation in SCET . . . 15

3 VFNS for classical DIS **17**
3.1 Kinematics of DIS . . . 17
3.2 The massless factorization theorem . . . 19
3.3 Mass effects at $\mathcal{O}(\alpha_s)$ . . . 22
3.3.1 Scenario I: $m \gtrsim Q$ . . . 24
3.3.2 Scenario II: $m \lesssim Q$ . . . 26
3.4 Secondary mass effects . . . 29
3.4.1 Dispersion relations . . . 30
3.4.2 Massive gluon computation at $\mathcal{O}(\alpha_s)$ . . . 32
3.4.3 Secondary massive quark effects at $\mathcal{O}(\alpha_s^2 C_F T_F)$ . . . 37

4 VFNS for DIS in the endpoint region **43**
4.1 The massless factorization theorem . . . 43
4.2 The mass factorization setup . . . 50
4.2.1 Scenario I: $m > Q > Q\lambda > Q\lambda^2$ . . . 53
4.2.2 Scenario II: $Q > m > Q\lambda > Q\lambda^2$ . . . 54
4.2.3 Scenario III: $Q > Q\lambda > m > Q\lambda^2$ . . . 56
4.2.4 Renormalization conditions and continuity . . . 58
4.2.5 Outline of the computations . . . 59
4.3 One-loop computations for secondary massive gluons . . . 60
4.3.1 Hard current matching coefficient and threshold correction . . . 61
4.3.2 Jet function and threshold correction . . . 67
4.3.3 Consistency relations . . . 71
4.3.4 Fixed-order expansion and comparison with full QCD result . . . 76
4.4 Two-loop computations for secondary massive quarks . . . 77
4.4.1 Hard current matching coefficient and threshold correction . . . 77
4.4.2 Jet function and threshold correction . . . 83
4.4.3 Consistency relations . . . 88
4.4.4 Fixed-order expansion and comparison with full QCD result . . . 92

5 VFNS for thrust in the dijet region **95**
5.1 Event shapes . . . 95
5.2 The massless factorization theorem . . . 96
5.3 The mass mode setup . . . 100
5.3.1 Scenario I: $m > Q > Q\lambda > Q\lambda^2$ . . . 101
5.3.2 Scenario II: $Q > m > Q\lambda > Q\lambda^2$ . . . 102
5.3.3 Scenario III: $Q > Q\lambda > m > Q\lambda^2$ . . . 102
5.3.4 Scenario IV: $Q > Q\lambda > Q\lambda^2 > m$ . . . 102
5.3.5 Gap subtraction, evolution and matching . . . 104
5.4 Two-loop soft function for secondary massive quarks . . . 107
5.4.1 Soft function for massive gluons at $\mathcal{O}(\alpha_s)$ . . . 109
5.4.2 Massive quark corrections with gluon hemisphere prescription . . . 110
5.4.3 Phase space misalignment correction . . . 111
5.4.4 Renormalon subtractions . . . 114
5.5 Consistency relations . . . 117
5.6 Singular fixed-order QCD result . . . 123
5.7 Numerical analysis . . . 124

6 Conclusions **133**

A Longitudinal structure function **135**
A.1 Massless results . . . 135
A.2 Mass effects at $\mathcal{O}(\alpha_s)$ . . . 135
A.3 Secondary mass effects . . . 136
A.3.1 Massive gluon results at $\mathcal{O}(\alpha_s)$ . . . 136
A.3.2 Secondary massive quark effects at $\mathcal{O}(\alpha_s^2 C_F T_F)$ . . . 137

B Identities for distributions **139**
B.1 Integer plus-distributions . . . 139
B.2 Noninteger plus-distributions . . . 140

C Evolution factors and anomalous dimensions **141**
C.1 Current evolution factor . . . 141
C.2 Evolution factors for the jet and soft functions . . . 142
C.3 PDF evolution factor for $x \to 1$ . . . 142
C.4 Coefficients of the β-function . . . 142
C.5 Anomalous dimensions of the matrix elements . . . 143

D Computation of the hemisphere misalignment correction **145**
D.1 Computation of the cumulant . . . 145
D.2 Asymptotic expansion for $\ell \gg m$ . . . 145

E Massive gluon radiation in thrust at $\mathcal{O}(\alpha_s)$ in full QCD **149**
E.1 General result . . . 149
E.2 Expansions . . . 152

F Secondary mass effects with primary massive quarks **155**
F.1 Factorization for primary massive quarks . . . 155
F.2 Current matching with secondary massive quarks . . . 156
F.2.1 One-loop computation for secondary massive gluons . . . 157
F.2.2 Two-loop computation for secondary massive quarks . . . 159
F.3 Consistency relations . . . 160

Chapter 1

Introduction

In the era of the Large Hadron Collider (LHC) we are investigating the mechanism of electroweak symmetry breaking, determining fundamental parameters of the Standard Model and looking for new physics beyond the Standard Model at the TeV scale. One of the main requirements for this search is a good understanding of collider phenomenology, in particular a thorough analysis of QCD at different energy scales is necessary. This includes a precise description of the strongly interacting initial state on the one hand and of the hard scattering interactions and final state cross talks on the other hand, which affects the complete energy range between the hadronization scale Λ_{QCD} and the center-of-mass (c.m.) energy $Q \gg \Lambda_{\mathrm{QCD}}$. One of the most common objects observed in collider experiments are jets, i.e. bunches of very energetic collimated hadrons. Their distribution and shape provide many information about the high-energy process, such that a good understanding of jets is the basis of carrying out measurements at all modern colliders. In the recent years many advances have been achieved in this field thanks to higher order loop calculations and summation of large logarithmic terms allowing for an accurate description of many strong interaction processes. In this context one cannot neglect the quark masses at sufficient high accuracy, which concerns in particular the top mass at the LHC. Depending on the hierarchy between the relevant mass scales and the kinematic energy scales in the process, different descriptions for the massive quark can be appropriate. In this field substantial progress is required to take full advantage of present and upcoming data, since currently mass effects are in many cases not treated in a coherent way concerning resummation and the incorporation of fixed-order matrix elements.

One example where the treatment of massive quark effects raises a lot of interest is deep-inelastic scattering (DIS), the benchmark process for the extraction of parton distribution functions (PDFs). These are one main input for the analysis of all processes at hadron colliders, such that a precise determination including the effects of the charm and bottom quark masses is necessary. A first systematic approach to incorporate heavy quarks with arbitrary masses with respect to the other relevant scales has been provided in Refs. [1, 2], which laid the basis of a *variable flavor number scheme* (VFNS) for inclusive processes in hadron collisions. It is founded on the separation of close-to-mass-shell modes and offshell fluctuations and is thus in the spirit of effective field theory (EFT) factorization. Nowadays, different schemes have been developed to cope with this challenge, which are mainly based on this approach, but differ in their detailed implementation concerning formally subleading contributions (see Ref. [3] for a short overview).

Jets play a major role also at experiments beyond hadron colliders. In particular, due to the lack of a strongly interacting initial state, high energy processes at lepton colliders are very suitable for precision QCD measurements. Recent conceptual developments in EFTs and progress in theoretical calculations have made it possible to extract fundamental parameters of QCD like the strong coupling from LEP data for event shapes with unprecedented accuracy [4, 5]. In this context one also needs a good estimate of quark mass effects at the current accuracy of the predictions for a complete analysis. Furthermore, future lepton colliders like the ILC will allow to determine also the top mass, one of the most sensitive parameters for constraints of the Standard Model, with small uncertainties both via threshold scans [6, 7] and far away from threshold in the dijet region [8, 9].

In this thesis and the associated papers we propose a general factorization framework to include massive quark corrections loops in inclusive hard scattering processes with several dynamical scales. In particular we develop a VFNS for final state jets, which are initiated by massless quarks and where massive quarks are produced through the radiation of gluons that split into massive quark-antiquark pairs, i.e. via *secondary* radiation. This concerns both real radiation effects and heavy quark loops. Since the corresponding fixed-order corrections start contributing at $\mathcal{O}(\alpha_s^2)$ they give numerically quite small effects. Nevertheless, their treatment provides important conceptual background for the full consistent treatment of massive quark effects in differential cross sections including direct (*primary*) production, in particular concerning the treatment of large logarithmic terms, which might have a significant impact in future phenomenological studies.

In processes with jets one faces a multiscale problem with the different invariant mass scales corresponding to the hard momentum transfer, the collinear radiation within the jets, the low-energetic soft radiation between the jets and the hadronic scale $\Lambda_{\rm QCD}$, which can be widely separated depending on the process and the kinematic regime under investigation. Our setup allows to deal with all possible hierarchies between the mass and the above-mentioned scales. It resums all large logarithms between these scales due to flavor number dependent evolution, converges smoothly to the correct limiting behavior, namely the decoupling limit for large masses and the massless limit for small masses, and provides a continuous description in between. We illustrate the features of the VFNS on two examples, namely DIS in the endpoint region $x \to 1$ and the thrust distribution in the dijet limit $\tau \to 0$, and provide the corresponding computations for the secondary massive quark corrections at $\mathcal{O}(\alpha_s^2 C_F T_F)$. The incorporation of massive quarks into cross section allows to resolve real and virtual radiation and can also shed light on the case of massless quarks.

The outline of this thesis is as follows: First we will describe in chapter 2 an appropriate EFT framework for the investigation of jet processes that disentangles the physics at the different kinematic scales, namely *Soft-Collinear Effective Theory* (SCET). Here we provide the language and the basic concepts for the factorization theorems in the later chapters. In chapter 3 we describe factorization in DIS in the classical region $1 - x \sim \mathcal{O}(1)$ and explain how a VFNS for inclusive processes in hadron collisions, is constructed. We will show how the flavor number dependent resummation of logarithms is related to the proper choice of renormalization conditions. In particular we will also perform the required computations for secondary massive quark radiation at $\mathcal{O}(\alpha_s^2 C_F T_F)$ explicitly, which to our knowledge have not been displayed in the literature before. These results are directly obtained from the corresponding results for the radiation of a massive gauge boson with vector coupling at $\mathcal{O}(\alpha_s)$ with the help of dispersion relations.

The chapters 4 and 5 contain the main results of this thesis. In chapter 4 we generalize the setup to the endpoint region of DIS with $1 - x \ll 1$, where the final state becomes a single jet with an invariant mass that is much smaller than the momentum transfer energy. We explain how the factorization theorem changes compared to the region $1 - x \sim \mathcal{O}(1)$ and what consequence this has for the incorporation of massive quarks. We will distinguish massive quark modes with a collinear and a soft scaling and show how either of them contributes for different hierarchies with respect to the kinematic scales. The computations of the secondary massive quark corrections at $\mathcal{O}(\alpha_s^2 C_F T_F)$ in the factorization theorem are described explicitly, again first at the level of a "massive gluon" at $\mathcal{O}(\alpha_s)$, where most relevant conceptual and technical issues can be already dealt with. We will encounter divergences which are not regularized by dimensional regularization and corresponding potentially large logarithms for contributions around the mass shell, which are not resummed by the usual renormalization group (RG) evolution. We will discuss the "rapidity evolution" to resum these both at $\mathcal{O}(\alpha_s)$ and $\mathcal{O}(\alpha_s^2 C_F T_F)$. Another interesting aspect is that the virtual structures at different scales are related to each other via consistency conditions of RG running which we will check by explicit computations.

In chapter 5 we switch process to e^+e^--collisions and investigate the thrust distribution in the dijet limit as an example for an event shape, where secondary massive quarks may also have a significant phenomenological impact. The factorization setup for both massless and massive quarks is in fact related to DIS for $x \to 1$ due to crossing symmetry and the universality of some involved components of the factorization theorem. The only additional ingredient which needs to be calculated is the perturbative soft function describing low-energetic radiation between the jets, which is a more involved computation and deserves a devoted discussion. This also includes the computation of the corresponding renormalon subtractions to remove the $\mathcal{O}(\Lambda_{\rm QCD})$ ambiguity in the perturbative expansion in dimensional regularization. Finally, to estimate the impact of the mass corrections we carry out a numerical analysis for secondary massive bottom and top quarks on thrust distributions at different c.m. energies.

In chapter 6 we summarize our results and give an outlook on future work on mass effects with exciting possible applications in hadron collider physics. Some prospects concern top loop effects for the primary production of massive top quarks, which is discussed using the example of the thrust distribution in appendix F.

Much of the content of this thesis has been already published in papers in collaboration with Simon Gritschacher, Andre Hoang, Ilaria Jemos and Vicent Mateu concerning the development of the mass mode setup and the application to the thrust distribution [10–12]. Large parts in chapter 4 and in particular in chapter 5 are adopted from these papers. The application to the case of both primary and secondary massive quarks and the resummation of rapidity logarithms will be discussed in a future publication in collaboration with Andre Hoang, Aditya Pathak and Iain Stewart [13]. The application to DIS is ongoing work with Andre Hoang and Daniel Samitz [14] which has been already presented partially at different conferences [15].

We will usually perform the calculations in Feynman gauge and in dimensional regularization for the regularization of UV divergences with $d = 4 - 2\epsilon$ and $\tilde{\mu}^{2\epsilon} = (\frac{\mu^2 e^{\gamma_E}}{4\pi})^{2\epsilon}$ for the extension of the integration measure, which is convenient when the $\overline{\rm MS}$ scheme is employed for renormalization. Most of the computations and plots were performed using *Mathematica 9* [16]. For the expansion of hypergeometric functions, which frequently appear in our computations, we use the *HypExp* package [17]. The Feynman diagrams and many illustrations were drawn in *Jaxodraw 2* [18].

Chapter 2

SCET: An EFT for jet physics

In this chapter we describe an EFT for hard scattering processes with widely separated scales, namely SCET. First we briefly outline what EFTs are, what benefits one gains in using them and why an EFT framework is useful in jet physics. Further information about EFTs can be found in many sources, e.g. in Refs. [19, 20]. We then highlight the main steps in the construction of SCET at leading order in the expansion parameter and its most important features as described in Refs. [21–24]. The emphasis lies on the applications in the chapters 3, 4 and 5, where we in particular need to understand the relevant degrees of freedom and types of interactions that can appear, and the way how factorization and resummation works in SCET. We recommend Iain Stewart's online lectures for a detailed overview over SCET [25].

2.1 Effective Field Theories

The language of particle physics is the one of quantum field theories (QFTs) that describe the degrees of freedom and their interactions up to some particular scale. Basically all phenomenologically relevant QFTs are not UV finite, which implies a validity range up to some high scale $\Lambda_{\rm UV}$ where the description in terms of these theories breaks down and has to be replaced by a more general picture. This holds in particular for the Standard Model, where the high energy scale $\Lambda_{\rm UV}$ might correspond to the Planck scale, the scale of grand unification or a much lower scale (the TeV scale?), which could be probed at the LHC. Since the former scales are out of range, experimentally testable QFTs in particle physics are in principle EFTs. The lack of knowledge about the UV behavior, which causes divergent expressions in the amplitudes does not lead, however, to an inability to describe the physics at a typical low energy scale Λ. This is related to the fact that all building blocks in the QFT, i.e. the couplings, fields and operators can be renormalized in a controlled way, such that meaningful predictions can be obtained. EFTs are intrinsically nonrenormalizable, since they are an infinite series in a power counting parameter corresponding to $\Lambda/\Lambda_{\rm UV}$, which implies that an infinite number of operators have to be renormalized. However, at any order in the power counting parameter $\Lambda/\Lambda_{\rm UV}$ we need only a finite amount of operators and corresponding coefficients related to the high energy behavior which can be determined from experiment. This means that we can make quantitative descriptions at the scale Λ to any precision we want without referring to the details of the full underlying theory. [1]

On the other hand, we do not always want to use the full QFT for describing processes at low energy scales, even if we know the more general structure at high energies. This concerns situations where the full QFT does not give stable quantitative results, e.g. in a perturbative expansion containing large logarithms, or is practically difficult to handle, e.g. the description of atoms and molecules using the full information of QCD and QED. In these cases EFTs are useful to perform simplified computations with reduced degrees of freedom and number of scales in agreement with the infrared structure of the full theory. As described above this does not result in an uncontrolled loss of precision, due to the possibility of a systematic incorporation of higher order effects in the power counting. Since EFTs separate the degrees of freedom at the relevant scales from the beginning they allow to disentangle the quantum fluctuations in a physical quantity at different energies in the form of a factorization theorem. EFTs provide operator based definitions for the matrix elements in factorization theorems in terms of the corresponding degrees

[1] However, symmetries and patterns in the Wilson coefficients can help us to identify main features of the underlying theory. This is exploited in particular in B physics.

of freedom. These components are often highly constrained by the emerging symmetries in the EFT, so that they appear frequently as universal ingredients for different processes. In the context of QCD, factorization is in particular important to separate perturbative and nonperturbative physics. Usually we can exploit our knowledge about the full QCD description and determine the process-dependent high-energy coefficients in the EFT by an explicit calculation. [2] This allows to extract the nonperturbative operator matrix elements in a benchmark process, which can be then used as an input in the description of a different reaction where they appear. Finally, all EFT operators contributing to the corresponding matrix elements in the factorization theorem have to be renormalized, which provides a natural framework for the resummation of large logarithms between widely separated physical scales via RG evolution, a particularly important benefit of EFTs.

Within the Standard Model we often encounter large hierarchies between different scales, e.g. the masses of the particles are very different from each other. In this context, a frequently discussed example is the study of processes at the bottom mass scale which does not require a detailed description of the electroweak interaction and of the top quark. It is then more appropriate to adopt an effective description with a power counting parameter corresponding to m_b/m_W, where the exchange of the gauge bosons in the electroweak theory is incorporated only via local four-fermion operators at leading order in the EFT. The EFT constructed in this way is called Fermi theory. Also in QCD large hierarchies of scales corresponding to masses, momenta, binding energies and the hadronization scale Λ_{QCD} lead to the development of different EFTs. Prominent and very successful examples are Chiral Perturbation Theory (ChPT), Non-Relativistic QCD (NRQCD), Heavy Quark Effective Theory (HQET) and Soft Collinear Effective Theory (SCET), which is the one we will discuss in the following.

The basic ingredients of any EFT are always the same: First one has to find the relevant scales and appropriate degrees of freedom for the given process one wants to describe, which become the fields (modes) in the EFT. The symmetries which are inherited from the full theory or which can arise additionally in the specific kinematic regime guide us what operators are allowed and which possible interactions appear between the modes. Finally, the power counting parameter corresponding to the ratio of the generic scales of the modes we kept in the theory and the ones we integrated out tells us, at which order we can truncate the infinite series expansion of the full theory to reach the intended precision. In the following we will see the most relevant steps explicitly for the case of jet processes described by SCET.

2.2 Momenta and modes in SCET I

SCET is an EFT for jets and light, energetic hadrons that was first developed for B decays. It is different from most EFTs in the respect that it separates the modes according to the scaling of the momentum components of all particles instead of to the particle content. One integrates out far off-shell modes, but keeps the low-energy modes with different invariant masses that can communicate with each other via nonlocal interactions. The ultimate goal of SCET is to factorize cross sections into single scale structures and resum large logarithms between the corresponding kinematic scales.

Let us first investigate the scales appearing in collider processes with narrow jets. In this collinearly enhanced region the typical invariant mass of the jets becomes much smaller than the hard scale Q corresponding to the momentum transfer. In addition soft particle radiation can appear between the jets. This is illustrated in Fig. 2.1 for the endpoint region of the decay $B \to X_s\gamma$ in the heavy meson rest frame, where the final state X contains a single narrow jet of invariant mass $\sim m_b\Lambda_{\mathrm{QCD}}$. Due to the fact that the hard scale $Q \sim m_b$ and the invariant mass scales of the collinear and soft radiation can be widely separated the language of EFT is appropriate to describe this process in the kinematic regime where the jets are narrow.

To describe low invariant mass fluctuations for highly boosted objects, we introduce appropriate coordinates which make the hierarchies in the momentum components obvious. These are the lightcone coordinates which are defined by the lightlike vectors $n^\mu = (1, \vec{n})$ and $\bar{n}^\mu = (1, -\vec{n})$ satisfying $n^2 = \bar{n}^2 = 0$

[2] This is not always possible in an analytic way, since the Wilson coefficients can be nonperturbative. In these cases one has to match to experiments or rely on computations from lattice QCD.

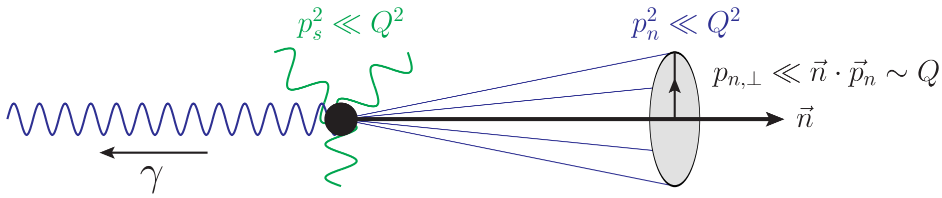

Figure 2.1: Sketch of the decay $B \to X_s \gamma$ in the endpoint region, where the invariant mass of the collinear and soft radiation is much smaller than the c.m. energy $Q \sim m_b$.

and $n \cdot \bar{n} = 2$ and where $\vec{n}$ indicates the direction of the jet. [3] The decomposition of the momenta in terms of the lightcone vectors and the three-momentum perpendicular to the jet axis $\vec{n}$ reads

$$p^\mu = \frac{\bar{n}^\mu}{2} p^+ + \frac{n^\mu}{2} p^- + p_\perp^\mu \equiv (p^+, p^-, p_\perp) \tag{2.1}$$

with $p^+ \equiv n \cdot p$ and $p^- \equiv \bar{n} \cdot p$. The energy of a particle reads in terms of these coordinates

$$E = p_0 = \frac{1}{2}(p^+ + p^-)\,. \tag{2.2}$$

The invariant mass of a particle can be written as

$$p^2 = p^+ p^- + p_\perp^2\,. \tag{2.3}$$

We define hard momenta by the generic scaling $p_h^\mu \sim Q(1,1,1)$. Since these have a large offshellness, they only appear in the local interaction denoted by the blob in Fig. 2.1 and will not be associated with degrees of freedom in SCET. The momentum components of (massless) boosted collinear particles in the jet direction $\vec{n}$ satisfy $p_n^- \gg p_n^+$ and $p_n^- \gg |\vec{p}_\perp|$, such that $p_n^- \sim 2E_n \sim Q$. The invariant mass of the jet $s \sim (\sum_{i \in \text{jet}} p_{n,i})^2$ is much smaller than Q^2, characterizes the width of the jet and depends on the (inclusive) observable we want to measure. The SCET power counting parameter can be defined by the ratio of the jet invariant mass and the momentum transfer scale, i.e. $\lambda^2 \sim s/Q^2$. Frequently one encounters the specific scaling $\lambda \sim \sqrt{\Lambda_{\text{QCD}}/Q}$ or $\lambda \sim \Lambda_{\text{QCD}}/Q$ corresponding to soft radiation at the hadronic scale, but depending on the process and the kinematic regime s can adopt also a scaling unrelated to Λ_{QCD}. To describe the momentum components of the collinear fluctuations the natural counting in terms of the power counting parameter is $p^+p^- \sim p_\perp^2 \sim Q\lambda^2$. Thus the n-collinear momenta scale like $p_n^\mu \sim Q(\lambda^2, 1, \lambda)$. The momenta of the soft radiation have uniformly scaling components, but invariant masses that depend on the corresponding physical observable. If the soft invariant mass scale is of order $Q^2\lambda^4$ we call the momenta ultrasoft and they satisfy $p_{us}^\mu \sim Q(\lambda^2, \lambda^2, \lambda^2)$. On the other hand if the soft invariant mass scale is of the same order as the jet scale, the soft momenta scale as $p_s^\mu \sim Q(\lambda, \lambda, \lambda)$. The corresponding theories are then usually called SCET I and SCET II, respectively. [4] In this thesis we will encounter both theories. Since SCET II can be obtained from integrating out (hard) collinear modes with larger virtuality from SCET I, we will first sketch the construction of SCET I, and come back to SCET II in Sec. 2.5.

We have now seen that the relevant degrees of freedom for jet processes, the collinear and soft particles, are characterized by their momentum scalings. The corresponding fields can be obtained from the full QCD fields by disentangling short-range from long-distance quantum fluctuations. There are different technical ways to perform this: One can either distinguish the large and small momenta by introducing "labels" in a hybrid momentum-position space picture [22–24] or one can stay in position space and perform a full multipole expansion there [27, 28]. In the following we will adopt the first approach. We

[3] We will investigate only processes with a single jet or two jets going back-to-back. Therefore, a single jet axis is enough for our purposes, so that we can choose $\bar{n}_1^\mu = n_2^\mu$ in dijet processes with $\vec{n}_2 = -\vec{n}_1$ for convenience. In the case of several jet directions this description can be generalized.

[4] For some observables, e.g. arbitrary angularities, the jet and soft scales can be also separated by noninteger powers of the expansion parameter λ. We will not consider this situation in the following.

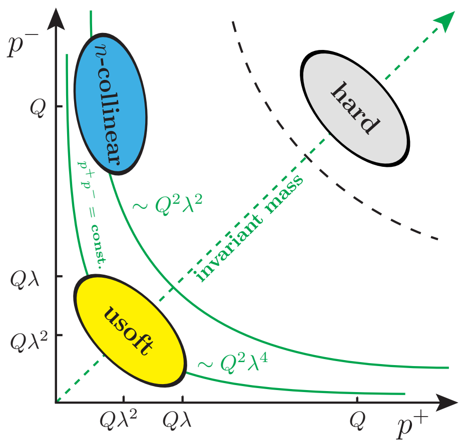

mode	$p^\mu = (+, -, \perp)$	p^2	fields
hard	$Q(1, 1, 1)$	Q^2	–
n-collinear	$Q(\lambda^2, 1, \lambda)$	$Q^2\lambda^2$	ξ_n, A_n^μ
ultrasoft	$Q(\lambda^2, \lambda^2, \lambda^2)$	$Q^2\lambda^4$	q_{us}, A_{us}^μ

Figure 2.2: Momentum modes and scaling in the p^+-p^- plane in SCET I for a process with a single jet like $B \to X_s\gamma$ with $Q \sim m_b$. Hard modes with offshellness $\sim Q^2$ are integrated out and only ultrasoft and collinear modes at different scales remain. Adapted from Ref. [26].

decompose the momentum of a n-collinear particle into a "discrete" large label momentum $\tilde{p}_n^\mu$ with respect to the n-collinear direction of order Q and $Q\lambda$ and a small residual momentum k^μ of order $Q\lambda^2$

$$p_n^\mu = \tilde{p}_n^\mu + k^\mu\,, \quad \tilde{p}_n^\mu \sim Q(0, 1, \lambda)\,, \quad k^\mu \sim Q(\lambda^2, \lambda^2, \lambda^2)\,. \tag{2.4}$$

Both types of momenta will be (overall) conserved individually in any interaction. We want to separate quantum fluctuations corresponding to these momenta in a gauge-invariant way and therefore decompose the quark fields $q(x)$ and the gluon field $A^\mu(x)$ such that they contain only the dependence on the residual momentum, [5]

$$q(x) = \sum_{\tilde{p}\neq 0} e^{-i\tilde{p}x} q_{n,\tilde{p}}(x) + q_{us}(x)\,, \quad A^\mu(x) = \sum_{\tilde{p}\neq 0} e^{-i\tilde{p}x} A_{n,\tilde{p}}^\mu(x) + A_{us}^\mu(x)\,. \tag{2.5}$$

For $p^- \gg p_\perp \gg p^+$ the collinear quark field $q_{n,\tilde{p}}(x)$ contains one large spinor component $\xi_{n,\tilde{p}}(x)$ and one small spinor component $\hat{\xi}_{\bar{n},\tilde{p}}(x)$. These can be obtained by applying the orthogonal projectors

$$P_n = \frac{\not{n}\not{\bar{n}}}{4}\,, \quad P_{\bar{n}} = \frac{\not{\bar{n}}\not{n}}{4} \quad \text{with } P_n + P_{\bar{n}} = 1 \tag{2.6}$$

on $q_{n,\tilde{p}}$ via

$$\xi_{n,\tilde{p}}(x) = P_n\, q_{n,\tilde{p}}(x)\,, \quad \hat{\xi}_{\bar{n},\tilde{p}}(x) = P_{\bar{n}}\, q_{n,\tilde{p}}(x)\,. \tag{2.7}$$

The small component $\hat{\xi}_{\bar{n},\tilde{p}}(x)$ has a power suppressed kinetic term, will be therefore not treated as a dynamic field and is integrated out in the construction of SCET. The location of the relevant fields in the p^+p^- plane in the case of one single jet in SCET I and the scaling of the corresponding momenta is summarized in Fig. 2.2. Note that $\xi_{n,\tilde{p}}(x)$ represents both quark and antiquark fields, which can then be treated together for internal states. Writing out the mode expansion of the Dirac spinor

$$q(x) = \int \mathrm{d}^4p\, \delta(p^2)\, \theta(p^+ + p^-)\, \big(u(p)\, a(p)\, e^{-ipx} + v(p)\, b^\dagger(p)\, e^{ipx}\big) \equiv q^+(x) + q^-(x)\,, \tag{2.8}$$

and following the decomposition in Eq. (2.5) and the projection in Eq. (2.7) particle fields with a positive label p^- and antiparticle fields with a negative label p^- can be combined to the collinear field $\xi_{n,\tilde{p}}(x)$,

$$\xi_{n,\tilde{p}}(x) = \theta(p^-)\, \xi_{n,\tilde{p}}^+(x) + \theta(-p^-)\, \xi_{n,-\tilde{p}}^-(x)\,. \tag{2.9}$$

[5] In the second relation also terms with multiple gauge fields $A^\mu(x)$ appear to preserve gauge symmetries at higher orders in the power counting. Since we are here just interested in the leading order terms in λ we neglect them.

An important thing to notice is that the ultrasoft fields $q_{us}(x)$ and $A^\mu_{us}(x)$ are related to a vanishing label. In contrast the collinear fields imply a nonvanishing label. In practice, however, it is much simpler to perform calculations with a continuous integration over all momenta. In this case one has to take care of double counting between the collinear and ultrasoft sector, which can be achieved by performing a subtraction of the amplitudes with an additional expansion of the collinear momenta in the ultrasoft region, called zero-bin subtractions [29].

2.3 The Lagrangian in SCET I

To perform computations in SCET we need the Lagrangian and the corresponding Feynman rules. In this thesis we will just consider the leading order in the expansion parameter λ. Power suppressed contributions were considered e.g. in Refs. [27,30]. We start with the QCD Lagrangian including a quark mass,

$$\mathcal{L}_{\rm QCD} = \bar{q}\,(i\not{D} - m)\,q - \frac{1}{4}F_{\mu\nu}F^{\mu\nu} \tag{2.10}$$

with $D_\mu = \partial_\mu + igT^a A^a_\mu$ and the gluon field strength tensor $F_{\mu\nu} = -\frac{i}{g}[D_\mu, D_\nu]$. To find the relevant operators in the SCET Lagrangian we have to consider the scaling of the collinear and ultrasoft fields. It is convenient to let the kinetic terms of the dynamic fields scale like λ^0, and count the interaction terms in powers of λ with respect to them. The n-collinear fields fluctuate over a distance $\Delta x^\mu_n \sim Q^{-1}(\lambda^{-2}, 1, \lambda^{-1})$, which yields a phase space measure $\mathrm{d}^4x_n \sim (Q\lambda)^{-4}$. Performing the field redefinitions in Eq. (2.5) in the Lagrangian (2.10) and investigating the derivative terms (related to the residual momentum component) leads to the scaling relations for the collinear fields, [6]

$$\xi_{n,\tilde{p}} \sim q_{n,\tilde{p}} \sim Q^{3/2}\lambda\,, \quad A^\mu_{n,\tilde{p}} \sim Q(\lambda^2, 1, \lambda)\,, \tag{2.11}$$

The ultrasoft fields fluctuate over a distance $\Delta x^\mu_{us} \sim Q^{-1}(\lambda^{-2}, \lambda^{-2}, \lambda^{-2})$, which yields a phase space measure $\mathrm{d}^4x_{us} \sim (Q\lambda^2)^{-4}$, and satisfy the scaling

$$q_{us} \sim Q^{3/2}\lambda^3\,, \quad A^\mu_{us} \sim Q(\lambda^2, \lambda^2, \lambda^2)\,. \tag{2.12}$$

Note that the gauge fields scale like the corresponding momenta, so that derivatives acting on a collinear quark field can be recombined to covariant derivatives.

Let us study the collinear quark Lagrangian in SCET. Applying Eqs. (2.5) and (2.7) in the QCD quark Lagrangian yields

$$\begin{aligned}\mathcal{L}_{q,n} = \sum_{\tilde{p},\tilde{p}'\neq 0} e^{-i(\tilde{p}-\tilde{p}')x}\Big[&\bar{\xi}_{n,\tilde{p}'}\, in\cdot D\,\frac{\not{\bar{n}}}{2}\xi_{n,\tilde{p}} + \bar{\hat{\xi}}_{\bar{n},\tilde{p}'}\left(\not{\tilde{p}}_\perp + i\not{D}_\perp - m\right)\xi_{n,\tilde{p}} \\ &+ \bar{\xi}_{n,\tilde{p}'}\left(\not{\tilde{p}}_\perp + i\not{D}_\perp - m\right)\hat{\xi}_{\bar{n},\tilde{p}} + \bar{\hat{\xi}}_{\bar{n},\tilde{p}'}\,(\tilde{p} + i\bar{n}\cdot D)\,\frac{\not{n}}{2}\hat{\xi}_{\bar{n},\tilde{p}}\Big]\,.\end{aligned} \tag{2.13}$$

As already stated in Sec. 2.2 the field $\hat{\xi}_{\bar{n},\tilde{p}} \sim Q^{3/2}\lambda^2$ is static in SCET due to the fact that the kinetic term involving the partial derivative $\bar{n}\cdot\partial \sim Q\lambda^2$ is suppressed. We can therefore integrate it out via the equation of motion

$$(\tilde{p} + i\bar{n}\cdot D)\,\frac{\not{n}}{2}\hat{\xi}_{\bar{n},\tilde{p}} = -\left(\not{\tilde{p}}_\perp + i\not{D}_\perp - m\right)\xi_{n,\tilde{p}}\,, \tag{2.14}$$

and the corresponding one for $\bar{\hat{\xi}}_{\bar{n},\tilde{p}}$. Thus the Lagrangian at tree level reads

$$\mathcal{L}_{q,n} = \sum_{\tilde{p},\tilde{p}'\neq 0} e^{-i(\tilde{p}-\tilde{p}')x}\bar{\xi}_{n,\tilde{p}'}\left[in\cdot D + (\not{\tilde{p}}_\perp + i\not{D}_\perp + m)\frac{1}{\tilde{p}_- + i\bar{n}\cdot D}(\not{\tilde{p}}_\perp + i\not{D}_\perp - m)\right]\frac{\not{\bar{n}}}{2}\xi_{n,\tilde{p}}\,. \tag{2.15}$$

[6]For the collinear gauge field one can impose the constraint that all components of the propagator scale according to the momenta in a general covariant gauge.

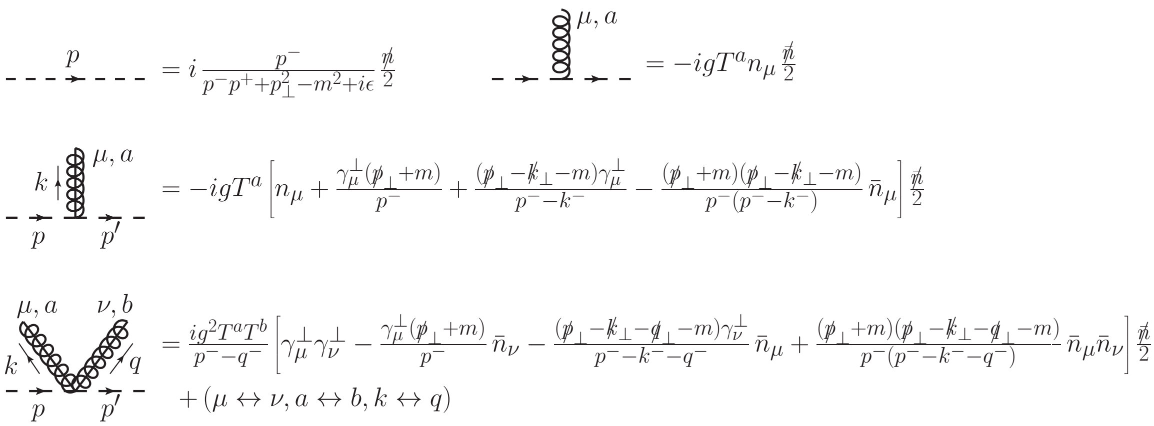

Figure 2.3: The SCET Feynman rules corresponding to the n-collinear massive quark Lagrangian in Eq. (2.18) at leading order in λ up to $\mathcal{O}(g^2)$ in the strong coupling. Here we have combined the label momenta with the residual momenta. Zero-bin subtractions are implied for the collinear momenta.

This expression is still exact when considering a single collinear sector which is just boosted QCD. Note that due to the interactions with collinear gluons the label momentum of the quark changes. It is convenient to suppress the explicit dependence on the labels to simplify the notation. For this purpose we introduce the label operator $\mathcal{P}^\mu$, which extracts the large label momentum out of any collinear field $\phi_{n,\tilde{p}}(x)$, i.e.

$$\mathcal{P}^\mu \phi_{n,\tilde{p}}(x) = \tilde{p}^\mu \phi_{n,\tilde{p}}(x)\,, \quad \mathcal{P}^\mu \phi^\dagger_{n,\tilde{p}}(x) = -\tilde{p}^\mu \phi^\dagger_{n,\tilde{p}}(x)\,. \tag{2.16}$$

The remaining partial derivatives are only acting on the residual x-dependence in contrast to the full QCD fields,

$$i\partial^\mu\left[P_n q(x)\right] \to e^{-i\mathcal{P}\cdot x}\left(\mathcal{P}^\mu + i\partial^\mu\right)\xi_n(x) \quad \text{with } \xi_n(x) \equiv \sum_{\tilde{p}\neq 0} \xi_{n,\tilde{p}}(x)\,, \tag{2.17}$$

with $\partial^\mu \sim Q\lambda^2$ in SCET. In the following we will imply overall label conservation, so that the exponentials $e^{-i\mathcal{P}x}$ will not be written out explicitly. To obtain the Lagrangian at LO we have to expand Eq. (2.15) using the scaling of the momenta in Eq. (2.4) and the scaling of the fields in Eqs. (2.11) and (2.12). After these steps the collinear quark Lagrangian reads [22, 31]

$$\mathcal{L}_{q,n} = \bar{\xi}_n(x)\left[in\cdot D + \left(iD\!\!\!\!/_{n\perp} + m\right)\frac{1}{i\bar{n}\cdot D_n}\left(iD\!\!\!\!/_{n\perp} - m\right)\right]\frac{\bar{n}\!\!\!/}{2}\xi_n(x)\,, \tag{2.18}$$

which is still local in the residual coordinate x. In Eq. (2.18) we have used besides the full covariant derivative in $n\cdot D$ also the multipole expanded components denoted by $D^\mu_{n\perp}$ and $\bar{n}\cdot D_n$, which are given by

$$in\cdot D = in\cdot\partial - gn\cdot A_n - gn\cdot A_{us}\,, \tag{2.19}$$
$$iD^\mu_{n\perp} = \mathcal{P}^\mu_\perp - gA^\mu_{n,\perp}\,, \tag{2.20}$$
$$i\bar{n}\cdot D_n = \bar{n}\cdot\mathcal{P} - g\bar{n}\cdot A_n\,. \tag{2.21}$$

We note that the label n is conserved corresponding to the fact that only a hard external interaction can alter the direction of the collinear quark. The Feynman rules corresponding to the Lagrangian in Eq. (2.18) expanded up to $\mathcal{O}(g^2)$ in the strong coupling are displayed in Fig. 2.3.

The derivation of the leading order (i.e. $\mathcal{O}(\lambda^4)$) Lagrangian density has been performed here just at tree level. In principle loop corrections could enter in Wilson coefficients and could involve also other

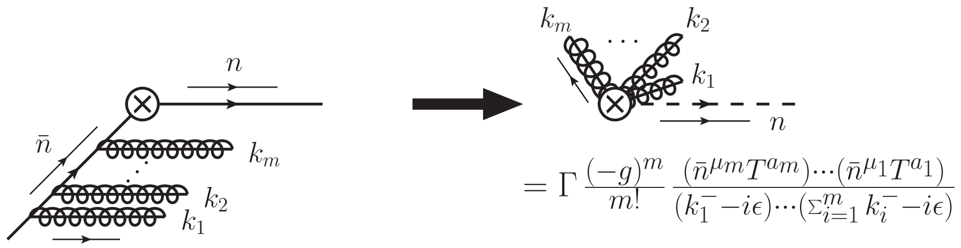

Figure 2.4: The Feynman rule corresponding to the Wilson line in Eq. (2.28) contributing to the SCET current operator in Eq. (2.24) for one configuration of m outgoing n-collinear gluons.

operators. However, investigating the symmetries of SCET it turns out that the Lagrangian (2.18) is exact to any order in α_s: On the one hand, SCET can be constructed such that the collinear and ultrasoft sectors do not mix under gauge transformations, i.e. are separately gauge-invariant [24] as we will discuss in Sec. 2.4, which puts constraints on the form of the possible operators involving several gluon fields. On the other hand, although Lorentz invariance is explicitly broken by a fixed jet direction $\vec{n}$, there is still a degree of arbitrariness in picking the coordinates n^μ and $\bar{n}^\mu$. This residual symmetry is called reparametrization invariance, excludes any additional operators in the Lagrangian at leading order and fixes all remaining Wilson coefficients [32].

Including also all collinear gluon and ultrasoft interactions the complete Lagrangian reads

$$\mathcal{L}_{\mathrm{SCET}} = \mathcal{L}_{q,n}(\xi_n, A_n^\mu, A_{us}^\mu) + \mathcal{L}_{g,n}(A_n^\mu, A_{us}^\mu) + \mathcal{L}_{us}(q_{us}, A_{us}^\mu)\,. \tag{2.22}$$

The ultrasoft Lagrangian $\mathcal{L}_{us}$ has uniformly scaling components, does not contain interactions with the collinear fields and is thus the same as in QCD with the fields replaced by ultrasoft quarks and gluons. The purely gluonic collinear Lagrangian $\mathcal{L}_{g,n}$ can be derived in a similar way as the collinear quark Lagrangian and can be found with the corresponding Feynman rules in Ref. [24]. Note that the Lagrangian (2.22) can be generalized easily for multiple jets by including copies of $\mathcal{L}_{q,n_i}$ and $\mathcal{L}_{g,n_i}$ with the corresponding jet axes $\vec{n}_i$.

2.4 Wilson lines and gauge symmetries

We discuss collinear and ultrasoft Wilson lines which have the appropriate gauge transformations to construct fundamental building blocks of SCET operators.

2.4.1 Collinear Wilson lines

We have seen in the SCET Lagrangian (2.22) that n is a conserved label, i.e. collinear particles in different directions cannot interact with each other directly. This is related to the fact that their sum of the momenta and their invariant mass satisfy (here displayed for an n- and $\bar{n}$-collinear particle)

$$p_n^\mu + p_{\bar{n}}^\mu \sim Q(1,1,\lambda)\,, \quad (p_n + p_{\bar{n}})^2 \sim Q^2\,, \tag{2.23}$$

such that these interactions generate large virtualities (i.e. invariant masses) which we have integrated out in the matching process to SCET and which are encaptured in local Wilson coefficients. Thus only interactions within one collinear sector and with the low-momentum ultrasoft modes are possible.

However, in hard scattering processes we will encounter interactions, which are not described by the Lagrangian in Eq. (2.22), in our examples mainly mediated via the electromagnetic force. In the corresponding external current operators fields with different collinear directions can appear. Let us investigate a scattering process with an incoming $\bar{n}$-collinear and an outgoing n-collinear quark field as displayed in Fig. 2.4. [7] The corresponding current reads in full QCD and in SCET

$$\bar{q}(x)\,\Gamma\,q(x) \to \bar{\xi}_n(x)\,\Gamma\,\xi_{\bar{n}}(x)\,[1+\mathcal{O}(g)]\;, \tag{2.24}$$

where Γ is an arbitrary 4×4 spin matrix. The current operator on the RHS can contain an arbitrary number of n-collinear ($\bar{n}$-collinear) gluons emitted from the incoming $\bar{n}$-collinear (outgoing n-collinear quark) since operators with $\bar{n}\cdot A_n$ ($n\cdot A_{\bar{n}}$) are not suppressed by the power counting parameter λ in the corresponding collinear sector. However, this interaction pushes the intermediate quark propagators far offshell, as shown in Eq. (2.23) resulting in local interactions in the effective theory.

The form of these local interactions is restricted by gauge-invariance. In SCET the fields fluctuate over different distances, which is a fact that should be preserved under gauge transformations U such that the EFT is closed and different degrees of freedom do not mix with each other. Therefore the fields change under gauge transformations according to their corresponding momentum scaling. We define n-collinear, $\bar{n}$-collinear and ultrasoft gauge transformations by

$$\partial^\mu U_n(x)\sim Q(\lambda^2,1,\lambda)\,,\quad \partial^\mu U_{\bar{n}}(x)\sim Q(1,\lambda^2,\lambda)\,,\quad \partial^\mu U_{us}(x)\sim Q(\lambda^2,\lambda^2,\lambda^2)\,. \tag{2.25}$$

The n-collinear quark field transforms according to [24] [8]

$$\xi_n(x)\xrightarrow{U_n} U_n(x)\xi_n(x)\,,\quad \xi_n(x)\xrightarrow{U_{\bar{n}}}\xi_n(x)\,,\quad \xi_n(x)\xrightarrow{U_{us}} U_{us}(x)\xi_n(x)\,, \tag{2.26}$$

and analogously for the $\bar{n}$-collinear field with the replacement $n\to\bar{n}$. The n-collinear ($\bar{n}$-collinear) field does not change under $\bar{n}$-collinear (n-collinear) gauge transformations. Therefore, the current operator on the RHS of Eq. (2.24) is not invariant under collinear gauge transformations and we need gauge-links in terms of the collinear gluon fields to restore this symmetry. These are provided by Wilson lines, which are given in position space by

$$\tilde{W}_n(x,-\infty) = \mathrm{P}\exp\left[-ig\int_{-\infty}^{0} ds\,\bar{n}\cdot A_n\,(s\bar{n}^\mu + x^\mu)\right] \tag{2.27}$$

for the n-collinear sector and a related definition for the $\bar{n}$-collinear Wilson line $\tilde{W}_{\bar{n}}$. Here P denotes the path-ordering operator. Performing a Fourier transformation to label space we obtain for the n-collinear sector

$$W_n(x) = \left[\sum_{\text{perms}} \exp\left\{-\frac{g}{\bar{n}\cdot\mathcal{P}}\,\bar{n}\cdot A_n(x)\right\}\right]\,. \tag{2.28}$$

Here and in the following the label operator acts only inside the square bracket. This label space Wilson line agrees with the direct computation of the matching between the QCD to SCET currents. The corresponding Feynman rule at LO in λ for one configuration of m outgoing n-collinear gluons is shown in Fig. (2.4). By summing over all permutations and different numbers of emitted gluons one obtains Eq. (2.28). Note that we have dropped the $i\epsilon$ prescription in Eq. (2.28), since it does not play a role for the collinear sector once the corresponding zero-bin subtractions are taking into account. In this respect $W_{\bar{n}}(x)$ is in analogy to Eq. (2.27) with n replaced by $\bar{n}$ irrespective of the origin of the collinear Wilson line. [9]

The Wilson lines transform under the gauge transformations according to

$$W_n(x)\xrightarrow{U_n} U_n(x)W_n(x)\,,\quad W_n(x)\xrightarrow{U_{\bar{n}}} W_n(x)\,,\quad W_n(x)\xrightarrow{U_{us}} U_{us}(x)W_n(x)U_{us}^\dagger(x)\,, \tag{2.29}$$

With the transformation rules in Eqs. (2.26) and (2.29) one can construct the collinearly gauge-invariant *quark jet fields* $\chi_n(x)$, $\chi_{\bar{n}}(x)$ defined by

$$\chi_n(x)\equiv W_n^\dagger(x)\xi_n(x)\,,\quad \chi_{\bar{n}}(x)\equiv W_{\bar{n}}^\dagger(x)\xi_{\bar{n}}(x)\,, \tag{2.30}$$

[7] The remaining cases with incoming or/and outgoing antiquarks can be treated analogously and correspond to inversions of the momenta and the ordering of the emitted gluons.

[8] The n-collinear transformation changes the label of the quark field, i.e. $\xi_{n,\tilde{p}}(x)\to U_{n,\tilde{p}-\tilde{p}'}(x)\,\xi_{n,\tilde{p}'}(x)$, which we have hidden in our notation.

[9] This does not hold any more for ultrasoft Wilson lines, see Sec. 2.4.2.

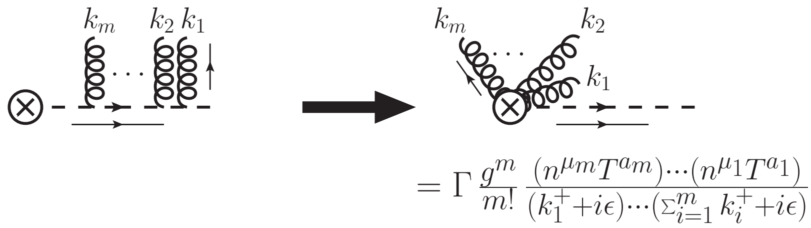

Figure 2.5: The Feynman rule for the Wilson line $Y^\dagger_{n,+}$ corresponding to Eq. (2.40) contributing to the SCET current operator in Eq. (2.35) for one configuration of m outgoing soft gluons and an n-collinear outgoing quark.

as building blocks for SCET operators. The corresponding current

$$\mathcal{J}_\Gamma = \bar{\chi}_n(x)\,\Gamma\,\chi_{\bar{n}}(x) \tag{2.31}$$

is then gauge-invariant with respect to both collinear and ultrasoft transformations.

In a similar way to the quark fields, one can also construct collinearly gauge-invariant *gluon jet fields* with the help of the Wilson lines, e.g. for the n-collinear sector one has

$$\mathcal{B}^\mu_{n\perp}(x) = \frac{1}{g}\left[W_n^\dagger(x) iD^\mu_{n\perp}(x) W_n(x)\right] . \tag{2.32}$$

The label of a quark or gluon jet field is the sum of the labels of the particles in the jet initiated by the corresponding parton, such that these fields are the appropriate ones to describe the dynamics of a jet.

2.4.2 Ultrasoft Wilson lines

So far the collinear fields in the SCET Lagrangian (2.22) are still interacting with the ultrasoft fields. It is, however, possible and convenient (though not mandatory) to decouple also the collinear and ultrasoft sectors there. This can be achieved by the following field redefinitions [24],

$$\xi_n(x) = Y_n(x)\xi_n^{(0)}(x)\,, \quad A_n^\mu(x) = Y_n(x) A_n^{\mu(0)}(x) Y_n^\dagger(x)\,, \tag{2.33}$$

where $Y_n(x)$ is an ultrasoft Wilson line and the computations with the decoupled fields $\xi_n^{(0)}(x)$ and $A_n^{\mu(0)}(x)$ yield the same S-matrix elements as with $\xi_n(x)$ and $A_n^\mu(x)$. Using the defining equation of the ultrasoft Wilson line, $(in\cdot\partial + gn\cdot A_{us})Y_n = 0$, and its unitarity, $Y_n Y_n^\dagger = 1$, the ultrasoft interactions cancel in the collinear Lagrangian and all sectors are separated (and of course gauge-invariant), i.e.

$$\mathcal{L}_{\text{SCET}} = \mathcal{L}_{q,n}(\xi_n, A_n^\mu) + \mathcal{L}_{g,n}(A_n^\mu) + \mathcal{L}_{us}(q_{us}, A_{us}^\mu)\,. \tag{2.34}$$

The interactions between the collinear and ultrasoft fields are now encoded in external current operators, e.g. for the SCET current in Eq. (2.31) we obtain

$$\mathcal{J}_\Gamma = \bar{\chi}_n \Gamma \chi_{\bar{n}}(x) \to \bar{\chi}_n^{(0)} Y_n^\dagger\,\Gamma\,Y_{\bar{n}} \chi_{\bar{n}}^{(0)}(x)\,. \tag{2.35}$$

In the remainder of this thesis we will drop the superscript (0), since it will be clear from the context when we use the collinear fields after having decoupled the ultrasoft fields.

For external incoming/outgoing particles and antiparticles the precise prescriptions for the ultrasoft Wilson line $Y_n(x)$ differ. For the case of an incoming and outgoing n-collinear quark the Wilson lines reads in position space

$$Y_{n,+}(x) \equiv Y_n(x,-\infty) = \mathrm{P}\exp\left[-ig\int_{-\infty}^0 ds\, n\cdot A_{us}(sn^\mu + x^\mu)\right] , \tag{2.36}$$

$$Y^\dagger_{n,+}(x) \equiv Y_n(\infty,x) = \mathrm{P}\exp\left[-ig\int_0^{\infty} ds\, n\cdot A_{us}(sn^\mu + x^\mu)\right] , \tag{2.37}$$

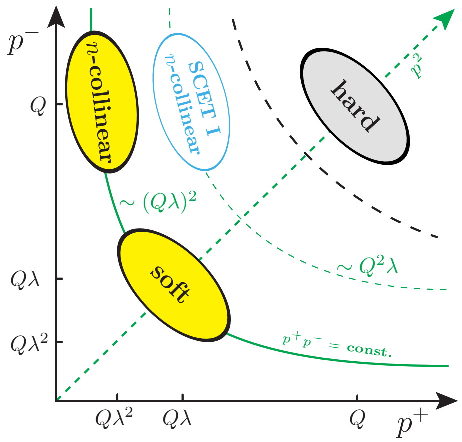

mode	$p^\mu = (+,-,\perp)$	p^2	fields
hard	$Q(1,1,1)$	Q^2	$-$
n-collinear	$Q(\lambda^2,1,\lambda)$	$Q^2\lambda^2$	$\xi_n,\ A_n^\mu$
soft	$Q(\lambda,\lambda,\lambda)$	$Q^2\lambda^2$	$q_s,\ A_s^\mu$

Figure 2.6: Momentum modes and scaling in SCET II in the p^+-p^- plane e.g. for an exclusive decay with one collinear hadron in the final state like in $B \to D\pi$ with $Q \sim m_b$. Hard modes with offshellness $\sim Q^2$ are integrated out and only soft and collinear modes at different scales remain. We have also indicated the scaling of the corresponding hard collinear SCET I modes, which have to be integrated out to obtain SCET II.

where the subscript n stands for the direction of the Wilson line and not the encoded fields, and $Y^\dagger_{n,+}(x)$ should be read as $(Y^\dagger_n)_+(x)$ and not as $(Y_{n,+}(x))^\dagger$. For the case of an outgoing and incoming n-collinear antiparticle we obtain instead

$$Y_{n,-}(x) \equiv \overline{Y}_n(\infty, x) = \overline{\mathrm{P}} \exp\left[ig \int_0^\infty ds\, n \cdot A_{us}(sn^\mu + x^\mu)\right], \tag{2.38}$$

$$Y^\dagger_{n,-}(x) \equiv \overline{Y}_n(x, -\infty) = \overline{\mathrm{P}} \exp\left[ig \int_{-\infty}^0 ds\, n \cdot A_{us}(sn^\mu + x^\mu)\right], \tag{2.39}$$

where $\overline{\mathrm{P}}$ denotes anti-path-ordering. Note that we get $(Y_{n,+}(x))^\dagger = Y^\dagger_{n,-}(x)$ and $(Y_{n,-}(x))^\dagger = Y^\dagger_{n,+}(x)$. Performing a Fourier transform to momentum space the Wilson line for n-collinear outgoing quarks and gluons with outgoing momenta k_i one obtains

$$Y^\dagger_{n,+} = \sum_{m=0}^\infty \sum_{\text{perms}} \frac{g^m}{m!} \frac{n \cdot A^{a_m}_{us} T^{a_m} \cdots n \cdot A^{a_1}_{us} T^{a_1}}{(k_1^+ + i\epsilon) \cdots (\sum_{i=1}^m k_i^+ + i\epsilon)} \tag{2.40}$$

with the corresponding Feynman rule illustrated in Fig. 2.5 for one configuration of m soft gluons. The other configurations have similar expressions. A thorough analysis for the appropriate soft Wilson lines in different processes can be found in Ref. [33]. Finally, we note that the ultrasoft fields do not change under collinear gauge transformations, in particular we obtain

$$Y_n(x) \xrightarrow{U_n} Y_n(x)\,, \quad Y_n(x) \xrightarrow{U_{\bar{n}}} Y_n(x)\,, \quad Y_n(x) \xrightarrow{U_{us}} U_{us}(x) Y_n(x)\,. \tag{2.41}$$

2.5 SCET II

So far we have discussed SCET with collinear and ultrasoft modes. For some processes like exclusive decays into hadrons or for some production mechanisms of massive particles this is, however, not the appropriate theory. In these cases fluctuations of *soft* and collinear modes can take place at the same invariant mass scale. This is sketched in Fig. 2.6 for the decay $B \to D\pi$ in the B meson rest frame, where the pion is strongly boosted and large fluctuations around the heavy quark mass scales have been integrated out, so that the remaining fluctuations have an invariant mass of $\mathcal{O}(\Lambda^2_{\text{QCD}})$. Note that the distinction of soft and collinear modes is frame dependent, since they are just separated by boosts and not by invariant masses as in SCET I.

SCET II can be obtained from SCET I with the expansion parameter λ_{I} by integrating out hard collinear modes with the momentum scaling $p_{hc,n} \sim Q(\lambda_{\mathrm{I}}^2, 1, \lambda_{\mathrm{I}})$ for the n-direction [34]. In terms of the SCET II scaling parameter $\lambda_{\mathrm{II}} = \lambda_{\mathrm{I}}^2$ the corresponding low-energy collinear modes adopt the usual scaling $p_n \sim Q(\lambda_{\mathrm{II}}^2, 1, \lambda_{\mathrm{II}})$, whereas the ultrasoft modes in SCET I become soft, i.e. they scale like $p_s \sim Q(\lambda_{\mathrm{II}}, \lambda_{\mathrm{II}}, \lambda_{\mathrm{II}})$. Note that soft and collinear particles in SCET II cannot interact with each other directly, since the corresponding invariant mass would scale like $(p_n + p_s)^2 \sim Q^2\lambda_{\mathrm{II}} \gg Q^2\lambda_{\mathrm{II}}^2$ and is thus far offshell. Therefore, intermediate offshell particles have to be integrated out giving rise to soft Wilson lines $S_n(x)$. These can be also obtained directly from SCET I using the field redefinitions with the ultrasoft Wilson lines $Y_n(x)$ (see Sec. 2.4.2) and with the replacement $A^\mu_{us} \to A^\mu_s$. Note that the collinear fields now do not change under soft gauge transformations and also soft fields are not affected by collinear gauge transformations.

There are some subtleties in SCET II computations compared to SCET I: First, the collinear fields in SCET II require now a soft-bin subtraction to avoid double counting with the soft sector, i.e. the subtraction of contributions with an additional expansion in the soft region [29,35]. Second, the fact that soft and collinear modes are not separated by invariant masses but by rapidity y (with $e^{2y} = p^-/p^+$) leads to a new type of divergence in the overlap region for individual sectors, which is called *rapidity divergence*. This divergence cannot be regularized with dimensional regularization, but needs an additional regulator that breaks boost invariance. In the sum of all contributions the rapidity divergences cancel, but can leave behind a large logarithm.

2.6 Factorization and resummation in SCET

The main aim of the separation of the hard, collinear and soft modes in SCET is to factorize differential cross sections $\mathrm{d}\sigma$ into structures depending only on one single scale, schematically

$$\mathrm{d}\sigma \sim \mathcal{H} \otimes \mathcal{J} \otimes \mathcal{S}\,[1 + \mathcal{O}(\lambda)]\,, \tag{2.42}$$

where $\mathcal{H}$ denotes a hard function corresponding to the mismatch between SCET and QCD at the hard scale, $\mathcal{J}$ stands for a jet function in terms of the collinear modes and $\mathcal{S}$ corresponds to a soft function in terms of the ultrasoft (or soft) modes. We will see in the next chapters examples for this type of factorization. Establishing a factorization theorem in QCD is often tedious and many “proofs” rely on the use of a specific gauge or are performed order by order in the strong coupling. In contrast, in EFTs factorization is simplified by the appropriate choice of modes. We just have to write down all possible operators at the given order in the power counting parameter that are consistent with the symmetries of the EFT. In SCET, a minimal basis of building blocks with n-collinear fields for operators satisfying gauge invariance and reparametrization invariance is given by [36]

$$\chi_n(x)\,, \quad \mathcal{B}^\mu_{n\perp}(x)\,, \quad \mathcal{P}^\mu_{n\perp}\,, \quad \bar{n}\cdot\mathcal{P}\,. \tag{2.43}$$

Note that the label operator $\bar{n}\cdot\mathcal{P}$ is not suppressed by powers of λ and can be attached as an arbitrary function $\mathcal{C}(\bar{n}\cdot\mathcal{P})$ to any collinear field, which can be interpreted as a Wilson coefficient feeding into $\mathcal{H}$. In general this gives rise to convolutions of the form [37]

$$\mathrm{d}\sigma \sim \int \mathrm{d}\omega_1 \cdots \int \mathrm{d}\omega_m\, \mathcal{C}_{ij}(\omega_1, \ldots, \omega_m)\, \mathcal{O}_j(\omega_1, \ldots, \omega_m)\,, \tag{2.44}$$

where the operators $\mathcal{O}_i$ encode the low-energy behavior and are decomposed out of the terms

$$\chi_{n,\omega}(x) = [\delta(\bar{n}\cdot\mathcal{P} - \omega)\chi_n(x)]\,, \quad \mathcal{B}^\mu_{n\perp,\omega}(x) = [\delta(\bar{n}\cdot\mathcal{P} - \omega)\mathcal{B}^\mu_{n\perp}(x)]\,, \quad \mathcal{P}^\mu_{n\perp}\,. \tag{2.45}$$

Eq. (2.44) means that the labels of the jet fields are associated to the momenta entering the perturbative hard function that can be obtained by a partonic matching calculation. In addition to this hard-collinear factorization one can also achieve soft-collinear factorization by the field redefinitions described in Sec. 2.4.2 and a decomposition of the operators $\mathcal{O}_i$ into separate color singlet structures corresponding to $\mathcal{J}$ and $\mathcal{S}$. Since the set of operators $\mathcal{O}_i$ which can built out of the collinear fields in Eq. (2.45) and

series in $\ln(\mathrm{d}\sigma)$		Γ	γ	β	matching
LL	$\alpha_s^n L^{n+1}$	1-loop	-	1-loop	tree
NLL	$\alpha_s^n L^n$	2-loop	1-loop	2-loop	tree
N^{2}LL	$\alpha_s^n L^{n-1}$	3-loop	2-loop	3-loop	1-loop
N^{3}LL	$\alpha_s^n L^{n-2}$	4-loop	3-loop	4-loop	2-loop

Table 2.1: Table with required ingredients at different orders in the resummation for processes with Sudakov double logarithms.

the (ultra-)soft fields is frequently strongly limited, in particular at lowest order in the power counting parameter λ, we get in many cases universal low-energy matrix elements in the EFT (like the PDFs) appearing in various processes.

After having established a factorization theorem the aim is to evaluate the cross section in a perturbative expansion with the required accuracy at some arbitrary renormalization scale. Since the scales of the functions corresponding to $\mathcal{H}$, $\mathcal{J}$ and $\mathcal{S}$ in Eq. (2.42) are, however, widely separated, one obtains large logarithms between these scales, which render the perturbative expansion unstable. In the case of collider processes we encounter in addition to single logarithms also Sudakov double logarithms of the form $\ln^2\lambda$. These arise as the remnants from the cancellation of overlapping IR collinear and soft divergences in full QCD. Since SCET turns IR divergences into UV divergences, it provides a way to resum the corresponding logarithms in terms of RG evolution.

Let us have a closer look at the way how resummation works in SCET, which logarithms are resummed at a particular order and which ingredients we need for this purpose. The perturbative expansion of a differential cross section in the SCET regime (i.e. with widely separated physical scales) has the typical form [10]

$$\begin{array}{lllllll} \ln(\mathrm{d}\sigma) \sim & \alpha_s L^2 & + \alpha_s L & + \alpha_s & & & \\ & + \alpha_s^2 L^3 & + \alpha_s^2 L^2 & + \alpha_s^2 L & + \alpha_s^2 & & \\ & + \alpha_s^3 L^4 & + \alpha_s^3 L^3 & + \alpha_s^3 L^2 & + \alpha_s^3 L & + \alpha_s^3 & \\ & + \vdots & \vdots & \vdots & \vdots & \vdots & \end{array} \tag{2.46}$$

Here $L \sim \ln\lambda$ corresponds to a large logarithm between two involved scales in the process. Using a fixed-order counting at a particular order in α_s one would take into account the corresponding number of rows in Eq. (2.46). In SCET, however, one wants to resum the logarithms using the counting $\alpha_s L \sim 1$. This effectively corresponds to the summation of all elements inside a column in Eq. (2.46), e.g. at LL the complete first column has to be taken into account with the elements being counted $\sim 1/\alpha_s$. The resummation is performed with RG equations for which the anomalous dimensions of the structures have to be determined. For SCET operators $\mathcal{O}_i$ depending just on a single label ω these read [11]

$$\mu\frac{\mathrm{d}}{\mathrm{d}\mu}\,\mathcal{O}_i(\mu,\omega) = \int \mathrm{d}\omega' \left(\frac{\Gamma_{ij}^{\mathcal{O}}}{\mu}\left[\frac{\mu\,\theta(\omega-\omega')}{\omega-\omega'}\right]_+ + \gamma_{ij}^{\mathcal{O}}\,\delta(\omega-\omega')\right)\mathcal{O}_j(\mu,\omega')\,, \tag{2.47}$$

where $\Gamma_{ij}^{\mathcal{O}}$ and $\gamma_{ij}^{\mathcal{O}}$ are called the cusp and noncusp anomalous dimensions. Note that if the remaining label ω in Eq. (2.47) is fixed kinematically we obtain a simple multiplication instead of a convolution and the plus-distribution is replaced by a single logarithm. The required ingredients for a determination of cross sections in SCET up to N^{3}LL resummation are displayed in Table 2.1.

At the very end, we have to remark that the "rapidity logarithms" arising in SCET II from the interface between collinear and soft modes as described in Sec. 2.5 cannot be resummed by the usual RG evolution with respect to the invariant mass scale. These logarithms appear in $\ln(\mathrm{d}\sigma)$ as single logarithms at any order in the strong coupling and are therefore known to simply exponentiate in differential cross sections [38,39]. In fact they can be also resummed formally via a RG evolution in rapidity space [40,41] which provides a way to assign scale ambiguities for perturbative error estimates. We will encounter rapidity logarithms in Chapter 4 and 5 and discuss their resummation there explicitly.

[10] Taking the logarithm of the cross section makes the counting more transparent.
[11] We could have equivalently written this RG equation also for the Wilson coefficients $\mathcal{C}_{ij}$.

Chapter 3

VFNS for classical DIS

As a first hard scattering process we investigate DIS, i.e. the scattering of a lepton off a hadron, for a differential cross section in the inclusive OPE region $1-x \sim \mathcal{O}(1)$. This process contains only two relevant scales, the hard momentum transfer scale Q and the hadronization scale $\Lambda_{\rm QCD}$ and is thus one of the simplest examples for a multiscale problem in QCD discussed in many textbooks (see e.g. [42]). Here factorization plays the crucial role of separating perturbative and nonperturbative physics in terms of hard matching coefficients and PDFs, which will be discussed first for the massless case in Sec. 3.2 in the language of SCET. In spite of its simplicity DIS has a rich and interesting phenomenology which needs to be understood at high accuracy to extract PDFs for the use at hadron colliders. In this context massive quark effects have an important impact, which has lead to the development of many approaches for their treatment. We outline in Sec. 3.3 how massive quarks are incorporated at $\mathcal{O}(\alpha_s)$ and compute in Sec. 3.4 the contributions from secondary massive quark radiation at $\mathcal{O}(\alpha_s^2 C_F T_F)$ explicitly via dispersion relations from corresponding massive gluon results at $\mathcal{O}(\alpha_s)$.

3.1 Kinematics of DIS

We consider the scattering of an electron off a proton P via photon exchange as displayed in Fig. 3.1. We denote the proton momentum by P_P^μ, the momentum of the incoming (outgoing) electron by k^μ (k'^μ), the incoming momentum of the virtual photon by $q^\mu = k'^\mu - k^\mu$ with spacelike invariant mass $q^2 = -Q^2 < 0$ and the momentum of the outgoing final state X by P_X^μ. The Lorentz invariant Bjorken scaling variable x is defined by

$$x = -\frac{q^2}{2P_P \cdot q} = \frac{Q^2}{2P_P \cdot q} \tag{3.1}$$

with the kinematic constraint $0 \leq x \leq 1$. We will work in the Breit frame, where q^μ does not have an energy component and the initial state proton is $\bar{n}$-collinear. This frame will be particularly convenient in the endpoint region $x \to 1$ to obtain a transparent power counting. The relevant momenta in the Breit frame read in terms of lightcone coordinates, see Eq. (2.1), [1]

$$q^\mu = Q(-1,1,0)\,, \quad P_P^\mu = \frac{Q}{x}(1,0,0)\,, \quad P_X^\mu = P_P^\mu + q^\mu = Q\left(\frac{1-x}{x},1,0\right)\,. \tag{3.2}$$

Note that the invariant mass of the final state is

$$P_X^2 = \frac{Q^2(1-x)}{x}\,. \tag{3.3}$$

In this chapter we consider the classical OPE region, where $1-x \sim \mathcal{O}(1)$, and thus $P_X^2 \sim Q^2$ resulting in a two-scale problem. The endpoint region $1-x \ll 1$, where the additional scale $Q^2(1-x) \ll Q^2$ appears, will be discussed in chapter 4.

[1] Here we neglect the proton mass $m_P \sim \Lambda_{\rm QCD}$ which is consistent with the power expansion in $\Lambda_{\rm QCD}/Q$ in Sec. 3.2. For a discussion of target mass effects we refer to Ref. [43].

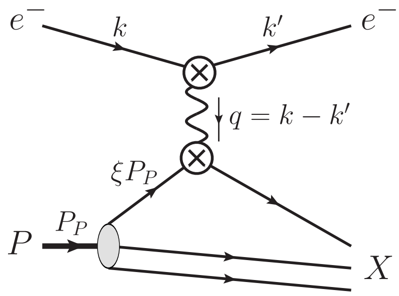

Figure 3.1: The kinematics of $e^- P \to e^- X$ via virtual photon exchange.

We will see that at leading order in the hard scattering process in fact only a single parton with momentum p^μ initiates the hard interaction. The corresponding partonic Bjorken variable reads

$$\hat{x} \equiv \frac{x}{\xi} = \frac{Q^2}{2p \cdot q}\,, \tag{3.4}$$

where the longitudinal momentum component of the parton is the fraction ξ of the corresponding proton momentum, i.e. $p^\mu = \xi P_P^\mu$ for massless partons.

In the following we will consider the spin-averaged differential cross section

$$\frac{\mathrm{d}\sigma}{\mathrm{d}Q^2 dx} = \frac{4\pi\alpha_{\rm em}^2}{Q^2 x^2 s^2}\, L^{\mu\nu}(k,k') W_{\mu\nu}(P_P, q)\,, \tag{3.5}$$

where s denotes the c.m. energy $(P_P + k)^2$. The leptonic tensor $L^{\mu\nu}(k,k')$ can be described in QED and does not contain strong interaction effects at leading order in the electromagnetic coupling $\alpha_{\rm em}$. We will concentrate on the hadronic tensor containing in particular the nonperturbative physics which is defined by

$$\begin{aligned} W^{\mu\nu}(P_P, q) &= \frac{1}{4\pi} \sum_X \mathrm{d}\Pi_X \langle P(P_P)|J^{\mu\dagger}(0)|X\rangle\langle X|J^\nu(0)|P(P_P)\rangle\, (2\pi)^4\, \delta^{(4)}(P_P + q - P_X) \\ &= \frac{1}{2\pi}\, \mathrm{Im}\left[i \int \mathrm{d}^4 z\, e^{iqz} \langle P(P_P)|\, T[J^{\mu\dagger}(z) J^\nu(0)]\, |P(P_P)\rangle\right]\,, \end{aligned} \tag{3.6}$$

with the current $J^\mu(z) = \sum_{q_i} e_{q_i}^2\, \bar{q}_i \gamma^\mu q_i(z)$ summed over all quark flavors q_i with corresponding electric charges e_{q_i} and $\mathrm{d}\Pi_X$ denoting the integration over the complete phase space. We will just consider unpolarized DIS, so that a spin average is always implied. Using current conservation, which implies $q^\mu W_{\mu\nu} = 0$, one can decompose the hadronic tensor for the parity conserving vector current into two structure functions $F_1(x, Q^2)$ and $F_2(x, Q^2)$,

$$\begin{aligned} W^{\mu\nu}(P_P, q) &= \left(-g_{\mu\nu} - \frac{q^\mu q^\nu}{q^2}\right) F_1(x, Q^2) + \frac{1}{P_P \cdot q} \left(P_P^\mu + \frac{q^\mu}{2x}\right)\left(P_P^\nu + \frac{q^\nu}{2x}\right) F_2(x, Q^2) \\ &= -g_\perp^{\mu\nu} F_1(x, Q) + \frac{1}{2}\left(\frac{n^\mu}{2} + \frac{\bar{n}^\mu}{2}\right)\left(\frac{n^\nu}{2} + \frac{\bar{n}^\nu}{2}\right) F_L(x, Q)\,. \end{aligned} \tag{3.7}$$

with $g_\perp^{\mu\nu} = g^{\mu\nu} - 1/2(n^\mu \bar{n}^\nu + \bar{n}^\mu n^\nu)$. Here the longitudinal structure function $F_L(x, Q)$ reads in terms of $F_1(x, Q)$ and $F_2(x, Q)$

$$F_L(x, Q) = \frac{1}{x} F_2(x, Q) - 2F_1(x, Q)\,. \tag{3.8}$$

In the following we consider the factorization and mass effects for the form factor $F_1(x, Q)$ for definiteness and present a summary of the results for $F_L(x, Q)$ in appendix A. In analogy to the hadronic tensor we can also define the partonic tensor $\hat{W}_{qi}^{\mu\nu}(p, q)$ with corresponding partonic structure functions $\hat{F}_{1,qi}(z, Q)$ and $\hat{F}_{L,qi}(z, Q)$, where in Eq. (3.6) the initial state proton is replaced by a parton $i = q, \bar{q}, g$ with momentum p^μ.

3.2 The massless factorization theorem

The way how the structure functions factorize has been known for a long time in QCD [44, 45]. Within SCET the demonstration of the factorization theorem turns out to be very simple and provides immediately an operator based definition for the low energy matrix elements, the PDFs. In the Breit frame the incoming proton can be described as a $\bar{n}$-collinear initial state at the invariant mass scale Λ^2_{QCD}, whereas the final state does not contain relevant degrees of freedom at the low-energy scale and is integrated out. Thus the corresponding SCET scaling parameter satisfies $\lambda = \Lambda_{\mathrm{QCD}}/Q$ and the low-energy operators can be described by the $\bar{n}$-collinear SCET II-type jet fields $\chi_{\bar{n}}$ and $\mathcal{B}^{\mu}_{\bar{n}\perp}$ defined in analogy to Eqs. (2.30) and (2.32). [2] The only possible operators which are consistent with the symmetries, i.e. gauge invariance and reparametrization invariance, and thus constructed from the building blocks in Eq. (2.45) are at lowest order in the power counting, i.e. at $\mathcal{O}(\lambda^2)$ corresponding to twist two, given by [37, 46]

$$\mathcal{O}_q(\omega) = \bar{\chi}_{\bar{n}}(0)\frac{\not{n}}{2}\chi_{\bar{n},\omega}(0)\,, \tag{3.9}$$

$$\mathcal{O}_g(\omega) = -\frac{\omega}{T_F}\,\mathrm{Tr}\left[\mathcal{B}_{\bar{n}\perp\mu}(0)\mathcal{B}^{\mu}_{\bar{n}\perp,\omega}(0)\right]\,, \tag{3.10}$$

where the trace is over the suppressed color indices. Although the relevant operators contain two jet fields they effectively just depend only on one single label ω due to momentum conservation, which is already explicit in Eqs. (3.9) and (3.10). Note that these operators are local with respect to the residual coordinate (but nonlocal with respect to the label momentum). They are normalized such that the nonvanishing results for the tree level matrix elements with initial partonic states having the momentum p^μ give $\delta(1-\omega/p^+)$. All ultrasoft fields cancel each other in SCET I after performing the field redefinitions described in Sec. 2.4.2, so that the operators in SCET II depend only on collinear physics in the Breit frame.

The quark, antiquark and gluon PDFs are the probability distributions for extracting out of the proton the corresponding parton jet with the momentum fraction ξ, which is carried to the hard interaction. They are forward matrix elements of the operators in Eqs. (3.9) and (3.10),

$$\phi^{\mathrm{bare}}_{q/P}(\xi) = \theta(\xi)\langle P(P_P)|\mathcal{O}^{\mathrm{bare}}_q(\xi P_P^+)|P(P_P)\rangle\,, \tag{3.11}$$

$$\phi^{\mathrm{bare}}_{\bar{q}/P}(\xi) = -\theta(-\xi)\langle P(P_P)|\mathcal{O}^{\mathrm{bare}}_q(-\xi P_P^+)|P(P_P)\rangle = -\phi^{\mathrm{bare}}_{q/P}(-\xi)\,, \tag{3.12}$$

$$\phi^{\mathrm{bare}}_{g/P}(\xi) = \theta(\xi)\langle P(P_P)|\mathcal{O}^{\mathrm{bare}}_g(\xi P_P^+)|P(P_P)\rangle\,. \tag{3.13}$$

These definitions in terms of collinear field operators are equivalent to the full QCD definitions in Ref. [47]. Note that the quark PDFs are associated with a positive label momentum $\omega > 0$, whereas the antiquark PDFs correspond to a negative label momentum $\omega < 0$ in agreement with Eq. (2.9).

The hard collinear factorization has the form of Eq. (2.44), where only one label momentum enters the convolution. Reparametrization invariance implies that the convolution involves ratios of the large label momenta. Following Ref. [37] the factorization theorem for the structure functions reads for n_f massless quarks to all orders in α_s up to higher orders in the power counting parameter [3]

$$F_1(x,Q) = \sum_{i=q}\frac{e_i^2}{2}\sum_{j,k=q,g}\int\frac{\mathrm{d}\xi}{\xi}\int\frac{\mathrm{d}\xi'}{\xi'}\,\mathcal{C}^{(n_f)}_{ij}\left(\frac{x}{\xi},Q,\mu_H\right)U^{(n_f)}_{\phi,jk}\left(\frac{\xi}{\xi'},\mu_H,\mu_\phi\right)\phi^{(n_f)}_{k/P}(\xi',\mu_\phi)\,. \tag{3.14}$$

Here the sum over q includes the massless quark flavors as well as the corresponding antiquarks and the subscript (n_f) indicates that the $\overline{\mathrm{MS}}$ scheme with n_f dynamic flavors is used for all renormalized quantities, as common when only massless quarks are involved. The factorization theorem allows for parton mixing, which means that the parton generated out of the PDF is not necessarily the one directly interacting with the photon.

[2] Since we will not encounter any soft or ultrasoft modes in this example, we can actually be ignorant about whether we deal with SCET I or SCET II.

[3] In fact the next corrections arise from twist-four operators and appear only at $\mathcal{O}(\lambda^2) = \mathcal{O}(\Lambda^2_{\mathrm{QCD}}/Q^2)$ in the factorization theorem (3.14).

In Eq. (3.14) the hard matching coefficients $\mathcal{C}_{ij}^{(n_f)}(z,Q,\mu\sim Q)$ contain the mismatch between the full QCD structure function and the low-energy operator matrix elements in SCET, i.e. the PDFs $\phi_{k/P}^{(n_f)}(z,\mu)$, and are known up to three loops [48]. They can be computed with a partonic initial state j at the scale $\mu_H\sim Q$, where the quark flavor $i=q$ is interacting with the photon. The results can be directly deduced from a pure QCD calculation since the partonic PDF diagrams for massless partons are scaleless in dimensional regularization and vanish. Since both theories contain the same IR behavior the dependence on any low-energy scale cancels in the matching coefficient. Note that the matching coefficients for initial quarks and antiquarks are related to each other via charge conjugation like the PDFs (see Eq. (3.12)) and enter Eq. (3.14) with the same expression. The functions $\mathcal{C}_{ij}^{(n_f)}(z,Q,\mu)$ depend implicitly on n_f at $\mathcal{O}(\alpha_s)$ through the strong coupling constant. The explicit dependence on n_f apart from the possible values of the indices ij starts at $\mathcal{O}(\alpha_s^2)$. The expansion of the matching coefficient up to this order has the form

$$\begin{aligned}\mathcal{C}_{ij}^{(n_f)}(z,Q,\mu)&=\delta(1-z)+\mathcal{C}_{ij}^{(n_f,1)}(z,Q,\mu)+\Big[\mathcal{C}_{ij,C_F}^{(n_f,2)}(z,Q,\mu)+\mathcal{C}_{ij,C_A}^{(n_f,2)}(z,Q,\mu)+n_f\,\mathcal{C}_{ij,T_F}^{(n_f,2)}(z,Q,\mu)\Big]\\&\quad+\mathcal{O}(\alpha_s^3)\,,\end{aligned}\tag{3.15}$$

where $\mathcal{C}_{ij}^{(n_f,1)}$, $\mathcal{C}_{ij,C_F}^{(n_f,2)}$, $\mathcal{C}_{ij,C_A}^{(n_f,2)}$ and $\mathcal{C}_{ij,T_F}^{(n_f,2)}$ denote the contributions at $\mathcal{O}(\alpha_s)$, $\mathcal{O}(\alpha_s^2C_F^2)$, $\mathcal{O}(\alpha_s^2C_FC_A)$ and $\mathcal{O}(\alpha_s^2C_FT_F)$, respectively. We use a similar notation for all other perturbative expressions throughout this thesis. The additional dependence on a finite quark mass will be indicated in the arguments. We will frequently also drop the reference to the number of quark flavors when it is not relevant, in particular when we discuss the case of a massive gluon, where a similar self-explaining notation is used.

The nonvanishing hard matching coefficients at $\mathcal{O}(\alpha_s)$ read [49] ($\alpha_s^{(n_f)}\equiv\alpha_s^{(n_f)}(\mu)$)

$$\begin{aligned}\mathcal{C}_{qq}^{(n_f,1)}(z,Q,\mu)&=\frac{\alpha_s^{(n_f)}C_F}{4\pi}\,\theta(z)\,\theta(1-z)\bigg\{\delta(1-z)\left[3L_Q-9-\frac{2\pi^2}{3}\right]+\left[\frac{1}{1-z}\right]_+[4L_Q-3]\\&\quad+4\left[\frac{\ln(1-z)}{1-z}\right]_+-2(1+z)\left[L_Q+\ln(1-z)\right]-\frac{2(1+z^2)}{1-z}\ln(z)+6\bigg\}\,,\end{aligned}\tag{3.16}$$

$$\mathcal{C}_{qg}^{(n_f,1)}(z,Q,\mu)=\frac{\alpha_s^{(n_f)}T_F}{4\pi}\,\theta(z)\,\theta(1-z)\bigg\{2(1-2z+2z^2)\left[L_Q+\ln(1-z)-\ln(z)\right]-2+8z-8z^2\bigg\}\,,\tag{3.17}$$

with $L_Q\equiv\ln(Q^2/\mu^2)$. For later comparison with our results for secondary massive quarks we also display the flavor diagonal contribution at $\mathcal{O}(\alpha_s^2C_FT_F)$, where the initial quark is also the one interacting with the photon and where any other flavor just appears via "secondary" production, obtained in Refs. [50,51], [4]

$$\begin{aligned}\mathcal{C}_{qq,T_F}^{(n_f,2)}(z,Q,\mu)&=\frac{\big(\alpha_s^{(n_f)}\big)^2C_FT_F}{16\pi^2}\,\theta(z)\,\theta(1-z)\bigg\{\delta(1-z)\left[2L_Q^2-\left(\frac{38}{3}+\frac{16\pi^2}{9}\right)L_Q+\frac{457}{18}+\frac{38\pi^2}{9}+\frac{8}{3}\zeta_3\right]\\&\quad+\left[\frac{1}{1-z}\right]_+\left[\frac{8}{3}L_Q^2-\frac{116}{9}L_Q+\frac{494}{27}-\frac{8\pi^2}{9}\right]+\left[\frac{\ln(1-z)}{1-z}\right]_+\left[\frac{16}{3}L_Q-\frac{116}{9}\right]\\&\quad+\frac{8}{3}\left[\frac{\ln^2(1-z)}{1-z}\right]_+-\frac{8(1+z^2)}{3(1-z)}\,\mathrm{Li}_2(1-z)+\frac{10(1+z^2)}{3(1-z)}\ln^2(z)-\frac{4}{3}(1+z)\ln^2(1-z)\\&\quad-\frac{16(1+z^2)}{3(1-z)}\ln(z)\ln(1-z)+\frac{4}{3(1-z)}\ln(z)\left[6+2z+11z^2-4(1+z)L_Q\right]\\&\quad+\frac{8}{9}\ln(1-z)\left[8+11z-3(1+z)L_Q\right]-\frac{4}{3}(1+z)L_Q^2+\frac{8}{9}(8+11z)L_Q-\frac{460}{27}-\frac{376}{27}z\\&\quad+\frac{4\pi^2}{9}(1+z)\bigg\}\,.\end{aligned}\tag{3.18}$$

[4] This correction corresponds to the matching coefficient in the "nonsinglet" part of the structure function at $\mathcal{O}(\alpha_s^2C_FT_F)$.

Since the PDFs are matrix elements of EFT operators they need to be renormalized. [5] The bare PDFs in Eqs. (3.11) – (3.13) and the renormalized PDFs entering Eq. (3.14) are related via

$$\phi_{i/P}^{\mathrm{bare}}(z) = \sum_{j=q,g} \int \frac{\mathrm{d}\xi}{\xi}\, Z_{\phi,ij}^{(n_f)}\left(\frac{z}{\xi},\mu\right) \phi_{j/P}^{(n_f)}(\xi,\mu)\,. \tag{3.19}$$

The corresponding counterterms $Z_{\phi,qj}^{(n_f)}$ for the production of a quark out of the PDF read at $\mathcal{O}(\alpha_s)$

$$Z_{\phi,qq}^{(n_f,1)}(z,\mu) = \frac{\alpha_s^{(n_f)} C_F}{4\pi}\,\theta(z)\,\theta(1-z)\,\frac{1}{\epsilon}\left\{3\,\delta(1-z) + 4\left[\frac{1}{1-z}\right]_+ - 2(1+z)\right\}, \tag{3.20}$$

$$Z_{\phi,qg}^{(n_f,1)}(z,\mu) = \frac{\alpha_s^{(n_f)} T_F}{4\pi}\,\theta(z)\,\theta(1-z)\,\frac{1}{\epsilon}\left\{2(1-2z+2z^2)\right\}, \tag{3.21}$$

and for the contribution at $\mathcal{O}(\alpha_s^2 C_F T_F)$

$$\begin{aligned} Z_{\phi,qq,T_F}^{(n_f,2)}(z,\mu) = \frac{\big(\alpha_s^{(n_f)}\big)^2 C_F T_F}{16\pi^2}\,\theta(z)\,\theta(1-z)\,\Bigg\{&\delta(1-z)\left[\frac{2}{\epsilon^2} - \frac{1}{\epsilon}\left(\frac{1}{3}+\frac{4\pi^2}{9}\right)\right] + \left[\frac{1}{1-z}\right]_+\left[\frac{8}{3\epsilon^2} - \frac{40}{9\epsilon}\right] \\ &- \frac{4}{3\epsilon^2}(1+z) - \frac{1}{\epsilon}\left[\frac{4(1+z^2)}{3(1-z)}\ln(z) + \frac{4}{9} - \frac{44}{9}z\right]\Bigg\}\,. \end{aligned} \tag{3.22}$$

The flavor mixing evolution factors $U_{\phi,ij}^{(n_f)}$ resum the logarithms between the characteristic renormalization scale of the PDFs $\mu_\phi \sim \Lambda_{\mathrm{QCD}}$ and the hard scale $\mu_H \sim Q$ and satisfy the DGLAP evolution equations [52–54]

$$\mu\frac{\mathrm{d}}{\mathrm{d}\mu}\, U_{\phi.ij}^{(n_f)}(z,\mu,\mu_0) = \sum_{k=q,g}\int\frac{\mathrm{d}\xi}{\xi}\,\gamma_{\phi,ik}^{(n_f)}\left(\frac{z}{\xi}\right) U_{\phi,kj}^{(n_f)}(\xi,\mu,\mu_0)\,. \tag{3.23}$$

Note that the evolution factors are already at LL sensitive to the number of active flavors both through the dependence on α_s as well as due to the summation over the quarks q. Thus, modifying the number of active quark flavors in the evolution affects the form factor already at LL, which happens when a mass threshold is crossed. The anomalous dimensions $\gamma_{\phi,ij}^{(n_f)}(z)$ can be derived from the counterterms $Z_{\phi,ij}^{(n_f)}(z)$ via

$$\gamma_{\phi,ij}^{(n_f)}(z,\mu) = -\sum_{k=q,g}\int\frac{\mathrm{d}\xi}{\xi}\left(Z_\phi^{(n_f)}\right)^{-1}_{ik}\left(\frac{z}{\xi},\mu\right)\mu\frac{\mathrm{d}}{\mathrm{d}\mu}\,Z_{\phi,kj}^{(n_f)}(\xi,\mu)\,. \tag{3.24}$$

The terms at $\mathcal{O}(\alpha_s)$ and $\mathcal{O}(\alpha_s^2 C_F T_F)$ can be easily computed from Eqs. (3.20) - (3.22) and read

$$\gamma_{\phi,qq(g)}^{(n_f,1)}(z,\mu) = \frac{\alpha_s^{(n_f)} C_F}{4\pi}\,P_{qq(g)}^{(1)}(z)\,,\quad \gamma_{\phi,qq,T_F}^{(n_f,2)}(z,\mu) = \frac{\big(\alpha_s^{(n_f)}\big)^2 C_F T_F}{16\pi^2}\,P_{qq,T_F}^{(2)}(z) \tag{3.25}$$

with the splitting functions given by [6]

$$P_{qq}^{(1)}(z) = 2\,\theta(z)\,\theta(1-z)\left\{3\,\delta(1-z) + 4\left[\frac{1}{1-z}\right]_+ - 2(1+z)\right\}, \tag{3.26}$$

$$P_{qg}^{(1)}(z) = 4\,\theta(z)\,\theta(1-z)\left\{1-2z+2z^2\right\}, \tag{3.27}$$

[5] Strictly speaking we renormalize the corresponding operators. However, since the external state does not play a role for the UV behavior, we can equivalently talk about the renormalization of the matrix elements. Note that sometimes we will also associate the counterterms with the corresponding Wilson coefficients instead of the operators, which is technically equivalent.

[6] Since we display perturbative expansions in terms of $\alpha_s/4\pi$, the splitting functions defined here differ from the more common ones in the literature by a factor of 4.

and

$$P^{(2)}_{qq,T_F}(z) = 4\,\theta(z)\,\theta(1-z)\,\left\{\delta(1-z)\left[-\frac{1}{3}-\frac{4\pi^2}{9}\right]-\frac{40}{9}\left[\frac{1}{1-z}\right]_+-\frac{4(1+z^2)}{3(1-z)}\ln(z)-\frac{4}{9}+\frac{44}{9}z\right\}. \tag{3.28}$$

The splitting functions are nowadays known up to 3-loop [55, 56]. We note that even at one-loop the DGLAP equations cannot be solved fully analytically, but require a numerical treatment either directly in x-space or in the frequently used Mellin moment space.

3.3 Mass effects at $\mathcal{O}(\alpha_s)$

Let us investigate the situation where a massive quark is included into DIS. In the following we consider a setup with n_l massless flavors and one heavy quark with mass $m \gg \Lambda_{\rm QCD}$, which we want to incorporate into the factorization theorem of Eq. (3.14). This can be easily generalized to the case of several massive quark flavors with different masses appearing in practical considerations where both the mass of the charm and bottom quark may be relevant. We remark that we will not consider the possibility of having an intrinsic charm contribution with $m \gtrsim \Lambda_{\rm QCD}$ generated nonperturbatively out of the proton.

The massive quark can in general not be treated in the same way as the massless quarks, since the mass represents an additional scale in the setup which has to be taken into account. In the literature massive quarks are usually treated with different approaches, either based on a *fixed flavor number scheme* (FFNS), which treats the massive quark as heavy and does not include it in the RG evolution, or based on a *variable flavor number scheme* (VFNS), which accounts for the massive quark as heavy or light depending on the hierarchies with respect to the other scales implying a RG evolution with a variable number of flavors. The latter is in the spirit of EFTs and we will describe in the following a VFNS which coincides with the FFNS for the case of heavy quarks with $m \gtrsim Q$.

A VFNS for DIS has to exhibit the following features: (i) it has to sum all large logarithms between the mass, the hard scale and $\Lambda_{\rm QCD}$, and (ii) to recover the correct limiting behavior, i.e. the decoupling limit for $m \gg Q$ and the massless limit for $m \ll Q$. A VFNS valid for arbitrary quark masses should (iii) continuously interpolate between these two limits keeping the full mass dependence because in practice large hierarchies between the hard scale and the mass scale might not be reached. This has been achieved for the first time in the ACOT scheme [1, 2]. The crucial ingredient is the use of proper renormalization conditions for the massive quark PDFs depending on the hierarchy with respect to the hard scale Q [57], whereas for the massless quark corrections always $\overline{\rm MS}$-renormalization is employed. This renormalization procedure is analogous to the one for the strong coupling in the presence of massive quarks [58].

We will describe the massive quark with additional degrees of freedom in SCET, which we call *mass modes* and which carry in particular fluctuations around the mass shell. The latter can be described for small masses with the parameter $\lambda_m = m/Q$. Since at leading order in the power counting only $\bar{n}$-collinear modes contribute to the factorization theorem, the only relevant mass shell fluctuations adopt the scaling $Q(1, \lambda_m^2, \lambda_m)$ for small masses $m \ll Q$. When the mass threshold is crossed in the evolution these contributions should be integrated out. [7] For large masses $m \gtrsim Q$ the mass modes should not enter the SCET description at all and should be rather taken into account in the matching process to QCD. The corresponding factorization theorems for the two hierarchies $m \ll Q$ and $m \gtrsim Q$ lead to the correct physical description, but might suggest that we rely on a large hierarchy for the first case, so that the range of applicability of the mass mode method would be constrained to the cases $\lambda_m \ll 1$ and $\lambda_m \gtrsim 1$ separately, but might miss either power corrections or the resummation of large logarithms in between. However, in fact the two cases can be merged continuously without any power corrections in the transition region, since one can instead take the viewpoint of having the mass modes always included in the setup, but impose different renormalization conditions for the massive quark PDFs, as we will see in the following. The mass mode picture will be in particular helpful to discuss setups involving several SCET modes at different invariant mass scales (see chapters 4 and 5).

[7] Throughout this work we adopt the convention that the effects of the massive quark flavor in the factorization theorems are integrated out globally at the scale $\mu_m \sim m$.

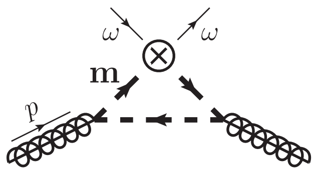

Figure 3.2: Feynman diagram at $\mathcal{O}(\alpha_s)$ for the collinear PDF operator $\mathcal{O}_Q(\omega)$ corresponding to Eq. (3.9) with a massive quark field Q for a collinear gluon in the initial state.

To show the impact of the renormalization scheme we discuss the renormalization of the massive quark PDF operator, which is defined in analogy to Eq. (3.9), where the corresponding collinear quark fields have a mass. We are interested in the perturbative generation of a massive quark from a light parton state which can be found inside the proton at the scale Λ_{QCD}. At $\mathcal{O}(\alpha_s)$ only initial state gluons can contribute to the operator $\mathcal{O}_Q(\omega)$ giving rise to the Feynman diagram in Fig. 3.2. Applying the Feynman rules in Fig. 2.3 and performing a computation in analogy to Ref. [46] we obtain for the spin-averaged matrix element

$$\hat{\phi}^{(\mathrm{bare},1)}_{Q/g}(z,m,\mu) \equiv \langle g_n(p)|\mathcal{O}^{\mathrm{bare}}_Q(zp^+)|g_n(p)\rangle^{(1)} = \frac{\alpha_s T_F}{4\pi}\,\frac{P^{(1)}_{qg}(z)}{2}\left[\frac{1}{\epsilon} - L_m + \mathcal{O}(\epsilon)\right], \tag{3.29}$$

with $L_m = \ln(m^2/\mu^2)$. Here α_s is still the unrenormalized coupling. Note that the mass regulates all IR divergences so that the computation can be carried out without any additional IR regulator. The subtractions of the region where the collinear modes become soft, i.e. the soft-bin subtractions, do not have to be taken into account, since soft (and also ultrasoft) modes do not play any role in the OPE region of DIS. In fact all contributions associated to the soft modes and soft-bins are scaleless and would vanish anyway. We will employ two different renormalization conditions for the massive quark corrections to the PDF operator, but always $\overline{\mathrm{MS}}$-renormalization for the light parton corrections: Using on-shell (OS) renormalization for the massive quark contributions indicated by the superscript (n_l), which corresponds to a low-momentum subtraction, the counterterm cancels the whole contribution leaving behind no correction to the matrix element of the renormalized operator $\mathcal{O}^{\mathrm{OS}}_Q$, i.e. $(\alpha_s^{(n_l)} = \alpha_s^{(n_l)}(\mu))$

$$Z^{(n_l,1)}_{\phi,Qg}(z,m,\mu) = \frac{\alpha_s^{(n_l)} T_F}{4\pi}\,\frac{P^{(1)}_{qg}(z)}{2}\left[\frac{1}{\epsilon} - L_m\right], \quad \hat{\phi}^{(n_l,1)}_{Q/g}(z,m,\mu) = 0\,. \tag{3.30}$$

Due to this fact the corresponding anomalous dimension vanishes, i.e. $\gamma^{(n_l,1)}_{\phi,Qg}(z,\mu) = 0$ at $\mathcal{O}(\alpha_s)$, so that the massive quark is a passive flavor with respect to the RG evolution. This statement holds to any order in perturbation theory. Here we have also used the OS scheme for the massive quark corrections to α_s which leads to the anomalous dimension $\beta = \beta^{(n_l)}$, i.e. a running with only n_l flavors. Therefore, the OS renormalization scheme will turn out to be appropriate if the quark mass is large or comparable to the evolution scale μ, where the virtual contributions can be integrated out. In contrast, the $\overline{\mathrm{MS}}$ renormalization indicated by the superscript (n_l+1) implies that only the divergent piece is absorbed into the counterterm, i.e. we have $(\alpha_s^{(n_l+1)} = \alpha_s^{(n_l+1)}(\mu))$

$$Z^{(n_l+1,1)}_{\phi,Qg}(z,\mu) = \frac{\alpha_s^{(n_l+1)} T_F}{4\pi}\,\frac{P^{(1)}_{qg}(z)}{2}\,\frac{1}{\epsilon}, \quad \hat{\phi}^{(n_l+1,1)}_{Q/g}(z,m,\mu) = -\frac{\alpha_s^{(n_l+1)} T_F}{4\pi}\,\frac{P^{(1)}_{qg}(z)}{2}\,L_m\,. \tag{3.31}$$

The corresponding anomalous dimension is the same as for the case of massless quarks, i.e. $\gamma^{(n_l+1,1)}_{\phi,Qg}(z,\mu) = \gamma^{(n_l+1,1)}_{\phi,qg}(z,\mu)$ (see Eq. (3.25)) at $\mathcal{O}(\alpha_s)$, which also holds to any order in α_s, so that the massive quark is an active flavor with respect to the RG evolution. Here we have also used the $\overline{\mathrm{MS}}$ scheme for the massive quark corrections to α_s which leads to the anomalous dimension $\beta = \beta^{(n_l+1)}$, i.e. a running with n_l+1 flavors. Therefore, the $\overline{\mathrm{MS}}$ renormalization scheme gives a good description if the quark mass is small or comparable to the evolution scale μ, where its finite virtual contributions should contribute to the renormalized matrix elements.

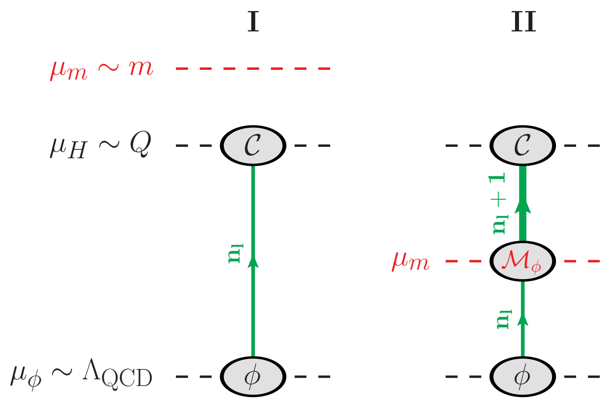

Figure 3.3: Illustration of the ACOT scheme for DIS for the hierarchies $m \gtrsim Q$ and $m \lesssim Q$. The green arrows indicate the RG running of the PDFs $\phi_{i/P}$ and α_s to the natural scale of the matching coefficients $\mathcal{C}_{ij}$ with the respective appropriate number of active flavors. When the mass threshold is crossed we obtain a matching condition and the number of active flavors changes.

A VFNS like the ACOT scheme combines these two renormalization schemes as illustrated in Fig. 3.3. When $m \gtrsim Q$ (scenario I) OS renormalization is employed for the massive quark contributions to the PDFs and α_s, which implies that the RG evolution for the PDFs and α_s is performed just with the n_l massless flavors. Here the decoupling limit for the hard matching coefficients $\mathcal{C}_{ij}$ is reached for $m \gg Q$. On the other hand, for $m \lesssim Q$ (scenario II) the renormalization scheme is switched from OS to $\overline{\rm MS}$ above the mass scale $\mu_m \sim m$. Taking into account that the quark mass does not affect the UV divergences for the mass-independent $\overline{\rm MS}$-scheme this implies that the RGE is performed with $n_l + 1$ flavors above μ_m and with n_l flavors below μ_m. Due to the fact that the dependence on IR low-energy scales cancels in the matching between full QCD and the effective theory description, the Wilson coefficients $\mathcal{C}_{ij}$ in $\overline{\rm MS}$ reach the massless limit for $m \to 0$. The difference between OS- and $\overline{\rm MS}$-renormalized PDFs constitutes threshold corrections denoted by $\mathcal{M}_\phi$ in Fig. 3.3 similar to the decoupling relation of α_s, which render the description of the structure functions continuous. [8]

We remark that the ACOT scheme is usually interpreted in the literature in a different way which is rather based on the strict EFT paradigm that the massive quark is either present in the theory or integrated out. This viewpoint is perfectly legitimate, but obscures the origin of the continuity between the two descriptions, where one might expect large power counting breaking terms of $\mathcal{O}(m^2/Q^2)$ in the transition region $\mu \sim m \sim Q$. This is not the case which is intrinsically manifest in the construction of the VFNS scheme based on different renormalization conditions for the massive quark corrections.

We will now describe the mass factorization setups in scenario I and II in more detail and discuss the contributions for an NLL analysis requiring fixed-order corrections at $\mathcal{O}(\alpha_s)$. For the explicit computations we refer to Ref. [59].

3.3.1 Scenario I: $m \gtrsim Q$

When the mass is larger than the momentum transfer energy Q, the factorization theorem is the same as for n_l massless quarks except for the fact that the matching coefficients between QCD and SCET are now mass dependent, i.e.

$$F_1^{(n_l)}(x,Q,m) = \sum_{i=q,Q} \frac{e_i^2}{2} \sum_{j,k=q,g} \int \frac{\mathrm{d}\xi}{\xi} \int \frac{\mathrm{d}\xi'}{\xi'}\, \mathcal{C}_{ij}^{(n_l)}\left(\frac{x}{\xi}, Q, m, \mu_H\right) U_{\phi,jk}^{(n_l)}\left(\frac{\xi}{\xi'}, \mu_H, \mu_\phi\right) \phi_{k/P}^{(n_l)}(\xi', \mu_\phi)\,. \tag{3.32}$$

Since OS renormalization is employed for the massive quark PDF, the quark is not generated at a low

[8]We mean continuity up to higher order perturbative corrections which are not enhanced by large logarithms.

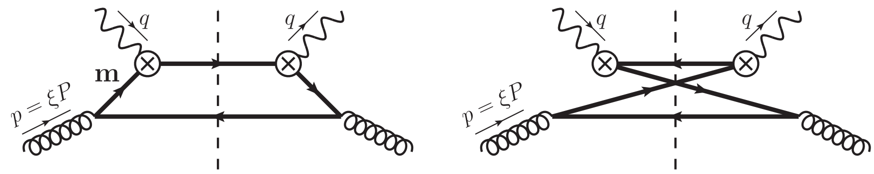

Figure 3.4: Massive quark contributions to the hard matching coefficient $\mathcal{C}_{Qg}^{(n_l,1)}$ in full QCD.

energy scale and cannot enter the hard interaction as an initial state. The only contributing diagrams at $\mathcal{O}(\alpha_s)$ arise via gluon splitting in the hard coefficient $\mathcal{C}_{Qg}^{(n_l,1)}$ and are shown in Fig. 3.4 for the full QCD contributions in the partonic structure function $\hat{F}_{1,Qg}^{(n_l,1)}$. They yield the correction [60] [9]

$$\hat{F}_{1,Qg}^{(n_l,1)}(z,Q,m) = \frac{\alpha_s^{(n_l)}T_F}{4\pi}\,\frac{e_Q^2}{2}\,\theta(z)\,\theta\left(\frac{Q^2}{Q^2+4m^2}-z\right)\left\{-2v\left(1-4z+4z^2+\frac{4m^2}{Q^2}z(1-z)\right)\right.$$
$$\left.+2\left(1-2z+2z^2+\frac{4m^2}{Q^2}z(1-z)-\frac{8m^4}{Q^4}z^2\right)\ln\left(\frac{1+v}{1-v}\right)\right\}, \tag{3.33}$$

where $z \leq Q^2/(Q^2+4m^2)$ is the kinematic condition for the massive quark pair production and the final state massive quark velocity in the partonic quark-photon c.m. frame v is given by

$$v = \sqrt{1-\frac{4m^2z}{Q^2(1-z)}}\,. \tag{3.34}$$

The matching coefficients can be obtained from the partonic structure function and the partonic PDFs by the relation

$$\hat{F}_{1,ij}^{(n_l)}(z,Q,m) = \frac{e_Q^2}{2}\int\frac{\mathrm{d}\xi}{\xi}\,\mathcal{C}_{ij}^{(n_l)}\left(\frac{z}{\xi},Q,m,\mu\right)\hat{\phi}_{j/k}^{(n_l)}(\xi,m,\mu)\,. \tag{3.35}$$

Since the SCET contributions to the partonic PDF $\hat{\phi}_{Q/g}^{(n_l,1)}$ vanish in OS renormalization corresponding to the fact that there are no relevant massive modes in the effective theory we obtain the matching correction [10]

$$\mathcal{C}_{Qg}^{(n_l,1)}(z,Q,m) = \frac{2}{e_Q^2}\hat{F}_{1,Qg}^{(n_l,1)}(z,Q,m) - \hat{\phi}_{Q/g}^{(n_l,1)}(z,m,\mu) = \frac{2}{e_Q^2}\hat{F}_{1,Qg}^{(n_l,1)}(z,Q,m)\,. \tag{3.36}$$

Note that $\mathcal{C}_{Qg}^{(n_l,1)}$ vanishes for $4m^2 > Q^2(1-z)/z$, so that the heavy quark automatically decouples for sufficiently large masses. In the massless limit we obtain

$$\mathcal{C}_{Qg}^{(n_l,1)}(z,Q,m) \overset{m\to 0}{\longrightarrow} \frac{\alpha_s^{(n_l)}T_F}{4\pi}\,\theta(z)\,\theta(1-z)\left\{-\frac{P_{qg}^{(1)}(z)}{2}\ln\left(\frac{m^2z}{Q^2(1-z)}\right)-2+8z-8z^2\right\}, \tag{3.37}$$

which does not correspond to the massless expression in Eq. (3.17). Eq. (3.37) contains unresummed mass logarithms related to the splitting function $P_{qg}^{(1)}(z)$, which spoil the perturbative expansion in powers of α_s for large hierarchies between m and Q. This tells us that using the OS scheme, where the massive quark is treated as a UV degree of freedom concerning RG evolution, is not appropriate for small masses. Instead one should switch the scheme and incorporate the massive quark as dynamic light degree of freedom.

[9] Throughout the thesis we usually suppress the dependence on the renormalization scale μ in the arguments of fixed-order corrections which are just implicitly depending on the renormalization scale through α_s or the mass m indicating that the corresponding contribution to the anomalous dimension is vanishing at the given order.

[10] Here we have used the fact that $\mathcal{C}_{gg}^{(n_l,0)}(z) = \hat{\phi}_{g/g}^{(n_l,0)}(z) = \delta(1-z)$.

3.3.2 Scenario II: $m \lesssim Q$

When the mass is smaller than the momentum transfer energy Q, the massive quark contributes to all structures above the matching scale μ_m and the factorization theorem reads

$$F_1^{(n_l+1)}(x,Q,m) = \sum_{i=q,Q} \frac{e_i^2}{2} \sum_{j,k=q,Q,g} \sum_{l,m=q,g} \int \frac{\mathrm{d}\xi}{\xi} \int \frac{\mathrm{d}\xi'}{\xi'} \int \frac{\mathrm{d}\xi''}{\xi''} \int \frac{\mathrm{d}\xi'''}{\xi'''} \mathcal{C}_{ij}^{(n_l+1)}\left(\frac{x}{\xi}, Q, m, \mu_H\right) \\ \times U_{\phi.jk}^{(n_l+1)}\left(\frac{\xi}{\xi'}, \mu_H, \mu_m\right) \mathcal{M}_{\phi,kl}\left(\frac{\xi'}{\xi''}, m, \mu_m\right) U_{\phi,lm}^{(n_l)}\left(\frac{\xi''}{\xi'''}, \mu_m, \mu_\phi\right) \phi_{m/P}^{(n_l)}(\xi''', \mu_\phi)\,. \tag{3.38}$$

Employing $\overline{\mathrm{MS}}$ renormalization above μ_m implies that the massive flavor can contribute to the running of the PDFs. At the mass scale we now get threshold corrections $\mathcal{M}_{\phi,ij}$ that relate the PDF operators in the $\overline{\mathrm{MS}}$ renormalization scheme to the ones in the OS scheme,

$$\phi_{i/P}^{(n_l+1)}(z,m,\mu_m) = \sum_{j=q,g} \int \frac{\mathrm{d}\xi}{\xi} \mathcal{M}_{\phi,ij}\left(\frac{z}{\xi}, m, \mu_m\right) \phi_{j/P}^{(n_l)}(\xi, \mu_m)\,. \tag{3.39}$$

The matching conditions for the PDFs are thus the analogues of the well known relations between the strong coupling schemes with $n_l + 1$ and n_l running dynamic flavors, $\alpha_s^{(n_l+1)}$ and $\alpha_s^{(n_l)}$ respectively. However, they do not involve simple products, but rather convolutions in x-space. We now also obtain a "massive quark PDF" due to this matching relation since $i = q, Q, g$ includes the massive quark flavor, which can then appear as an initial state of the hard interaction. Relating the bare PDFs to the renormalized ones in the two schemes,

$$\phi_{i/P}^{\mathrm{bare}}(z,m) = \sum_{j=q,g} \int \frac{\mathrm{d}\xi}{\xi} Z_{\phi,ij}^{(n_l)}\left(\frac{z}{\xi}, m, \mu\right) \phi_{j/P}^{(n_l)}(\xi,\mu) = \sum_{j=q,Q,g} \int \frac{\mathrm{d}\xi}{\xi} Z_{\phi,ij}^{(n_l+1)}\left(\frac{z}{\xi}, \mu\right) \phi_{j/P}^{(n_l+1)}(\xi, m, \mu)\,, \tag{3.40}$$

we can write the threshold factors $\mathcal{M}_{\phi,ij}$ as

$$\mathcal{M}_{\phi,ij}\left(z,m,\mu_m\right) = \sum_{k=q,Q,g} \int \frac{\mathrm{d}\xi}{\xi} \left(Z_\phi^{(n_l+1)}\right)^{-1}_{ik} \left(\frac{z}{\xi}, \mu\right) Z_{\phi,kj}^{(n_l)}\left(\xi, m, \mu\right)\,. \tag{3.41}$$

The contribution due to initial state gluons reads at $\mathcal{O}(\alpha_s)$

$$\begin{aligned} \mathcal{M}_{\phi,Qg}^{(1)}(z,m,\mu) &= Z_{\phi,Qg}^{(n_l,1)}(z,m,\mu) - Z_{\phi,Qg}^{(n_l+1,1)}(z,\mu) = \hat{\phi}_{Q/g}^{(n_l+1,1)}(z,m,\mu) - \hat{\phi}_{Q/g}^{(n_l,1)}(z,m,\mu) \\ &= -\frac{\alpha_s^{(n_l+1)} T_F}{4\pi}\,\theta(z)\,\theta(1-z)\,\frac{P_{qg}^{(1)}(z)}{2}\,L_m\,, \end{aligned} \tag{3.42}$$

where we have used Eqs. (3.30) and (3.31) as well as the tree level results $\hat{\phi}_{Q/Q}^{(n_l+1,0)}(z) = \hat{\phi}_{g/g}^{(n_l,0)}(z) = \delta(1-z)$. Note that we have here the freedom to display α_s either in the n_l or (n_l+1)-scheme, where the connection between these two schemes is just the decoupling relation which does not contain any large logarithm for $\mu = \mu_m \sim m$. The only other nonvanishing matching contribution at $\mathcal{O}(\alpha_s)$ is due to self-energy diagrams for the gluon PDF (with initial state gluons),

$$\mathcal{M}_{gg}^{(1)}(z,m,\mu) = \frac{\alpha_s^{(n_l+1)} T_F}{3\pi}\,\delta(1-z)\,L_m\,. \tag{3.43}$$

Note that both $\mathcal{M}_{\phi,Qg}^{(1)}$ and $\mathcal{M}_{gg}^{(1)}$ vanish for $\mu_m = m$, which has been exploited in some analyses to disregard the massive threshold correction factors. However, this feature does not hold in general and one gets already at $\mathcal{O}(\alpha_s^2)$ nonvanishing contributions for $\mu_m = m$. Furthermore, it is desirable to keep μ_m different from m allowing for a reliable assignment of perturbative errors via scale variations.

The hard coefficients $\mathcal{C}_{ij}^{(n_l+1)}$ in Eq. (3.38) are obtained by performing a matching in analogy to Eq. (3.35) in the $\overline{\mathrm{MS}}$ scheme with partonic (onshell) initial states, which include now both massless and

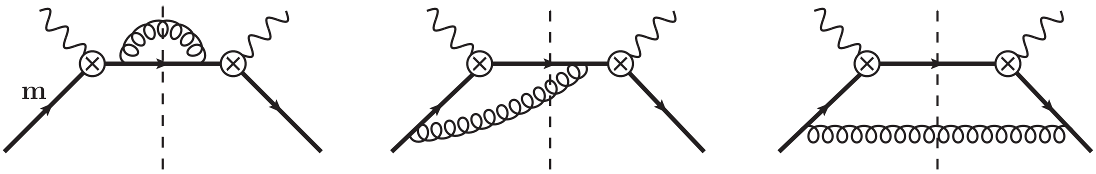

Figure 3.5: Massive quark contributions to the hard matching coefficient $\mathcal{C}_{QQ}^{(n_l+1,1)}$ in full QCD. The cuts indicated by the dashed lines have to be placed at all possible positions. Symmetric diagrams and wave function renormalization corrections have to be added.

massive quarks. The partonic structure function $\hat{F}_{1,Qg}^{(n_l,1)}$ gives the same result as in Eq. (3.33) except for the fact that the strong coupling is now evaluated with n_l+1 flavors, i.e.

$$\hat{F}_{1,Qg}^{(n_l+1,1)}(z,Q,m) = \hat{F}_{1,Qg}^{(n_l,1)}(z,Q,m)\Big|_{\alpha_s^{(n_l)}\to\alpha_s^{(n_l+1)}} . \tag{3.44}$$

The corresponding PDF contribution $\hat{\phi}_{Q/g}^{(n_l+1,1)}$ has been already given in Eq. (3.31). Thus the matching coefficient $\mathcal{C}_{Qg}^{(n_l+1,1)}$ reads

$$\begin{aligned}\mathcal{C}_{Qg}^{(n_l+1,1)}(z,Q,m,\mu) &= \frac{2}{e_Q^2}\hat{F}_{1,Qg}^{(n_l+1,1)}(z,Q,m) - \hat{\phi}_{Q/g}^{(n_l+1,1)}(z,m,\mu)\\ &= \mathcal{C}_{Qg}^{(n_l+1,1)}(z,Q,\mu) + \frac{2}{e_Q^2}\left(\hat{F}_{1,Qg}^{(n_l+1,1)}(z,Q,m) - \hat{F}_{1,Qg}^{(n_l+1,1)}(z,Q,m)\Big|_{m\to 0}\right) , \end{aligned}\tag{3.45}$$

This expression clearly shows that the SCET matching subtracts the mass singular terms in the Wilson coefficient and that therefore the massless limit is reached for $m \to 0$, i.e.

$$\mathcal{C}_{Qg}^{(n_l+1,1)}(z,Q,m,\mu) \overset{m\to 0}{\longrightarrow} \mathcal{C}_{Qg}^{(n_l+1,1)}(z,Q,\mu) . \tag{3.46}$$

Note that the same correction $\hat{\phi}_{Q/g}^{(n_l+1,1)}$ is swapped between $\mathcal{C}_{Qg}^{(n_l+1,1)}$ in Eq. (3.45) and $\mathcal{M}_{\phi,Qg}^{(1)}$ in Eq. (3.42), which guarantees that we get a continuous transition to the factorization of scenario I in Eq. (3.32) at fixed order, i.e. for $\mu_H = \mu_m = \mu$,

$$\sum_{j=q,Q,g}\int\frac{\mathrm{d}\xi}{\xi}\,\mathcal{C}_{Qj}^{(n_l+1)}\left(\frac{z}{\xi},Q,m,\mu\right)\mathcal{M}_{\phi,jg}(\xi,m,\mu) = \mathcal{C}_{Qg}^{(n_l)}(z,Q,m) , \tag{3.47}$$

which can be easily checked explicitly at $\mathcal{O}(\alpha_s)$ using the tree level results $\mathcal{M}_{\phi,gg}^{(0)}(z) = \mathcal{C}_{QQ}^{(n_l+1,0)}(z) = \delta(1-z)$ and the expressions in Eqs. (3.33), (3.42) and (3.45). The difference with respect to scenario I is that the corrections $\hat{\phi}_{Q/g}^{(n_l+1,1)}$ are evaluated at different scales, namely μ_m and μ_H. The flavor number dependent evolution together with this feature allow us to resum the large mass logarithms appearing in Eq. (3.37), but to give still the same result in the fixed-order expansion without having to drop terms of $\mathcal{O}(m^2/Q^2)$.

By discussing $\mathcal{M}_{\phi,Qg}^{(1)}$ and $\mathcal{C}_{Qg}^{(n_l+1,1)}$ we have in fact already considered all relevant contributions in the factorization theorem appearing at $\mathcal{O}(\alpha_s)$ in the fixed-order expansion. For completeness, let us also display the one-loop hard matching coefficient with initial state massive quarks, i.e. $\mathcal{C}_{QQ}^{(n_l+1,1)}$, which contributes at $\mathcal{O}(\alpha_s^2)$ in the factorization theorem since one matching relation at $\mathcal{O}(\alpha_s)$ has to be involved to generate the massive quark PDF. The corresponding full QCD diagrams for the partonic tensor are shown in Fig. 3.5. These have been calculated in Refs. [59, 61] and yield lengthy expressions. We only display the massless limit,

$$\begin{aligned}\hat{F}_{1,QQ}^{(n_l+1,1)}(z,Q,m) \overset{m\to 0}{\longrightarrow} \frac{\alpha_s^{(n_l+1)}C_F}{4\pi}\frac{e_Q^2}{2}\,\theta(z)\,\theta(1-z)\Bigg\{&\frac{P_{qq}^{(1)}(z)}{2}\ln\left(\frac{Q^2}{m^2}\right) - \delta(1-z)\left[5+\frac{2\pi^2}{3}\right] - 7\left[\frac{1}{1-z}\right]_+\\ &- 4\left[\frac{\ln(1-z)}{1-z}\right]_+ + 2(1+z)\ln(1-z) - \frac{2(1+z^2)}{1-z}\ln(z) + 8 + 2z\Bigg\} . \end{aligned}\tag{3.48}$$

Figure 3.6: Feynman diagrams at $\mathcal{O}(\alpha_s)$ for the collinear PDF operator $\mathcal{O}_Q(\omega)$ corresponding to Eq. (3.9) for a massive quark field Q in the initial state. Symmetric diagrams and wave function renormalization corrections have to be added.

This expression contains also logarithmic mass singularities, which are related to the splitting function and suggest a resummation via RG evolution performed in SCET. For the matching we have to take into account the SCET subtractions given by the partonic PDF diagrams with a massive quark in the initial state displayed in Fig. 3.6, which yield

$$\hat{\phi}^{(n_l+1,1)}_{Q/Q}(z,m,\mu) = \frac{\alpha_s^{(n_l+1)} C_F}{4\pi}\,\theta(z)\,\theta(1-z)\left\{-\frac{P^{(1)}_{qq}(z)}{2}L_m + 4\,\delta(1-z) - 4\left[\frac{1}{1-z}\right]_+ - 8\left[\frac{\ln(1-z)}{1-z}\right]_+ \right.$$
$$\left. + 4(1+z)\ln(1-z) + 2 + 2z\right\}. \tag{3.49}$$

In the matching coefficient the IR low-mass dependence cancels and we get in analogy to Eq. (3.45)

$$\begin{aligned}\mathcal{C}^{(n_l+1,1)}_{QQ}(z,Q,m,\mu) &= \frac{2}{e_Q^2}\hat{F}^{(n_l+1,1)}_{1,Qg}(z,Q,m) - \hat{\phi}^{(n_l+1,1)}_{Q/Q}(z,m,\mu)\\ &= \mathcal{C}^{(n_l+1,1)}_{QQ}(z,Q,\mu) + \frac{2}{e_Q^2}\left(\hat{F}^{(n_l+1,1)}_{1,QQ}(z,Q,m) - \hat{F}^{(n_l+1,1)}_{1,QQ}(z,Q,m)\Big|_{m\to 0}\right)\,,\end{aligned} \tag{3.50}$$

which yields the massless limit for $m \to 0$,

$$\mathcal{C}^{(n_l+1,1)}_{QQ}(z,Q,m,\mu) \overset{m\to 0}{\longrightarrow} \mathcal{C}^{(n_l+1,1)}_{QQ}(z,Q,\mu)\,. \tag{3.51}$$

Thus, if $Q \gg m$ the mass dependence in the hard matching coefficient can be dropped and the only place where the mass enters explicitly is in the threshold corrections. This approach is frequently called zero-mass VFNS (ZM-VFNS).

Let us at the end of this section comment on different quark mass implementations in the literature concerning this scenario. First we note that keeping the exact mass dependence the momentum of an onshell initial state massive parton reads in terms of the partonic Bjorken variable in Eq. (3.4)

$$p^\mu = Q\left(\frac{1}{\eta}, \frac{m^2\eta}{Q^2}, 0\right) \qquad \text{with } \eta \equiv \frac{2\hat{x}}{1+\sqrt{1+\frac{4m^2\hat{x}^2}{Q^2}}}\,. \tag{3.52}$$

In the discussion above with massive quark fluctuations scaling as $\sim Q(1,\lambda_m^2,\lambda_m)$, the residual momenta are of $\mathcal{O}(m^2/Q)$ such that the label momentum is not affected by the presence of the mass, i.e. $\tilde{p}^+ = Q/\hat{x}$. In contrast, in the ACOT approach (see Ref. [2]) translated to the language of SCET the mass dependence is fully incorporated in the label momentum component $\tilde{p}^+$, i.e. $\tilde{p}^+ = Q/\eta$, but p^- is still treated as residual momentum. The corresponding matching coefficients denoted by $\tilde{\mathcal{C}}_{ij}$ with an initial massive quark state are then obtained from the partonic relation

$$\hat{F}^{(n_l+1)}_{1,iQ}(\hat{x},Q,m) = \frac{e_i^2}{2}\sum_{j=q,Q,g}\int\frac{\mathrm{d}\xi}{\xi}\,\tilde{\mathcal{C}}^{(n_l+1)}_{ij}\left(\frac{\eta}{\xi},Q,m,\mu\right)\,\hat{\phi}^{(n_l+1)}_{j/Q}(\xi,m,\mu)\,, \tag{3.53}$$

which yields e.g. at tree level the relation

$$\tilde{\mathcal{C}}^{(n_l+1,0)}_{QQ}(\eta(\hat{x})) = \delta(1-\hat{x})\,. \tag{3.54}$$

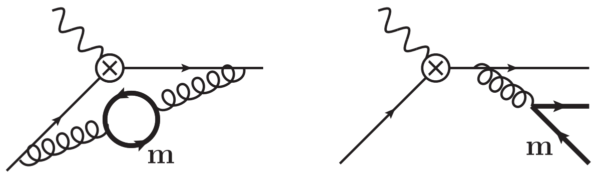

Figure 3.7: Exemplary diagrams for secondary massive quark production in DIS at $\mathcal{O}(\alpha_s^2 C_F T_F)$.

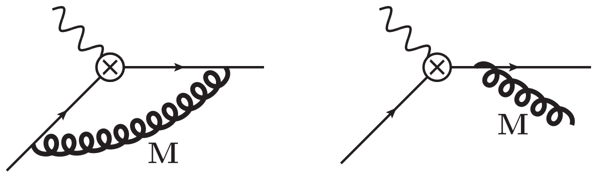

Figure 3.8: Exemplary diagrams for secondary massive gluon production in DIS at $\mathcal{O}(\alpha_s)$.

Incorporating this matching coefficient back into the original convolution for the hadronic structure function with a massless initial state proton gives a tedious form for the involved Wilson coefficients, which can be considerably simplified by displaying them in terms of the rescaled variable [2, 59, 61]

$$\chi = \frac{x}{2}\left(1+\sqrt{1+\frac{4m^2}{Q^2}}\right) . \tag{3.55}$$

Note that the ACOT approach resums the same logarithms at $\mathcal{O}(\frac{m^0}{Q^0}\ln(\frac{m^2}{Q^2}))$ as Eq. (3.38) and coincides in the fixed-order expansion with Eq. (3.38), since both approaches exhibit a continuous transition to the common fixed flavor result in Eq. (3.32). Concerning our discussion outlined at NLL the difference therefore amounts to the treatment of terms at $\mathcal{O}(\alpha_s^2 \frac{m^2}{Q^2}\ln(\frac{m^2}{Q^2}))$ and is thus parametrically of higher order, both for $m \ll Q$ and $m \sim Q$. We also mention that Eq. (3.38) and also the ACOT approach in Ref. [2] yield nonvanishing contributions for the hard matching coefficients beyond the kinematically allowed threshold for the production of two heavy quarks, $z = 1/(1+4m^2/Q^2)$, related to the subtraction terms. This has lead to the implementation of the correct threshold behavior by hand due to a different rescaling variable [62]. The difference concerns again terms of $\mathcal{O}(\alpha_s^2 \frac{m^2}{Q^2}\ln(\frac{m^2}{Q^2}))$ and is thus formally of higher order. The ambiguity to deal with these terms has been first pointed out in Ref. [63] and lead to the emergence of many more different schemes. Extending our systematic SCET approach to subleading order one can in principle clarify conceptually how to unambiguously assign m^2/Q^2 suppressed terms between the Wilson coefficients and mass threshold corrections.

3.4 Secondary mass effects

We now turn to the computation of massive quark effects initiated by massless quarks and where massive quarks are produced through the radiation of gluons splitting into massive quark-antiquark pairs and do not interact with the hard photon directly, see Fig. 3.7. We call this type of heavy quark production mechanism, which starts at $\mathcal{O}(\alpha_s^2)$, *secondary* in contrast to the case where massive quarks interact directly with the hard photon, which is the situation discussed in the previous section at $\mathcal{O}(\alpha_s)$ and which we call *primary*. We will see in chapter 4 that in the endpoint region $x \to 1$ the primary mass effects are suppressed by $\mathcal{O}(1-x)$ and thus the secondary mass effects give the dominant mass corrections there. It is instructive to investigate these corrections also for $1-x \sim \mathcal{O}(1)$ to illustrate the computations with the dispersive method frequently used throughout the remainder of this thesis and for the sake of comparison to the results in the endpoint region in chapter 4.

We will see that the problem of secondary heavy quark production with mass m is closely related to the production of gauge bosons with vector coupling and mass M, i.e. "massive gluons", see Fig. 3.8. The

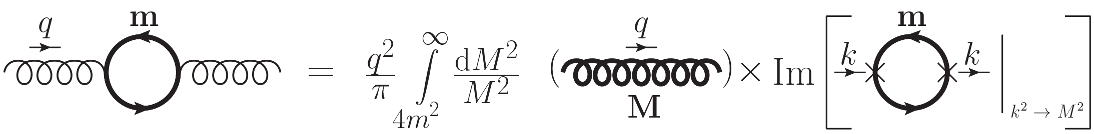

Figure 3.9: Figure illustrating the dispersion method for the vacuum polarization correction to the gluon propagator in the subtracted version with $\Pi^{\rm OS}(m^2, p^2 = 0) = 0$ suitable for situations where the massive quark is not contributing to the renormalization group evolution.

connection is given by the invariant mass which a massless offshell gluon has to carry to split up into a quark-antiquark pair. In the following we will adopt a notation for the massive gluon that agrees with the one for the QCD results, which facilitates the interpretation of the results at $\mathcal{O}(\alpha_s)$ and allows to compare with the results for massless gluons given in Sec. 3.2.

Here we perform the calculations at $\mathcal{O}(\alpha_s^2 C_F T_F)$ for the mass mode contributions to the infrared-safe hard Wilson coefficient and the massive threshold corrections explicitly within the factorization theorems of the VFNS described in Sec. 3.3 in Eqs. (3.32) and (3.38) and discuss the main features. We remind the reader that we use Feynman gauge and dimensional regularization as UV regulator. For the computation of the SCET diagrams we need the integration measure in light-cone coordinates, which reads

$$\frac{\mathrm{d}^d k}{(2\pi)^d} \quad\longrightarrow\quad \frac{1}{2}\frac{\mathrm{d}k^+}{2\pi}\frac{\mathrm{d}k^-}{2\pi}\frac{2^{3-d}\pi^{1-d/2}}{\Gamma\left(\frac{d-2}{2}\right)}\,\mathrm{d}|\vec{k}_\perp|\,|\vec{k}_\perp|^{d-3} \tag{3.56}$$

for integrals not depending on the angles between the transverse momenta. For convenience we abbreviate the ratios between the masses M and m and the momentum transfer energy Q via

$$\hat{M} \equiv \frac{M}{Q}\,, \quad \hat{m} \equiv \frac{m}{Q}\,. \tag{3.57}$$

3.4.1 Dispersion relations

Instead of performing the two-loop integrations for the secondary massive quarks directly we will first calculate the results for the radiation of a massive gluon at $\mathcal{O}(\alpha_s)$ and then relate them to the contributions at $\mathcal{O}(\alpha_s^2 C_F T_F)$ via a dispersive integration. This way is both technically simpler and conceptually more instructive, since most of the interesting features for secondary massive quarks can be already discussed at the one-loop level with the massive gluon.

We explain the dispersive method for a secondary massive quark-antiquark pair starting from the gluonic vacuum polarization $\Pi(m^2, p^2)$ due to a massive quark-antiquark bubble,

$$\begin{aligned}\Pi^{AB}_{\mu\nu}(m^2, p^2) &= -\,i\left(p^2 g_{\mu\nu} - p_\mu p_\nu\right)\Pi(m^2, p^2)\,\delta^{AB}\\ &\equiv \int \mathrm{d}^4 x\, e^{ipx}\,\langle 0|T\,[J^A_\mu(x) J^B_\nu(0)]|0\rangle\,,\end{aligned} \tag{3.58}$$

with the vector current $J^A_\mu(x) = ig\,\bar{q}(x)T^A\gamma_\mu q(x)$. The vacuum polarization function $\Pi(m^2, p^2)$ can be rewritten as a dispersion integral over its absorptive part. The unsubtracted (unrenormalized) dispersion integral reads

$$\Pi(m^2, p^2) = -\,\frac{1}{\pi}\int \mathrm{d}M^2\,\frac{\mathrm{Im}\big[\Pi(m^2, M^2)\big]}{p^2 - M^2 + i\epsilon}\,, \tag{3.59}$$

and the subtracted (on-shell and finite) dispersion relation has the form

$$\begin{aligned}\Pi^{\rm OS}(m^2, p^2) &= \Pi(m^2, p^2) - \Pi(m^2, 0)\\ &= -\,\frac{p^2}{\pi}\int \frac{\mathrm{d}M^2}{M^2}\,\frac{\mathrm{Im}\big[\Pi(m^2, M^2)\big]}{p^2 - M^2 + i\epsilon}\,.\end{aligned} \tag{3.60}$$

The absorptive part in d dimensions reads

$$\mathrm{Im}\big[\Pi(m^2,p^2)\big] = \theta(p^2-4m^2)\, g^2 T_F \tilde{\mu}^{2\epsilon} (p^2)^{(d-4)/2}\, \frac{2^{3-2d}\pi^{(3-d)/2}}{\Gamma\Big(\frac{d+1}{2}\Big)} \Big(d-2+\frac{4m^2}{p^2}\Big)\Big(1-\frac{4m^2}{p^2}\Big)^{(d-3)/2}. \tag{3.61}$$

Eqs. (3.59) and (3.60) together with Eq. (3.61) are valid for any d. The subtracted vacuum polarization function $\Pi^{\rm OS}(m^2,p^2)$ has the important feature that its insertion into the gluon line can be rewritten as a dispersion integration over a "massive gluon" propagator,

$$\frac{-\,i\,g^{\mu\rho}}{p^2+i\epsilon}\,\Pi^{\rm OS}_{\rho\sigma}(m^2,p^2)\,\frac{-\,i\,g^{\sigma\nu}}{p^2+i\epsilon} = \frac{1}{\pi}\int\frac{\mathrm{d}M^2}{M^2}\,\frac{-\,i\left(g^{\mu\nu}-\frac{p^\mu p^\nu}{p^2}\right)}{p^2-M^2+i\epsilon}\,\mathrm{Im}\big[\Pi(m^2,M^2)\big]\;, \tag{3.62}$$

where p^μ denotes the external gluon momentum, and we have dropped the overall color conserving Kronecker δ^{AB}. Note that in Eq. (3.62) the propagator becomes transverse from the insertion of the vacuum polarization. In our calculations the contributions from the additional $p^\mu p^\nu$ term vanish due to gauge invariance and can be ignored. The insertion of the full unsubtracted vacuum polarization function $\Pi(m^2,p^2)$ can be recovered by subtracting a term with the massless gluon propagator times the vacuum polarization function at zero momentum transfer,

$$\begin{aligned}\frac{-\,i\,g^{\mu\rho}}{p^2+i\epsilon}\,\Pi_{\rho\sigma}(m^2,p^2)\,\frac{-\,i\,g^{\sigma\nu}}{p^2+i\epsilon} =& \frac{1}{\pi}\int\frac{\mathrm{d}M^2}{M^2}\,\frac{-\,i\left(g^{\mu\nu}-\frac{p^\mu p^\nu}{p^2}\right)}{p^2-M^2+i\epsilon}\,\mathrm{Im}\big[\Pi(m^2,M^2)\big]\\ &-\frac{-\,i\left(g^{\mu\nu}-\frac{p^\mu p^\nu}{p^2}\right)}{p^2+i\epsilon}\,\Pi(m^2,0)\,.\end{aligned} \tag{3.63}$$

Note that the RHS of the equalities in Eqs. (3.62) and (3.63) stays the same in any gauge used for the propagators on the LHS. The zero momentum vacuum polarization function at $\mathcal{O}(\alpha_s)$ in d dimensions reads

$$\Pi(m^2,0) \;=\; \frac{\alpha_s T_F}{3\pi}\left(\frac{\mu^2 e^{\gamma_E}}{m^2}\right)^{2-\frac{d}{2}}\Gamma\Big(2-\frac{d}{2}\Big)\,. \tag{3.64}$$

Using the on-shell vacuum polarization insertion via Eq. (3.62) automatically implements the on-shell subtraction for the renormalization of the strong coupling with respect to the effects of the massive quark. So using Eq. (3.60) implies that we employ the strong coupling in the n_l flavor scheme, i.e. $\alpha_s^{(n_l)}$. The subtracted dispersion relation has the computational advantage that the integration over the virtual gluon mass is suppressed by an additional inverse power of M^2. This can make the dispersion integration UV finite and may allow us to carry out the integral directly in $d=4$ dimensions. Using the full vacuum polarization insertion of Eq. (3.63) implies that the strong coupling is still unrenormalized with respect to the effects of the massive quark flavor.

The relations in Eqs. (3.62) and (3.63) show explicitly that we can obtain the result for the massive quark-antiquark pair from a dispersion integral over the corresponding result for a gluon with mass M. We note that the dispersion relation method may not only be used to determine the effects of secondary virtual massive quarks, but also for real radiation corrections as long as the momenta of the massive quark and antiquark enter a quantity coherently (i.e. only the sum of their momenta is relevant in the observable), which is the case for inclusive DIS. Even if this is not the case the dispersion integration may be useful to determine the dominant corrections or to the deal with singular or divergent parts of the result, see e.g. Sec. 5.4 for such an application in the calculation of the $\mathcal{O}(\alpha_s^2 C_F T_F)$ massive quark contributions to the soft function for the thrust distribution describing large angle soft radiation. Furthermore, besides the treatment of massive quarks dispersion relations can be applied for the study of other secondary colored particles, see e.g. Ref. [26] for a study of massive gluino effects.

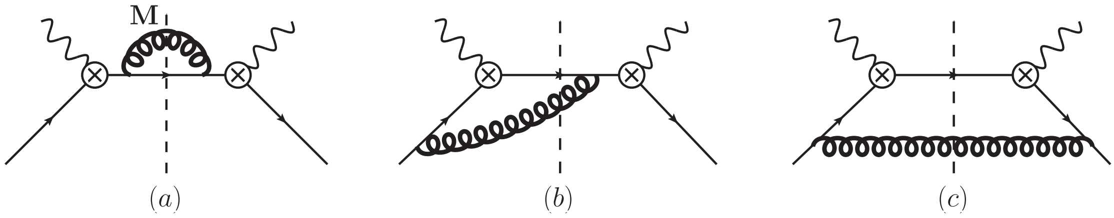

Figure 3.10: Full QCD contributions to the partonic tensor with a massless initial state quark and a massive gluon at $\mathcal{O}(\alpha_s)$. The cuts indicated by the dashed lines can be also placed at different positions. Symmetric diagrams and wave function corrections have to be added.

3.4.2 Massive gluon computation at $\mathcal{O}(\alpha_s)$

We compute the hard matching coefficients $\mathcal{C}_{qq}^{(\mathrm{OS},1)}(z,Q,M)$ and $\mathcal{C}_{qq}^{(\overline{\mathrm{MS}},1)}(z,Q,M,\mu)$ for the structure function $F_1(x,Q,M)$ in the scenarios I and II described in Sec. 3.3, respectively, for the radiation of a massive gluon at $\mathcal{O}(\alpha_s)$, as well as the threshold correction $\mathcal{M}_{\phi,qq}^{(1)}(z,M,\mu)$. The corresponding results for the longitudinal structure function $F_L(x,Q,M)$ can be found again in appendix A. First we will display the full QCD computation of the partonic tensor, then the corresponding SCET calculation for the PDF and discuss the complete massive gluon corrections to the factorization theorems (3.32) and (3.38) at the end of this subsection. In general we will need the full d-dimensional result to carry out the dispersive integral in Eq. (3.60) to obtain the results for secondary massive quarks $\mathcal{O}(\alpha_s^2 C_F T_F)$ in the next step.

Full QCD computation

We start with the calculation of the partonic tensor $\hat{W}_{qq}^{\mu\nu}(p,q)$ in full QCD, for which the corresponding Feynman diagrams are shown in Fig. 3.10. After applying the QCD Feynman rules we have performed this calculation using *FeynCalc* [64] for the spin traces coming from the spin average and the decomposition into elementary one-loop scalar integrals, which could be evaluated with the help of Refs. [65, 66]. At the end the imaginary part was taken, which corresponds to all cuts of the diagrams in Fig. 3.10, and the appropriate projections of the partonic tensor have been applied to obtain the partonic structure functions $\hat{F}_{1,qq}^{(1)}$ and $\hat{F}_{L,qq}^{(1)}$. Note that no IR divergences occur in the calculation since the gluon mass acts as an IR regulator. In the following we display the results for each diagram separately already expanded for $\epsilon \to 0$. [11]

The first diagram in Fig. 3.10 yields both a virtual self-energy correction and a real radiation contribution from the final state quark with the kinematic threshold $z = 1/(1+\hat{M}^2)$,

$$\hat{F}_{1,qq}^{(1,a)} = \frac{\alpha_s C_F}{4\pi}\,\frac{e_q^2}{2}\left\{\delta(1-z)\left[-\frac{1}{\epsilon}+L_M+\frac{1}{2}\right]+\theta(z)\,\theta(1-z-\hat{M}^2 z)\,\frac{(1-z-\hat{M}^2 z)^2}{(1-z)^3}\right\}, \tag{3.65}$$

with $L_M = \ln(M^2/\mu^2)$. In this section we will not specify the renormalization conditions for the massive gluon coupling α_s. The second diagram gives a virtual vertex correction as well as a real radiation contribution emitted from the initial state quark with the same threshold as before,

$$\begin{aligned}\hat{F}_{1,qq}^{(1,b)} = \frac{\alpha_s C_F}{4\pi}\,\frac{e_q^2}{2}\Bigg\{&\delta(1-z)\bigg[\frac{1}{\epsilon}-L_M+(1-\hat{M}^2)^2\left(2\,\mathrm{Li}_2(\hat{M}^2)-\ln^2(\hat{M}^2)+2\ln(1-\hat{M}^2)\ln(\hat{M}^2)-\frac{2\pi^2}{3}\right)\\ &-(3-2\hat{M}^2)\ln(\hat{M}^2)-4+2\hat{M}^2\bigg]+\theta(z)\,\theta(1-z-\hat{M}^2 z)\,\frac{2z}{1-z}\bigg[\ln\left(\frac{(1-\hat{M}^2 z)(1-z)}{\hat{M}^2 z^2}\right)\\ &\times\Big(1-\hat{M}^2(1+z)+\hat{M}^4 z\Big)-\frac{1}{1-z}\Big(1-z-\hat{M}^2+\hat{M}^4 z\Big)\bigg]\Bigg\}.\end{aligned} \tag{3.66}$$

[11] Since the full QCD result decouples automatically for $M \gg Q$ the onshell dispersion integral in Eq. (3.62) is convergent and dimensional regularization will not be needed as a regulator at this stage.

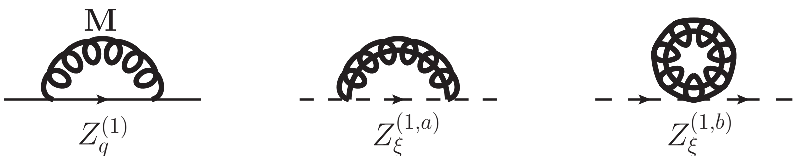

Figure 3.11: The quark wave function renormalization diagrams for an interaction with a massive gluon at one loop in full QCD (first diagram) and in SCET (second and third diagram).

The third diagram yields a pure real radiation correction,

$$\hat{F}^{(1,c)}_{1,qq} = \frac{\alpha_s C_F}{4\pi}\,\frac{e_q^2}{2}\,\theta(z)\,\theta(1-z-\hat{M}^2 z)\left\{2\ln\left(\frac{(1-\hat{M}^2 z)(1-z)}{\hat{M}^2 z^2}\right)\left[1-z+4\hat{M}^2 z^2-6\hat{M}^4 z^3\right]\right. \\ \left. -\frac{2(1-z-\hat{M}^2 z)}{(1-z)^2(1-\hat{M}^2 z)}\left[(1-z)(1-2z)-\hat{M}^2 z(2-10z+7z^2)+\hat{M}^4 z^2(2-9z+6z^2)\right]\right\}. \tag{3.67}$$

Finally we also need the quark wave-function renormalization graph displayed in Fig. 3.11, which yields

$$Z_q^{(1)} = \frac{\alpha_s C_F}{4\pi}\,\delta(1-z)\left\{\frac{1}{\epsilon}-L_M-\frac{1}{2}\right\}. \tag{3.68}$$

Summing up all contributions and taking into account all symmetric configurations yields

$$\hat{F}^{(1)}_{1,qq}(z,Q,M) = \hat{F}^{(1,a)}_{1,qq} + 2\hat{F}^{(1,b)}_{1,qq} + \hat{F}^{(1,c)}_{1,qq} - Z_q^{(1)}\,\frac{e_q^2}{2}\,\delta(1-z) \\ = e_q^2\,\delta(1-z)\,\hat{F}^{(1)}_{M,\mathrm{QCD}}(Q,M) + \theta(z)\,\theta(1-z-\hat{M}^2 z)\,\frac{e_q^2}{2}\,\hat{F}^{(1)}_{M,\mathrm{QCD},\theta}(z,Q,M). \tag{3.69}$$

Here $\hat{F}^{(1)}_{M,\mathrm{QCD}}(Q,M)$ denotes the partonic current form factor in a spacelike QCD process for the interaction with a massive gluon and is given by (see also Refs. [67,68] for the timelike analytic continuation)

$$\hat{F}^{(1)}_{M,\mathrm{QCD}}(Q,M) = \frac{\alpha_s C_F}{4\pi}\left\{(1-\hat{M}^2)^2\left[2\,\mathrm{Li}_2(\hat{M}^2)-\ln^2(\hat{M}^2)+2\ln(1-\hat{M}^2)\ln(\hat{M}^2)-\frac{2\pi^2}{3}\right]\right. \\ \left. -(3-2\hat{M}^2)\ln(\hat{M}^2)+2\hat{M}^2-\frac{7}{2}\right\}. \tag{3.70}$$

The real radiation correction $\hat{F}^{(1)}_{M,\mathrm{QCD},\theta}(z,Q,M)$ with the threshold $z = 1/(1+\hat{M}^2)$ reads

$$\hat{F}^{(1)}_{M,\mathrm{QCD},\theta}(z,Q,M) = \frac{\alpha_s C_F}{4\pi}\,\frac{1}{1-z}\left\{2\ln\left(\frac{(1-\hat{M}^2 z)(1-z)}{\hat{M}^2 z^2}\right)\left[1+z^2-2\hat{M}^2 z(1-z+2z^2)\right.\right. \\ \left. +2\hat{M}^4 z^2(1-3z+3z^2)\right] + \frac{1-z-\hat{M}^2 z}{(1-z)^2(1-\hat{M}^2 z)}\left[-1+3z-6z^2+4z^3\right. \\ \left.\left. +\hat{M}^2 z(6-23z+30z^2-14z^3)+\hat{M}^4 z^2(-7+26z-30z^2+12z^3)\right]\right\}. \tag{3.71}$$

Since the QCD current is conserved all UV divergences have cancelled in the calculation and the contributions to the structure function do not require renormalization. We remark that in the heavy quark limit the full QCD corrections decouple, i.e. $\hat{F}^{(1)}_{1,qq}(z,Q,M) \to 0$ for $\hat{M} \to \infty$. In contrast to the one-loop massive quark correction $\hat{F}^{(n_l,1)}_{1,Qg}(z,Q,m)$ in Eq. (3.33) there is, however, always a virtual contributions for arbitrary masses $M > Q$ that does not vanish above a certain threshold. In the small mass limit

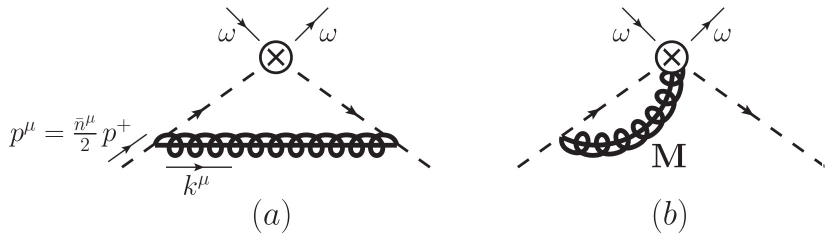

Figure 3.12: Feynman diagrams for the collinear PDF operator $\mathcal{O}_q(\omega)$ with a massless quark field in the initial state and a massive gluon at $\mathcal{O}(\alpha_s)$. Special care has to be taken in the diagram (b) concerning the label momentum which extracted in the local interaction. Symmetric diagrams and wave function corrections have to be added.

$\hat{M} \to 0$, on the other hand, we obtain [12]

$$\begin{aligned}\hat{F}^{(1)}_{1,qq}(z,Q,M) \stackrel{\hat{M}\to 0}{\longrightarrow} \frac{\alpha_s C_F}{4\pi}\,\frac{e_q^2}{2}\,\theta(z)\,\theta(1-z)\biggl\{&\delta(1-z)\left[-3\ln(\hat{M}^2)-\frac{9}{2}-\frac{4\pi^2}{3}\right]\\ &+\left[\frac{1}{1-z}\right]_+\left[-4\ln(\hat{M}^2)-3\right]+4\left[\frac{\ln(1-z)}{1-z}\right]_+ +2(1+z)\ln(\hat{M}^2)\\ &-2(1+z)\ln(1-z)-\frac{4(1+z^2)}{1-z}\ln(z)+2+4z\biggr\}\,,\end{aligned} \tag{3.72}$$

which exhibits again infrared mass-singularities.

SCET computation

We turn to the computation of the partonic PDF corrections in SCET corresponding to the diagrams displayed in Fig. 3.12, which we will describe in more detail here. We note that we could in principle also perform the calculation with the full QCD Feynman rules, since for one single boosted collinear sector SCET is equivalent to QCD. Applying the SCET Feynman rules given in Fig. 2.3 for the matrix element of the PDF operator $\mathcal{O}_q(\omega)$ in Eq. (3.9) with massless external quarks the spin average of the first diagram yields in close analogy to the computation in Ref. [46]

$$\hat{\phi}^{(1,a)}_{q/q} = -ig^2 C_F \tilde{\mu}^{2\epsilon}(d-2)\,p^+\theta(z)\int\frac{\mathrm{d}^d k}{(2\pi)^d}\,\frac{k_\perp^2}{[(p-k)^2+i\epsilon]^2}\,\frac{1}{[k^2-M^2+i\epsilon]}\,\delta(p^+-k^+-zp^+)\,. \tag{3.73}$$

For convenience, we use a frame for the initial onshell particle, where the perpendicular momentum component vanishes, i.e. $p^\mu = (Q,0,0)$. Employing the scaling $k^\mu \sim Q(1,\lambda_M^2,\lambda_M)$ for the $\bar{n}$-collinear loop momentum we obtain

$$\begin{aligned}\hat{\phi}^{(1,a)}_{q/q} =& ig^2 C_F\tilde{\mu}^{2\epsilon}(d-2)\,\theta(z)\int\frac{\mathrm{d}^d k}{(2\pi)^d}\,\frac{\vec{k}_\perp^2}{[k^+k^- -\vec{k}_\perp^2-Qk^+ +i\epsilon]^2}\,\frac{1}{[k^+k^- -\vec{k}_\perp^2-M^2+i\epsilon]}\\ &\times\delta\left(1-z-\frac{k^+}{Q}\right)\,.\end{aligned} \tag{3.74}$$

We first carry out the k^- integration with the method of residues and then the $k_\perp$-integration. Finally, after integrating over the remaining δ-distribution in k^+ space we obtain

$$\hat{\phi}^{(1,a)}_{q/q} = \frac{\alpha_s C_F}{4\pi}\,\frac{(d-2)^2}{2}\,\Gamma\left(2-\frac{d}{2}\right)\left(\frac{\mu^2 e^{\gamma_E}}{M^2 z}\right)^{2-\frac{d}{2}}\theta(z)\,\theta(1-z)\,(1-z)\,. \tag{3.75}$$

[12]Note that the virtual current form factor $\hat{F}^{(1)}_{M,\mathrm{QCD}}$ and the real radiation correction $\hat{F}^{(1)}_{M,\mathrm{QCD},\theta}$ yield individually also Sudakov double logarithms in the massless limit, which cancel in the sum.

In principle we still have to take care of the corresponding soft-bin subtractions. In fact they give vanishing contributions due to the fact that the soft region is not relevant for the factorization of the structure functions and they can be decoupled by a field redefinition in the same way as (ultra-)soft fields. We will check this here by explicit computations. By further expanding Eq. (3.74) with the soft scaling $k^\mu \sim Q(\lambda_M, \lambda_M, \lambda_M)$ one gets

$$\left(\hat{\phi}^{(1,a)}_{q/q}\right)_{0M} = ig^2 C_F \tilde{\mu}^{2\epsilon}(d-2)\,\theta(z) \int \frac{\mathrm{d}^d k}{(2\pi)^d} \frac{\vec{k}_\perp^2}{[Qk^+ - i\epsilon]^2} \frac{1}{[k^2 - M^2 + i\epsilon]}\,\delta(1-z)\,, \tag{3.76}$$

which is parametrically suppressed by M^2/Q^2 and thus gives no contribution at leading order in λ_M.

In a similar way we can compute the second diagram. Here one has to be aware of the fact that a gluon field can be contracted both with the Wilson line in the jet field $\chi_{\bar{n}}(0)$ or the one in $\bar{\chi}_{\bar{n}}(0)$ in Eq. (3.9) giving rise to purely virtual and real radiation contributions with different extractions of the label momenta by the label operator. Taking into account both possibilities we get

$$\begin{aligned}\hat{\phi}^{(1,b)}_{q/q} =& 2ig^2 C_F \tilde{\mu}^{2\epsilon}\,\theta(z) \int \frac{\mathrm{d}^d k}{(2\pi)^d} \frac{Q-k^+}{k^+} \frac{1}{[k^+k^- - \vec{k}_\perp^2 - Qk^+ + i\epsilon]} \frac{1}{[k^+k^- - \vec{k}_\perp^2 - M^2 + i\epsilon]} \\ &\times \left[\delta\left(1-z\right) - \delta\left(1 - z - \frac{k^+}{Q}\right)\right]\,.\end{aligned} \tag{3.77}$$

After carrying out the integrations in k^- and $k_\perp$ and rescaling the integration variable k^+ in terms of $y = k^+/Q$ this yields

$$\hat{\phi}^{(1,b)}_{q/q} = \frac{\alpha_s C_F}{2\pi}\,\Gamma\left(2-\frac{d}{2}\right)\left(\frac{\mu^2 e^{\gamma_E}}{M^2}\right)^{2-\frac{d}{2}} \theta(z)\,\theta(1-z) \int_0^1 \frac{\mathrm{d}y}{y}\,(1-y)^{\frac{d}{2}-1}\left[\delta(1-z-y) - \delta(1-z)\right]\,. \tag{3.78}$$

Note that both phase space contributions are by themselves not well-defined in dimensional regularization. In fact they contain rapidity divergences which, however, cancel among these two collinear contributions and do not result in large logarithms for $1 - x \sim \mathcal{O}(1)$. With a proper recombination in terms of distributions we obtain [13]

$$\hat{\phi}^{(1,b)}_{q/q} = \frac{\alpha_s C_F}{2\pi}\,\Gamma\left(2-\frac{d}{2}\right)\left(\frac{\mu^2 e^{\gamma_E}}{M^2 z}\right)^{2-\frac{d}{2}} \theta(z)\,\theta(1-z)\left\{H_{\frac{d}{2}-1}\,\delta(1-z) + \left[\frac{1}{1-z}\right]_+ - 1\right\}\,, \tag{3.79}$$

where H_n denotes the n-th Harmonic number. We note that the corresponding soft-bin subtractions cancel due to the fact that the two δ-distributions in Eq. (3.77) become the same after performing an additional soft expansion.

Finally, we compute the wave function renormalization diagrams $Z_\xi^{(1,a)}$ and $Z_\xi^{(1,b)}$ in Fig. 3.11 for the external massless collinear quarks. This will give the same result as in full QCD, since the interactions within a single collinear sector correspond to the ones in full QCD in a boosted frame. The sum of both self-energy diagrams for arbitrary collinear external momentum p^μ can be readily combined and reads

$$Z_\xi^{(1,a)} + Z_\xi^{(1,b)} = -i\frac{\not{n}}{2} g^2 C_F (d-2)\tilde{\mu}^{2\epsilon} \frac{1}{Q} \int \frac{\mathrm{d}^d k}{(2\pi)^d} \frac{p^2 + Qk^-}{[p^2(1 + k^+/Q) + Qk^- + k^2 + i\epsilon]} \frac{1}{[k^2 - M^2 + i\epsilon]}\,. \tag{3.80}$$

The wave-function renormalization contribution $Z_\xi^{(1)}$ can be identified in the limit $p^2 \to 0$ giving

$$Z_\xi^{(1,a)} + Z_\xi^{(1,b)} \overset{p^2\to 0}{\longrightarrow} i\frac{\not{n}}{2}\frac{p^2}{p^+} Z_\xi^{(1)}\,. \tag{3.81}$$

[13] This can be achieved with the help of a rapidity regulator and will be described in chapter 4 explicitly.

In d dimensions $Z_\xi^{(1)}$ reads

$$Z_\xi^{(1)} = \frac{\alpha_s C_F}{4\pi}\,\Gamma\Big(2-\frac{d}{2}\Big)\Big(\frac{\mu^2 e^{\gamma_E}}{M^2}\Big)^{2-\frac{d}{2}}\,\frac{2(d-2)}{d}\,, \tag{3.82}$$

which reproduces the full theory self energy graph and in particular has the same expansion for $\epsilon \to 0$ as given in Eq. (3.68). The soft-bin subtraction for the wave function contribution turns out to be power suppressed by M/Q. To demonstrate this let us first consider the power counting of the collinear mass mode self-energy diagrams given in Eq. (3.80). The external massless collinear modes interacting with the collinear mass modes with the scaling $k^\mu \sim Q(1, \lambda_M^2, \lambda_M)$ obey the same scaling giving $p^2 \sim (p+k)^2 \sim M^2$. This yields $Z_\xi^{(1,a)} + Z_\xi^{(1,b)} \sim M^2/Q$ for the result in Eq. (3.80) and thus gives $p^2/Q \times Z_\xi^{(1)} \sim M^2/Q$ in Eq. (3.81). This demonstrates that $Z_\xi^{(1)} \sim \mathcal{O}(1)$ as we have obtained also in the explicit result shown in Eq. (3.82). For the soft-bin subtraction to Eq. (3.80) we have to apply the counting $k_s^\mu \sim (\lambda_M, \lambda_M, \lambda_M)$ for the loop momentum, which increases the typical invariant mass of the massless collinear quarks to $p^2 \sim (p+k_s)^2 \sim QM$. The mass mode bin integral that emerges therefore has the form of a simple tadpole graph,

$$\Big(Z_\xi^{(1,a)} + Z_\xi^{(1,b)}\Big)_{0M} = -i\frac{\not{n}}{2} g^2 C_F (d-2)\tilde{\mu}^{2\epsilon}\frac{1}{Q}\int \frac{\mathrm{d}^d k}{(2\pi)^d}\frac{1}{[k^2 - M^2 + i\epsilon]}\,. \tag{3.83}$$

with the counting $(Z_\xi^{(1,a)} + Z_\xi^{(1,b)})_{0M} \sim M^2/Q$. The same counting also applies to the resulting wave-function renormalization contribution, i.e. $p^2/Q \times (Z_\xi^{(1)})_{0M} \sim M^2/Q$, and because $p^2 \sim QM$ we find that $(Z_\xi^{(1)})_{0M} \sim M/Q$. This shows that the mass mode bin subtraction for the collinear wave function renormalization due to the mass modes belongs to a subleading treatment beyond the scope of the treatment discussed here. [14]

Adding all contributions and taking into account the symmetric configuration of diagram (b) in Fig. 3.12 yields

$$\begin{aligned}\hat\phi_{q/q}^{(\mathrm{bare},1)}(z,M,\mu) &= \hat\phi_{q/q}^{(1,a)} + 2\hat\phi_{q/q}^{(1,b)} - Z_\xi^{(1)}\delta(1-z)\\ &= \frac{\alpha_s C_F}{4\pi}\,\Gamma\Big(2-\frac{d}{2}\Big)\Big(\frac{\mu^2 e^{\gamma_E}}{zM^2}\Big)^{2-\frac{d}{2}}\theta(z)\,\theta(1-z)\,\bigg\{\delta(1-z)\,\bigg[4H_{\frac{d}{2}-1} - \frac{2(d-2)}{d}\bigg]\\ &\quad + 4\bigg[\frac{1}{1-z}\bigg]_+ + (1-z)\frac{(d-2)^2}{2} - 4\bigg\}\,.\end{aligned} \tag{3.84}$$

Expanding for $\epsilon \to 0$ gives

$$\begin{aligned}\hat\phi_{q/q}^{(\mathrm{bare},1)}(z,M,\mu) = \frac{\alpha_s C_F}{4\pi}\,\theta(z)\,\theta(1-z)\bigg\{\bigg[\frac{1}{\epsilon} - L_M\bigg]\frac{P_{qq}^{(1)}(z)}{2} + \delta(1-z)\bigg[\frac{9}{2} - \frac{2\pi^2}{3}\bigg] - \frac{2(1+z^2)}{1-z}\ln(z)\\ - 4(1-z)\bigg\}\,,\end{aligned} \tag{3.85}$$

with the one-loop splitting function $P_{qq}^{(1)}(z)$ defined in Eq. (3.26). The condition of decoupling requires that the massive quark contributions vanish for $M \to \infty$. Renormalizing the PDF operator in the OS scheme thus yields the counterterm

$$Z_{\phi,qq}^{(\mathrm{OS},1)}(z,M,\mu) = \hat\phi_{q/q}^{(\mathrm{bare},1)}\,, \tag{3.86}$$

[14] Since linear M/Q-suppressed terms do not exist in the non-singular collinear terms that can be obtained in the full theory calculation, the subleading effective field theory treatment contains a mechanism that makes these contributions vanish identically.

with a vanishing renormalized contribution, i.e. $\hat{\phi}^{(\mathrm{OS},1)}_{q/q}(z, M, \mu) = 0$. Using $\overline{\mathrm{MS}}$ renormalization we obtain the same counterterm as in Eq. (3.20) since the UV behavior is independent of any IR scale like the mass, which yields the renormalized contribution

$$\begin{aligned}\hat{\phi}^{(\overline{\mathrm{MS}},1)}_{q/q}(z, M, \mu) = \frac{\alpha_s C_F}{4\pi}\,\theta(z)\,\theta(1-z)\Bigg\{&\delta(1-z)\left[-3L_M + \frac{9}{2} - \frac{2\pi^2}{3}\right] - 4L_M\left[\frac{1}{1-z}\right]_+ \\ &+ 2(1+z)L_M - \frac{2(1+z^2)}{1-z}\ln(z) - 4(1-z)\Bigg\}\,. \end{aligned} \tag{3.87}$$

Results for hard matching coefficients and threshold correction

Now we have computed all required contributions to display the final results for the hard matching coefficients $\mathcal{C}^{(\mathrm{OS},1)}_{qq}$ in scenario I (for $M \gtrsim Q$) and $\mathcal{C}^{(\overline{\mathrm{MS}},1)}_{qq}$ in scenario II (for $M \lesssim Q$) and the threshold correction $\mathcal{M}^{(1)}_{\phi,qq}$. Due to the fact that the partonic PDF diagrams vanish in the OS scheme we obtain in scenario I using Eq. (3.35)

$$\mathcal{C}^{(\mathrm{OS},1)}_{qq}(z, Q, M) = \frac{2}{e_q^2}\,\hat{F}^{(1)}_{1,qq}(z, Q, M)\,, \tag{3.88}$$

which has the correct decoupling limit, see Eq. (3.69). In scenario II all infrared mass-singularities cancel between the QCD and SCET contributions in the $\overline{\mathrm{MS}}$ scheme, so that we get

$$\begin{aligned}\mathcal{C}^{(\overline{\mathrm{MS}},1)}_{qq}(z, Q, M, \mu) &= \frac{2}{e_q^2}\,\hat{F}^{(1)}_{1,qq}(z, Q, M) - \hat{\phi}^{(\overline{\mathrm{MS}},1)}_{q/q}(z, M, \mu) \\ &= \mathcal{C}^{(1)}_{qq}(z, Q, \mu) + \frac{2}{e_q^2}\left(\hat{F}^{(1)}_{1,qq}(z, Q, M) - \hat{F}^{(1)}_{1,qq}(z, Q, M)\Big|_{M\to 0}\right)\,,\end{aligned} \tag{3.89}$$

which has the correct massless limit in Eq. (3.16), i.e.

$$\mathcal{C}^{(\overline{\mathrm{MS}},1)}_{qq}(z, Q, M, \mu) \overset{M\to 0}{\longrightarrow} \mathcal{C}^{(1)}_{qq}(z, Q, \mu)\,. \tag{3.90}$$

The evolution for the massive gluon in the $\overline{\mathrm{MS}}$ scheme is performed above the mass mode matching scale μ_m with the same anomalous dimension as for the massless one in Eq. (3.25). At this scale the change of schemes between OS and $\overline{\mathrm{MS}}$ renormalization is performed leading to a threshold correction $\mathcal{M}^{(1)}_{\phi,qq}$ in analogy to Eq. (3.42),

$$\mathcal{M}^{(1)}_{\phi,qq}(z, M, \mu) = \hat{\phi}^{(\overline{\mathrm{MS}},1)}_{q/q}(z, M, \mu)\,, \tag{3.91}$$

with $\hat{\phi}^{(\overline{\mathrm{MS}},1)}_{q/q}(z, M, \mu)$ given in Eq. (3.87). We get a continuous transition between scenario I and II due to the fact that the contribution $\hat{\phi}^{(\overline{\mathrm{MS}},1)}_{q/q}$ is only swapped in the factorization theorem between the hard matching coefficient and the threshold correction for the purpose of resummation of logarithms. Note that the linearity of the dispersion integration entails that the continuity is carried over also to the contributions coming from the secondary massive quarks.

3.4.3 Secondary massive quark effects at $\mathcal{O}(\alpha_s^2 C_F T_F)$

Starting from the results at $\mathcal{O}(\alpha_s)$ for a massive gluon we can now compute the secondary massive quark corrections at $\mathcal{O}(\alpha_s^2 C_F T_F)$, which become more lengthy, but exhibit the same basic features. Following Eq. (3.62) we can obtain the unrenormalized $\mathcal{O}(\alpha_s^2 C_F T_F)$ contributions by the relations

$$\hat{F}^{(n_l,2)}_{1,qq,T_F}(z, Q, m) = \frac{1}{\pi}\int \frac{\mathrm{d}M^2}{M^2}\,\hat{F}^{(1)}_{1,qq}(z, Q, M)\,\mathrm{Im}\big[\Pi(m^2, M^2)\big]\,, \tag{3.92}$$

$$\hat{\phi}^{(n_l,\mathrm{bare},2)}_{q/q,T_F}(z, m, \mu) = \frac{1}{\pi}\int \frac{\mathrm{d}M^2}{M^2}\,\hat{\phi}^{(\mathrm{bare},1)}_{q/q}(z, M, \mu)\,\mathrm{Im}\big[\Pi(m^2, M^2)\big]\,, \tag{3.93}$$

where the superscripts (n_l) and (bare) remind us that the subtracted dispersion relation is used, i.e. that the strong coupling is given in n_l flavors, but that the PDF itself is still unrenormalized.

The full QCD result at $\mathcal{O}(\alpha_s^2 C_F T_F)$ is both IR- and UV-finite and can be decomposed in analogy to Eq. (3.69) into a purely virtual correction and a real radiation correction with the kinematic threshold $z = 1/(1+4\hat{m}^2)$,

$$\hat{F}^{(n_l,2)}_{1,qq,T_F}(z,Q,m) = e_q^2\,\hat{F}^{(n_l,2)}_{m,\mathrm{QCD}}(Q,m)\,\delta(1-z) + \theta(z)\,\theta(1-z-4\hat{m}^2 z)\,\frac{e_q^2}{2}\,\hat{F}^{(n_l,2)}_{m,\mathrm{QCD},\theta}(z,Q,m)\,. \tag{3.94}$$

The partonic QCD current form factor $\hat{F}^{(n_l,2)}_{m,\mathrm{QCD}}(Q,m)$ is in fact just a function of $\hat{m}$ and reads

$$\hat{F}^{(n_l,2)}_{m,\mathrm{QCD}}(Q,m) = \frac{\big(\alpha_s^{(n_l)}\big)^2 C_F T_F}{16\pi^2}\,f^{(2)}_{m,\mathrm{QCD}}(\hat{m}) \tag{3.95}$$

where the function $f^{(2)}_{m,\mathrm{QCD}}(\hat{m})$ is given by

$$\begin{aligned} f^{(2)}_{m,\mathrm{QCD}}(\hat{m}) = {}& \Big(-r^4 + 2r^2 + \frac{5}{3}\Big)\Big[\mathrm{Li}_3\Big(\frac{r+1}{r-1}\Big) + \mathrm{Li}_3\Big(\frac{r-1}{r+1}\Big) - 2\zeta_3\Big] + \Big(\frac{46}{9}r^3 + \frac{10}{3}r\Big) \\ & \times \left[\mathrm{Li}_2\Big(\frac{r-1}{r+1}\Big) - \mathrm{Li}_2\Big(\frac{r+1}{r-1}\Big)\right] + \left(\frac{110}{9}r^2 + \frac{200}{27}\right)\ln\Big(\frac{1-r^2}{4}\Big) + \frac{238}{9}r^2 + \frac{1213}{81}\,, \end{aligned} \tag{3.96}$$

where

$$r = \sqrt{1-4\hat{m}^2}\,. \tag{3.97}$$

This expression has been written in a way that allows easily for an analytical continuation from the spacelike DIS with $q^2 = -Q^2$ to timelike processes e.g. e^+e^- collisions with $q^2 = Q^2$ (see also the result in Refs. [68–70]). We also redefine the threshold term without the prefactors,

$$\hat{F}^{(n_l,2)}_{m,\mathrm{QCD},\theta}(z,Q,m) = \frac{\big(\alpha_s^{(n_l)}\big)^2 C_F T_F}{16\pi^2}\,f^{(2)}_{m,\mathrm{QCD},\theta}(z,\hat{m}) \tag{3.98}$$

where the real radiation function $f^{(2)}_{m,\mathrm{QCD},\theta}(z,\hat{m})$ reads

$$\begin{aligned} f^{(2)}_{m,\mathrm{QCD},\theta}(z,\hat{m}) = {}& \frac{1}{1-z}\left\{\frac{8}{3}\left[1+z^2-12\hat{m}^4 z^2(1-3z+3z^2)\right]\left[\mathrm{Li}_2\left(\frac{r_z-w_z}{r_z+1}\right) + \mathrm{Li}_2\left(\frac{r_z+w_z}{r_z-1}\right)\right.\right. \\ & \left. - \mathrm{Li}_2\left(\frac{r_z-w_z}{r_z-1}\right) - \mathrm{Li}_2\left(\frac{r_z+w_z}{r_z+1}\right) + \ln\left(\frac{1+r_z}{1-r_z}\right)\ln\left(\frac{r_z+w_z}{r_z-w_z}\right)\right] \\ & + \frac{8}{9}\,r_z\left[-8-11z^2+2\hat{m}^2 z(13-18z+28z^2)\right]\ln\left(\frac{r_z+w_z}{r_z-w_z}\right) \\ & + \frac{4}{3(1-z)^2}\left[1-3z^2+2z^3+6\hat{m}^4 z^2(1-2z)(7-12z+6z^2)\right]\ln\left(\frac{1+w_z}{1-w_z}\right) \\ & \left. + \frac{2w_z}{27(1-z)}\left[151-265z+436z^2-322z^3-2\hat{m}^2 z(491-1530z+2030z^2-996z^3)\right]\right\}. \end{aligned} \tag{3.99}$$

Here we have used the abbreviations

$$r_z = \sqrt{1-4\hat{m}^2 z}\,, \quad w_z = \sqrt{1-\frac{4\hat{m}^2 z}{1-z}}\,. \tag{3.100}$$

We remark that as for the one-loop case the QCD corrections decouple in the heavy quark limit using the n_l scheme for α_s, i.e. $\hat{F}^{(n_l,2)}_{1,qq,T_F}(z,Q,m) \to 0$ for $\hat{m} \to \infty$. In the small mass limit $\hat{m} \to 0$, on the other hand, we obtain

$$\begin{aligned}
\hat{F}^{(n_l,2)}_{1,qq,T_F}(z,Q,m) \overset{\hat{m}\to 0}{\longrightarrow}\ & \frac{\left(\alpha_s^{(n_l)}\right)^2 C_F T_F}{16\pi^2}\,\frac{e_q^2}{2}\,\theta(z)\,\theta(1-z)\left\{\delta(1-z)\left[2\ln^2(\hat{m}^2)+\left(\frac{38}{3}+\frac{16\pi^2}{9}\right)\ln(\hat{m}^2)\right.\right.\\
&\left.+\frac{265}{9}+\frac{134\pi^2}{27}\right]+\left[\frac{1}{1-z}\right]_+\left[\frac{8}{3}\ln^2(\hat{m}^2)+\frac{116}{9}\ln(\hat{m}^2)+\frac{718}{27}-\frac{8\pi^2}{9}\right]\\
&+\left[\frac{\ln(1-z)}{1-z}\right]_+\left[-\frac{16}{3}\ln(\hat{m}^2)-\frac{116}{9}\right]+\frac{8}{3}\left[\frac{\ln^2(1-z)}{1-z}\right]_+-\frac{8(1+z^2)}{3(1-z)}\,\mathrm{Li}_2(1-z)\\
&+\frac{4(1+z^2)}{1-z}\ln^2(z)-\frac{4}{3}(1+z)\ln^2(1-z)-\frac{16(1+z^2)}{3(1-z)}\ln(z)\ln(1-z)\\
&+\frac{4}{9(1-z)}\ln(z)\left[12\left(1+z^2\right)\ln(\hat{m}^2)+29-6z+44z^2\right]\\
&+\frac{8}{9}\ln(1-z)\left[3\left(1+z\right)\ln(\hat{m}^2)+8+11z\right]-\frac{4}{3}(1+z)\ln^2(\hat{m}^2)\\
&\left.-\frac{8}{9}(8+11z)\ln(\hat{m}^2)-\frac{416}{27}-\frac{644}{27}z+\frac{4\pi^2}{9}(1+z)\right\}. \qquad (3.101)
\end{aligned}$$

As we have already seen in the one-loop case this expression has infrared mass logarithms.

We turn to the computation of the corresponding PDF corrections. Carrying out the convolution in Eq. (3.93) in $d = 4-2\epsilon$ dimensions and expanding in ϵ we obtain ($L_m = \ln(m^2/\mu^2)$)

$$\begin{aligned}
\hat{\phi}^{(n_l,\mathrm{bare},2)}_{q/q,T_F}(z,m,\mu) =\ & \frac{\left(\alpha_s^{(n_l)}\right)^2 C_F T_F}{16\pi^2}\,\theta(z)\,\theta(1-z)\left\{\delta(1-z)\left[\frac{2}{\epsilon^2}+\frac{1}{\epsilon}\left(-4L_m-\frac{1}{3}-\frac{4\pi^2}{9}\right)+4L_m^2\right.\right.\\
&\left.+\left(\frac{2}{3}+\frac{8\pi^2}{9}\right)L_m+\frac{73}{18}+\frac{29\pi^2}{27}-\frac{8}{3}\zeta_3\right]+\left[\frac{1}{1-z}\right]_+\left[\frac{8}{3\epsilon^2}-\frac{1}{\epsilon}\left(\frac{16}{3}L_m+\frac{40}{9}\right)\right.\\
&\left.+\frac{16}{3}L_m^2+\frac{80}{9}L_m+\frac{224}{27}+\frac{4\pi^2}{9}\right]-\frac{4}{3\epsilon^2}(1+z)+\frac{1}{\epsilon}\left[\frac{8}{3}(1+z)L_m-\frac{4}{9}+\frac{44}{9}z\right.\\
&\left.-\frac{4(1+z^2)}{3(1-z)}\ln(z)\right]+\frac{2(1+z^2)}{3(1-z)}\ln^2(z)+\frac{\ln(z)}{1-z}\left[\frac{8}{3}L_m(1+z^2)+\frac{44}{9}-\frac{16}{3}z+\frac{44}{9}z^2\right]\\
&\left.-\frac{8}{3}L_m^2(1+z)+L_m\left(\frac{8}{9}-\frac{88}{9}z\right)+\frac{44}{27}-\frac{268}{27}z-\frac{2\pi^2}{9}(1+z)\right\}. \qquad (3.102)
\end{aligned}$$

In scenario I we renormalize the massive quark correction in the OS scheme, where the counterterm cancels all SCET contributions, i.e. [15]

$$Z^{(n_l,2)}_{\phi,qq,T_F}(z,m,\mu) = \hat{\phi}^{(n_l,\mathrm{bare},2)}_{q/q,T_F}(z,m,\mu)\,. \qquad (3.103)$$

Thus the hard matching coefficient in scenario I corresponds again only to the full theory contributions

$$\mathcal{C}^{(n_l,2)}_{qq,T_F}(z,Q,m) = \frac{2}{e_q^2}\,\hat{F}^{(n_l,2)}_{1,qq,T_F}(z,Q,m)\,, \qquad (3.104)$$

which decouples for $m\to\infty$. In scenario II we want to apply the $\overline{\mathrm{MS}}$ renormalization condition for the computation of the matching condition, i.e. for the corrections to the PDF operator, but also for the strong coupling. [16] Since $\hat{F}^{(n_l,2)}_{1,qq,T_F}$ and $\hat{\phi}^{(n_l,\mathrm{bare},2)}_{q/q,T_F}$ have been computed with the subtracted dispersion relation they correspond to expressions in the n_l flavor scheme for the strong coupling. To switch to the (n_l+1)-flavor scheme one can subtract, according to Eq. (3.63), the $\overline{\mathrm{MS}}$-subtracted vacuum polarization

[15]We remind the reader that the massless quark bubble contributions are still renormalized in the $\overline{\mathrm{MS}}$ scheme as usual.

[16]Note that the quark mass scheme does not play any role at this order and has to be only specified in the consideration of secondary mass effects at $\mathcal{O}(\alpha_s^3)$.

function at zero-momentum times the corresponding unrenormalized (massless) one-loop partonic structure function $\hat{F}^{(1)}_{1,qq}(z,Q,\mu,\Delta)$ and PDF $\hat{\phi}^{(\mathrm{bare},1)}_{q/q}(z,Q,\mu,\Delta)$ calculated with an arbitrary IR regulator Δ,

$$\hat{F}^{(n_l+1,2)}_{1,qq,T_F}(z,Q,m,\mu,\Delta) = \hat{F}^{(n_l,2)}_{1,qq,T_F}(z,Q,m) - \left(\Pi(m^2,0) - \frac{\alpha_s T_F}{3\pi}\,\frac{1}{\epsilon}\right)\hat{F}^{(1)}_{1,qq}(z,Q,\mu,\Delta)\,, \tag{3.105}$$

$$\hat{\phi}^{(n_l+1,\mathrm{bare},2)}_{q/q,T_F}(z,m,\mu,\Delta) = \hat{\phi}^{(n_l,\mathrm{bare},2)}_{q/q,T_F}(z,m,\mu) - \left(\Pi(m^2,0) - \frac{\alpha_s T_F}{3\pi}\,\frac{1}{\epsilon}\right)\hat{\phi}^{(\mathrm{bare},1)}_{q/q}(z,\mu,\Delta)\,. \tag{3.106}$$

To obtain the matching coefficient we should in principle first renormalize both quantities and then calculate their difference where the dependence on Δ cancels. Since the QCD structure function is UV finite, it is convenient to revert this procedure, i.e. to first determine the difference of the unrenormalized quantities and cancel the UV divergences in the PDF correction by the corresponding counterterm at the very end, such that the cancellation of the IR divergences can be made explicit from the beginning. The difference of the massless gluon one-loop QCD structure function and the PDF correction involved in the calculation of the matching coefficient yields [17]

$$\frac{2}{e_q^2}\,\hat{F}^{(1)}_{1,qq}(z,Q,\mu,\Delta) - \hat{\phi}^{(\mathrm{bare},1)}_{q/q}(z,\mu,\Delta) = \mathcal{C}^{(1)}_{qq}(z,Q,\mu) - Z^{(1)}_{\phi,qq}(z,\mu)\,. \tag{3.107}$$

Thus the additional term in the hard matching coefficient corresponding to the change from the n_l- to the (n_l+1)-flavor scheme for the strong coupling reads

$$\begin{aligned}
\mathcal{C}^{(n_l\to n_l+1,2)}_{qq}(z,Q,m,\mu) = &-\left(\Pi(m^2,0) - \frac{\alpha_s T_F}{3\pi}\,\frac{1}{\epsilon}\right)\left(\mathcal{C}^{(1)}_{qq}(z,Q,\mu) - Z^{(1)}_{\phi,qq}(z)\right)\\
= &\frac{\alpha_s^2 C_F T_F}{16\pi^2}\,\theta(z)\,\theta(1-z)\bigg\{\delta(1-z)\left[-\frac{4}{\epsilon}\,L_m + 2L_m^2 + 4L_Q L_m - \left(12+\frac{8\pi^2}{9}\right)L_m\right.\\
&\left.+\frac{\pi^2}{3}\right] + \left[\frac{1}{1-z}\right]_+\left[-\frac{16}{3\epsilon}\,L_m + \frac{8}{3}L_m^2 + \frac{16}{3}L_Q L_m - 4L_m + \frac{4\pi^2}{9}\right]\\
&+\frac{16}{3}\,L_m\left[\frac{\ln(1-z)}{1-z}\right]_+ + \frac{8}{3\epsilon}(1+z)L_m - \frac{4}{3}(1+z)L_m^2 - \frac{8}{3}(1+z)L_m L_Q\\
&-\frac{8}{3}(1+z)L_m\ln(1-z) - \frac{8(1+z^2)}{3(1-z)}L_m\ln(z) + 8L_m - \frac{2\pi^2}{9}(1+z)\bigg\}\,.
\end{aligned} \tag{3.108}$$

Combining all contributions and including the $\overline{\mathrm{MS}}$ current counterterm contribution $Z^{(n_l+1,2)}_{\phi,qq,T_F}$ given in Eq. (3.22), the result for the $\mathcal{O}(\alpha_s^2 C_F T_F)$ secondary massive quark contributions to the hard matching coefficient for scenario II, i.e. in the (n_l+1)-flavor scheme for the strong coupling and PDF, reads ($\alpha_s = \alpha_s^{(n_l+1)}(\mu)$)

$$\begin{aligned}
\mathcal{C}^{(n_l+1,2)}_{qq,T_F}(z,Q,m,\mu) &= \frac{2}{e_q^2}\,\hat{F}^{(n_l,2)}_{1,qq,T_F}(z,Q,m) - \hat{\phi}^{(n_l,\mathrm{bare},2)}_{q/q,T_F}(z,m,\mu) + \mathcal{C}^{(n_l\to n_l+1,2)}_{qq}(z,Q,m,\mu) + Z^{(n_l+1,2)}_{\phi,qq,T_F}(z,\mu)\\
&= \mathcal{C}^{(n_l+1,2)}_{qq,T_F}(z,Q,\mu) + \frac{2}{e_q^2}\left(\hat{F}^{(n_l,2)}_{1,qq,T_F}(z,Q,m) - \hat{F}^{(n_l,2)}_{1,qq,T_F}(z,Q,m)\Big|_{m\to 0}\right)\,,
\end{aligned} \tag{3.109}$$

which yields the massless limit for $m \to 0$, i.e.

$$\mathcal{C}^{(n_l+1,2)}_{qq,T_F}(z,Q,m,\mu) \stackrel{m\to 0}{\longrightarrow} \mathcal{C}^{(n_l+1,2)}_{qq,T_F}(z,Q,\mu) \tag{3.110}$$

with $\mathcal{C}^{(n_f,2)}_{qq,T_F}(z,Q,\mu)$ given in Eq. (3.18).

[17] Using dimensional regularization for both UV and IR divergences the SCET contributions for massless gluons vanish identically.

Finally, we also compute the PDF matching coefficient starting from Eq. (3.41). Due to the fact that the scheme dependence cancels between the matching coefficients and low-energy operators, this relation can be equivalently written in terms of the renormalized matching coefficients in the OS and $\overline{\mathrm{MS}}$ scheme

$$\mathcal{M}_{\phi,ij}\left(z,m,\mu_m\right) = \sum_{k=q,Q,g} \int \frac{\mathrm{d}\xi}{\xi} \left(\mathcal{C}^{(n_l+1)}\right)^{-1}_{ik} \left(\frac{z}{\xi},Q,m,\mu\right) \mathcal{C}^{(n_l)}_{kj}\left(\xi,Q,m,\mu\right) . \tag{3.111}$$

Since the difference in the factorization theorems for scenario I and II concerns just the matching conditions and the PDF evolution, Eq. (3.111) makes it evident that the condition for the threshold correction automatically implements a continuous transition between these two scenarios for $m \sim \mu_m \sim \mu_H \sim Q$. Due to the fact that the expressions in Eq. (3.111) are written in different schemes for α_s one has to relate them by the decoupling relation for α_s [18]

$$\alpha_s^{(n_l)}(\mu_m) = \alpha_s^{(n_l+1)}(\mu_m)\left[1 + \frac{\alpha_s^{(n_l+1)}(\mu_m)T_F}{3\pi}\,L_m + \mathcal{O}(\alpha_s^2)\right] . \tag{3.112}$$

Using the structure of the Wilson coefficients in Eqs. (3.104) and (3.109) we obtain up to $\mathcal{O}(\alpha_s^2)$

$$\begin{aligned}\mathcal{M}_{\phi,qq}(z,m,\mu) = {}& \delta(1-z) + \hat{\phi}^{(n_l,\mathrm{bare},2)}_{q/q,T_F}(z,m,\mu) - \mathcal{C}^{(n_l\to n_l+1,2)}_{qq}(z,Q,m,\mu) - Z^{(n_l+1,2)}_{\phi,qq,T_F}(z,\mu) \\ &+ \frac{\alpha_s^{(n_l+1)}T_F}{3\pi}\,L_m\,\mathcal{C}^{(n_l+1,1)}_{qq}(z,Q,\mu) + \mathcal{O}(\alpha_s^3) \,.\end{aligned} \tag{3.113}$$

Inserting all explicit expressions gives at $\mathcal{O}(\alpha_s^2 C_F T_F)$

$$\begin{aligned}\mathcal{M}^{(2)}_{\phi,qq}(z,m,\mu_m) = {}& \frac{\left(\alpha_s^{(n_l+1)}\right)^2 C_F T_F}{(4\pi)^2}\,\theta(z)\,\theta(1-z)\left\{\delta(1-z)\left[2L_m^2 + \left(\frac{2}{3}+\frac{8\pi^2}{9}\right)L_m + \frac{73}{18} + \frac{20\pi^2}{27} - \frac{8}{3}\zeta_3\right]\right. \\ &+ \left[\frac{1}{1-z}\right]_+\left[\frac{8}{3}L_m^2 + \frac{80}{9}L_m + \frac{224}{27}\right] - \frac{4}{3}L_m^2(1+z) + L_m\left[\frac{8}{9} - \frac{88}{9}z + \frac{8(1+z^2)}{3(1-z)}\ln(z)\right] \\ &\left.+ \frac{2(1+z^2)}{3(1-z)}\ln^2(z) + \frac{\ln(z)}{1-z}\left[\frac{44}{9} - \frac{16}{3}z + \frac{44}{9}z^2\right] + \frac{44}{27} - \frac{268}{27}z\right\} ,\end{aligned} \tag{3.114}$$

where the scheme for α_s does not necessarily need to be specified at this order. The result in Eq. (3.114) is in agreement with Ref. [71] and completes our discussion of the secondary massive quark effects in the OPE region in DIS.

[18] Using the ratio of the counterterms in Eq. (3.41) instead of the ratio of the renormalized matching coefficients in Eq. (3.111) we would need in Eq. (3.112) terms up to $\mathcal{O}(\epsilon^2)$. These can be easily determined from the result for $\Pi(m^2,0)$ in Eq. (3.64) in d dimensions. Otherwise the calculation is straightforward and completely equivalent to the one based on the renormalized expressions.

Chapter 4

VFNS for DIS in the endpoint region

After having discussed the VFNS in the OPE region of DIS we now turn to the endpoint region $x \to 1$. This region is experimentally difficult to investigate due to the strong suppression of the PDFs, so that small corrections due to massive quark effects are unlikely to play an important phenomenological role. However, this region is conceptually interesting since the limit $x \to 1$ constrains the final state to contain one single jet with a small invariant mass, which modifies the factorization theorem as will be explained in Sec. 4.1. The emerging structures are to some extent universal and appear also in other processes involving jets.

We will see that at leading order in $1 - x$ heavy quark contributions to the structure functions arise in the endpoint region exclusively from secondary massive quark radiation. Here, we will extend our discussion about mass modes in SCET initiated in Sec. 3.3 and show in Sec. 4.2 how to embed them into a factorization setup from the EFT perspective depending on the hierarchy between the involved scales. Here we elucidate the resulting factorization theorems in this EFT picture, although technically we just impose different renormalization conditions in analogy to our discussion in chapter 3, which is the underlying reason why the VFNS is continuous.

We perform the associated computations at $\mathcal{O}(\alpha_s^2 C_F T_F)$ relevant for an analysis at N^{3}LL order again with the help of dispersion relations discussing first the calculation of the matrix elements and threshold corrections at $\mathcal{O}(\alpha_s)$ for the radiation of a massive gluon in Sec. 4.3 and performing the dispersive integral to obtain the results for secondary massive quarks afterwards in Sec. 4.4. One interesting aspect in the calculations is the appearance of rapidity divergences, which arise due to the separation of fluctuations with different rapidity but same invariant mass and can be treated completely at the one-loop level with the massive gluon. In the threshold corrections at the mass scale these generate associated large logarithms, which were already mentioned in Sec. 2.6 and whose resummation will be also discussed here in detail.

The mass mode setup is quite generic and can be applied to other, less inclusive processes, where the computations may be more challenging. We will face such an example in chapter 5.

4.1 The massless factorization theorem

Let us first discuss the massless factorization setup in the endpoint region $x \to 1$ for the most singular contributions, highlight the main features and give explicit results at $\mathcal{O}(\alpha_s)$ and $\mathcal{O}(\alpha_s^2 C_F T_F)$ for comparison and reference concerning the massive gluon and massive quark contributions discussed in later sections. Due to consistency the massive quark results must yield the massless expressions for vanishing quark mass.

For $x \to 1$ the collinear parton entering the hard interaction carries almost the full momentum fraction of the proton leaving behind only soft beam remnants. We have shown in Eq. (3.3) that in this region the invariant mass of the final state X becomes much smaller than the momentum transfer scale Q^2. As can be seen in Eq. (3.2) the final state is boosted in n-direction in the Breit frame and therefore corresponds to a n-collinear jet. This situation is sketched in Fig. 4.1. The emergence of the additional jet invariant mass scale $Q^2(1 - x)$ implies that the factorization theorem in Eq. (3.14) is not any more applicable. In particular this can be seen in the hard matching coefficient $\mathcal{C}_{ij}^{(n_f)}(z, Q, \mu)$, where in the endpoint region

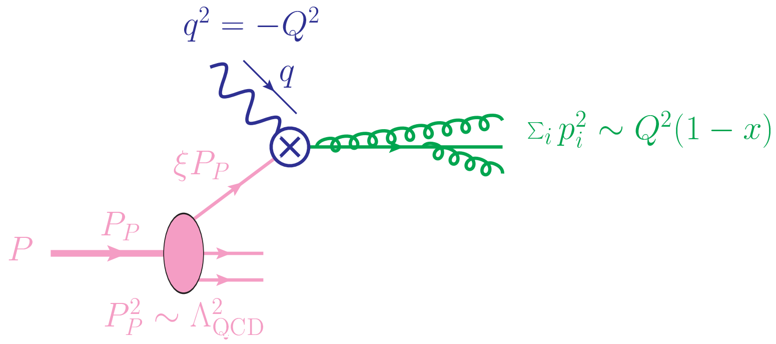

Figure 4.1: The scales in DIS close to the endpoint $x \approx 1$. The different colors correspond to structures with different invariant masses.

large Sudakov logarithms $\sim \ln^2(1-z)$ arise. [1] These are implicit in the distributions in $1-z$ and can be made obvious e.g. for $\mathcal{C}_{qq}^{(n_f,1)}$ in Eq. (3.16) by a proper rescaling in terms of the jet scale $s = Q^2(1-z)$,

$$\frac{\mu^2}{Q^2}\,\mathcal{C}_{qq}^{(n_f,1)}(z,Q,\mu) \overset{z\to 1}{\longrightarrow} \frac{\alpha_s^{(n_f)} C_F}{4\pi}\left\{\delta(\bar s)\left[-2L_Q^2 + 6L_Q - 9 - \frac{2\pi^2}{3}\right] - 3\left[\frac{\theta(\bar s)}{\bar s}\right]_+ + 4\left[\frac{\theta(\bar s)\ln \bar s}{\bar s}\right]_+\right\} \quad (4.1)$$

with $L_Q = \ln(Q^2/\mu^2)$ and $\bar s = s/\mu^2$. Setting $\mu^2 \sim Q^2(1-x)$ which is required to minimize implicit logarithms in the distributions generates a large logarithm for L_Q. Therefore the n-collinear dynamics has to be separated from the hard function leading to the emergence of an additional matrix element, which is sometimes called “refactorization” [72]. We will assume that the jet scale is a perturbative scale, i.e. $1-x \gg \Lambda_{\rm QCD}^2/Q^2$. Generically the emission of soft hadronic radiation will push the final state invariant mass up to scales of $Q\Lambda_{\rm QCD} \gg \Lambda_{\rm QCD}^2$ (except if directly a hadronic resonance is probed which is then not a jet), so that this condition does not impose a significant constraint.

The relevant SCET modes for the endpoint region in DIS are displayed in Fig. 4.2. Note that we have both SCET I-type modes, namely the final state n-collinear modes with invariant mass $\sim Q^2(1-x)$, and SCET II-type modes corresponding to the initial collinear proton and the beam remnants with invariant mass $\sim \Lambda_{\rm QCD}^2$ which can interact with the final state jet via its residual momentum component scaling like $Q(1-x)$. The general scaling of the beam remnants, which has to our knowledge not been stated explicitly in this form before, allows the derivation of the factorization theorem without any assumption on the relation between $\Lambda_{\rm QCD}$ and $Q(1-x)$. In the following we will adopt the scaling $1-x \sim \Lambda_{\rm QCD}/Q$ for convenience, which is the common way to define the endpoint region in the literature. We emphasize, however, that the outcome for the factorization theorem and the results presented in this chapter do not rely on this counting since there is no physical structure associated to the invariant mass scale $Q^2(1-x)^2$, so that we will later not correlate the (rapidity) scale $Q(1-x)$ with $\Lambda_{\rm QCD}$ any more. This point has been already stated in several papers, e.g. in Refs. [73–75].[2]

Due to the fact that the final state is described in SCET and not integrated out as for $1-x \sim \mathcal{O}(1)$ the derivation of the factorization theorem has to be modified. As a first step the full QCD hadronic tensor in Eq. (3.6) is matched onto the corresponding SCET I operators, which involves the matching of the SCET current in Eq. (2.35) to the QCD current,

$$J_\mu(x) \longrightarrow \int {\rm d}\omega \int {\rm d}\omega'\, C(\omega,\omega')\, \bar\chi_{n,\omega'} Y_n^\dagger \gamma_\mu Y_{\bar n} \chi_{\bar n,\omega}(x)\,. \quad (4.2)$$

We remark that currents constructed out of the gluon jet fields in Eq. (2.32), which would be among the allowed gauge-invariant building blocks, vanish due to current conservation [76]. Following a similar derivation as for event shapes [8] one can separate the dynamics of the gauge-invariant fields by

[1] Note that $x \to 1$ implies that the longitudinal momentum fractions in all structures are close to 1 since $x \le z \le 1$.

[2] We remark that concerning the mode setup we disagree with Ref. [74] which assumes nonperturbative messenger modes for the beam remnants at the invariant mass scale $\Lambda_{\rm QCD}^2(1-x) \ll \Lambda_{\rm QCD}^2$.

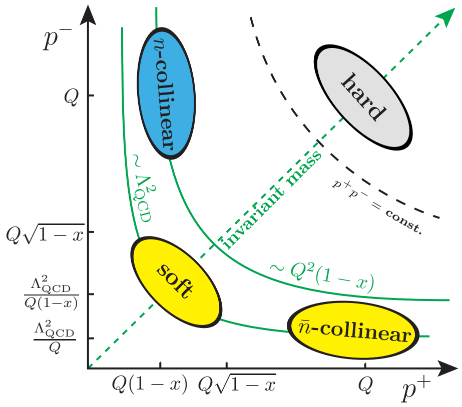

mode	$p^\mu = (+,-,\perp)$	p^2	fields
n-coll.	$Q\left(\lambda_{\rm I}^2, 1, \lambda_{\rm I}\right)$	$Q^2\lambda_{\rm I}^2$	$\xi_n,\, A_n^\mu$
$\bar{n}$-coll.	$Q\left(1, \lambda_{\rm II}^2, \lambda_{\rm II}\right)$	$Q^2\lambda_{\rm II}^2$	$\xi_{\bar{n}},\, A_{\bar{n}}^\mu$
soft	$Q\left(\lambda_{\rm I}^2, \lambda_{\rm II}^2/\lambda_{\rm I}^2, \lambda_{\rm II}\right)$	$Q^2\lambda_{\rm II}^2$	$q_s,\, A_s^\mu$

Figure 4.2: Relevant momentum modes for DIS in the endpoint region. Here we show the general case, where $\lambda_{\rm I} = \sqrt{1-x}$ and $\lambda_{\rm II} = \Lambda_{\rm QCD}/Q$ are the uncorrelated expansion parameters in SCET I and II, respectively. Note that for $\lambda_{\rm I}^2 \gg \lambda_{\rm II}$ also the soft modes are boosted in $\bar{n}$-collinear direction. For the discussion of the factorization theorem we assume $\lambda_{\rm I}^2 \sim \lambda_{\rm II}$, where the soft modes adopt the familiar SCET II scaling $p_s^\mu \sim Q(\lambda_{\rm II}, \lambda_{\rm II}, \lambda_{\rm II})$.

decomposing the final state into collinear and ultrasoft states, [3]

$$|X\rangle = |X_{\bar{n}}\rangle\, |X_n\rangle\, |X_{us}\rangle\,. \tag{4.3}$$

By performing Fierz-transformations for color and spin one can disentangle the hadronic tensor into color singlet structures inside which the Dirac indices are contracted with each other. The contributions to the hadronic tensor from one single primary quark flavor read

$$\begin{aligned}
W^q_{\mu\nu}(P,q) = &-\frac{e_q^2}{2}\, g^\perp_{\mu\nu}\, (2\pi)^4\, \delta^{(4)}\left(P + q - P_{X_{\bar{n}}} - P_{X_n} - P_{X_{us}}\right) \int {\rm d}\omega \int {\rm d}\omega'\, \left|C(\omega,\omega')\right|^2 \\
&\times \sum_{X_{\bar{n}}} \langle P(P_P)|\bar{\chi}_{\bar{n}}|X_{\bar{n}}\rangle\langle X_{\bar{n}}|\frac{\not{n}}{2}\chi_{\bar{n},\omega}|P(P_P)\rangle \sum_{X_n} \frac{1}{4\pi N_c}\, {\rm Tr}\left\{\langle 0|\frac{\not{\bar{n}}}{2}\chi_n|X_n\rangle\langle X_n|\bar{\chi}_{n,\omega'}|0\rangle\right\} \\
&\times \sum_{X_{us}} \frac{1}{N_c}\, {\rm Tr}\left\{\langle 0|\overline{T}\left[\overline{Y}_{\bar{n}}(0,-\infty)\overline{Y}_n(\infty,0)\right]|X_{us}\rangle\langle X_{us}|T\left[Y_n(\infty,0)Y_{\bar{n}}(0,-\infty)\right]|0\rangle\right\}.
\end{aligned} \tag{4.4}$$

For a primary antiquark we obtain an analogous expression. In Eq. (4.4) all fields are evaluated at $x^\mu = 0$ for the residual coordinate, all color and spin indices are summed over and the integration over the phase space is implicit in the sums over the final states. Due to momentum conservation only one relevant label appears in each gauge-invariant collinear sector. We have used the appropriate ultrasoft Wilson lines defined in Eqs. (2.36) – (2.39), which are in fact already properly time-ordered, so that the (anti)-time ordering operators T ($\overline{T}$) can be dropped in Eq. (4.4). Note that the hadronic tensor becomes transverse in the limit $x \to 1$, such that $F_L(x,Q^2) = 0$ and the Callan-Gross relation $F_2(x,Q^2) = 2xF_1(x,Q^2)$ is satisfied to all orders in α_s.

The kinematics in the Breit frame prohibits the appearance of a final $\bar{n}$-collinear state, as can be seen from Eq. (3.2), so that $|X_{\bar{n}}\rangle = |0\rangle$, $P^\mu_{X_{\bar{n}}} = 0$ and the label momentum ω is fixed to Q. This has the important consequence that the $\bar{n}$-collinear sector just enters the factorization theorem as a component which is local both in label space as well as in the residual coordinate, as has been also pointed out in Ref. [78].

In the following one employs the multipole expansion of the final state momenta according to Eq. (2.4), i.e. $P^\mu_{X_n} = \tilde{P}^\mu_{X_n} + K^\mu_{X_n}$ and $P^\mu_{X_{us}} = K^\mu_{X_{us}}$ with $\tilde{P}^\mu_{X_n}$ being the label momentum of the n-collinear state and $K^\mu_{X_n}$, $K^\mu_{X_{us}}$ being residual momenta, to make the power counting manifest. We can already see in

[3]This assumption is based on the fact that the Lagrangian factorizes and therefore the energy eigenstates of the corresponding Hamiltonian do as well. It is in fact not crucial as shown in [77].

Eq. (4.4) that the collinear and ultrasoft modes communicate with each other via the residual component in the condition for momentum conservation, which finally yields a convolution between the corresponding structures. We can relate the momenta in the final state sectors to the corresponding matrix elements introducing the identity

$$\begin{aligned} 1 &= \int \mathrm{d}^4\tilde{p}_n\, \delta^{(4)}(\tilde{p}_n - \tilde{P}_{X_n}) \int \mathrm{d}^4 k_n\, \mathrm{d}^4 k_{us}\, \delta^{(4)}(k_n - K_{X_n})\, \delta^{(4)}(k_{us} - K_{X_{us}}) \\ &= \int \mathrm{d}\tilde{p}_n^-\, \mathrm{d}^2\tilde{p}_n^\perp\, \delta(\tilde{p}_n^- - Q)\, \delta^{(2)}(\tilde{p}_n^\perp) \int \mathrm{d}^4 k_n\, \mathrm{d}^4 k_{us} \int \frac{\mathrm{d}^4 y}{(2\pi)^4}\, e^{i(k_n - K_{X_n})y} \int \frac{\mathrm{d}^4 z}{(2\pi)^4}\, e^{i(k_{us} - K_{X_{us}})z}\,, \end{aligned} \tag{4.5}$$

where we have displayed the label momenta in terms of continuous variables and used the expression for the final state momentum in the Breit frame in Eq. (3.2) in the second line. This fixes in particular the label momentum ω', so that the corresponding Wilson coefficient $C(\omega,\omega') \to C(Q)$ just depends on the momentum transfer energy Q and no convolution between the hard and collinear structures appears. Eq. (4.5) can be used to translate n-collinear and ultrasoft fields in Eq. (4.4) from 0 to a position y and z, respectively, which allows to write the corresponding matrix elements as imaginary parts of vacuum correlation functions. Finally, in going from a SCET I to a SCET II description, the jet invariant mass scale $Q^2(1-x)$ is integrated out, so that the corresponding n-collinear function becomes a matching coefficient and the ultrasoft Wilson lines become soft Wilson lines with respect to the $\bar{n}$-collinear modes, which are then defined with a soft-bin subtraction. [4] All in all we obtain the factorization theorem for n_f massless quarks (to all orders in α_s and up to higher orders in $1-x$) [73, 74, 78–81]

$$\begin{aligned} F_1(x,Q) = \sum_{i=q} \frac{e_i^2}{2} \left|C^{(n_f)}(Q,\mu_H)\right|^2 \left|U_C^{(n_f)}(Q,\mu_H,\mu)\right|^2 \int \mathrm{d}s \int \mathrm{d}s'\, J^{(n_f)}(s',\mu_J)\, U_J^{(n_f)}(s-s',\mu,\mu_J) \\ \times \int \mathrm{d}\xi\, \tilde{\phi}_{i/P}^{(n_f)}\left(\xi - x - \frac{s}{Q^2}, \mu_\phi\right) U_{\tilde{\phi}}^{(n_f)}(1-\xi,\mu,\mu_\phi)\,, \end{aligned} \tag{4.6}$$

where the sum over q includes both quark and antiquark flavors. In the following we only display explicit definitions of the matrix elements in terms of the quark flavors, the antiquarks lead to analogous expressions with the same perturbative expansions.

In Eq. (4.6) the matching coefficient between SCET I and SCET II, $J^{(n_f)}(s,\mu)$, is a vacuum correlator of the hard collinear fields in SCET I and describes the production rate of an inclusive jet with invariant mass s. Therefore, it is usually called the jet function. It is defined in terms of the n-collinear fields as

$$J^{(n_f)}(Qr_n^+,\mu) \equiv \frac{-1}{2\pi N_c Q}\, \mathrm{Im}\left[i \int d^4 z\, e^{ir_n\cdot z} \langle 0|\mathrm{T}\left\{\bar{\chi}_{n,Q}(0)\frac{\bar{n}\!\!\!/}{2}\chi_n(z)\right\}|0\rangle\right]\,, \tag{4.7}$$

where the invariant mass is $r_n^2 \simeq Qr_n^+$. All color and spin indices are traced implicitly. Since the jet invariant mass s varies according to the Bjorken variable x, the renormalization scale should depend on the evaluation point in the spectrum, i.e. $\mu_J = \mu_J(x)$.

The definition of the PDF in the endpoint region, which we denote by $\tilde{\phi}_{i/P}^{(n_f)}(1-z,\mu)$, has to be modified compared to Eq. (3.11), since now the emitted real radiation cannot be any more collinear, but has to be soft. Thus the collinear matrix element describing the initial state proton yields only purely virtual corrections, whereas we have in addition a soft matrix element describing the remaining beam remnants as can be already seen from Eq. (4.4). Therefore, the PDF is decomposed according to

$$\tilde{\phi}_{i/P}^{(n_f)}(1-z,\mu) = Q \int \mathrm{d}\ell'\, f_{i/P}^{(n_f)}\left(Q(1-z)-\ell',\mu\right) S_\phi^{(n_f)}(\ell',\mu)\,. \tag{4.8}$$

Here the local collinear quark PDF function is defined as

$$f_{q/P}^{(n_f)}(\ell,\mu) = \langle P(P_P)|\bar{\chi}_{\bar{n}}(0)\frac{n\!\!\!/}{2}\chi_{\bar{n},Q}(0)|P(P_P)\rangle\, \delta(\ell)\,. \tag{4.9}$$

[4] The n-collinear gauge-singlet structure is the only matching coefficient in this step since all sectors are fully factorized in Eq. (4.4) and the Lagrangian (2.34), so that except for the n-collinear fields no offshell modes have to be integrated out.

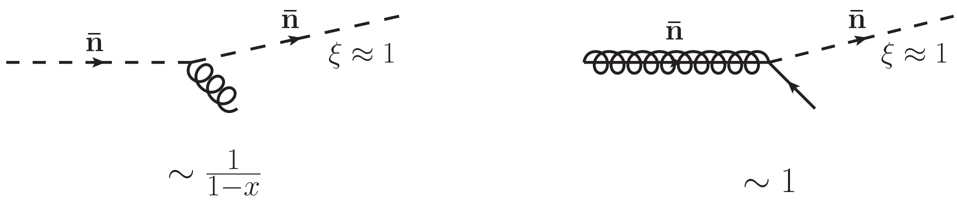

Figure 4.3: Illustration of the underlying argument, why no flavor mixing occurs in the EFT contributions to the factorization theorem (4.6): The emission of an (ultra)soft gluon by a collinear quark is enhanced with respect to other splitting interactions with a final parton with $\xi \approx 1$.

The nonlocal soft function reads [5]

$$S_\phi^{(n_f)}(\ell,\mu) = \frac{1}{4\pi N_c}\,\mathrm{Im}\left[i\int \mathrm{d}y\, e^{\frac{i}{2}\ell y}\,\langle 0|S^\dagger_{\bar{n},-}\left(\frac{n^\mu}{2}y\right) S_{n,-}\left(\frac{n^\mu}{2}y\right) S^\dagger_{n,+}(0)\, S_{\bar{n},+}(0)|0\rangle\right], \tag{4.10}$$

or equivalently,

$$S_\phi^{(n_f)}(\ell,\mu) = \frac{1}{N_c}\sum_{X_s}\delta(\ell-k_s^+)\,\langle 0|S^\dagger_{\bar{n},-}(0)\,S_{n,-}(0)|X_s\rangle\langle X_s|S^\dagger_{n,+}(0)\,S_{\bar{n},+}(0)|0\rangle\,, \tag{4.11}$$

where again all color indices are traced implicitly. We will see explicitly that both $f_{i/P}^{(n_f)}(\ell,\mu)$ and $S_\phi^{(n_f)}(\ell,\mu)$ individually contain rapidity divergences. These cancel in the PDF defined as in Eq. (4.8). The soft function encodes also information on the interactions with the final state, which has lead to a reconsideration of the PDF definition [78]. From our viewpoint it seems natural to include these interactions due to the nonperturbative soft beam remnants into the PDF, even if this restricts its universality, and we will therefore stay with the definition in Eq. (4.8). Finally, we remark that Eq. (4.8) can be obtained from the full QCD definition in Ref. [47] by appropriate expansions (see e.g. Ref. [59]). The crucial difference with respect to the conventional definition for the OPE region in Eq. (3.11) is that the fields are separated by a typical distance $y \sim \frac{1}{Q(1-x)}$ instead of $y \sim \frac{1}{Q} \to 0$, which results in the nonlocality in the soft function definition, and that the collinear momentum $\omega = Qz$ has been set to Q.

An important feature of the factorization theorem in Eq. (4.6) is that there are no flavor mixing terms between quarks and gluons in any of the EFT contributions in the hard current matching, the jet function, the PDF and their evolution factors. One can easily explain this using the possible interactions in SCET at leading order in the power counting parameter, e.g. for the PDF evolution one can make the following intuitive argument as illustrated in Fig. 4.3: Flavor mixing requires the splitting of an initial state collinear quark or gluon into two partons. To stay in the endpoint regime one of the final partons has to carry the longitudinal momentum fraction $\xi > x \approx 1$, i.e. almost the whole momentum, implying that the remaining parton is (ultra)soft. The only available interaction of this kind at leading order in SCET is the emission of an (ultra)soft gluon from a collinear quark, whereas the splitting of a collinear gluon into a collinear and (ultra)soft quark is suppressed by $\mathcal{O}(1-x)$. This means that the parton extracted out of the PDF at the low scale $\sim \Lambda_{\mathrm{QCD}}$ is also the one interacting with the photon and entering the final state jet, and thus cannot be a gluon. However, we note that in the full QCD current contributions to the hard matching coefficient there are in fact flavor mixing diagrams appearing at $\mathcal{O}(\alpha_s^3)$ for the electromagnetic vector current, which are not explicit in our notation and will not be relevant for the later discussion.

Now we give the perturbative expansions of the functions $C^{(n_f)}(Q,\mu)$ and $J^{(n_f)}(s,\mu)$ for massless quarks and the corresponding counterterms for later comparison and reference in the discussion of the massive quark corrections. In particular we collect the results at $\mathcal{O}(\alpha_s)$, which are implicitly depending on n_f through the strong coupling constant, and at $\mathcal{O}(\alpha_s^2 C_F T_F)$, where the explicit dependence on n_f

[5] Our prescriptions for the Wilson lines are consistent with Ref. [75], but differ with respect to Ref. [78].

appears. [6] We will stick to the notation introduced in Eq. (3.15).

The current matching coefficient for massless quarks corresponds to the finite terms of the partonic form factor in full QCD with dimensional regularization as IR regulator and is known up to three loops [82]. The renormalized contributions at $\mathcal{O}(\alpha_s)$ and $\mathcal{O}(\alpha_s^2 C_F T_F)$ read ($\alpha_s^{(n_f)} \equiv \alpha_s^{(n_f)}(\mu)$)

$$C^{(n_f,1)}(Q,\mu) = \frac{\alpha_s^{(n_f)} C_F}{4\pi}\left\{-L_Q^2 + 3L_Q - 8 + \frac{\pi^2}{6}\right\}, \tag{4.12}$$

$$C_{T_F}^{(n_f,2)}(Q,\mu) = \frac{\big(\alpha_s^{(n_f)}\big)^2 C_F T_F}{16\pi^2}\left\{-\frac{4}{9}L_Q^3 + \frac{38}{9}L_Q^2 - \left(\frac{418}{27} + \frac{4\pi^2}{9}\right)L_Q + \frac{4085}{162} + \frac{23\pi^2}{27} + \frac{4}{9}\zeta_3\right\}. \tag{4.13}$$

The associated contributions to the renormalization factor read [7]

$$Z_C^{(n_f,1)}(Q,\mu) = \frac{\alpha_s^{(n_f)} C_F}{4\pi}\left\{-\frac{2}{\epsilon^2} + \frac{2}{\epsilon}\,L_Q + \frac{3}{\epsilon}\right\}, \tag{4.14}$$

$$Z_{C,n_f}^{(n_f,2)}(Q,\mu) = \frac{\big(\alpha_s^{(n_f)}\big)^2 C_F T_F n_f}{16\pi^2}\left\{-\frac{2}{\epsilon^3} + \frac{1}{\epsilon^2}\left[\frac{4}{3}\,L_Q - \frac{8}{9}\right] + \frac{1}{\epsilon}\left[-\frac{20}{9}\,L_Q + \frac{65}{27} + \frac{\pi^2}{3}\right]\right\}. \tag{4.15}$$

The jet function $J^{(n_f)}(s,\mu)$ is known up to two loops [83]. The renormalized expressions at $\mathcal{O}(\alpha_s)$ and $\mathcal{O}(\alpha_s^2 C_F T_F)$ read

$$\mu^2 J^{(n_f,1)}(s,\mu^2) = \frac{\alpha_s^{(n_f)} C_F}{4\pi}\left\{\delta(\bar{s})\left(7-\pi^2\right) - 3\left[\frac{\theta(\bar{s})}{\bar{s}}\right]_+ + 4\left[\frac{\theta(\bar{s})\ln\bar{s}}{\bar{s}}\right]_+\right\}, \tag{4.16}$$

$$\begin{aligned}\mu^2 J_{T_F}^{(n_f,2)}(s,\mu) = \frac{\big(\alpha_s^{(n_f)}\big)^2 C_F T_F}{16\pi^2}\Bigg\{&\delta(\bar{s})\left[-\frac{4057}{162} + \frac{68\pi^2}{27} + \frac{16}{9}\zeta_3\right] + \left[\frac{\theta(\bar{s})}{\bar{s}}\right]_+\left[\frac{494}{27} - \frac{8\pi^2}{9}\right]\\ &-\frac{116}{9}\left[\frac{\theta(\bar{s})\ln\bar{s}}{\bar{s}}\right]_+ + \frac{8}{3}\left[\frac{\theta(\bar{s})\ln^2\bar{s}}{\bar{s}}\right]_+\Bigg\},\end{aligned} \tag{4.17}$$

with $\bar{s} \equiv s/\mu^2$. The corresponding contributions to the renormalization factor read

$$\mu^2 Z_J^{(n_f,1)}(s,\mu) = \frac{\alpha_s^{(n_f)} C_F}{4\pi}\left\{\delta(\bar{s})\left[\frac{4}{\epsilon^2} + \frac{3}{\epsilon}\right] - \frac{4}{\epsilon}\left[\frac{\theta(\bar{s})}{\bar{s}}\right]_+\right\}, \tag{4.18}$$

$$\mu^2 Z_{J,T_F}^{(n_f,2)}(s,\mu) = \frac{\big(\alpha_s^{(n_f)}\big)^2 C_F T_F}{16\pi^2}\left\{\delta(\bar{s})\left[\frac{4}{\epsilon^3} - \frac{2}{9\epsilon^2} - \frac{1}{\epsilon}\left(\frac{121}{27} + \frac{2\pi^2}{9}\right)\right] - \left[\frac{\theta(\bar{s})}{\bar{s}}\right]_+\left[\frac{8}{3\epsilon^2} - \frac{40}{9\epsilon}\right]\right\}. \tag{4.19}$$

For completeness, we display also the counterterm contributions at $\mathcal{O}(\alpha_s)$ and $\mathcal{O}(\alpha_s^2 C_F T_F)$ for the PDFs in the endpoint region, which can be read off from Eqs. (3.20) and (3.22) by identifying the singular terms in the limit $z \to 1$

$$Z_{\tilde{\phi}}^{(n_f,1)}(1-z,\mu) = \frac{\alpha_s^{(n_f)} C_F}{4\pi}\left\{\frac{3}{\epsilon}\,\delta(1-z) + \frac{4}{\epsilon}\left[\frac{\theta(1-z)}{1-z}\right]_+\right\}, \tag{4.20}$$

$$Z_{\tilde{\phi},T_F}^{(n_f,2)}(1-z,\mu) = \frac{\big(\alpha_s^{(n_f)}\big)^2 C_F T_F}{16\pi^2}\left\{\delta(1-z)\left[\frac{2}{\epsilon^2} - \frac{1}{\epsilon}\left(\frac{1}{3} + \frac{4\pi^2}{9}\right)\right] + \left[\frac{\theta(1-z)}{1-z}\right]_+\left[\frac{8}{3\epsilon^2} - \frac{40}{9\epsilon}\right]\right\}. \tag{4.21}$$

Large logarithms between the characteristic scales of each sector, μ_H, μ_J and μ_ϕ, and the final, common renormalization scale of the factorization theorem μ are summed by the evolution factors $U_C^{(n_f)}$,

[6] Here we only cite the references with the most up-to-date results and refer to [4] for a comprehensive list of original literature for the closely related functions in e^+e^- collisions.

[7] Here we use $C^{\rm bare} = Z_C C$ as common in literature. The counterterm of the SCET current operator $\mathcal{J}$ in Eq. (2.35) is related to this definition by taking the inverse.

$U_J^{(n_f)}$ and $U_{\tilde{\phi}}^{(n_f)}$. The evolution factors are already at LL sensitive to the number of active flavors n_f due to the running of α_s. The evolution factors satisfy the RG equations

$$\mu\frac{\mathrm{d}}{\mathrm{d}\mu}\,U_C^{(n_f)}(Q,\mu_H,\mu) = \gamma_C^{(n_f)}(Q,\mu)\,U_C^{(n_f)}(Q,\mu_H,\mu)\,, \tag{4.22}$$

$$\mu\frac{\mathrm{d}}{\mathrm{d}\mu}\,U_J^{(n_f)}(s,\mu,\mu_J) = \int \mathrm{d}s'\,\gamma_J^{(n_f)}(s-s',\mu)\,U_J^{(n_f)}(s',\mu,\mu_J)\,, \tag{4.23}$$

$$\mu\frac{\mathrm{d}}{\mathrm{d}\mu}\,U_{\tilde{\phi}}^{(n_f)}(1-z,\mu,\mu_\phi) = \int \mathrm{d}z'\,\gamma_{\tilde{\phi}}^{(n_f)}(z'-z,\mu)\,U_{\tilde{\phi}}^{(n_f)}(1-z',\mu,\mu_\phi)\,. \tag{4.24}$$

The anomalous dimensions can be easily derived from the corresponding counterterm contributions,

$$\gamma_C(Q,\mu) = -Z_C^{-1}(Q,\mu)\,\mu\frac{\mathrm{d}}{\mathrm{d}\mu}\,Z_C(Q,\mu)\,, \tag{4.25}$$

$$\mu^2\gamma_J(s,\mu) = -\int \mathrm{d}s'\,Z_J^{-1}(s-s',\mu)\,\mu\frac{\mathrm{d}}{\mathrm{d}\mu}\,Z_J(s',\mu) \tag{4.26}$$

$$\gamma_{\tilde{\phi}}(1-z,\mu) = -\int \mathrm{d}z'\,Z_{\tilde{\phi}}^{-1}(z'-z,\mu)\,\mu\frac{\mathrm{d}}{\mathrm{d}\mu}\,Z_{\tilde{\phi}}(1-z',\mu)\,. \tag{4.27}$$

For the current we obtain

$$\gamma_C^{(n_f,1)}(Q,\mu) = \frac{\alpha_s^{(n_f)}C_F}{4\pi}\left\{\Gamma^{(1)}L_Q - 6\right\}\,, \tag{4.28}$$

$$\gamma_{C,T_F}^{(n_f,2)}(Q,\mu) = \frac{\left(\alpha_s^{(n_f)}\right)^2 C_F T_F}{16\pi^2}\left\{\Gamma_{T_F}^{(2)}L_Q + \frac{260}{27} + \frac{4\pi^2}{3}\right\}\,, \tag{4.29}$$

with $\Gamma^{(1)} = 4$ and $\Gamma_{T_F}^{(2)} = -80/9$ being the $\mathcal{O}(\alpha_s)$ and $\mathcal{O}(\alpha_s^2 C_F T_F)$ coefficients of the cusp anomalous dimension $\Gamma_{\mathrm{cusp}}^{(n_f)}$. For the jet function one gets

$$\mu^2\gamma_J^{(n_f,1)}(s,\mu) = \frac{\alpha_s^{(n_f)}C_F}{4\pi}\left\{-2\,\Gamma^{(1)}\left[\frac{\theta(\bar{s})}{\bar{s}}\right]_+ + 6\,\delta(\bar{s})\right\}\,, \tag{4.30}$$

$$\mu^2\gamma_{J,T_F}^{(n_f,2)}(s,\mu) = \frac{\left(\alpha_s^{(n_f)}\right)^2 C_F T_F}{16\pi^2}\left\{-2\,\Gamma_{T_F}^{(2)}\left[\frac{\theta(\bar{s})}{\bar{s}}\right]_+ - \left(\frac{484}{27} + \frac{8\pi^2}{9}\right)\delta(\bar{s})\right\}\,. \tag{4.31}$$

Finally, the anomalous dimensions for the PDF read

$$\gamma_{\tilde{\phi}}^{(n_f,1)}(1-z,\mu) = \frac{\alpha_s^{(n_f)}C_F}{4\pi}\left\{2\,\Gamma^{(1)}\left[\frac{\theta(1-z)}{1-z}\right]_+ + 6\,\delta(1-z)\right\}\,, \tag{4.32}$$

$$\gamma_{\tilde{\phi},T_F}^{(n_f,2)}(1-z,\mu) = \frac{\left(\alpha_s^{(n_f)}\right)^2 C_F T_F}{16\pi^2}\left\{2\,\Gamma_{T_F}^{(2)}\left[\frac{\theta(1-z)}{1-z}\right]_+ - \left(\frac{4}{3} + \frac{16\pi^2}{9}\right)\delta(1-z)\right\}\,. \tag{4.33}$$

The anomalous dimensions are of the form of Eq. (2.47) involving a cusp anomalous dimension and thus resum the Sudakov double logarithms in $(1-z)$ arising in Eq. (4.1). In contrast to the OPE region the specific structure of the anomalous dimensions in the endpoint region allows us to solve the RG equations in Eqs. (4.22) – (4.24) fully analytically up to any arbitrary order in α_s in terms of the coefficients of the anomalous dimensions and the β function. Since the RG equations for the jet function and the PDF involve convolutions it is convenient to solve them in Fourier- or Laplace-space and transform the resulting expression back into momentum space at the end [74]. We show the generic solutions in appendix C.

In Eq. (4.6) the choice of μ is arbitrary, and the dependence on μ cancels exactly working to any given order in perturbation theory. In the following we will present our results adopting the choice $\mu = \mu_\phi$, such that the evolution factor satisfies $U_{\tilde{\phi}}(1-z,\mu_\phi,\mu_\phi) = \delta(1-z)$ and can be dropped from Eq. (4.6).

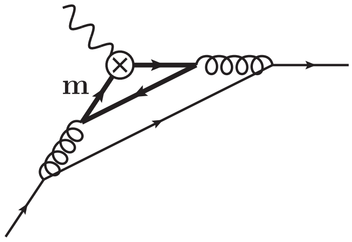

Figure 4.4: Flavor mixing contribution at $\mathcal{O}(\alpha_s^2 C_F T_F)$ with massive quarks in the full QCD current. For a vector current this correction vanishes.

The fact that any other choice for μ can be implemented leads to a consistency relation between the renormalization group factors, which reads [74]

$$Q^2 \left|U_C^{(n_f)}(Q, \mu_0, \mu)\right|^2 U_J^{(n_f)}(Q^2(1-z), \mu, \mu_0) = U_{\tilde{\phi}}^{(n_f)}(1-z, \mu_0, \mu)\,. \tag{4.34}$$

It can be also written as a relation for the μ-anomalous dimensions,

$$2\gamma_C^{(n_f)}(Q, \mu)\, \delta(1-z) + Q^2 \gamma_J^{(n_f)}(Q^2(1-z), \mu) + \gamma_{\tilde{\phi}}^{(n_f)}(1-z, \mu) \,=\, 0\,. \tag{4.35}$$

In the massive quark case this consistency relation remains intact since the UV divergences are mass independent. However, since the quark mass represents an additional relevant scale, the factorization theorem exhibits a richer structure due to the increased number of scales and additional consistency relations emerge between threshold corrections when massive quark modes are integrated out.

4.2 The mass factorization setup

In the following we will construct a VFNS in the endpoint region of DIS with the same features as in the classical OPE region, see Sec. 3.3. This includes (i) the resummation of all large logarithms, (ii) the correct limiting behavior of the perturbative structures, i.e. the hard matching coefficient and the jet function, for very small and large masses and (iii) a continuous description for arbitrary hierarchies of the dynamic scales with respect to the mass keeping the full mass dependence of the singular terms (i.e. at the lowest order in the power counting parameter λ).

The fact that the factorization theorem (4.6) does not show any flavor mixing terms for the EFT contributions is maintained in the presence of massive quarks. Due to the same argument as given above the massive quark contributions in SCET to the hard and jet functions, their evolution as well as additional threshold corrections at the mass scale related to different renormalization conditions of the matrix elements in analogy to Eq. (3.41) are also flavor diagonal. Since we assume $m \gg \Lambda_{\mathrm{QCD}}$, so that the heavy quarks are not produced nonperturbatively out of the proton, this has the consequence that massive quarks enter the EFT components of the factorization theorem only via secondary corrections, i.e. via contributions which are initiated by massless quarks and where massive quarks are produced through the radiation of virtual gluons that split into a massive quark-antiquark pair, see Fig. 3.7. We mention that in the full QCD current there are also flavor mixing corrections with massive quarks, see Fig. 4.4 for an example, which in general start contributing also at $\mathcal{O}(\alpha_s^2)$ like the secondary corrections. Since these types of corrections do not have a corresponding EFT counterpart, they can be easily included in the hard matching coefficient, and we will not consider them specifically in our discussion. For the case of the electromagnetic vector current the diagram in Fig. 4.4 in fact vanishes due to charge conjugation, so that these effects also do not show up at $\mathcal{O}(\alpha_s^2 C_F T_F)$ relevant for N^{3}LL resummation, which is the order where we give explicit results.

It is convenient to discuss the hierarchies appearing in the treatment of secondary mass effects by means of the mass modes briefly introduced in Sec. 3.3. We will outline the corresponding setup that is based on three different EFT scenarios associated to the hierarchies between the hard and jet scales and

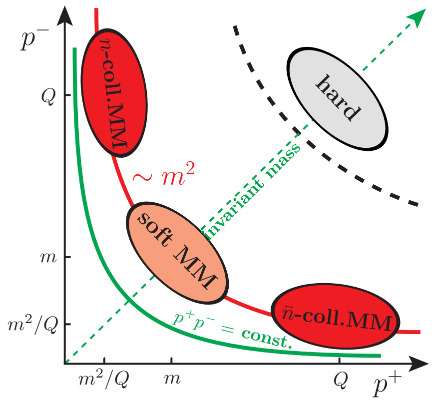

Figure 4.5: The intrinsic (SCET II-type) mass mode fluctuations around the mass-shell in the p^+p^--plane. Modes with the same invariant mass are located on the same mass hyperbola which is always the case for the collinear and soft mass-shell fluctuations. Adapted from Ref. [26].

the quark mass, which leads in an intuitive way to the correct form of the resulting factorization theorems. Here we will not carry out a formal "derivation", since this does not lead to any new insights. Before performing the explicit computations in Secs. 4.3 and 4.4 we already present the final results for all mass dependent perturbative corrections to explain the main features without getting lost in details concerning calculational steps. Since the strict EFT setup assumes large hierarchies, it does not, however, explain the continuity between two neighboring scenarios in a satisfactory way. In Sec. 4.2.4 we will therefore adopt a similar view as in chapter 3 based only on SCET with the massless power counting parameter λ, but with renormalization schemes for the different components of the factorization theorem that vary according to the relation between the hard and jet scales and the mass.

For the discussion of the mass mode method we consider again a generic setup with *one* massive quark flavor with mass m in addition to n_l massless flavors, and our notation is set up accordingly. In addition to the power counting parameters $\lambda_{\mathrm{I}} \sim \sqrt{1-x}$ and $\lambda_{\mathrm{II}} \sim \Lambda_{\mathrm{QCD}}/Q$ in the massless setup, which we decide to correlate via $\lambda \equiv \lambda_{\mathrm{I}} = \sqrt{\lambda_{\mathrm{II}}}$ for simplicity, we define the ratio

$$\lambda_m = \frac{m}{Q}\,. \tag{4.36}$$

From the field theoretic point of view we consider n-, $\bar{n}$-collinear and soft mass modes in addition to the corresponding massless modes with the scaling $p_n^\mu \sim Q(\lambda^2, 1, \lambda)$, $p_{\bar{n}}^\mu \sim Q(1, \lambda^4, \lambda^2)$ and $p_s^\mu \sim Q(\lambda^2, \lambda^2, \lambda^2)$. If kinematically allowed, the mass modes can have the momentum scaling and virtualities of their massless counterparts, but in addition one has to account for the fluctuations around their mass-shell which have the scaling $p_n^\mu \sim Q(\lambda_m^2, 1, \lambda_m)$, $p_{\bar{n}}^\mu \sim Q(1, \lambda_m^2, \lambda_m)$ for the n-, $\bar{n}$-collinear mass modes, respectively, and $p_s^\mu \sim Q(\lambda_m, \lambda_m, \lambda_m)$ for the soft mass modes. Note that the invariant mass fluctuations around the mass shell of the collinear and the soft mass modes are of the same order and thus just separated by boosts with different rapidity y (with $e^{2y} = p^-/p^+$), see Fig. 4.5. Since the typical invariant masses of the mass modes are bounded from below by $p_n^2 \sim p_{\bar{n}}^2 \sim p_s^2 \sim Q^2\lambda_m^2 \sim m^2$, dynamical real radiation effects can only occur if the typical collinear scale is bigger than m^2. Thus, $\bar{n}$-collinear and soft mass mode fluctuations will only contribute via virtual effects. Since the relation between the mass scale and the hard and jet scales can vary substantially, the treatment of the mass modes has to be adapted from case to case. There are also different scenario-dependent threshold corrections when the RG evolution crosses the mass scale and the massive quark flavor is integrated out.

The different scenarios can be ordered according to where the mass scale is situated with respect to the hard and jet scales, see Fig. 4.6 for graphical illustrations. Each scaling situation corresponds in principle to a different EFT setup. In the following we briefly summarize the different EFT scenarios: [8]

[8]For the scenarios II and III we require besides the condition $\lambda \ll 1$ in principle also large hierarchies between λ_m and the massless parameters 1, λ and λ^2. In fact the latter conditions can be abandoned as will become obvious in Sec. 4.2.4.

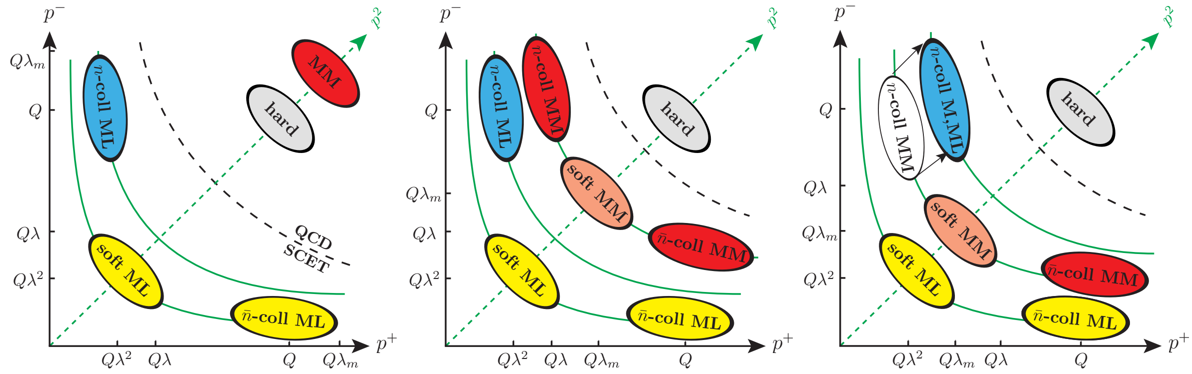

(a) $\lambda_m > 1 > \lambda > \lambda^2$ (b) $1 > \lambda_m > \lambda > \lambda^2$ (c) $1 > \lambda > \lambda_m > \lambda^2$

Figure 4.6: Localization of massless (ML) and massive (M) modes together with their mass-shell fluctuations (MM) in the p^+-p^--plane according to their generic scaling for different hierarchies between λ and λ_m.

I) $m > Q > Q\lambda > Q\lambda^2$ ($\lambda_m > 1 > \lambda > \lambda^2$): The mass m is larger than the hard scale Q and the mass modes are not described by SCET, but integrated out when SCET is matched to full QCD. Thus the factorization theorem is the one for massless fermions up to the hard current matching coefficient which acquires an additional contribution due to the mass modes. The mass effects decouple for $\lambda_m \to \infty$.

II) $Q > m > Q\lambda > Q\lambda^2$ ($1 > \lambda_m > \lambda > \lambda^2$): In this scenario the mass m is between the hard scale and the jet scale. The mass mode effects are virtual because the jet scale $Q\lambda$, the typical invariant mass for real collinear particle radiation, is below m. However, the mass modes contribute to the matching condition at the scale Q and the evolution of the current for scales above m. The mass-shell fluctuations are integrated out at the scale m. The factorization theorem is the one for the massless quarks concerning the jet function but receives mass mode corrections in the matching and evolution of the production current. The matching condition of the production current at the hard scale Q reproduces the result for massless quarks for $\lambda_m \to 0$, since all infrared mass-shell contributions have been removed from it in the matching procedure.

III) $Q > Q\lambda > m > Q\lambda^2$ ($1 > \lambda > \lambda_m > \lambda^2$): The mass is below the jet scale. Therefore, massless and massive collinear modes both can fluctuate in the n-collinear sector yielding real and virtual contributions to the jet function, whereas the $\bar{n}$-collinear and soft mass modes only arise through their virtual effects. The mass mode contributions to the current matching and evolution are exactly the same as in scenario II. Analogously to the previous scenario the mass-shell fluctuations are integrated out at the scale $\mu_m \sim m$ leading to an additional massive threshold correction for the jet function.

Concerning Feynman rules, the collinear massive quark interactions are determined from the collinear Lagrangian in Eq. (2.18). In practice, since the collinear sector is essentially just a boosted version of usual QCD, the effects of the secondary massive quarks in the collinear sector can be calculated using regular QCD Feynman rules. We emphasize, however, that the consistency for calculations in the collinear sector with massive modes involves additional (non-vanishing) soft mass mode bin subtractions [35] in the collinear loop integrations to avoid double-counting with the soft sector and to maintain collinear gauge invariance. These soft-bin subtractions are essential to obtain meaningful and gauge-invariant results. Concerning the interactions within the soft sector, the Feynman rules are anyway given by the usual QCD interactions and Feynman rules. This is sufficient for the treatment of the secondary soft massive quarks in this work.

Note that some of the notation, the formulation of the factorization theorems and the organization of the RG evolution we use for the presentation of the results in this section are related to the choice that

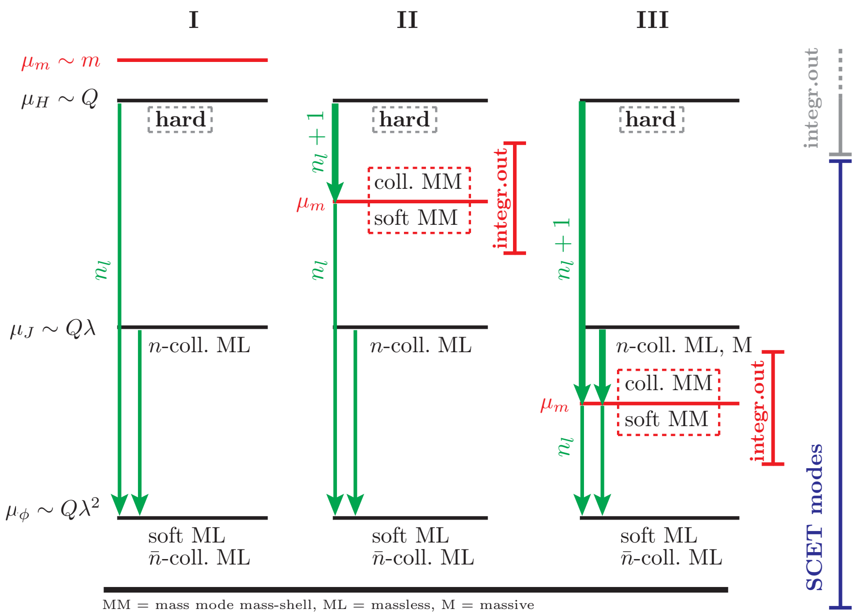

Figure 4.7: The different scenarios depending on the hierarchy between the mass scale μ_m and the hard, jet and PDF scale. MM indicates mass-shell scaling, ML the massless one. With M we denote modes that have a mass m but scale as their massless counterparts. The renormalization group evolution is also shown in the top-down evolution from the hard scale μ_H down to $\mu = \mu_\phi$. When the mass scale is crossed the mass-shell fluctuations are integrated out (dashed box). This leads to a matching condition and to a change in the evolution factor.

the final renormalization scale μ is set equal to the PDF scale. Thus only the current and jet function RG evolution factors U_C and U_J, respectively, appear. The RG pattern of this "top-down approach" together with a graphical display of how the collinear and soft massive modes give contributions are illustrated in Fig. 4.7. Clearly, any other choice for μ is possible and can significantly affect the form as well as the interpretation of the various components of the factorization theorems in the different scenarios. We postpone a more general discussion of different choices of μ to Secs. 4.3.3 and 4.4.3, where we focus more on the RG properties of the hard coefficient, the jet function and the PDF rather than on the full factorization theorem. This allows to streamline the discussion significantly and to generalize our results to other processes.

4.2.1 Scenario I: $m > Q > Q\lambda > Q\lambda^2$

The massive quark is integrated out at the hard scale. The factorization theorem is the one for n_l massless fermions in analogy to Eq. (4.6) up to the hard current matching coefficient which acquires an additional contribution due to the heavy quark,

$$F_1(x,Q,m) = \sum_{i=q} \frac{e_i^2}{2} \left|C^{(n_l)}(Q,m,\mu_H)\right|^2 \left|U_C^{(n_l)}(Q,\mu_H,\mu_\phi)\right|^2 \int \mathrm{d}s \int \mathrm{d}s'\, J^{(n_l)}(s',\mu_J) \\ \times U_J^{(n_l)}(s-s',\mu_\phi,\mu_J)\, \tilde{\phi}_{i/P}^{(n_l)}\left(1-x-\frac{s}{Q^2},\mu_\phi\right), \tag{4.37}$$

where

$$C^{(n_l)}(Q,m,\mu) = C^{(n_l)}(Q,\mu) + \hat{F}_{m,\mathrm{QCD}}^{(n_l,2)}(Q,m)\,. \tag{4.38}$$

The term $\hat{F}_{m,\mathrm{QCD}}^{(n_l,2)}$ represents the massive quark bubble contribution to the QCD current form factor, see the first diagram in Fig. 3.7, which has been already computed in Sec. 3.4 with the result given in

Eq. (3.95). The imposed OS renormalization condition for the strong coupling concerning the massive quark bubble contributions implies the massive quark is not an active dynamic flavor and does not contribute to the RG evolution of the strong coupling. Together with the fact that the form factor is evaluated with external on-shell states this guarantees that scenario I shows manifest decoupling in the infinite mass limit, i.e.

$$C^{(n_l)}(Q,m,\mu) \overset{m\to\infty}{\longrightarrow} C^{(n_l)}(Q,\mu)\,. \tag{4.39}$$

due to the the decoupling property of the zero-momentum subtracted result, $\hat{F}^{(n_l,2)}_{m,\mathrm{QCD}}(Q,m) \to 0$ for $\hat{m} \equiv m/Q \to \infty$. For light fermions, i.e. $\hat{m} \to 0$, we find ($\alpha_s^{(n_l)} = \alpha_s^{(n_l)}(\mu)$)

$$\begin{aligned} F^{(n_l,2)}_{m,\mathrm{QCD}}(Q,m) \overset{\hat{m}\to 0}{\longrightarrow} \frac{\big(\alpha_s^{(n_l)}\big)^2 C_F T_F}{16\pi^2} \bigg\{ & \frac{4}{9}\ln^3(\hat{m}^2) + \frac{38}{9}\ln^2(\hat{m}^2) + \bigg(\frac{530}{27} + \frac{4\pi^2}{9}\bigg)\ln(\hat{m}^2) + \frac{3355}{81} \\ & + \frac{38\pi^2}{27} - \frac{16}{3}\zeta_3 \bigg\}\,, \end{aligned} \tag{4.40}$$

with subleading corrections going as $\mathcal{O}(\hat{m}^2)$. Eq. (4.40) does not bear any similarity to the massless result of Eq. (4.13) and further exhibits large unresummed mass logarithms. Thus the QCD result of Eq. (3.95) is not suitable for taking the massless limit. This is because Eq. (3.95) still contains the mass-shell contributions which must be subtracted prior to taking the limit $m \ll Q$. This procedure is described in scenario II.

4.2.2 Scenario II: $Q > m > Q\lambda > Q\lambda^2$

The mass m is below the hard scale, but still above the jet scale. It is the aim (i) to resum the mass logarithms in Eq. (4.40) and (ii) to determine the hard current matching coefficient such that it contains no mass-singularities and in particular approaches the massless limit for $m \to 0$. The collinear and soft mass modes are included into the SCET setup, so that they render the hard coefficient IR safe by subtracting the mass-shell contributions in the matching procedure. They contribute as dynamic degrees of freedom to the RG evolution above m. In the RG evolution of the current from the hard to the jet scale the mass-shell fluctuations are finally integrated out at the scale m. The mass mode effects are purely virtual because the jet scale $Q\lambda$, the typical invariant mass for real collinear particle radiation is below m. Therefore, the jet function as well as its RG evolution factor towards scales smaller than m coincides with the one for n_l massless quarks. The factorization theorem reads

$$\begin{aligned} F_1(x,Q,m) = \sum_{i=q} \frac{e_i^2}{2} & \left|C^{(n_l+1)}(Q,m,\mu_H)\right|^2 \left|U_C^{(n_l+1)}(Q,\mu_H,\mu_m)\right|^2 \left|\mathcal{M}_C(Q,m,\mu_m)\right|^2 \left|U_C^{(n_l)}(Q,\mu_m,\mu_\phi)\right|^2 \\ & \times \int \mathrm{d}s \int \mathrm{d}s'\, J^{(n_l)}(s',\mu_J)\, U_J^{(n_l)}(s-s',\mu_\phi,\mu_J)\, \tilde{\phi}^{(n_l)}_{i/P}\left(1-x-\frac{s}{Q^2},\mu_\phi\right)\,. \end{aligned} \tag{4.41}$$

Compared to $C^{(n_l)}(Q,m,\mu_H)$ in Eq. (4.38) the hard current coefficient $C^{(n_l+1)}(Q,m,\mu_H)$ acquires a subtractive contribution arising from the non-vanishing SCET diagrams involving virtual collinear and soft mass modes and contributions related to the use of the $\overline{\mathrm{MS}}$ renormalization prescription for the strong coupling rather than the OS one concerning the massive quark bubble. The latter correction means that the massive quark now contributes to the RG evolution and that we employ $\alpha_s^{(n_l+1)}$. The result reads

$$C^{(n_l+1)}(Q,m,\mu) = C^{(n_l+1)}(Q,\mu) + \hat{F}^{(n_l+1,2)}_{\Delta m}(Q,m)\,. \tag{4.42}$$

The term $\hat{F}^{(n_l+1,2)}_{\Delta m}(Q,m)$ represents the corrections due to the non-vanishing mass of the heavy quark and can be written with the help of Eq. (3.95) as ($\alpha_s^{(n_l+1)} = \alpha_s^{(n_l+1)}(\mu)$)

$$\hat{F}^{(n_l+1,2)}_{\Delta m}(Q,m) = \frac{\big(\alpha_s^{(n_l+1)}\big)^2 C_F T_F}{16\pi^2} \left[f^{(2)}_{m,\mathrm{QCD}}(\hat{m}) - f^{(2)}_{m,\mathrm{QCD}}(\hat{m})\Big|_{m\to 0}\right]\,, \tag{4.43}$$

which can be read off explicitly from Eqs. (3.96) and (4.40). All calculational steps leading to this results are explained in detail in Secs. 4.3.1 and 4.4.1. One can check explicitly that all of the IR divergent mass-shell contributions are removed and that the massless limit for Eq. (4.42) is recovered for $m \to 0$, i.e. $\hat{F}^{(n_l+1,2)}_{\Delta m}(Q,m) \overset{m\to 0}{\longrightarrow} 0$. We will see that in the results of the collinear, the soft and the soft-bin contributions there are rapidity divergences that cancel in the sum of all terms. We stress, however, that for $\mu \sim Q$ no large (rapidity) logarithm remains in the hard current matching.

Note that the UV divergences of the bare SCET form factor are insensitive to the non-vanishing quark mass, such that we get in total the UV divergences from Eq. (4.15) for $n_f = n_l + 1$. This argument does not rely on a specific order in α_s, so that the evolution factor $U_C^{(n_l+1)}$ obeys the RG equation

$$\mu \frac{\mathrm{d}}{\mathrm{d}\mu}\, U_C^{(n_l+1)}(Q,\mu_H,\mu) = \gamma_C^{(n_l+1)}(Q,\mu)\, U_C^{(n_l+1)}(Q,\mu_H,\mu) \tag{4.44}$$

to all orders in perturbative QCD.

At the scale μ_m the mass-shell fluctuations of the collinear and soft mass modes are integrated out in the RG evolution of the current coefficient leading to the current mass mode matching coefficient $\mathcal{M}_C(Q,m,\mu_m)$, which is the analogue of the PDF matching coefficient which we have encountered in chapter 3. Using the counting $\alpha_s \ln(m^2/Q^2) \sim \mathcal{O}(1)$ the result has the structure

$$\begin{aligned}
\mathcal{M}_C(Q,m,\mu_H,\mu_m) = 1 &+ \left[\frac{\big(\alpha_s^{(n_l+1)}\big)^2}{(4\pi)^2} \ln\left(\frac{\mu_H^2}{\mu_m^2}\right) \mathcal{M}^{(2)}_{C,\ln}(m,\mu_m)\right]_{\mathcal{O}(\alpha_s)} \\
&+ \left[\frac{\big(\alpha_s^{(n_l+1)}\big)^2}{(4\pi)^2} \mathcal{M}^{(2)}_{C,1}(Q,m,\mu_m,\mu_H) + \frac{\big(\alpha_s^{(n_l+1)}\big)^3}{(4\pi)^3} \ln\left(\frac{\mu_H^2}{\mu_m^2}\right) \mathcal{M}^{(3)}_{C,\ln}(m,\mu_m)\right. \\
&\left. + \frac{\big(\alpha_s^{(n_l+1)}\big)^4}{(4\pi)^4} \ln^2\left(\frac{\mu_H^2}{\mu_m^2}\right) \mathcal{M}^{(4)}_{C,\ln^2}(m,\mu_m)\right]_{\mathcal{O}(\alpha_s^2)} + \mathcal{O}(\alpha_s^3)\,,
\end{aligned} \tag{4.45}$$

We display the corresponding results for $\alpha_s^{(n_l+1)} = \alpha_s^{(n_l+1)}(\mu_m)$ and $m \equiv \overline{m}(\mu_m)$ given in the $\overline{\mathrm{MS}}$ scheme. The two-loop functions in the fixed-order expansion, i.e. $\mathcal{M}^{(2)}_{C,\ln}$ and $\mathcal{M}^{(2)}_{C,1}$, read explicitly ($L_m \equiv \ln\big(m^2/\mu_m^2\big)$)

$$\mathcal{M}^{(2)}_{C,\ln}(m,\mu_m) = C_F T_F \left\{-\frac{4}{3}L_m^2 - \frac{40}{9}L_m - \frac{112}{27}\right\}, \tag{4.46}$$

$$\begin{aligned}
\mathcal{M}^{(2)}_{C,1}(Q,m,\mu_m,\mu_H) = C_F T_F &\left\{\frac{4}{9}L_m^3 + \frac{38}{9}L_m^2 + \left(\frac{242}{27} + \frac{2\pi^2}{3}\right)L_m - \ln\left(\frac{Q^2}{\mu_H^2}\right)\left[\frac{4}{3}L_m^2 + \frac{40}{9}L_m + \frac{112}{27}\right]\right. \\
&\left. + \frac{875}{54} + \frac{5\pi^2}{9} - \frac{52}{9}\zeta_3\right\}.
\end{aligned} \tag{4.47}$$

The three-loop function $\mathcal{M}^{(3)}_{C,\ln}$ is given by

$$\begin{aligned}
\mathcal{M}^{(3)}_{C,\ln}(m,\mu_m) = C_F T_F &\left\{L_m^3\left[\frac{88}{27}C_A - \frac{32}{27}T_F n_l - \frac{64}{27}T_F\right] + L_m^2\left[\left(-\frac{92}{9} + \frac{8\pi^2}{9}\right)C_A + 12\,C_F - \frac{160}{27}T_F\right]\right. \\
&+ L_m\left[\left(-\frac{620}{81} + \frac{80\pi^2}{27} - \frac{112}{3}\zeta_3\right)C_A + \left(-\frac{4}{3} + 32\zeta_3\right)C_F - \frac{1088}{81}T_F n_l - \frac{992}{81}T_F\right] \\
&+ C_A\left(\frac{17726}{729} - \frac{824\pi^2}{243} - 30\zeta_3 + \frac{88\pi^4}{135} - \frac{16}{3}B_4\right) + C_F\left(-\frac{3337}{27} + \frac{604}{9}\zeta_3 - \frac{8\pi^4}{15} + \frac{32}{3}B_4\right) \\
&\left. + T_F n_l\left(\frac{12032}{729} - \frac{256}{27}\zeta_3\right) + T_F\left(-\frac{6032}{729} + \frac{448}{27}\zeta_3\right)\right\},
\end{aligned} \tag{4.48}$$

where

$$B_4 = \frac{2}{3}\ln^4(2) - \frac{2\pi^2}{3}\ln^2(2) - \frac{13\pi^4}{180} + 16\,\mathrm{Li}_4\left(\frac{1}{2}\right). \tag{4.49}$$

Finally, the relevant four-loop function $\mathcal{M}^{(4)}_{C,\ln^2}(m,\mu_m)$ reads

$$\mathcal{M}^{(4)}_{C,\ln^2}(m,\mu_m) = \frac{\Big(\mathcal{M}^{(2)}_{C,\ln}(m,\mu_m)\Big)^2}{2} = C_F^2 T_F^2 \left\{\frac{8}{9}\,L_m^4 + \frac{160}{27}\,L_m^3 + \frac{416}{27}L_m^2 + \frac{4480}{243}\,L_m + \frac{6272}{729}\right\}. \tag{4.50}$$

The result for the threshold correction in Eq. (4.45) deserves some discussion. We see that the mass mode matching coefficient contains large logarithms $\ln(\mu_m^2/\mu_H^2)$, which are not summed by the RG μ-evolution of the current. These logarithms are related to rapidity singularities that arise in the overlap region between the collinear and soft mass modes, all having invariant masses of order m^2. Carrying out the corresponding computations in Sec. 4.4.1 we will discuss how these logarithms can be resummed. The outcome is just a simple exponentiation which yields the term at $\mathcal{O}(\alpha_s^4\ln^2(m^2/Q^2))$ corresponding to the function $\mathcal{M}^{(4)}_{C,\ln^2}$ in Eq. (4.50). We note that through the rapidity RG evolution $\mathcal{M}_C$ depends at each order on two rapidity scales. For simplicity we have correlated them with the two invariant mass scales μ_H and μ_m. We stress, however, that the dependence of $\mathcal{M}_C$ on the hard matching scale μ_H is actually spurious and cancels in an expansion at fixed-order in α_s. The existence of the large logarithms has the important consequence that the $\mathcal{O}(\alpha_s^2\ln(m^2/Q^2))$ corrections in Eq. (4.45) corresponding to $\mathcal{M}^{(2)}_{C,\ln}$ in Eq. (4.46) enter at the same order as the $\mathcal{O}(\alpha_s)$ fixed-order corrections based on the counting $\alpha_s\ln(m^2/Q^2)\sim\mathcal{O}(1)$ and thus contribute already at N^{2}LL order where one-loop fixed-order corrections to the hard coefficient and the jet and the soft function are accounted for. At N^{3}LL order we therefore need the terms at $\mathcal{O}(\alpha_s^3\ln(m^2/Q^2))$ and $\mathcal{O}(\alpha_s^4\ln^2(m^2/Q^2))$. [9] We have indicated this counting by using the subscripts "$\mathcal{O}(\alpha_s)$" and "$\mathcal{O}(\alpha_s^2)$" in the result of Eq. (4.45). In Eq. (4.48) we display the full form of the $\mathcal{O}(\alpha_s^3\ln(m^2/Q^2))$. We can derive the μ_m dependent terms by consistency of RG running as explained in Sec. 4.4.1. We have not computed the term multiplying the rapidity logarithm that is physically unrelated to logarithms of μ_m. However, it can be directly determined from a corresponding term in the PDF threshold correction computed in Ref. [84] due to a consistency relation as explained in Sec. 4.4.3.

4.2.3 Scenario III: $Q > Q\lambda > m > Q\lambda^2$

The mass is between the jet scale and $\Lambda_{\rm QCD}$. The current evolution is the same as the one in scenario II and the PDF still includes only the effects of the n_l massless quarks. Since the massless as well as the massive n-collinear modes both can now fluctuate in the jet sector the difference to scenario II concerns the jet function, where additional massive real and virtual contributions arise. The setup is constructed such that it (i) sums all mass logarithms that arise in the evolution of the jet function and (ii) ensures that the jet function approaches the known massless result for n_l+1 flavors in the limit $m\to 0$. In analogy to the current, the RG evolution of the jet function is performed with n_l+1 flavors above the mass threshold. Collinear mass-shell fluctuations are integrated out at the mass scale yielding a threshold correction $\mathcal{M}_J$ for the jet function, and the evolution continues with n_l light quarks down to the PDF scale. Overall the factorization theorem in this scenario has the form

$$\begin{aligned}F_1(x,Q,m) = \sum_{i=q}\frac{e_i^2}{2}\,&\big|C^{(n_l+1)}(Q,m,\mu_H)\big|^2\,\big|U_C^{(n_l+1)}(Q,\mu_H,\mu_m)\big|^2\big|\mathcal{M}_C(Q,m,\mu_m)\big|^2\,\big|U_C^{(n_l)}(Q,\mu_m,\mu_\phi)\big|^2\\ &\times\int\!{\rm d}s\int\!{\rm d}s'\int\!{\rm d}s''\int\!{\rm d}s'''\,J^{(n_l+1)}(s''',m,\mu_J)\,U_J^{(n_l+1)}(s''-s''',\mu_m,\mu_J)\\ &\times\mathcal{M}_J(s'-s'',m,\mu_m)\,U_J^{(n_l)}(s-s',\mu_\phi,\mu_m)\,\tilde\phi_{i/P}^{(n_l)}\left(1-x-\frac{s}{Q^2},\mu_\phi\right),\end{aligned} \tag{4.51}$$

where the matching coefficients $C^{(n_l+1)}(Q,m,\mu_H)$ and $\mathcal{M}_C(Q,m,\mu_m)$ are the same as in scenario II, see Eqs. (4.42) and (4.45). The jet function $J^{(n_l+1)}(s,m,\mu)$ contains contributions related to virtual and real

[9] In the primed counting one might also distinguish between terms enhanced by rapidity logarithms (and related to terms summed by the rapidity RGE) and the remaining terms in the series for the mass mode threshold factors. This can have a sizeable numerical effect.

radiation of the massive secondary quarks and has the form

$$J^{(n_l+1)}(s,m,\mu) = J^{(n_l+1)}(s,\mu) + J^{(n_l+1,2)}_{\Delta m,\mathrm{dist}}(s,m,\mu) + J^{(n_l+1,2)}_{m,\mathrm{real}}(s,m)\,. \tag{4.52}$$

Here the last two terms represent the corrections due to a nonvanishing quark mass, the corresponding computations are described in Secs. 4.3.2 and 4.4.2. The expression for $J^{(n_l+1,2)}_{\Delta m,\mathrm{dist}}(s,m,\mu)$ contains only distributions and corresponds to collinear massive virtual corrections (including soft-bin subtractions) as well as terms related to the subtraction of the massless quark result already contained in $J^{(n_l+1)}(s,\mu)$ (see Eq. (4.17)). Its renormalized expression reads ($\bar{s} = s/\mu^2$)

$$\begin{aligned}\mu^2 J^{(n_l+1,2)}_{\Delta m,\mathrm{dist}}(s,m,\mu) = \frac{\big(\alpha_s^{(n_l+1)}\big)^2 C_F T_F}{16\pi^2}&\bigg\{\delta(\bar{s})\left[\frac{8}{9}L_m^3 + \frac{58}{9}L_m^2 + \left(\frac{718}{27} - \frac{8\pi^2}{9}\right)L_m + \frac{4325}{81} - \frac{58\pi^2}{27} - \frac{32}{3}\zeta_3\right]\\ &+\left[\frac{\theta(\bar{s})}{\bar{s}}\right]_+\left[-\frac{8}{3}L_m^2 - \frac{116}{9}L_m - \frac{718}{27} + \frac{8\pi^2}{9}\right] + \left[\frac{\theta(\bar{s})\ln\bar{s}}{\bar{s}}\right]_+\left[\frac{16}{3}L_m + \frac{116}{9}\right]\\ &- \frac{8}{3}\left[\frac{\theta(\bar{s})\ln^2\bar{s}}{\bar{s}}\right]_+\bigg\}\,.\end{aligned} \tag{4.53}$$

The term $J^{(n_l+1,2)}_{m,\mathrm{real}}(s,m)$ in Eq. (4.52) contributes only when the jet invariant mass is above the threshold $4m^2$ and thus corresponds to real production of the massive quarks. It is given by

$$\begin{aligned}\mu^2 J^{(n_l+1,2)}_{m,\mathrm{real}}(s,m) = \frac{\big(\alpha_s^{(n_l+1)}\big)^2 C_F T_F}{16\pi^2}\frac{1}{\bar{s}}\,\theta(s-4m^2)&\bigg\{-\frac{32}{3}\,\mathrm{Li}_2\!\left(\frac{b-1}{1+b}\right) + \frac{16}{3}\ln\!\left(\frac{1-b^2}{4}\right)\ln\!\left(\frac{1-b}{1+b}\right)\\ &- \frac{8}{3}\ln^2\!\left(\frac{1-b}{1+b}\right) + \left(\frac{1}{2}b^4 - b^2 + \frac{241}{18}\right)\ln\!\left(\frac{1-b}{1+b}\right) - \frac{5}{27}b^3 + \frac{241}{9}b - \frac{8\pi^2}{9}\bigg\}\,,\end{aligned} \tag{4.54}$$

with

$$b = \sqrt{1 - \frac{4m^2}{s}}\,. \tag{4.55}$$

Due to its physical character it is UV-finite and does not contain any explicit logarithmic μ-dependence. Furthermore, $J^{(n_l+1,2)}_{m,\mathrm{real}}$ and its first two derivatives in s vanish at the threshold, so that no discontinuity arises due to real radiation. Note that the range in τ where scenario III is employed may be chosen such that it includes the threshold of collinear massive real radiation at $\tau = 4m^2/Q^2$, so that the threshold is properly accounted for through the analytic form of $J^{(n_l+1,2)}_{m,\mathrm{real}}$. For $m \to 0$ the jet function $J^{(n_l+1)}(s,m,\mu)$ yields correctly the fully massless jet function at $\mathcal{O}(\alpha_s^2)$, i.e.

$$J^{(n_l+1)}(s,m,\mu) \overset{m\to 0}{\longrightarrow} J^{(n_l+1)}(s,\mu)\,. \tag{4.56}$$

We note that in the calculation of $J^{(n_l+1,2)}_{\Delta m,\mathrm{dist}}$ rapidity divergences arise which cancel in the sum of the collinear diagrams and the corresponding soft-bin subtractions. We stress that for $\mu^2 \sim s$ all associated logarithms cancel completely in the sum of $J^{(n_l+1,2)}_{m,\mathrm{real}}$ and $J^{(n_l+1,2)}_{\Delta m,\mathrm{dist}}$, so that no (large) rapidity logarithm remains in the jet function.

The UV divergences of the bare jet function $J^{(n_l+1,\mathrm{bare})}(s,m,\mu)$ are mass independent and agree with the known massless ones for n_l+1 dynamic flavors. The $\mathcal{O}(\alpha_s^2 C_F T_F)$ contributions to the jet function counterterm are the ones from Eq. (4.19) for $n_f = n_l+1$. This statement holds to any order in α_s, so that the jet function evolution factor $U_J^{(n_l+1)}$ obeys

$$\mu\frac{\mathrm{d}}{\mathrm{d}\mu}\,U_J^{(n_l+1)}(s,\mu,\mu_J) = \int \mathrm{d}s'\,\gamma_J^{(n_l+1)}(s-s',\mu)\,U_J^{(n_l+1)}(s',\mu,\mu_J)\,. \tag{4.57}$$

When crossing the scale μ_m in the RG evolution of the jet function down to the soft scale the mass-shell fluctuations of the collinear mass modes are integrated out. These contributions are encoded in the jet mass mode matching coefficient $\mathcal{M}_J(s,m,\mu_m)$ and contain all virtual effects of the massive flavor such that for the scales $\mu < \mu_m$ all massive collinear effects decouple. Using the counting $\alpha_s \ln(m^2/s) \sim \mathcal{O}(1)$ the result has the structure

$$\begin{aligned}
\mu_J^2\,\mathcal{M}_J(s,m,\mu_J,\mu_m) = \delta(\tilde{s}) + &\left[\frac{\big(\alpha_s^{(n_l+1)}\big)^2}{(4\pi)^2}\,\delta(\tilde{s})\ln\left(\frac{\mu_J^2}{\mu_m^2}\right)\,\mathcal{M}_{J,\ln}^{(2)}(m,\mu_m)\right]_{\mathcal{O}(\alpha_s)} \\
&+\left[\frac{\big(\alpha_s^{(n_l+1)}\big)^2}{(4\pi)^2}\left(\delta(\tilde{s})\,\mathcal{M}_{J,1}^{(2)}(m,\mu_m) + \left[\frac{\theta(\tilde{s})}{\tilde{s}}\right]_+\mathcal{M}_{J,\ln}^{(2)}(m,\mu_m)\right)\right. \\
&+\frac{\big(\alpha_s^{(n_l+1)}\big)^3}{(4\pi)^3}\,\delta(\tilde{s})\,\ln\left(\frac{\mu_J^2}{\mu_m^2}\right)\mathcal{M}_{J,\ln}^{(3)}(m,\mu_m) \\
&\left.+\frac{\big(\alpha_s^{(n_l+1)}\big)^4}{(4\pi)^4}\,\delta(\tilde{s})\ln^2\left(\frac{\mu_J^2}{\mu_m^2}\right)\mathcal{M}_{J,\ln^2}^{(4)}(m,\mu_m)\right]_{\mathcal{O}(\alpha_s^2)} + \mathcal{O}(\alpha_s^3)\,.
\end{aligned} \tag{4.58}$$

We display the corresponding results for $\alpha_s^{(n_l+1)} = \alpha_s^{(n_l+1)}(\mu_m)$ and $m \equiv \overline{m}(\mu_m)$ given in the $\overline{\text{MS}}$ scheme. The functions multiplying the logarithm $\ln(\mu_J^2/\mu_m^2)$ are related to the ones entering the current mass mode matching correction (see Eqs. (4.46), (4.48) and (4.50)),

$$\mathcal{M}_{J,\ln}^{(2)}(m,\mu_m) = -\,2\,\mathcal{M}_{C,\ln}^{(2)}(m,\mu_m)\,, \tag{4.59}$$

$$\mathcal{M}_{J,\ln}^{(3)}(m,\mu_m) = -\,2\,\mathcal{M}_{C,\ln}^{(3)}(m,\mu_m)\,, \tag{4.60}$$

$$\mathcal{M}_{J,\ln}^{(4)}(m,\mu_m) = 4\,\mathcal{M}_{C,\ln^2}^{(4)}(m,\mu_m)\,. \tag{4.61}$$

The intrinsic relation between the current and jet threshold corrections is based on the consistency of RG running and will be elucidated in Sec. 4.4.3. The less universal two-loop function $\mathcal{M}_{J,1}^{(2)}$ reads

$$\mathcal{M}_{J,1}^{(2)}(m,\mu_m) = C_F T_F\left\{-\frac{8}{9}L_m^3 - \frac{58}{9}L_m^2 + \left(-\frac{466}{27} - \frac{4\pi^2}{9}\right)L_m - \frac{1531}{54} - \frac{10\pi^2}{27} + \frac{80}{9}\zeta_3\right\}\,. \tag{4.62}$$

It is interesting to note that the result in Eq. (4.58) is a non-trivial distributive function of the jet invariant mass s and thus differs substantially from the local mass mode matching coefficient of the current (see Eq. (4.45)) or the strong coupling which do not depend on any kinematic scale. As for the case of the current mass mode matching coefficient, $\mathcal{M}_J$ contains large logarithms involving the ratio of the jet scale $s \sim \mu_J$ and the mass scale $m \sim \mu_m$ which are not summed by the RG μ-evolution of the jet function. They are related to rapidity-type singularities that arise for the massive virtual corrections in the overlap region between the collinear mass mode contributions and the soft-bin subtractions. These logarithms exponentiate as in the case of the current mass mode matching coefficient. We note that, through the rapidity RG evolution, $\mathcal{M}_J$ depends at each order on two rapidity scales, which we correlate to the jet and mass scales μ_J and μ_m. We stress, however, that the dependence of $\mathcal{M}_J$ on the jet scale μ_J is spurious and cancels at fixed order. Using the counting $\alpha_s \ln(m^2/s) \sim \mathcal{O}(1)$ concerning rapidity logarithms the $\mathcal{O}(\alpha_s^2 \ln(m^2/s))$ corrections in Eq. (4.58) are counted as $\mathcal{O}(\alpha_s)$, while at $\mathcal{O}(\alpha_s^2)$ one has to include the terms of $\mathcal{O}(\alpha_s^4 \ln^2(m^2/s))$ and $\mathcal{O}(\alpha_s^3 \ln(m^2/s))$. We refer to Sec. 4.4.2 for the explicit computations.

4.2.4 Renormalization conditions and continuity

So far we have discussed the mass mode setup in terms of three different EFT scenarios resulting in different factorization theorems. This description might suggest that we imply large hierarchies between the hard and jet scale on the one hand and the mass scale on the other hand for each of these descriptions. In fact this requirement is not necessary. Instead of using different effective theories that follow the strict guideline of having the massive quark modes either as fluctuating fields or excluded completed (i.e. integrated out) we can use only a single theory which contains the massive quark modes, but employs different renormalization conditions for the quantum corrections arising from the massive quark modes, which is along the lines of the discussion in chapter 3. Since the hard current, the jet function and the PDFs are gauge-invariant quantities, they can also be renormalized independently. These renormalization conditions are again either the $\overline{\text{MS}}$ prescription or the OS prescription (concerning the massive quark corrections). The former leads to the usual $\overline{\text{MS}}$ feature that massless quarks and the massive flavor all contribute to the RG evolution in the same way, so one uses the $(n_l + 1)$ running flavor scheme. The latter is defined by the condition that the mass corrections vanish for invariant mass scales much smaller than the quark mass and also subtracts finite and scale-dependent contributions such that the massive flavor does not lead to any contribution in the RG evolution, so there are only n_l running flavors. This concerns the strong coupling α_s as well as the hard coefficient, the jet function and the PDFs.

Obviously the $\overline{\text{MS}}$ prescription is suitable to cover the situation where the quark mass becomes small (where suitable means that no large mass logarithms arise in the massless limit) and leads to results which give the known results for massless quarks in the limit $m \to 0$. The on-shell prescription is suitable to cover the decoupling limit, such that the effects of the massive quark vanish in the infinite mass limit. This method of using different renormalization conditions for the RG evolution schemes with (n_l+1) and n_l running flavors also has the advantage that the kinematically dependent threshold of the jet function due to the quark mass is fully contained in the prediction regardless of which type of renormalization scheme is used. This is unlike for the case of using the effective theory method, where the massive quark is completely excluded from the n_l flavor theory, and one is forced to take care of the fact that the real radiation thresholds are always located in the $(n_l + 1)$-flavor theory.

The differences of the renormalized quantities with respect to both of these renormalization prescriptions constitute matching conditions that uniquely define the massive threshold correction factors $\mathcal{M}_C$ and $\mathcal{M}_J$ in analogy to the PDF threshold factors $\mathcal{M}_{\phi,ij}$ in Eq. (3.41). Since the hard current coefficient, the jet function and the PDFs are independent and in principle not tied to the particular factorization theorem for DIS in the endpoint region, the important outcome is that the threshold correction factors can be determined from these quantities themselves and do not rely on knowing the perturbative "full theory" results in the classical OPE region.

The fact that the hard coefficient, the jet function, the PDFs and the massive quark threshold corrections factors that appear in the factorization theorems in the three scenarios (in schemes with either n_l or $n_l + 1$ running flavors) are conceptually connected through different choices of renormalization schemes and not related in any way to expansions in either small or large quantities makes it evident that the predictions of the different factorization theorems at their respective borders of validity have an overlap region and are continuous. In the case of marginal or non-existent hierarchies (such as $Q \gg m \gtrsim Q\lambda \gg Q\lambda^2$ or $Q \gtrsim m \gg Q\lambda \gg Q\lambda^2$) the RG evolution between close-by scales is equivalent to a perturbative treatment, so that the factors of concern might be simply expanded out. Since this might be as well applied to the two neighboring scenarios within some range, we have continuity between the two descriptions, and the transition point where one switches between them can be picked freely within this range. The continuity of the theoretical description for differential cross sections depending on some external kinematic scales is particularly important for practical applications, since different hierarchies between the mass scale and the kinematic scales can arise within a single spectrum when the kinematic variables are varied within their allowed ranges.

4.2.5 Outline of the computations

In the following sections we will perform the computations corresponding to the results summarized before. We have seen in Sec. 3.4.1 that for sufficiently inclusive observables dispersion relations can be used to obtain the results for secondary massive quark radiation (with mass m) at $\mathcal{O}(\alpha_s^2 C_F T_F)$ from the results for "massive gluon" radiation (with mass M) at $\mathcal{O}(\alpha_s)$, which allows to deal with the technically simpler one-loop computations for the latter instead of performing the two-loop integration directly. Due to the fact that the scaling $M \sim m$ is inherited in the dispersion integration also the field theoretic setups in both cases are closely related to each other, which provides the opportunity to investigate many conceptual features of the VFNS already with secondary massive gluons. In Sec. 4.3 we will therefore first compute the hard coefficient, the jet function and the corresponding mass mode threshold corrections at $\mathcal{O}(\alpha_s)$ and discuss the factorization theorems at this level. In Sec. 4.4 we will then use the dispersion relation in Eq. (3.63) to obtain the results at $\mathcal{O}(\alpha_s^2 C_F T_F)$ for massive secondary quarks.

4.3 One-loop computations for secondary massive gluons

We discuss the massive gluon corrections within a toy theory where these gauge bosons are distinct degrees of freedom and exist in parallel to the common massless collinear and ultrasoft gluons. We will consider massive collinear as well as soft gluon modes with mass M, all of which can have mass-shell fluctuations of equal typical virtuality of $\mathcal{O}(M^2)$ in addition to fluctuations at the hard and jet scale depending on the kinematic situation. While they primarily adopt the role of placeholders for the secondary massive quarks (and the gluonic modes they can interact with) the setup can be of direct interest by itself and might well serve for concrete applications for example related to the electroweak theory. We use a notation for the massive gluon that is analogous with the one for the QCD results (with massless gluons) and facilitates the interpretation of the results for the dispersion integration used to implement the corrections due to the gluon splitting. Before we describe the computations for a massive gluon explicitly, let us write down the factorization theorems in the three different scenarios for later reference. Instead of following the strict EFT guideline we adopt this time a notation in which the mass modes are always dynamical degrees of freedom, but different renormalization conditions are employed concerning the massive gluon effects. Including the massless gluons the factorization theorem in scenario I ($M \gtrsim Q$) reads

$$F_1(x,Q,M) = \sum_{i=q} \frac{e_i^2}{2} \left|C^{(\mathrm{OS})}(Q,M,\mu_H)\right|^2 \left|U_C^{(\mathrm{OS})}(Q,\mu_H,\mu_\phi)\right|^2 \int \mathrm{d}s \int \mathrm{d}s'\, J^{(\mathrm{OS})}(s',M,\mu_J) \\ \times U_J^{(\mathrm{OS})}(s-s',\mu_\phi,\mu_J)\, \tilde{\phi}_{i/P}^{(\mathrm{OS})}\left(1-x-\frac{s}{Q^2},\mu_\phi\right), \tag{4.63}$$

The superscript (OS) in the matrix elements and matching coefficients indicates that the OS scheme is used for the massive gluon corrections, which implies in particular that the running is only due to the massless gluon contributions. In scenario II ($Q \gtrsim M$ and $M \gtrsim Q\sqrt{1-x}$) we have

$$F_1(x,Q,M) = \sum_{i=q} \frac{e_i^2}{2} \left|C^{(\overline{\mathrm{MS}})}(Q,M,\mu_H)\right|^2 \left|U_C^{(\overline{\mathrm{MS}})}(Q,\mu_H,\mu_M)\right|^2 \left|\mathcal{M}_C(Q,M,\mu_M)\right|^2 \left|U_C^{(\mathrm{OS})}(Q,\mu_M,\mu_\phi)\right|^2 \\ \times \int \mathrm{d}s \int \mathrm{d}s'\, J^{(\mathrm{OS})}(s',M,\mu_J)\, U_J^{(\mathrm{OS})}(s-s',\mu_\phi,\mu_J)\, \tilde{\phi}_{i/P}^{(\mathrm{OS})}\left(1-x-\frac{s}{Q^2},\mu_\phi\right). \tag{4.64}$$

The superscript ($\overline{\mathrm{MS}}$) in the matrix elements and matching coefficients indicates that the $\overline{\mathrm{MS}}$ scheme is used for the massive gluon contributions, which implies in particular that the running is both due to the massless and massive gluon contributions. In scenario III ($Q\sqrt{1-x} \gtrsim M$) the factorization theorem reads

$$F_1(x,Q,M) = \sum_{i=q} \frac{e_i^2}{2} \left|C^{(\overline{\mathrm{MS}})}(Q,M,\mu_H)\right|^2 \left|U_C^{(\overline{\mathrm{MS}})}(Q,\mu_H,\mu_M)\right|^2 \left|\mathcal{M}_C(Q,M,\mu_M)\right|^2 \left|U_C^{(\mathrm{OS})}(Q,\mu_M,\mu_\phi)\right|^2 \\ \times \int \mathrm{d}s \int \mathrm{d}s' \int \mathrm{d}s'' \int \mathrm{d}s'''\, J^{(\overline{\mathrm{MS}})}(s''',M,\mu_J)\, U_J^{(\overline{\mathrm{MS}})}(s''-s''',\mu_M,\mu_J) \\ \times \mathcal{M}_J(s'-s'',M,\mu_M)\, U_J^{(\mathrm{OS})}(s-s',\mu_\phi,\mu_m)\, \tilde{\phi}_{i/P}^{(\mathrm{OS})}\left(1-x-\frac{s}{Q^2},\mu_\phi\right). \tag{4.65}$$

In the following we describe the calculations for the mass mode contributions to the hard Wilson coefficients $C^{(\mathrm{OS})}(Q,M,\mu)$ and $C^{(\overline{\mathrm{MS}})}(Q,M,\mu)$, the jet functions $J^{(\mathrm{OS})}(s,M,\mu)$ and $J^{(\overline{\mathrm{MS}})}(s,M,\mu)$ and the mass-mode matching coefficients and $\mathcal{M}_C(Q,M,\mu)$ and $\mathcal{M}_J(s,M,\mu)$ entering the factorization theorems at $\mathcal{O}(\alpha_s)$.

An important technical point is that we encounter rapidity divergences in single diagrams mentioned in Sec. 2.5 which are not associated to the UV or IR behavior, but rather to large rapidity separations of the collinear and soft mass modes, and are not regularized by dimensional regularization. In the calculations of the mass-mode contributions to the hard current Wilson coefficient (at $\mu_H \sim Q$) and the jet function (at $\mu_J \sim Q\sqrt{1-x}$) these divergences turn out to cancel among the proper set of diagrams and, if needed, the soft-bin subtractions, and do not result in large logarithms. For the threshold corrections that arise when the mass modes are integrated out (at $\mu_M \sim M$) the rapidity divergences also cancel, but they leave behind large logarithmic terms that in general cannot be summed within the μ-evolution formalism based on dimensional regularization. For the current threshold correction these logarithms are known to exponentiate [40, 41]. In Sec. 4.3.1 we reproduce this result using the evolution method from [41] and demonstrate that analogous exponentiations arise for the jet and PDF mass mode matching coefficients, respectively.

To resum the rapidity logarithms we need an additional regulator that breaks boost invariance. Here we display the corresponding results for individual diagrams employing the analytic "α-regulator" [85, 86] for the k^- integrations, i.e. [10]

$$\frac{\mathrm{d}k^-}{k^-} \to \mathrm{d}k^- \frac{\nu^\alpha}{(k^-)^{1+\alpha}} \,. \tag{4.66}$$

In this context the scale ν is an auxiliary scale to maintain the dimensions of the regulated integrals which adopts a similar role as the μ scale in dimensional regularization. In particular, also the strong coupling adopts a ν-scaling proportional to α. The α-regulator treats the n-and $\bar{n}$-collinear sectors as well as the soft boundaries towards the two collinear sectors in an asymmetric way. Note that the α-regulator as defined in Eq. (4.66) entails the occurrence of spurious $\ln(Q)$-terms that are not supposed to be confused with the analytic $\ln(Q^2)$-terms. Only the latter are altered in the analytic continuation from the timelike momentum transfer in DIS to the spacelike momentum transfer in e^+e^- collisions discussed in chapter 5.

We present all calculations in Feynman gauge. We have checked explicitly that the contributions coming from longitudinal polarizations of the massive gauge bosons vanish due to gauge invariance in all matrix elements and matching corrections.[11] To achieve this for the calculations involving collinear mass modes the inclusion of soft-bin subtractions turned out to be crucial. Thus the soft-bin subtractions are essential to isolate gauge-invariant structures and to achieve factorization, as has also been stressed in Ref. [35].

4.3.1 Hard current matching coefficient and threshold correction

Current matching coefficient

We compute the hard current matching coefficient with a massive gluon at one-loop using quarks as external states. The virtual full QCD result $\hat{F}^{(1)}_{M,\mathrm{QCD}}(Q, M)$ corresponds to the first diagram in Fig. 3.8 and has been already given in Eq. (3.70). We therefore focus on the calculation of the collinear and soft mass mode corrections to the effective theory vertex. The relevant diagrams are shown in Fig. 4.8, where p (p') denotes the momentum of the collinear massless external incoming (outgoing) quark. The corrections for antiquarks in the initial state can be derived in complete analogy and yield the same result. The computations are valid for all scenarios where the mass scale M is below the hard scale Q. This can be understood from the fact that the way how collinear and soft mass modes are distributed with respect to the massless modes below the hard scale Q does not affect the hard contribution itself. [12]

Applying the SCET Feynman rules in Fig. 2.3 gives for the coefficient multiplying the current $\bar{\xi}_{n,p}\gamma^\mu\xi_{\bar{n},p'}$ in the soft mass mode diagram

$$V_s = -2ig^2 C_F \tilde{\mu}^{2\epsilon} \int \frac{\mathrm{d}^d k}{(2\pi)^d} \frac{p^+ - k^+}{[(p-k)^2 + i\epsilon]} \frac{p'^- - k^-}{[(p'-k)^2 + i\epsilon]} \frac{1}{[k^2 - M^2 + i\epsilon]} \,. \tag{4.67}$$

Using $p^\mu = (Q, 0, 0)$ and $p'^\mu = (0, Q, 0)$ and the soft scaling $k^\mu \sim Q(\lambda_M, \lambda_M, \lambda_M)$ for the soft momentum

[10] We use the α-regulator in a way more general than advocated in Ref. [86] since we apply it not only for phase space integrations but also for loop diagrams, so that some of the properties of this regulator for phase space integrals as stated in Ref. [86] might not hold.

[11] For the resummation of rapidity logarithms we decompose the matrix elements into components which are sometimes gauge-dependent. However, the rapidity divergences and the resulting ν-anomalous dimensions are always gauge-invariant.

[12] We carry out the calculations for external massless collinear quarks which are on-shell. This leads to exactly the same calculations for all scenarios with $M < Q$.

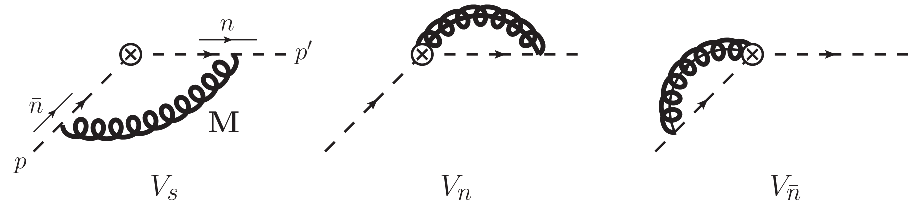

Figure 4.8: Non-vanishing EFT vertex diagrams for the computation of the hard matching coefficient. Soft mass mode bin subtractions are implied for the collinear diagrams.

we obtain for $\lambda_M \ll 1$

$$V_s = -2ig^2 C_F \tilde{\mu}^{2\epsilon} \int \frac{\mathrm{d}^d k}{(2\pi)^d} \frac{1}{[k^- - i\epsilon]} \frac{1}{[k^+ - i\epsilon]} \frac{1}{[k^2 - M^2 + i\epsilon]} \,. \tag{4.68}$$

The expression in Eq. (4.68) can as well be obtained directly from the SCET Feynman rules upon field redefinition in SCET I (or equivalently in SCET II) such that the soft mass mode gauge bosons couple to the collinear massless quarks through Wilson lines. The n-collinear diagram yields

$$V_n = 2ig^2 C_F \tilde{\mu}^{2\epsilon} \int \frac{\mathrm{d}^d k}{(2\pi)^d} \frac{p'^- - k^-}{[(p-k)^2 + i\epsilon]} \frac{1}{[k^- - i\epsilon]} \frac{1}{[k^2 - M^2 + i\epsilon]} \,, \tag{4.69}$$

and using the form of the external momenta (and likewise the collinear scaling $k^\mu \sim Q(\lambda_M^2, 1, \lambda_M)$) we obtain

$$V_n = 2ig^2 C_F \tilde{\mu}^{2\epsilon} \int \frac{\mathrm{d}^d k}{(2\pi)^d} \frac{Q - k^-}{[k^+(k^- - Q) - \vec{k}_\perp^2 + i\epsilon]} \frac{1}{[k^- - i\epsilon]} \frac{1}{[k^2 - M^2 + i\epsilon]} \,. \tag{4.70}$$

The $\bar{n}$-collinear diagram is obtained in an analogous manner and involves the function $V_{\bar{n}}$. It is obtained from the n-collinear diagram by swapping the plus- with the minus-components as well as p' with p. To avoid double counting and achieve gauge-invariance it is crucial to subtract the soft-bin contributions, which arise from the soft scaling regions of the collinear diagrams. Expanding the n-collinear diagram of Eq. (4.70) in the soft mass mode regime $k^\mu \sim Q(\lambda_M, \lambda_M, \lambda_M)$ we obtain the soft-bin subtraction contribution,

$$V_{n,0M} = -2ig^2 C_F \tilde{\mu}^{2\epsilon} \int \frac{\mathrm{d}^d k}{(2\pi)^d} \frac{1}{[k^+ - i\epsilon]} \frac{1}{[k^- - i\epsilon]} \frac{1}{[k^2 - M^2 + i\epsilon]} \,, \tag{4.71}$$

with the analogous expression for the $\bar{n}$-collinear sector, which we call $V_{\bar{n},0M}$. Note that $V_{n,0M} = V_{\bar{n},0M} = V_s$ holds for rapidity regulators that do not act differently on soft graphs and soft-bin subtractions from collinear graphs, e.g. the α-regulator defined in Eq. (4.66). The sum of all vertex diagrams including the soft-bin subtractions and the wave function renormalization computed in Eq. (3.82) gives [35]

$$\begin{aligned} \hat{F}^{(\text{bare},1)}_{M,\text{SCET}}(Q,M,\mu) &= (V_n - V_{n,0M}) + (V_{\bar{n}} - V_{\bar{n},0M}) + V_s - Z_\xi^{(1)} \\ &= V_n + V_{\bar{n}} - V_s - Z_\xi^{(1)} \,, \end{aligned} \tag{4.72}$$

as for the massless case with 0-bin subtractions [87]. We note that the second identity in Eq. (4.72) does not hold for arbitrary IR regulators, e.g. the η regulator employed for the Wilson lines [41] yields different results for the soft graphs and the soft-bin subtractions.

We compute the integrals for $V_n, V_{\bar{n}}$ and V_s by first performing the k^+-integration with the method of residues and then the $k_\perp$-integration. Finally, the rapidity divergences in the k^--integration are regularized with the α-regulator in Eq. (4.66), and the limit $\alpha \to 0$ is implied at the end. Note that the integrals V_n and $V_{\bar{n}}$ are not treated symmetrically and lead to different analytic expressions for the remaining k^- integral. We start from the integral V_n given in Eq. (4.70). Carrying out the k^+- and $k_\perp$-integration as described above we obtain

$$\begin{aligned} V_n &= -\frac{\alpha_s C_F}{(4\pi)^2}\,\Gamma\left(2-\frac{d}{2}\right)\left(\frac{\mu^2 e^{\gamma_E}}{M^2}\right)^{2-\frac{d}{2}}\left(\frac{\nu}{Q}\right)^{\alpha}\int_0^1 \mathrm{d}z\,\frac{(1-z)^{\frac{d}{2}-1}}{z^{1+\alpha}} \\ &= \frac{\alpha_s C_F}{2\pi}\,\Gamma\left(2-\frac{d}{2}\right)\left(\frac{\mu^2 e^{\gamma_E}}{M^2}\right)^{2-\frac{d}{2}}\left\{\frac{1}{\alpha}+\ln\left(\frac{\nu}{Q}\right)+H_{\frac{d}{2}-1}\right\}, \end{aligned} \tag{4.73}$$

where $z \equiv k^-/Q$. After performing the k^+- and $k_\perp$-integrations for $V_{\bar n}$ we arrive at [13]

$$\begin{aligned} V_{\bar n} &= \frac{\alpha_s C_F}{2\pi}\,\Gamma\left(2-\frac{d}{2}\right)\left(\frac{\mu^2 e^{\gamma_E}}{M^2}\right)^{2-\frac{d}{2}}\left[\left(\frac{Q\,\nu}{M^2}\right)^{\alpha}\int_0^\infty \frac{\mathrm{d}z}{z^\alpha}\,\frac{1-z^{\frac{d}{2}-2}}{1-z}+\int_0^1 \mathrm{d}z\,(1-z)^{\frac{d}{2}-2}\right] \\ &= \frac{\alpha_s C_F}{2\pi}\,\Gamma\left(2-\frac{d}{2}\right)\left(\frac{\mu^2 e^{\gamma_E}}{M^2}\right)^{2-\frac{d}{2}}\left\{-\frac{1}{\alpha}-\ln\left(\frac{Q^2}{M^2}\right)-\ln\left(\frac{\nu}{Q}\right)-\frac{\Gamma\left(\frac{d}{2}\right)^2\Gamma\left(1-\frac{d}{2}\right)^2}{2\,\Gamma(d)\,\Gamma(1-d)}+\frac{2}{d-2}\right\}. \end{aligned} \tag{4.74}$$

The result differs from Eq. (4.73) since the integrations for V_n and $V_{\bar n}$ were performed in an asymmetric way. Note that upon summing the contributions from V_n and $V_{\bar n}$ according to Eq. (4.72) the rapidity divergences cancel exactly. Finally, we compute V_s given in Eq. (4.68) in the same way and obtain

$$V_s = V_{n,0M} = V_{\bar n,0M} = -\frac{\alpha_s C_F}{2\pi}\,\Gamma\left(2-\frac{d}{2}\right)\left(\frac{\mu^2 e^{\gamma_E}}{M^2}\right)^{2-\frac{d}{2}}\int_0^\infty \frac{\mathrm{d}z}{z^{1+\alpha}} = 0\,. \tag{4.75}$$

Combining Eqs. (4.73), (4.74), (4.75) and including the contribution due to the wave function renormalization in Eq. (3.82) we arrive at the final d-dimensional result

$$\begin{aligned} \hat F^{(\mathrm{bare},1)}_{M,\mathrm{SCET}}(Q,M,\mu) = \frac{\alpha_s C_F}{4\pi}\,\Gamma\left(2-\frac{d}{2}\right)\left(\frac{\mu^2 e^{\gamma_E}}{M^2}\right)^{2-\frac{d}{2}}&\left\{2H_{\frac{d}{2}-1}-\frac{\Gamma\left(\frac{d}{2}\right)^2\Gamma\left(1-\frac{d}{2}\right)^2}{\Gamma(d)\,\Gamma(1-d)}-\frac{2(d^2-6d+4)}{d(d-2)}\right. \\ &\left.+\ln\left(\frac{M^2}{Q^2}\right)\right\}. \end{aligned} \tag{4.76}$$

The logarithm in the second line arises as a remnant from the cancellation of the rapidity divergences. Expanding in ϵ gives ($L_Q = \ln(Q^2/\mu^2)$, $L_M = \ln(M^2/\mu^2)$)

$$\hat F^{(\mathrm{bare},1)}_{M,\mathrm{SCET}}(Q,M,\mu) = \frac{\alpha_s C_F}{4\pi}\left\{\frac{2}{\epsilon^2}+\frac{3}{\epsilon}-\frac{2}{\epsilon}L_Q+2L_M L_Q-L_M^2-3L_M+\frac{9}{2}-\frac{5\pi^2}{6}\right\}. \tag{4.77}$$

The same result apart from a trivial analytic continuation to a timelike process (see also chapter 5) has been obtained before in Refs. [35, 38, 41, 88] using different regulators and in Refs. [10, 26] without any regulator by properly recombining the integrals, such that the rapidity divergences cancel implicitly. In Eq. (4.77) the UV-divergences do not depend on the mass and agree exactly with those of the sum of the corresponding collinear and soft effective theory diagrams for massless gluons, see Eq. (4.14). If we renormalize the matching coefficient in $\overline{\mathrm{MS}}$ using Eq. (4.14) we obtain the result for the massive gluon contributions to the current in SCET

$$\begin{aligned} \hat F^{(\overline{\mathrm{MS}},1)}_{M,\mathrm{SCET}}(Q,M,\mu) &= \hat F^{(\mathrm{bare},1)}_{M,\mathrm{SCET}}(Q,M,\mu)+Z_C^{(\overline{\mathrm{MS}},1)}(Q,\mu) \\ &= \frac{\alpha_s C_F}{4\pi}\left\{2L_M L_Q-L_M^2-3L_M+\frac{9}{2}-\frac{5\pi^2}{6}\right\}, \end{aligned} \tag{4.78}$$

[13]The contour integration in the k^+-component requires some care concerning the pole structure for $k^- \approx 0$. To be safe, one can determine the relevant residues by including a small p^--component which can be set to 0 after the contour integration.

which has large logarithms for $M \ll Q$ and $M \gg Q$. Using OS renormalization which implies $\hat{F}^{(\mathrm{OS},1)}_{M,\mathrm{SCET}} = 0$ for $M/Q \to \infty$ the counterterm absorbs the complete contribution, i.e.

$$Z_C^{(\mathrm{OS},1)}(Q,M,\mu) = -\hat{F}^{(\mathrm{bare},1)}_{M,\mathrm{SCET}}(Q,M,\mu)\,. \tag{4.79}$$

We are now able to write down the full matching coefficients in all scenarios. In scenario I we use OS renormalization with respect to the massive gluon corrections which gives after including also the massless gluon contributions in Eq. (4.12)

$$C^{(\mathrm{OS},1)}(Q,M,\mu) = C^{(1)}(Q,\mu) + \hat{F}^{(1)}_{M,\mathrm{QCD}}(Q,M)\,, \tag{4.80}$$

where the massive gluon decouples in the heavy gluon limit, i.e. $C^{(\mathrm{OS},1)}(Q,M,\mu) \to C^{(1)}(Q,\mu)$ for $\hat{M} \to \infty$. In the small mass limit $\hat{M} \to 0$, on the other hand, we obtain

$$C^{(\mathrm{OS},1)}(Q,M,\mu) \overset{\hat{M}\to 0}{\longrightarrow} C^{(1)}(Q,\mu) - \frac{\alpha_s C_F}{4\pi}\left\{\ln^2(\hat{M}^2) + 3\ln(\hat{M}^2) + \frac{7}{2} + \frac{2\pi^2}{3}\right\}, \tag{4.81}$$

which shows infrared sensitivity to the small mass scale. However, this limit belongs to the realm of the scenarios II and III where $\overline{\mathrm{MS}}$ renormalization for the mass mode contributions in SCET should be used yielding

$$C^{(\overline{\mathrm{MS}},1)}(Q,M,\mu) = C^{(1)}(Q,\mu) + \hat{F}^{(1)}_{M,\mathrm{QCD}}(Q,M) - \hat{F}^{(\overline{\mathrm{MS}},1)}_{M,\mathrm{SCET}}(Q,M,\mu)\,. \tag{4.82}$$

For $\mu_H \sim Q$ the large logarithms that occur in the full theory form factor $\hat{F}^{(1)}_{M,\mathrm{QCD}}$ for $M \ll Q$ in Eq. (4.81) cancel entirely with the corresponding logarithms in the SCET contributions $\hat{F}^{(\overline{\mathrm{MS}},1)}_{M,\mathrm{SCET}}$ in Eq. (4.78), and $C^{(\overline{\mathrm{MS}},1)}$ reaches the massless limit, i.e. in our toy theory with both massive and massless gluon corrections

$$C^{(\overline{\mathrm{MS}},1)}(Q,M,\mu) \overset{M\to 0}{\longrightarrow} 2C^{(1)}(Q,\mu)\,. \tag{4.83}$$

Note that although we have encountered rapidity divergences in intermediate stages of the calculation they do not produce a large logarithm in the final result which is not suppressed by $\hat{M}$. This is also valid for the jet function and the results with secondary massive quarks.

Hard current threshold correction

The mass mode threshold factor $\mathcal{M}_C(Q,M,\mu_M)$ arises when the RG evolution of the hard current coefficient crosses the massive quark threshold, i.e. in the factorization theorems of scenario II and III in Eqs. (4.64) and (4.65), respectively. As already mentioned in Sec. 4.2 and in analogy to the discussion of the PDF threshold correction in Eq. (3.41), it is constituted by the difference in the renormalization conditions for the hard matching coefficient

$$\mathcal{M}_C(Q,M,\mu_M) = \frac{C^{(\mathrm{OS})}(Q,M,\mu_M)}{C^{(\overline{\mathrm{MS}})}(Q,M,\mu_M)} = \frac{Z_C^{(\overline{\mathrm{MS}})}(Q,\mu_M)}{Z_C^{(\mathrm{OS})}(Q,M,\mu_M)} = \frac{Z_{\mathcal{J}}^{(\mathrm{OS})}(Q,\mu_M)}{Z_{\mathcal{J}}^{(\overline{\mathrm{MS}})}(Q,M,\mu_M)}\,. \tag{4.84}$$

In the latter equality we have written the threshold correction in terms of the renormalization constants of the SCET current $\mathcal{J}$ which is more convenient for the discussion of the rapidity evolution. Since the difference in the factorization theorems for scenario I and II in Eqs. (4.63) and (4.64) concerns just the current matching coefficients and evolution, Eq. (4.84) makes it evident that the condition for the current mass mode matching coefficient automatically implements a continuous transition between these two scenarios for $M \sim \mu_M \sim \mu_H \sim Q$. Thus we obtain up to $\mathcal{O}(\alpha_s)$ in the fixed-order expansion

$$\begin{aligned}\mathcal{M}_C(Q,M,\mu) &= 1 + \hat{F}^{(\overline{\mathrm{MS}},1)}_{M,\mathrm{SCET}}(Q,M,\mu) + \mathcal{O}(\alpha_s^2)\\ &= 1 + \frac{\alpha_s C_F}{4\pi}\left\{2L_M \ln\left(\frac{Q^2}{M^2}\right) + L_M^2 - 3L_M - \frac{5\pi^2}{6} + \frac{9}{2}\right\} + \mathcal{O}(\alpha_s^2)\,.\end{aligned} \tag{4.85}$$

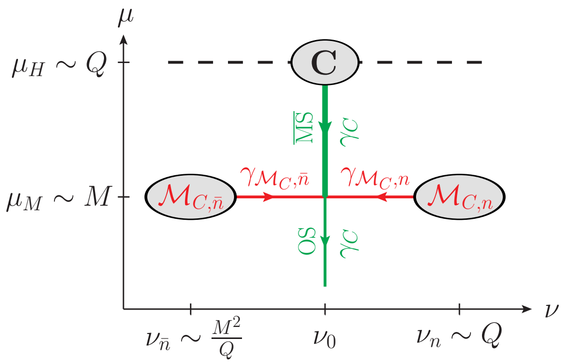

Figure 4.9: Evolution in μ-ν-space for the current: We first perform the running of the Wilson coefficient $C(Q, M, \mu)$ in μ from the hard scale $\mu_H \sim Q$ to the mass scale $\mu_M \sim M$. The evolution to a common ν-scale (ν_0) is then employed for the n- and $\bar{n}$-collinear matching corrections at this fixed invariant mass scale before the μ-evolution down to lower scales continues. Note that the soft contributions vanish with our choice of regulator. Since path independence holds [40, 41], other choices of running are equivalent, but may lead to more involved analytic structures of the evolution factors.

The mass mode contributions $\hat{F}^{(\overline{\text{MS}},1)}_{M,\text{SCET}}$, which are subtracted from the scenario I hard matching coefficient (at μ_H) to obtain the infrared-safe expression $C^{(\overline{\text{MS}},1)}$, are added back in the current threshold factor (at μ_M) when the mass modes are integrated out. This is exactly the analogue of the situation realized for hard coefficients in the VFNS for classical DIS in chapter 3.

Notice that for $M \ll Q$ the mass mode matching coefficient $\mathcal{M}_C$ contains a large logarithmic term $\sim \ln(M^2/\mu_M^2)\ln(Q^2/M^2)$, which can be traced back to the rapidity divergences contained in the collinear and soft mass mode diagrams. For $\mu_M = M$ this logarithm is resummed by the current evolution factors with respect to the invariant mass, but not any more for a generic choice $\mu_M \sim M$. This feature holds generically just for the one-loop case, at higher orders one encounters logarithmic terms which cannot be resummed in this way [38, 89].

We follow the method of Refs. [40, 41] for setting up the rapidity RG evolution. The summation of these logarithms can be carried out independently after the μ-evolution has been settled, and this is the approach we are adopting here, see Fig. 4.9. The result will be a simple exponentiation. In Refs. [40, 41] it has been pointed out that the μ-evolution and the summation of rapidity logarithms can also be carried out simultaneously via a two-dimensional evolution merging RG evolution in virtuality (within dimensional regularization) with RG evolution in rapidity.

We first decompose the current corrections into n-, $\bar{n}$-collinear and soft contributions, which has been in fact one step in the derivation of the factorization theorem [14]

$$\hat{F}_{\text{SCET}} = \hat{F}_{\text{SCET},n} \times \hat{F}_{\text{SCET},\bar{n}} \times \hat{F}_{\text{SCET},s} \,. \tag{4.86}$$

Here we include implicitly the wave function contributions $Z_{\xi_n}/2$ and $Z_{\xi_{\bar{n}}}/2$ in the terms for the corresponding collinear sectors. Let us consider the corresponding one-loop contributions. With the α-regulator the soft mass mode as well as the soft-bin subtraction diagrams lead to vanishing scaleless integrals, i.e. $\hat{F}^{(1)}_{M,\text{SCET},s} = 0$. Starting from Eq. (4.73), including half of the wave function renormalization in Eq. (3.82) and taking the limit $\alpha \to 0$ prior to $\epsilon \to 0$, we obtain for the "bare" n-collinear

[14] The zero-bin contributions might be decoupled in SCET I via a field redefinition [87, 90] and recombined in SCET II with the soft contributions to $\hat{F}_{\text{SCET},s}$. We also emphasize that the individual expressions for each of the factors on the RHS of Eq. (4.86) is regulator dependent.

contribution [15]

$$\hat{F}^{(\text{bare},1)}_{M,\text{SCET},n} = \frac{\alpha_s C_F}{4\pi}\left\{\frac{2}{\alpha}\left[\frac{1}{\epsilon} - L_M + \mathcal{O}(\epsilon)\right] + \frac{1}{\epsilon}\left[2\ln\left(\frac{\nu}{Q}\right) + \frac{3}{2}\right] - 2L_M\ln\left(\frac{\nu}{Q}\right) - \frac{3}{2}L_M + \frac{9}{4} - \frac{\pi^2}{3}\right\}, \tag{4.87}$$

and for the $\bar{n}$-collinear contribution

$$\begin{aligned}\hat{F}^{(\text{bare},1)}_{M,\text{SCET},\bar{n}} = \frac{\alpha_s C_F}{4\pi}\bigg\{&-\frac{2}{\alpha}\left[\frac{1}{\epsilon} - L_M + \mathcal{O}(\epsilon)\right] + \frac{2}{\epsilon^2} - \frac{1}{\epsilon}\left[2\ln\left(\frac{Q^2}{M^2}\right) + 2\ln\left(\frac{\nu}{Q}\right) + 2L_M - \frac{3}{2}\right]\\ &+ L_M^2 + 2L_M\left[\ln\left(\frac{Q^2}{M^2}\right) + \ln\left(\frac{\nu}{Q}\right)\right] - \frac{3}{2}L_M + \frac{9}{4} - \frac{\pi^2}{2}\bigg\}.\end{aligned} \tag{4.88}$$

We see that $F^{(\text{bare},1)}_{M,\text{SCET},n}$ is free of large logarithms for $\nu = \nu_n \sim Q$, and $F^{(\text{bare},1)}_{M,\text{SCET},\bar{n}}$ is free of large logarithms for $\nu = \nu_{\bar{n}} \sim M^2/Q$. It is then possible to set up an evolution in ν between ν_n and $\nu_{\bar{n}}$. The resulting current renormalization constants read

$$Z^{(\overline{\text{MS}},1)}_{\mathcal{J},n} = \frac{\alpha_s(\mu,\nu)C_F}{4\pi}\left\{\frac{2}{\alpha}\left[\frac{1}{\epsilon} - L_M + \mathcal{O}(\epsilon)\right] + \frac{1}{\epsilon}\left[2\ln\left(\frac{\nu}{Q}\right) + \frac{3}{2}\right]\right\}, \tag{4.89}$$

$$Z^{(\overline{\text{MS}},1)}_{\mathcal{J},\bar{n}} = \frac{\alpha_s(\mu,\nu)C_F}{4\pi}\left\{-\frac{2}{\alpha}\left[\frac{1}{\epsilon} - L_M + \mathcal{O}(\epsilon)\right] + \frac{2}{\epsilon^2} - \frac{1}{\epsilon}\left[2\ln\left(\frac{Q^2}{M^2}\right) + 2\ln\left(\frac{\nu}{Q}\right) + 2L_M - \frac{3}{2}\right]\right\}. \tag{4.90}$$

We note that the renormalized strong coupling depends on the scale ν only due to the dimensional extension of the k^--integration and satisfies $\mathrm{d}\alpha_s/\mathrm{d}\ln\nu = -\alpha\,\alpha_s$. The sum of the individual counterterm contributions gives the complete current counterterm corresponding to Eq. (4.14),

$$Z^{(1)}_C(Q,\mu) = -\left(Z^{(\overline{\text{MS}},1)}_{\mathcal{J},n} + Z^{(\overline{\text{MS}},1)}_{\mathcal{J},\bar{n}}\right), \tag{4.91}$$

which yields the correct μ-anomalous dimension for the hard current. The ν-evolution equation for the soft, n- and $\bar{n}$-collinear contributions of the threshold correction denoted by $\mathcal{M}_{C,s}$, $\mathcal{M}_{C,n}$ and $\mathcal{M}_{C,\bar{n}}$, respectively, can be directly obtained from Eq. (4.84) applied to each sector and reads

$$\nu\frac{\mathrm{d}}{\mathrm{d}\nu}\,\mathcal{M}_{C,i}(Q,M,\mu,\nu) = \left(\gamma_{\mathcal{J},i,\nu} - \gamma^{(\text{OS})}_{\mathcal{J},i,\nu}\right)\mathcal{M}_{C,i}(Q,M,\mu,\nu) \equiv \gamma_{\mathcal{M}_C,i}\,\mathcal{M}_{C,i}(Q,M,\mu,\nu), \tag{4.92}$$

where $i = s, n, \bar{n}$ and the anomalous dimensions $\gamma^{(\text{OS})}_{\mathcal{J},i,\nu}$ corresponding to counterterms in the OS scheme employed below the mass threshold vanish for the massive gluon at $\mathcal{O}(\alpha_s)$. [16] The ν-anomalous dimensions in the $\overline{\text{MS}}$ scheme employed above the mass threshold can be read off at $\mathcal{O}(\alpha_s)$ from the counterterm contributions in Eqs. (4.89) and (4.90), [17]

$$\gamma^{(1)}_{\mathcal{J},s,\nu} = -\,\nu\frac{\mathrm{d}}{\mathrm{d}\nu}\,Z^{(\overline{\text{MS}},1)}_{\mathcal{J},s} = 0\,, \tag{4.93}$$

$$\gamma^{(1)}_{\mathcal{J},n,\nu} = -\,\nu\frac{\mathrm{d}}{\mathrm{d}\nu}\,Z^{(\overline{\text{MS}},1)}_{\mathcal{J},n} = -\frac{\alpha_s C_F}{4\pi}\,2L_M = -\frac{\Gamma^{(1)}_{\text{cusp}}}{2}\,L_M\,, \tag{4.94}$$

$$\gamma^{(1)}_{\mathcal{J},\bar{n},\nu} = -\,\nu\frac{\mathrm{d}}{\mathrm{d}\nu}\,Z^{(\overline{\text{MS}},1)}_{\mathcal{J},\bar{n}} = \frac{\alpha_s C_F}{4\pi}\,2L_M = -\gamma^{(1)}_{\mathcal{J},n,\nu}\,. \tag{4.95}$$

[15] Here the ϵ-dependence in the expression proportional to $1/\alpha$ should be in principle kept unexpanded to avoid terms going like ϵ/α in the μ-anomalous dimension. However, for convenience we show only the terms up to $\mathcal{O}(\epsilon^0)$.

[16] The anomalous dimensions with respect to the massless gluon contributions cancel exactly at $\mathcal{O}(\alpha_s)$ in the difference between the two anomalous dimensions in Eq. (4.92). This does not hold when considering higher order corrections in the strong coupling due to the scheme dependence of α_s as we will see in Sec. 4.4.1.

[17] Using instead the symmetric Wilson line regulator η in Refs. [40,41] the corresponding anomalous dimensions $\gamma^{(\overline{\text{MS}},1,\eta)}_{\mathcal{J},i,\nu}$ satisfy in terms of the one Eq. (4.94): $\gamma^{(\overline{\text{MS}},1,\eta)}_{\mathcal{J},s,\nu} = -2\gamma^{(\overline{\text{MS}},1)}_{\mathcal{J},n,\nu}$ and $\gamma^{(\overline{\text{MS}},1,\eta)}_{\mathcal{J},n,\nu} = \gamma^{(\overline{\text{MS}},1,\eta)}_{\mathcal{J},\bar{n},\nu} = \gamma^{(\overline{\text{MS}},1)}_{\mathcal{J},n,\nu}$.

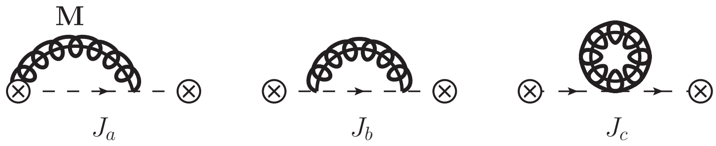

Figure 4.10: Non-vanishing EFT diagrams for the computation of the jet function. The required soft-bin subtractions are implicit. Concerning J_a also the right-symmetric diagram has to be taken into account. At the end the imaginary part has to be taken.

We note that the coefficient multiplying $L_M = \ln(M^2/\mu^2)$ is related to the one-loop cusp anomalous dimension due to the path-independence of the evolution in μ-ν-space, which holds to all orders in α_s. Solving Eq. (4.92) and expanding out the terms that do not involve large logarithms leads to

$$\mathcal{M}_C(Q, M, \mu_M, \nu_n, \nu_{\bar{n}}) = \exp\left[\frac{\alpha_s C_F}{2\pi} L_M \ln\left(\frac{\nu_n}{\nu_{\bar{n}}}\right)\right] \left(1 + \frac{\alpha_s C_F}{4\pi}\left\{-L_M\left[\ln\left(\frac{\nu_n^2}{Q^2}\right) - \ln\left(\frac{Q^2\nu_{\bar{n}}^2}{M^4}\right)\right]\right.\right.$$
$$\left.\left. + L_M^2 - 3L_M + \frac{9}{2} - \frac{5\pi^2}{6}\right\}\right). \tag{4.96}$$

This expression is also suitable for an analytic continuation to timelike processes e.g. in $e^+e^- \to$ jets via the replacement $Q^2 \to -(Q^2 + i0)$.

4.3.2 Jet function and threshold correction

Jet function

We calculate the $\mathcal{O}(\alpha_s)$ massive gluon contributions to the massless quark jet function. The corresponding diagrams are listed in Fig. 4.10. The mass mode contributions to the jet function arise in the situation $\lambda_M \sim \lambda$, where the collinear mass modes can yield real and virtual effects with typical invariant mass $Q^2\lambda^2$, so we can use the scaling $k^\mu \sim Q(\lambda^2, 1, \lambda)$ for the n-collinear massive gluon keeping the full mass dependence. The jet momentum and its invariant mass are denoted with p^μ and $s \equiv p^2 = Qp^+ + p_\perp^2$, where the prescription $s \to s + i0$ is understood in the following. We keep p^+ explicitly non-zero in the subsequent computations to account for the non-vanishing offshellness s of the jet sector and use a frame with $p_\perp^\mu = 0$.

Taking into account the trace and the prefactors of the jet function matrix element in Eq. (4.7) we obtain for diagram J_a (before taking the imaginary part)

$$J_a = -\frac{2g^2 C_F}{\pi s}\tilde{\mu}^{2\epsilon}\int \frac{\mathrm{d}^d k}{(2\pi)^d}\frac{p^- - k^-}{[(p-k)^2 + i\epsilon]}\frac{1}{[k^- - i\epsilon]}\frac{1}{[k^2 - M^2 + i\epsilon]}. \tag{4.97}$$

For our choice of the external momenta this yields

$$J_a = -\frac{2g^2 C_F}{\pi s}\tilde{\mu}^{2\epsilon}\int \frac{\mathrm{d}^d k}{(2\pi)^d}\frac{Q - k^-}{[s(1 - k^-/Q) - Qk^+ + k^2 + i\epsilon]}\frac{1}{[k^- - i\epsilon]}\frac{1}{[k^2 - M^2 + i\epsilon]}. \tag{4.98}$$

The corresponding soft mass mode bin subtraction with the scaling $k^\mu \sim Q(\lambda_M, \lambda_M, \lambda_M)$ gives

$$J_{a,0M} = -\frac{2g^2 C_F}{\pi s}\tilde{\mu}^{2\epsilon}\int \frac{\mathrm{d}^d k}{(2\pi)^d}\frac{Q}{[s - Qk^+ + i\epsilon]}\frac{1}{[k^- - i\epsilon]}\frac{1}{[k^2 - M^2 + i\epsilon]}. \tag{4.99}$$

Note that the invariant mass term s is maintained as an infrared scale to account for the non-zero jet invariant mass. This is related to the fact that the typical invariant mass of the massless collinear quark increases from $Q^2\lambda^2$ to $Q^2\lambda_M$ by an interaction with a virtual soft mass mode which also changes the parametric counting of s for the soft-bin contribution. In close analogy to the wave function contributions discussed in Sec. 3.4.2 the sum of the self-energy diagrams J_b and J_c reads

$$J_b + J_c = -\frac{g^2 C_F (d-2)}{\pi s}\tilde{\mu}^{2\epsilon}\int \frac{\mathrm{d}^d k}{(2\pi)^d}\,\frac{1}{[k^2 - M^2 + i\epsilon]}\,\frac{1 + Qk^+/s}{[s(1 + k^-/Q) + Qk^+ + k^2 + i\epsilon]}\,. \tag{4.100}$$

As we have discussed below Eq. (3.82), the soft-bin subtraction terms to the self-energy diagrams belong to a subleading effective theory treatment and are thus not considered.

To compute the integrals, we apply the same technique as in Sec. 4.3.1, i.e. we first carry out the k^+- and $k_\perp$-integrations. We will encounter rapidity singularities in the collinear mass mode contributions and the soft-bin subtractions, for which we employ the α-regulator in Eq. (4.66) in the k^- integration. For J_a we then obtain

$$\begin{aligned}
J_a &= -\frac{i}{\pi s}\frac{\alpha_s C_F}{2\pi}\,\Gamma\left(2-\frac{d}{2}\right)\left(\frac{\mu^2 e^{\gamma_E}}{M^2}\right)^{2-\frac{d}{2}}\left(\frac{\nu}{Q}\right)^{\alpha}\int_0^1 \frac{\mathrm{d}z}{z^{1+\alpha}}\,(1-z)^{\frac{d}{2}-1}\left(1-\frac{s}{M^2}z\right)^{\frac{d}{2}-2}\\
&= -\frac{i}{\pi s}\frac{\alpha_s C_F}{2\pi}\left\{\Gamma\left(2-\frac{d}{2}\right)\left(\frac{\mu^2 e^{\gamma_E}}{M^2}\right)^{2-\frac{d}{2}}\left[-\frac{1}{\alpha} - \ln\left(\frac{\nu}{Q}\right) - H_{\frac{d}{2}-1}\right]\right.\\
&\quad\left. + \mathrm{Li}_2\left(\frac{s}{M^2}\right) + \left(1 - \frac{M^2}{s}\right)\ln\left(1-\frac{s}{M^2}\right) - 1\right\}
\end{aligned} \tag{4.101}$$

with $z \equiv k^-/Q$. In the second line we have also isolated the structures which are singular at $s = 0$ yielding distributive pieces, for which we will need the full d-dimensional expressions, from structures which vanish for $M \to \infty$. The latter yield UV and IR-finite real radiation pieces which we have expanded for $d \to 4$ in the last line.

The corresponding soft mass mode bin subtraction yields

$$\begin{aligned}
J_{a,0M} &= -\frac{i}{\pi s}\frac{\alpha_s C_F}{2\pi}\,\Gamma\left(2-\frac{d}{2}\right)\left(\frac{\mu^2 e^{\gamma_E}}{M^2}\right)^{2-\frac{d}{2}}\left(\frac{\nu}{Q}\right)^{\alpha}\int_0^\infty \frac{\mathrm{d}z}{z^{1+\alpha}}\left(1-\frac{s}{M^2}z\right)^{\frac{d}{2}-2}\\
&= -\frac{i}{\pi s}\frac{\alpha_s C_F}{2\pi}\,\Gamma\left(2-\frac{d}{2}\right)\left(\frac{\mu^2 e^{\gamma_E}}{M^2}\right)^{2-\frac{d}{2}}\left\{-\frac{1}{\alpha} - \ln\left(\frac{\nu}{Q}\right) - H_{1-\frac{d}{2}} - \ln\left(-\frac{s}{M^2}\right)\right\}.
\end{aligned} \tag{4.102}$$

In the difference of J_a and $J_{a,0M}$ all rapidity divergences cancel and one obtains a finite result in dimensional regularization. We note that the rapidity divergences we encounter only affect the virtual (distributive) contribution to the jet function. Note that the soft-bin contributions do not lead to any real radiative terms, consistently with the counting argument given after Eq. (4.99).

Next, we proceed to the calculation of the self energy diagrams $J_b + J_c$. Here rapidity divergences do not occur and we will thus not employ any regulator besides dimensional regularization. Defining $z \equiv -k^+/p^+$ we arrive at the expression

$$\begin{aligned}
J_b + J_c &= -\frac{i}{\pi s}\frac{\alpha_s C_F}{4\pi}\,(d-2)\,\Gamma\left(2-\frac{d}{2}\right)\left(\frac{\mu^2 e^{\gamma_E}}{M^2}\right)^{2-\frac{d}{2}}\int_0^1 \mathrm{d}z\,(1-z)^{\frac{d}{2}-1}\left(1-\frac{s}{M^2}z\right)^{\frac{d}{2}-2}\\
&= -\frac{i}{\pi s}\frac{\alpha_s C_F}{2\pi}\left\{\Gamma\left(2-\frac{d}{2}\right)\left(\frac{\mu^2 e^{\gamma_E}}{M^2}\right)^{2-\frac{d}{2}}\frac{d-2}{d} - \frac{(M^2-s)^2}{2s^2}\ln\left(1-\frac{s}{M^2}\right) + \frac{3}{4} - \frac{M^2}{2s}\right\}.
\end{aligned} \tag{4.103}$$

Here we have again expanded out a finite real radiation piece for $d \to 4$.

The sum of all diagrams before taking the imaginary part yields

$$\begin{aligned}
2(J_a - J_{a,0M}) + J_b + J_c = &-\frac{i}{\pi s}\frac{\alpha_s C_F}{4\pi}\left\{4\,\Gamma\left(2-\frac{d}{2}\right)\left(\frac{\mu^2 e^{\gamma_E}}{M^2}\right)^{2-\frac{d}{2}}\left[H_{1-\frac{d}{2}} - H_{\frac{d}{2}-1} + \frac{d-2}{2d} + \ln\left(\frac{-s}{M^2}\right)\right]\right.\\
&\left. + 4\,\mathrm{Li}_2\left(\frac{s}{M^2}\right) + \frac{(s-M^2)(3s+M^2)}{s^2}\ln\left(1-\frac{s}{M^2}\right) - \frac{M^2}{s} - \frac{5}{2}\right\}.
\end{aligned} \tag{4.104}$$

The same result was also obtained in Refs. [10, 26] without any regulator by properly recombining the integrals, such that the rapidity divergences cancel implicitly. We can take the absorptive part with the help of the relations in the appendix of Ref. [9] (which are partially also displayed in appendix B), which leads to the mass mode contributions to the jet function. Including the massless gluon contributions we write the unrenormalized jet function as

$$J^{(\text{bare},1)}(s,M,\mu) = J^{(\text{bare},1)}(s,\mu) + J^{(\text{bare},1)}_{M,\text{virt}}(s,M,\mu) + J^{(1)}_{M,\text{real}}(s,M)\,. \tag{4.105}$$

Here the unrenormalized virtual contribution $J^{(\text{bare},1)}_{M,\text{virt}}(s,M,\mu)$ containing only distributions is given in d dimensions by ($\bar{s} = s/\mu^2$)

$$\mu^2 J^{(\text{bare},1)}_{M,\text{virt}}(s,M,\mu) = \frac{\alpha_s C_F}{4\pi}\,\Gamma\Big(2-\frac{d}{2}\Big)\Big(\frac{\mu^2 e^{\gamma_E}}{M^2}\Big)^{2-\frac{d}{2}}\bigg\{\delta(\bar{s})\left[4H_{\frac{d}{2}-1} - 4H_{1-\frac{d}{2}} + 4L_M - \frac{2(d-2)}{d}\right] \\ -4\left[\frac{\theta(\bar{s})}{\bar{s}}\right]_+\bigg\}\,. \tag{4.106}$$

The UV- and IR-finite correction $J^{(1)}_{M,\text{real}}(s,M)$ contributes only when the jet invariant mass is above the threshold M and thus corresponds to real production of the massive gluons,

$$J^{(1)}_{M,\text{real}}(s,M) = \frac{\alpha_s C_F}{4\pi}\,\theta(s-M^2)\left\{\frac{(M^2-s)(3s+M^2)}{s^3} + \frac{4}{s}\ln\Big(\frac{s}{M^2}\Big)\right\}\,. \tag{4.107}$$

Expanding for $\epsilon \to 0$ the virtual contributions read

$$\mu^2 J^{(\text{bare},1)}_{M,\text{virt}}(s,M,\mu) = \frac{\alpha_s C_F}{4\pi}\left\{\delta(\bar{s})\left[\frac{4}{\epsilon^2} + \frac{3}{\epsilon} - 2L_M^2 - 3L_M + \frac{9}{2} - \pi^2\right] + \left[\frac{\theta(\bar{s})}{\bar{s}}\right]_+\left[-\frac{4}{\epsilon} + 4L_M\right]\right\}\,. \tag{4.108}$$

We see that the UV-divergences are mass independent and agree with those from the purely massless jet function in Eq. (4.18). Therefore, using $\overline{\text{MS}}$ renormalization for both massless and massive gluon contributions the jet function reads

$$J^{(\overline{\text{MS}},1)}(s,M,\mu) = J^{(1)}(s,\mu) + J^{(1)}_{M,\text{virt}}(s,M,\mu) + J^{(1)}_{M,\text{real}}(s,M)\,. \tag{4.109}$$

with

$$\begin{aligned} J^{(1)}_{M,\text{virt}}(s,M,\mu) &= J^{(\text{bare},1)}_{M,\text{virt}}(s,M,\mu) - Z^{(1)}_J(s,\mu) \\ &= \frac{\alpha_s C_F}{4\pi}\left\{\delta(\bar{s})\left[-2L_M^2 - 3L_M + \frac{9}{2} - \pi^2\right] + 4L_M\left[\frac{\theta(\bar{s})}{\bar{s}}\right]_+\right\}\,. \end{aligned} \tag{4.110}$$

Note that for $\mu^2 = \mu_J^2 \sim s$ the large logarithms that arise for $M^2 \ll s$ cancel between the real and virtual mass mode contributions and we obtain the massless limit

$$J^{(\overline{\text{MS}},1)}(s,M,\mu) \overset{M\to 0}{\longrightarrow} 2J^{(1)}(s,\mu)\,. \tag{4.111}$$

In contrast, if OS renormalization is employed for the massive gluon corrections we obtain the corresponding counterterm contribution [18]

$$Z^{(\text{OS},1)}_{J,M}(s,M,\mu) = J^{(\text{bare},1)}_{M,\text{virt}}(s,M,\mu)\,, \tag{4.112}$$

which results in the renormalized jet function

$$J^{(\text{OS},1)}(s,M,\mu) = J^{(1)}(s,\mu) + J^{(1)}_{M,\text{real}}(s,M)\,. \tag{4.113}$$

Since the real radiation contribution contains a threshold it is obvious that the massive gluon terms decouple for $s \gg M$.

[18] For the massless gluon contributions we still employ $\overline{\text{MS}}$ renormalization with the counterterm in Eq. (4.18).

Jet function threshold correction

The mass mode threshold factor $\mathcal{M}_J(s,M,\mu_M)$ arises when the RG evolution of the jet function crosses the massive quark threshold. The derivation goes along the lines of the current mass mode threshold factor. The matching procedure is accounting for the difference between the jet functions in the OS and $\overline{\text{MS}}$ scheme, thus the mass mode matching coefficient is obtained by the relation

$$\begin{aligned}\mathcal{M}_J(s,M,\mu_M) &= \int \mathrm{d}s'\, J^{(\text{OS})}(s-s',M,\mu_M)\left(J^{(\overline{\text{MS}})}\right)^{-1}(s',M,\mu_M)\\ &= \int \mathrm{d}s'\, Z_J^{(\overline{\text{MS}})}(s-s',\mu_M)\left(Z_J^{(\text{OS})}\right)^{-1}(s',M,\mu_M)\,. \end{aligned}\tag{4.114}$$

Since the difference in the factorization theorems for the scenarios II and III in Eqs. (4.64) and (4.65) concerns just the jet function and its evolution, Eq. (4.114) shows that the matching condition for the jet function automatically implements a continuous transition between these two scenarios at $M^2 \sim \mu_M^2 \sim \mu_J^2 \sim s$. Note that real radiation terms are fully included in both scenarios. Thus we obtain up to $\mathcal{O}(\alpha_s)$

$$\begin{aligned}\mu_J^2\,\mathcal{M}_J(s,M,\mu_M) &= \delta(\tilde{s}) - J^{(1)}_{\text{virt}}(s,M,\mu_M) + \mathcal{O}(\alpha_s^2)\\ &= \delta(\tilde{s}) + \frac{\alpha_s C_F}{4\pi}\left\{\delta(\tilde{s})\left[-4L_M\ln\left(\frac{\mu_J^2}{\mu_M^2}\right) + 2L_M^2 + 3L_M - \frac{9}{2} + \pi^2\right]\right.\\ &\qquad \left. - 4L_M\left[\frac{\theta(\tilde{s})}{\tilde{s}}\right]_+\right\} + \mathcal{O}(\alpha_s^2)\,. \end{aligned}\tag{4.115}$$

Similar to the mass mode matching coefficient of the current $\mathcal{M}_C$, also $\mathcal{M}_J$ contains a large logarithm $\sim \ln(s/M^2)$ for $\mu_M \ll \mu_J$, which is manifest when using the normalized jet invariant mass variable $\tilde{s} \equiv s/\mu_J^2$. For the discussion of its resummation we closely follow the method outlined in Sec. 4.3.1. We decompose the jet function as

$$J = J_n \otimes J_{0M} \tag{4.116}$$

for the collinear and soft-bin mass mode contributions. [19] Note that J_{0M} as it is defined here will have an opposite sign compared to the soft-bin contributions in the jet function calculation (which were subtracted). In the following we will not explicitly write out the real radiation corrections and the massless gluon contributions, since they cancel in the ratio of Eq. (4.114).

Using the α-regulator and taking the limit $\alpha \to 0$ prior to $\epsilon \to 0$, we obtain for the bare virtual collinear mass mode contributions from Eqs. (4.101) and (4.103)

$$\begin{aligned}\mu_J^2\, J^{(\text{bare},1)}_{M,\text{virt},n} = \frac{\alpha_s C_F}{4\pi}\,\delta(\tilde{s})&\left\{\frac{4}{\alpha}\left[\frac{1}{\epsilon} - L_M + \mathcal{O}(\epsilon)\right] + \frac{1}{\epsilon}\left[4\ln\left(\frac{\nu}{Q}\right) + 3\right] - 4L_M\ln\left(\frac{\nu}{Q}\right) - 3L_M\right.\\ &\left. + \frac{9}{2} - \frac{2\pi^2}{3}\right\}. \end{aligned}\tag{4.117}$$

Using Eq. (4.102) the contributions due to the soft-bin subtractions yield

$$\begin{aligned}\mu_J^2\, J^{(\text{bare},1)}_{M,\text{virt},0M} = \frac{\alpha_s C_F}{4\pi}&\left\{\delta(\tilde{s})\left[-\frac{4}{\alpha}\left(\frac{1}{\epsilon} - L_M + \mathcal{O}(\epsilon)\right) + \frac{4}{\epsilon^2} - \frac{4}{\epsilon}\ln\left(\frac{\nu\,\mu_J^2}{Q\,\mu^2}\right) + 4L_M\ln\left(\frac{\nu\,\mu_J^2}{Q\,\mu^2}\right)\right.\right.\\ &\left.\left. - 2L_M^2 - \frac{\pi^2}{3}\right] + \left[\frac{\theta(\tilde{s})}{\tilde{s}}\right]_+\left[-\frac{4}{\epsilon} + 4L_M\right]\right\}. \end{aligned}\tag{4.118}$$

We see that for $\mu = \mu_M \sim M$ the contribution $J^{(\text{bare},1)}_{M,\text{virt},n}$ is free of large logarithms for $\nu = \nu_n \sim Q$, and $J^{(\text{bare},1)}_{M,\text{virt},0M}$ is free of large logarithms for $\nu = \nu_{0M} \sim QM^2/s$. The resulting renormalization constants for

[19] Zero-bin subtractions can be formally decoupled in SCET I via field redefinitions [87,90]. Therefore we can in principle also factorize the soft-bin subtractions in SCET II.

the jet threshold corrections read

$$\mu_J^2\, Z^{(\overline{\rm MS},1)}_{J,M,n} = \frac{\alpha_s C_F}{4\pi}\,\delta(\tilde{s})\left\{\frac{4}{\alpha}\left[\frac{1}{\epsilon} - L_M + \mathcal{O}(\epsilon)\right] + \frac{1}{\epsilon}\left[4\ln\left(\frac{\nu}{Q}\right) + 3\right]\right\}, \tag{4.119}$$

$$\mu_J^2\, Z^{(\overline{\rm MS},1)}_{J,M,0M} = \frac{\alpha_s C_F}{4\pi}\left\{\delta(\tilde{s})\left(-\frac{4}{\alpha}\left[\frac{1}{\epsilon} - L_M + \mathcal{O}(\epsilon)\right] + \frac{4}{\epsilon^2} - \frac{4}{\epsilon}\ln\left(\frac{\nu\,\mu_J^2}{Q\,\mu^2}\right)\right) + \frac{4}{\epsilon}\left[\frac{\theta(\tilde{s})}{\tilde{s}}\right]_+\right\}. \tag{4.120}$$

The sum of the individual counterterm contributions yields the complete jet function counterterm corresponding to Eq. (4.18)

$$Z^{(1)}_{J,M}(s,\mu) = Z^{(1)}_{J,M,n} + Z^{(1)}_{J,M,0M}\,, \tag{4.121}$$

which is in particular free of rapidity divergences and yields the correct μ-anomalous dimension for the jet function. The ν-evolution equation for the collinear and soft-bin contributions to the threshold correction denoted by $\mathcal{M}_{J,n}$ and $\mathcal{M}_{J,0M}$, respectively, can be derived from Eq. (4.114) for each sector and reads

$$\nu\frac{\mathrm{d}}{\mathrm{d}\nu}\,\mathcal{M}_{J,i}(s,M,Q,\mu,\nu) = -\left(\gamma_{J,i,\nu} - \gamma^{(\rm OS)}_{J,i,\nu}\right)\mathcal{M}_{J,i}(s,M,Q,\mu,\nu) \equiv \gamma_{\mathcal{M}_J,i}\,\mathcal{M}_{J,i}(s,M,Q,\mu,\nu)\,, \tag{4.122}$$

where $i = n, 0M$ and the anomalous dimensions $\gamma^{(\rm OS)}_{J,i,\nu}$ corresponding to counterterms in the OS scheme employed below the mass threshold vanish for the massive gluon contributions at $\mathcal{O}(\alpha_s)$. Note that the RGE in Eq. (4.122) does not involve a convolution in contrast to the RGE equation for μ, see Eq. (4.23). This is due to the fact that the ν-anomalous dimension does not involve a cusp (see Ref. [38]) and is thus purely local in the convolution variable. The ν-anomalous dimensions at $\mathcal{O}(\alpha_s)$ can be read off from the counterterm contributions in Eqs. (4.119) and (4.120), [20]

$$\gamma^{(1)}_{J,n,\nu} = -\,\nu\frac{\mathrm{d}}{\mathrm{d}\nu}\,Z^{(\overline{\rm MS},1)}_{J,M,n} = -\frac{\alpha_s C_F}{4\pi}\,4L_M = -\Gamma^{(1)}_{\rm cusp}\,L_M\,, \tag{4.123}$$

$$\gamma^{(1)}_{J,0M,\nu} = -\,\nu\frac{\mathrm{d}}{\mathrm{d}\nu}\,Z^{(\overline{\rm MS},1)}_{J,M,0M} = \frac{\alpha_s C_F}{4\pi}\,4L_M = -\gamma^{(1)}_{J,n,\nu}\,. \tag{4.124}$$

As for the current mass mode matching coefficient, there is no ν-evolution for $\mu_M = M$. Solving Eq. (4.122), which leads to the anticipated exponentiation, and expanding out the terms that do not involve large logarithms leads to the final form of the jet function threshold correction,

$$\begin{aligned}\mu_J^2\,\mathcal{M}_J(s,M,\mu_M,\nu_n,\nu_{0M}) = \exp\left[\frac{\alpha_s C_F}{\pi}\,L_M\ln\left(\frac{\nu_{0M}}{\nu_n}\right)\right]\Bigg(1 + \frac{\alpha_s C_F}{4\pi}\Bigg\{\delta(\tilde{s})\Bigg[4L_M\left(\ln\left(\frac{\nu_n}{Q}\right) - \ln\left(\frac{\nu_{0M}\mu_J^2}{QM^2}\right)\right)\\ - 2L_M^2 + 3L_M - \frac{9}{2} + \pi^2\Bigg] - 4L_M\left[\frac{\theta(\tilde{s})}{\tilde{s}}\right]_+\Bigg\}\Bigg)\,.\end{aligned} \tag{4.125}$$

4.3.3 Consistency relations

The fact of having four different scales relevant for setting up the RG evolution (μ_H, μ_J, μ_ϕ and μ_M) leads to another interesting feature related to the possibilities to pick the final renormalization scale $\mu = \mu_{\rm final}$ which the hard current coefficient, the jet function and the PDF are being evolved to in the different factorization theorems. In Fig. 4.11 we show an illustration of two equivalent choices for scenario III ($\mu_J > \mu_M > \mu_\phi$), where we display the situations that (a) $\mu_{\rm final}$ lies between the mass and the PDF scale and (b) between the jet and the mass scale. The equivalence concerning physical predictions for the differential cross section leads to statements about the intrinsic connections between the components of the factorization theorems. On the one hand, they imply the well-known consistency conditions between the RG evolution factors U_C, U_J and $U_{\tilde{\phi}}$. However, in the context of the RG evolution crossing a massive quark threshold they also imply a consistency relation between the mass mode threshold factors $\mathcal{M}_C$, $\mathcal{M}_J$

[20] The Wilson line regulator η in Refs. [40, 41] acts on the n-collinear sector and the soft-bin subtraction in the same way as the α-regulator and thus yields the same result for the anomalous dimensions.

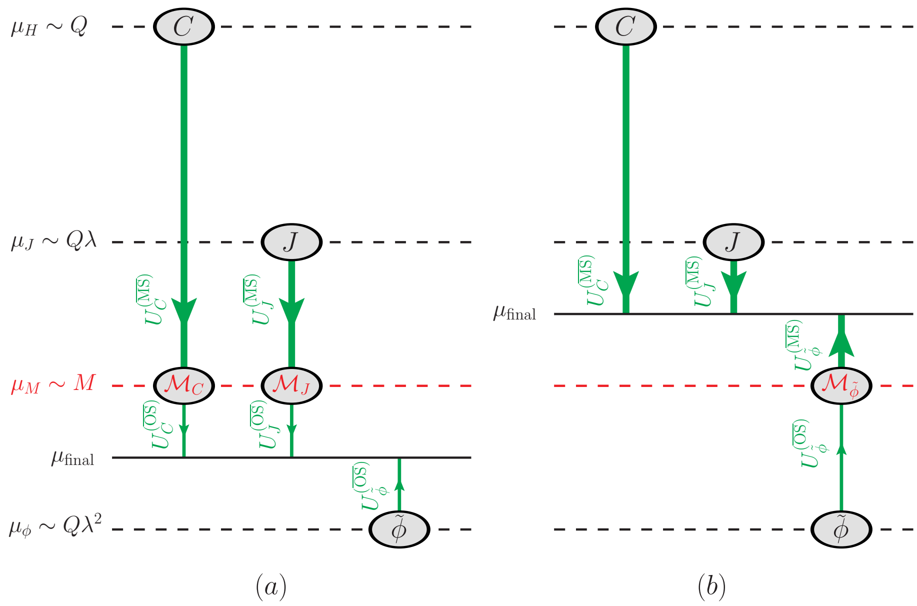

Figure 4.11: Illustration of the different RG setups for scenario III ($\mu_J > \mu_M > \mu_\phi$) leading to the consistency relations mentioned in the text. We display the cases where the final renormalization scale $\mu_{\rm final}$ satisfies (a) $\mu_M > \mu_{\rm final} > \mu_\phi$ and (b) $\mu_J > \mu_{\rm final} > \mu_M$.

and $\mathcal{M}_{\tilde\phi}$, the analogue for the PDF $\tilde\phi$. This can be used to gain interesting general insights into properties of mass singularities, and at the practical level, may be used as a non-trivial tool for consistency checks.

Apart from providing consistency checks of theoretical calculations, these relations have also computational power, as they can be used to calculate properties of independent gauge-invariant field theoretic objects once it has become clear that they represent building blocks of a factorization theorem. In the case of DIS these building blocks are the hard current coefficient, the jet function and the PDF. Hereby, one of the most interesting aspects is that the various building blocks can appear in different factorization theorems, as we will see in the discussion of event shapes in chapter 5, and one may gain insights into the mass-singularities of apparently unrelated quantities.

To be specific let us consider the factorization theorem in scenario III for a different choice of the final renormalization scale, namely the jet scale $\mu_{\rm final} = \mu_J$,

$$\begin{aligned} F_1(x,Q,M) = \sum_{i=q} \frac{e_i^2}{2} \left|C^{(\overline{\rm MS})}(Q,M,\mu_H)\right|^2 \left|U_C^{(\overline{\rm MS})}(Q,\mu_H,\mu_J)\right|^2 \\ \times \int {\rm d}s \int {\rm d}z \int {\rm d}z' \int {\rm d}z'' J^{(\overline{\rm MS})}(s,M,\mu_J)\, U_{\tilde\phi}^{(\overline{\rm MS})}(1-z-\frac{s}{Q^2},\mu_J,\mu_M) \\ \times \mathcal{M}_{\tilde\phi}(z-z',M,\mu_M)\, U_{\tilde\phi}^{(\rm OS)}(z'-z'',\mu_M,\mu_\phi)\, \tilde\phi_{i/P}^{(\rm OS)}\left(z''-x,\mu_\phi\right). \end{aligned} \tag{4.126}$$

Here the mass mode threshold factor $\mathcal{M}_{\tilde\phi}(1-z,M,\mu_M)$ arises since the RG evolution of the PDF $\tilde\phi$ crosses the massive quark threshold. This does not happen in the RG setup we discussed in Sec. 4.2, since there the final renormalization scale has always been set to the PDF scale. $\mathcal{M}_{\tilde\phi}$ differs from $\mathcal{M}_C$ and $\mathcal{M}_J$ in the fact that it corresponds to the correction when the mass modes are integrated in, i.e. that the threshold is crossed from below instead from above. [21]

The equivalence of the factorization theorems in Eqs. (4.65) and (4.126) implies, besides the relation between the evolution factors and anomalous dimensions shown in Eqs. (4.34) and (4.35) for n_f =

[21] In this respect we could have also defined either $\mathcal{M}_{\tilde\phi}$ or $\mathcal{M}_C$ and $\mathcal{M}_J$ via their inverse. However, it will be always clear from the context how we define the mass mode threshold corrections.

n_l, n_l+1, also a relation between the mass mode threshold factors,

$$\mathcal{M}_{\tilde{\phi}}(1-z, M, \mu) = Q^2 \,|\mathcal{M}_C(Q, M, \mu)|^2\, \mathcal{M}_J(Q^2(1-z), M, \mu)\,. \tag{4.127}$$

We have computed the PDF threshold condition for the radiation of a massive gluon at $\mathcal{O}(\alpha_s)$ already in the classical region in Sec. 3.4.2. The result in the endpoint region can be easily obtained from Eq. (3.91) by expanding for $z \to 1$,

$$\mathcal{M}^{(1)}_{\tilde{\phi}}(1-z, M, \mu) = \frac{\alpha_s C_F}{4\pi}\left\{\delta(1-z)\left[-3L_M + \frac{9}{2} - \frac{2\pi^2}{3}\right] - 4L_M\left[\frac{\theta(1-z)}{1-z}\right]_+\right\}. \tag{4.128}$$

Similar to the mass mode matching coefficient of the current and the jet function also $\mathcal{M}_{\tilde{\phi}}$ contains a large logarithm $\sim \ln(1-z)$, which is manifest when rescaling the plus-distribution using the identity in Eq. (B.3) in terms of the normalized soft momentum variable $\tilde{\ell} \equiv \ell/\nu_\phi$ with $\ell = Q(1-z)$ and the profile scale $\nu_\phi \sim Q(1-z) \sim \mu_J^2/\mu_H$,

$$\frac{\nu_\phi}{Q}\,\mathcal{M}^{(1)}_{\tilde{\phi}}\left(\frac{\ell}{Q}, M, Q, \mu, \nu_\phi\right) = \frac{\alpha_s C_F}{4\pi}\left\{\delta(\tilde{\ell})\left[-4L_M \ln\left(\frac{\nu_\phi}{Q}\right) - 3L_M + \frac{9}{2} - \frac{2\pi^2}{3}\right] - 4L_M\left[\frac{\theta(\tilde{\ell})}{\tilde{\ell}}\right]_+\right\}. \tag{4.129}$$

Note that the argument of the large logarithm is not depending on the mass scale μ_M or on the PDF scale μ_ϕ, but only on the ratio between the scales $\nu_\phi \sim Q(1-z)$ and Q related to the separation of the soft and $\bar{n}$-collinear modes in rapidity. Using the explicit fixed-order expressions for $\mathcal{M}^{(1)}_C$ in Eq. (4.85) and $\mathcal{M}^{(1)}_J$ in Eq. (4.115) one can check that the relation (4.127) is indeed satisfied at $\mathcal{O}(\alpha_s)$. Note that Eq. (4.127) shows in particular that the rapidity logarithms (and singularities) that arise in the current, jet and PDF sectors are intrinsically related to each other, which implies also that an exponentiation of the large logarithms also takes place in $\mathcal{M}_{\tilde{\phi}}$.

In the following we will compute the PDF threshold condition directly in the endpoint region and confirm that it gives the same fixed-order result as the one derived from $\mathcal{M}^{(1)}_{\phi,qq}$ in the classical regime. Since, however, for $x \to 1$ the collinear and soft contributions can be explicitly separated, the definition in Eq. (4.8) provides a way to resum the rapidity logarithm in Eq. (4.128) via the rapidity RGE.

PDF threshold correction

For the computation of the PDF threshold correction we have to consider both the collinear PDF function $f_{q/P}(\ell, \mu)$ and the soft function $S_\phi(\ell, \mu)$ defined in Eqs. (4.9) and (4.10), respectively. Since we are interested in the matching correction related to different employed schemes, we can perform the computation with partonic initial states. In the following we consider only the massive gluon contributions.

Let us start with the computation of the partonic collinear contribution $\hat{f}^{(1)}_{q/q}$, where the only contribution for massive gluon radiation at $\mathcal{O}(\alpha_s)$ is given by the virtual gluon contribution of the diagram in Fig. 3.12 (b) and which we denote by $f_{\bar{n}}$. After performing the k^-- and $k_\perp$-integrations we get in analogy to Eq. (3.78)

$$f_{\bar{n}} = -\frac{\alpha_s C_F}{2\pi}\,\delta(\ell)\,\Gamma\left(2-\frac{d}{2}\right)\left(\frac{\mu^2 e^{\gamma_E}}{M^2}\right)^{2-\frac{d}{2}} \int_0^Q \frac{\mathrm{d}k^+}{k^+}\left(1-\frac{k^+}{Q}\right)^{\frac{d}{2}-1}. \tag{4.130}$$

This piece is not regularized by dimensional regularization and in contrast to the computation in Sec. 3.4.2 there is no collinear real radiation contribution to cancel the corresponding rapidity divergences. Employing the α-regulator for the k^+-component in analogy to Eq. (4.66) and expanding for $\alpha \to 0$ gives the same result for the integral as for the current matching contribution in Eq. (4.73),

$$f_{\bar{n}} = \frac{\alpha_s C_F}{2\pi}\,\delta(\ell)\,\Gamma\left(2-\frac{d}{2}\right)\left(\frac{\mu^2 e^{\gamma_E}}{M^2}\right)^{2-\frac{d}{2}}\left\{\frac{1}{\alpha} + \ln\left(\frac{\nu}{Q}\right) + H_{\frac{d}{2}-1}\right\}. \tag{4.131}$$

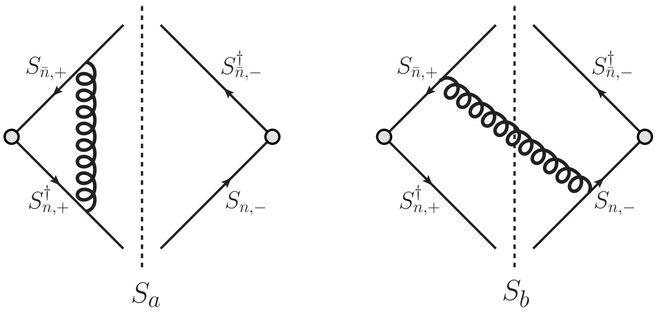

Figure 4.12: Non-vanishing Feynman diagrams for the computation of the one-loop massive gluon contributions to the soft function $S_\phi(\ell,\mu)$. The corresponding symmetric configurations are implied.

Now a corresponding function $f_{\bar n,0M}$ for the soft-bin subtractions has to be taken into account, which in general yields some additional contributions. [22] However, with our choice of regulator it vanishes in analogy to Eq. (4.75). Including the contribution from the wave function renormalization in Eq. (3.82) we obtain in total for the bare partonic collinear function

$$\begin{aligned}\hat f^{(\mathrm{bare},1)}_{q/q}(\ell,M,Q,\mu,\nu) &= 2\,(f_{\bar n} - f_{\bar n,0M}) - Z^{(1)}_\xi\,\delta(\ell)\\ &= \frac{\alpha_s C_F}{4\pi}\,\delta(\ell)\,\Gamma\left(2-\frac{d}{2}\right)\left(\frac{\mu^2 e^{\gamma_E}}{M^2}\right)^{2-\frac{d}{2}}\left\{\frac{4}{\alpha}+4\ln\left(\frac{\nu}{Q}\right)+4H_{\frac{d}{2}-1}-\frac{2(d-2)}{d}\right\}.\end{aligned} \tag{4.132}$$

Expanding for $d\to 4$ gives the unrenormalized correction

$$\begin{aligned}\hat f^{(\mathrm{bare},1)}_{q/q}(\ell,M,Q,\mu,\nu) = \frac{\alpha_s C_F}{4\pi}\,\delta(\ell)\bigg\{&\frac{4}{\alpha}\left[\frac{1}{\epsilon}-L_M+\mathcal{O}(\epsilon)\right]+\frac{1}{\epsilon}\left[4\ln\left(\frac{\nu}{Q}\right)+3\right]-4L_M\ln\left(\frac{\nu}{Q}\right)-3L_M\\ &+\frac{9}{2}-\frac{2\pi^2}{3}\bigg\}.\end{aligned} \tag{4.133}$$

Let us turn to the computation of the (partonic) soft matrix element $\hat S^{(1)}_\phi$, where the corresponding diagrams are shown in Fig. 4.12. The virtual diagram S_a is the analogue to the current diagram V_s in Eq. (4.68) and reads

$$S_a = V_s\,\delta(\ell)\,. \tag{4.134}$$

Using the α-regulator entails therefore, that S_a vanishes. The real radiation diagram S_b yields

$$S_b = 2ig^2 C_F\tilde\mu^{2\epsilon}\int\frac{\mathrm{d}^d k}{(2\pi)^d}\,\frac{1}{[k^- - i\epsilon]}\,\frac{1}{[k^+ - i\epsilon]}\,(-2\pi i)\,\theta(k^+ + k^-)\,\delta(k^2-M^2)\,\delta(\ell-k^+)\,. \tag{4.135}$$

Employing the α-regulator for the k^+ component and performing the k^+- and $k_\perp$-integrations gives

$$S_b = \frac{\alpha_s C_F}{2\pi}\,\frac{\left(\mu^2 e^{\gamma_E}\right)^{2-\frac{d}{2}}}{\Gamma\left(\frac{d}{2}-1\right)}\,\frac{\nu^\alpha}{\ell^{1+\alpha}}\int_{\frac{M^2}{\ell}}^\infty\frac{\mathrm{d}k^-}{k^-}\,\left(\ell\,k^- - M^2\right)^{\frac{d}{2}-2}\,. \tag{4.136}$$

Finally, expanding in α after the k^--integration yields (with $\bar\ell\equiv\ell/\nu$)

$$\nu\,S_b = \frac{\alpha_s C_F}{2\pi}\,\Gamma\left(2-\frac{d}{2}\right)\left(\frac{\mu^2 e^{\gamma_E}}{M^2}\right)^{2-\frac{d}{2}}\left\{-\frac{1}{\alpha}\,\delta(\bar\ell)+\left[\frac{\theta(\bar\ell)}{\bar\ell}\right]_+\right\}. \tag{4.137}$$

[22] Concerning the resummation of rapidity logarithms $f_{\bar n,0M}$ might be also associated with the soft function than with the collinear function.

Summing up all contributions the bare soft function reads in terms of $\tilde{\ell} \equiv \ell/\nu_\phi$

$$\begin{aligned}\nu_\phi\, S_\phi^{(\text{bare},1)}(\ell, M, \mu, \nu) &= 2\,\nu_\phi\,(S_a + S_b)\\ &= \frac{\alpha_s C_F}{4\pi}\,\Gamma\left(2-\frac{d}{2}\right)\left(\frac{\mu^2 e^{\gamma_E}}{M^2}\right)^{2-\frac{d}{2}}\left\{\delta(\tilde{\ell})\left[-\frac{4}{\alpha} - 4\ln\left(\frac{\nu}{\nu_\phi}\right)\right] + 4\left[\frac{\theta(\tilde{\ell})}{\tilde{\ell}}\right]_+\right\}.\end{aligned} \tag{4.138}$$

We emphasize that the computation of the soft diagrams does not require any collinear-bin subtractions in contrast to the calculation in Ref. [78]. [23] Expanding for $d \to 4$ yields

$$\begin{aligned}\nu_\phi\, S_\phi^{(\text{bare},1)}(\ell, M, \mu, \nu) = \frac{\alpha_s C_F}{4\pi}&\left\{\delta(\tilde{\ell})\left(-\frac{1}{\alpha}\left[\frac{4}{\epsilon} - 4L_M + \mathcal{O}(\epsilon)\right] - \left[\frac{4}{\epsilon} - 4L_M\right]\ln\left(\frac{\nu}{\nu_\phi}\right)\right)\right.\\ &\left.+\left[\frac{\theta(\tilde{\ell})}{\tilde{\ell}}\right]_+\left[\frac{4}{\epsilon} - 4L_M\right]\right\}.\end{aligned} \tag{4.139}$$

Upon combining the collinear and soft function the rapidity divergences cancel and the unrenormalized partonic PDF at $\mathcal{O}(\alpha_s)$ reads (see also Ref. [78])

$$\hat{\tilde{\phi}}_{q/q}^{(\text{bare},1)}(1-z, M, \mu) = \frac{\alpha_s C_F}{4\pi}\left\{\delta(1-z)\left[\frac{3}{\epsilon} - 3L_M + \frac{9}{2} - \frac{2\pi^2}{3}\right] + \left[\frac{\theta(1-z)}{1-z}\right]_+\left[\frac{4}{\epsilon} - 4L_M\right]\right\}. \tag{4.140}$$

Renormalizing the PDF in the $\overline{\text{MS}}$ scheme implies that the same counterterm is used as for massless quarks given in Eq. (4.20), whereas in OS renormalization the counterterm is

$$Z_{\tilde{\phi}}^{(\text{OS},1)}(1-z, M, \mu) = \hat{\tilde{\phi}}_{q/q}^{(\text{bare},1)}(1-z, M, \mu)\,. \tag{4.141}$$

The threshold correction for the PDF is related to the difference in the employed schemes in analogy to Eq. (3.42) and is thus given at one loop by

$$\mathcal{M}_{\tilde{\phi}}^{(1)}(1-z, M, \mu) = \hat{\tilde{\phi}}_{q/q}^{(\text{bare},1)}(1-z, M, \mu) - Z_{\tilde{\phi}}^{(1)}(1-z, M, \mu)\,, \tag{4.142}$$

which yields Eq. (4.128).

In the same way as for the hard current and jet threshold correction we can also resum the rapidity logarithms in the PDF matching factor. We see that $\hat{f}_{q/q}^{(1)}$ is free of large logarithms for $\nu = \nu_f \sim Q$, and $\hat{S}_\phi^{(1)}$ is free of large logarithms for $\nu = \nu_S \sim \nu_\phi \sim Q(1-x)$. The resulting counterterms associated to the PDF mass mode matching coefficient read

$$\nu_\phi\, Z_{\tilde{\phi},f}^{(\overline{\text{MS}},1)} = \frac{\alpha_s C_F}{4\pi}\,\delta(\tilde{\ell})\left\{\frac{4}{\alpha}\left[\frac{1}{\epsilon} - L_M + \mathcal{O}(\epsilon)\right] + \frac{1}{\epsilon}\left[4\ln\left(\frac{\nu}{Q}\right) + 3\right]\right\}, \tag{4.143}$$

$$\nu_\phi\, Z_{\tilde{\phi},S}^{(\overline{\text{MS}},1)} = \frac{\alpha_s C_F}{4\pi}\left\{\delta(\tilde{\ell})\left(-\frac{4}{\alpha}\left[\frac{1}{\epsilon} - L_M + \mathcal{O}(\epsilon)\right] - \frac{4}{\epsilon}\ln\left(\frac{\nu}{\nu_\phi}\right)\right) + \frac{4}{\epsilon}\left[\frac{\theta(\tilde{\ell})}{\tilde{\ell}}\right]_+\right\}. \tag{4.144}$$

The ν-evolution equation for the collinear and soft function contributions ($i = f, S$) to the threshold correction reads

$$\nu\frac{\mathrm{d}}{\mathrm{d}\nu}\,\mathcal{M}_{\tilde{\phi},i}(\ell, M, Q, \mu, \nu) = \left(\gamma_{\tilde{\phi},i,\nu} - \gamma_{\tilde{\phi},i,\nu}^{(\text{OS})}\right)\mathcal{M}_{\tilde{\phi},i}(\ell, M, Q, \mu, \nu) \equiv \gamma_{\mathcal{M}_{\tilde{\phi},i}}\,\mathcal{M}_{\tilde{\phi},i}(\ell, M, Q, \mu, \nu)\,, \tag{4.145}$$

[23] This is not related to the fact that in the computation in Ref. [78] the Wilson line regulator η was used. Repeating their calculation we obtain a different result for the soft real radiation contribution that yields with the corresponding virtual contribution (with which we agree) directly the soft function in Eq. (4.138).

where the anomalous dimensions $\gamma^{(\rm OS)}_{\tilde\phi,i,\nu}$ corresponding to counterterms in the OS scheme employed below the mass threshold vanish for the massive gluon at $\mathcal{O}(\alpha_s)$. We see that the RGE in Eq. (4.145) is again local. The ν-anomalous dimensions at $\mathcal{O}(\alpha_s)$ can be read off from the counterterm contributions in Eqs. (4.143) and (4.144), [24]

$$\gamma^{(1)}_{\tilde\phi,f,\nu} = -\,\nu\frac{\mathrm{d}}{\mathrm{d}\nu}\,Z^{(\overline{\rm MS},1)}_{\tilde\phi,f} = -\frac{\alpha_s C_F}{4\pi}\,4L_M = -\Gamma^{(1)}_{\rm cusp}\,L_M\,, \tag{4.146}$$

$$\gamma^{(1)}_{\tilde\phi,S,\nu} = -\,\nu\frac{\mathrm{d}}{\mathrm{d}\nu}\,Z^{(\overline{\rm MS},1)}_{\tilde\phi,S} = \frac{\alpha_s C_F}{4\pi}\,4L_M = -\gamma^{(1)}_{\tilde\phi,f,\nu}\,. \tag{4.147}$$

Solving Eq. (4.145), which leads to the anticipated exponentiation, and expanding out the terms that do not involve large logarithms leads to (with $\nu_S = \nu_\phi$)

$$\frac{\nu_\phi}{Q}\,\mathcal{M}_{\tilde\phi}\Big(\frac{\ell}{Q},M,Q,\mu_M,\nu_f,\nu_\phi\Big) = \exp\left[\frac{\alpha_s C_F}{\pi}\,L_M\ln\Big(\frac{\nu_f}{\nu_\phi}\Big)\right]\Bigg(1+\frac{\alpha_s C_F}{4\pi}\bigg\{\delta(\tilde\ell)\left[-4L_M\ln\Big(\frac{\nu_f}{Q}\Big)\right.$$
$$\left. -\,3L_M+\frac{9}{2}-\frac{2\pi^2}{3}\right]-4L_M\left[\frac{\theta(\tilde\ell)}{\tilde\ell}\right]_+\bigg\}\Bigg)\,. \tag{4.148}$$

4.3.4 Fixed-order expansion and comparison with full QCD result

Each of the factorization theorems discussed at the beginning of Sec. 4.3 contains all information about the singular $\mathcal{O}(\alpha_s)$ secondary massive gluon corrections to the structure function $F_1(x,Q,m)$ in the fixed-order expansion. Besides the virtual contributions in QCD, which are fully contained in the SCET description, the singular perturbative fixed-order corrections consist also of the singular collinear real radiation contributions which arise for $1-x\sim M^2/Q^2\ll 1$. Setting $\mu=\mu_H=\mu_J=\mu_M$ we obtain in any scenario

$$F_1(x,Q,M)\big|_{\rm FO} = \sum_{i=q}\frac{e_i^2}{2}\int\mathrm{d}\xi\,\underbrace{Q^2\big|C^{(\rm OS)}(Q,M,\mu)\big|^2\,J^{(\rm OS)}(Q^2(1-\xi),M,\mu)}_{\equiv\,\mathcal{C}^{(\rm OS)}_{x\to1}(\xi,Q,M,\mu)}\,\tilde\phi^{(\rm OS)}_{i/P}\Big(\xi-x,\mu\Big)\,. \tag{4.149}$$

where the massive gluon contributions to the fixed-order matching coefficient $\mathcal{C}^{(\rm OS)}_{x\to1}$ at $\mathcal{O}(\alpha_s)$ read

$$\mathcal{C}^{(\rm OS,1)}_{x\to1,M}(z,Q,M) = 2\hat F^{(1)}_{M,\rm QCD}(Q,M)\,\delta(1-z)+Q^2J^{(1)}_{M,\rm real}(Q^2(1-z),M) \tag{4.150}$$

with $\hat F^{(1)}_{M,\rm QCD}(Q,M)$ and $J^{(1)}_{M,\rm real}(s,M)$ given in Eqs. (3.70) and (4.107), respectively. In the following we show as a cross-check that this result can be obtained from the corresponding full QCD fixed-order computation in Sec. 3.4.2, i.e.

$$\mathcal{C}^{(\rm OS,1)}_{qq}(z,Q,M)\xrightarrow{z\to1}\mathcal{C}^{(\rm OS,1)}_{x\to1,M}(z,Q,M) \tag{4.151}$$

with $\mathcal{C}^{(\rm OS,1)}_{qq}(z,Q,M)$ given in Eq. (3.88), and discuss the required expansion for $z\to1$. As stated before, we see that the terms in the δ-distributions agree, which means that the SCET does not perform any expansion for the virtual contributions. The term $\hat F^{(1)}_{M,\rm QCD,\theta}(z,Q,M)$ in the full QCD fixed-order result in Eq. (3.88), which contains the threshold $\theta(1-z-\hat M^2 z)$ (with $\hat M\equiv M/Q$), contains the collinear real radiation contributions. In the endpoint region the jet invariant mass $Q\sqrt{1-z}$ and the mass M have to be considered of the same order to account for real radiation effects in the singular expression. Thus we have to expand in terms of $1-z\sim\hat M^2\ll1$ and obtain

$$\theta(1-z-\hat M^2 z)\,\hat F^{(1)}_{M,\rm QCD,\theta}(z,Q,M)\xrightarrow{z\to1}\frac{\alpha_s C_F}{4\pi}\,\theta(1-z-\hat M^2)\left\{-\frac{\Big(1-z-\hat M^2\Big)\Big(3(1-z)+\hat M^2\Big)}{(1-z)^3}\right.$$
$$\left.+\,\frac{4}{1-z}\ln\Big(\frac{1-z}{\hat M^2}\Big)\right\}+\mathcal{O}\Big((1-z)^0,\hat M^0\Big)\,, \tag{4.152}$$

[24]The Wilson line regulator η yields the same result for the anomalous dimensions, see also Ref. [78].

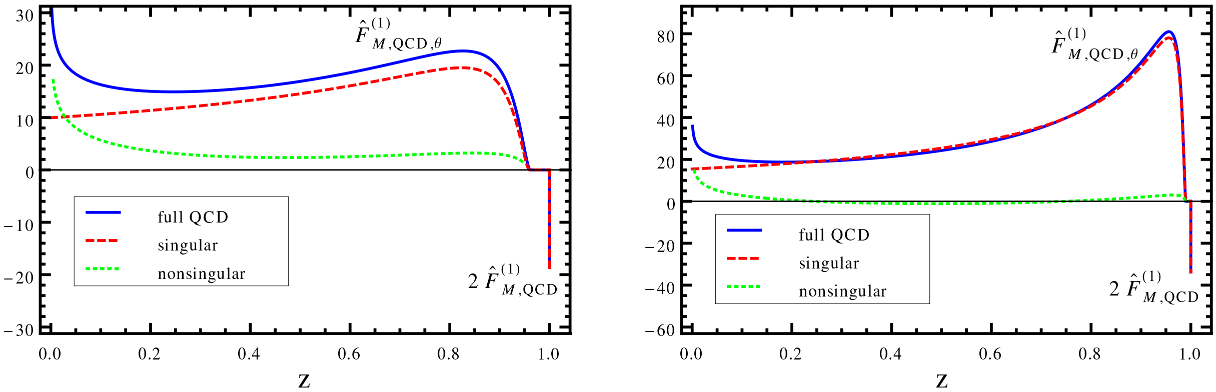

Figure 4.13: Massive gluon contributions at $\mathcal{O}(\alpha_s)$ in full QCD (blue, solid) together with the singular result for $z \to 1$ in the fixed-order expansion (red, dashed) and the nonsingular terms (green, dotted) for $\hat{M} = 0.2$ (left panel) and $\hat{M} = 0.1$ (right panel), all normalized by $\alpha_s C_F/(4\pi)$.

which is equivalent to the term $Q^2 J^{(1)}_{M,\mathrm{real}}(Q^2(1-z), M)$.

In Fig. 4.13 we display the full fixed-flavor QCD term $\mathcal{C}^{(\mathrm{OS},1)}_{qq}(z, Q, M)$ (blue, solid line), the singular fixed-order terms corresponding to the SCET result in Eq. (4.150) (red, dashed line) and the remaining nonsingular terms (green, dotted line) for $\hat{M} = 0.2$ and $\hat{M} = 0.1$. Here the singular contributions are in fact dominant even up to small z. For small masses we see that the fixed-order expansion of the fixed flavor result undergoes big changes related to large mass logarithms which render the perturbative expansion unstable and which should be resummed by a proper VFNS description.

An important difference of the factorization theorems in the SCET setup compared to the fixed-order QCD expansion is that in the former the various components are calculated in different renormalization schemes to allow for the summation of logarithms involving ratios of the scales Q^2, $Q^2(1-x)$ and M^2, as discussed at the beginning of Sec. 4.3. A maybe even more notable difference is that the consistent and IR-safe definition of the jet function entails that virtual corrections have non-vanishing support for finite values of $1-z$, so that they do not only arise in coefficients of $\delta(1-z)$, but also in coefficients involving plus-distributions $(\ln^n(1-z)/(1-z))_+$. In contrast, the fixed-order expansion contains only real radiation corrections for finite values of $1-z$ and virtual corrections proportional to $\delta(1-z)$ each of which is individually IR-divergent for $M \to 0$. The rearrangement of virtual and mass-singular corrections, which is intrinsically connected to the consistency relation of Eq. (4.127), is the basis of rendering the hard coefficient and the jet function in the factorization theorems IR-safe in the limit $M \to 0$. This may provide a guideline to understand the factorization from the point of view of the fixed-order expansion.

4.4 Two-loop computations for secondary massive quarks

After having calculated all secondary massive gluon results at $\mathcal{O}(\alpha_s)$ we are now able to apply the dispersion relations in Sec. 3.4.1 to obtain the secondary massive quark corrections at $\mathcal{O}(\alpha_s^2 C_F T_F)$ to the hard current coefficient, the jet function and the corresponding massive threshold corrections, which were already given in the discussion of the factorization theorems in Sec. 4.2.

4.4.1 Hard current matching coefficient and threshold correction

Current matching coefficient

Following Eq. (3.62) we can obtain the $\mathcal{O}(\alpha_s^2 C_F T_F)$ secondary massive quark form factor corrections relevant for the hard current matching calculation with the on-shell subtraction for the strong coupling by the relations

$$\hat{F}^{(n_l,2)}_{m,\mathrm{QCD}}(Q,m) = \frac{1}{\pi}\int \frac{\mathrm{d}M^2}{M^2}\,\hat{F}^{(1)}_{M,\mathrm{QCD}}(Q,M)\,\mathrm{Im}\left[\Pi(m^2,M^2)\right]\,, \tag{4.153}$$

$$\hat{F}^{(n_l,\mathrm{bare},2)}_{m,\mathrm{SCET}}(Q,m,\mu) = \frac{1}{\pi}\int \frac{\mathrm{d}M^2}{M^2}\,\hat{F}^{(\mathrm{bare},1)}_{M,\mathrm{SCET}}(Q,M,\mu)\,\mathrm{Im}\left[\Pi(m^2,M^2)\right]\,, \tag{4.154}$$

where $\hat{F}^{(1)}_{M,\mathrm{QCD}}(Q,M)$ ($\hat{F}^{(\mathrm{bare},1)}_{M,\mathrm{SCET}}(Q,M,\mu)$) denotes the one-loop massive gluon form factor in QCD (SCET) computed in Eqs. (3.70) (in Eq. (4.76)). The full QCD correction at two loop, $\hat{F}^{(n_l,2)}_{m,\mathrm{QCD}}$, is both IR- and UV-finite, has been computed in Sec. 3 and is given in Eq. (3.95).

Carrying out the convolution in Eq. (4.154) for the bare SCET form factor in $d = 4-2\epsilon$ dimensions and expanding in ϵ we obtain ($L_Q \equiv \ln(Q^2/\mu^2), \hat{m} \equiv m/Q$)

$$\begin{aligned}
\hat{F}^{(n_l,\mathrm{bare},2)}_{m,\mathrm{SCET}}(Q,m,\mu) = \frac{\big(\alpha_s^{(n_l)}\big)^2 C_F T_F}{(4\pi)^2}\bigg\{&\frac{2}{\epsilon^3} + \frac{1}{\epsilon^2}\left[-\frac{8}{3}\ln(\hat{m}^2) - 4L_Q + \frac{8}{9}\right] + \frac{1}{\epsilon}\left[\frac{4}{3}\ln^2(\hat{m}^2) + \frac{16}{3}\ln(\hat{m}^2)L_Q\right.\\
&\left. + 4L_Q^2 - 4\ln(\hat{m}^2) - \frac{16}{9}L_Q - \left(\frac{65}{27}+\frac{\pi^2}{9}\right)\right] - \frac{8}{3}\ln^2(\hat{m}^2)\,L_Q - \frac{16}{3}\ln(\hat{m}^2)L_Q^2\\
&- \frac{8}{3}L_Q^3 + \frac{56}{9}\ln^2(\hat{m}^2) + 8\ln(\hat{m}^2)\,L_Q + \frac{16}{9}L_Q^2 + \left(\frac{242}{27}+\frac{4\pi^2}{9}\right)\ln(\hat{m}^2)\\
&+ \left(\frac{130}{27}+\frac{2\pi^2}{9}\right)L_Q + \frac{875}{54} + \frac{8\pi^2}{9} - \frac{20}{3}\zeta_3\bigg\}\,.
\end{aligned} \tag{4.155}$$

If we renormalize the current using the OS condition, the corresponding counterterm contribution associated to the Wilson coefficient reads

$$Z^{(n_l,2)}_{C,m}(Q,m,\mu) = -\hat{F}^{(n_l,\mathrm{bare},2)}_{m,\mathrm{SCET}}(Q,m,\mu)\,, \tag{4.156}$$

such that no finite corrections remain in the renormalized SCET result and the hard matching coefficient just contains the full QCD corrections in the n_l-scheme,

$$C^{(n_l,2)}_{T_F}(Q,m,\mu) = C^{(n_l,2)}_{T_F}(Q,\mu) + \hat{F}^{(n_l,2)}_{m,\mathrm{QCD}}(Q,m)\,. \tag{4.157}$$

This Wilson coefficient corresponds to the one used for scenario I in Sec. 4.2.

Since $\hat{F}^{(n_l,2)}_{m,\mathrm{QCD}}$ and $\hat{F}^{(n_l,2)}_{m,\mathrm{SCET}}$ have been computed with the subtracted dispersion relation they correspond to expressions in the n_l flavor scheme for the strong coupling. To switch to the (n_l+1)-flavor scheme one has to add the $\overline{\mathrm{MS}}$-subtracted vacuum polarization function at zero-momentum times the corresponding one-loop form factor, i.e.

$$\hat{F}^{(n_l+1,2)}_{m,\mathrm{QCD}}(Q,m,\mu,\Delta) = \hat{F}^{(n_l,2)}_{m,\mathrm{QCD}}(Q,m) - \left(\Pi(m^2,0) - \frac{\alpha_s T_F}{3\pi}\,\frac{1}{\epsilon}\right)\hat{F}^{(1)}_{\mathrm{QCD}}(Q,\mu,\Delta)\,, \tag{4.158}$$

$$\hat{F}^{(n_l+1,\mathrm{bare},2)}_{m,\mathrm{SCET}}(Q,m,\mu,\Delta) = \hat{F}^{(n_l,\mathrm{bare},2)}_{m,\mathrm{SCET}}(Q,m,\mu) - \left(\Pi(m^2,0) - \frac{\alpha_s T_F}{3\pi}\,\frac{1}{\epsilon}\right)\hat{F}^{(\mathrm{bare},1)}_{\mathrm{SCET}}(Q,\mu,\Delta)\,, \tag{4.159}$$

where $\hat{F}^{(1)}_{\mathrm{QCD}}(Q,\mu,\Delta)$ ($\hat{F}^{(\mathrm{bare},1)}_{\mathrm{SCET}}(Q,\mu,\Delta)$) is the (bare) massless gluon one-loop QCD (SCET) form factor calculated with an IR regulator Δ. To obtain the matching coefficient one should in principle first renormalize both quantities and then calculate their difference where the dependence on Δ cancels. Since the QCD current is UV finite, it is convenient to revert this procedure in analogy to the computation in Sec. 3.4.3, i.e. to first determine the difference of the unrenormalized quantities and renormalize the UV divergences in the SCET contribution at the very end, such that the cancellation of the IR divergences can be made explicit from the beginning. The difference of the massless gluon one-loop QCD and SCET form factors has the form [25]

$$\hat{F}^{(1)}_{\mathrm{QCD}}(Q,\mu,\Delta) - \hat{F}^{(\mathrm{bare},1)}_{\mathrm{SCET}}(Q,\mu,\Delta) = Z^{(1)}_C(Q,\mu) + C^{(1)}(Q,\mu)\,, \tag{4.160}$$

[25] Using dimensional regularization for both UV and IR divergences the SCET form factor for massless gluons vanishes identically.

where the hard matching coefficient at one-loop $C^{(1)}(Q,\mu)$ and the corresponding counterterm $Z_C^{(1)}(Q,\mu)$ are given in Eqs. (4.12) and (4.14), respectively. The additional term corresponding to the change from the n_l- to the (n_l+1)-flavor scheme thus reads

$$\begin{aligned}
C^{(n_l\to n_l+1,2)}(Q,m,\mu) &= -\left(\Pi(m^2,0)-\frac{\alpha_s T_F}{3\pi}\frac{1}{\epsilon}\right)\left(Z_C^{(1)}(Q,\mu)+C^{(1)}(Q,\mu)\right)\\
&=\frac{\alpha_s^2 C_F T_F}{(4\pi)^2}\bigg\{\frac{1}{\epsilon^2}\left[-\frac{8}{3}\ln(\hat m^2)-\frac{8}{3}L_Q\right]+\frac{1}{\epsilon}\bigg[\frac{4}{3}\ln^2(\hat m^2)+\frac{16}{3}\ln(\hat m^2)L_Q+4L_Q^2\\
&\quad-4\ln(\hat m^2)-4L_Q+\frac{2\pi^2}{9}\bigg]-\frac{4}{9}\ln^3(\hat m^2)-\frac{8}{3}\ln^2(\hat m^2)L_Q-\frac{16}{3}\ln(\hat m^2)L_Q^2\\
&\quad-\frac{28}{9}L_Q^3+2\ln^2(\hat m^2)+8\ln(\hat m^2)L_Q+6L_Q^2-\frac{32}{3}\ln(\hat m^2)-\left(\frac{32}{3}+\frac{2\pi^2}{9}\right)L_Q\\
&\quad+\frac{\pi^2}{3}-\frac{8}{9}\zeta_3\bigg\}\,. \qquad (4.161)
\end{aligned}$$

Combining all contributions and including the $\overline{\rm MS}$ current counterterm contribution $Z_{C,T_F}^{(n_l+1,2)}$ given in Eq. (4.15), the result for the $\mathcal{O}(\alpha_s^2 C_F T_F)$ secondary massive quark contributions to the hard current coefficient in the (n_l+1)-flavor scheme, denoted by $\delta C_m^{(n_l+1,2)}$, reads

$$\delta C_m^{(n_l+1,2)}(Q,m,\mu)=\hat F_{m,\rm QCD}^{(n_l,2)}(Q,m)-\hat F_{m,\rm SCET}^{(n_l,\rm bare,2)}(Q,m,\mu)+C^{(n_l\to n_l+1,2)}(Q,m,\mu)-Z_{C,T_F}^{(n_l+1,2)}(Q,\mu)\,, \qquad (4.162)$$

with $\alpha_s=\alpha_s^{(n_l+1)}(\mu)$ employed in $\delta C_m^{(n_l+1,2)}$ at the end. Inserting Eqs. (4.15), (4.155) and (4.161) gives (see also Ref. [26])

$$\begin{aligned}
\delta C_m^{(n_l+1,2)}(Q,m,\mu) &= \hat F_{m,\rm QCD}^{(n_l,2)}(Q,m)+\frac{\big(\alpha_s^{(n_l+1)}\big)^2 C_F T_F}{(4\pi)^2}\bigg\{-\frac{4}{9}\ln^3(\hat m^2)-\frac{4}{9}L_Q^3-\frac{38}{9}\ln^2(\hat m^2)+\frac{38}{9}L_Q^2\\
&\quad+\left(\frac{530}{27}+\frac{4\pi^2}{9}\right)\ln(\hat m^2)-\left(\frac{418}{27}+\frac{4\pi^2}{9}\right)L_Q-\frac{875}{54}-\frac{5\pi^2}{9}+\frac{52}{9}\zeta_3\bigg\}\,, \qquad (4.163)
\end{aligned}$$

Subtracting from Eq. (4.162) the massless limit in Eq. (4.13) we obtain the mass corrections to the form factor in $\overline{\rm MS}$ renormalization for the scenarios II and III in Sec. 4.2, $\hat F_{\Delta m}(Q,m)$, defined in Eq. (4.42). We see from the result of Eq. (4.43) that the SCET matching procedure in the (n_l+1)-flavor scheme does in principle nothing else than exactly subtracting the asymptotic massless limit from the full QCD on-shell form factor correction. This is expected since the IR sensitivity has to cancel at leading order in m/Q if the factorization in Sec. (4.1) has been set up properly, such that the SCET calculation can be seen as consistency check without providing new essential information.

Hard current threshold correction

The mass mode threshold factor $\mathcal{M}_C(Q,m,\mu_m)$ is straightforward to determine from the relation between the renormalized hard current coefficients in the OS and $\overline{\rm MS}$ scheme at the scale μ_m. The matching accounts for the difference between the two schemes and is obtained by the relation

$$\mathcal{M}_C(Q,m,\mu_m)=\frac{C^{(n_l)}(Q,m,\mu_m)}{C^{(n_l+1)}(Q,m,\mu_m)}=\frac{Z_C^{(n_l+1)}(Q,\mu_m)}{Z_C^{(n_l)}(Q,m,\mu_m)}=\frac{Z_{\mathcal{J}}^{(n_l)}(Q,\mu_m)}{Z_{\mathcal{J}}^{(n_l+1)}(Q,m,\mu_m)}\,. \qquad (4.164)$$

Since the difference in the factorization theorems for scenario I and II in Eqs. (4.37) and (4.41) concerns just the current matching coefficient and evolution, Eq. (4.164) makes it evident that the condition for the current mass mode matching coefficient automatically implements a continuous transition between these two scenarios. In the border region between the two scenarios, i.e. $m\sim\mu_m\sim\mu_H\sim Q$, the same mass-shell contributions are just swapped between the Wilson coefficient and the mass mode matching coefficient.

Since the expressions in Eq. (4.164) are written in different schemes for α_s one has to relate them by the decoupling relation for α_s in Eq. (3.112). Using the structure of the Wilson coefficients in Eqs. (4.38) and (4.42), we obtain at $\mathcal{O}(\alpha_s^2)$ in the fixed-order counting ($L_m = \ln(m^2/\mu^2)$)

$$\mathcal{M}_C(Q,m,\mu) = 1 + \hat{F}^{(n_l,2)}_{m,\mathrm{QCD}}(Q,m) - \delta C_m^{(n_l+1,2)}(Q,m,\mu) + \frac{\alpha_s^{(n_l+1)}T_F}{3\pi}\, L_m C^{(n_l+1,1)}(Q,\mu) + \mathcal{O}(\alpha_s^3)\,. \tag{4.165}$$

Inserting all explicit expressions gives at $\mathcal{O}(\alpha_s^2)$ in the fixed-order counting we find

$$\begin{aligned}\mathcal{M}_C^{(2)}(Q,m,\mu_m) = \frac{\alpha_s^2 C_F T_F}{16\pi^2}\bigg\{&\bigg[\frac{4}{3}L_m^2 + \frac{40}{9}L_m + \frac{112}{27}\bigg]\ln\!\bigg(\frac{m^2}{Q^2}\bigg) - \frac{8}{9}L_m^3 - \frac{2}{9}L_m^2 + \bigg(\frac{130}{27} + \frac{2\pi^2}{3}\bigg)L_m \\ &+ \frac{875}{54} + \frac{5\pi^2}{9} - \frac{52}{9}\zeta_3\bigg\}\,.\end{aligned} \tag{4.166}$$

Since there are no $\mathcal{O}(\alpha_s)$ one-loop corrections the schemes of α_s and the mass appearing in Eq. (4.166) do not need to be specified at this point. In Eq. (4.166) we see explicitly the large rapidity logarithm $\ln\big(m^2/Q^2\big)$ which enforces the counting $\alpha_s \ln(m^2/Q^2) \sim 1$.

We will now set up a RG evolution in rapidity space to resum the associated higher order logarithms in analogy to the one-loop case described in Sec. 4.3.1. As in Eq. (4.86) we decompose the bare SCET form factor in terms of n-collinear, $\bar{n}$-collinear and soft contributions. Note that the scheme difference of the strong coupling above and below threshold requires that also the one-loop corrections for the radiation of a massless gluon have to be accounted for and should be decomposed in the same way. To achieve this goal we will use a gluon mass $\Lambda \ll m$ as an infrared regulator which allows us to apply the results in Sec. 4.3.1. We write the two-loop contributions as

$$\begin{aligned}\hat{F}^{(n_l+1,\mathrm{bare},2)}_{m,\mathrm{SCET},i}(Q,m,\Lambda,\mu,\nu) = &\frac{1}{\pi}\int\frac{\mathrm{d}M^2}{M^2}\,\hat{F}^{(\mathrm{bare},1)}_{M,\mathrm{SCET},i}(Q,M,\mu,\nu)\,\mathrm{Im}\left[\Pi(m^2,M^2)\right] \\ &-\bigg(\Pi(m^2,0) - \frac{\alpha_s^{(n_l+1)}T_F}{3\pi}\frac{1}{\epsilon}\bigg)\hat{F}^{(\mathrm{bare},1)}_{M,\mathrm{SCET,i}}(Q,\Lambda,\mu,\nu)\,,\end{aligned} \tag{4.167}$$

with $i = n, \bar{n}, s$ and the nonvanishing one-loop massive gluon corrections $\hat{F}^{(\mathrm{bare},1)}_{M,\mathrm{SCET},i}$ given in Eqs. (4.87) and (4.88). We will display the rapidity divergent collinear and soft contributions using the α-regulator in Eq. (4.66). After performing the subtracted dispersion relation and including the scheme change contribution we obtain for the individual sectors ($L_\Lambda = \ln(\Lambda^2/\mu^2)$)

$$\begin{aligned}\hat{F}^{(n_l+1,\mathrm{bare},2)}_{m,\mathrm{SCET},n} = &\frac{\big(\alpha_s^{(n_l+1)}\big)^2 C_F T_F}{16\pi^2}\bigg\{\frac{1}{\alpha}\bigg[\frac{4}{3\epsilon^2} - \frac{20}{9\epsilon} - \frac{8}{3}L_m L_\Lambda + \frac{4}{3}L_m^2 + \frac{40}{9}L_m + \frac{112}{27} + \mathcal{O}(\epsilon)\bigg] \\ &+ \frac{1}{\epsilon^2}\bigg[\frac{4}{3}\ln\!\bigg(\frac{\nu}{Q}\bigg) + 1\bigg] + \frac{1}{\epsilon}\bigg[-\frac{20}{9}\ln\!\bigg(\frac{\nu}{Q}\bigg) - \frac{1}{6} - \frac{2\pi^2}{9}\bigg] + \bigg(-\frac{8}{3}L_m L_\Lambda + \frac{4}{3}L_m^2 \\ &+ \frac{40}{9}L_m + \frac{112}{27}\bigg)\ln\!\bigg(\frac{\nu}{Q}\bigg) - 2L_m L_\Lambda + L_m^2 + \frac{10}{3}L_m + \frac{73}{36} + \frac{10\pi^2}{27} - \frac{4}{3}\zeta_3\bigg\}\,,\end{aligned} \tag{4.168}$$

$$\begin{aligned}\hat{F}^{(n_l+1,\mathrm{bare},2)}_{m,\mathrm{SCET},\bar{n}} = &\frac{\big(\alpha_s^{(n_l+1)}\big)^2 C_F T_F}{16\pi^2}\bigg\{\frac{1}{\alpha}\bigg[-\frac{4}{3\epsilon^2} + \frac{20}{9\epsilon} + \frac{8}{3}L_m L_\Lambda - \frac{4}{3}L_m^2 - \frac{40}{9}L_m - \frac{112}{27} + \mathcal{O}(\epsilon)\bigg] \\ &+ \frac{2}{\epsilon^3} + \frac{1}{\epsilon^2}\bigg[-\frac{4}{3}\ln\!\bigg(\frac{\nu}{Q}\bigg) - \frac{4}{3}L_Q - \frac{1}{9}\bigg] + \frac{1}{\epsilon}\bigg[\frac{20}{9}\ln\!\bigg(\frac{\nu}{Q}\bigg) + \frac{20}{9}L_Q - \frac{121}{54} - \frac{\pi^2}{9}\bigg] \\ &+ \bigg(\frac{8}{3}L_m L_\Lambda - \frac{4}{3}L_m^2 - \frac{40}{9}L_m - \frac{112}{27}\bigg)\bigg[\ln\!\bigg(\frac{\nu}{Q}\bigg) + L_Q\bigg] - \frac{4}{3}L_m L_\Lambda^2 - 2L_m L_\Lambda + \frac{4}{9}L_m^3 \\ &+ \frac{29}{9}L_m^2 + \bigg(\frac{314}{27} - \frac{4\pi^2}{9}\bigg)L_m + \frac{1531}{108} + \frac{5\pi^2}{27} - \frac{40}{9}\zeta_3\bigg\}\,,\end{aligned} \tag{4.169}$$

and $\hat{F}^{(n_l+1,\mathrm{bare},2)}_{m,\mathrm{SCET},s} = 0$. Therefore, the nonvanishing two-loop counterterm contributions above threshold, where we use $\overline{\mathrm{MS}}$-renormalization, read for the current [26]

$$\begin{aligned}
Z^{(n_l+1,2)}_{\mathcal{J},n,T_F} = & \frac{\alpha_s^{(n_l+1)}(\mu,\nu)\,\alpha_s^{(n_l+1)}(\mu)\,C_F T_F}{16\pi^2}\left\{\frac{1}{\alpha}\left[\frac{4}{3\epsilon^2} - \frac{20}{9\epsilon} - \frac{8}{3}L_m L_\Lambda + \frac{4}{3}L_m^2 + \frac{40}{9}L_m + \frac{112}{27} + \mathcal{O}(\epsilon)\right]\right. \\
& \left. + \frac{1}{\epsilon^2}\left[\frac{4}{3}\ln\left(\frac{\nu}{Q}\right) + 1\right] + \frac{1}{\epsilon}\left[-\frac{20}{9}\ln\left(\frac{\nu}{Q}\right) - \frac{1}{6} - \frac{2\pi^2}{9}\right]\right\}, \qquad (4.170)\\
Z^{(n_l+1,2)}_{\mathcal{J},\bar{n},T_F} = & \frac{\alpha_s^{(n_l+1)}(\mu,\nu)\,\alpha_s^{(n_l+1)}(\mu)\,C_F T_F}{16\pi^2}\left\{\frac{1}{\alpha}\left[-\frac{4}{3\epsilon^2} + \frac{20}{9\epsilon} + \frac{8}{3}L_m L_\Lambda - \frac{4}{3}L_m^2 - \frac{40}{9}L_m - \frac{112}{27} + \mathcal{O}(\epsilon)\right]\right. \\
& \left. + \frac{2}{\epsilon^3} + \frac{1}{\epsilon^2}\left[-\frac{4}{3}\ln\left(\frac{Q\,\nu}{\mu^2}\right) - \frac{1}{9}\right] + \frac{1}{\epsilon}\left[\frac{20}{9}\ln\left(\frac{Q\,\nu}{\mu^2}\right) - \frac{121}{54} - \frac{\pi^2}{9}\right]\right\}. \qquad (4.171)
\end{aligned}$$

The sum of the individual counterterm contributions gives the complete current counterterm for one flavor corresponding to Eq. (4.15),

$$Z^{(n_l+1,2)}_{C,T_F}(Q,\mu) = -\left(Z^{(n_l+1,2)}_{\mathcal{J},n,T_F} + Z^{(n_l+1,2)}_{\mathcal{J},\bar{n},T_F}\right). \qquad (4.172)$$

This yields together with the corresponding contributions at $\mathcal{O}(\alpha_s)$, for which the analogous relation holds, the correct μ-anomalous dimension for the current at $\mathcal{O}(\alpha_s^2 C_F T_F)$ in Eq. (4.29). The ν-anomalous dimensions for the soft, n- and $\bar{n}$-collinear contributions in the $\overline{\mathrm{MS}}$-scheme satisfy [27]

$$\begin{aligned}
\gamma^{(n_l+1,2)}_{\mathcal{J},s,\nu,T_F} &= -\,\nu\frac{\mathrm{d}}{\mathrm{d}\nu}\,Z^{(n_l+1,2)}_{\mathcal{J},s,T_F} = 0\,, \qquad (4.173)\\
\gamma^{(n_l+1,2)}_{\mathcal{J},n,\nu,T_F} &= -\,\nu\frac{\mathrm{d}}{\mathrm{d}\nu}\,Z^{(n_l+1,2)}_{\mathcal{J},n,T_F} = \frac{\left(\alpha_s^{(n_l+1)}\right)^2 C_F T_F}{16\pi^2}\left\{-\frac{8}{3}L_m L_\Lambda + \frac{4}{3}L_m^2 + \frac{40}{9}L_m + \frac{112}{27}\right\}, \qquad (4.174)\\
\gamma^{(n_l+1,2)}_{\mathcal{J},\bar{n},\nu,T_F} &= -\,\nu\frac{\mathrm{d}}{\mathrm{d}\nu}\,Z^{(n_l+1,2)}_{\mathcal{J},\bar{n},T_F} = -\gamma^{(n_l+1,2)}_{\mathcal{J},n,\nu,T_F}\,. \qquad (4.175)
\end{aligned}$$

Note that these anomalous dimensions are depending on the infrared regulator Λ. However, this dependence drops out in the ν-evolution of the massive threshold correction, which is decomposed in terms of n-, $\bar{n}$-collinear and soft contributions satisfying in analogy to Eq. (4.92)

$$\nu\frac{\mathrm{d}}{\mathrm{d}\nu}\,\mathcal{M}_{C,i}(Q,m,\mu,\nu) = \left(\gamma^{(n_l+1)}_{\mathcal{J},i,\nu} - \gamma^{(n_l)}_{\mathcal{J},i,\nu}\right)\mathcal{M}_{C,i}(Q,m,\mu,\nu) \equiv \gamma_{\mathcal{M}_C,i}\,\mathcal{M}_{C,i}(Q,m,\mu,\nu) \qquad (4.176)$$

with $i = n,\bar{n},s$. This is due to the fact that the difference of the scheme for α_s in the $\overline{\mathrm{MS}}$ and OS anomalous dimensions affects the terms at $\mathcal{O}(\alpha_s^2 C_F T_F)$,

$$\begin{aligned}
\gamma^{(n_l+1)}_{\mathcal{J},i,\nu} - \gamma^{(n_l)}_{\mathcal{J},i,\nu} &= \left(\gamma^{(n_l+1,1)}_{\mathcal{J},i,\nu} - \gamma^{(n_l,1)}_{\mathcal{J},i,\nu}\right) + \left(\gamma^{(n_l+1,2)}_{\mathcal{J},i,\nu,T_F} - \gamma^{(n_l,2)}_{\mathcal{J},i,\nu,T_F}\right) + \mathcal{O}(\alpha_s^3)\\
&= \gamma^{(n_l+1,2)}_{\mathcal{J},i,\nu,T_F} - \frac{\alpha_s^{(n_l+1)}T_F}{3\pi}\,L_m\,\gamma^{(n_l+1,1)}_{\mathcal{J},i,\nu} + \mathcal{O}(\alpha_s^3)\,, \qquad (4.177)
\end{aligned}$$

where we have used the decoupling relation of α_s in Eq. (3.112) and the fact that the OS counterterms lead to vanishing anomalous dimensions for the massive quark contributions, i.e. $\gamma^{(n_l,2)}_{\mathcal{J},i,\nu,T_F} = 0$. Using the result for the gluon mass dependent one-loop anomalous dimensions $\gamma^{(1)}_{\mathcal{J},i,\nu}$ in Eqs. (4.93) – (4.95) we obtain $\gamma^{(2)}_{\mathcal{M}_C,s} = 0$ and

$$\gamma^{(2)}_{\mathcal{M}_C,n} = -\gamma^{(2)}_{\mathcal{M}_C,\bar{n}} = \frac{\alpha_s^2 C_F T_F}{16\pi^2}\left\{\frac{4}{3}L_m^2 + \frac{40}{9}L_m + \frac{112}{27}\right\} + \mathcal{O}(\alpha_s^3)\,. \qquad (4.178)$$

[26] We indicate explicitly that only the strong coupling related to the interactions of the gluon to the primary quarks is affected by the rapidity regularization procedure and adopts a ν-dependence. The interactions due to gluon splitting within a single sector do not contain any rapidity divergences and therefore do not need additional regularization.

[27] Using the symmetric Wilson line regulator η in Refs. [40,41] one obtains the same relations for the anomalous dimensions as in the one-loop case, i.e. $\gamma^{(n_l+1,2,\eta)}_{\mathcal{J},s,\nu,T_F} = -2\gamma^{(n_l+1,2)}_{\mathcal{J},n,\nu,T_F}$ and $\gamma^{(n_l+1,2,\eta)}_{\mathcal{J},n,\nu,T_F} = \gamma^{(n_l+1,2,\eta)}_{\mathcal{J},\bar{n},\nu,T_F} = \gamma^{(n_l+1,2)}_{\mathcal{J},n,\nu,T_F}$.

The solution of Eq. (4.176) is the anticipated exponentiation which allows to determine the required term at $\mathcal{O}(\alpha_s^4 \ln^2(m^2/Q^2)) \sim \mathcal{O}(\alpha_s^2)$ in the logarithmic counting $\alpha_s \ln(m^2/Q^2) \sim 1$.

For a complete analysis at N^{3}LL we would also need the term at $\mathcal{O}(\alpha_s^3 \ln(m^2/Q^2)) \sim \mathcal{O}(\alpha_s^2)$. We can determine its μ_m-dependent contribution from the identity

$$\mathcal{M}_C(Q,m,\mu_m) = U_C^{(n_l+1)}(Q,\mu_m,m)\,\mathcal{M}_C(Q,m,m)\,U_C^{(n_l)}(Q,m,\mu_m)\,, \tag{4.179}$$

or equivalently,

$$\mu\frac{\mathrm{d}}{\mathrm{d}\mu}\,\mathcal{M}_C(Q,m,\mu) = -\Big(\gamma_C^{(n_l+1)}(Q,\mu) - \gamma_C^{(n_l)}(Q,\mu)\Big)\,\mathcal{M}_C(Q,m,\mu)\,. \tag{4.180}$$

Expanding in α_s gives the perturbative result for the μ_m-dependent terms. Including the relevant term at $\mathcal{O}(\alpha_s^3 \ln(m^2/Q^2))$ in the exponent the structure of the mass mode matching coefficient reads [28] ($\alpha_s^{(n_l+1)} = \alpha_s^{(n_l+1)}(\mu_m)$, $m = m(\mu_m)$)

$$\begin{aligned}
\mathcal{M}_C(Q,m,\mu_m) = {} & \bigg\{1 + \frac{\big(\alpha_s^{(n_l+1)}\big)^2}{(4\pi)^2}\bigg[\frac{L_m^3}{12}\,\Gamma_0^C\Delta\beta_0 + \frac{L_m^2}{4}\big(\Delta\Gamma_1^C + \gamma_0^C\Delta\beta_0\big) + \frac{L_m}{2}\Big(\Delta\gamma_1^C + 2\mathcal{M}_2^{C,+}\Big) + \mathcal{M}_2^C\bigg]\bigg\} \\
& \times \exp\bigg\{\frac{\big(\alpha_s^{(n_l+1)}\big)^2}{(4\pi)^2}\,L_Q\bigg[-\frac{L_m^2}{4}\,\Gamma_0^C\Delta\beta_0 - \frac{L_m}{2}\,\Delta\Gamma_1^C - \mathcal{M}_2^{C,+}\bigg] \\
& + \frac{\big(\alpha_s^{(n_l+1)}\big)^3}{(4\pi)^3}\,L_Q\bigg[\frac{L_m^3}{6}\,\Gamma_0^C\Delta\beta_0(\beta_0 + \Delta\beta_0) + \frac{L_m^2}{4}\Big(2\,\Delta\Gamma_1^C(\beta_0+\Delta\beta_0) - 2\,\Gamma_1^C\Delta\beta_0 \\
& - \Gamma_0^C\Delta\beta_1 + 4\,\Gamma_0^C\Delta\beta_0\gamma_0^m\Big) + \frac{L_m}{2}\Big(-\Delta\Gamma_2^C + 2\,\Delta\Gamma_1^C\gamma_0^m + \Gamma_0^C c_{\mathrm{dec}} + 4\beta_0\mathcal{M}_2^{C,+}\Big) \\
& - \mathcal{M}_3^{C,+}\bigg]\bigg\}\,.
\end{aligned} \tag{4.181}$$

Here $\Delta\eta \equiv \eta^{(n_l+1)} - \eta^{(n_l)}$ is the difference between an evolution constant η in the (n_l+1)- and n_l-scheme. The terms Γ_i^C, γ_i^C, γ_i^m and β_i denote the coefficients of the cusp and noncusp current anomalous dimensions, the mass anomalous dimension and the beta function with n_l+1 light quarks, respectively,

$$\mu\frac{\mathrm{d}}{\mathrm{d}\mu}\,C^{(n_l+1)}(Q,\mu) = \sum_{i\geq 0}\left(\frac{\alpha_s^{(n_l+1)}(\mu)}{4\pi}\right)^{i+1}\big[-\Gamma_i^C L_Q + \gamma_i^C\big]\,C^{(n_l+1)}(Q,\mu)\,, \tag{4.182}$$

$$\mu\frac{\mathrm{d}}{\mathrm{d}\mu}\,m^{(n_l+1)}(\mu) = -\,2\sum_{i\geq 0}\left(\frac{\alpha_s^{(n_l+1)}(\mu)}{4\pi}\right)^{i+1}\gamma_i^m\,m^{(n_l+1)}(\mu)\,, \tag{4.183}$$

$$\mu\frac{\mathrm{d}}{\mathrm{d}\mu}\,\alpha_s^{(n_l+1)}(\mu) = -\,2\sum_{i\geq 0}\left(\frac{\alpha_s^{(n_l+1)}(\mu)}{4\pi}\right)^{i+1}\beta_i\,\alpha_s^{(n_l+1)}(\mu)\,, \tag{4.184}$$

where $\gamma_0^m = 3C_F$ for the $\overline{\mathrm{MS}}$ scheme and the remaining required anomalous dimensions in the $\overline{\mathrm{MS}}$ scheme are displayed in appendix C. The terms $\mathcal{M}_i^{C,+}$ ($\mathcal{M}_i^C$) indicate the renormalization scale independent constants, which multiply (do not multiply) the rapidity logarithm $\ln(m^2/Q^2)$ in the matching coefficient. Note that we have not determined the relevant constant $\mathcal{M}_3^{C,+}$ at this stage. We will see in Sec. 4.4.3 how to relate it to an existing result for the PDF threshold correction. The constant c_{dec} is the mass scheme dependent coefficient of the two-loop correction in the decoupling relation between the strong couplings in the n_l and the (n_l+1)-flavor schemes at the scale of the mass, that is being employed, i.e.

$$\alpha_s^{(n_l)}(m) = \alpha_s^{(n_l+1)}(m)\bigg[1 + \left(\frac{\alpha_s^{(n_l+1)}(m)}{4\pi}\right)^2 c_{\mathrm{dec}}\bigg]. \tag{4.185}$$

[28] For simplicity we set $\nu_n = Q$ and $\nu_{\bar{n}} = \mu_m$ here. For a phenomenological error estimate the ν-dependence can be easily restored.

For the $\overline{\rm MS}$ mass $m = \overline{m}(\mu_m)$ we have (see e.g. Ref. [91])

$$c_{\rm dec}^{\overline{\rm MS}} = \frac{32}{9} C_A T_F - \frac{13}{3} C_F T_F \,. \tag{4.186}$$

Inserting the values for all of the constants and expanding Eq. (4.181) using the logarithmic counting $\alpha_s \ln(m^2/Q^2) \sim 1$ gives our final result in Eq. (4.45).

4.4.2 Jet function and threshold correction

Jet function

The calculation of the $\mathcal{O}(\alpha_s^2 C_F T_F)$ secondary massive quark corrections to the jet function in the (n_l+1)-flavor scheme goes along the lines of the hard current coefficient. In the n_l-flavor scheme for α_s they can be obtained from the one-loop jet function for the radiation of a massive gluon with the subtracted dispersion relation

$$\begin{aligned} J_m^{(n_l,\text{bare},2)}(s,m,\mu) &= J_{m,\text{virt}}^{(n_l,\text{bare},2)}(s,m,\mu) + J_{m,\text{real}}^{(n_l,2)}(s,m) \\ &= \frac{1}{\pi}\int \frac{\mathrm{d}M^2}{M^2}\Big(J_{M,\text{virt}}^{(\text{bare},1)}(s,M,\mu) + J_{M,\text{real}}^{(1)}(s,M)\Big)\,\mathrm{Im}\big[\Pi(m^2,M^2)\big]\,, \end{aligned} \tag{4.187}$$

where the $\mathcal{O}(\alpha_s)$ results for the virtual emission in d dimensions and the real emission in 4 dimensions, $J_{M,\text{virt}}^{(\text{bare},1)}(s,M,\mu)$ and $J_{M,\text{real}}^{(1)}(s,M)$, are given in Eqs. (4.106) and (4.107), respectively. The convolution is performed separately for these terms, where for the real radiation correction no divergences arise in the M-integration and thus the $d=4$ version of the absorptive part of the vacuum polarization function in Eq. (3.61) can be used. This yields Eq. (4.54) for the real radiation term $J_{m,\text{real}}^{(n_l,2)}(s,m)$ (where the n_l-scheme for α_s is implied) and ($\bar{s} = s/\mu_m^2$)

$$\begin{aligned} \mu^2 J_{m,\text{virt}}^{(n_l,\text{bare},2)}(s,m,\mu) = \frac{\big(\alpha_s^{(n_l)}\big)^2 C_F T_F}{(4\pi)^2}\bigg\{&\delta(\bar{s})\bigg[\frac{4}{\epsilon^3} + \frac{1}{\epsilon^2}\bigg(-\frac{16}{3}L_m - \frac{2}{9}\bigg) + \frac{1}{\epsilon}\bigg(\frac{8}{3}L_m^2 - 4L_m - \frac{121}{27} + \frac{2\pi^2}{9}\bigg) \\ &+ \frac{76}{9}L_m^2 + \frac{466}{27}L_m + \frac{1531}{54} + \frac{19\pi^2}{27} - \frac{32}{3}\zeta_3\bigg] + \bigg[\frac{\theta(\bar{s})}{\bar{s}}\bigg]_+\bigg[-\frac{8}{3\epsilon^2} \\ &+ \frac{1}{\epsilon}\bigg(\frac{16}{3}L_m + \frac{40}{9}\bigg) - \frac{16}{3}L_m^2 - \frac{80}{9}L_m - \frac{224}{27} - \frac{4\pi^2}{9}\bigg]\bigg\}\,. \end{aligned} \tag{4.188}$$

If we renormalize the jet function using the OS condition, the corresponding counterterm contribution reads

$$Z_{J,m}^{(n_l,2)}(s,m,\mu) = J_{m,\text{virt}}^{(n_l,\text{bare},2)}(s,m,\mu)\,, \tag{4.189}$$

and the complete renormalized jet function contains besides the massless quark corrections just the real radiation contributions,

$$J_{T_F}^{(n_l,2)}(s,m,\mu) = J_{T_F}^{(n_l,2)}(s,\mu) + J_{m,\text{real}}^{(n_l,2)}(s,m)\,. \tag{4.190}$$

We switch to the (n_l+1)-flavor scheme for α_s by adding the $\overline{\rm MS}$-renormalized $\Pi(0)$ times the (unrenormalized) massless one-loop contribution to the jet function

$$J^{(\text{bare},1)}(s,\mu) = J^{(1)}(s,\mu) + Z_J^{(1)}(s,\mu)\,, \tag{4.191}$$

with $J^{(1)}(s,\mu)$ and $Z_J^{(1)}(s,\mu)$ given in Eqs. (4.16) and (4.18), respectively. Thus the corresponding contribution needed to change from the n_l to the (n_l+1)-flavor scheme reads

$$\begin{aligned}\mu^2 J^{(n_l\to n_l+1,2)}(s,m,\mu) =& -\bigg(\Pi(m^2,0)-\frac{\alpha_s T_F}{3\pi}\,\frac{1}{\epsilon}\bigg)\Big(\mu^2 J^{(1)}(s,\mu)+\mu^2 Z_J^{(1)}(s,\mu)\Big)\\ =& \frac{\alpha_s^2 C_F T_F}{(4\pi)^2}\bigg\{\delta(\bar s)\bigg[\frac{16}{3\epsilon^2}L_m+\frac{1}{\epsilon}\bigg(-\frac{8}{3}L_m^2+4L_m-\frac{4\pi^2}{9}\bigg)+\frac{8}{9}L_m^3-4L_m^2\\ &+\bigg(\frac{28}{3}-\frac{8\pi^2}{9}\bigg)L_m-\frac{\pi^2}{3}+\frac{16}{9}\zeta_3\bigg]+\bigg[\frac{\theta(\bar s)}{\bar s}\bigg]_+\bigg[-\frac{16}{3\epsilon}L_m+\frac{8}{3}L_m^2-4L_m+\frac{4\pi^2}{9}\bigg]\\ &+\frac{16}{3}L_m\bigg[\frac{\theta(\bar s)\ln\bar s}{\bar s}\bigg]_+\bigg\}\,. \end{aligned} \tag{4.192}$$

Combining all virtual massive quark contributions and renormalizing the result with the jet counterterm contribution $Z_{J,T_F}^{(n_l+1,2)}$ in Eq. (4.19) finally gives

$$J_{m,\mathrm{virt}}^{(n_l+1,2)}(s,m,\mu) = J_{m,\mathrm{virt}}^{(n_l,\mathrm{bare},2)}(s,m,\mu)+\delta J^{(n_l\to n_l+1,2)}(s,m,\mu)-Z_{J,T_F}^{(n_l+1,2)}(s,\mu) \tag{4.193}$$

with $\alpha_s=\alpha_s^{(n_l+1)}(\mu)$ employed at the end in $J_{m,\mathrm{virt}}^{(n_l+1,2)}$. Inserting Eqs. (4.19), (4.188) and (4.192) we obtain (see also Ref. [26])

$$\begin{aligned}J_{m,\mathrm{virt}}^{(n_l+1,2)}(s,m,\mu) =& \frac{\big(\alpha_s^{(n_l+1)}\big)^2 C_F T_F}{16\pi^2}\bigg\{\delta(\bar s)\bigg[\frac{8}{9}L_m^3+\frac{58}{9}L_m^2+\bigg(\frac{718}{27}-\frac{8\pi^2}{9}\bigg)L_m+\frac{1531}{54}+\frac{10\pi^2}{27}-\frac{80}{9}\zeta_3\bigg]\\ &+\bigg[\frac{\theta(\bar s)}{\bar s}\bigg]_+\bigg[-\frac{8}{3}L_m^2-\frac{116}{9}L_m-\frac{224}{27}\bigg]+\frac{16}{3}L_m\bigg[\frac{\theta(\bar s)\ln\bar s}{\bar s}\bigg]_+\bigg\}\,. \end{aligned} \tag{4.194}$$

Subtracting from Eq. (4.194) the massless limit of Eq. (4.17) we obtain the distributive mass corrections to the jet function given in Eq. (4.53).

Jet function threshold correction

The mass mode threshold factor $\mathcal{M}_J(s,m,\mu_m)$ is straightforward to determine from the relation between the renormalized jet functions in the OS and $\overline{\mathrm{MS}}$ scheme at the scale μ_m. The matching accounts for the difference between the two schemes and is obtained by the relation

$$\begin{aligned}\mathcal{M}_J(s,m,\mu_m) &= \int \mathrm{d}s'\,J^{(n_l)}(s-s',m,\mu_m)\,\Big(J^{(n_l+1)}\Big)^{-1}(s',m,\mu_m)\\ &= \int \mathrm{d}s'\,Z_J^{(n_l+1)}(s-s',\mu_m)\,\Big(Z_J^{(n_l)}\Big)^{-1}(s',m,\mu_m)\,. \end{aligned} \tag{4.195}$$

Since the difference in the factorization theorems for the scenarios II and III in Eqs. (4.41) and (4.51) concerns just the jet function and its evolution, Eq. (4.195) shows that the matching condition for the jet function automatically implements a continuous transition between these two scenarios for $m^2\sim\mu_m^2\sim\mu_J^2\sim s$, in particular at $\mathcal{O}(\alpha_s^2)$ also due to the fact that the real radiation terms $J_{m,\mathrm{real}}^{(n_l,2)}$ and $J_{m,\mathrm{real}}^{(n_l+1,2)}$, respectively, are fully included in each of the two scenarios.

Relating the schemes of α_s via Eq. (3.112), we obtain at $\mathcal{O}(\alpha_s^2)$ in fixed-order counting

$$\mathcal{M}_J(s,m,\mu_m) = \delta(s) - J_{m,\mathrm{virt}}^{(n_l+1,2)}(s,m,\mu) + \frac{\alpha_s^{(n_l+1)}T_F}{3\pi}\,L_m\,J^{(n_l+1,1)}(s,\mu_m)+\mathcal{O}(\alpha_s^3)\,. \tag{4.196}$$

Note that using the renormalized jet functions for the matching calculation the real radiation terms cancel in Eq. (4.195) and do not contribute to the threshold correction factor. [29] Inserting all explicit

[29]This should hold to any order in perturbation theory which is technically satisfied due to mixed virtual-real massive quark corrections in the (n_l+1)-scheme at higher orders.

expressions gives at $\mathcal{O}(\alpha_s^2)$ in the fixed-order counting

$$\mu_m^2\,\mathcal{M}_J^{(2)}(s,m,\mu_m) = \frac{\alpha_s^2 C_F T_F}{16\pi^2}\bigg\{\delta(\bar{s})\left[-\frac{8}{9}L_m^3-\frac{58}{9}L_m^2-\left(\frac{466}{27}+\frac{4\pi^2}{9}\right)L_m-\frac{1531}{54}-\frac{10\pi^2}{27}+\frac{80}{9}\zeta_3\right] + \left[\frac{\theta(\bar{s})}{\bar{s}}\right]_+\left[\frac{8}{3}L_m^2+\frac{80}{9}L_m+\frac{224}{27}\right]\bigg\}\,. \tag{4.197}$$

Since there are no $\mathcal{O}(\alpha_s)$ one-loop corrections the schemes of α_s and the mass appearing in Eq. (4.197) do not need to be specified at this point. Eq. (4.197) contains a large logarithm $\ln(m^2/s)$, which can be better seen by a rescaling of the invariant mass variable $\bar{s}=s/\mu_m^2$ in terms of $\tilde{s}=s/\mu_J^2\sim\mathcal{O}(1)$ with the help of Eq. (B.3),

$$\mu_J^2\,\mathcal{M}_J^{(2)}(s,m,\mu_m) = \frac{\alpha_s^2 C_F T_F}{16\pi^2}\bigg\{\delta(\tilde{s})\bigg[\left(\frac{8}{3}L_m^2+\frac{80}{9}L_m+\frac{224}{27}\right)\ln\left(\frac{\mu_J^2}{\mu_m^2}\right)-\frac{8}{9}L_m^3-\frac{58}{9}L_m^2 -\left(\frac{466}{27}+\frac{4\pi^2}{9}\right)L_m-\frac{1531}{54}-\frac{10\pi^2}{27}+\frac{80}{9}\zeta_3\bigg]+\left[\frac{\theta(\tilde{s})}{\tilde{s}}\right]_+\left[\frac{8}{3}L_m^2+\frac{80}{9}L_m+\frac{224}{27}\right]\bigg\}\,. \tag{4.198}$$

As for the current mass mode matching coefficient this is a rapidity logarithm which enforces the counting $\alpha_s\ln(m^2/s)\sim\mathcal{O}(1)$.

We will now set up a RG evolution in rapidity space to resum the associated higher order logarithms in analogy the one-loop case described in Sec. 4.3.2. As in Eq. (4.116) we decompose the bare jet function in terms of n-collinear and the soft-bin contributions. Note that the scheme difference of the strong coupling above and below threshold requires that also the one-loop corrections for the radiation of a massless gluon have to be accounted for and should be decomposed in the same way. For this purpose we will again use a gluon mass $\Lambda\ll m$ as an infrared regulator which allows us to apply the results in Sec. 4.3.2. We write the two-loop contributions for virtual massive quarks as

$$J_{m,\mathrm{virt},i}^{(n_l+1,2,\mathrm{bare})}(s,m,Q,\Lambda,\mu,\nu) = \frac{1}{\pi}\int\frac{\mathrm{d}M^2}{M^2}\,J_{M,\mathrm{virt},i}^{(\mathrm{bare},1)}(s,M,Q,\mu,\nu)\,\mathrm{Im}\left[\Pi(m^2,M^2)\right] - \left(\Pi(m^2,0)-\frac{\alpha_s^{(n_l+1)}T_F}{3\pi}\,\frac{1}{\epsilon}\right)J_{M,\mathrm{virt},i}^{(\mathrm{bare},1)}(s,Q,\Lambda,\mu,\nu)\,, \tag{4.199}$$

with $i=n,0m$ denoting the n-collinear and the soft-bin contributions and the one-loop massive gluon corrections $J_{M,\mathrm{virt},i}^{(\mathrm{bare},1)}$ given in Eqs. (4.117) and (4.118). After performing the subtracted dispersion relation and including the scheme change contribution we obtain for the individual contributions [30] $(L_\Lambda=\ln(\Lambda^2/\mu^2))$

$$\mu^2 J_{m,\mathrm{virt},n}^{(n_l+1,\mathrm{bare},2)} = \frac{\left(\alpha_s^{(n_l+1)}\right)^2 C_F T_F}{16\pi^2}\,\delta(\bar{s})\bigg\{\frac{1}{\alpha}\left[\frac{8}{3\epsilon^2}-\frac{40}{9\epsilon}-\frac{16}{3}L_m L_\Lambda+\frac{8}{3}L_m^2+\frac{80}{9}L_m+\frac{224}{27}+\mathcal{O}(\epsilon)\right] +\frac{1}{\epsilon^2}\left[\frac{8}{3}\ln\left(\frac{\nu}{Q}\right)+2\right]+\frac{1}{\epsilon}\left[-\frac{40}{9}\ln\left(\frac{\nu}{Q}\right)-\frac{1}{3}-\frac{4\pi^2}{9}\right]+\bigg(-\frac{16}{3}L_m L_\Lambda+\frac{8}{3}L_m^2 +\frac{80}{9}L_m+\frac{224}{27}\bigg)\ln\left(\frac{\nu}{Q}\right)-4L_m L_\Lambda+2L_m^2+\frac{20}{3}L_m+\frac{73}{18}+\frac{20\pi^2}{27}-\frac{8}{3}\zeta_3\bigg\}\,, \tag{4.200}$$

[30] Note that the virtual n-collinear correction is equivalent to the corresponding current contribution in Eq. (4.168), i.e. $J_{m,\mathrm{virt},n}^{(n_l+1,\mathrm{bare},2)}=2\hat{F}_{m,\mathrm{SCET},n}^{(n_l+1,\mathrm{bare},2)}\,\delta(s)$, which are both described by the same types of diagrams.

and

$$\begin{aligned}
\mu^2 J^{(n_l+1,\mathrm{bare},2)}_{m,\mathrm{virt},0m} &= \frac{\big(\alpha_s^{(n_l+1)}\big)^2 C_F T_F}{16\pi^2}\bigg\{\delta(\bar{s})\bigg(\frac{1}{\alpha}\bigg[-\frac{8}{3\epsilon^2}+\frac{40}{9\epsilon}+\frac{16}{3}L_m L_\Lambda-\frac{8}{3}L_m^2-\frac{80}{9}L_m-\frac{224}{27}+\mathcal{O}(\epsilon)\bigg] \\
&\quad+\frac{4}{\epsilon^3}+\frac{1}{\epsilon^2}\bigg[-\frac{8}{3}\ln\Big(\frac{\nu}{Q}\Big)-\frac{20}{9}\bigg]+\frac{1}{\epsilon}\bigg[\frac{40}{9}\ln\Big(\frac{\nu}{Q}\Big)-\frac{112}{27}+\frac{2\pi^2}{9}\bigg] \\
&\quad+\bigg(-\frac{16}{3}L_m L_\Lambda+\frac{8}{3}L_m^2+\frac{80}{9}L_m+\frac{224}{27}\bigg)\ln\Big(\frac{\nu}{Q}\Big)-\frac{8}{3}L_m L_\Lambda^2+\frac{8}{9}L_m^3+\frac{40}{9}L_m^2 \\
&\quad+\bigg(\frac{448}{27}-\frac{8\pi^2}{9}\bigg)L_m+\frac{656}{27}-\frac{10\pi^2}{27}-\frac{56}{9}\zeta_3\bigg)+\bigg[\frac{\theta(\bar{s})}{\bar{s}}\bigg]_+\bigg(-\frac{8}{3\epsilon^2}+\frac{40}{9\epsilon}+\frac{16}{3}L_m L_\Lambda \\
&\quad-\frac{8}{3}L_m^2-\frac{80}{9}L_m-\frac{224}{27}\bigg)\bigg\}\,. \qquad (4.201)
\end{aligned}$$

Therefore, the nonvanishing two-loop counterterm contributions above threshold, where we use $\overline{\mathrm{MS}}$-renormalization, read

$$\begin{aligned}
\mu^2 Z^{(n_l+1,2)}_{J,n,T_F} &= \frac{\alpha_s^{(n_l+1)}(\mu,\nu)\,\alpha_s^{(n_l+1)}(\mu)\,C_F T_F}{16\pi^2}\,\delta(\bar{s})\bigg\{\frac{1}{\alpha}\bigg[\frac{8}{3\epsilon^2}-\frac{40}{9\epsilon}-\frac{16}{3}L_m L_\Lambda+\frac{8}{3}L_m^2+\frac{80}{9}L_m \\
&\quad+\frac{224}{27}+\mathcal{O}(\epsilon)\bigg]+\frac{1}{\epsilon^2}\bigg[\frac{8}{3}\ln\Big(\frac{\nu}{Q}\Big)+2\bigg]+\frac{1}{\epsilon}\bigg[-\frac{40}{9}\ln\Big(\frac{\nu}{Q}\Big)-\frac{1}{3}-\frac{4\pi^2}{9}\bigg]\bigg\}\,, \qquad (4.202) \\
\mu^2 Z^{(n_l+1,2)}_{J,0m,T_F} &= \frac{\alpha_s^{(n_l+1)}(\mu,\nu)\,\alpha_s^{(n_l+1)}(\mu)\,C_F T_F}{16\pi^2}\bigg\{\delta(\bar{s})\bigg(\frac{1}{\alpha}\bigg[-\frac{8}{3\epsilon^2}+\frac{40}{9\epsilon}-\frac{16}{3}L_m L_\Lambda-\frac{8}{3}L_m^2-\frac{80}{9}L_m \\
&\quad-\frac{224}{27}+\mathcal{O}(\epsilon)\bigg]+\frac{4}{\epsilon^3}+\frac{1}{\epsilon^2}\bigg[-\frac{8}{3}\ln\Big(\frac{\nu}{Q}\Big)-\frac{20}{9}\bigg]+\frac{1}{\epsilon}\bigg[\frac{40}{9}\ln\Big(\frac{\nu}{Q}\Big)-\frac{112}{27}+\frac{2\pi^2}{9}\bigg]\bigg) \\
&\quad+\bigg[\frac{\theta(\bar{s})}{\bar{s}}\bigg]_+\bigg(-\frac{8}{3\epsilon^2}+\frac{40}{9\epsilon}\bigg)\bigg\}\,. \qquad (4.203)
\end{aligned}$$

The sum of the individual counterterm contributions gives the complete jet function counterterm at $\mathcal{O}(\alpha_s C_F T_F)$ corresponding to Eq. (4.19),

$$Z^{(n_l+1,2)}_{J,T_F}(s,\mu) = Z^{(n_l+1,2)}_{J,n,T_F} + Z^{(n_l+1,2)}_{J,0m,T_F}\,. \qquad (4.204)$$

This yields together with the corresponding contributions at $\mathcal{O}(\alpha_s)$, for which the analogous relation holds, the correct μ-anomalous dimension for the jet function at $\mathcal{O}(\alpha_s^2 C_F T_F)$ in Eq. (4.31). The ν-anomalous dimensions for the pure n-collinear and the soft-bin contributions in the $\overline{\mathrm{MS}}$-scheme satisfy [31]

$$\begin{aligned}
\gamma^{(n_l+1,2)}_{J,n,\nu,T_F} &= -\,\nu\frac{\mathrm{d}}{\mathrm{d}\nu}\,Z^{(n_l+1,2)}_{J,n,T_F} = \frac{\big(\alpha_s^{(n_l+1)}\big)^2 C_F T_F}{16\pi^2}\bigg\{-\frac{16}{3}L_m L_\Lambda+\frac{8}{3}L_m^2+\frac{80}{9}L_m+\frac{224}{27}\bigg\}\,, \qquad (4.205) \\
\gamma^{(n_l+1,2)}_{J,0m,\nu,T_F} &= -\,\nu\frac{\mathrm{d}}{\mathrm{d}\nu}\,Z^{(n_l+1,2)}_{J,0m,T_F} = -\gamma^{(n_l+1,2)}_{J,n,\nu,T_F}\,. \qquad (4.206)
\end{aligned}$$

As for the current threshold correction the dependence on the infrared regulator Λ cancels in the ν-evolution of the jet function threshold correction, which is decomposed in terms of n-collinear and soft-bin contributions satisfying in analogy to Eq. (4.122)

$$\nu\frac{\mathrm{d}}{\mathrm{d}\nu}\,\mathcal{M}_{J,i}(s,m,\mu,\nu) = -\Big(\gamma^{(n_l+1)}_{J,i,\nu}-\gamma^{(n_l)}_{J,i,\nu}\Big)\,\mathcal{M}_{J,i}(s,m,\mu,\nu) \equiv \gamma_{\mathcal{M}_J,i}\,\mathcal{M}_{J,i}(s,m,\mu,\nu) \qquad (4.207)$$

with $i=n,0m$. The difference between the anomalous dimensions in $\overline{\mathrm{MS}}$ and OS renormalization reads

$$\gamma^{(n_l+1)}_{J,i,\nu}-\gamma^{(n_l)}_{J,i,\nu} = \gamma^{(n_l+1,2)}_{J,i,\nu}-\frac{\alpha_s^{(n_l+1)}T_F}{3\pi}\,L_m\,\gamma^{(n_l+1,1)}_{J,i,\nu}+\mathcal{O}(\alpha_s^3)\,. \qquad (4.208)$$

[31] The same results hold when the η-regulator in Refs. [40,41] is employed.

Using the results for the gluon mass dependent one-loop anomalous dimensions in Eqs. (4.93) – (4.95) we obtain

$$\gamma_{\mathcal{M}_J,n} = -\gamma_{\mathcal{M}_J,0m} = \frac{\alpha_s^2 C_F T_F}{16\pi^2}\left\{-\frac{8}{3}L_m^2 - \frac{80}{9}L_m - \frac{224}{27}\right\} + \mathcal{O}(\alpha_s^3)\,. \tag{4.209}$$

The solution of Eq. (4.207) is the anticipated exponentiation which allows to determine the required term at $\mathcal{O}(\alpha_s^4\ln^2(m^2/s)) \sim \mathcal{O}(\alpha_s^2)$ in the logarithmic counting $\alpha_s\ln(m^2/s) \sim 1$.

For a complete analysis at N^{3}LL we also need the term at $\mathcal{O}(\alpha_s^3\ln(m^2/s)) \sim \mathcal{O}(\alpha_s^2)$. We can determine its μ_m-dependent contribution from the identity

$$\mathcal{M}_J(s,m,\mu_m) = \int \mathrm{d}s' \int \mathrm{d}s''\, U_J^{(n_l+1)}(s-s',m,\mu_m)\,\mathcal{M}_J(s'-s'',m,m)\,U_J^{(n_l)}(s'',\mu_m,m)\,. \tag{4.210}$$

or equivalently,

$$\mu\frac{\mathrm{d}}{\mathrm{d}\mu}\mathcal{M}_J(s,m,\mu) = -\int \mathrm{d}s'\,\left(\gamma_J^{(n_l+1)}(s-s',\mu) - \gamma_J^{(n_l)}(s-s',\mu)\right)\mathcal{M}_J(s',m,\mu)\,. \tag{4.211}$$

Expanding in α_s gives the perturbative result for the μ_m-dependent terms. Including the relevant term at $\mathcal{O}(\alpha_s^3\ln(s/m^2))$ in the exponent the structure of the mass mode matching coefficient reads [32] ($\alpha_s^{(n_l+1)} = \alpha_s^{(n_l+1)}(\mu_m)$, $m = m(\mu_m)$)

$$\begin{aligned}
\mu_J^2\,\mathcal{M}_J(s,m,\mu_J,\mu_m) = &\Bigg\{\delta(\tilde{s}) + \frac{\left(\alpha_s^{(n_l+1)}\right)^2}{(4\pi)^2}\Bigg(\delta(\tilde{s})\left[\frac{L_m^3}{12}\,\Gamma_0^J\Delta\beta_0 + \frac{L_m^2}{4}\left(\Delta\Gamma_1^J + \gamma_0^J\Delta\beta_0\right)\right.\\
&\left.+\frac{L_m}{2}\left(\Delta\gamma_1^J - 2\mathcal{M}_2^{J,+}\right) + \mathcal{M}_2^J\right] + \left[\frac{\theta(\tilde{s})}{\tilde{s}}\right]_+\left[-\frac{L_m^2}{4}\,\Gamma_0^J\Delta\beta_0 - \frac{L_m}{2}\,\Delta\Gamma_1^J + \mathcal{M}_2^{J,+}\right]\Bigg)\Bigg\}\\
&\times\exp\Bigg\{\frac{\left(\alpha_s^{(n_l+1)}\right)^2}{(4\pi)^2}\ln\!\left(\frac{\mu_J^2}{\mu_m^2}\right)\left[-\frac{L_m^2}{4}\,\Gamma_0^J\Delta\beta_0 - \frac{L_m}{2}\,\Delta\Gamma_1^J + \mathcal{M}_2^{J,+}\right]\\
&+\frac{\left(\alpha_s^{(n_l+1)}\right)^3}{(4\pi)^3}\ln\!\left(\frac{\mu_J^2}{\mu_m^2}\right)\Bigg[\frac{L_m^3}{6}\,\Gamma_0^J\Delta\beta_0(\beta_0+\Delta\beta_0) + \frac{L_m^2}{4}\Big(2\,\Delta\Gamma_1^J(\beta_0+\Delta\beta_0)\\
&-2\,\Gamma_1^J\Delta\beta_0 - \Gamma_0^J\Delta\beta_1 + 4\,\Gamma_0^J\Delta\beta_0\gamma_0^m\Big) + \frac{L_m}{2}\Big(-\Delta\Gamma_2^J + 2\,\Delta\Gamma_1^J\gamma_0^m + \Gamma_0^J c_{\mathrm{dec}}\\
&-4\beta_0\mathcal{M}_2^{J,+}\Big) + \mathcal{M}_3^{J,+}\Bigg]\Bigg\}\,,
\end{aligned}\tag{4.212}$$

The terms Γ_i^J and γ_i^J denote the coefficients of the cusp and non-cusp jet function anomalous dimensions with n_l+1 flavors defined by (see appendix C for explicit expressions)

$$\mu\frac{\mathrm{d}}{\mathrm{d}\mu}\,J^{(n_l+1)}(s,\mu) = \sum_{i\geq 0}\left(\frac{\alpha_s^{(n_l+1)}(\mu)}{4\pi}\right)^{i+1}\int \mathrm{d}s'\left(-\frac{\Gamma_i^J}{\mu^2}\left[\frac{\mu^2\theta(s-s')}{s-s'}\right]_+ + \gamma_i^J\,\delta(s-s')\right)J^{(n_l+1)}(s',\mu)\,. \tag{4.213}$$

The terms $\mathcal{M}_i^{J,+}$ ($\mathcal{M}_i^J$) indicate the μ_m-independent coefficients of the plus-distribution $\frac{1}{m^2}\left[\frac{m^2\theta(s)}{s}\right]_+$ and delta-distribution $\delta(s)$ in the matching coefficient $\mathcal{M}_J(s,m,m)$ (i.e. for $\mu_m = m$), respectively. Note that we have not determined the relevant constant $\mathcal{M}_3^{J,+}$ at this stage. We will see in Sec. 4.4.3 how to relate it to an existing result for the PDF threshold correction. The remaining constants appearing in Eq. (4.212) are defined below Eq. (4.181). Inserting the values for all of the constants and expanding Eq. (4.212) using the logarithmic counting $\alpha_s\ln(m^2/s) \sim \mathcal{O}(1)$ gives our final result in Eq. (4.58).

[32] For simplicity we set $\nu_n = Q$ and $\nu_{0M} = Q\mu_m^2/\mu_J^2$ here. For a phenomenological error estimate the ν-dependence can be easily restored.

4.4.3 Consistency relations

We have seen in the discussion of secondary massive gluon effects in Sec. 4.3.3 that the corresponding threshold corrections appearing in different setups for RG running are related to each other via the consistency condition in Eq. (4.127). An equivalent relation holds in the presence of secondary massive quarks, where the PDF matching correction $\mathcal{M}_{\tilde{\phi}}$ arises, when the PDF evolution crosses the mass threshold, e.g. if the final renormalization in scenario III is the jet scale $\mu_{\rm final} = \mu_J$,

$$\begin{aligned} F_1(x, Q, m) = & \sum_{i=q} \frac{e_i^2}{2} \left|C^{(n_l+1)}(Q, m, \mu_H)\right|^2 \left|U_C^{(n_l+1)}(Q, \mu_H, \mu_J)\right|^2 \\ & \times \int \mathrm{d}s \int \mathrm{d}z \int \mathrm{d}z' \int \mathrm{d}z''\, J^{(n_l+1)}(s, m, \mu_J)\, U_{\tilde{\phi}}^{(n_l+1)}(1 - z - \frac{s}{Q^2}, \mu_J, \mu_m) \\ & \times \mathcal{M}_{\tilde{\phi}}(z - z', m, \mu_m)\, U_{\tilde{\phi}}^{(n_l)}(z' - z'', \mu_m, \mu_\phi)\, \tilde{\phi}_{i/P}^{(n_l)}\Big(z'' - x, \mu_\phi\Big)\,. \end{aligned} \tag{4.214}$$

We have already computed the PDF threshold condition at $\mathcal{O}(\alpha_s^2)$ in the OPE region in Sec. 3.4.2. The result in the endpoint region can be easily obtained from Eq. (3.114) by expanding for $z \to 1$,

$$\begin{aligned} \mathcal{M}_{\tilde{\phi}}^{(2)}(1 - z, m, \mu_m) = & \frac{\alpha_s^2 C_F T_F}{(4\pi)^2} \left\{ \delta(1 - z) \left[2L_m^2 + \left(\frac{2}{3} + \frac{8\pi^2}{9}\right) L_m + \frac{73}{18} + \frac{20\pi^2}{27} - \frac{8}{3}\zeta_3 \right] \right. \\ & \left. + \left[\frac{\theta(1 - z)}{1 - z}\right]_+ \left[\frac{8}{3}L_m^2 + \frac{80}{9}L_m + \frac{224}{27}\right] \right\}. \end{aligned} \tag{4.215}$$

Eq. (4.215) contains a large logarithm $\sim \ln(1 - z)$ as for the massive gluon case (see Eq. (4.129)), that is manifest when rescaling the plus-distribution in terms of a normalized soft momentum variable $\tilde{\ell} \equiv \ell/\nu_\phi$ with $\ell = Q(1 - z)$ and $\nu_\phi \sim Q(1 - z) \sim \mu_J^2/\mu_H$ (using the identity in Eq. (B.3)),

$$\begin{aligned} \frac{\nu_\phi}{Q} \mathcal{M}_{\tilde{\phi}}^{(2)}\left(\frac{\ell}{Q}, m, Q, \mu, \nu_\phi\right) = & \frac{\alpha_s^2 C_F T_F}{(4\pi)^2} \left\{ \delta(\tilde{\ell}) \left[\left(\frac{8}{3}L_m^2 + \frac{80}{9}L_m + \frac{224}{27}\right) \ln\left(\frac{\nu_\phi}{Q}\right) + 2L_m^2 + \left(\frac{2}{3} + \frac{8\pi^2}{9}\right) L_m \right.\right. \\ & \left.\left. + \frac{73}{18} + \frac{20\pi^2}{27} - \frac{8}{3}\zeta_3 \right] + \left[\frac{\theta(\tilde{\ell})}{\tilde{\ell}}\right]_+ \left[\frac{8}{3}L_m^2 + \frac{80}{9}L_m + \frac{224}{27}\right] \right\}. \end{aligned} \tag{4.216}$$

Using the explicit fixed-order expressions for $\mathcal{M}_C$ in Eq. (4.166) and $\mathcal{M}_J$ in Eq. (4.197) one can check that the consistency relation

$$\mathcal{M}_{\tilde{\phi}}(1 - z, m, \mu) = Q^2 \left|\mathcal{M}_C(Q, m, \mu)\right|^2 \mathcal{M}_J(Q^2(1 - z), m, \mu) \tag{4.217}$$

is indeed satisfied at $\mathcal{O}(\alpha_s^2)$. The relation (4.217) implies also that the rapidity logarithms (and singularities) in the hard, collinear and PDF sectors are intrinsically related to each other. We emphasize again that the form of the threshold factors and the validity of the consistency relation are not restricted to DIS in the endpoint region, but arise in analogous form for other observables, which exhibit factorization theorems with a similar structure, i.e. involving a hard current coefficient, a jet function and a soft function as building blocks, as we will see in chapter 5.

In the following we will compute the PDF threshold condition directly from the definition in Eq. (4.8) for the PDF in the endpoint region, which confirms the fixed-order result derived from $\mathcal{M}_{\phi,qq}^{(2)}$ in the classical regime, and resum the rapidity logarithms in Eq. (4.215) via the rapidity RGE.

PDF threshold correction

We determine the PDF threshold correction from the difference of the $\overline{\rm MS}$- and OS-renormalized collinear and soft PDF functions, $f_{q/P}(\ell, m, \mu)$ and $S_\phi(\ell, m, \mu)$ defined in Eqs. (4.9) and (4.10), respectively. Since we have already seen in Eq. (4.215) that a large rapidity logarithm arises we will directly compute the corresponding contributions individually to be able to resum it via the rapidity RGE. Therefore, we calculate the massive quark corrections at $\mathcal{O}(\alpha_s^2 C_F T_F)$ in terms of the (partonic) results for the radiation of a massive gluon at $\mathcal{O}(\alpha_s)$ in Eqs. (4.132) and (4.138) as

$$\begin{aligned}\hat{f}_{q/q,T_F}^{(n_l+1,\text{bare},2)}(\ell,m,Q,\Lambda,\mu,\nu) &= \frac{1}{\pi}\int \frac{\mathrm{d}M^2}{M^2}\,\hat{f}_{q/q}^{(\text{bare},1)}(\ell,M,Q,\mu,\nu)\,\mathrm{Im}\left[\Pi(m^2,M^2)\right] \\ &\quad - \left(\Pi(m^2,0) - \frac{\alpha_s^{(n_l+1)} T_F}{3\pi}\frac{1}{\epsilon}\right)\hat{f}_{q/q}^{(\text{bare},1)}(\ell,\Lambda,Q,\mu,\nu)\,, \qquad (4.218)\\ \hat{S}_{\phi,T_F}^{(n_l+1,\text{bare},2)}(\ell,m,\Lambda,\mu,\nu) &= \frac{1}{\pi}\int \frac{\mathrm{d}M^2}{M^2}\,\hat{S}_{\phi}^{(\text{bare},1)}(\ell,M,\mu,\nu)\,\mathrm{Im}\left[\Pi(m^2,M^2)\right] \\ &\quad - \left(\Pi(m^2,0) - \frac{\alpha_s^{(n_l+1)} T_F}{3\pi}\frac{1}{\epsilon}\right)\hat{S}_{\phi}^{(\text{bare},1)}(\ell,\Lambda,\mu,\nu)\ . \qquad (4.219)\end{aligned}$$

For the massless contributions we use again a gluon mass $\Lambda \ll m$ as an infrared regulator which also allows us to apply the results from Sec. 4.3.3.

After performing the subtracted dispersion relation and including the scheme change contribution we obtain [33] ($\bar{\ell} = \ell/\nu$)

$$\begin{aligned}\nu\,\hat{f}_{q/q,T_F}^{(n_l+1,\text{bare},2)} &= \frac{\left(\alpha_s^{(n_l+1)}\right)^2 C_F T_F}{16\pi^2}\,\delta(\bar{\ell})\left\{\frac{1}{\alpha}\left[\frac{8}{3\epsilon^2} - \frac{40}{9\epsilon} - \frac{16}{3}L_m L_\Lambda + \frac{8}{3}L_m^2 + \frac{80}{9}L_m + \frac{224}{27} + \mathcal{O}(\epsilon)\right]\right. \\ &\quad + \frac{1}{\epsilon^2}\left[\frac{8}{3}\ln\left(\frac{\nu}{Q}\right) + 2\right] + \frac{1}{\epsilon}\left[-\frac{40}{9}\ln\left(\frac{\nu}{Q}\right) - \frac{1}{3} - \frac{4\pi^2}{9}\right] + \left(-\frac{16}{3}L_m L_\Lambda + \frac{8}{3}L_m^2\right. \\ &\quad \left.\left. + \frac{80}{9}L_m + \frac{224}{27}\right)\ln\left(\frac{\nu}{Q}\right) - 4L_m L_\Lambda + 2L_m^2 + \frac{20}{3}L_m + \frac{73}{18} + \frac{20\pi^2}{27} - \frac{8}{3}\zeta_3\right\}\,, \qquad (4.220)\\ \mu\,\hat{S}_{\phi,T_F}^{(n_l+1,\text{bare},2)} &= \frac{\left(\alpha_s^{(n_l+1)}\right)^2 C_F T_F}{16\pi^2}\left\{\frac{1}{\alpha}\,\delta(\bar{\ell})\left[-\frac{8}{3\epsilon^2} + \frac{40}{9\epsilon} + \frac{16}{3}L_m L_\Lambda - \frac{8}{3}L_m^2 - \frac{80}{9}L_m - \frac{224}{27} + \mathcal{O}(\epsilon)\right]\right. \\ &\quad \left. + \left[\frac{\theta(\bar{\ell})}{\bar{\ell}}\right]_+\left[\frac{8}{3\epsilon^2} - \frac{40}{9\epsilon} - \frac{16}{3}L_m L_\Lambda + \frac{8}{3}L_m^2 + \frac{80}{9}L_m + \frac{224}{27}\right]\right\}\,. \qquad (4.221)\end{aligned}$$

Therefore, the nonvanishing two-loop counterterm contributions above the quark mass threshold, where we use $\overline{\text{MS}}$-renormalization, read

$$\begin{aligned}\nu\,Z_{\tilde{\phi},f,T_F}^{(n_l+1,2)} &= \frac{\alpha_s^{(n_l+1)}(\mu,\nu)\,\alpha_s^{(n_l+1)}(\mu)\,C_F T_F}{16\pi^2}\,\delta(\bar{\ell})\left\{\frac{1}{\alpha}\left[\frac{8}{3\epsilon^2} - \frac{40}{9\epsilon} - \frac{16}{3}L_m L_\Lambda + \frac{8}{3}L_m^2 + \frac{80}{9}L_m\right.\right. \\ &\quad \left.\left. + \frac{224}{27} + \mathcal{O}(\epsilon)\right] + \frac{1}{\epsilon^2}\left[\frac{8}{3}\ln\left(\frac{\nu}{Q}\right) + 2\right] + \frac{1}{\epsilon}\left[-\frac{40}{9}\ln\left(\frac{\nu}{Q}\right) - \frac{1}{3} - \frac{4\pi^2}{9}\right]\right\}\,, \qquad (4.222)\\ \nu\,Z_{\tilde{\phi},S,T_F}^{(n_l+1,2)} &= \frac{\alpha_s^{(n_l+1)}(\mu,\nu)\,\alpha_s^{(n_l+1)}(\mu)\,C_F T_F}{16\pi^2}\left\{\frac{1}{\alpha}\,\delta(\bar{\ell})\left[-\frac{8}{3\epsilon^2} + \frac{40}{9\epsilon} + \frac{16}{3}L_m L_\Lambda - \frac{8}{3}L_m^2 - \frac{80}{9}L_m\right.\right. \\ &\quad \left.\left. - \frac{224}{27} + \mathcal{O}(\epsilon)\right] + \left[\frac{\theta(\bar{\ell})}{\bar{\ell}}\right]_+\left[\frac{8}{3\epsilon^2} - \frac{40}{9\epsilon}\right]\right\}\,. \qquad (4.223)\end{aligned}$$

The sum of the individual counterterm contributions yields the complete PDF counterterm for one flavor corresponding to Eq. (4.21),

$$Z_{\tilde{\phi},T_F}^{(n_l+1,2)}(1-z,\mu) = Q\left(Z_{\tilde{\phi},f,T_F}^{(n_l+1,2)} + Z_{\tilde{\phi},S,T_F}^{(n_l+1,2)}\right)\,. \qquad (4.224)$$

This yields together with the corresponding contributions at $\mathcal{O}(\alpha_s)$, for which the analogous relation holds, the correct μ-anomalous dimension for the PDF at $\mathcal{O}(\alpha_s^2 C_F T_F)$ in Eq. (4.33). The ν-anomalous

[33] Note that the virtual n-collinear correction is equivalent to the corresponding current contribution in Eq. (4.168), i.e. $\hat{f}_{q/q,T_F}^{(n_l+1,\text{bare},2)} = 2\hat{F}_{m,\text{SCET},n}^{(n_l+1,\text{bare},2)}\,\delta(\ell)$, which are both described by the same types of diagrams.

dimensions for the pure collinear and the soft PDF contributions in the $\overline{\text{MS}}$-scheme satisfy

$$\gamma^{(n_l+1,2)}_{\tilde{\phi},f,\nu,T_F} = -\nu\frac{\mathrm{d}}{\mathrm{d}\nu}\,Z^{(n_l+1,2)}_{\tilde{\phi},f,T_F} = \frac{\big(\alpha_s^{(n_l+1)}\big)^2 C_F T_F}{16\pi^2}\left\{-\frac{16}{3}L_m L_\Lambda + \frac{8}{3}L_m^2 + \frac{80}{9}L_m + \frac{224}{27}\right\}, \tag{4.225}$$

$$\gamma^{(n_l+1,2)}_{\tilde{\phi},S,\nu,T_F} = -\nu\frac{\mathrm{d}}{\mathrm{d}\nu}\,Z^{(n_l+1,2)}_{\tilde{\phi},S,T_F} = -\gamma^{(n_l+1,2)}_{\tilde{\phi},f,\nu,T_F}\,. \tag{4.226}$$

Below the mass threshold OS renormalization is employed for both the strong coupling and the massive quark contribution to the collinear and soft PDF functions. The threshold corrections correspond to the resulting difference to the $\overline{\text{MS}}$ renormalized quantities,

$$\begin{aligned}\mathcal{M}_{\tilde{\phi}}(1-z,m,\mu_m) &= \int \mathrm{d}z'\,\hat{\tilde{\phi}}^{(n_l+1)}(1-z',m,\mu_m)\left(\hat{\tilde{\phi}}^{(n_l)}\right)^{-1}(z'-z,m,\mu_m)\\ &= \int \mathrm{d}z'\,Z^{(n_l)}_{\tilde{\phi}}(1-z',m,\mu_m)\left(Z^{(n_l+1)}_{\tilde{\phi}}\right)^{-1}(z'-z,\mu_m)\,,\end{aligned} \tag{4.227}$$

and analogously for the individual components $\mathcal{M}_{\tilde{\phi},f}$ and $\mathcal{M}_{\tilde{\phi},S}$. For the collinear PDF threshold correction at $\mathcal{O}(\alpha_s^2 C_F T_F)$ we obtain in analogy to Eqs. (4.165) and (4.196) with $\nu_\phi \sim Q(1-x)\sim \ell$

$$\begin{aligned}\nu_\phi\,\mathcal{M}^{(2)}_{\tilde{\phi},f}(\ell,m,Q,\mu_m,\nu) &= \nu_\phi\,\hat{f}^{(n_l+1,\text{bare},2)}_{q/q,T_F} - \nu_\phi\,Z^{(n_l+1,2)}_{\tilde{\phi},f,T_F} - \frac{\alpha_s^{(n_l+1)}T_F}{3\pi}\,L_m\,\nu_\phi\,\hat{f}^{(n_l+1,1)}_{q/q}\\ &= \frac{\big(\alpha_s^{(n_l+1)}\big)^2 C_F T_F}{16\pi^2}\,\delta(\tilde{\ell})\left\{\left(\frac{8}{3}L_m^2+\frac{80}{9}L_m+\frac{224}{27}\right)\ln\left(\frac{\nu}{Q}\right)\right.\\ &\qquad \left. + 2L_m^2 + \left(\frac{2}{3}+\frac{8\pi^2}{9}\right)L_m + \frac{73}{18} + \frac{20\pi^2}{27} - \frac{8}{3}\zeta_3\right\},\end{aligned} \tag{4.228}$$

Here we have used Eq. (4.133) with a gluon mass Λ as an infrared regulator resulting in the renormalized one-loop collinear PDF function $\hat{f}^{(n_l+1,1)}_{q/q}$. Similarly, for the soft PDF threshold correction at $\mathcal{O}(\alpha_s^2 C_F T_F)$ one gets

$$\begin{aligned}\nu_\phi\,\mathcal{M}^{(2)}_{\tilde{\phi},S}(\ell,m,\mu_m,\nu) &= \nu_\phi\,S^{(n_l+1,\text{bare},2)}_{\tilde{\phi}} - \nu_\phi\,Z^{(n_l+1,2)}_{\tilde{\phi},S,T_F} - \frac{\alpha_s^{(n_l+1)}T_F}{3\pi}\,L_m\,\nu_\phi\,S^{(n_l+1,1)}_{\tilde{\phi}}\\ &= \frac{\big(\alpha_s^{(n_l+1)}\big)^2 C_F T_F}{16\pi^2}\left(\delta(\tilde{\ell})\ln\left(\frac{\nu_\phi}{\nu}\right)+\left[\frac{\theta(\tilde{\ell})}{\tilde{\ell}}\right]_+\right)\left[\frac{8}{3}L_m^2+\frac{80}{9}L_m+\frac{224}{27}\right],\end{aligned} \tag{4.229}$$

where the one-loop result in Eq. (4.138) with a gluon mass Λ was used. Upon summing up $\mathcal{M}^{(2)}_{\tilde{\phi},f}$ and $\mathcal{M}^{(2)}_{\tilde{\phi},S}$ we obtain the total PDF threshold correction in Eq. (4.215).

For the ν-evolution of the threshold corrections we obtain ($i=f,S$)

$$\nu\frac{\mathrm{d}}{\mathrm{d}\nu}\,\mathcal{M}_{\tilde{\phi},i}(\ell,m,Q,\mu,\nu) = \left(\gamma^{(n_l+1)}_{\tilde{\phi},i,\nu} - \gamma^{(n_l)}_{\tilde{\phi},i,\nu}\right)\mathcal{M}_{\tilde{\phi},i}(\ell,m,Q,\mu,\nu) \equiv \gamma_{\mathcal{M}_{\tilde{\phi},i}}\,\mathcal{M}_{\tilde{\phi},i}(\ell,m,Q,\mu,\nu)\,, \tag{4.230}$$

where the ν-anomalous dimensions for the mass mode matching coefficients read

$$\gamma^{(2)}_{\mathcal{M}_{\tilde{\phi},f}} = -\gamma^{(2)}_{\mathcal{M}_{\tilde{\phi},S}} = \frac{\alpha_s^2 C_F T_F}{16\pi^2}\left\{\frac{8}{3}L_m^2+\frac{80}{9}L_m+\frac{224}{27}\right\}. \tag{4.231}$$

As for the case of the current and jet function threshold correction the solution of Eq. (4.230) is a simple exponentiation which allows us to determine the required term at $\mathcal{O}(\alpha_s^4\ln^2(1-x))\sim\mathcal{O}(\alpha_s^2)$ in the PDF threshold correction (in the logarithmic counting $\alpha_s\ln(1-x)\sim 1$).

For a complete analysis at N^{3}LL we also need the term at $\mathcal{O}(\alpha_s^3\ln(1-x))\sim\mathcal{O}(\alpha_s^2)$. We can determine its μ_m-dependent contribution from the identity

$$\mathcal{M}_{\tilde{\phi}}(1-z,m,\mu_m) = \int\mathrm{d}z'\int\mathrm{d}z''\,U^{(n_l)}_{\tilde{\phi}}(z'-z,m,\mu_m)\,\mathcal{M}_{\tilde{\phi}}(z''-z',m,m)\,U^{(n_l+1)}_{\tilde{\phi}}(1-z'',\mu_m,m)\,. \tag{4.232}$$

or equivalently,

$$\mu\frac{\mathrm{d}}{\mathrm{d}\mu}\,\mathcal{M}_{\tilde\phi}(1-z,m,\mu) = \int \mathrm{d}z'\,\Big(\gamma_{\tilde\phi}^{(n_l+1)}(z'-z,\mu) - \gamma_{\tilde\phi}^{(n_l)}(z'-z,\mu)\Big)\,\mathcal{M}_{\tilde\phi}(1-z',m,\mu)\,. \tag{4.233}$$

Expanding in α_s gives the perturbative result for the μ_m-dependent terms. Including the relevant term at $\mathcal{O}(\alpha_s^3\ln(1-x))$ in the exponent the structure of the mass mode matching coefficient reads [34] ($\alpha_s^{(n_l+1)} = \alpha_s^{(n_l+1)}(\mu_m)$, $m=\overline{m}(\mu_m)$)

$$\begin{aligned}
\frac{\nu_\phi}{Q}\,\mathcal{M}_{\tilde\phi}\Big(\frac{\ell}{Q},m,Q,\mu_m,\nu_\phi\Big) =& \Bigg\{\delta(\tilde\ell) + \frac{\big(\alpha_s^{(n_l+1)}\big)^2}{(4\pi)^2}\,\Bigg(\delta(\tilde\ell)\Big[-\frac{L_m^2}{4}\,\gamma_0^{\tilde\phi}\Delta\beta_0 - \frac{L_m}{2}\,\Delta\gamma_1^{\tilde\phi} + \mathcal{M}_2^{\tilde\phi}\Big] \\
&+ \Bigg[\frac{\theta(\tilde\ell)}{\tilde\ell}\Bigg]_+\,\Big[\frac{L_m^2}{2}\,\Gamma_0^{\tilde\phi}\,\Delta\beta_0 + L_m\,\Delta\Gamma_1^{\tilde\phi} + \mathcal{M}_2^{\tilde\phi,+}\Big]\Bigg)\Bigg\} \\
&\times\exp\Bigg\{\frac{\big(\alpha_s^{(n_l+1)}\big)^2}{(4\pi)^2}\,\ln\Big(\frac{\nu_\phi^2}{Q^2}\Big)\Bigg[\frac{L_m^2}{4}\,\Gamma_0^{\tilde\phi}\,\Delta\beta_0 + \frac{L_m}{2}\,\Delta\Gamma_1^{\tilde\phi} + \frac{\mathcal{M}_2^{\tilde\phi,+}}{2}\Bigg] \\
&+ \frac{\big(\alpha_s^{(n_l+1)}\big)^3}{(4\pi)^3}\,\ln\Big(\frac{\nu_\phi^2}{Q^2}\Big)\,\Bigg[-\frac{L_m^3}{6}\,\Gamma_0^{\tilde\phi}\Delta\beta_0(\beta_0+\Delta\beta_0) \\
&+ \frac{L_m^2}{4}\,\Big(-2\Delta\Gamma_1^{\tilde\phi}(\beta_0+\Delta\beta_0) + 2\,\Gamma_1^{\tilde\phi}\Delta\beta_0 + \Gamma_0^{\tilde\phi}\Delta\beta_1 - 4\,\Gamma_0^{\tilde\phi}\Delta\beta_0\gamma_0^m\Big) \\
&+ \frac{L_m}{2}\Big(\Delta\Gamma_2^{\tilde\phi} - 2\Delta\Gamma_1^{\tilde\phi}\gamma_0^m - \Gamma_0^{\tilde\phi}c_{\rm dec} - 2\beta_0\mathcal{M}_2^{\tilde\phi,+}\Big) + \frac{\mathcal{M}_3^{\tilde\phi,+}}{2}\Bigg]\Bigg\}\,.
\end{aligned} \tag{4.234}$$

The terms $\Gamma_i^{\tilde\phi}$ and $\gamma_i^{\tilde\phi}$ denote the coefficients of the cusp and non-cusp PDF anomalous dimensions with n_l+1 flavors defined by (see appendix C to obtain explicit expressions)

$$\mu\frac{\mathrm{d}}{\mathrm{d}\mu}\,\tilde\phi^{(n_l+1)}(1-z,\mu) = \sum_{i\geq 0}\Big(\frac{\alpha_s^{(n_l+1)}(\mu)}{4\pi}\Big)^{i+1}\int\mathrm{d}z'\,\Bigg[-2\,\Gamma_i^{\tilde\phi}\,\Bigg[\frac{\theta(z'-z)}{z'-z}\Bigg]_+ + \gamma_i^{\tilde\phi}\,\delta(z'-z)\Bigg]\,\tilde\phi^{(n_l+1)}(1-z',\mu)\,. \tag{4.235}$$

The terms $\mathcal{M}_i^{\tilde\phi,+}$ ($\mathcal{M}_i^{\tilde\phi}$) indicate the μ_m-independent constants in the plus-distribution (delta-distribution) terms. The (nonsinglet) PDF threshold correction in the OPE region has been recently computed up to $\mathcal{O}(\alpha_s^3)$ in Ref. [84]. The corresponding expanded result for $x\to 1$ agrees with our computation for the μ_m-dependent terms at fixed order, but allows additionally to extract the relevant constant $\mathcal{M}_3^{\tilde\phi,+}$. It reads

$$\begin{aligned}
\mathcal{M}_3^{\tilde\phi,+} =& C_F T_F\,\Bigg\{C_A\Big(-\frac{35452}{729} + \frac{1648\pi^2}{243} + 60\zeta_3 - \frac{176\pi^4}{135} + \frac{32}{3}B_4\Big) + C_F\Big(\frac{6674}{27} - \frac{1208}{9}\zeta_3 + \frac{16\pi^4}{15} - \frac{64}{3}B_4\Big) \\
&+ T_F n_l\Big(-\frac{24064}{729} + \frac{512}{27}\zeta_3\Big) + T_F\Big(\frac{12064}{729} - \frac{896}{27}\zeta_3\Big)\Bigg\}\,,
\end{aligned} \tag{4.236}$$

with B_4 defined in Eq. (4.49). The remaining constants appearing in Eq. (4.234) are defined below Eq. (4.181). Using the explicit form of the threshold corrections in Eqs. (4.181), (4.212) and (4.234) and the relation between the anomalous dimensions in Eq. (4.35) one can check that the consistency condition in Eq. (4.217) is satisfied exactly for $\nu_\phi = \mu_J^2/Q$ for the μ_m-dependent terms, and for $\nu_\phi \sim \mu_J^2/Q$ up to terms of higher orders in the logarithmic counting. Furthermore, Eq. (4.217) allows to predict the constants $\mathcal{M}_3^{C,+}$ and $\mathcal{M}_3^{J,+}$, which are enhanced by a rapidity logarithm and therefore directly tied to

[34] For simplicity we set $\nu_f = Q$ and $\nu_S = \nu_\phi$ here. For a phenomenological error estimate the ν-dependence can be easily restored.

$\mathcal{M}_3^{\tilde{\phi},+}$ via

$$\mathcal{M}_3^{J,+} = 2\,\mathcal{M}_3^{C,+} = \mathcal{M}_3^{\tilde{\phi},+}\,. \tag{4.237}$$

Inserting the values for all of the constants and expanding Eq. (4.234) using the logarithmic counting $\alpha_s \ln(1-x) \sim \mathcal{O}(1)$ gives the following result for the PDF threshold correction

$$\begin{aligned}\frac{\nu_\phi}{Q}\,\mathcal{M}_{\tilde{\phi}}\bigg(\frac{\ell}{Q}, m, Q, \mu_m, \nu_\phi\bigg) = \delta(\tilde{\ell}) &+ \Bigg[\frac{\big(\alpha_s^{(n_l+1)}\big)^2}{(4\pi)^2}\,\delta(\tilde{\ell})\ln\bigg(\frac{\nu_\phi^2}{Q^2}\bigg)\,\mathcal{M}^{(2)}_{\phi,\ln}(m,\mu_m)\Bigg]_{\mathcal{O}(\alpha_s)} \\ &+ \Bigg[\frac{\big(\alpha_s^{(n_l+1)}\big)^2}{(4\pi)^2}\Bigg(\delta(\tilde{\ell})\,\mathcal{M}^{(2)}_{\tilde{\phi},1}(m,\mu_m) + \bigg[\frac{\theta(\tilde{\ell})}{\tilde{\ell}}\bigg]_+ 2\mathcal{M}^{(2)}_{\tilde{\phi},\ln}(m,\mu_m)\Bigg) \\ &+ \frac{\big(\alpha_s^{(n_l+1)}\big)^3}{(4\pi)^3}\,\delta(\tilde{\ell})\ln\bigg(\frac{\nu_\phi^2}{Q^2}\bigg)\,\mathcal{M}^{(3)}_{\tilde{\phi},\ln}(m,\mu_m) \\ &+ \frac{\big(\alpha_s^{(n_l+1)}\big)^4}{(4\pi)^4}\,\delta(\tilde{\ell})\ln^2\bigg(\frac{\nu_\phi^2}{Q^2}\bigg)\,\mathcal{M}^{(4)}_{\tilde{\phi},\ln^2}(m,\mu_m)\Bigg]_{\mathcal{O}(\alpha_s^2)} + \mathcal{O}(\alpha_s^3)\,. \end{aligned} \tag{4.238}$$

We display the corresponding results for $\alpha_s^{(n_l+1)} = \alpha_s^{(n_l+1)}(\mu_m)$ and $m \equiv \overline{m}(\mu_m)$ given in the $\overline{\rm MS}$ scheme. The functions multiplying the logarithm $\ln(\nu_\phi^2/Q^2)$ are related to the ones entering the current mass mode matching correction (see Eqs. (4.46), (4.48) and (4.50))

$$\mathcal{M}^{(2)}_{\tilde{\phi},\ln}(m,\mu_m) = -\,\mathcal{M}^{(2)}_{C,\ln}(m,\mu_m)\,, \tag{4.239}$$

$$\mathcal{M}^{(3)}_{\tilde{\phi},\ln}(m,\mu_m) = -\,\mathcal{M}^{(3)}_{C,\ln}(m,\mu_m)\,, \tag{4.240}$$

$$\mathcal{M}^{(4)}_{\tilde{\phi},\ln^2}(m,\mu_m) = \mathcal{M}^{(4)}_{C,\ln^2}(m,\mu_m)\,. \tag{4.241}$$

Finally, the less universal two-loop function $\mathcal{M}^{(2)}_{\tilde{\phi},1}$ which is not related to a rapidity logarithm can be easily identified from Eq. (4.215),

$$\mathcal{M}^{(2)}_{\tilde{\phi},1}(m,\mu_m) = C_F T_F\left\{2L_m^2 + \bigg(\frac{2}{3} + \frac{8\pi^2}{9}\bigg)L_m + \frac{73}{18} + \frac{20\pi^2}{27} - \frac{8}{3}\zeta_3\right\}. \tag{4.242}$$

4.4.4 Fixed-order expansion and comparison with full QCD result

The factorization theorems discussed in Sec. 4.2 each contain all information about the singular $\mathcal{O}(\alpha_s^2 C_F T_F)$ secondary massive quark corrections to the structure function $F_1(x,Q,m)$ in the fixed-order expansion in full QCD. Besides the virtual contributions in QCD, which are fully contained in the SCET description, the singular perturbative fixed-order corrections also consist of the singular collinear real radiation contributions which arise for $1-x \sim m^2/Q^2 \ll 1$. Setting $\mu = \mu_H = \mu_J = \mu_m$ we obtain in any scenario

$$F_1(x,Q,m)\big|_{\rm FO} = \sum_{i=q}\frac{e_i^2}{2}\int {\rm d}\xi\; \underbrace{Q^2\big|C^{(n_l)}(Q,m,\mu)\big|^2\, J^{(n_l)}(Q^2(1-\xi),m,\mu)}_{\equiv\, \mathcal{C}^{(n_l)}_{x\to1}(\xi,Q,m,\mu)}\;\tilde{\phi}^{(n_l)}_{i/P}\Big(\xi - x,\mu\Big)\,. \tag{4.243}$$

where the massive quark contributions to the fixed-order matching coefficient $\mathcal{C}^{(n_l)}_{x\to1}$ at $\mathcal{O}(\alpha_s^2 C_F T_F)$ read

$$\mathcal{C}^{(n_l,2)}_{x\to1,m}(z,Q,m) = 2\hat{F}^{(n_l,2)}_{m,{\rm QCD}}(Q,m)\,\delta(1-z) + Q^2 J^{(n_l,2)}_{m,{\rm real}}(Q^2(1-z),m)\,. \tag{4.244}$$

with $\hat{F}^{(n_l,2)}_{m,{\rm QCD}}(Q,m)$ and $J^{(n_l,2)}_{m,{\rm real}}(s,m)$ given in Eqs. (3.95) and (4.54) with $\alpha_s = \alpha_s^{(n_l)}(\mu)$. In analogy to Sec. 4.3.4 we can obtain this result also from the corresponding full QCD fixed-order computation in Sec. 3. Since the virtual contributions in the $\delta(1-z)$ distribution agree, we only have to consider the

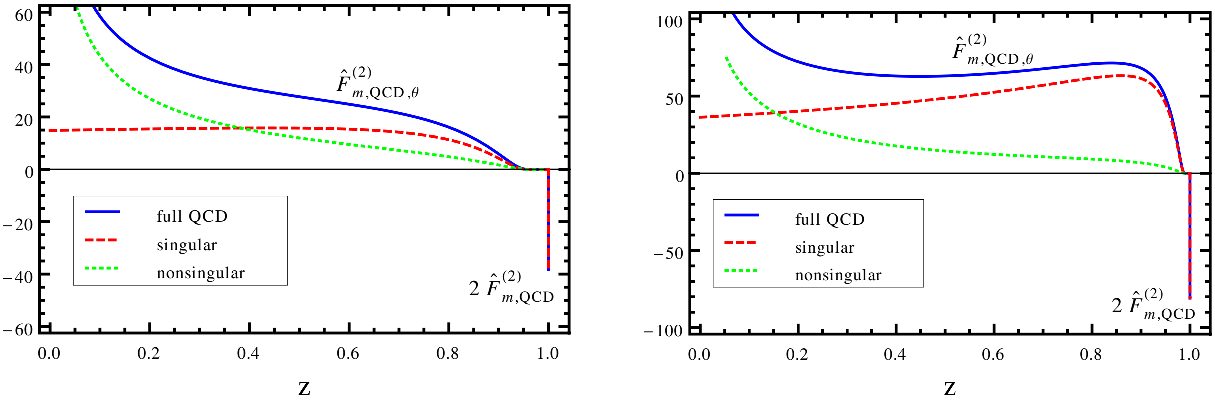

Figure 4.14: Secondary massive quark contributions at $\mathcal{O}(\alpha_s^2 C_F T_F)$ in full QCD (blue, solid) together with the singular result for $z \to 1$ in the fixed-order expansion (red, dashed) and the nonsingular terms (green, dotted) for $\hat{m} = 0.1$ (left panel) and $\hat{m} = 0.05$ (right panel), all normalized by $\alpha_s^2 C_F T_F/(4\pi)^2$.

expansion of the real radiation term $\hat{F}^{(n_l,2)}_{m,\mathrm{QCD},\theta}(z,Q,m)$ in Eq. (3.98) for $1-z \sim \hat{m}^2 \ll 1$ (with $\hat{m} = m/Q$), which yields indeed the correct term,

$$\theta(1-z-4\hat{m}^2 z)\,\hat{F}^{(n_l,2)}_{m,\mathrm{QCD},\theta}(z,Q,m) \xrightarrow{z\to 1} Q^2 \delta J^{(n_l,2)}_{m,\mathrm{real}}(Q^2(1-z),m) + \mathcal{O}((1-z)^0,\hat{m}^0)\,, \tag{4.245}$$

In Fig. 4.14 we display the full fixed-flavor QCD term $\mathcal{C}^{(n_l,2)}_{qq,T_F}(z,Q,m)$ (blue, solid line), the singular fixed-order terms corresponding to the SCET result in Eq. (4.244) (red, dashed line) and the remaining nonsingular terms (green, dotted line) for $\hat{m} = 0.1$ and $\hat{m} = 0.05$. We note that compared to the massive gluon results in Sec. 4.3.4 the singular fixed-order terms do not provide a good approximation of the full QCD result away from the endpoint unless the mass is very small, so that a phenomenological analysis will necessarily have to take care of the nonsingular terms in $1-x$, even in the vicinity of the endpoint for not very large hierarchies between the m and Q. The nonsingular terms can be included together with the singular terms in a combined description $F_1^{\mathrm{tot}}(x,Q,m)$,

$$F_1^{\mathrm{tot}}(x,Q,m) = F_1^{\mathrm{s}}(x,Q,m) + F_1^{\mathrm{ns}}(x,Q,m)\,. \tag{4.246}$$

Here $F_1^{\mathrm{s}}(x,Q,m)$ denotes the factorized SCET structure function in its scenario-dependent appearance as discussed in Sec. 4.2, which treats the most singular terms and resums all logarithms $\sim \ln(1-x)$, and $F_1^{\mathrm{ns}}(x,Q,m)$ corresponds to the difference between the factorized QCD structure function discussed in Sec. 3.4 and the SCET structure function evaluated at fixed order concerning $1-x$, i.e. for $\mu_J = \mu_H$. Here we will not carry out a numerical analysis of secondary massive quark effects, since in practice they will unlikely play any role in any phenomenological discussion of the endpoint region, where currently only few data with large uncertainties are present. In the following chapter we will discuss the example of the thrust distribution, where these effects are phenomenologically more relevant and where their numerical impact will be determined in relation to the complete massless result.

Chapter 5

VFNS for thrust in the dijet region

We turn to the discussion of secondary massive quark effects for event shapes in e^+e^- collisions. Here we will consider the most prominent event shape, namely thrust. The setup of most other inclusive soft-recoil insensitive observables is very similar, but the computations can be significantly more involved.

After a short introduction to event shapes in Sec. 5.1 we discuss the massless factorization theorem for thrust in the dijet limit in Sec. 5.2. Its structure and ingredients resemble the ones for DIS in the endpoint region $x \to 1$. The main difference is the appearance of a soft scale that is not necessarily related to $\Lambda_{\rm QCD}$ and can generate a perturbative soft function. As explained in Sec. 5.3 this also leads to the only major extension of the mass mode setup discussed for DIS in Sec. 4.2, namely to an additional EFT scenario where the mass is below the soft scale. This requires the computation of the massive quark corrections to the soft function which we describe in detail in Sec. 5.4. Since the thrust soft function depends on individual projections and not just the sum of all final state particle momenta the dispersive technique cannot be used directly to obtain the complete result, but provides a good starting point for the more involved computation. The soft function can have large nonperturbative power corrections and suffers from a renormalon problem in dimensional regularization which can be cured in the gap formalism of Ref. [92] by appropriate subtractions and the infrared evolution of the corresponding gap parameter. Here the required components are computed for the secondary massive quark case. Finally, we show a numerical analysis for secondary massive bottom and top quark effects at different c.m. energies. In particular we give estimates for the impact of the mass corrections on phenomenological analyses in relation to the massless approximation.

5.1 Event shapes

Infrared and collinear safe observables at e^+e^--colliders provide a clean environment to study QCD at the high precision. Among these observable event shapes are particularly simple and suitable to describe geometrically the final state in an inclusive way. Instead of relying on jet algorithms, that introduce cutoff scales, event shapes measure the "jettiness" of an event (i.e. usually how dijet-like the final state is) in a continuous way and are more practical for analytic calculations. On the experimental side there has been a large amount of data taken at LEP and at PETRA at different c.m. energies (between 14 and 207 GeV) with small uncertainties. On the theoretical side the description of event shape distributions has recently seen substantial progress concerning the treatment of higher-order QCD corrections [93–96], the techniques concerning the summation of large logarithmic terms [40, 41, 97–100] and the implementation of schemes that avoid renormalon ambiguities together with the definition of nonperturbative parameters [92, 101]. These developments have contributed to an improved theoretical accuracy for the description of event shape distributions and to precise measurements of QCD parameters such as the strong coupling [4, 5, 97, 100, 102].

Popular examples for event shapes are angularities [103] including thrust [104] and jet broadening [105], heavy jet mass [106] and the C-parameter [107]. All of these have the generic property that their values continuously interpolate between the dijet region with narrow back-to-back jets in one limit and the isotropic region with uniform radiation in the other limit. Note that this can be also generalized for N jets [108]. Many examples and specific features of several event shapes can be found in [109].

As a concrete event shape we will discuss in the following thrust, where we define the thrust variable

Figure 5.1: Illustration of the kinematic scales for thrust. The different colors indicate radiation at different invariant masses.

τ via

$$\tau \,=\, 1 - T \,=\, 1 - \max_{\vec{n}} \frac{\sum_i |\vec{n}\cdot\vec{p}_i|}{\sum_j |E_j|} \,=\, 1 - \max_{\vec{n}} \sum_i \frac{|\vec{n}\cdot\vec{p}_i|}{Q}\,. \tag{5.1}$$

Here the sum is performed over all final state particles with momenta $\vec{p}_i$ and energies E_i. The axis that maximizes the moduli of the momentum projections is called thrust axis. Note that we define the thrust variable τ normalized with respect to the c.m. energy Q, which is the sum of all energies, in contrast to the original definition [104], where the sum of the modula of the momenta $\vec{p}_i$ appears in the denominator. [1] In the massless case both definition coincide, but in the massive case our definition simplifies the analytical computations significantly. Thrust is related to the invariant masses from all particles in each of the two hemispheres $(+,-)$ separated by the plane perpendicular to the thrust axis via

$$\tau = \frac{s_+ + s_-}{Q^2} + \mathcal{O}\left(\frac{s_{+,-}^2}{Q^4}\right) \tag{5.2}$$

in the dijet limit, where the invariant masses in both hemispheres vanish and $\tau \to 0$. The isotropic multi-particle limit is reached for $\tau \to 1/2$ (for massless primary quarks).

For thrust and any soft-recoil insensitive event shapes (i.e. not for jet broadening) the dijet region $\tau \ll 1$ is governed by three different scales, see Fig. 5.1: the hard scale Q corresponding to the c.m. energy, the jet scale $Q\lambda$ related to the invariant mass of collinear fluctuations and the soft scale $Q\lambda^2$, where low energetic ultrasoft radiation between the jets takes place. In the peak region, where $\tau \sim \Lambda_{\rm QCD}/Q$, the ultrasoft radiation saturates at a hadronic scale such that $\lambda \sim \sqrt{\Lambda_{\rm QCD}/Q}$, whereas in the tail region $\Lambda_{\rm QCD}/Q \ll \tau \ll 1$ the ultrasoft scale can exceed the hadronic scale contributing to an invariant mass in each hemisphere of order $Q^2\tau$, such that $\lambda \sim \sqrt{\tau}$ and structures at the hadronic scale appear only via power corrections. Finally, if $\tau \sim 1/2$ the distinction into hard, jet and ultrasoft scales becomes artificial and perturbative radiation can be always described in a fixed-order description at the scale Q.

Note that the thrust distribution exhibits a power law behavior making it large in the extreme dijet limit, in particular in the peak region, such that this region, where the resummation of infrared soft and collinear logarithms needs to be performed, is phenomenologically very relevant. This is in contrast to DIS in the endpoint region where we had a suppression due to the small values of the PDFs.

5.2 The massless factorization theorem

In this section we briefly review the known massless factorization theorem for the most singular contributions of the thrust distribution in the dijet limit, which are the dominant terms for small values of τ. The relevant SCET modes for $\tau \to 0$ are displayed in Fig. 5.2. This time we have only SCET I-type modes, the n- and $\bar{n}$-collinear modes corresponding to the quark and antiquark initiated jets along the thrust

[1] Our definition agrees also with the event shape variable 2-jettiness [108].

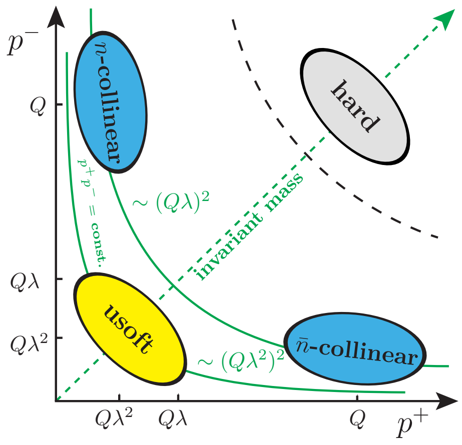

mode	$p^\mu = (+,-,\perp)$	p^2	fields
hard	$Q(1,1,1)$	Q^2	$-$
n-collinear	$Q(\lambda^2,1,\lambda)$	$Q^2\lambda^2$	$\xi_n,\ A_n^\mu$
$\bar{n}$-collinear	$Q(1,\lambda^2,\lambda)$	$Q^2\lambda^2$	$\xi_{\bar{n}},\ A_{\bar{n}}^\mu$
ultrasoft	$Q(\lambda^2,\lambda^2,\lambda^2)$	$Q^2\lambda^4$	$q_{us},\ A_{us}^\mu$

Figure 5.2: Relevant momentum modes for thrust in the dijet limit $\tau \to 0$. Adapted from Ref. [26].

axis with invariant mass of $\mathcal{O}(Q^2\lambda^2)$ and the ultrasoft modes with invariant mass $\mathcal{O}(Q^2\lambda^4)$. The factorization proceeds in a similar way as for DIS in the endpoint region, see Sec. 4.1, where now, however, no matching onto SCET II is required at the end. As a first step of the factorization we match the currents in the full QCD hadronic tensor, which is defined in analogy to Eq. (3.6), onto the corresponding SCET currents in Eq. (4.2) resulting in the Wilson coefficient $\tilde{C}(\omega,\omega')$. After the final state is decomposed into n-, $\bar{n}$-collinear and ultrasoft states and the different gauge structures are disentangled into spin and color singlets, the cross section in the SCET limit reads

$$\begin{aligned}\sigma \sim\; & (2\pi)^4\,\delta^{(4)}\left(q - P_{X_{\bar{n}}} - P_{X_n} - P_{X_{us}}\right)\int \mathrm{d}\omega \int \mathrm{d}\omega'\ \left|C(\omega,\omega')\right|^2 \\ & \times \sum_{X_{\bar{n}}} \frac{1}{4\pi N_c}\,\mathrm{Tr}\left\{\langle 0|\bar{\chi}_{\bar{n}}|X_{\bar{n}}\rangle\langle X_{\bar{n}}|\frac{\not{n}}{2}\chi_{\bar{n},\omega}|0\rangle\right\}\sum_{X_n}\frac{1}{4\pi N_c}\,\mathrm{Tr}\left\{\langle 0|\frac{\not{\bar{n}}}{2}\chi_n|X_n\rangle\langle X_n|\bar{\chi}_{n,\omega'}|0\rangle\right\} \\ & \times \sum_{X_{us}}\frac{1}{N_c}\,\mathrm{Tr}\Big\{\langle 0|\overline{T}\left[Y_{\bar{n}}(\infty,0)\overline{Y}_n(\infty,0)\right]|X_{us}\rangle\langle X_{us}|T\left[Y_n(\infty,0)\overline{Y}_{\bar{n}}(\infty,0)\right]|0\rangle\Big\}\,. \end{aligned} \tag{5.3}$$

Then the details on the particular event shape are implemented and the expansions for the restricted dijet-like final state are performed. The corresponding algebra has been performed in Ref. [8] for the double hemisphere invariant mass distribution and thrust, which are related via Eq. (5.2).

The resulting factorization theorem for n_f massless quarks reads to all orders in α_s up to the higher orders in $\lambda \sim \max\{\tau^{1/2}, (\Lambda_{\rm QCD}/Q)^{1/2}\}$ [8, 77, 103, 110, 111] [2]

$$\begin{aligned}\frac{1}{\sigma_0}\frac{\mathrm{d}\sigma}{\mathrm{d}\tau} =\, & Q\left|\tilde{C}^{(n_f)}(Q,\mu_H)\right|^2\left|U_{\tilde{C}}^{(n_f)}(Q,\mu_H,\mu)\right|^2\int \mathrm{d}s\int \mathrm{d}s'\ J_\tau^{(n_f)}(s',\mu_J)\,U_{J_\tau}^{(n_f)}(s-s',\mu,\mu_J) \\ & \times \int \mathrm{d}\ell\ S_\tau^{(n_f)}(Q\tau - \frac{s}{Q} - \ell,\mu_S)\,U_{S_\tau}^{(n_f)}(\ell,\mu,\mu_S)\,. \end{aligned} \tag{5.4}$$

Here σ_0 denotes the total partonic e^+e^- cross-section at tree-level. The local hard matching coefficient $\tilde{C}^{(n_f)}(Q,\mu)$ is the same as $C^{(n_f)}(Q,\mu)$ appearing in the factorization theorem for DIS in the endpoint region in Eq. (4.6) up to an analytic continuation from spacelike to timelike momentum transfer, $q^2_{\rm DIS} = -Q^2 \to q^2_{\rm e^+e^-} = Q^2$. This amounts to a simple replacement of $L_Q = \ln(Q^2/\mu^2)$ to $L_{-Q} = \ln(-Q^2/\mu^2)$ (with $Q^2 = Q^2 + i0$) in Eqs. (4.12) – (4.15).

The thrust jet function $J_\tau^{(n_f)}(s,\mu)$ describes the dynamics of the n- and $\bar{n}$-collinear modes and takes into account both final state jets in n and $\bar{n}$ direction,

$$J_\tau^{(n_f)}(s,\mu) \equiv \int \mathrm{d}s'\ J_n^{(n_f)}(s-s',\mu)\,J_{\bar{n}}^{(n_f)}(s',\mu)\,, \tag{5.5}$$

[2] In fact the first nonvanishing power corrections are again of $\mathcal{O}(\lambda^2)$.

where $J_n^{(n_f)}(s,\mu)$ is the same hemisphere jet function as the one appearing in the DIS factorization theorem for $x \to 1$ in Eq. (4.6) and defined in Eq. (4.7). The $\bar{n}$-collinear antiquark jet function is given in analogy by

$$J_{\bar{n}}^{(n_f)}(Qr_{\bar{n}}^{-},\mu) \equiv \frac{1}{2\pi N_c Q}\,\mathrm{Im}\left[i\int \mathrm{d}^4x\, e^{ir_{\bar{n}}\cdot x}\langle 0|\mathrm{T}\{\bar{\chi}_{\bar{n}}(x)\frac{\not{n}}{2}\chi_{\bar{n},-Q}(0)\}|0\rangle\right], \tag{5.6}$$

which has the same perturbative expansion as $J_n^{(n_f)}(s,\mu)$ due to charge conjugation symmetry. Therefore, the corrections to the thrust jet function at $\mathcal{O}(\alpha_s)$ and $\mathcal{O}(\alpha_s^2 C_F T_F)$ amount to a multiplication of Eqs. (4.16) – (4.19) by a factor of 2.

The thrust soft function $S_\tau^{(n_f)}(\ell,\mu)$ describes ultrasoft radiation between the two jets and reads

$$S_\tau^{(n_f)}(\ell,\mu) = \frac{1}{N_c}\sum_{X_{us}}\delta(\ell - n\cdot k_s^R - \bar{n}\cdot k_s^L)\,\langle 0|\tilde{Y}_{\bar{n},+}^{\dagger}(0)\,Y_{n,-}(0)|X_{us}\rangle\langle X_{us}|Y_{n,+}^{\dagger}(0)\,\tilde{Y}_{\bar{n},-}(0)|0\rangle\,, \tag{5.7}$$

where we have defined the (anti-)time-ordered Wilson lines $\tilde{Y}_{n,-}(x) \equiv T[Y_{n,-}(x)]$ and $\tilde{Y}_{\bar{n},+}^{\dagger}(x) \equiv \overline{T}[Y_{\bar{n},+}^{\dagger}(x)]$. Furthermore, k_s^R (k_s^L) denotes the momentum of the ultrasoft final state $|X_{us}\rangle$ in the right (left) hemisphere and again all color indices are traced implicitly. [3] It is convenient to write the complete soft function as a convolution of the partonic soft function describing perturbative corrections at the ultrasoft scale and the nonperturbative hadronic soft function $S_\tau^{\mathrm{mod}}(\ell)$ [92], i.e.

$$S_\tau^{(n_f)}(\ell,\mu) = \int \mathrm{d}\ell'\,\hat{S}_\tau^{(n_f)}(\ell-\ell',\mu)\,S_\tau^{\mathrm{mod}}(\ell')\,. \tag{5.8}$$

The renormalized expressions for the partonic soft function are known up to two loops [112,113] and read at $\mathcal{O}(\alpha_s)$ and $\mathcal{O}(\alpha_s^2 C_F T_F)$

$$\mu\,\hat{S}_\tau^{(n_f,1)}(\ell,\mu) = \frac{\alpha_s^{(n_f)}C_F}{4\pi}\left\{\frac{\pi^2}{3}\,\delta(\bar{\ell}) - 16\left[\frac{\theta(\bar{\ell})\ln\bar{\ell}}{\bar{\ell}}\right]_+\right\}, \tag{5.9}$$

$$\begin{aligned}\mu\,\hat{S}_{\tau,T_F}^{(n_f,2)}(\ell,\mu) = \frac{\big(\alpha_s^{(n_f)}\big)^2 C_F T_F}{16\pi^2}&\left\{\delta(\bar{\ell})\left[\frac{80}{81}+\frac{74\pi^2}{27}-\frac{232}{9}\zeta_3\right]+\left[\frac{\theta(\bar{\ell})}{\bar{\ell}}\right]_+\left[-\frac{448}{27}+\frac{16\pi^2}{9}\right]\right.\\ &\left.+\frac{320}{9}\left[\frac{\theta(\bar{\ell})\ln\bar{\ell}}{\bar{\ell}}\right]_+ - \frac{64}{3}\left[\frac{\theta(\bar{\ell})\ln^2\bar{\ell}}{\bar{\ell}}\right]_+\right\},\end{aligned} \tag{5.10}$$

with $\bar{\ell} \equiv \ell/\mu$. The corresponding contributions to the renormalization factor read

$$\mu\,Z_{S_\tau}^{(n_f,1)}(\ell,\mu) = \frac{\alpha_s^{(n_f)}C_F}{4\pi}\left\{-\frac{4}{\epsilon^2}\,\delta(\bar{\ell}) + \frac{8}{\epsilon}\left[\frac{\theta(\bar{\ell})}{\bar{\ell}}\right]_+\right\}, \tag{5.11}$$

$$\mu\,Z_{S_\tau,T_F}^{(n_f,2)}(\ell,\mu) = \frac{\big(\alpha_s^{(n_f)}\big)^2 C_F T_F}{16\pi^2}\left\{\delta(\bar{\ell})\left[-\frac{4}{\epsilon^3}+\frac{20}{9\epsilon^2}+\frac{1}{\epsilon}\left(\frac{112}{27}-\frac{2\pi^2}{9}\right)\right]+\left[\frac{\theta(\bar{\ell})}{\bar{\ell}}\right]_+\left[\frac{16}{3\epsilon^2}-\frac{80}{9\epsilon}\right]\right\}. \tag{5.12}$$

Large UV logarithms between the characteristic scales of each sector, μ_H, μ_J and μ_S, and the final, common renormalization scale of the factorization theorem μ are summed by the evolution factors $U_{\tilde{C}}^{(n_f)}(Q,\mu_0,\mu)$, $U_{J_\tau}^{(n_f)}(s,\mu,\mu_0)$ and $U_{S_\tau}^{(n_f)}(\ell,\mu,\mu_0)$ satisfying RG equations analogous to Eqs. (4.22) and (4.23), and by

$$\mu\frac{\mathrm{d}}{\mathrm{d}\mu}\,U_{S_\tau}^{(n_f)}(\ell,\mu,\mu_S) = \int \mathrm{d}\ell'\,\gamma_{S_\tau}^{(n_f)}(\ell-\ell',\mu)\,U_{S_\tau}^{(n_f)}(\ell',\mu,\mu_S)\,. \tag{5.13}$$

[3] The thrust soft function cannot be written as imaginary part of a time-ordered product in contrast to the PDF soft function (see Eq. 4.10) since the momenta of the final state particles enter the definition incoherently.

We display for completeness the anomalous dimensions of the soft function at $\mathcal{O}(\alpha_s)$ and $\mathcal{O}(\alpha_s^2 C_F T_F)$,

$$\mu\,\gamma_{S_\tau}^{(n_f,1)}(\ell,\mu) = = \frac{\alpha_s C_F}{4\pi}\left\{4\,\Gamma^{(1)}\left[\frac{\theta(\bar\ell)}{\bar\ell}\right]_+\right\}, \tag{5.14}$$

$$\mu\,\gamma_{S_\tau,T_F}^{(n_f,2)}(\ell,\mu) = \frac{\big(\alpha_s^{(n_f)}\big)^2 C_F T_F}{16\pi^2}\left\{4\,\Gamma_{T_F}^{(2)}\left[\frac{\theta(\bar\ell)}{\bar\ell}\right]_+ + \left(\frac{448}{27}-\frac{8\pi^2}{9}\right)\delta(\bar\ell)\right\}, \tag{5.15}$$

with $\Gamma^{(1)} = 4$ and $\Gamma_{T_F}^{(2)} = -80/9$ being the $\mathcal{O}(\alpha_s)$ and $\mathcal{O}(\alpha_s^2 C_F T_F)$ coefficients of the cusp anomalous dimension $\Gamma_{\rm cusp}^{(n_f)}$. We mention that in analogy to Eq. (4.34) one obtains a consistency relation between the anomalous dimensions, which reads here

$$2\,{\rm Re}\big[\gamma_{\tilde C}^{(n_f)}(Q,\mu)\big]\delta(\bar\ell) + Q\,\mu\,\gamma_{J_\tau}^{(n_f)}(Q\ell,\mu) + \mu\,\gamma_{S_\tau}^{(n_f)}(\ell,\mu) = 0\,. \tag{5.16}$$

The overlap between the partonic and the nonperturbative contributions in dimensional regularization leads to an infrared sensitivity of the perturbative corrections implying factorially enhanced coefficients called *renormalons*. These are formally defined as a type of singularities in the Borel transform of the perturbative series and the divergent behavior of the corresponding coefficients can be related to the ambiguities in performing the back transform arising from the pole structure in the Borel plane, see Ref. [114] for more information. Introducing a gap parameter $\Delta \sim \Lambda_{\rm QCD}$ in the hadronic soft model function related to a minimal hadronic energy deposit in each hemisphere together with properly defined perturbative subtractions in the partonic soft function, one can eliminate the renormalon problem for the leading $\mathcal{O}(\Lambda_{\rm QCD})$ power correction that arises in the operator production expansion (OPE) of the soft function for $\ell \gg \Lambda_{\rm QCD}$ rendering it order-by-order IR stable [92, 115]. Effectively, one switches to a short distance scheme, which depends on an IR "cutoff" scale R. The complete function including the renormalon-subtractions has the form

$$S_\tau^{(n_f)}(\ell,\mu) = \int {\rm d}\ell'\,\hat S_\tau^{(n_f)}\Big(\ell-\ell'-2\delta^{(n_f)}(R,\mu),\mu\Big)\,S_\tau^{\rm mod}\Big(\ell'-2\bar\Delta^{(n_f)}(R,\mu)\Big)\,, \tag{5.17}$$

where $\delta^{(n_f)}(R,\mu)$ is the subtraction series, and $\bar\Delta^{(n_f)}(R,\mu)$ is the gap parameter which is free of the $\mathcal{O}(\Lambda_{\rm QCD})$ renormalon. A convenient definition for $\delta^{(n_f)}(R,\mu)$ with consistent RG properties has been given in Ref. [115] and has the form

$$\delta^{(n_f)}(R,\mu) = \frac{R}{2}\,e^{\gamma_E}\frac{\rm d}{{\rm d}\ln(ix)}\,\ln\tilde S_\tau^{(n_f)}(x,\mu)\Big|_{x=(iRe^{\gamma_E})^{-1}}\,, \tag{5.18}$$

where $\tilde S_\tau^{(n_f)}(x,\mu)$ is the partonic soft function in configuration space, $\tilde S_\tau^{(n_f)}(x,\mu) = \int {\rm d}\ell\,\hat S_\tau^{(n_f)}(\ell,\mu)\,e^{-i\ell x}$. The $\mathcal{O}(\alpha_s)$ and $\mathcal{O}(\alpha_s^2 C_F T_F)$ corrections read

$$\delta^{(n_f,1)}(R,\mu) = \frac{\alpha_s^{(n_f)} C_F}{4\pi}\,R\,e^{\gamma_E}\left\{-4\ln\left(\frac{\mu^2}{R^2}\right)\right\}, \tag{5.19}$$

$$\delta_{T_F}^{(n_f,2)}(R,\mu) = \frac{\big(\alpha_s^{(n_f)}\big)^2 C_F T_F}{16\pi^2}\,R\,e^{\gamma_E}\left\{\frac{8}{3}\ln^2\left(\frac{\mu^2}{R^2}\right) + \frac{80}{9}\ln\left(\frac{\mu^2}{R^2}\right) + \frac{224}{27} + \frac{8\pi^2}{9}\right\}. \tag{5.20}$$

The renormalon-free gap parameter $\bar\Delta^{(n_f)}(R,\mu)$ is related to the ambiguous, but scale-independent "bare" gap parameter Δ by the relation [4]

$$\Delta = \bar\Delta^{(n_f)}(R,\mu) + \delta^{(n_f)}(R,\mu)\,. \tag{5.21}$$

Thus $\bar\Delta^{(n_f)}(R,\mu)$ is now scale- and subtraction scheme-dependent. The natural choice for the scale R of the nonperturbative gap is $R \gtrsim \Lambda_{\rm QCD}$. On the other hand, the renormalon subtraction $\delta^{(n_f)}(R,\mu)$ should

[4] The "bare" gap parameter Δ is conceptually analogous to the heavy quark pole mass parameter, so all renormalon-free gap schemes can be related to each other unambiguously through their relation to the bare Δ.

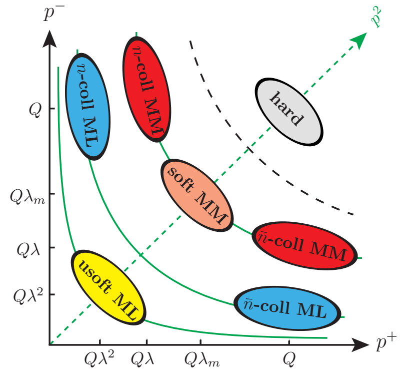

(a) $1 > \lambda_m > \lambda > \lambda^2$

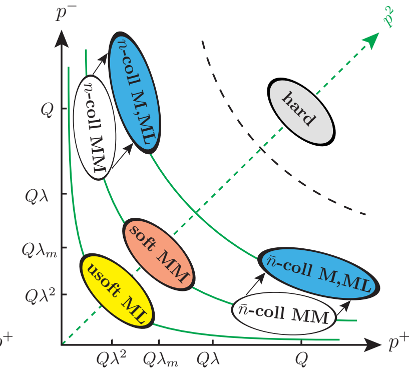

(b) $1 > \lambda > \lambda_m > \lambda^2$

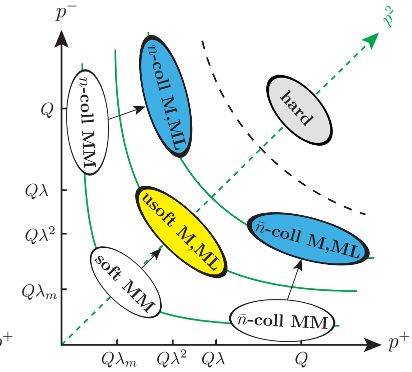

(c) $1 > \lambda > \lambda^2 > \lambda_m$

Figure 5.3: Localization of massless (ML) and massive (M) modes together with their mass-shell fluctuations (MM) in the p^+-p^- phase space according to their generic scaling for different hierarchies between λ and λ_m for $\lambda_m < 1$.

be evaluated for $\mu = \mu_S$, which is much larger than $\Lambda_{\rm QCD}$ in the tail region, in order to achieve a proper cancellation with the IR sensitive terms in the soft function. This requires the resummation of large logarithms $\sim \ln(\mu_S/\Lambda_{\rm QCD})$ which can be performed by solving the evolution equations [92, 101, 115, 116]

$$R\frac{\mathrm{d}}{\mathrm{d}R}\,\bar\Delta^{(n_f)}(R,R) \equiv -R\,\gamma_R^{(n_f)}[\alpha_s^{(n_f)}(R)] = -R\frac{\mathrm{d}}{\mathrm{d}R}\,\delta^{(n_f)}(R,R)\,, \tag{5.22}$$

$$\mu\frac{\mathrm{d}}{\mathrm{d}\mu}\,\bar\Delta^{(n_f)}(R,\mu) \equiv -R\,\gamma_{\Delta,\mu}^{(n_f)} = 2R\,e^{\gamma_E}\,\Gamma_{\rm cusp}^{(n_f)}[\alpha_s^{(n_f)}(\mu)]\,. \tag{5.23}$$

Note that the R-anomalous dimension $\gamma_R^{(n_f)}$, which is responsible for relating $\bar\Delta^{(n_f)}(R,\mu)$ at different values of R to each other in a way free of the $\mathcal{O}(\Lambda_{\rm QCD})$ renormalon and free of large IR logarithms, happens to vanish at $\mathcal{O}(\alpha_s)$, i.e. $\gamma_R^{(n_f,1)} = 0$. Thus the leading anomalous dimension at $\mathcal{O}(\alpha_s^2)$ depends both linearly and via the strong coupling constant on the number of active flavors n_f. The contribution at $\mathcal{O}(\alpha_s^2 C_F T_F)$ reads

$$\gamma_{R,T_F}^{(n_f,2)} = \frac{\left(\alpha_s^{(n_f)}\right)^2 C_F T_F}{16\pi^2}\,e^{\gamma_E}\left\{\frac{224}{27}+\frac{8\pi^2}{9}\right\}. \tag{5.24}$$

Note that the first moment of the soft model function Ω_1^τ, related to the more standard moment of the model function for the double hemisphere invariant mass distribution Ω_1 via $\Omega_1^\tau \equiv 2\,\Omega_1$, becomes also a scheme- and scale-dependent quantity once we employ a renormalon-free gap scheme. The moment parameter $\bar\Omega_1^{(n_f)}(R,\mu)$ is then related to the gap parameter $\bar\Delta^{(n_f)}(R,\mu)$ via

$$\bar\Omega_1^{(n_f)}(R,\mu) \equiv \frac{1}{2}\int_0^\infty \mathrm{d}\ell\,\ell\,S_\tau^{\rm mod}\big(\ell - 2\,\bar\Delta^{(n_f)}(R,\mu)\big) = \bar\Delta^{(n_f)}(R,\mu) + \frac{1}{2}\int_0^\infty \mathrm{d}\ell\,\ell\,S_\tau^{\rm mod}(\ell)\,. \tag{5.25}$$

5.3 The mass mode setup

We turn to the discussion of secondary massive quark effects initiated by light quarks. We have described already the setup dealing with this question in Sec. 4.2 by means of the example of DIS in the endpoint region. Here the involved mass modes are the same as before giving also rise to the EFT scenarios I, II and III which we will briefly show in the following and where we just highlight the changes compared to the DIS case discussed in Sec. 4.2. The main difference concerns an additional hierarchy the mass scale can have with respect to the ultrasoft scale. Since the typical ultrasoft scale in the tail region is $\mu_S \sim Q\tau \gg \Lambda_{\rm QCD}$ the heavy quark mass can be also of the order of μ_S or even smaller. We call the

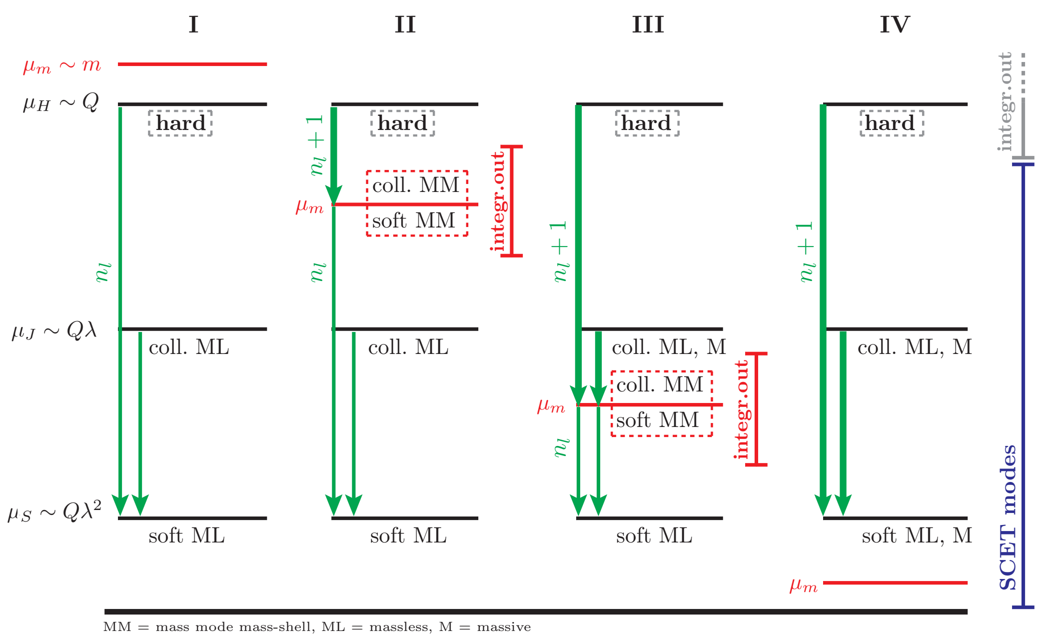

Figure 5.4: The different scenarios depending on the hierarchy between the mass scale μ_m and the hard, jet and ultrasoft scale. MM indicates mass-shell scaling, ML the massless one. With M we denote modes that have a mass m but scale as their massless counterparts. The renormalization group evolution is also shown in the top-down evolution from the hard scale μ_H down to $\mu = \mu_S$. When the mass scale is crossed the mass-shell fluctuations are integrated out (dashed box). This leads to a matching condition and to a change in the evolution factor.

corresponding EFT setup to this scaling situation scenario IV. In this case the mass-shell fluctuations of the mass modes merge into those of the massless quarks and gluons and in principle do not have to be separated. Both the collinear and soft fluctuations of the mass modes are treated at the same footing as those of the massless collinear and ultrasoft quarks and gluons, in particular the soft mass modes adopt the same invariant mass scaling as the massless ultrasoft degrees of freedom. However, their mass still has to be taken into account in the calculations. In this last scenario the mass-shell fluctuations are not integrated out. The hierarchies between the modes for $\lambda_m < 1$ are displayed in Fig. 5.3.

The factorization theorems in each scenario will be described again in the top-down running as shown in Fig. 5.4. For convenience we will discuss only the EFT picture that entails that the mass modes either contribute or are completely integrated out. It is implied that using the OS renormalization condition massive real radiation effects may still be present in matrix elements in boundary regions between two scenarios.

5.3.1 Scenario I: $m > Q > Q\lambda > Q\lambda^2$

When the mass m is larger than the hard scale Q the massive quark is integrated out in the matching process between SCET and QCD. The factorization theorem is the one for n_l massless fermions in analogy to Eq. (5.4) up to the hard current coefficient which acquires an additional contribution due to the heavy quark, i.e.

$$\begin{aligned}\frac{1}{\sigma_0}\frac{\mathrm{d}\sigma}{\mathrm{d}\tau} &= Q\left|\tilde{C}^{(n_l)}(Q,m,\mu_H)\right|^2\left|U_{\tilde{C}}^{(n_l)}(Q,\mu_H,\mu_S)\right|^2\int\mathrm{d}s\int\mathrm{d}s'\,J_\tau^{(n_l)}(s',\mu_J)\,U_{J_\tau}^{(n_l)}(s-s',\mu_S,\mu_J)\\&\quad\times S_\tau^{(n_l)}\Big(Q\tau-\frac{s}{Q},\mu_S\Big)\,,\end{aligned}\tag{5.26}$$

where the massive contribution to the Wilson coefficient $\tilde{C}^{(n_l)}(Q,m,\mu_H)$ at $\mathcal{O}(\alpha_s^2 C_F T_F)$ corresponds to Eq. (4.38) with the replacement $Q^2 \to -(Q^2 + i0)$ (or equivalently $\hat{m}^2 \to -\hat{m}^2 + i0$).

5.3.2 Scenario II: $Q > m > Q\lambda > Q\lambda^2$

The mass m is below the hard scale, but still above the jet and the ultrasoft scale. The collinear and soft mass modes are included into the SCET setup and contribute as dynamic degrees of freedom to the RG evolution above m, but not yet via real radiation. In the RG evolution of the current from the hard to the jet scale the mass-shell fluctuations are finally integrated out at the scale $\mu_m \sim m$. The factorization theorem reads

$$\begin{aligned}\frac{1}{\sigma_0}\frac{\mathrm{d}\sigma}{\mathrm{d}\tau} &= Q\left|\tilde{C}^{(n_l+1)}(Q,m,\mu_H)\right|^2\left|U_{\tilde{C}}^{(n_l+1)}(Q,\mu_H,\mu_m)\right|^2\left|\mathcal{M}_{\tilde{C}}(Q,m,\mu_m)\right|^2\left|U_{\tilde{C}}^{(n_l)}(Q,\mu_m,\mu_S)\right|^2 \\ &\quad\times\int\mathrm{d}s\int\mathrm{d}s'\,J_\tau^{(n_l)}(s',\mu_J)\,U_{J_\tau}^{(n_l)}(s-s',\mu_S,\mu_J)\,S_\tau^{(n_l)}\Big(Q\tau-\frac{s}{Q},\mu_S\Big)\,. \end{aligned}\tag{5.27}$$

The hard current coefficient acquires a subtractive contribution arising from the non-vanishing SCET diagrams and contributions related to the change of the renormalization prescription for the strong coupling, and the threshold correction $\mathcal{M}_{\tilde{C}}(Q,m,\mu_m)$ arises, when the current evolution crosses the mass scale. Both terms at $\mathcal{O}(\alpha_s^2 C_F T_F)$ are the same as the expressions in Eqs. (4.42) and (4.45) after the replacement $Q^2 \to -(Q^2+i0)$.

5.3.3 Scenario III: $Q > Q\lambda > m > Q\lambda^2$

The mass is between the jet and the ultrasoft scale. Since the massless as well as the massive collinear modes both can now fluctuate in the collinear sector additional massive real and virtual contributions arise in the jet sector. In analogy to the current, the RG evolution of the jet function is performed with n_l+1 flavors above the mass threshold and collinear mass-shell fluctuations are integrated out at the mass scale. Overall the factorization theorem in this scenario has the form

$$\begin{aligned}\frac{1}{\sigma_0}\frac{\mathrm{d}\sigma}{\mathrm{d}\tau} &= Q\left|\tilde{C}^{(n_l+1)}(Q,m,\mu_H)\right|^2\left|U_{\tilde{C}}^{(n_l+1)}(Q,\mu_H,\mu_m)\right|^2\left|\mathcal{M}_{\tilde{C}}(Q,m,\mu_m)\right|^2\left|U_{\tilde{C}}^{(n_l)}(Q,\mu_m,\mu_S)\right|^2 \\ &\quad\times\int\mathrm{d}s\int\mathrm{d}s'\int\mathrm{d}s''\int\mathrm{d}s'''\,J_\tau^{(n_l+1)}(s''',m,\mu_J)\,U_{J_\tau}^{(n_l+1)}(s''-s''',\mu_m,\mu_J) \\ &\quad\times\mathcal{M}_{J_\tau}(s'-s'',m,\mu_m)\,U_{J_\tau}^{(n_l)}(s-s',\mu_S,\mu_m)\,S_\tau^{(n_l)}\Big(Q\tau-\frac{s}{Q},\mu_S\Big)\,, \end{aligned}\tag{5.28}$$

The virtual and real mass corrections to the thrust jet function at $\mathcal{O}(\alpha_s^2 C_F T_F)$ are simply twice the ones of the hemisphere jet function contributions given in Eqs. (4.53) and (4.54). The jet mass mode matching coefficient can be decomposed into a n- and $\bar{n}$-collinear factor, $\mathcal{M}_{J_\tau} = \mathcal{M}_{J_\tau,n}\otimes\mathcal{M}_{J_\tau,\bar{n}}$, which yields with respect to the hemisphere jet threshold correction in Eq. (4.58) a factor of two for the terms at $\mathcal{O}(\alpha_s^2)$ and $\mathcal{O}(\alpha_s^3)$ in the fixed-order counting, and a factor of four at $\mathcal{O}(\alpha_s^4 C_F^2 T_F^2)$.

5.3.4 Scenario IV: $Q > Q\lambda > Q\lambda^2 > m$

The mass is below the ultrasoft scale. There is no separation between the collinear and soft mass modes and the corresponding collinear and ultrasoft massless modes since the RG evolution following the top-down approach of Fig. 5.4 never crosses the massive quark threshold and all evolution is carried out for n_l+1 active dynamic flavors. So compared to scenario III there are no mass mode matching coefficients, and the soft function accounts for the secondary massive contributions. The factorization theorem reads

$$\begin{aligned}\frac{1}{\sigma_0}\frac{\mathrm{d}\sigma}{\mathrm{d}\tau} &= Q\left|\tilde{C}^{(n_l+1)}(Q,m,\mu_H)\right|^2\left|U_{\tilde{C}}^{(n_l+1)}(Q,\mu_H,\mu_S)\right|^2\int\mathrm{d}s\int\mathrm{d}s'\,J_\tau^{(n_l+1)}(s',m,\mu_J)\,U_{J_\tau}^{(n_l+1)}(s-s',\mu_S,\mu_J) \\ &\quad\times S_\tau^{(n_l+1)}\Big(Q\tau-\frac{s}{Q},m,\mu_S\Big)\,, \end{aligned}\tag{5.29}$$

where the hard current matching coefficient $\tilde{C}^{(n_l+1)}(Q,m,\mu_H)$ is the same as in scenarios II and III, and the jet function $J_\tau^{(n_l+1)}(s,m,\mu_J)$ is the same as in scenario III. The soft function $S_\tau^{(n_l+1)}(\ell,m,\mu_S)$ contains virtual as well as real radiation contributions related to the massive quark. The partonic contribution can be written up to $\mathcal{O}(\alpha_s^2 C_F T_F)$ as

$$\hat{S}_\tau^{(n_l+1)}(\ell,m,\mu) = \hat{S}_\tau^{(n_l+1)}(\ell,\mu) + \hat{S}_{\tau,\Delta m,\mathrm{dist}}^{(n_l+1,2)}(\ell,m,\mu) + \hat{S}_{\tau,m,\theta}^{(n_l+1,2)}(\ell,m) + \hat{S}_{\tau,m,\Delta}^{(n_l+1,2)}(\ell,m)\,, \tag{5.30}$$

where $\hat{S}_\tau^{(n_l+1)}(\ell,\mu)$ is the partonic soft function for n_l+1 massless quark flavors. The other terms represent the $\mathcal{O}(\alpha_s^2 C_F T_F)$ corrections due to the non-zero quark mass. Their computation will be presented explicitly in Sec. 5.4.

The expression for $\hat{S}_{\tau,\Delta m,\mathrm{dist}}^{(n_l+1,2)}(\ell,m,\mu)$ contains only distributions and corresponds to virtual massive quark radiation as well as to the terms related to the subtractions of the massless quark result (see Eq. (5.10)) to avoid double counting with the full massless result in the first term of Eq. (5.30). The renormalized expression reads ($\bar{\ell}=\ell/\mu$, $\alpha_s^{(n_l+1)}=\alpha_s^{(n_l+1)}(\mu)$)

$$\begin{aligned}\mu\,\hat{S}_{\tau,\Delta m,\mathrm{dist}}^{(n_l+1,2)}(\ell,m,\mu) = \frac{\big(\alpha_s^{(n_l+1)}\big)^2 C_F T_F}{16\pi^2}\bigg\{&\delta(\bar{\ell})\bigg[-\frac{8}{9}L_m^3-\frac{40}{9}L_m^2-\bigg(\frac{448}{27}-\frac{8\pi^2}{9}\bigg)L_m-\frac{2048}{81}-\frac{64\pi^2}{27}+32\zeta_3\bigg]\\ &+\bigg[\frac{\theta(\bar{\ell})}{\bar{\ell}}\bigg]_+\bigg[\frac{16}{3}L_m^2+\frac{160}{9}L_m+\frac{896}{27}-\frac{16\pi^2}{9}\bigg]+\bigg[\frac{\theta(\bar{\ell})\ln\bar{\ell}}{\bar{\ell}}\bigg]_+\bigg[-\frac{64}{3}L_m-\frac{320}{9}\bigg]\\ &+\frac{64}{3}\bigg[\frac{\theta(\bar{\ell})\ln^2\bar{\ell}}{\bar{\ell}}\bigg]_+\bigg\}.\end{aligned} \tag{5.31}$$

The term $\hat{S}_{\tau,m,\theta}^{(n_l+1,2)}(\ell,m)$ describes real massive quark radiation for the prescription that the coherent sum of the massive quark and antiquark momentum (i.e. the virtual gluon momentum) enters the thrust definition. This prescription can be easily calculated analytically with the dispersive method and agrees with the regular thrust prescription except when quark and antiquark enter different hemispheres. $\hat{S}_{\tau,m,\theta}^{(n_l+1,2)}$ contains a threshold at $\ell=2m$ and reads

$$\begin{aligned}\mu\,\hat{S}_{\tau,m,\theta}^{(n_l+1,2)}(\ell,m) = \frac{\big(\alpha_s^{(n_l+1)}\big)^2 C_F T_F}{16\pi^2}\,\theta(\ell-2m)\,\frac{1}{\ell}\bigg\{&\frac{64}{3}\,\mathrm{Li}_2\bigg(\frac{w-1}{w+1}\bigg)-\frac{32}{3}\ln\Big(\frac{1-w^2}{4}\Big)\ln\bigg(\frac{1-w}{1+w}\bigg)\\ &+\frac{16}{3}\ln^2\bigg(\frac{1-w}{1+w}\bigg)-\frac{160}{9}\ln\bigg(\frac{1-w}{1+w}\bigg)+\frac{64}{27}w^3-\frac{320}{9}w+\frac{16\pi^2}{9}\bigg\},\end{aligned} \tag{5.32}$$

with

$$w=\sqrt{1-\frac{4m^2}{\ell^2}}\,. \tag{5.33}$$

$\hat{S}_{\tau,m,\theta}^{(n_l+1,2)}(\ell,m)$ and its first two derivatives in ℓ vanish at the threshold, so that no discontinuity arises due to real radiation. Since the momenta of the quark and antiquark contribute to the thrust prescription as different respective projections on one of the two lightcone axes if they enter different hemispheres, $\hat{S}_{\tau,m,\theta}^{(n_l+1,2)}(\ell,m)$ does not represent the correct real radiation contribution. For the phase space region where the massive quark and antiquark propagate into opposite hemispheres, one has to account for the additional, numerically small *hemisphere misalignment contribution* $\hat{S}_{\tau,m,\Delta}^{(n_l+1,2)}(\ell,m)$ that consists out of the difference between the correct thrust prescription and the one leading to $\hat{S}_{\tau,m,\theta}^{(n_l+1,2)}(\ell,m)$. This correction does not have a threshold and is nonvanishing for all positive thrust momenta ℓ. In the massless limit $\hat{S}_{\tau,m,\Delta}^{(n_l+1,2)}(\ell,m)$ approaches a δ-distribution. We give a parametrization for $\hat{S}_{\tau,m,\Delta}^{(n_l+1,2)}$ that approximates this contribution up to better than 2% relative accuracy ($\hat{\ell}\equiv\ell/m$),

$$\hat{S}_{\tau,m,\Delta}^{(n_l+1,2)}(\ell,m)\Big|_{\mathrm{param.}} = \frac{\big(\alpha_s^{(n_l+1)}\big)^2 C_F T_F}{16\pi^2}\,\frac{\hat{\ell}^5}{m}\,\frac{a\ln^2\Big(1+\hat{\ell}^2\Big)+b\ln\Big(1+\hat{\ell}^2\Big)+c}{d\,\hat{\ell}^8+e\,\hat{\ell}^7+f\,\hat{\ell}^6+g\,\hat{\ell}^4+h\,\hat{\ell}^3+j\,\hat{\ell}^2+1}\,. \tag{5.34}$$

with $a=8\,d$, $b=-80\,d$, $c=8/15$ and $d=6/(2400+360\pi+73\pi^2)$ being fixed from imposing the correct asymptotic behavior for $m\gg\ell$ and $m\ll\ell$. The remaining 5 parameters were obtained using a fit with the constraint of satisfying the correct normalization corresponding to the massless analytic limit,

$$e = 0.0117\,,\quad f = 0.100\,,\quad g = -0.502\,,\quad h = 0.747\,,\quad j = -0.180\,. \tag{5.35}$$

Note that both real radiation contributions are UV finite. For $m \to 0$ the soft function $\hat{S}_\tau^{(n_l+1)}(\ell, m, \mu)$ yields correctly the fully massless partonic soft function at $\mathcal{O}(\alpha_s^2)$, i.e.

$$\hat{S}_\tau^{(n_l+1)}(\ell, m, \mu) \overset{m\to 0}{\longrightarrow} \hat{S}_\tau^{(n_l+1)}(\ell, \mu)\,. \tag{5.36}$$

We note that in the calculation of $\hat{S}_{\tau,\Delta m,\mathrm{dist}}^{(n_l+1,2)}$ rapidity divergences arise in the contributions coming from the different hemispheres which cancel in the sum of the terms. We stress, however, that for $\mu \sim \ell$ all associated logarithmic mass-singularities cancel in the sum of $\hat{S}_{\tau,\Delta m,\mathrm{dist}}^{(n_l+1,2)}$ and $\hat{S}_{\tau,m,\theta}^{(n_l+1,2)}$, so that no (large) rapidity logarithm remains in the soft function.

The UV divergences of the bare soft function $\hat{S}_\tau^{(n_l+1,\mathrm{bare},2)}$ are mass independent and agree with the known massless ones for n_l+1 dynamic flavors in Eq. (5.12) with the replacement $n_f = n_l + 1$. The evolution factor $U_{S_\tau}^{(n_l+1)}$ obeys

$$\mu\frac{\mathrm{d}}{\mathrm{d}\mu}\, U_{S_\tau}^{(n_l+1)}(\ell, \mu, \mu_S) = \int \mathrm{d}\ell'\, \gamma_{S_\tau}^{(n_l+1)}(\ell-\ell', \mu)\, U_{S_\tau}^{(n_l+1)}(\ell', \mu, \mu_S)\,, \tag{5.37}$$

which holds to any order in the strong coupling.

5.3.5 Gap subtraction, evolution and matching

Since in the scenarios I to III the quark mass is above the ultrasoft scale, the massive quark does not affect the soft function. Thus the gap subtraction agrees with the one from the factorization theorem for $n_f = n_l$ massless quarks as described in Sec. 5.2. [5] In scenario IV, for $m > \Lambda_{\mathrm{QCD}}$ the finite quark mass provides an infrared cutoff for the virtuality of the exchanged gluon in the partonic soft function such that the factorial growth of the coefficients related to the massive flavor at large orders in perturbation theory is suppressed and, in principle, a corresponding subtraction in the gap series $\delta(R, \mu)$ might be unnecessary. However, implementing the gap scheme along the lines of Eqs. (5.17) and (5.18) including the effects of the secondary massive quarks is useful in order to have a smooth interpolation of the gap scheme parameters to the massless quark limit. Since the resulting subtraction series $\delta^{(n_l+1)}(R, m, \mu)$ encodes infrared-sensitive perturbative contributions, it now becomes mass dependent. Thus the complete soft function in scenario IV reads

$$S_\tau^{(n_l+1)}(\ell, m, \mu) = \int \mathrm{d}\ell'\, \hat{S}_\tau^{(n_l+1)}(\ell-\ell'-2\,\delta^{(n_l+1)}(R,m,\mu), m, \mu)\, S_\tau^{\mathrm{mod}}(\ell' - 2\,\bar{\Delta}^{(n_l+1)}(R,m,\mu))\,. \tag{5.38}$$

The renormalon subtractions $\delta^{(n_l+1)}(R, m, \mu)$ can be written as

$$\delta^{(n_l+1)}(R, m, \mu) = \delta^{(n_l+1)}(R, \mu) + \delta_{\Delta m}^{(n_l+1,2)}(R, m)\,, \tag{5.39}$$

where $\delta^{(n_l+1)}(R, \mu)$ is the series for n_l+1 massless quark flavors and $\delta_{\Delta m}^{(n_l+1,2)}(R, m/R)$ represents the correction to the massless result at $\mathcal{O}(\alpha_s^2 C_F T_F)$ due to the finite quark mass. The result can be parametrized by ($y = m/R$)

$$\delta_{\Delta m}^{(n_l+1,2)}(R, R\,y)\Big|_{\mathrm{param.}} = \frac{\big(\alpha_s^{(n_l+1)}\big)^2 C_F T_F}{16\pi^2}\, R\, e^{\gamma_E} \left\{ \tilde{h}(y) - \frac{\tilde{h}(y) + a y}{1 + b y + c y^2}\, e^{-\alpha y^\beta} \right\}, \tag{5.40}$$

[5] If we do not use the strict EFT picture, but rather the OS renormalized soft function in the scenarios I to III we would also have mass dependent real radiation terms there and could define corresponding renormalon subtractions (which decouple for $m \gg R$). This would modify the R-evolution below the mass threshold and the matching condition in Eq. (5.49). Since, however, we do not have to cancel any renormalon for a heavy quark in the first place, we have some freedom concerning this point. For our purposes it is more convenient to define the renormalon subtractions such that gap parameter in the n_l scheme is not mass dependent.

where

$$\alpha = 0.634\,, \quad \beta = 1.035\,, \quad a = 23.6\,, \quad b = -\,0.481\,, \quad c = 1.19\,, \tag{5.41}$$

and

$$\tilde{h}(y) = -\,\frac{8}{3}\ln^2 y^2 - \frac{80}{9}\ln y^2 - \frac{448}{27} - \frac{8\pi^2}{9}\,. \tag{5.42}$$

The expression in Eq. (5.40) provides an approximation with a relative deviation of much less than 1% that is constructed such that the massless limit in Eq. (5.39) is recovered for $m \to 0$, i.e. $\delta_{\Delta m}^{(n_l+1,2)}(R,m) \stackrel{m\to 0}{\longrightarrow} 0$. Moreover, for $m/R \to \infty$ the parametrization yields the correct limit,

$$\delta_{\Delta m}^{(n_l+1,2)}(R, R\,y)\Big|_{\text{para}} \stackrel{y\to\infty}{\longrightarrow} \frac{\big(\alpha_s^{(n_l+1)}\big)^2 C_F T_F}{16\pi^2}\, R\, e^{\gamma_E}\,\tilde{h}(y)\,, \tag{5.43}$$

The μ-evolution of the gap parameter $\bar{\Delta}^{(n_l+1)}(R,m,\mu)$ is mass independent and thus the same as for the massless gap parameter as given in Eq. (5.23) with the replacement $n_f = n_l + 1$. With the quark mass dependent gap subtraction at $\mathcal{O}(\alpha_s^2 C_F T_F)$, however, the gap evolution in R becomes mass dependent, and one can determine the R-evolution equation directly from Eq. (5.39) using Eq. (5.22). The R-anomalous dimension can then be written as

$$\gamma_R^{(n_l+1)}\left(\frac{m}{R}\right) = \gamma_R^{(n_l+1)} + \gamma_{R,\Delta m}^{(n_l+1,2)}\left(\frac{m}{R}\right)\,. \tag{5.44}$$

Using the parametrization of Eq. (5.40) the result for the $\mathcal{O}(\alpha_s^2 C_F T_F)$ massive quark correction $\gamma_{R,m}^{(n_l+1,2)}(m/R)$ can be easily computed,

$$\gamma_{R,\Delta m}^{(n_l+1,2)}\left(\frac{m}{R}\right)\Big|_{\text{param.}} = \frac{\mathrm{d}}{\mathrm{d}R}\,\delta_{\Delta m}^{(n_l+1,2)}(R,m)\Big|_{\text{param.}}\,. \tag{5.45}$$

It approximates the exact result within 2% (except for $m/R < 0.1$, where the correction is anyway tiny) and yields the correct massless limit in Eq. (5.44) for $m \to 0$, i.e. $\gamma_{R,\Delta m}^{(n_l+1,2)}(m/R) \stackrel{m\to 0}{\longrightarrow} 0$.

The explicit solution for the μ- and R-evolution for $\bar{\Delta}^{(n_f)}(R,\mu)$ with massless quarks can be found in Eq. (41) of Ref. [4]. The quark mass just modifies the R-evolution terms of that solution. It affects the function $D^{(k)}(\alpha_s(R_1),\alpha_s(R_0))$, defined for massless quarks in Eq. (A.31) of Ref. [4], where R_0 (R_1) is the initial (final) scale of the R-evolution. [6] Mass effects start contributing at N^{2}LL order and modify the corresponding function $D^{(n_l+1,2)}(\alpha_s(R_0),\alpha_s(R_1))$ defined in the (n_l+1)-scheme in the following way:

$$\begin{aligned} D^{(n_l+1,2)}(\alpha_s^{(n_l+1)}(R_0),\alpha_s^{(n_l+1)}(R_1),m) &= D^{(n_l+1,2)}(\alpha_s^{(n_l+1)}(R_0),\alpha_s^{(n_l+1)}(R_1)) \\ &\quad + \frac{1}{4\beta_0^2}\int_{t_0}^{t_1}\mathrm{d}t\, e^{-t}(-t)^{-2-\frac{\beta_1}{2\beta_0^2}}\gamma_{R,\Delta m}^{(n_l+1,2)}\left(\frac{m\,e^{G^{(2)}(t)}}{\Lambda_{\text{QCD}}^{(n_l+1,2)}}\right), \end{aligned} \tag{5.46}$$

with $t_i = -\,2\pi/(\beta_0\,\alpha_s^{(n_l+1)}(R_i))$ and β_i being the coefficients of the perturbative expansion of the β function in the (n_l+1)-scheme as defined in Eq. (4.184). $\Lambda_{\text{QCD}}^{(n_l+1,2)} = R\,e^{G^{(2)}(t)} = R_i\,e^{G^{(2)}(t_i)}$ is the scale coming from dimensional transmutation of the strong coupling running with (n_l+1) flavors at N^{2}LL order. The function $G^{(2)}(t)$ is given by

$$G^{(2)}(t) = t + \frac{\beta_1}{2\beta_0^2}\ln(-\,t) - \frac{\beta_1^2 - \beta_0\beta_2}{4\beta_0^4}\,\frac{1}{t}\,, \tag{5.47}$$

Eq. (5.46) can be obtained following the changes of variables as explained in Ref. [116]. A generalization to higher orders is straightforward.

[6] We note again that the R-evolution is performed diagonally in μ-R-space such that the running of α_s is accounted for.

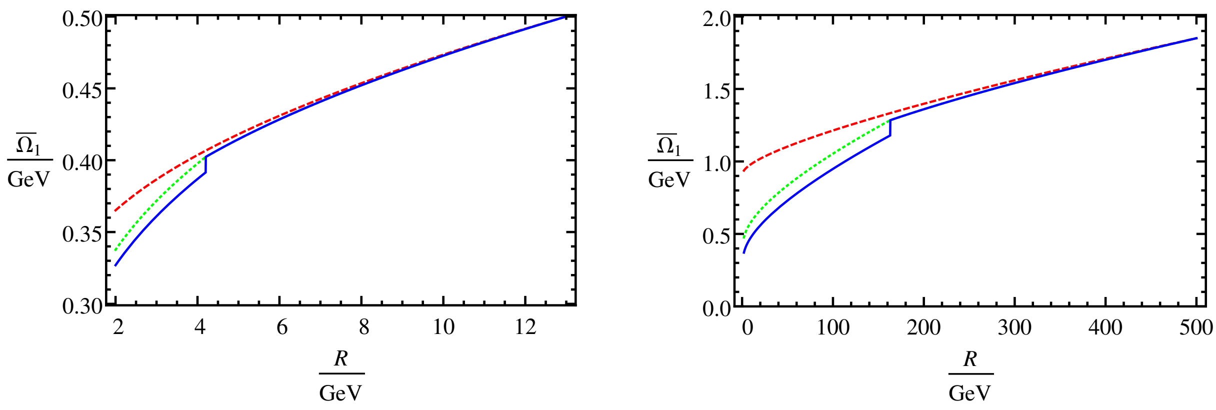

Figure 5.5: R-evolution of $\bar{\Omega}_1(R, \mu = R)$ with a massive bottom (left) and a massive top quark (right) at $\mathcal{O}(\alpha_s^3)$ as described in the text. The curves represent purely massless evolution (red, dashed), massive evolution including threshold matching (blue, solid) at $\overline{m}_b(\overline{m}_b)$ and $\overline{m}_t(\overline{m}_t)$, respectively, and massive evolution without threshold matching (green, dotted).

To complete the discussion on the evolution of the gap parameter we have to consider the matching relation between $\bar{\Delta}^{(n_l+1)}(R, m, \mu)$ for $R, \mu > \mu_m \sim m$, where the massive quark is an active dynamic flavor, and $\bar{\Delta}^{(n_l)}(R, \mu)$ for $R, \mu < \mu_m \sim m$, where the massive quark is integrated out. The matching relation is most easily derived using the fact that the "bare" gap parameter is scheme-independent very much like the massive quark pole mass. This gives the relation

$$\Delta = \bar{\Delta}^{(n_l)}(R, \mu) + \delta^{(n_l)}(R, \mu) = \bar{\Delta}^{(n_l+1)}(R, m, \mu) + \delta^{(n_l+1)}(R, m, \mu)\,. \tag{5.48}$$

We thus obtain ($L_m = \ln(m^2/\mu^2)$)

$$\begin{aligned}\bar{\Delta}^{(n_l)}(R, \mu) = \bar{\Delta}^{(n_l+1)}(R, m, \mu) &+ \delta_{T_F}^{(n_l+1,2)}(R, \mu) + \delta_{\Delta m}^{(n_l+1,2)}(R, m, \mu) \\ &- \frac{\alpha_s^{(n_l+1)} T_F}{3\pi}\, L_m\, \delta^{(n_l+1,1)}(R, \mu) + \mathcal{O}(\alpha_s^3)\end{aligned} \tag{5.49}$$

with the one-loop gap subtraction given in Eq. (5.19). The latter term arises from the matching relation of the strong coupling between the n_l- and (n_l+1)-scheme. To avoid large logarithms, the gap matching relation should be employed for $R \sim \mu \sim m$.

In Fig. 5.5 (left panel) we show $\bar{\Omega}_1(R, \mu = R)$ (see Eq. (5.25)) as a function of R in the range between 2 and 13 GeV using $\bar{\Omega}_1^{(5)}(13\,\text{GeV}, 13\,\text{GeV}) = 0.5\,\text{GeV}$ and $\alpha_s^{(5)}(m_Z) = 0.114$ as initial conditions. The choice of these initial conditions is motivated by recent fits for α_s and $\bar{\Omega}_1$ in Refs. [4,5] which involved only experimental data related to R-scale values above 10 GeV despite the fact that values for $\bar{\Omega}_1$ at $R = 2\,\text{GeV}$ were quoted in the final result. The red, dashed curve shows the purely massless evolution using the R-anomalous dimension at $\mathcal{O}(\alpha_s^3)$. The blue, solid curve shows the R-dependence accounting for the finite bottom quark mass taking $\overline{m}_b(\overline{m}_b) = 4.2\,\text{GeV}$ as an input for the $\overline{\text{MS}}$ bottom quark mass and using the threshold matching relation of Eq. (5.49) at $R = \mu = \overline{m}_b(\overline{m}_b)$ when switching from the $n_f = 5$ to the $n_f = 4$ flavor scheme for the gap parameter. The difference between the blue and the red curve illustrates the impact of the finite bottom mass corrections on the R-dependence. We see that the mass effects are relatively small for $R > \overline{m}_b(\overline{m}_b)$, which indicates that the mass corrections in the anomalous dimension in R represent only a minor effect. On the other hand, for $R < \overline{m}_b(\overline{m}_b)$, the bottom mass effects, which arise from the threshold matching corrections and from using the $n_f = 4$ flavor anomalous dimension, are quite sizeable. These belong also to the most important effects due to the finite bottom mass in the complete thrust distribution. To visualize the impact of the bottom mass on the R-evolution alone we have also displayed the dependence on R when the threshold matching correction is ignored (green, dotted curve). Overall, we see that the impact due to the finite bottom quark mass is sizeable and non-negligible particularly for scales below the bottom quark mass.

In the right panel of Fig. 5.5 we display $\bar{\Omega}_1(R, \mu = R)$ as a function of R in the range up to 500 GeV showing the same type of curves as described before in order to illustrate the impact of the finite top quark mass. All curves have the common input value $\bar{\Omega}_1^{(6)}(500\,\mathrm{GeV}, 500\,\mathrm{GeV}) = 1.85\,\mathrm{GeV}$ using again $\alpha_s^{(5)}(m_Z) = 0.114$. The switch from the $n_f = 6$ to the $n_f = 5$ flavor scheme has been carried out exactly at the top quark mass $\overline{m}_t(\overline{m}_t) = 163\,\mathrm{GeV}$. We can make observations that are very similar to the ones already discussed for the bottom quark threshold region. The difference is that the impact of the finite top quark mass effects are even more dramatic than for the bottom quark case leading to a discrepancy of a factor of two between the appropriate mass dependent evolution and the running for a massless top quark when $\bar{\Omega}_1$ is evolved down to the bottom quark scale. This is related to the linear dependence of the gap parameter on $R \sim m_t$ in the threshold matching relation and the R-evolution.

Note that the mass dependence of the R-evolution equations at $\mathcal{O}(\alpha_s^3)$ is currently unknown. For the numerical analysis in Sec. 5.7 we have therefore employed at $\mathcal{O}(\alpha_s^3)$ the known massless corrections with the appropriate number of flavors. As the $\mathcal{O}(\alpha_s^3)$ corrections amount to at most 25 % of the $\mathcal{O}(\alpha_s^2)$ terms, and – as we have just shown above – the mass dependence in the R-evolution equation only represents a minor effect, this approach is certainly justified. We have checked that using the R-evolution equation at $\mathcal{O}(\alpha_s^2)$ (disregarding $\mathcal{O}(\alpha_s^3)$-terms) leads to a deviation in the bottom quark mass correction for the thrust distribution that is less than half of the one generated by the variation of μ_m discussed in our numerical analysis of Sec. 5.7. This indicates that the missing quark mass corrections at $\mathcal{O}(\alpha_s^3)$ might be safely ignored at this stage.

5.4 Two-loop soft function for secondary massive quarks

In this section we compute the secondary massive quark contributions to the thrust soft function at $\mathcal{O}(\alpha_s^2 C_F T_F)$. For a generalization to the related soft function for the double differential hemisphere distribution we refer to Ref. [11]. We emphasize that the definition of the soft function in Eq. (5.7) also applies to the case when the primary quarks are massive [8,9] as long as the c.m. energy Q is much larger than their mass (i.e. in the boosted regime) since the emergence of the Wilson lines in the soft eikonal approximation is mass independent. Thus our result is also valid for massive secondary quark effects in massive primary quark production, where masses of primary and secondary quarks can differ, up to potential trivial modifications concerning the scheme for α_s.

We need to compute the diagrams in Fig. 5.6 for a quark flavor with mass m. While the phase space for the diagrams (a) – (d) is simple, the computation of the diagrams (e) and (f) is highly non-trivial corresponding to the case, when the massive quark and antiquark with momenta k and q, respectively, enter the final state. Taking into account the corresponding symmetry factors, one can obtain their contributions to the soft function in the form analogously to the massless case [112]

$$S_{e+f}(\ell, m) = \int \frac{\mathrm{d}^d k}{(2\pi)^d} \int \frac{\mathrm{d}^d q}{(2\pi)^d} F^{(qq)}(k, q, \ell, m)\, s(k, q)\,, \tag{5.50}$$

where $s(k, q)$ is the matrix element calculated by conventional Feynman rules,

$$s(k, q) = g^4 C_F T_F \tilde{\mu}^{2\epsilon} \frac{4(k^+q^- + k^-q^+ - 2k\cdot q)}{(k^+ + q^+)(k^- + q^-)(k+q)^4}\,. \tag{5.51}$$

The phase space constraints and the on-shell condition for the massive quarks are given by the *quark hemisphere prescription* $F^{(qq)}(k, q, \ell, m)$,

$$\begin{aligned} F^{(qq)}(k, q, \ell, m) = {} & (-2\pi i)^2\, \delta(k^2 - m^2)\, \delta(q^2 - m^2)\, \theta(k^+ + k^-)\, \theta(q^+ + q^-) \\ & \times \big[\theta(k^+ - k^-)\, \theta(q^- - q^+)\, \delta(\ell - k^- - q^+) + \theta(k^- - k^+)\, \theta(q^+ - q^-)\, \delta(\ell - k^+ - q^-) \\ & + \theta(k^- - k^+)\, \theta(q^- - q^+)\, \delta(\ell - k^+ - q^+) + \theta(k^+ - k^-)\, \theta(q^+ - q^-)\, \delta(\ell - k^- - q^-)\big]\,. \end{aligned} \tag{5.52}$$

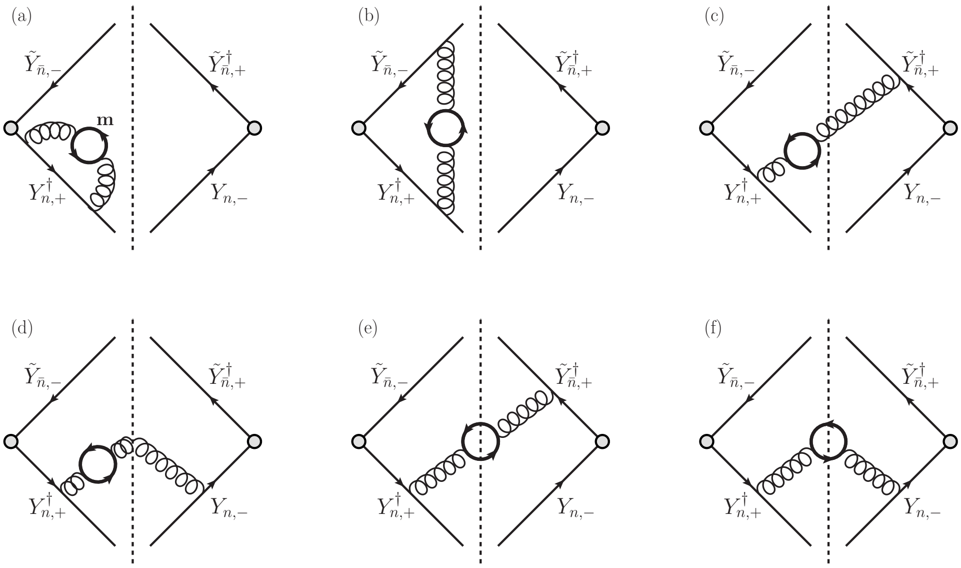

Figure 5.6: The types of Feynman diagrams for the $\mathcal{O}(\alpha_s^2 C_F T_F)$ contributions to the soft function with corresponding symmetric configurations. (a) and (b) are purely virtual, (c) and (d) contain the contributions to real gluon radiation and (e) and (f) the contributions for the real radiation of a quark-antiquark pair. (a) and (d) vanish in Feynman gauge due to $n \cdot n = 0$.

Solving the integral (5.50) directly with this phase space constraint turns out to be an extraordinarily difficult task due to the mass dependence together with the complications that arise from the parts of the phase space where the quark and antiquark enter different hemispheres. Instead of approaching with brute force, we therefore apply the following strategy: We first calculate a soft function (over the full physical phase space) with a much simpler momentum assignment (but the same matrix element),

$$S^{(g)}_{e+f}(\ell, m) = \int \frac{\mathrm{d}^d k}{(2\pi)^d} \int \frac{\mathrm{d}^d q}{(2\pi)^d}\, F^{(g)}(k, q, \ell, m)\, s(k, q)\,, \tag{5.53}$$

where the phase space constraints are given by the *gluon hemisphere prescription* $F^{(g)}(k, q, \ell, m)$,

$$\begin{aligned} F^{(g)}(k, q, \ell, m) &= (-2\pi i)^2\, \delta(k^2 - m^2)\, \delta(q^2 - m^2)\, \theta(k^+ + k^-)\, \theta(q^+ + q^-) \\ &\quad \times \left[\theta(k^+ + q^+ - k^- - q^-)\, \delta(\ell - k^- - q^-) + \theta(k^- + q^- - k^+ - q^+)\, \delta(\ell - k^+ - q^+)\right]\,. \end{aligned} \tag{5.54}$$

This phase space assigns the soft hemisphere momenta coherently to the components of the gluon momentum $k + q$, so that the massive quark and antiquark momenta always contribute together and homogeneously to ℓ. The soft function obtained in this way only keeps track of the hemisphere, into which the virtual gluon propagated, and therefore differs from the actual physical thrust soft function we aim to calculate, where the final state partons each are accounted for in the hemisphere they propagate. Since both prescriptions are compatible with soft-collinear factorization and lead to the same hard current and jet functions, the consistency of the renormalization group evolution forces both soft functions to have the same UV divergences. So the required additional correction arising from the difference between the quark hemisphere and gluon hemisphere prescription, which we call *phase space misalignment correction*, can be computed in four dimensions, which can be tackled numerically. Due to the finite quark masses the resulting calculations are also IR-finite and straightforward to carry out.

The advantage of introducing the gluon hemisphere prescription is that the kinematics is only governed by the gluon momenta weighted by the gluon virtuality. So in the calculation the physical effects associated to the fact that a massive quark pair is produced from virtual gluon decay can be separated from the computation of the phase space. This makes the gluon hemisphere prescription quite simple to compute because it allows us to perform the computation with the help of dispersion integrations over the gluon virtuality as described in Sec. 3.4.1. In the following we will therefore as a first step calculate the $\mathcal{O}(\alpha_s)$ corrections to the partonic soft function coming from the radiation of a massive gluon with momentum $k+q$. Then, by convoluting the massive gluon result with the imaginary part of the gluon vacuum polarization function related to the massive quark cuts in diagrams (e) and (f) one obtains the $\mathcal{O}(\alpha_s^2 C_F T_F)$ massive quark corrections in the gluon hemisphere prescription. The calculation is very generic and it is simple to determine the effects of gluon splitting into any other kind of final state, such as gluino pairs just to mention one example.

5.4.1 Soft function for massive gluons at $\mathcal{O}(\alpha_s)$

The non-vanishing diagrams at $\mathcal{O}(\alpha_s)$ are similar to the ones displayed in Fig. 4.12 for the computation of the PDF soft function and we will also refer to them as S_a and S_b. However, note that the involved Wilson lines and in particular the phase space are different for the thrust soft function, which is based on a hemisphere momentum definition. As in the computation of Sec. 4.3.3 we encounter rapidity divergences in the soft function. In contrast to the PDF soft function, however, these cancel among themselves and no further recombination with other structures is required. We calculate the massive gluon contributions using again the α-regulator defined in Eq. (4.66), which implies that the diagram S_a vanishes. Diagram S_b and its symmetric configuration give two contributions related to the cases $k^+ > k^-$ and $k^+ < k^-$ for the massive gluon momentum k^μ,

$$2S_b = S_+ + S_- \,, \tag{5.55}$$

which are treated asymmetrically with the α-regulator,

$$S_+ = 8\pi g^2 C_F \tilde{\mu}^{2\epsilon} \int \frac{\mathrm{d}^d k}{(2\pi)^d} \frac{\nu^\alpha}{(k^-)^{1+\alpha}} \frac{1}{k^+} \,\theta(k^+ + k^-)\,\delta(k^2 - M^2)\,\theta(k^+ - k^-)\,\delta(\ell - k^-)\,, \tag{5.56}$$

$$S_- = 8\pi g^2 C_F \tilde{\mu}^{2\epsilon} \int \frac{\mathrm{d}^d k}{(2\pi)^d} \frac{\nu^\alpha}{(k^-)^{1+\alpha}} \frac{1}{k^+} \,\theta(k^+ + k^-)\,\delta(k^2 - M^2)\,\theta(k^- - k^+)\,\delta(\ell - k^+)\,. \tag{5.57}$$

Applying the hemisphere constraints and performing the $k_\perp$-integration, one obtains the expressions

$$S_+ = \frac{\alpha_s C_F}{\pi} \frac{\left(\mu^2 e^{\gamma_E}\right)^{2-\frac{d}{2}}}{\Gamma\left(\frac{d}{2}-1\right)} \int_\ell^\infty \mathrm{d}k^+ \,\frac{\nu^\alpha}{\ell^\alpha} \frac{\left(\ell\, k^+ - M^2\right)^{\frac{d}{2}-2}}{\ell\, k^+} \,\theta(\ell\, k^+ - M^2)\,, \tag{5.58}$$

$$S_- = \frac{\alpha_s C_F}{\pi} \frac{\left(\mu^2 e^{\gamma_E}\right)^{2-\frac{d}{2}}}{\Gamma\left(\frac{d}{2}-1\right)} \int_\ell^\infty \mathrm{d}k^- \,\frac{\nu^\alpha}{(k^-)^\alpha} \frac{\left(\ell\, k^- - M^2\right)^{\frac{d}{2}-2}}{\ell\, k^-} \,\theta(\ell\, k^- - M^2)\,. \tag{5.59}$$

Performing the last integration and taking the limit $\alpha \to 0$ we obtain ($\bar{\ell} = \ell/\mu$)

$$\mu\, S_+ = \frac{\alpha_s C_F}{\pi} \left\{ \Gamma\left(2 - \frac{d}{2}\right) \left(\frac{\mu^2 e^{\gamma_E}}{M^2}\right)^{2-\frac{d}{2}} \left(\delta(\bar{\ell}) \left[-\frac{1}{\alpha} - \ln\left(\frac{\nu}{\mu}\right) \right] + \left[\frac{\theta(\bar{\ell})}{\bar{\ell}}\right]_+ \right) - \theta(\ell - M)\, \frac{1}{\bar{\ell}} \ln\left(\frac{\ell^2}{M^2}\right) \right\}, \tag{5.60}$$

and ($L_M = \ln(M^2/\mu^2)$)

$$\begin{aligned}\mu\, S_- = \frac{\alpha_s C_F}{\pi} &\left\{ \Gamma\left(2 - \frac{d}{2}\right) \left(\frac{\mu^2 e^{\gamma_E}}{M^2}\right)^{2-\frac{d}{2}} \left(\delta(\bar{\ell}) \left[\frac{1}{\alpha} + \ln\left(\frac{\nu}{\mu}\right) - L_M + H_{1-\frac{d}{2}} \right] + \left[\frac{\theta(\bar{\ell})}{\bar{\ell}}\right]_+ \right) \right. \\ &\left. - \theta(\ell - M)\, \frac{1}{\bar{\ell}} \ln\left(\frac{\ell^2}{M^2}\right) \right\}.\end{aligned} \tag{5.61}$$

Note that the threshold terms involving the θ-function correspond to the real radiation contributions for the massive gluon. They have been given for $d = 4$ ($\epsilon = 0$) because they only contain IR and UV finite integrals within the subtracted dispersion integral (3.62). In the sum all α-singularities and the dependence on ν cancels between the two hemisphere contributions. [7] We write the unrenormalized mass mode contributions to the thrust soft function as

$$\hat{S}^{(\text{bare},1)}_{\tau,M}(\ell,M,\mu) = \hat{S}^{(\text{bare},1)}_{\tau,M,\text{virt}}(\ell,M,\mu) + \hat{S}^{(1)}_{\tau,M,\text{real}}(\ell,M)\,. \tag{5.62}$$

with the virtual massive gluon corrections given by

$$\mu\,\hat{S}^{(\text{bare},1)}_{\tau,M,\text{virt}}(\ell,M,\mu) = \frac{\alpha_s C_F}{4\pi}\,\Gamma\left(2-\frac{d}{2}\right)\left(\frac{\mu^2 e^{\gamma_E}}{M^2}\right)^{2-\frac{d}{2}}\left\{4\,\delta(\bar{\ell})\left[-L_M + H_{1-\frac{d}{2}}\right] + 8\left[\frac{\theta(\bar{\ell})}{\bar{\ell}}\right]_+\right\}, \tag{5.63}$$

and the real massive gluon corrections given by

$$\mu\,\hat{S}^{(1)}_{\tau,M,\text{real}}(\ell,M,\mu) = -\,\frac{\alpha_s C_F}{4\pi}\,\theta(\ell-M)\,\frac{8}{\bar{\ell}}\ln\left(\frac{\ell^2}{M^2}\right). \tag{5.64}$$

Furthermore, expanding for $\epsilon\to 0$ we obtain

$$\mu\,\hat{S}^{(\text{bare},1)}_{\tau,M,\text{virt}}(\ell,M,\mu) = \frac{\alpha_s C_F}{4\pi}\left\{\delta(\bar{\ell})\left[-\frac{4}{\epsilon^2} + 2L_M^2 + \frac{\pi^2}{3}\right] + \left[\frac{\theta(\bar{\ell})}{\bar{\ell}}\right]_+\left[\frac{8}{\epsilon} - 8L_M\right]\right\}. \tag{5.65}$$

We see that the UV-divergences are mass independent and agree exactly with the well known divergences of the massless gluon contributions to the soft function in Eq. (5.11). Subtracting the divergences with the counterterm of Eq. (5.11) leads to a renormalized expression of the thrust soft function which has the correct massless limit in Eq. (5.9), i.e. $\hat{S}^{(1)}_{\tau,M}(\ell,M,\mu) \to \hat{S}^{(1)}_{\tau}(\ell,\mu)$ for $M\to 0$. Note that for $\mu=\mu_S\sim\ell\sim Q\lambda^2$ all large logarithms that arise for $M\ll\ell$ in individual corrections cancel in the sum of the real and virtual mass mode contributions.

5.4.2 Massive quark corrections with gluon hemisphere prescription

We use the dispersive technique for the calculation of the $\mathcal{O}(\alpha_s^2 C_F T_F)$ massive quark contributions to the soft function with the gluon hemisphere prescription. In the n_l-flavor scheme for α_s they can be obtained from the one-loop soft function for the radiation of a massive gluon with the subtracted dispersion relation

$$\begin{aligned}\hat{S}^{(g,n_l,\text{bare},2)}_{\tau,m}(\ell,m,\mu) &= \hat{S}^{(n_l,\text{bare},2)}_{\tau,m,\text{virt}}(\ell,m,\mu) + \hat{S}^{(n_l,2)}_{\tau,m,\theta}(\ell,m)\\ &= \frac{1}{\pi}\int\frac{\mathrm{d}M^2}{M^2}\left(\hat{S}^{(\text{bare},1)}_{\tau,M,\text{virt}}(\ell,M,\mu) + \hat{S}^{(1)}_{\tau,M,\text{real}}(\ell,M)\right)\text{Im}\big[\Pi(m^2,M^2)\big]\,.\end{aligned} \tag{5.66}$$

The convolution is performed separately for the virtual gluon emission term $\hat{S}^{(\text{bare},1)}_{\tau,M,\text{virt}}$ in Eq. (5.63) and the UV and IR finite real radiation term $\hat{S}^{(1)}_{\tau,M,\text{real}}$ in Eq. (5.64), where for the latter the $d=4$ version of the absorptive part of the vacuum polarization function in Eq. (3.61) can be used. We obtain the result in Eq. (5.32) for the real radiation term $\hat{S}^{(n_l,2)}_{\tau,m,\theta}$ (with $\alpha_s=\alpha_s^{(n_l)}(\mu)$) and for the virtual radiation term

$$\begin{aligned}\mu\,\hat{S}^{(n_l,\text{bare},2)}_{\tau,m,\text{virt}}(\ell,m,\mu) = \frac{\big(\alpha_s^{(n_l)}\big)^2 C_F T_F}{16\pi^2}\Bigg\{&\delta(\bar{\ell})\Bigg[-\frac{4}{\epsilon^3} + \frac{1}{\epsilon^2}\left(\frac{16}{3}L_m + \frac{20}{9}\right) + \frac{1}{\epsilon}\left(-\frac{8}{3}L_m^2 + \frac{112}{27} - \frac{2\pi^2}{3}\right)\\ &- \frac{40}{9}L_m^2 + \left(-\frac{448}{27} + \frac{8\pi^2}{9}\right)L_m - \frac{656}{27} + \frac{10\pi^2}{27} + 8\zeta_3\Bigg] + \left[\frac{\theta(\bar{\ell})}{\bar{\ell}}\right]_+\Bigg[\frac{16}{3\epsilon^2}\\ &+ \frac{1}{\epsilon}\left(-\frac{32}{3}L_m - \frac{80}{9}\right) + \frac{32}{3}L_m^2 + \frac{160}{9}L_m + \frac{448}{27} + \frac{8\pi^2}{9}\Bigg]\Bigg\}\,.\end{aligned} \tag{5.67}$$

[7] Using the symmetric Wilson line regulator η in Refs. [40,41] the diagram S_a does not vanish and the rapidity divergences cancel between S_a and S_b within one hemisphere instead of between S_+ and S_-.

We switch to the (n_l+1)-flavor scheme for α_s by adding the $\overline{\text{MS}}$-renormalized $\Pi(0)$ times the (unrenormalized) massless one-loop contribution to the soft function

$$\hat{S}_\tau^{(n_l+1,\text{bare},1)}(\ell,\mu) = \hat{S}_\tau^{(n_l+1,1)}(\ell,\mu) + Z_{S_\tau}^{(n_l+1,1)}(\ell,\mu)\,, \tag{5.68}$$

with $\hat{S}_\tau^{(n_l+1,1)}(\ell,\mu)$ and $Z_{S_\tau}^{(n_l+1,1)}(\ell,\mu)$ given in Eqs. (5.9) and (5.11), respectively. Thus the corresponding contribution needed to change from the n_l to the (n_l+1)-flavor scheme reads

$$\begin{aligned}\mu\,\hat{S}_\tau^{(n_l\to n_l+1,2)}(\ell,m,\mu) &= -\left(\Pi(m^2,0) - \frac{\alpha_s T_F}{3\pi}\frac{1}{\epsilon}\right)\left(\hat{S}_\tau^{(n_l+1,1)}(\ell,\mu) + Z_{S_\tau}^{(n_l+1,1)}(\ell,\mu)\right)\\ &= \frac{\alpha_s^2 C_F T_F}{(4\pi)^2}\left\{\delta(\bar\ell)\left[-\frac{16}{3\epsilon^2}L_m + \frac{1}{\epsilon}\left(\frac{8}{3}L_m^2 + \frac{4\pi^2}{9}\right) - \frac{8}{9}L_m^3 - \frac{16}{9}\zeta_3\right]\right.\\ &\quad\left. + \left[\frac{\theta(\bar\ell)}{\bar\ell}\right]_+\left[\frac{32}{3\epsilon}L_m - \frac{16}{3}L_m^2 - \frac{8\pi^2}{9}\right] - \frac{64}{3}L_m\left[\frac{\theta(\bar\ell)\ln\bar\ell}{\bar\ell}\right]_+\right\}.\end{aligned} \tag{5.69}$$

Note that the contributions in Eq. (5.69) contain only the virtual distributive pieces and do not affect the massive quark real radiation corrections. Combining all contributions and renormalizing the result with the soft counterterm contribution $Z_{S_\tau,T_F}^{(n_l+1,2)}$ in Eq. (5.12) finally gives

$$\hat{S}_{\tau,m,\text{virt}}^{(n_l+1,2)}(\ell,m,\mu) = \hat{S}_{\tau,m,\text{virt}}^{(n_l,\text{bare},2)}(\ell,m,\mu) + \hat{S}_\tau^{(n_l\to n_l+1,2)}(\ell,m,\mu) - Z_{S_\tau,T_F}^{(n_l+1,2)}(\ell,\mu) \tag{5.70}$$

with $\alpha_s = \alpha_s^{(n_l+1)}(\mu)$ employed in the final result. Inserting Eqs. (5.12), (5.67) and (5.69) yields

$$\begin{aligned}\mu\,\hat{S}_{\tau,m,\text{virt}}^{(n_l+1,2)}(\ell,m,\mu) &= \frac{\big(\alpha_s^{(n_l+1)}\big)^2 C_F T_F}{16\pi^2}\left\{\delta(\bar\ell)\left[-\frac{8}{9}L_m^3 - \frac{40}{9}L_m^2 + \left(-\frac{448}{27} + \frac{8\pi^2}{9}\right)L_m - \frac{656}{27} + \frac{10\pi^2}{27}\right.\right.\\ &\quad\left.\left. + \frac{56}{9}\zeta_3\right] + \left[\frac{\theta(\bar\ell)}{\bar\ell}\right]_+\left[\frac{16}{3}L_m^2 + \frac{160}{9}L_m + \frac{448}{27}\right] - \frac{64}{3}L_m\left[\frac{\theta(\bar\ell)\ln\bar\ell}{\bar\ell}\right]_+\right\}\end{aligned} \tag{5.71}$$

Subtracting from Eq. (5.71) the massless limit in Eq. (5.10) we obtain the distributive mass corrections to the soft function given in Eq. (5.31).

From Eq. (5.66) one can take the massless limit by expanding the real radiation contribution $\hat{S}_{\tau,m,\theta}^{(n_l+1,2)}$ into delta- and plus-distribution, which leads for the renormalized result

$$\begin{aligned}\mu\,\hat{S}_{\tau,m}^{(g,n_l+1,2)}(\ell,m,\mu) \overset{m\to 0}{\longrightarrow} \frac{\big(\alpha_s^{(n_l+1)}\big)^2 C_F T_F}{16\pi^2}&\left\{\delta(\bar\ell)\left[\frac{656}{81} - \frac{10\pi^2}{9} - \frac{40}{9}\zeta_3\right] + \left[\frac{\theta(\bar\ell)}{\bar\ell}\right]_+\left[-\frac{448}{27} + \frac{16\pi^2}{9}\right]\right.\\ &\left. + \frac{320}{9}\left[\frac{\theta(\bar\ell)\ln\bar\ell}{\bar\ell}\right]_+ - \frac{64}{3}\left[\frac{\theta(\bar\ell)\ln^2\bar\ell}{\bar\ell}\right]_+\right\}.\end{aligned} \tag{5.72}$$

This agrees with a corresponding computation for the gluon hemisphere soft function, where the mass is set to zero from the beginning, but does not yield the full massless thrust soft function correction at $\mathcal{O}(\alpha_s^2 C_F T_F)$ (with the quark hemisphere prescription) in Eq. (5.10). Thus the additional phase space misalignment contribution which we compute in the following is required to achieve the correct massless limit of the thrust soft function.

5.4.3 Phase space misalignment correction

We now determine the $\mathcal{O}(\alpha_s^2 C_F T_F)$ massive quark corrections to the thrust soft function for the physical quark hemisphere prescription. After having obtained the results for the gluon hemisphere prescription $\hat{S}_{\tau,m}^{(g,n_l+1,2)}$ in Sec. 5.4.2, what remains to be calculated are the corrections due to the phase space misalignment to the physical quark hemisphere prescription, which we call $\hat{S}_{\tau,m,\Delta}^{(n_l+1,2)}$. The result for the full $\mathcal{O}(\alpha_s^2 C_F T_F)$ massive quark corrections to the renormalized thrust soft function reads

$$\hat{S}_{\tau,m}^{(n_l+1,2)}(\ell,m,\mu) = \hat{S}_{\tau,m}^{(g,n_l+1,2)}(\ell,m,\mu) + \hat{S}_{\tau,m,\Delta}^{(n_l+1,2)}(\ell,m)\,. \tag{5.73}$$

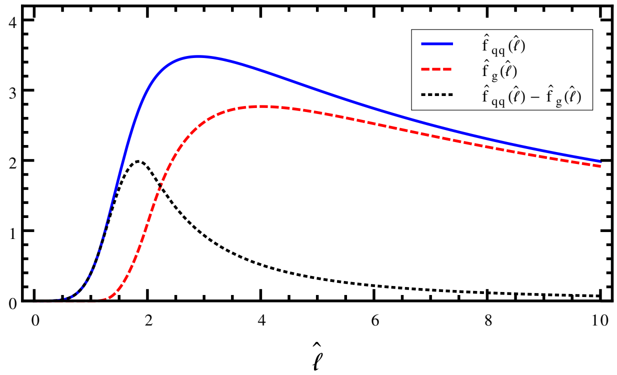

Figure 5.7: The contributions to the thrust soft function from the opposite hemisphere phase space, for the quark hemisphere prescription $\hat{f}_{qq}(\hat{\ell})$ (blue, solid), gluon hemisphere prescription $\hat{f}_g(\hat{\ell})$ (red, dashed) and the difference which is proportional to $m\,\hat{S}^{(n_l+1,2)}_{\tau,m,\Delta}(\ell, m)$ (black, dotted).

The phase space misalignment correction $\hat{S}^{(n_l+1,2)}_{\tau,m,\Delta}$ contains only phase space contributions, where the two quarks enter different hemispheres, since quark and gluon hemisphere prescriptions act in the same way when the quarks enter the same hemisphere. After having performed the integrations over the transverse momenta in Eqs. (5.50) and (5.53) we obtain

$$\begin{aligned}\hat{S}^{(n_l+1,2)}_{\tau,m,\Delta}(\ell, m) = \frac{\big(\alpha_s^{(n_l+1)}\big)^2 C_F T_F}{16\pi^2} &\int \mathrm{d}q^- \int \mathrm{d}k^+ \int \mathrm{d}q^+ \int \mathrm{d}k^-\, \theta(k^- - k^+)\,\theta(q^+ - q^-) \\ &\times \theta(k^+k^- - m^2)\,\theta(q^+q^- - m^2)\,\theta(k^- + k^+)\,\theta(q^+ + q^-)\,\big[\delta(\ell - k^+ - q^-) \\ &- \theta(k^- + q^- - k^+ - q^+)\,\delta(\ell - k^+ - q^+) - \theta(k^+ + q^+ - k^- - q^-)\,\delta(\ell - k^- - q^-)\big] \\ &\times f_m(k^+, k^-, q^+, q^-, m) \end{aligned} \tag{5.74}$$

with the integrand

$$\begin{aligned} f_m(k^+, k^-, q^+, q^-, m) = &\left[\left(\frac{k^+q^+}{(q^+ + k^+)^2} + \frac{k^-q^-}{(q^- + k^-)^2}\right)(q^+k^- + k^+q^-) - \frac{4(k^+k^- - m^2)(q^+q^- - m^2)}{(q^+ + k^+)(q^- + k^-)}\right] \\ &\times \frac{16}{[(q^+k^- + k^+q^-)^2 - 4(k^+k^- - m^2)(q^+q^- - m^2)]^{3/2}}\,. \end{aligned} \tag{5.75}$$

In fact the results of both, quark and gluon hemisphere prescriptions entering $\hat{S}^{(n_l+1,2)}_{\tau,m,\Delta}$ are individually free of UV divergences. Conceptually this is related to the consistency of soft-collinear factorization and the exponentiation properties of the hemisphere soft function [92, 115], which imply that at $\mathcal{O}(\alpha_s^2)$ UV-divergent contributions depending simultaneously on both momentum projections in the two hemispheres in a non-trivial way can only have C_F^2 color-structures. For the massive quark corrections we calculate, there are also no IR divergences for both hemisphere prescriptions individually since the mass acts as an IR regulator. [8] Therefore we do not have to employ any additional regularization and a numerical computation can be easily performed. Furthermore, since these contributions to the soft function correspond to real emission diagrams, no distributions are generated for nonvanishing quark masses.

Using Eq. (5.74) we can cast the result for the phase space misalignment correction into the form ($\hat{\ell} = \ell/m$)

$$m\,\hat{S}^{(n_l+1,2)}_{\tau,m,\Delta}(\ell, m) = \frac{\big(\alpha_s^{(n_l+1)}\big)^2 C_F T_F}{16\pi^2}\left(\hat{f}_{qq}(\hat{\ell}) - \hat{f}_g(\hat{\ell})\right). \tag{5.76}$$

[8] In the massless computation of the hemisphere soft function in Refs. [112, 117] infrared $1/\epsilon$ divergences arise for the phase space, where the two quarks enter opposite hemispheres, as well as for the one, where they enter the same hemisphere. These cancel in the sum.

The term $\hat{f}_{qq}$ is the contribution due to the quark hemisphere prescription,

$$\hat{f}_{qq}(\hat{\ell}) = \int_0^\infty dy^- \int_0^\infty dy^+ \int_0^\infty dx^- \,\theta(x^- + y^- - \hat{\ell})\,\theta(y^+ - y^-)\,\theta(\hat{\ell}x^- - y^-x^- - 1)\,\theta(y^+y^- - 1) \times f_m(\hat{\ell} - y^-, x^-, y^+, y^-, 1) \tag{5.77}$$

in rescaled variables with $x^\pm = k^\pm/m$ and $y^\pm = q^\pm/m$. Since $\hat{f}_{qq}$ is dimensionless we have recombined the scales and written f_m as a dimensionless function in terms of these rescaled momenta. The term $\hat{f}_g$ is related to the gluon hemisphere prescription and reads

$$\hat{f}_g(\hat{\ell}) = \int_0^\infty dy^- \int_0^\infty dy^+ \int_0^\infty dx^- \,\theta(x^- + y^+ - \hat{\ell})\,\theta(y^+ - y^-)\,\theta(\hat{\ell}x^- - y^+x^- - 1)\,\theta(y^+y^- - 1) \times f_m(\hat{\ell} - y^+, x^-, y^+, y^-, 1)\,. \tag{5.78}$$

Writing out the phase space in Eq. (5.77) and (5.78) in terms of separate integration domains, one can evaluate $\hat{f}_{qq}$ and $\hat{f}_g$ numerically. Using the Cuba library [118] we obtained the same result for both deterministic as well as Monte-Carlo algorithms. The resulting functions are displayed in Fig. 5.7 together with their difference resulting in the complete hemisphere misalignment contribution. $\hat{f}_g(\hat{\ell})$ contains a threshold at the scale $\hat{\ell} = 1$, at which it turns on smoothly. Indeed the momentum deposit ℓ in the gluon prescription for the opposite hemisphere phase space is a sum of one large lightcone component, say q^+, and a small lightcone component k^+. Since the invariant mass of each real particle is fixed by the on-shell condition, it follows that $q^+q^- \geq m^2$. Taking into account that in this case $q^+ > q^-$ we get $\ell^2 = (q^+ + k^+)^2 \geq (q^+)^2 \geq q^+q^- \geq m^2$. For $\hat{f}_{qq}$ no threshold arises, since just the small lightcone components contribute.

Let us investigate the asymptotic behavior of the hemisphere misalignment correction analytically and show the results for very heavy and light quarks explicitly. For large masses, i.e. $\ell \ll m$, the expansion of $\hat{f}_{qq}$ gives the only contribution to $\hat{S}^{(n_l+1,2)}_{\tau,m,\Delta}$, since $\hat{f}_g$ vanishes, resulting in

$$m\,\hat{S}^{(n_l+1,2)}_{\tau,m,\Delta}(\ell, m) \overset{\ell \ll m}{\longrightarrow} \frac{\big(\alpha_s^{(n_l+1)}\big)^2 C_F T_F}{16\pi^2}\,\frac{8}{15}\,\hat{\ell}^5\left[1 + \mathcal{O}(\hat{\ell}^2)\right]\,. \tag{5.79}$$

This gives a strong suppression of mass effects in the decoupling limit.

For $\ell \gg m$ we obtain for the expansion of both $\hat{f}_{qq}$ and $\hat{f}_g$ at leading order

$$\hat{f}_{qq}(\hat{\ell}),\; \hat{f}_g(\hat{\ell}) \overset{\hat{\ell} \gg 1}{\longrightarrow} \left(-\frac{16}{3} + \frac{32\pi^2}{9}\right)\frac{1}{\hat{\ell}}\left[1 + \mathcal{O}\left(\frac{1}{\hat{\ell}}\right)\right]\,. \tag{5.80}$$

Thus for large values of ℓ/m the hemisphere misalignment correction involves strong cancellations in the difference between its quark and gluon hemisphere contributions as can be also seen in Fig. 5.7, which can lead to numerical instabilities. An alternative way to compute $\hat{S}^{(n_l+1,2)}_{\tau,m,\Delta}$ for large values of ℓ/m can be achieved by evaluating the cumulant, where the quark and gluon hemisphere contributions can be combined prior to integration, and by differentiating numerically afterwards (see appendix D). The asymptotic expansion for large thrust momenta is also outlined in appendix D and gives

$$m\,\hat{S}^{(n_l+1,2)}_{\tau,m,\Delta}(\ell, m) \overset{\ell \gg m}{\longrightarrow} \frac{\big(\alpha_s^{(n_l+1)}\big)^2 C_F T_F}{16\pi^2}\,\frac{1}{\hat{\ell}^3}\left[8\ln^2\hat{\ell}^2 - 80\ln\hat{\ell} + \frac{640}{3} + \frac{292\pi^2}{45} + 32\pi\right]\left[1 + \mathcal{O}\left(\frac{1}{\hat{\ell}}\right)\right]\,. \tag{5.81}$$

In the massless limit the hemisphere misalignment correction becomes a delta-distribution and gives

$$\mu\,\hat{S}^{(n_l+1,2)}_{\tau,m,\Delta}(\ell, m) \overset{m \to 0}{\longrightarrow} \frac{\big(\alpha_s^{(n_l+1)}\big)^2 C_F T_F}{16\pi^2}\,\delta(\bar{\ell})\left\{-\frac{64}{9} + \frac{104\pi^2}{27} - \frac{64}{3}\zeta_3\right\}\,. \tag{5.82}$$

Together with the massless limits of the soft function with gluon hemisphere prescription in Eqs. (5.72) this yields the massless result in Eq. (5.10).

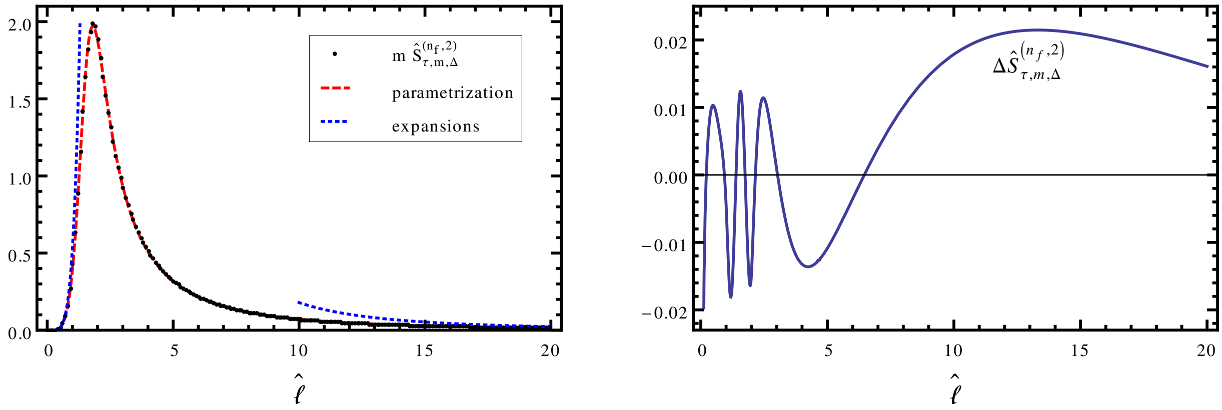

Figure 5.8: Left panel: Phase space misalignment correction $m\,\hat{S}^{(n_f,2)}_{\tau,m,\Delta}(\ell,m)$ (black dots) together with the parametrization in Eq. (5.34) (red, dashed) and its asymptotic expansions (blue, dotted), all normalized by the prefactor $(\alpha_s^{(n_f)})^2 C_F T_F/16\pi^2$ (with $n_f = n_l$ or $n_f = n_l + 1$). The fit is almost indistinguishable from the exact function. Right panel: The relative deviation of the parametrization with respect to an interpolation of the exact function for $\hat{S}^{(n_f,2)}_{\tau,m,\Delta}$, denoted by $\Delta\hat{S}^{(n_f,2)}_{\tau,m,\Delta}$.

A possible parametrization of $\hat{S}^{(n_l+1,2)}_{\tau,m,\Delta}$ can be given by a Padé-type rational function multiplying some logarithmic terms, see Eq. (5.34). We have adopted an analytic ansatz that is capable of yielding the asymptotic behaviors of Eqs. (5.79) and (5.81) and has the finite normalization given by Eq. (5.82). We have also already displayed the parameters fixed by the asymptotic expansion and the fitted values corresponding to a local minimum of the χ^2-function in Sec. 5.3 (above and in Eq. (5.35)). The exact and fitted results together with the asymptotic expansions are shown in Fig. 5.8, where we clearly see that the parametrization yields an excellent approximation of the actual function and is certainly more than adequate for phenomenological applications in the near future.

Finally, we also display the three components of the $\mathcal{O}(\alpha_s^2 C_F T_F)$ massive quark corrections to the renormalized thrust soft function, their sum and the massless limit together with the cumulants in Fig. 5.9 for $\mu = m$ as a function of $\hat{\ell} = \ell/m$ and $\hat{L} = L/m$, respectively. We see that the phase space misalignment correction represents a relatively small contribution.

5.4.4 Renormalon subtractions

We compute the leading renormalon subtraction for massive secondary quarks for $m \lesssim Q\tau$ in the gap formalism. The subtraction series defined by Eq. (5.18) is now mass dependent. Following the form of Eqs. (5.66) and (5.73) we parametrize the gap subtraction coming from the $\mathcal{O}(\alpha_s^2 C_F T_F)$ massive quark corrections in the form

$$\delta^{(n_l+1,2)}_{m}(R,m,\mu) = \delta^{(n_l+1,2)}_{m,\mathrm{virt}}(R,m,\mu) + \delta^{(n_l+1,2)}_{m,\theta}(R,m) + \delta^{(n_l+1,2)}_{m,\Delta}(R,m)\,, \tag{5.83}$$

where the three terms in the brackets arise from the results for $\hat{S}^{(n_l+1,2)}_{\tau,m,\mathrm{virt}}$, $\hat{S}^{(n_l+1,2)}_{\tau,m,\theta}$ and $\hat{S}^{(n_l+1,2)}_{\tau,m,\Delta}$ given in Eqs. (5.71), (5.32) and (5.74). We emphasize that the results are given here in the scheme with $n_l + 1$ dynamical quark flavors. We obtain

$$\delta^{(n_l+1,2)}_{m,\mathrm{virt}}(R,m,\mu) = -\,\frac{\left(\alpha_s^{(n_l+1)}\right)^2 C_F T_F}{(4\pi)^2}\,R\,e^{\gamma_E}\left\{\frac{16}{3}L_m \ln\left(\frac{\mu^2}{R^2}\right) - \frac{8}{3}L_m^2 - \frac{80}{9}L_m - \frac{224}{27}\right\}, \tag{5.84}$$

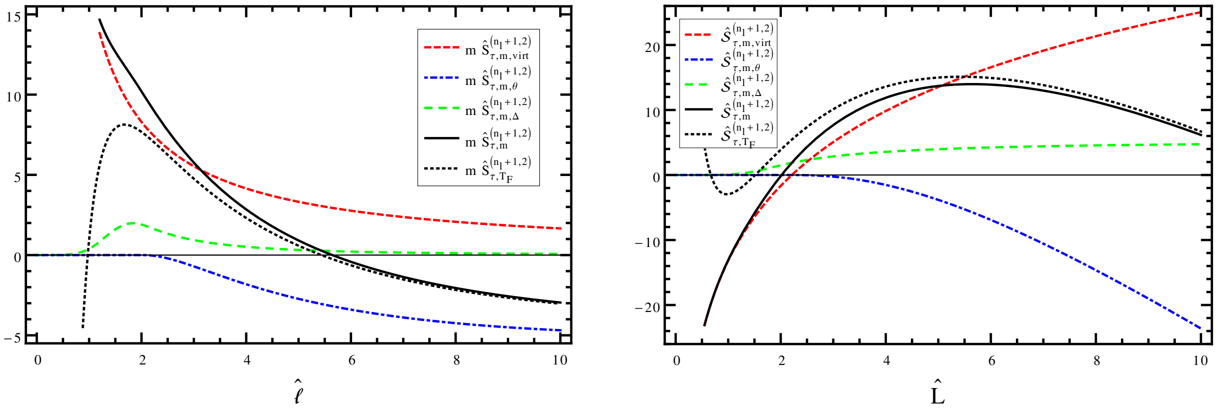

Figure 5.9: Plots of the massive quark contributions to the thrust soft function (left panel) and its cumulant (right panel) for $\mu = m$, normalized by the prefactor $(\alpha_s^{(n_l+1)})^2 C_F T_F/16\pi^2$. $\hat{S}^{(n_l+1,2)}_{\tau,m,\mathrm{virt}}$, $\hat{S}^{(n_l+1,2)}_{\tau,m,\theta}$ and $\hat{S}^{(n_l+1,2)}_{\tau,m,\Delta}$ denote the virtual, real radiation and phase space misalignment contributions described in the text, $\hat{S}^{(n_l+1,2)}_{\tau,m}$ is their sum, i.e. the full massive contribution, and $\hat{S}^{(n_l+1,2)}_{\tau,T_F}$ is the massless contribution at $\mathcal{O}(\alpha_s^2 C_F T_F)$ for one single flavor. The corresponding descriptions also hold for the cumulant terms $\hat{\mathcal{S}}_\tau$.

and after some lengthy analytical calculation

$$\begin{aligned}
\delta^{(n_l+1,2)}_{m,\theta}(R,m) =& \frac{\left(\alpha_s^{(n_l+1)}\right)^2 C_F T_F}{(4\pi)^2}\, R\, e^{\gamma_E} \left\{ \frac{16}{3} G^{3,0}_{1,3}\left(\begin{matrix} 1 \\ 0,0,0 \end{matrix} \middle| \frac{z^2}{4} \right) - \frac{160}{9} K_0(z) + z\left[\frac{160}{9} K_1(z) - 8\pi \right] \right. \\
&+ z^2 \left[-\frac{16}{27} K_2(z) + 8\pi\big(K_0(z) L_{-1}(z) + K_1(z) L_0(z)\big) \right] + z^3 \left[\frac{16}{27} K_1(z) - \frac{8\pi}{27} \right] \\
&\left. + \frac{8\pi}{27} z^4 \Big[K_0(z) L_{-1}(z) + K_1(z) L_0(z) \Big] \right\}, \qquad (5.85)
\end{aligned}$$

where $z \equiv 2m/(Re^{\gamma_E})$ and K_n being the familiar Bessel functions. $G^{m,n}_{p,q}$ and L_n denote the less known Meijer G and Struve functions. For $z > 0$ the corresponding explicit integral representations of these functions read

$$G^{3,0}_{1,3}\left(\begin{matrix} 1 \\ 0,0,0 \end{matrix} \middle| \frac{z^2}{4} \right) = 4 \int_1^\infty \frac{\mathrm{d}t}{t} K_0(zt)\,, \qquad (5.86)$$

$$L_n(z) = I_{-n}(z) - \frac{2^{1-n} z^n}{\sqrt{\pi}\,\Gamma\left(n+\frac{1}{2}\right)} \int_0^\infty dt\, \left(t^2+1\right)^{n-\frac{1}{2}} \sin(tz)\,, \qquad (5.87)$$

where I_n indicate the better known Bessel functions. Computing the integral in Eq. (5.86) numerically is faster and more stable than evaluating $G^{3,0}_{1,3}$ directly in *Mathematica* (in particular for large vales of the argument). We refer to Ref. [119] for further information about these functions.

The contribution from the phase space misalignment correction can again not be given in closed analytic form and, using Eqs. (5.18) and (5.74), reads

$$\begin{aligned}
\delta^{(n_l+1,2)}_{m,\Delta}(R,m) =& -\frac{\left(\alpha_s^{(n_l+1)}\right)^2 C_F T_F}{(4\pi)^2} \frac{1}{2} \int \mathrm{d}q^- \int \mathrm{d}k^+ \int \mathrm{d}q^+ \int \mathrm{d}k^-\, \theta(k^- - k^+)\, \theta(q^+ - q^-) \\
&\times \theta(k^+k^- - m^2)\, \theta(q^+q^- - m^2)\, \theta(k^+ + k^-)\, \theta(q^+ + q^-) \left[(q^- + k^+)\, e^{-\frac{q^- + k^+}{Re^{\gamma_E}}} \right. \\
&\left. - \theta(k^- + q^- - k^+ - q^+)(k^+ + q^+)\, e^{-\frac{k^+ + q^+}{Re^{\gamma_E}}} - \theta(k^+ + q^+ - k^- - q^-)\,(k^- + q^-)\, e^{-\frac{k^- + q^-}{Re^{\gamma_E}}} \right] \\
&\times f_m(k^+, k^-, q^+, q^-, m)\,. \qquad (5.88)
\end{aligned}$$

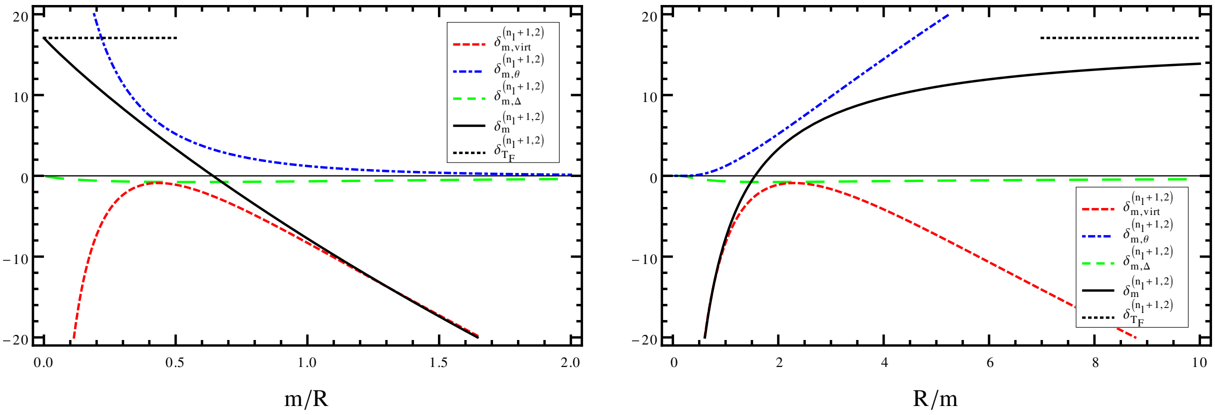

Figure 5.10: Gap subtractions $\delta^{(n_l+1,2)}_{m,\mathrm{virt}}(R,m,\mu=R)$, $\delta^{(n_l+1,2)}_{m,\theta}(R,m)$ and $\delta^{(n_l+1,2)}_{m,\Delta}(R,m)$ coming from massive quark virtual (red dashed line) and real (blue dotted-dashed line) contributions to the gluon hemisphere soft function and from the phase space misalignment correction (green wide-dashed line) at $\mathcal{O}(\alpha_s^2 C_F T_F)$, all normalized by the prefactor $Re^{\gamma_E}(\alpha_s^{(n_l+1)})^2 C_F T_F/16\pi^2$. The black solid line $\delta^{(n_l+1,2)}_{m}(R,m,\mu=R)$ denotes the sum of all terms and the black dotted line $\delta^{(n_l+1,2)}_{T_F}(R,\mu=R)$ the well known massless limit.

The results for $\delta^{(n_l+1,2)}_{m,\mathrm{virt}}(R,m,\mu=R)$, $\delta^{(n_l+1,2)}_{m,\theta}(R,m)$, $\delta^{(n_l+1,2)}_{m,\Delta}(R,m)$ and their sum are shown in Fig. 5.10 as a function of m/R and R/m. We see that $\delta^{(n_l+1,2)}_{m,\Delta}$, which contains only the phase space contribution where the quark and antiquark enter different hemispheres, is very small. This is not unexpected since this phase space configuration is related to larger gluon invariant masses and therefore less sensitive to infrared renormalon-type contributions than the phase space contributions in $\delta^{(n_l+1,2)}_{m,\mathrm{virt}}$ and $\delta^{(n_l+1,2)}_{m,\theta}$. One can also see that in the massless limit $R/m \gg 1$ there are large cancellations between the virtual and real radiation contributions $\delta^{(n_l+1,2)}_{m,\mathrm{virt}}$ and $\delta^{(n_l+1,2)}_{m,\theta}$. This is related to the fact that the real and virtual massive quark corrections to the soft function each contain mass-singularities, and the sum of both is needed to reach the known massless limit (indicated by the black dotted line),

$$\delta^{(n_l+1,2)}_{m,\mathrm{virt}}(R,m,\mu) + \delta^{(n_l+1,2)}_{m,\theta}(R,m) \overset{m\to 0}{\longrightarrow} \delta^{(n_l+1,2)}_{T_F}(R,\mu)\,, \tag{5.89}$$

with the massless renormalon subtraction $\delta^{(n_l+1,2)}_{T_F}$ given in Eq. (5.20) for $n_f = n_l+1$. Including the first non-vanishing correction to the massless limit we obtain for the whole renormalon subtraction [9]

$$\delta^{(n_l+1,2)}_{m}(R,m,\mu) \overset{m\to 0}{\longrightarrow} \delta^{(n_l+1,2)}_{T_F}(R,\mu) - \frac{\left(\alpha_s^{(n_l+1)}\right)^2 C_F T_F}{(4\pi)^2}\, 66.1\, m + \mathcal{O}\left(\frac{m^2}{R}\right). \tag{5.90}$$

The fact that a term linear in m arises is directly tied to the existence of the $\mathcal{O}(\Lambda_{\mathrm{QCD}})$ renormalon in the soft function indicating a linear sensitivity to small momenta [120–122]. For large masses the virtual contribution gives the leading order behavior, while the real radiation contributions decouple exponentially and power-like,

$$\delta^{(n_l+1,2)}_{m,\theta}(R,m) \overset{m\gg R}{\longrightarrow} \frac{\left(\alpha_s^{(n_l+1)}\right)^2 C_F T_F}{(4\pi)^2}\, R\, e^{\gamma_E}\, 16\sqrt{2\pi}\, z^{-\frac{5}{2}}\, e^{-z}\left[1 - \frac{49}{8z} + \mathcal{O}\left(\frac{1}{z^2}\right)\right], \tag{5.91}$$

$$\delta^{(n_l+1,2)}_{m,\Delta}(R,m) \overset{m\gg R}{\longrightarrow} \frac{\left(\alpha_s^{(n_l+1)}\right)^2 C_F T_F}{(4\pi)^2}\, R\, e^{\gamma_E}\, 12288\, z^{-6}\left[1 + \mathcal{O}\left(\frac{1}{z^2}\right)\right]. \tag{5.92}$$

[9] The small mass expansion is proportional to $-16\pi\, m$ for $\delta^{(n_l+1,2)}_{m,\theta}$ and to $\approx -15.8\, m$ for $\delta^{(n_l+1,2)}_{m,\Delta}$ at linear order in m.

This leads to

$$\delta_m^{(n_l+1,2)}(R,m,\mu) \overset{m\to\infty}{\longrightarrow} \delta_{m,\text{virt}}^{(n_l+1,2)}(R,m,\mu)\left[1+\mathcal{O}\left(\frac{R^6}{m^6}\right)\right], \tag{5.93}$$

which is equivalent to Eq. (5.43), where the massless result in Eq. (5.20) has been subtracted from $\delta_m^{(n_l+1,2)}$ to give the mass corrections to the massless limit. Thus the gap subtraction does not decouple by itself, indicating that the evolution in R of the renormalon-free gap parameter $\bar{\Delta}$ has a decoupling relation when the evolution crosses the mass threshold. This has been already discussed in detail in Sec. 5.3.5.

Since $\delta_{m,\theta}^{(n_l+1,2)}$ is cumbersome to evaluate in a numerical code and $\delta_{m,\Delta}^{(n_l+1,2)}$ is not known analytically, we have provided a parametrization for the mass corrections with the correct leading asymptotic behavior given in Eq. (5.40).

The $\mathcal{O}(\alpha_s^2 C_F T_F)$ massive quark corrections to the gap subtractions give contributions to the R-evolution of the subtracted gap parameter $\bar{\Delta}^{(n_l+1)}$, which is free of the $\mathcal{O}(\Lambda_{\text{QCD}})$ renormalon. The $\mathcal{O}(\alpha_s^2 C_F T_F)$ massive quark contributions can be determined from Eq. (5.83) giving

$$\gamma_{R,m}^{(n_l+1,2)} = \gamma_{R,m,\text{virt}}^{(n_l+1,2)} + \gamma_{R,m,\theta}^{(n_l+1,2)} + \gamma_{R,m,\Delta}^{(n_l+1,2)}, \tag{5.94}$$

where

$$\gamma_{R,m,\text{virt}}^{(n_l+1,2)} = \frac{\left(\alpha_s^{(n_l+1)}\right)^2 C_F T_F}{(4\pi)^2}\, e^{\gamma_E}\left\{-\frac{8}{3}\ln^2\left(\frac{m^2}{R^2}\right)+\frac{16}{9}\ln\left(\frac{m^2}{R^2}\right)+\frac{256}{27}\right\}, \tag{5.95}$$

$$\begin{aligned}\gamma_{R,m,\theta}^{(n_l+1,2)} = {}& \frac{\left(\alpha_s^{(n_l+1)}\right)^2 C_F T_F}{(4\pi)^2}\, e^{\gamma_E}\left\{\frac{16}{3}G_{1,3}^{3,0}\left(\begin{matrix}1\\0,0,0\end{matrix}\middle|\frac{z^2}{4}\right)+\frac{32}{9}K_0(z)-\frac{32}{27}zK_1(z)+\frac{32}{27}z^2K_0(z)+\frac{16\pi}{27}z^3\right.\\ &\left.-\frac{16\pi}{27}z^4\left[K_1(z)L_{-2}(z)+K_2(z)L_{-1}(z)\right]\right\}.\end{aligned} \tag{5.96}$$

The term $\gamma_{R,m,\Delta}^{(n_l+1,2)}$ cannot be given in analytic form and has to be computed numerically from Eq. (5.88). Its contribution is, however, very small and might be insignificant for practical applications. Alternatively, the complete $\mathcal{O}(\alpha_s^2 C_F T_F)$ massive quark contributions to the R-evolution can be determined from the parametrization in Eq. (5.40) which yields the correct result up to a deviation of much less than 1%.

5.5 Consistency relations

In the same way as already discussed in chapter 4, the threshold factors $\mathcal{M}_{\tilde{C}}$ for the hard current mass mode matching, $\mathcal{M}_{J_\tau}$ for the jet mass mode matching and $\mathcal{M}_{S_\tau}$ for the soft mass mode matching are related by consistency of RG running. The latter arises when the RG evolution of the soft function crosses the massive quark threshold. This does not happen in the RG setup we discussed in section 5.3, since there the final renormalization scale has always been set to the soft scale. However, if we choose a different final renormalization scale, say the jet scale μ_J, we can get a factorization theorem depending on $\mathcal{M}_{S_\tau}(\ell,m,\mu_m)$. This happens e.g. in scenario III ($\mu_J > \mu_m > \mu_S$),

$$\begin{aligned}\frac{1}{\sigma_0}\frac{\mathrm{d}\sigma}{\mathrm{d}\tau} = {}& Q\left|\tilde{C}^{(n_l+1)}(Q,m,\mu_H)\right|^2\left|U_{\tilde{C}}^{(n_l+1)}(Q,\mu_H,\mu_J)\right|^2\int\mathrm{d}s\int\mathrm{d}\ell\int\mathrm{d}\ell'\int\mathrm{d}\ell''\,J_\tau^{(n_l+1)}(s,m,\mu_J)\\ &\times U_{S_\tau}^{(n_l+1)}\Big(\ell-\frac{s}{Q},\mu_J,\mu_m\Big)\mathcal{M}_{S_\tau}(\ell'-\ell,m,\mu_m)\,U_{S_\tau}^{(n_l)}(\ell''-\ell',\mu_m,\mu_S)\,S_\tau^{(n_l)}(Q\tau-\ell'',\mu_S).\end{aligned} \tag{5.97}$$

The consistency relation can be easily read off from Eqs. (5.28) and (5.97), which show the factorization theorems in scenario III with the final renormalization scale μ set equal to the soft and the jet scale, respectively. It reads

$$\mathcal{M}_{S_\tau}(\ell,m,\mu) = Q\left|\mathcal{M}_{\tilde{C}}(Q,m,\mu)\right|^2\mathcal{M}_{J_\tau}(Q\ell,m,\mu). \tag{5.98}$$

The relation implies in particular that the rapidity logarithms (and singularities) that arise in the hard, collinear and soft sectors are intrinsically related to each other. We will check that this relation holds at $\mathcal{O}(\alpha_s^2 C_F T_F)$ by explicitly calculating the soft threshold factor $\mathcal{M}_{S_\tau}(\ell,m,\mu_m)$ in the following.

Soft mass mode matching

The derivation of $\mathcal{M}_{S_\tau}(\ell, m, \mu_m)$ proceeds along the lines of the mass mode threshold factors in Sec. 4.4. The matching procedure takes care of the difference between the renormalized soft functions in the $\overline{\text{MS}}$ and OS scheme concerning the massive quark contributions, such that the mass mode matching coefficient at the mass scale μ_m is obtained by the relation

$$\begin{aligned}\mathcal{M}_{S_\tau}(\ell, m, \mu_m) &= \int \mathrm{d}\ell' \, \hat{S}_\tau^{(n_l+1)}(\ell-\ell', m, \mu_m)\Big(\hat{S}_\tau^{(n_l)}\Big)^{-1}(\ell', m, \mu_m) \\ &= \int \mathrm{d}\ell' \, Z_{S_\tau}^{(n_l)}(\ell-\ell', m, \mu_m)\Big(Z_{S_\tau}^{(n_l+1)}\Big)^{-1}(\ell', \mu_m)\,. \end{aligned} \tag{5.99}$$

For scales $\mu > m$ we use the (n_l+1)-flavor scheme, so we employ the $\overline{\text{MS}}$ subtractions for the UV divergent contributions to the strong coupling and the soft function. We have displayed the $\overline{\text{MS}}$ renormalized soft function $\hat{S}_\tau^{(n_l+1)}(\ell, m, \mu)$ in Eq. (5.30) and the corresponding counterterm is given in Eq. (5.12) with $n_f = n_l + 1$. Using the OS scheme implies that the massive quark contributions decouple for $m \to \infty$, so that the counterterm has to cancel all virtual massive corrections, i.e.

$$Z_{S_\tau, T_F}^{(n_l,2)}(\ell, m, \mu) = \hat{S}_{\tau,m,\text{virt}}^{(n_l,\text{bare},2)}(\ell, m, \mu)\,, \tag{5.100}$$

with $\hat{S}_{\tau,m,\text{virt}}^{(n_l,\text{bare},2)}(\ell, m, \mu)$ given in Eq. (5.67). The OS renormalized soft function at $\mathcal{O}(\alpha_s^2 C_F T_F)$ contains only real radiation corrections, which vanish for $m \gg \ell$, and thus reads

$$\hat{S}_{\tau,m}^{(n_l,2)}(\ell, m, \mu) = \hat{S}_{\tau,m,\theta}^{(n_l,2)}(\ell, m) + \hat{S}_{\tau,m,\Delta}^{(n_l,2)}(\ell, m)\,, \tag{5.101}$$

with $\hat{S}_{\tau,m,\theta}^{(n_l,2)}(\ell, m)$ and $\hat{S}_{\tau,m,\Delta}^{(n_l,2)}(\ell, m)$ given in analogy to Eqs. (5.32) and (5.34), respectively, with $\alpha_s = \alpha_s^{(n_l)}(\mu)$ also renormalized in the OS scheme. The renormalized soft function in this scheme is the one to be used for $\mu_m \gtrsim \mu_S$ (in the scenarios I, II and III).

Relating the schemes of α_s via Eq. (3.112), which leads to addional terms involving the one-loop contributions to the soft function, we obtain at $\mathcal{O}(\alpha_s^2)$ in the fixed-order counting ($\alpha_s^{(n_l+1)} = \alpha_s^{(n_l+1)}(\mu_m)$)

$$\mathcal{M}_{S_\tau}(\ell, m, \mu_m) = \delta(\ell) - \frac{\alpha_s^{(n_l+1)} T_F}{3\pi}\, L_m\, \hat{S}_\tau^{(n_l+1,1)}(\ell, \mu_m) + \hat{S}_{\tau,m,\text{virt}}^{(n_l+1,2)}(\ell, m, \mu) + \mathcal{O}(\alpha_s^3)\,. \tag{5.102}$$

Note that the real radiation terms cancel in the ratio in Eq. (5.99) and do not contribute to the threshold correction factor. Inserting the explicit expressions in Eqs. (5.9) and (5.71), this gives at $\mathcal{O}(\alpha_s^2)$ in the fixed-order counting ($\bar{\ell} = \ell/\mu_m$, $L_m = \ln(m^2/\mu^2)$)

$$\begin{aligned}\mu_m\, \mathcal{M}_{S_\tau}^{(2)}(\ell, m, \mu_m) = \frac{\alpha_s^2 C_F T_F}{16\pi^2}\bigg\{&\delta(\bar{\ell})\bigg[-\frac{8}{9}L_m^3 - \frac{40}{9}L_m^2 + \bigg(-\frac{448}{27} + \frac{4\pi^2}{9}\bigg)L_m - \frac{656}{27} + \frac{10\pi^2}{27} + \frac{56}{9}\zeta_3\bigg] \\ &+ \bigg[\frac{\theta(\bar{\ell})}{\bar{\ell}}\bigg]_+ \bigg[\frac{16}{3}L_m^2 + \frac{160}{9}L_m + \frac{448}{27}\bigg]\bigg\}\,. \end{aligned} \tag{5.103}$$

Since there are no $\mathcal{O}(\alpha_s)$ corrections the schemes of α_s and the mass appearing in Eq. (5.103) do not need to be specified at this point. Eq. (5.103) contains a large logarithm, which can be better seen using the rescaled soft energy variable $\tilde{\ell} = \ell/\mu_S \sim \mathcal{O}(1)$ rather than $\bar{\ell} = \ell/\mu_m$. As for the other mass mode matching coefficients this is a rapidity logarithm which enforces the counting $\alpha_s \ln(m/\ell) \sim \mathcal{O}(1)$.

We will now set up a RG evolution in rapidity space to resum the associated higher order logarithms in analogy to the mass mode threshold corrections in chapter 4. First we decompose the bare soft function in terms of the two hemisphere contributions $(+,-)$ each having rapidity divergences if the α-regulator is used. Note that the scheme difference of the strong coupling above and below threshold requires that also the one-loop corrections for the radiation of a massless gluon have to be accounted for and should be decomposed in this way. For this purpose we will again use a gluon mass $\Lambda \ll m$ as an infrared regulator which allows us to apply the results in Sec. 5.4.1. We write the two-loop contributions for virtual massive quarks as

$$\hat{S}^{(n_l+1,\text{bare},2)}_{\tau,m,\text{virt},i}(\ell,m,\Lambda,\mu,\nu) = \frac{1}{\pi}\int\frac{\mathrm{d}M^2}{M^2}\,\hat{S}^{(\text{bare},1)}_{\tau,M,\text{virt},i}(\ell,M,\mu,\nu)\,\text{Im}\left[\Pi(m^2,M^2)\right] - \left(\Pi(m^2,0) - \frac{\alpha_s^{(n_l+1)}T_F}{3\pi}\,\frac{1}{\epsilon}\right)\hat{S}^{(\text{bare},1)}_{\tau,M,\text{virt},i}(\ell,\Lambda,\mu,\nu)\,, \tag{5.104}$$

with $i=+,-$ corresponding to either of the two hemispheres where the gluon containing the virtual massive quark polarization propagates. After performing the subtracted dispersion integral and including the scheme change contribution we obtain for the individual corrections ($L_\Lambda = \ln(\Lambda^2/\mu^2)$, $L_m = \ln(m^2/\mu^2)$)

$$\begin{aligned}\mu_S\,\hat{S}^{(n_l+1,\text{bare},2)}_{\tau,m,\text{virt},+} &= \frac{\big(\alpha_s^{(n_l+1)}\big)^2 C_F T_F}{16\pi^2}\left\{\delta(\tilde\ell)\left(\frac{1}{\alpha}\left[-\frac{8}{3\epsilon^2}+\frac{40}{9\epsilon}+\frac{16}{3}L_mL_\Lambda-\frac{8}{3}L_m^2-\frac{80}{9}L_m-\frac{224}{27}+\mathcal{O}(\epsilon)\right]\right.\right.\\&\quad -\frac{8}{3\epsilon^2}\ln\left(\frac{\nu}{\mu_S}\right)+\frac{40}{9\epsilon}\ln\left(\frac{\nu}{\mu_S}\right)+\left(\frac{16}{3}L_mL_\Lambda-\frac{8}{3}L_m^2-\frac{80}{9}L_m-\frac{224}{27}\right)\ln\left(\frac{\nu}{\mu_S}\right)\bigg)\\&\quad\left.+\left[\frac{\theta(\tilde\ell)}{\tilde\ell}\right]_+\left(\frac{8}{3\epsilon^2}-\frac{40}{9\epsilon}-\frac{16}{3}L_mL_\Lambda+\frac{8}{3}L_m^2+\frac{80}{9}L_m+\frac{224}{27}\right)\right\},\end{aligned} \tag{5.105}$$

$$\begin{aligned}\mu_S\,\hat{S}^{(n_l+1,\text{bare},2)}_{\tau,m,\text{virt},-} &= \frac{\big(\alpha_s^{(n_l+1)}\big)^2 C_F T_F}{16\pi^2}\left\{\delta(\tilde\ell)\left(\frac{1}{\alpha}\left[\frac{8}{3\epsilon^2}-\frac{40}{9\epsilon}-\frac{16}{3}L_mL_\Lambda+\frac{8}{3}L_m^2+\frac{80}{9}L_m+\frac{224}{27}+\mathcal{O}(\epsilon)\right]\right.\right.\\&\quad -\frac{4}{\epsilon^3}+\frac{1}{\epsilon^2}\left[\frac{8}{3}\ln\left(\frac{\nu\,\mu_S}{\mu^2}\right)+\frac{20}{9}\right]+\frac{1}{\epsilon}\left[-\frac{40}{9}\ln\left(\frac{\nu\,\mu_S}{\mu^2}\right)+\frac{112}{27}-\frac{2\pi^2}{9}\right]\\&\quad+\left(-\frac{16}{3}L_mL_\Lambda+\frac{8}{3}L_m^2+\frac{80}{9}L_m+\frac{224}{27}\right)\ln\left(\frac{\nu\,\mu_S}{\mu^2}\right)+\frac{8}{3}L_mL_\Lambda^2-\frac{8}{9}L_m^3-\frac{40}{9}L_m^2\\&\quad-\left(\frac{448}{27}-\frac{8\pi^2}{9}\right)L_m-\frac{656}{27}+\frac{10\pi^2}{27}+\frac{56}{9}\zeta_3\bigg)\\&\quad\left.+\left[\frac{\theta(\tilde\ell)}{\tilde\ell}\right]_+\left(\frac{8}{3\epsilon^2}-\frac{40}{9\epsilon}-\frac{16}{3}L_mL_\Lambda+\frac{8}{3}L_m^2+\frac{80}{9}L_m+\frac{224}{27}\right)\right\}.\end{aligned} \tag{5.106}$$

We see that for $\mu=\mu_m$ the correction $\hat{S}^{(n_l+1,\text{bare},2)}_{\tau,m,\text{virt},+}$ is free of large logarithms for $\nu=\nu_+\sim\mu_S$, and $\hat{S}^{(n_l+1,\text{bare},2)}_{\tau,m,\text{virt},-}$ is free of large logarithms for $\nu=\nu_-\sim\mu_m^2/\mu_S$. It is then possible to set up an evolution in ν between ν_+ and ν_-. The nonvanishing two-loop counterterm contributions above threshold, where we use $\overline{\text{MS}}$-renormalization, read

$$\begin{aligned}\mu\,Z^{(n_l+1,2)}_{S_\tau,+,T_F} &= \frac{\alpha_s^{(n_l+1)}(\mu,\nu)\,\alpha_s^{(n_l+1)}(\mu)\,C_FT_F}{16\pi^2}\left\{\delta(\bar\ell)\left(\frac{1}{\alpha}\left[-\frac{8}{3\epsilon^2}+\frac{40}{9\epsilon}+\frac{16}{3}L_mL_\Lambda-\frac{8}{3}L_m^2-\frac{80}{9}L_m\right.\right.\right.\\&\quad\left.-\frac{224}{27}+\mathcal{O}(\epsilon)\right]-\frac{8}{3\epsilon^2}\ln\left(\frac{\nu}{\mu}\right)+\frac{40}{9\epsilon}\ln\left(\frac{\nu}{\mu}\right)\bigg)+\left[\frac{\theta(\bar\ell)}{\bar\ell}\right]_+\left(\frac{8}{3\epsilon^2}-\frac{40}{9\epsilon}\right)\bigg\}\,,\\ \mu\,Z^{(n_l+1,2)}_{S_\tau,-,T_F} &= \frac{\alpha_s^{(n_l+1)}(\mu,\nu)\,\alpha_s^{(n_l+1)}(\mu)\,C_FT_F}{16\pi^2}\left\{\delta(\bar\ell)\left(\frac{1}{\alpha}\left[\frac{8}{3\epsilon^2}-\frac{40}{9\epsilon}-\frac{16}{3}L_mL_\Lambda+\frac{8}{3}L_m^2+\frac{80}{9}L_m\right.\right.\right.\\&\quad\left.+\frac{224}{27}+\mathcal{O}(\epsilon)\right]-\frac{4}{\epsilon^3}+\frac{1}{\epsilon^2}\left[\frac{8}{3}\ln\left(\frac{\nu}{\mu}\right)+\frac{20}{9}\right]+\frac{1}{\epsilon}\left[-\frac{40}{9}\ln\left(\frac{\nu}{\mu}\right)+\frac{112}{27}-\frac{2\pi^2}{9}\right]\bigg)\\&\quad\left.+\left[\frac{\theta(\bar\ell)}{\bar\ell}\right]_+\left(\frac{8}{3\epsilon^2}-\frac{40}{9\epsilon}\right)\right\}.\end{aligned} \tag{5.107}$$

The sum of the individual counterterm contributions gives the complete current counterterm corresponding to Eq. (5.12),

$$Z^{(n_l+1,2)}_{S_\tau,T_F}(\ell,\mu) = Z^{(n_l+1,2)}_{S_\tau,+,T_F} + Z^{(n_l+1,2)}_{S_\tau,-,T_F}\,. \tag{5.108}$$

This yields together with the corresponding contributions at $\mathcal{O}(\alpha_s)$, for which the analogous relation holds, the correct μ-anomalous dimension for the soft function at $\mathcal{O}(\alpha_s^2 C_F T_F)$ in Eq. (5.15). The ν-anomalous dimensions for the two hemisphere contributions in the $\overline{\text{MS}}$-scheme satisfy

$$\gamma^{(n_l+1,2)}_{S_\tau,+,\nu,T_F} = -\,\nu\frac{\mathrm{d}}{\mathrm{d}\nu}\,Z^{(n_l+1,2)}_{S_\tau,+,T_F} = \frac{\big(\alpha_s^{(n_l+1)}\big)^2 C_F T_F}{16\pi^2}\left\{\frac{16}{3}L_m L_\Lambda - \frac{8}{3}L_m^2 - \frac{80}{9}L_m - \frac{224}{27}\right\}, \tag{5.109}$$

$$\gamma^{(n_l+1,2)}_{S_\tau,-,\nu,T_F} = -\,\nu\frac{\mathrm{d}}{\mathrm{d}\nu}\,Z^{(n_l+1,2)}_{S_\tau,-,T_F} = -\gamma^{(n_l+1,2)}_{S_\tau,+,\nu,T_F}\,. \tag{5.110}$$

The corresponding threshold corrections $\mathcal{M}_{S_\tau,+}$ and $\mathcal{M}_{S_\tau,-}$ in the two hemispheres can be directly obtained from Eq. (5.99) applied to each sector and satisfy the equation

$$\nu\frac{\mathrm{d}}{\mathrm{d}\nu}\,\mathcal{M}_{S_\tau,i}(\ell,m,\mu,\nu) = \Big(\gamma^{(n_l+1)}_{S_\tau,i,\nu} - \gamma^{(n_l)}_{S_\tau,i,\nu}\Big)\,\mathcal{M}_{S_\tau,i}(\ell,m,\mu,\nu) \equiv \gamma^{(n_l)}_{\mathcal{M}_{S_\tau,i}}\,\mathcal{M}_{S_\tau,i}(\ell,m,\mu,\nu)\,. \tag{5.111}$$

The difference of the anomalous dimensions can be written as

$$\begin{aligned}\gamma^{(n_l+1)}_{S_\tau,i,\nu} - \gamma^{(n_l)}_{S_\tau,i,\nu} &= \gamma^{(n_l+1,1)}_{S_\tau,i,\nu} - \gamma^{(n_l,1)}_{S_\tau,i,\nu} + \Big(\gamma^{(n_l+1,2)}_{S_\tau,i,\nu,T_F} - \gamma^{(n_l,2)}_{S_\tau,i,\nu,T_F}\Big) + \mathcal{O}(\alpha_s^3)\\ &= \gamma^{(n_l+1,2)}_{S_\tau,i,\nu,T_F} - \frac{\alpha_s^{(n_l+1)}T_F}{3\pi}\,L_m\,\gamma^{(n_l+1,1)}_{S_\tau,i,\nu} + \mathcal{O}(\alpha_s^3)\,.\end{aligned} \tag{5.112}$$

The one-loop anomalous dimensions $\gamma^{(n_l+1,1)}_{S_\tau,i,\nu}$ can be easily computed from the results in Sec. 5.4.1. Expanding Eqs. (5.60) and (5.61) and absorbing all divergences, the one-loop counterterms with the infrared regulator Λ read

$$\mu\,Z^{(n_l+1,1)}_{S_\tau,+} = \frac{\alpha_s^{(n_l+1)}(\mu,\nu)C_F}{4\pi}\left\{\delta(\bar\ell)\left[-\frac{4}{\alpha}\left(\frac{1}{\epsilon} - L_\Lambda + \mathcal{O}(\epsilon)\right) - \frac{4}{\epsilon}\ln\left(\frac{\nu}{\mu}\right)\right] + \frac{4}{\epsilon}\left[\frac{\theta(\bar\ell)}{\bar\ell}\right]_+\right\}, \tag{5.113}$$

$$\mu\,Z^{(n_l+1,1)}_{S_\tau,-} = \frac{\alpha_s^{(n_l+1)}(\mu,\nu)C_F}{4\pi}\left\{\delta(\bar\ell)\left[\frac{4}{\alpha}\left(\frac{1}{\epsilon} - L_\Lambda + \mathcal{O}(\epsilon)\right) - \frac{4}{\epsilon^2} + \frac{4}{\epsilon}\ln\left(\frac{\nu}{\mu}\right)\right] + \frac{4}{\epsilon}\left[\frac{\theta(\bar\ell)}{\bar\ell}\right]_+\right\}, \tag{5.114}$$

which yields the anomalous dimensions

$$\gamma^{(n_l+1,1)}_{S_\tau,+,\nu} = -\,\nu\frac{\mathrm{d}}{\mathrm{d}\nu}\,Z^{(n_l+1,1)}_{S_\tau,+} = \frac{\alpha_s^{(n_l+1)}C_F}{4\pi}\,4L_\Lambda = -\gamma^{(n_l+1,1)}_{S_\tau,-,\nu}\,. \tag{5.115}$$

As in the computation of the current, jet function and PDF threshold corrections in Sec. 4.4 the dependence on the infrared regulator Λ cancels in the evolution of the soft function threshold correction which has the anomalous dimension

$$\gamma_{\mathcal{M}_{S_\tau,+}} = -\,\gamma_{\mathcal{M}_{S_\tau,-}} = \frac{\alpha_s^2 C_F T_F}{16\pi^2}\left\{-\frac{8}{3}L_m^2 - \frac{80}{9}L_m - \frac{224}{27}\right\} + \mathcal{O}(\alpha_s^3)\,. \tag{5.116}$$

The solution of Eq. (5.111) is the anticipated exponentiation which allows to determine the required term at $\mathcal{O}(\alpha_s^4\ln^2(m^2/\ell^2)) \sim \mathcal{O}(\alpha_s^2)$ in the logarithmic counting $\alpha_s\ln(m^2/\ell^2) \sim 1$.

For a complete analysis at N^{3}LL we also need the term at $\mathcal{O}(\alpha_s^3\ln(m/\ell)) \sim \mathcal{O}(\alpha_s^2)$. We can determine its μ_m-dependent contribution from the identity

$$\mathcal{M}_{S_\tau}(\ell,m,\mu_m) = \int\!\mathrm{d}\ell'\int\!\mathrm{d}\ell''\,U^{(n_l)}_{S_\tau}(\ell-\ell',m,\mu_m)\,\mathcal{M}_{S_\tau}(\ell'-\ell'',m,m)\,U^{(n_l+1)}_{S_\tau}(\ell'',\mu_m,m)\,. \tag{5.117}$$

or equivalently,

$$\mu\frac{\mathrm{d}}{\mathrm{d}\mu}\,\mathcal{M}_{S_\tau}(\ell,m,\mu) = \int\!\mathrm{d}\ell'\,\Big(\gamma^{(n_l+1)}_{S_\tau}(\ell-\ell',\mu) - \gamma^{(n_l)}_{S_\tau}(\ell-\ell',\mu)\Big)\,\mathcal{M}_{S_\tau}(\ell',m,\mu)\,. \tag{5.118}$$

Expanding in α_s gives the perturbative result for the μ_m-dependent terms. Including the term at $\mathcal{O}(\alpha_s^3 \ln(\ell^2/m^2))$ in the exponent the structure of the threshold factor reads [10]

$$\begin{aligned}
\mu_S\,\mathcal{M}_S(\ell,m,\mu_m,\mu_S) = \Bigg\{&\delta(\tilde\ell) + \frac{\big(\alpha_s^{(n_l+1)}\big)^2}{(4\pi)^2}\,\Bigg(\delta(\tilde\ell)\,\bigg[-\frac{L_m^3}{12}\,\Gamma_0^S\Delta\beta_0 - \frac{L_m^2}{4}\,(\Delta\Gamma_1^S+\gamma_0^S\Delta\beta_0)\\
&- \frac{L_m}{2}\,\Big(\Delta\gamma_1^S+\mathcal{M}_2^{S_\tau,+}\Big)+\mathcal{M}_2^{S_\tau}\bigg] + \bigg[\frac{\theta(\tilde\ell)}{\tilde\ell}\bigg]_+\bigg[\frac{L_m^2}{2}\,\Gamma_0^S\Delta\beta_0 + L_m\,\Delta\Gamma_1^S + \mathcal{M}_2^{S_\tau,+}\bigg]\Bigg)\Bigg\}\\
&\times\exp\Bigg\{\frac{\big(\alpha_s^{(n_l+1)}\big)^2}{(4\pi)^2}\ln\!\bigg(\frac{\mu_S^2}{\mu_m^2}\bigg)\bigg[\frac{L_m^2}{4}\,\Gamma_0^S\Delta\beta_0 + \frac{1}{2}\,L_m\Delta\Gamma_1^S + \frac{\mathcal{M}_2^{S_\tau,+}}{2}\bigg]\\
&+\frac{\big(\alpha_s^{(n_l+1)}\big)^3}{(4\pi)^3}\ln\!\bigg(\frac{\mu_S^2}{\mu_m^2}\bigg)\bigg[-\frac{L_m^3}{6}\,\Gamma_0^S\Delta\beta_0(\beta_0+\Delta\beta_0)\\
&+\frac{L_m^2}{4}\big(-2\,\Delta\Gamma_1^S(\beta_0+\Delta\beta_0)+2\,\Gamma_1^S\Delta\beta_0+\Gamma_0^S\,\Delta\beta_1-4\,\Gamma_0^S\Delta\beta_0\gamma_0^m\big)\\
&+\frac{L_m}{2}(\Delta\Gamma_2^S-2\,\Delta\Gamma_1^S\gamma_0^m-\Gamma_0^S c_{\rm dec}-2\Delta\beta_0\mathcal{M}_2^{S_\tau,+})+\frac{\mathcal{M}_3^{S_\tau,+}}{2}\bigg]\Bigg\}\,. \qquad (5.119)
\end{aligned}$$

The terms Γ_i^S and γ_i^S denote the coefficients of the cusp and non-cusp jet function anomalous dimensions with n_l+1 flavors defined by (see appendix C to obtain explicit expressions)

$$\mu\frac{\mathrm{d}}{\mathrm{d}\mu}\,S_\tau^{(n_l+1)}(\ell,\mu) = \sum_{i\geq 0}\bigg(\frac{\alpha_s^{(n_l+1)}(\mu)}{4\pi}\bigg)^{i+1}\int\mathrm{d}\ell'\,\bigg[-\frac{2\,\Gamma_i^S}{\mu}\,\bigg[\frac{\mu\,\theta(\ell-\ell')}{\ell-\ell'}\bigg]_+ + \gamma_i^S\,\delta(\ell-\ell')\bigg]\,S_\tau^{(n_l+1)}(\ell',\mu)\,. \qquad (5.120)$$

The terms $\mathcal{M}_i^{S_\tau,+}$ and $\mathcal{M}_i^{S_\tau}$ indicate the μ_m-independent coefficients of the plus-distribution $\frac{1}{m}\Big[\frac{m\,\theta(\ell)}{\ell}\Big]_+$ and delta-distribution $\delta(\ell)$ in the matching coefficient $\mathcal{M}_S(\ell,m,m)$ (i.e. for $\mu_m=m$), respectively. Note that we have not determined the relevant constant $\mathcal{M}_3^{S_\tau,+}$ at this stage. However, the consistency relation in Eq. (5.98) implies that it is related to the rapidity logarithm enhanced constants $\mathcal{M}_3^{\tilde C,+}$ and $\mathcal{M}_3^{J_\tau,+}$ in the current and jet function threshold corrections. These are closely related to the corresponding constants in DIS which have been determined by consistency from the PDF threshold correction (see Eq. (4.237)). Thus we obtain

$$\mathcal{M}_3^{S_\tau,+} = 2\,\mathcal{M}_3^{\tilde\phi,+}\,, \qquad (5.121)$$

with $\mathcal{M}_3^{\tilde\phi,+}$ given in Eq. (4.236). The remaining constants appearing in Eq. (5.119) are defined below Eq. (4.181). Inserting the values for all of the constants and expanding Eq. (5.119) using the logarithmic counting $\alpha_s\ln(m^2/\ell^2)\sim\mathcal{O}(1)$ gives the result ($\alpha_s^{(n_l+1)}=\alpha_s^{(n_l+1)}(\mu_m)$, $m=m(\mu_m)$)

$$\begin{aligned}
\mu_S\,\mathcal{M}_{S_\tau}(\ell,m,\mu_m,\mu_S) = \delta(\tilde\ell) &+ \bigg[\frac{\big(\alpha_s^{(n_l+1)}\big)^2}{(4\pi)^2}\,\delta(\tilde\ell)\ln\bigg(\frac{\mu_S^2}{\mu_m^2}\bigg)\,\mathcal{M}^{(2)}_{S_\tau,\ln}(m,\mu_m)\bigg]_{\mathcal{O}(\alpha_s)}\\
&+\bigg[\frac{\big(\alpha_s^{(n_l+1)}\big)^2}{(4\pi)^2}\,\bigg(\delta(\tilde\ell)\,\mathcal{M}^{(2)}_{S_\tau,1}(m,\mu_m)+\bigg[\frac{\theta(\tilde\ell)}{\tilde\ell}\bigg]_+\,2\mathcal{M}^{(2)}_{S_\tau,\ln}(m,\mu_m)\bigg)\\
&+\frac{\big(\alpha_s^{(n_l+1)}\big)^3}{(4\pi)^3}\,\delta(\tilde\ell)\ln\bigg(\frac{\mu_S^2}{\mu_m^2}\bigg)\,\mathcal{M}^{(3)}_{S_\tau,\ln}(m,\mu_m)\\
&+\frac{\big(\alpha_s^{(n_l+1)}\big)^4}{(4\pi)^4}\,\delta(\tilde\ell)\ln^2\bigg(\frac{\mu_S^2}{\mu_m^2}\bigg)\,\mathcal{M}^{(4)}_{S_\tau,\ln^2}(m,\mu_m)\bigg]_{\mathcal{O}(\alpha_s^2)} + \mathcal{O}(\alpha_s^3)\,. \qquad (5.122)
\end{aligned}$$

[10] Here we set $\nu_+=\mu_S$ and $\nu_-=\mu_m^2/\mu_S$. For a phenomenological error estimate the ν-dependence can be easily restored.

We display the corresponding results for $\alpha_s^{(n_l+1)} = \alpha_s^{(n_l+1)}(\mu_m)$ and $m \equiv \overline{m}(\mu_m)$ given in the $\overline{\text{MS}}$ scheme. The functions multiplying the logarithm $\ln(\mu_S^2/\mu_m^2)$ are related to the ones entering the current mass mode matching correction (see Eqs. (4.46), (4.48) and (4.50))

$$\mathcal{M}^{(2)}_{S_\tau,\ln}(m,\mu_m) = -\,2\,\mathcal{M}^{(2)}_{C,\ln}(m,\mu_m)\,, \tag{5.123}$$

$$\mathcal{M}^{(3)}_{S_\tau,\ln}(m,\mu_m) = -\,2\,\mathcal{M}^{(3)}_{C,\ln}(m,\mu_m)\,, \tag{5.124}$$

$$\mathcal{M}^{(4)}_{S_\tau,\ln}(m,\mu_m) = 4\,\mathcal{M}^{(4)}_{C,\ln^2}(m,\mu_m)\,. \tag{5.125}$$

Finally, the two-loop function $\mathcal{M}^{(2)}_{S_\tau,1}$ which is not related to a rapidity logarithm can be easily read off from Eq. (5.103),

$$\mathcal{M}^{(2)}_{S_\tau,1}(m,\mu_m) = C_F T_F \left\{ -\frac{8}{9}L_m^3 - \frac{40}{9}L_m^2 + \left(-\frac{448}{27} + \frac{4\pi^2}{9}\right)L_m - \frac{656}{27} + \frac{10\pi^2}{27} + \frac{56}{9}\zeta_3 \right\}. \tag{5.126}$$

Continuity

In the RG setup, where the final renormalization scale is the jet scale μ_J, the difference in the factorization theorems for scenario III, given in Eq. (5.97), and for scenario IV, given by

$$\begin{aligned}\frac{1}{\sigma_0}\frac{\mathrm{d}\sigma}{\mathrm{d}\tau} = {}& Q\left|\tilde{C}^{(n_l+1)}(Q,m,\mu_H)\right|^2 \left|U_{\tilde{C}}^{(n_l+1)}(Q,\mu_H,\mu_J)\right|^2 \int \mathrm{d}s \int \mathrm{d}\ell\, J_\tau^{(n_l+1)}(s,m,\mu_J) \\ & \times U_{S_\tau}^{(n_l+1)}\left(\ell - \frac{s}{Q},\mu_J,\mu_S\right) S_\tau^{(n_l+1)}\left(Q\tau - \ell, m, \mu_S\right)\,,\end{aligned} \tag{5.127}$$

concerns just the soft function and its evolution. Thus the condition for the soft function threshold correction in Eq. (5.99) automatically implements a continuous transition between these two scenarios in the region $m \sim \mu_m \sim \mu_S \sim \ell$, which happens at $\mathcal{O}(\alpha_s^2)$ in particular if the real radiation terms $\hat{S}^{(n_f,2)}_{\tau,m,\theta}(\ell,m)$ and $\hat{S}^{(n_f,2)}_{\tau,m,\Delta}(\ell,m)$ are included scenario III and IV with $n_f = n_l$ and $n_f = n_l+1$, respectively, and contribute when kinematically allowed. From the viewpoint of the factorization theorems in the top-down evolution to the soft scale given in Eqs. (5.28) and (5.29) the continuity seems less obvious. However, since the final renormalization scale is unphysical, these two RG setups are related to each other via consistency relations. Using the structure of the current and jet threshold corrections related to Eqs. (4.165) and (4.196), and the one for the soft threshold correction in Eq. (5.102), the consistency relation at $\mathcal{O}(\alpha_s^2)$ in the fixed-order expansion has the explicit form

$$\begin{aligned}&2\,\mathrm{Re}\left[\tilde{F}^{(n_l,2)}_{m,\mathrm{QCD}}(Q,m) - \delta\tilde{C}_m^{(n_l+1,2)}(Q,m,\mu_m)\right]\delta(\tau) - Q^2 J^{(n_l+1,2)}_{\tau,m,\mathrm{virt}}(Q^2\tau,m,\mu) - Q\,\hat{S}^{(n_l+1,2)}_{\tau,m,\mathrm{virt}}(Q\tau,m,\mu) \\ &+ \frac{\alpha_s T_F}{3\pi}\,L_m \left\{2\,\mathrm{Re}\left[\tilde{C}^{(n_l+1,1)}(Q,\mu)\right]\delta(\tau) + Q^2 J_\tau^{(n_l+1,1)}(Q^2\tau,\mu) + Q\,\hat{S}_\tau^{(n_l+1,1)}(Q\tau,\mu)\right\} = 0\,.\end{aligned} \tag{5.128}$$

The massive quark corrections given by $\tilde{F}^{(n_l+1,2)}_{m,\mathrm{QCD}}(Q,m)$, $\delta\tilde{C}_m^{(n_l+1,2)}(Q,\mu)$ and $J^{(n_l+1,2)}_{\tau,m,\mathrm{virt}}(s,m,\mu)$ are in complete analogy to the ones given for DIS in Eqs. (3.95), (4.163) and (4.194) with the appropriate analytic continuation for the hard current corrections and a factor of 2 for the jet function contribution, respectively, while the correction $\hat{S}^{(n_l+1,2)}_{\tau,m,\mathrm{virt}}(\ell,m,\mu)$ has been given in Eqs. (5.71). These do not involve terms related to real radiation of heavy quarks, but only the virtual quark contributions to the SCET current, the jet function and the soft function (in the $\overline{\text{MS}}$ scheme). Finally also the one-loop terms $\tilde{C}^{(n_l+1,1)}(Q,\mu)$, $J_\tau^{(n_l+1,1)}(s,\mu)$ and $\hat{S}_\tau^{(n_l+1,1)}(\ell,\mu)$, which can be read off from the Eqs. (4.12), (4.16) and (5.9), appear due to the virtual heavy quark contributions to the strong coupling encoded in the decoupling relation of α_s between the n_l and (n_l+1)-flavor scheme. Eq. (5.128) relates the virtual quark contributions to the hard current coefficient, the jet function, the soft function and α_s to one another and is a consequence of the consistency of the mass mode setup. Moreover, Eq. (5.128) is also the analytic relation behind the fact that the transition between the factorization theorems in Eqs. (5.28) and (5.29) for the scenarios III and IV, respectively, is continuous. [11]

[11] Note that also the gap parameter in the soft model function and the renormalon subtractions to the partonic soft function change. However, they compensate each other for $\mu_m \sim \mu_S$ due to the matching relation in Eq. (5.49).

5.6 Singular fixed-order QCD result

So far we have computed the secondary massive quark corrections in the SCET factorization theorems, i.e. the singular contributions of the full QCD result at the respective scales with the corresponding resummation of large logarithmic terms. Since the nonsingular contributions might have a significant impact even for small values of τ their calculation should be also done in order to perform a full phenomenological analysis with $\mathcal{O}(\alpha_s^2)$ corrections. In contrast to DIS, where the full QCD result at $\mathcal{O}(\alpha_s^2 C_F T_F)$ has been fairly easy to calculate via dispersion relations (see Sec. 3.4.3), it is extraordinarily difficult to find an analytic solution for the full QCD contributions, since in the corresponding computation the full four-particle phase space has to be dissected. We postpone this calculation, which will be rather tackled numerically instead with the help of an event generator, to a future work. In appendix E we present the (much simpler) calculation of the massive gluon corrections at $\mathcal{O}(\alpha_s)$ in full QCD in order to display some important features and to explain the required expansions to obtain the singular terms from the full QCD result.

In this section we present the singular $\mathcal{O}(\alpha_s^2 C_F T_F)$ secondary massive quark corrections to the thrust distribution in the fixed-order expansion, which are fully contained in each of the factorization theorems discussed in the previous sections. To our knowledge these have not been made available in the literature. Besides the virtual contributions the singular fixed-order corrections consist of the singular collinear and soft real radiation contributions which arise for $\tau \sim m^2/Q^2 \ll 1$ and $\tau \sim m/Q \ll 1$, respectively, in the dijet regime. Setting $\mu = \mu_H = \mu_J = \mu_S$, using the n_l-flavor scheme for α_s and ignoring the gap subtraction we obtain

$$\frac{1}{\sigma_0}\frac{\mathrm{d}\sigma}{\mathrm{d}\tau}\bigg|_{\mathcal{O}(\alpha_s^2 C_F T_F)} = 2\,\mathrm{Re}\Big[\tilde{F}^{(n_l,2)}_{m,\mathrm{QCD}}(Q,m)\Big]\delta(\tau) + Q^2 J^{(n_l,2)}_{\tau,m,\mathrm{real}}(Q^2\tau,m) + Q\,\hat{S}^{(n_l,2)}_{\tau,m,\theta}(Q\tau,m) + Q\,\hat{S}^{(n_l,2)}_{\tau,m,\Delta}(Q\tau,m)\,. \tag{5.129}$$

Using the explicit expressions for $\hat{F}^{(n_l,2)}_{m,\mathrm{QCD}}(Q,m)$ and $J^{(n_l,2)}_{m,\mathrm{real}}(s,m)$ in Eqs. (3.95) and (4.54) properly adapted from DIS to thrust, and for $\hat{S}^{(n_l,2)}_{\tau,m,\theta}(\ell,m)$ in Eq. (5.32) we obtain

$$\begin{aligned}
\frac{1}{\sigma_0}\frac{\mathrm{d}\sigma}{\mathrm{d}\tau}\bigg|_{\mathcal{O}(\alpha_s^2 C_F T_F)} &= \bigg(\frac{\alpha_s^{(n_l)}(\mu)}{4\pi}\bigg)^2 C_F T_F \\
\times \bigg\{ \delta(\tau)\bigg[&\bigg(-r^4+2r^2+\frac{5}{3}\bigg)\bigg(4\,\mathrm{Li}_3\Big(\frac{r-1}{r+1}\Big)+\frac{1}{3}\ln^3\Big(\frac{r-1}{r+1}\Big)-\frac{2\pi^2}{3}\ln\Big(\frac{r-1}{r+1}\Big)-4\zeta_3\bigg) \\
&+\bigg(\frac{46}{9}r^3+\frac{10}{3}r\bigg)\bigg(4\,\mathrm{Li}_2\Big(\frac{r-1}{r+1}\Big)+\ln^2\Big(\frac{r-1}{r+1}\Big)-\frac{2\pi^2}{3}\bigg)+\bigg(\frac{220}{9}+\frac{400}{27}r^2\bigg)\ln\Big(\frac{1-r^2}{4}\Big) \\
&+\frac{476}{9}r^2+\frac{2426}{81}\bigg] \\
+\frac{1}{\tau}\,\theta\Big(\tau-\frac{4m^2}{Q^2}\Big)\bigg[&-\frac{64}{3}\mathrm{Li}_2\Big(\frac{b-1}{b+1}\Big)+\frac{32}{3}\ln\Big(\frac{1-b^2}{4}\Big)\ln\Big(\frac{1-b}{1+b}\Big)-\frac{16}{3}\ln^2\Big(\frac{1-b}{1+b}\Big) \\
&+\bigg(b^4-2b^2+\frac{241}{9}\bigg)\ln\Big(\frac{1-b}{1+b}\Big)-\frac{10}{27}b^3+\frac{482}{9}b-\frac{16\pi^2}{9}\bigg] \\
+\frac{1}{\tau}\,\theta\Big(\tau-\frac{2m}{Q}\Big)\bigg[&\frac{64}{3}\mathrm{Li}_2\Big(\frac{w-1}{w+1}\Big)-\frac{32}{3}\ln\Big(\frac{1-w^2}{4}\Big)\ln\Big(\frac{1-w}{1+w}\Big)+\frac{16}{3}\ln^2\Big(\frac{1-w}{1+w}\Big)-\frac{160}{9}\ln\Big(\frac{1-w}{1+w}\Big) \\
&+\frac{64}{27}w^3-\frac{320}{9}w+\frac{16\pi^2}{9}\bigg]\bigg\} + Q\,\hat{S}^{(n_l,2)}_{\tau,m,\Delta}(Q\tau,m)\,,
\end{aligned} \tag{5.130}$$

with

$$r \equiv \sqrt{1+\frac{4m^2}{Q^2}}\,,\qquad b \equiv \sqrt{1-\frac{4m^2}{Q^2\tau}}\,,\qquad w \equiv \sqrt{1-\frac{4m^2}{Q^2\tau^2}}\,, \tag{5.131}$$

and where $\hat{S}^{(n_l,2)}_{\tau,m,\Delta}(\ell, m)$ can be read off from the parametrization in Eq. (5.34).

An important difference of the SCET setup to this fixed-order QCD expansion is that in the factorization theorems the various components are calculated in different flavor number schemes to allow for the summation of logarithms involving ratios of the scales Q, $Q\lambda$, $Q\lambda^2$ and m. A maybe even more notable difference is that the consistent and IR-safe definitions of the jet and the soft functions entail that virtual corrections have non-vanishing support for finite values of τ, so that they do not only arise in coefficients of $\delta(\tau)$, but also in coefficients involving plus-distributions $(\ln^n\tau/\tau)_+$. In contrast, the fixed-order expansion contains only real radiation corrections for finite values of τ and virtual corrections proportional to $\delta(\tau)$ each of which is individually IR-regular for $m \to 0$. The rearrangement of virtual and mass-singular corrections, which is intrinsically connected to the consistency relation of Eqs. (5.98) and (5.128), is the basis of rendering the hard coefficient and the jet and the soft functions in the factorization theorems infrared-safe in the limit $m \to 0$.

5.7 Numerical analysis

In the following we investigate the numerical effects of secondary bottom and top quarks in the thrust distribution related to the mass dependent factorization theorems we have described and presented in the previous sections. The emphasis is on a comparison to the predictions where the mass of the secondary quark is neglected. Since our analysis does not include the nonsingular contributions which might be sizeable in the tail and the far-tail region, some of the conclusions concerning the tail region, e.g. concerning the scale variations, are preliminary and final conclusions are postponed to a complete phenomenological analysis which also includes the effects of primary massive quark production.

The results in our analysis are calculated at N^{3}LL order in the usual SCET counting (with top-down running), see Table 2.1. [12] The perturbative corrections to the matrix elements and matching conditions are included up to $\mathcal{O}(\alpha_s^2)$ and expanded out within the factorized expressions to avoid higher order cross terms. In our analysis we have used the form of the RG evolution factors in appendix C and also all results for the matrix elements up to $\mathcal{O}(\alpha_s^2)$ not involving massive quark corrections, which can be found e.g. in Ref. [4] and the references therein. We have further checked that the massless limit of the factorization theorem for scenario IV agrees with the N^{3}LL thrust distribution given in Ref. [4] for massless quarks up to implementation-dependent higher order corrections.

For the renormalization scales of the individual structures and the renormalon subtraction scale we use the τ-dependent profile functions for the hard, jet, soft and R scale given in Ref. [4], which contain an appropriate generic scaling and smoothly interpolate between peak, tail and far-tail regimes. Adding an additional profile for the τ-independent mass mode matching scale the profile functions have the form

$$\mu_H = e_H\, Q\,, \tag{5.132}$$

$$\mu_S(\tau) = \begin{cases} \mu_0 + \frac{b}{2t_1}\tau^2\,, & 0 \le \tau \le t_1\,, \\ b\,\tau + d\,, & t_1 \le \tau \le t_2\,, \\ \mu_H - \frac{b}{1-2t_2}(\frac{1}{2}-\tau)^2\,, & t_2 \le \tau \le \frac{1}{2}\,, \end{cases} \tag{5.133}$$

$$\mu_J(\tau) = \left(1 + e_J\Big(\frac{1}{2}-\tau\Big)^2\right)\sqrt{\mu_H\,\mu_S(\tau)}\,, \tag{5.134}$$

$$R(\tau) = \begin{cases} R_0 + \mu_1\tau + \mu_2\tau^2\,, & 0 \le \tau \le t_1\,, \\ \mu_S(\tau) & t_1 \le \tau \le \frac{1}{2}\,, \end{cases} \tag{5.135}$$

$$\mu_m = e_m\, m_b\,. \tag{5.136}$$

[12] For the currently unknown four-loop cusp anomalous dimension $\Gamma_3^{\rm cusp}$, which has only a tiny impact on the numerical results, we use the Padé approximation of Ref. [4]. The remaining missing ingredient is the massive (noncusp) R-anomalous dimension at $\mathcal{O}(\alpha_s^3)$, for which we use the massless approximation (see the discussion in Sec. 5.3.5). Compared to Ref. [12] we have included the previously unknown logarithmically enhanced coefficients $\mathcal{M}_3^{\tilde{C},+}$ and $\mathcal{M}_3^{J_\tau,+}$ in the mass mode threshold factors at $\mathcal{O}(\alpha_s^3)$ in the fixed-order counting, which result only in a tiny change at the permille-level.

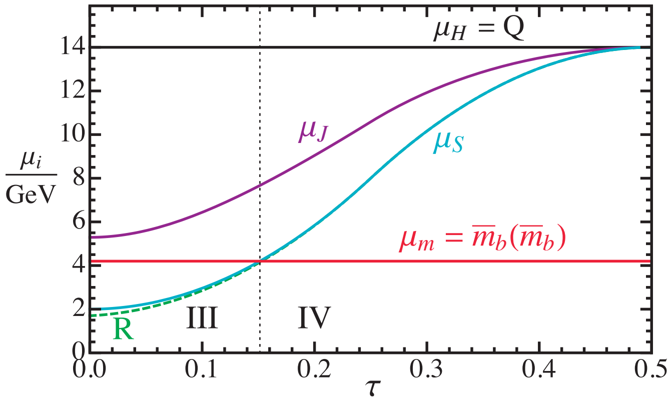

Figure 5.11: Default profiles for $Q = 14$ GeV. The transition value for τ between the scenarios III and IV is indicated by the dotted line.

As default values we use

$$e_H = e_m = 1\,,\; e_J = 0\,,\; \mu_0 = 2\,\mathrm{GeV}\,,\; R_0 = 0.85\,\mu_0\,,$$
$$t_2 = 0.25\,,\; n_1 \equiv \frac{Q\,t_1}{1\,\mathrm{GeV}} = \begin{cases} 5\,, & Q \geq \frac{5\,\mathrm{GeV}}{t_2}\,, \\ \frac{Q\,t_2}{1\,\mathrm{GeV}}\,, & Q \leq \frac{5\,\mathrm{GeV}}{t_2}\,, \end{cases} \tag{5.137}$$

and b, d, μ_1 and μ_2 are fixed by demanding smoothness of the profiles as in Ref. [4]. Compared to Ref. [4] we have modified the default value of the parameter n_1 for the case $Q \leq 5\,\mathrm{GeV}/t_2$ such that one always has $t_1 \leq t_2$, and the profiles can remain smooth for small values of Q.

We perform the convolution with the soft model function directly in momentum space since the mass dependent corrections to the jet and the soft function cannot be easily treated in Fourier space. This requires a thorough treatment of fractional plus-distributions of the form $[\ln^n(x)/x^{1+\omega}]_+$ appearing in the jet evolution factor (see Eq. (C.7)), where ω can be larger than 0. For convenience the corresponding rules are given in appendix B.2. As a model function we use

$$S_\tau^{\mathrm{mod}}(\ell) = \frac{128\,\ell^3}{3\lambda^4}\, e^{-4\ell/\lambda}\,, \tag{5.138}$$

which is properly normalized to unity. The parameter λ is a measure for the width of the function and therefore contributes as in Eq. (5.25) together with the gap parameter to the first nonperturbative moment, $\bar{\Omega}_1 = \bar{\Delta} + \lambda/2$. As a default we use the following parameters,

$$\bar{\Omega}_1^{(5)}(13\,\mathrm{GeV}, 13\,\mathrm{GeV}) = 0.5\,\mathrm{GeV}\,,\;\; \lambda = 0.65\,\mathrm{GeV}\,,$$
$$\alpha_s^{(5)}(m_Z) = 0.114\,,\;\; \overline{m}_b(\overline{m}_b) = 4.2\,\mathrm{GeV}\,,\;\; \overline{m}_t(\overline{m}_t) = 163\,\mathrm{GeV}\,. \tag{5.139}$$

We have checked that the basic characteristics of the results for the mass effects are depending rather weakly on these parameters within their known accuracy and on details of the shape of the soft model function, so our observations represent generic properties of the mass effects from secondary massive quarks.

An important aspect of the practical implementation of the VFNS concerns the prescription how the predictions within the various scenarios discussed in the previous sections are patched together to obtain the complete spectrum of the thrust distribution. As described in Sec. 5.3, one switches between neighboring scenarios when the mass scale is close to one of the kinematic scales related to the hard coefficient and the jet and the soft functions. It is therefore natural to tie the prescription for the transition to the τ-dependent profile functions for μ_m, μ_H, μ_J and μ_S. In Figs. 5.11 and 5.12 the default profile functions (including the subtraction scale R) are shown for $Q = 14$ GeV with $\mu_m = \overline{m}_b(\overline{m}_b)$ and $Q = 500$ GeV with $\mu_m = \overline{m}_t(\overline{m}_t)$, respectively. The prescription we adopt is that the transition

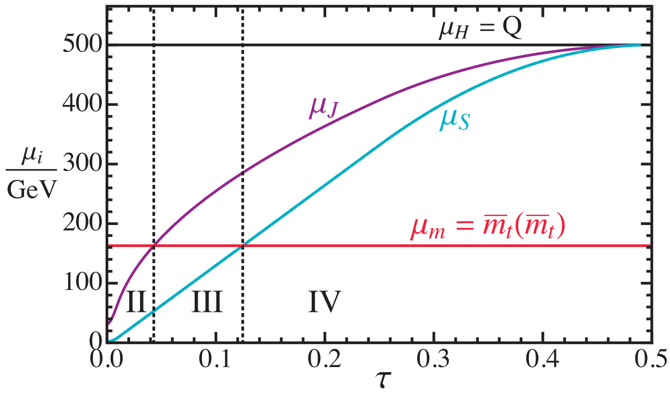

Figure 5.12: Default profiles for $Q = 500$ GeV. The transition values for τ between the scenarios II and III and between the scenarios III and IV are indicated by dotted lines.

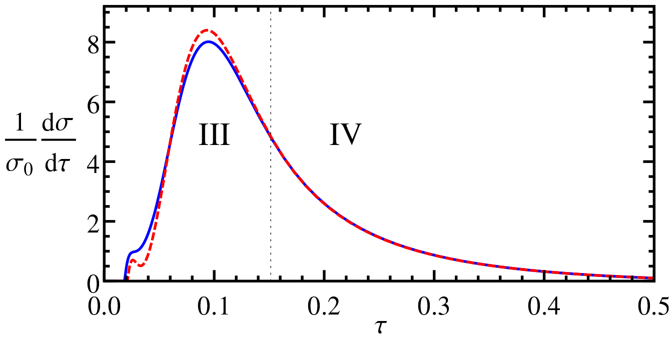

Figure 5.13: The thrust distribution at $Q = 14$ GeV including secondary massive bottom effects (blue, solid) compared to keeping the bottom quark massless (red, dashed).

concerning the scenarios II, III and IV is carried out when μ_m is equal to μ_J or μ_S, respectively. For each choice of the profile functions and the mass mode matching scale this leads to a unique value of τ for the transition. The resulting τ regions for the scenarios II, III and IV are indicated in Figs. 5.11 and 5.12 by the black dotted vertical lines. We note that the general freedom to choose the transition value for τ in some range causes variations in the predictions that are related to higher order corrections in the same way as changes of the renormalization and matching scales μ_m, μ_H, μ_J and μ_S in their respective ranges. Our prescription ties the choices made for their profile functions to the range in τ of the scenarios.

The practical implementation of the factorization theorems from the different scenarios at N^{3}LL involves a treatment of perturbative terms at higher orders that arise from cross terms of the perturbative series for the hard, jet and soft functions and the mass mode threshold factors. As mentioned above, we use the common approach to expand out the perturbative terms in the matrix elements and matching factors to $\mathcal{O}(\alpha_s^2)$, but to keep the RG evolution factors multiplying all expanded terms to the highest order. This approach has been proven advantageous to avoid spurious higher order corrections in the fixed-order expansion and to obtain reliable information on the remaining renormalization scale dependence at the corresponding order. This approach is also crucial to achieve a good numerical agreement of the factorization theorems in overlap regions where two different scenarios can be employed. In the same spirit, to avoid gaps at the transition points between neighboring scenarios related to spurious higher order terms and to obtain a continuous distribution, we also adopt as the default method an approach, where we expand in the series for the decoupling relations of the strong coupling and the gap parameter $\bar{\Delta}$ in Eqs. (3.112) and (5.49) up to $\mathcal{O}(\alpha_s^2)$.

In Fig. 5.13 the thrust distribution (for primary production of the four light quark flavors and secondary production of the light flavors and the bottom quark) normalized to the Born cross section σ_0

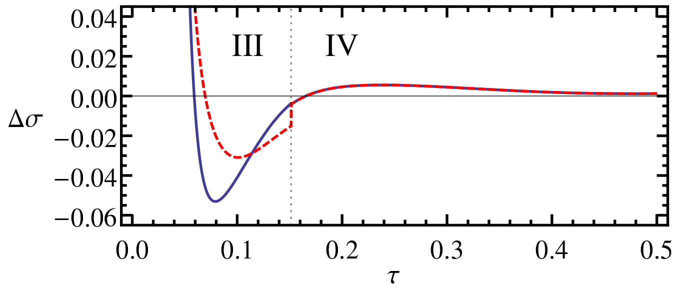

Figure 5.14: The relative deviations from the massless thrust distribution due to secondary massive bottom effects at $Q = 14$ GeV using our default fully expanded approach as described in the text (blue, solid) and the modified approach, where the decoupling relations for the gap and the strong coupling are not expanded out with the matrix elements (red, dashed).

is shown for $Q = 14$ GeV (a c.m. energy with collected data at PETRA) at N^{3}LL order, based on the factorization theorems for secondary massive bottom quarks with $\mu_m = \overline{m}_b(\overline{m}_b)$ (blue, solid line) and in the massless approximation (red, dashed line). We see that the finite bottom mass effects are significant at and below the peak, but small in the tail region. Overall the secondary quark mass effects lead to a significant decrease in the peak cross section.

Let us investigate the relative change due to the finite mass of the secondary massive bottom quarks $\Delta\sigma(m_b)$ defined by

$$\Delta\sigma(m) \equiv \frac{\frac{\mathrm{d}\sigma}{\mathrm{d}\tau}(m) - \frac{\mathrm{d}\sigma}{\mathrm{d}\tau}(m=0)}{\frac{\mathrm{d}\sigma}{\mathrm{d}\tau}(m=0)} \,. \tag{5.140}$$

Here $\frac{\mathrm{d}\sigma}{\mathrm{d}\tau}(m)$ is the complete thrust distribution at N^{3}LL for primary massless quarks and for secondary quark production which includes the proper number of light quarks and an additional flavor with mass m. In Fig. 5.14 we show $\Delta\sigma(m_b)$ for $Q = 14$ GeV using our default approach (blue, solid curve) and a modified approach where the decoupling relations for the gap parameter $\bar{\Delta}$ and the strong coupling are always taken into account up to the highest known order without expanding (red, dashed curve). We can see that $\Delta\sigma$ is up to $\sim -5\%$ ($\sim -3\%$) in the peak region in the default (modified) approach, whereas in the tail region the mass effects from secondary bottom quarks amount to relative corrections below 1%. Moreover, we can see that the default approach is continuous, [13] whereas the modified approach yields a numerically large discontinuity when the soft scale crosses the mass threshold due to the fact that the difference of the gap schemes is proportional to m at the mass scale, see Eq. (5.49). Furthermore, the variation of the mass mode matching scale μ_m turns out to be more unstable for the latter method. Therefore, we will present most of the remaining results in the default approach keeping in mind that for a phenomenological analysis a thorough investigation of the most appropriate description with the best way to assign uncertainties will have to be performed.

Interestingly at the peak the deviations are only weakly depending on the value of Q. This is illustrated in Fig. 5.15, where we display for $Q = 14$ GeV (blue, solid curve), $Q = 35$ GeV (red, dashed curve) and $Q = m_Z$ (green, dotted curve) the relative change due to the finite mass of the secondary massive bottom quarks $\Delta\sigma(m_b)$. We see that in the peak region $\Delta\sigma(m_b)$ is always up to -4%, whereas in the tail region the mass effects from secondary bottom quarks quickly decrease for larger values of Q.

It is also instructive to consider the relative mass effects at the partonic level and the changes due to the nonperturbative physics. This is shown in Fig. 5.16 for $Q = 14$ GeV, where we display $\Delta\sigma(m_b)$ for a purely partonic thrust distribution (red, dashed line), including a convolution with the soft model function $S_\tau^{\mathrm{mod}}(\ell)$ with $\Omega_1 = 0.5$ GeV without a gap (green, dotted line) and the full hadronic thrust distribution including the gap formalism with the associated renormalon subtractions (blue, solid line). We see that

[13] What appears to be a tiny gap around the scenario threshold is in fact only a change in slope in the small region $R < \mu_m < \mu_S$, where the mass threshold is crossed both in the R-evolution and in the μ-evolution from R to μ_S of the gap parameter.

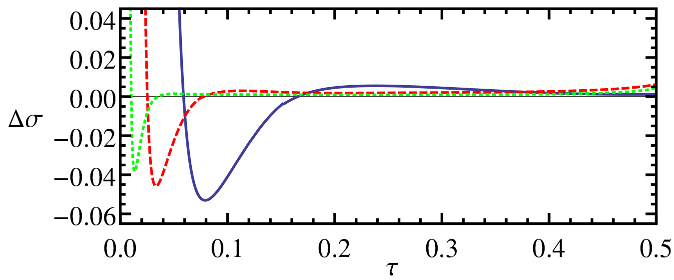

Figure 5.15: Relative secondary massive bottom effects for $Q = 14$ GeV (blue, solid), $Q = 35$ GeV (red, dashed) and $Q = m_Z$ (green, dotted).

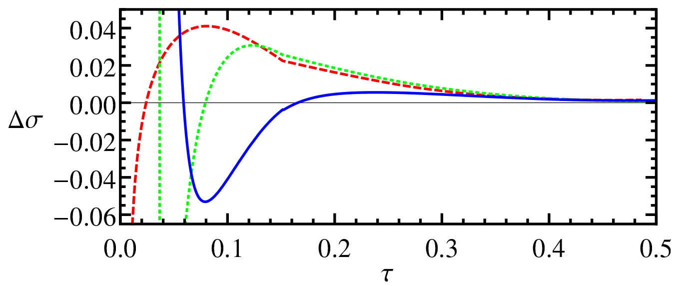

Figure 5.16: Relative secondary massive bottom effects for $Q = 14$ GeV at the partonic level (red, dashed) and including the nonperturbative soft model function $S_\tau^{\rm mod}(\ell)$ without (green, dotted) and with the incorporation of the gap formalism, which is the final default result (blue, solid).

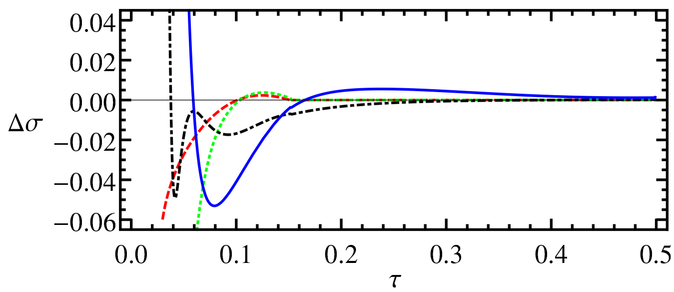

Figure 5.17: The relative deviations from the massless thrust distribution due to secondary massive bottom effects at $Q = 14$ GeV at different orders in the logarithmic counting, namely at LL (red, dashed), NLL (green, dotted), $\mathrm{N^2LL}$ (black, dashed-dotted) and $\mathrm{N^3LL}$ (blue, solid).

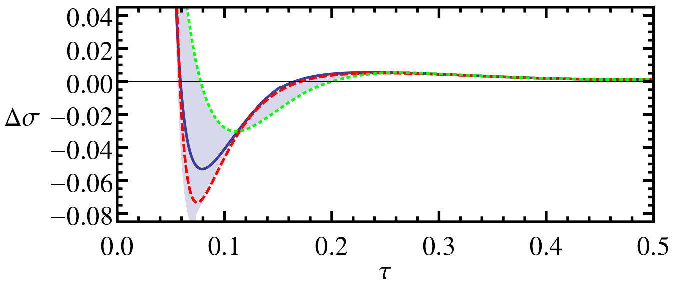

Figure 5.18: Dependence of $\Delta\sigma(m_b)$ on the mass mode matching scale μ_m for secondary bottom quarks for $Q = 14$ GeV: $\mu_m = m_b$ (blue, solid), $\mu_m = m_b/2$ (red, dashed), $\mu_m = 2m_b$ (green, dotted) with $m_b \equiv \overline{m}_b(\overline{m}_b)$. The variation in between is indicated by the shaded area.

at the partonic level the massive quark correction are significantly larger than at the nonperturbative level, reaching up to $\sim 4\%$ for $\tau \approx 0.1$. They are smeared out in the peak region by the convolution with the model which makes them smaller there. In the tail region the nonperturbative effects from $S_\tau^{\rm mod}$ enter only via the power correction Ω_1 (see Eq. 5.25) resulting in an overall shift of the distribution. Here the mass effects can be still quite significant reaching up to $2-3\%$ for $\tau \lesssim 0.2$. Finally, the inclusion of the gap formalism leads to a quite different shape of $\Delta\sigma(m_b)$. In the tail region the renormalon subtractions effectively remove the leading power corrections of $\mathcal{O}(m/Q\tau)$, which decreases $\Delta\sigma(m_b)$. The modified R-evolution has a large impact on the peak behavior.

In Fig. 5.17 we show $\Delta\sigma(m_b)$ for $Q = 14$ GeV at different orders in the logarithmic counting. At LL (red, dashed line) and NLL (green, dotted line) the massive quark effects enter only via different flavor numbers in the evolution, such that $\Delta\sigma(m_b) = 0$ in scenario IV, i.e. for $\tau \gtrsim 0.15$. At N^{2}LL (black, dashed-dotted line) $\Delta\sigma(m_b)$ changes its shape due to the appearance of the massive quark R-anomalous dimension, resulting in a nonvanishing value in scenario IV, and due to the inclusion of rapidity logarithms counting effectively as $\mathcal{O}(\alpha_s)$. Finally, at N^{3}LL (blue, solid line) for the first time mass dependent matrix elements enter corresponding to corrections at $\mathcal{O}(\alpha_s^2)$, which also alters $\Delta\sigma(m_b)$ significantly. Since at higher orders only corrections to the existing structures appear, we expect that $\Delta\sigma(m_b)$ does not change qualitatively and its uncertainties can be described by scale variations of the profile functions.

It is important to discuss the scale variations of the mass correction $\Delta\sigma$. In Fig. 5.18 the impact of the variations of μ_m is illustrated for the bottom quark case for $Q = 14$ GeV. We show the curves for $\mu_m = \overline{m}_b(\overline{m}_b)/2$ and $\mu_m = 2\,\overline{m}_b(\overline{m}_b)$ and the variation band between these two values. The μ_m dependence is quite small in the tail region and vanishes identically for $\mu_S > 2\,\overline{m}_b(\overline{m}_b)$. In the peak region, on the other hand, the variation of $\Delta\sigma(m_b)$ increases to 4% of the differential cross section and grows even further below the peak, where $\Delta\sigma$ changes sign. This behavior is generic for the bottom quark case and very similar for other values of Q. Since the finite mass of the secondary heavy quark leads to a modification of the peak behavior which represents a property of the complete thrust distribution, $\Delta\sigma$ should not be seen any more as a correction in this context. The result shows that variations of μ_m need to be accounted for when estimating perturbative uncertainties in the peak region.

In this context it is also relevant to examine the variations of $\Delta\sigma$ due to changes of the profile functions for μ_H, μ_J, μ_S as well as for R. In Fig. 5.19 $\Delta\sigma$ is shown for the bottom quark case at $Q = 14$ GeV for variations of the parameters e_H, e_J, μ_0, n_1 and t_2, see Eqs. (5.132) – (5.135), which parametrize changes of the profile functions. The ranges of variation are described in the figure caption and are identical to the ones used for the thrust analysis of Ref. [4] (except for n_1 which requires a lower range for low Q values). These variations induce visible changes in $\Delta\sigma$, but they are in general much smaller than the dependence on μ_m discussed just above. This outcome is again generic for other values of Q and also for the top quark case and shows that independent variations of the profile functions *and* of μ_m are essential for a thorough assessment of the scale variations of the complete thrust distribution including both massless and massive quark effects.

We continue our analysis by showing in Fig. 5.20 the thrust distribution for primary light quark production at $Q = 500$ GeV with $n_l = 5$ massless flavors and a secondary massive top quark (blue,

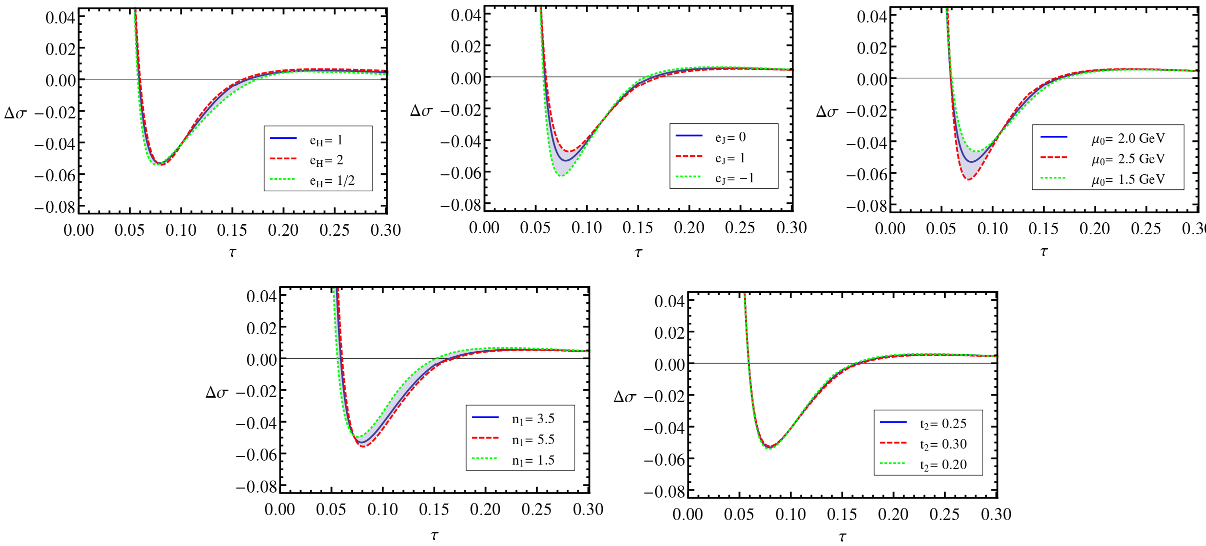

Figure 5.19: Relative secondary bottom mass effects for $Q = 14$ GeV under variation of the profile parameters for the hard, jet and soft scales.

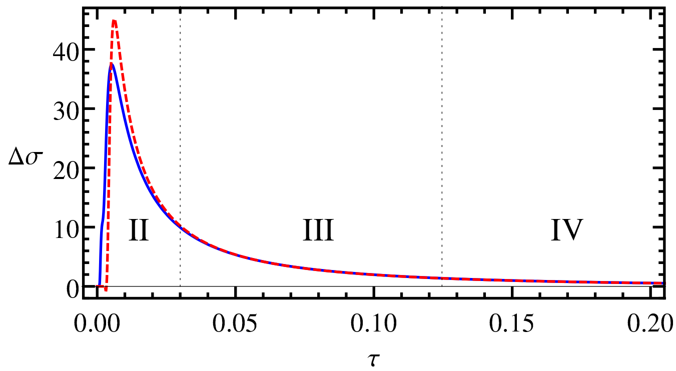

Figure 5.20: The thrust distribution at $Q = 500$ GeV including secondary massive top effects (blue, solid) compared to keeping the top quark massless (red, dashed).

solid line). The figure also shows the prediction for the case where the secondary top quark is treated as massless (red, dashed line). For all parameters the default values mentioned above are used. It is visible that the finite top quark mass causes, besides a reduction of the distribution at the peak, as we have already observed in the bottom quark case, also a shift of the peak to lower τ values. This effect is related to the top quark mass effects in the R-scale dependence of the gap parameter, which is significantly modified below the massive threshold as described in Sec. 5.3.5. In Fig. 5.21 $\Delta\sigma$ is shown for the top quark case for $Q = 500$ GeV (blue, solid line), $Q = 1000$ GeV (red, dashed line) and $Q = 3000$ GeV (green, dotted line). We find again sizable mass effects at and below the peak of the distribution even for large values of Q, where they amount to $10-20\%$. In the tail region, on the other hand, the top mass effects are relatively small. In contrast to the bottom quark case, the size of the top mass effects is much larger than the variations due changes of the mass mode matching scale μ_m which amount to $1-2\%$ in the differential cross section, see Fig. 5.22.

It is also interesting to compare the full mass dependent thrust distribution with other approximations that impose large hierarchies between the mass scale and the other involved scales except for the massless limit. We define the relative deviations between the full mass dependent result and these approximating

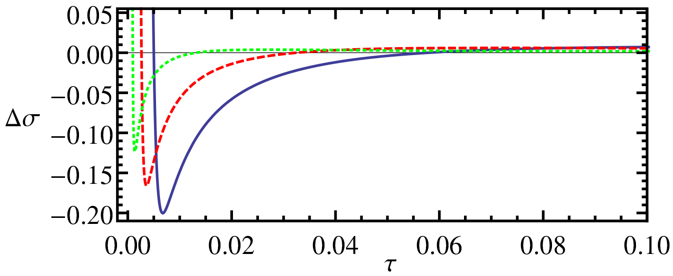

Figure 5.21: Relative secondary massive top effects for $Q = 500$ GeV (blue, solid), $Q = 1000$ GeV (red, dashed) and $Q = 3000$ GeV (green, dotted).

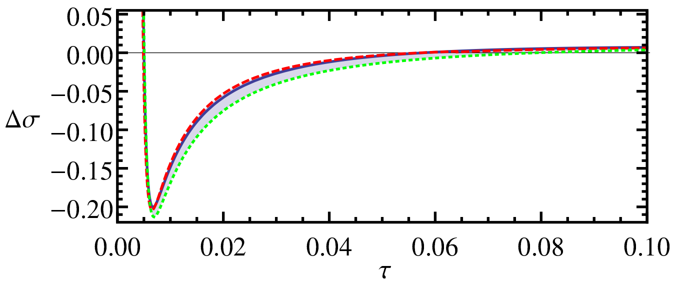

Figure 5.22: Dependence of $\Delta\sigma$ on the mass mode matching scale μ_m for secondary top quarks for $Q = 500$ GeV: $\mu_m = m_t$ (blue, solid), $\mu_m = m_t/2$ (red, dashed), $\mu_m = 2m_t$ (green, dotted).

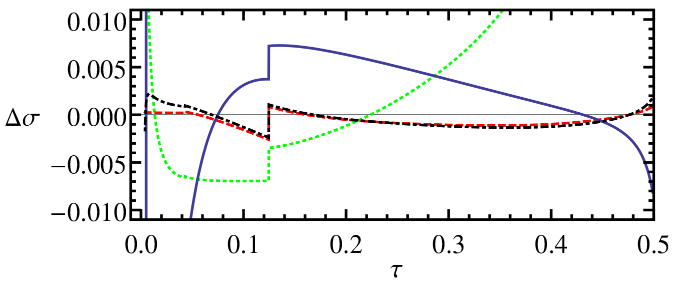

Figure 5.23: Relative deviation of the mass effects between the full mass dependent thrust distribution and four “schemes” assuming large hierarchies, i.e. the massless limit $m \ll Q\tau$ (blue, solid), the limit $Q\tau \ll m \ll Q\sqrt{\tau}$ (green, dotted), the limit $Q\sqrt{\tau} \ll m \ll Q$ (red, dashed) and the decoupling limit $Q \ll m$ (black, dashed-dotted).

"schemes" in analogy to Eq. (5.140) as

$$\Delta\sigma(m) = \frac{\frac{\mathrm{d}\sigma}{\mathrm{d}\tau}(m) - \left(\frac{\mathrm{d}\sigma}{\mathrm{d}\tau}\right)_{\text{approx}}(m)}{\left(\frac{\mathrm{d}\sigma}{\mathrm{d}\tau}\right)_{\text{approx}}(m)} \,. \tag{5.141}$$

In Fig. 5.23 we display $\Delta\sigma(m)$ at $Q = 500$ GeV for secondary massive top quarks. Besides the full massless limit $m \ll Q\lambda^2$ (blue, solid line) we display the decoupling limit $m \gg Q$ (black, dashed-dotted line), where the massive quark does not contribute at all. Furthermore, we show a zero-mass VFNS (ZM-VFNS) for scenario III assuming the hierarchy $Q\lambda^2 \ll m \ll Q\lambda$ (green, dotted line), i.e. with a hard and jet function in the massless limit and no massive quark contributions to the soft function. The only fixed-order components in the factorization theorem which contain any explicit mass dependence are the mass mode threshold corrections. Analogously we also display scenario II assuming $Q\lambda \ll m \ll Q$ (red, dashed line), i.e. with a massless hard function and no massive quark contributions to the jet and soft functions. Since we want to employ parameters both only defined in the n_l- as well as in the (n_l+1)-scheme corresponding to the decoupling and the massless limit we have employed here the more appropriate modified approach, where the decoupling relations for the gap parameter and the strong coupling are always taken into account up to their highest known order. We note that the decoupling limit, i.e. the thrust distribution with just 5 massless flavors, is at the peak much closer to the full massive prediction than the massless top approximation. This is due to the fact that the top mass is comparable to the hard scale and in the peak region significantly larger than the jet and the soft scales such that the decoupling approximation is more appropriate than the massless one. We emphasize that this statement has to be scrutinized case by case depending on the values of the involved scales and is e.g. not directly applicable in the bottom quark case for $Q = 14$ GeV, where the ratio between the mass scale and the c.m. energy is comparable to the top quark case with $Q = 500$ GeV.

At the end, let us mention that a thorough analysis of secondary mass effects in relation to experiment will face several subtleties. So far experiments have used the original definition for thrust [104], which is normalized by the sum of the modula of the momenta $\vec{p}_i$, in contrast to the definition applied here, which is normalized by the total c.m. energy (see Eq. (5.1)). Furthermore, we have considered the heavy quarks to be stable, whereas they decay in practice before reaching the detector and usually only the momenta of light hadrons are taken into account in the determination of the thrust value. In the SCET factorization setup this affects essentially the hemisphere momentum deposits in the soft function which would have to be reconsidered.

Chapter 6

Conclusions

In this work we provide for the first time a systematic factorization approach for secondary mass corrections, including effects from massive quark bubbles in the vacuum polarization function, in processes involving jets. The conceptual setup is nontrivial due to the emergence of different hierarchies between the mass scale and the involved kinematic scales for each of the field theoretical structures entering the corresponding factorization theorem. Using the language of SCET we have discussed for different examples a variable flavor number scheme (VFNS) which describes all of these hierarchies consistently. A properly defined VFNS can resum all large logarithms between the involved scales and obtain the correct limiting behavior, i.e. the decoupling limit for heavy quark masses and the massless limit for light quark masses. We find that to achieve these features a suitable choice of renormalization conditions for any component of a factorization theorem has to be imposed: On the one hand the use of the OS scheme for the massive quark corrections implies that the heavy quark does not contribute to the RG running. It is suitable, when the mass is larger than (or similar to) the relevant massless scale. On the other hand the $\overline{\text{MS}}$ scheme entails that the massive quark is active with respect to RG evolution, which can be applied if the mass of the quark is smaller than (or similar to) the relevant massless scales. The difference between these schemes contains only virtual massive quark corrections, which constitute mass threshold factors, the analogues of the matching correction of α_s regarding the matrix elements in the factorization theorem.

We have illustrated these properties on the well-known example of DIS in the classical region $1-x \sim \mathcal{O}(1)$, where a corresponding VFNS has been already developed in Ref. [1]. Apart from a more complicated analytic structure of the Wilson coefficient at the momentum transfer scale Q the massive quark affects the RG evolution of the PDF which is carried out with different flavor number above and below the quark mass scale and leads to a mass threshold correction factor when the RG evolution crosses the mass scale. Here we have explicitly calculated the full secondary massive quark contributions at $\mathcal{O}(\alpha_s^2 C_F T_F)$, which could be derived from the corresponding $\mathcal{O}(\alpha_s)$ corrections for the radiation of a "massive gluon" via dispersion relations.

In the following we have set up a VFNS for processes involving inclusive final state jets, where the number of relevant physical scales increases. We have discussed this situation in the endpoint region of DIS, $x \to 1$, where the final state invariant mass becomes small and thus a single jet emerges. Including the mass scale several possible scale hierarchies emerge and the VFNS has to deal with all of them. This is achieved by including additional modes to the theory, the collinear and soft "mass modes". The treatment of these mass modes differs for each scale hierarchy and leads to modifications of the known factorization for massless quarks. However, no assumption concerning a large hierarchy between the mass and the other scales has to be imposed and in a transition region between two neighboring hierarchical scaling scenarios both of their descriptions can be used which ensures that the transition is continuous (up to perturbative terms from beyond the order that is employed in the description). We have carried out the associated computations at $\mathcal{O}(\alpha_s)$ for the radiation of a massive gluon and at $\mathcal{O}(\alpha_s^2 C_F T_F)$ for the radiation of secondary massive quarks taking into account the resummation of so called rapidity logarithms arising from the interface between soft and collinear modes in the mass mode threshold factors. Furthermore, we have also found that the threshold corrections are not completely independent of each other, but related via consistency relations of RG running.

Finally, we have discussed also a VFNS for the thrust distribution in e^+e^- collisions in the dijet limit $\tau \to 0$. Since the field theoretic setup for the mass modes is generic and the structures at the hard and jet scale are to some extent universal the corresponding quantities in the factorization theorem can be read off easily from DIS in the endpoint region. Here only the structure describing the physics at the soft scale is different since we do not have a nonperturbative initial state and the radiation of low-energetic particles between the jets can take place at a perturbative scale, i.e. also above the mass scale. The corresponding observable dependent soft function has been calculated at $\mathcal{O}(\alpha_s^2 C_F T_F)$ including renormalon subtractions in the gap formalism. Finally, we have discussed the numerical impact of the secondary quark mass effects on the thrust distribution. These turn out to be generically small corrections in the tail region, but sizable at the peak, so that a phenomenological analysis of this region will have to take them into account. We emphasize that although the VFNS described here has been constructed for primary massless quarks, it can be applied also to the production of primary massive quarks as described in appendix F, which will lead to phenomenologically important improvements in the description of the full massive thrust distribution in a future work.

The conceptual results of this work can be applied far beyond the examples discussed here. Since the treatment of secondary massive quark or lepton effects and the incorporation of the associated threshold corrections is in several cases not complete or consistent, our results can help to clarify these issues and contribute to an improved phenomenological description of different observables in various processes. This concerns also QED processes like Bhabha scattering [123]. Certainly it will be particularly interesting to incorporate the mass mode method to physics at hadron-hadron colliders like the LHC. On the one hand one can investigate the impact of mass effects on other endpoint processes. This includes e.g. hard photon production at large transverse momentum in analogy to DIS, or event shapes in hadron colliders like beam thrust [76] applicable for Drell-Yan or Higgs production. On the other hand we can also scrutinize primary top quark production at the LHC, where questions concerning the implementation of massive top loops beyond a small or large mass approximation are still not resolved [124].

Appendix A

Longitudinal structure function

Here we summarize the results for the longitudinal structure function $F_L(x,Q^2)$ in the classical OPE region $1-x\sim\mathcal{O}(1)$, from which in combination with the results for $F_1(x,Q^2)$ in chapter 3 also the results for $F_2(x,Q^2)$ can be obtained via Eq. (3.8). We normalize the hard matching coefficients in the factorization theorem according to

$$F_L(x,Q)=\sum_{i=q}e_i^2\sum_{j,k=q,g}\int_x^1\frac{\mathrm{d}\xi}{\xi}\int_\xi^1\frac{\mathrm{d}\xi'}{\xi'}\,\mathcal{C}_{L,ij}^{(n_f)}\left(\frac{x}{\xi},Q,\mu_H\right)U_{jk}^{(n_f)}\left(\frac{\xi}{\xi'},\mu_H,\mu_\phi\right)\phi_{k/P}^{(n_f)}(\xi',\mu_\phi)\,. \tag{A.1}$$

A.1 Massless results

The tree level results for the hard matching coefficients $\mathcal{C}_{L,ij}^{(n_f)}$ with massless quarks vanish. At $\mathcal{O}(\alpha_s)$ we obtain

$$\mathcal{C}_{L,qq}^{(n_f,1)}(z)=\frac{\alpha_s^{(n_f)}C_F}{4\pi}\,\theta(z)\,\theta(1-z)\,4z\,, \tag{A.2}$$

$$\mathcal{C}_{L,qg}^{(n_f,1)}(z)=\frac{\alpha_s^{(n_f)}T_F}{4\pi}\,\theta(z)\,\theta(1-z)\,8z(1-z)\,. \tag{A.3}$$

The nonsinglet contribution for $\mathcal{C}_{L,qq}^{(n_f)}$ at $\mathcal{O}(\alpha_s^2C_FT_F)$ reads [51]

$$\mathcal{C}_{L,qq,T_F}^{(n_f,2)}(z,Q,\mu)=\frac{\left(\alpha_s^{(n_f)}\right)^2C_FT_F}{16\pi^2}\,\theta(z)\,\theta(1-z)\left\{\frac{16}{3}zL_Q-\frac{32}{3}z\ln(z)+\frac{16}{3}z\ln(1-z)+\frac{16}{3}-\frac{200}{9}z\right\}. \tag{A.4}$$

A.2 Mass effects at $\mathcal{O}(\alpha_s)$

The full QCD diagrams in Fig. (3.4) yield for the partonic tensor in the n_l scheme

$$\hat{F}_{L,Qg}^{(n_l,1)}(z,Q,m)=\frac{\alpha_s^{(n_l)}T_F}{4\pi}\,e_Q^2\,\theta(z)\,\theta\left(\frac{Q^2}{Q^2+4m^2}-z\right)\left\{8vz(1-z)-\frac{16m^2}{Q^2}z\ln\left(\frac{1+v}{1-v}\right)\right\}, \tag{A.5}$$

with v given in Eq. (3.34). Since the SCET contributions to the partonic PDF $\hat{\phi}_{Q/g}^{(n_l,1)}$ vanish in OS renormalization we obtain the matching correction

$$\mathcal{C}_{L,Qg}^{(n_l,1)}(z,Q,m)=\frac{1}{e_Q^2}\hat{F}_{L,Qg}^{(n_l,1)}(z,Q,m)\,. \tag{A.6}$$

It decouples for heavy quarks, i.e. $\mathcal{C}_{L,Qg}^{(n_l,1)}(z,Q,m)\to 0$ for $m\to\infty$. To obtain the result in the n_l+1 scheme let us first remark that the longitudinal hard matching coefficient $\mathcal{C}_{L,QQ}^{(n_l+1,0)}$ does not vanish at tree level as can be seen from a diagrammatic computation of the partonic structure function $\hat{F}^{(n_l+1,0)}_{L,QQ}$ with a massive onshell external quark. [1] We obtain

$$\mathcal{C}^{(n_l+1,0)}_{L,QQ}(z,Q,m) = \frac{4m^2}{Q^2}\,\delta(1-z)\,. \tag{A.7}$$

Together with the partonic PDF correction $\hat{\phi}^{(n_l+1,1)}_{Q/g}$ given in Eq. (3.31) this implies for the matching coefficient $\mathcal{C}^{(n_l+1,1)}_{L,Qg}$ obtained by the relation (3.35),

$$\begin{aligned}\mathcal{C}^{(n_l+1,1)}_{L,Qg}(z,Q,m,\mu) &= \frac{1}{e_Q^2}\,\hat{F}^{(n_l+1,1)}_{L,Qg}(z,Q,m) - \mathcal{C}^{(n_l+1,0)}_{L,QQ}\otimes\hat{\phi}^{(n_l+1,1)}_{Q/g}(z,Q,m,\mu)\\ &= \frac{1}{e_Q^2}\,\hat{F}^{(n_l+1,1)}_{L,Qg}(z,Q,m) + \frac{\alpha_s^{(n_l+1)}T_F}{4\pi}\,\theta(z)\,\theta(1-z)\,\frac{4m^2}{Q^2}\,\frac{P^{(1)}_{qg}(z)}{2}\,L_m\,,\end{aligned} \tag{A.8}$$

where $\hat{F}^{(n_l+1,1)}_{L,Qg}$ is defined in analogy to Eq. (3.44). This expression has the correct massless limit, [2]

$$\mathcal{C}^{(n_l+1,1)}_{L,Qg}(z,Q,m,\mu) \overset{m\to 0}{\longrightarrow} \mathcal{C}^{(n_l+1,1)}_{L,qg}(z)\,. \tag{A.9}$$

The transition between the factorization theorems for $m \gtrsim Q$ with $\mathcal{C}^{(n_l)}_{L,ij}$ and for $m \lesssim Q$ with $\mathcal{C}^{(n_l+1)}_{L,ij}$ and $\mathcal{M}_{\phi,ij}$ is continuous at $\mathcal{O}(\alpha_s)$ as can be checked by explicit computations.

The computation of the matching coefficient for a massive quark in the initial state can be carried out in analogy with the lengthy partonic structure function $\hat{F}^{(n_l+1,1)}_{L,QQ}$ which we do not display here explicitly. The matching relation reads

$$\mathcal{C}^{(n_l+1,1)}_{L,QQ}(z,Q,m,\mu) = \frac{1}{e_Q^2}\,\hat{F}^{(n_l+1,1)}_{L,QQ}(z,Q,m) - \mathcal{C}^{(n_l+1,0)}_{L,QQ}\otimes\hat{\phi}^{(n_l+1,1)}_{Q/Q}(z,Q,m,\mu)\,, \tag{A.10}$$

with $\hat{\phi}^{(n_l+1,1)}_{Q/Q}$ given in Eq. (3.49), which has the correct massless limit,

$$\mathcal{C}^{(n_l+1,1)}_{L,QQ}(z,Q,m,\mu) \overset{m\to 0}{\longrightarrow} \mathcal{C}^{(n_l+1,1)}_{L,qq}(z)\,. \tag{A.11}$$

A.3 Secondary mass effects

A.3.1 Massive gluon results at $\mathcal{O}(\alpha_s)$

We give the full QCD contributions to the matching coefficient for the longitudinal structure function $F_L(x,Q^2)$ for the radiation of a massive gluon at $\mathcal{O}(\alpha_s)$. Only the third diagram in Fig. 3.10 contributes to the computation of the partonic structure function giving rise to the real radiation contribution

$$\begin{aligned}\hat{F}^{(1)}_{L,qq}(z,Q,M) = \frac{\alpha_s C_F}{4\pi}\,e_q^2\,\theta(z)\,\theta(1-z-\hat{M}^2 z)\Bigg\{&8\hat{M}^2 z^2\ln\left(\frac{(1-\hat{M}^2 z)(1-z)}{\hat{M}^2 z^2}\right)\Big[2-3\hat{M}^2 z\Big]\\ &+\frac{4z(1-z-\hat{M}^2 z)}{(1-z)^2}\Big[1-z+\hat{M}^2(2-9z+6z^2)\Big]\Bigg\}\,.\end{aligned} \tag{A.12}$$

Due to the fact that the tree level result for $\hat{F}^{(0)}_{L,qq}$ vanishes, there are no additional subtraction terms involved in the computation of the matching coefficient via Eq. (3.35), so

$$\mathcal{C}^{(\mathrm{OS},1)}_{L,qq}(z,Q,M) = \mathcal{C}^{(\overline{\mathrm{MS}},1)}_{L,qq}(z,Q,M) = \frac{1}{e_q^2}\,\hat{F}^{(1)}_{L,qq}(z,Q,M)\,, \tag{A.13}$$

which has both the correct decoupling limit for large masses, i.e. $\mathcal{C}^{(\mathrm{OS},1)}_{L,qq}(z,Q,M)\to 0$ for $\hat{M}\to\infty$, and the correct massless limit given in Eq. (A.2), i.e. $\mathcal{C}^{(\overline{\mathrm{MS}},1)}_{L,qq}(z,Q,M)\to\mathcal{C}^{(1)}_{L,qq}(z)$ for $\hat{M}\to 0$.

[1]Note that there is in principle an ambiguity of $\mathcal{O}(m^2/Q^2)$ how to split up fixed-order corrections in the matching coefficients of the VFNS which cannot be resolved by SCET at leading order.

[2]Note that already the first term in Eq. (A.8) has the correct massless limit.

A.3.2 Secondary massive quark effects at $\mathcal{O}(\alpha_s^2 C_F T_F)$

The corresponding corrections due to secondary massive quarks can be easily obtained from the previous results by using the dispersion relation (3.62). We obtain for the partonic structure function in full QCD and the hard matching coefficient in the OS scheme

$$\begin{aligned}\hat{F}^{(n_l,2)}_{L,qq,T_F}(z,Q,m) &= e_q^2\, \mathcal{C}^{(n_l,2)}_{L,qq,T_F}(z,Q,m)\\ &= e_q^2\, \theta(z)\,\theta(1-z-4\hat{m}^2 z)\, \frac{\big(\alpha_s^{(n_l)}\big)^2 C_F T_F}{16\pi^2}\, f^{(2)}_{L,\mathrm{QCD},\theta}(z,\hat{m})\,, \end{aligned} \tag{A.14}$$

with the function ($r_z = \sqrt{1-4\hat{m}^2 z}$, $w_z = \sqrt{1-\frac{4\hat{m}^2 z}{1-z}}$)

$$\begin{aligned} f^{(2)}_{L,\mathrm{QCD},\theta}(z,\hat{m}) = {}& 192\,\hat{m}^4 z^3 \bigg[\mathrm{Li}_2\left(\frac{r_z-w_z}{r_z+1}\right) + \mathrm{Li}_2\left(\frac{r_z+w_z}{r_z-1}\right) - \mathrm{Li}_2\left(\frac{r_z-w_z}{r_z-1}\right) - \mathrm{Li}_2\left(\frac{r_z+w_z}{r_z+1}\right)\\ &+ \ln\left(\frac{1+r_z}{1-r_z}\right)\ln\left(\frac{r_z+w_z}{r_z-w_z}\right)\bigg] + \frac{16z}{3r_z}\left[1-26\,\hat{m}^2 z+88\,\hat{m}^4 z^2\right]\ln\left(\frac{r_z+w_z}{r_z-w_z}\right)\\ &+ \frac{32\,\hat{m}^4 z^2}{(1-z)^2}\left[2-9z+6z^2\right]\ln\left(\frac{1+w_z}{1-w_z}\right)\\ &+ \frac{8w_z}{9(1-z)}\left[6-31z+25z^2-\hat{m}^2 z(60-478z+372z^2)\right]. \end{aligned} \tag{A.15}$$

$\mathcal{C}^{(n_l,2)}_{L,qq,T_F}$ decouples for $\hat{m}^2 > (1-z)/(4z)$. In the massless limit one obtains the mass divergent expression

$$\begin{aligned} \mathcal{C}^{(n_l,2)}_{qq,T_F}(z,Q,m) \overset{\hat{m}\to 0}{\longrightarrow} {}& \frac{\big(\alpha_s^{(n_l)}\big)^2 C_F T_F}{16\pi^2}\,\theta(z)\,\theta(1-z)\bigg\{-\frac{16}{3}z\ln(\hat{m}^2) - \frac{32}{3}z\ln(z) + \frac{16}{3}z\ln(1-z)\\ &+ \frac{16}{3} - \frac{200}{9}z\bigg\}\,. \end{aligned} \tag{A.16}$$

Due to the fact that the tree level result for the longitudinal matching coefficient vanishes for massless quarks, i.e. $\mathcal{C}^{(0)}_{L,qq} = 0$, there are no pure SCET subtraction terms involved, but we get an additional term corresponding to the scheme change from the n_l- to the (n_l+1)-flavor scheme,

$$\begin{aligned} \mathcal{C}^{(n_l\to n_l+1,2)}_{L,qq}(z,m,\mu) &= -\left(\Pi(m^2,0) - \frac{\alpha_s T_F}{3\pi}\,\frac{1}{\epsilon}\right)\mathcal{C}^{(1)}_{L,qq}(z)\\ &= \frac{\alpha_s^2 C_F T_F}{16\pi^2}\,\theta(z)\,\theta(1-z)\,\frac{16}{3}z\,L_m\,. \end{aligned} \tag{A.17}$$

The matching coefficient in the (n_l+1)-scheme reads ($\alpha_s = \alpha_s^{(n_l+1)}(\mu)$)

$$\mathcal{C}^{(n_l+1,2)}_{L,qq,T_F}(z,Q,m,\mu) = \mathcal{C}^{(n_l,2)}_{L,qq,T_F}(z,Q,m) + \mathcal{C}^{(n_l\to n_l+1,2)}_{L,qq}(z,m,\mu)\,, \tag{A.18}$$

which has the correct massless limit, i.e.

$$\mathcal{C}^{(n_l+1,2)}_{L,qq,T_F}(z,Q,m,\mu) \overset{\hat{m}\to 0}{\longrightarrow} \mathcal{C}^{(n_l+1,2)}_{L,qq,T_F}(z,Q,\mu)\,, \tag{A.19}$$

with $\mathcal{C}^{(n_f,2)}_{L,qq,T_F}(z,Q,\mu)$ given in Eq. (A.4).

Appendix B

Identities for distributions

Here we summarize some helpful identities concerning plus-distributions which were frequently used throughout the thesis. We refer to Ref. [9] for a more extensive discussion.

B.1 Integer plus-distributions

We define the integer plus-distributions by the relation

$$\left[\frac{\theta(x)\ln^n(x)}{x}\right]_+ = \lim_{\epsilon\to 0}\left[\frac{\theta(x-\epsilon)\ln^n(x)}{x}\right] - \delta(x-\epsilon)\,\frac{\ln^{n+1}(\epsilon)}{n+1}\,, \tag{B.1}$$

which is equivalent to the integral prescription

$$\int_0^X \mathrm{d}x \left[\frac{\theta(x)\ln^n(x)}{x}\right]_+ f(x) = \int_0^X \mathrm{d}x\,\frac{\ln^n(x)}{x}\,[f(x)-f(0)] + f(0)\,\frac{\ln^{n+1}(X)}{n+1}\,. \tag{B.2}$$

In the thesis we apply several times the following rescaling identity to go from a variable with the parametric scaling $x \gg 1$ to a natural scaling by redefining $x = \kappa\tilde{x}$ with $\tilde{x}\sim 1$,

$$\left[\frac{\theta(x)\ln^n(x)}{x}\right]_+ = \frac{1}{\kappa}\,\frac{\ln^{n+1}(\kappa)}{n+1}\,\delta(\tilde{x}) + \frac{1}{\kappa}\sum_{k=0}^{n}\binom{n}{k}\ln^{n-k}(\kappa)\left[\frac{\theta(x)\ln^k(\tilde{x})}{\tilde{x}}\right]_+\,. \tag{B.3}$$

Plus-distributions are frequently obtained by the expansion of the function $\theta(x)/x^{1+\epsilon}$ (e.g. arising in dimensional regularization) for $\epsilon\to 0$,

$$\frac{\theta(x)}{x^{1+\epsilon}} \stackrel{\epsilon\to 0}{\longrightarrow} -\frac{1}{\epsilon}\,\delta(x) + \sum_{k=0}^{\infty}(-1)^k\,\frac{\epsilon^k}{k!}\left[\frac{\theta(x)\ln^k(x)}{x}\right]_+\,. \tag{B.4}$$

To perform convolutions between distributions it is convenient to have the corresponding Fourier transforms at hand. They can be easily derived from Eq. (B.4) by performing the transformation on both sides separately and comparing the results at each order in ϵ. We obtain for the first few distributive terms [115]

$$\int \mathrm{d}x\, e^{-ixy}\,\delta(x) = 1\,, \tag{B.5}$$

$$\int \mathrm{d}x\, e^{-ixy}\left[\frac{\theta(x)}{x}\right]_+ = -\ln\left(iye^{\gamma_E}\right)\,, \tag{B.6}$$

$$\int \mathrm{d}x\, e^{-ixy}\left[\frac{\theta(x)\ln(x)}{x}\right]_+ = \frac{1}{2}\ln^2\left(iye^{\gamma_E}\right) + \frac{\pi^2}{12}\,, \tag{B.7}$$

$$\int \mathrm{d}x\, e^{-ixy}\left[\frac{\theta(x)\ln^2(x)}{x}\right]_+ = -\frac{1}{3}\ln^3\left(iye^{\gamma_E}\right) - \frac{\pi^2}{6}\ln\left(iye^{\gamma_E}\right) - \frac{2}{3}\zeta_3\,. \tag{B.8}$$

The back-transform can be easily derived in the same way. For Feynman diagrams, which are performed by taking an imaginary part at the end corresponding to a real radiation cut, like in the computations of the hard matching coefficient in DIS in chapter 3 or the jet function in chapter 4 and appendix F, also the following identities are helpful,

$$\frac{1}{\pi}\,\mathrm{Im}\left[\frac{1}{x+i\epsilon}\right] = -\delta(x)\,, \tag{B.9}$$

$$\frac{1}{\pi}\,\mathrm{Im}\left[\frac{1}{(x+i\epsilon)^2}\right] = \delta'(x)\,, \tag{B.10}$$

$$\frac{1}{\pi}\,\mathrm{Im}\left[\frac{\ln(-x-i\epsilon)}{x+i\epsilon}\right] = -\left[\frac{\theta(x)}{x}\right]_+\,, \tag{B.11}$$

$$\frac{1}{\pi}\,\mathrm{Im}\left[\frac{\ln^2(-x-i\epsilon)}{x+i\epsilon}\right] = \frac{\pi^2}{3}\,\delta(x) - 2\left[\frac{\theta(x)\ln(x)}{x}\right]_+\,. \tag{B.12}$$

B.2 Noninteger plus-distributions

We give the definition and integral prescription for the plus-distributions appearing in the nonlocal evolution factors, denoted by $[\ln^n(x)/x^{1+\omega}]_+$, for arbitrary (non-vanishing) ω. The prescription of these plus-distributions is based on an analytic continuation to a domain with a well-behaved convergence [9]

$$\left[\frac{\theta(x)\ln^n(x)}{x^{1+\omega}}\right]_+ \xrightarrow{\omega<0} \frac{\theta(x)\ln^n(x)}{x^{1+\omega}}\,, \tag{B.13}$$

which gives the definition

$$\left[\frac{\theta(x)\ln^n(x)}{x^{1+\omega}}\right]_+ = \lim_{\epsilon\to 0}\left[\frac{\theta(x-\epsilon)\ln^n(x)}{x^{1+\omega}} - \delta(x-\epsilon)\frac{n!}{\omega^{n+1}}\,\epsilon^{-\omega}\sum_{l=0}^{n}\frac{\omega^l\ln^l(\epsilon)}{l!}\right]. \tag{B.14}$$

This expression can be rewritten as an integral prescription

$$\begin{aligned}\int_0^X \mathrm{d}x\left[\frac{\theta(x)\ln^n(x)}{x^{1+\omega}}\right]_+ f(x) &= \int_0^X \mathrm{d}x\,\frac{\ln^n(x)}{x^{1+\omega}}\left[f(x) - \sum_{k=0}^{\infty} f^{(k)}(0)\frac{x^k}{k!}\right]\\ &\quad - \sum_{k=0}^{\infty} f^{(k)}(0)\frac{1}{k!}\,\frac{\Gamma(n+1,(\omega-k)\ln(X))}{(\omega-k)^{n+1}}\,,\end{aligned} \tag{B.15}$$

where the sums can be truncated for $k = N$ if $\omega < N$. Eq. (B.15) allows for numerically stable convolutions with noninteger plus-distributions for arbitrary ω and has been used in the numerical analysis in Sec. 5.7. We note that the noninteger plus-distributions defined here are of a different type than the integer ones defined in appendix B.1, in particular we obtain for $\omega = 0$ different subtraction terms.

Finally, we conclude with an useful identity concerning the Fourier transformation of noninteger plus-distributions,

$$\begin{aligned}\int\frac{\mathrm{d}y}{2\pi}\,e^{ixy}\,(iy)^\omega\ln^n(iy) &= \frac{\partial^n}{\partial\omega^n}\left[\int\frac{\mathrm{d}y}{2\pi}\,e^{ixy}\,(iy)^\omega\right]\\ &= \frac{\partial^n}{\partial\omega^n}\left[\frac{1}{\Gamma(-\omega)}\,\left[\frac{\theta(x)}{x^{1+\omega}}\right]_+\right]\\ &= \sum_{k=0}^{n}\binom{n}{k}(-1)^k\left[\frac{\theta(x)\ln^k(x)}{x^{1+\omega}}\right]_+\frac{\partial^{n-k}}{\partial\omega^{n-k}}\,\frac{1}{\Gamma(-\omega)}\,.\end{aligned} \tag{B.16}$$

This formula can be applied when performing the back transformation of an evolution factor (e.g. of the jet or soft functions) in position space of the form (C.6) multiplying some logarithmic terms arising from distributions in matrix elements into momentum space.

Appendix C

Evolution factors and anomalous dimensions

Here we display the solutions of the RG equations for DIS in the endpoint $x \to 1$ and event shapes for $\tau \to 0$, see Eqs. (4.22) – (4.24) and Eq. (5.13), and give also explicit expressions for the anomalous dimensions. We refer to Refs. [4, 9] for further details and explicit derivations.

C.1 Current evolution factor

First we discuss the form of the local evolution factor $U_{C_Q}(Q, \mu_H, \mu)$ of the hard current coefficient, which reads [22]

$$U_C(Q, \mu_0, \mu) = e^{K(\Gamma_C, \mu, \mu_0) + \frac{1}{2}\omega(\gamma_C, \mu, \mu_0)} \left(\frac{\mu_0}{Q}\right)^{\omega(\Gamma_C, \mu, \mu_0)} . \tag{C.1}$$

The functions ω and K read for N^{3}LL resummation

$$\begin{aligned}
\omega(\Gamma, \mu, \mu_0) =& 2\int_{\alpha_s(\mu_0)}^{\alpha_s(\mu)} \frac{\mathrm{d}\alpha}{\beta(\alpha)}\,\Gamma(\alpha) \\
=& -\frac{\Gamma_0}{\beta_0}\bigg\{\ln r + \frac{\alpha_s(\mu_0)}{4\pi}\left(\frac{\Gamma_1}{\Gamma_0} - \frac{\beta_1}{\beta_0}\right)(r-1) + \frac{\alpha_s^2(\mu_0)}{(4\pi)^2}\left(\frac{\Gamma_2}{\Gamma_0} - \frac{\Gamma_1\beta_1}{\Gamma_0\beta_0} - \frac{\beta_2}{\beta_0} + \frac{\beta_1^2}{\beta_0^2}\right)\frac{(r^2-1)}{2} \\
&+ \frac{\alpha_s^3(\mu_0)}{(4\pi)^3}\left[\frac{\Gamma_3}{\Gamma_0} - \frac{\Gamma_2\beta_1}{\Gamma_0\beta_0} - \frac{\Gamma_1}{\Gamma_0}\left(\frac{\beta_2}{\beta_0} - \frac{\beta_1^2}{\beta_0^2}\right) - \frac{\beta_3}{\beta_0} + \frac{2\beta_2\beta_1}{\beta_0^2} - \frac{\beta_1^3}{\beta_0^3}\right]\frac{r^3-1}{3}\bigg\} ,
\end{aligned} \tag{C.2}$$

and

$$\begin{aligned}
K(\Gamma, \mu, \mu_0) =& 2\int_{\alpha_s(\mu_0)}^{\alpha_s(\mu)} \frac{\mathrm{d}\alpha}{\beta(\alpha)}\,\Gamma(\alpha)\int_{\alpha_s(\mu_0)}^{\alpha} \frac{\mathrm{d}\alpha'}{\beta(\alpha')} \\
=& -\frac{\Gamma_0}{2\beta_0^2}\bigg\{\frac{4\pi}{\alpha_s(\mu_0)}\left(1 - \frac{1}{r} - \ln r\right) - \left(\frac{\Gamma_1}{\Gamma_0} - \frac{\beta_1}{\beta_0}\right)(r - 1 - \ln r) + \frac{\beta_1}{2\beta_0}\ln^2 r \\
&+ \frac{\alpha_s(\mu_0)}{4\pi}\bigg[\left(\frac{\Gamma_1\beta_1}{\Gamma_0\beta_0} - \frac{\beta_2}{\beta_0} + \left(\frac{\Gamma_1\beta_1}{\Gamma_0\beta_0} - \frac{\beta_1^2}{\beta_0^2}\right)(r-1)\right)\ln r + \left(\frac{\Gamma_2}{\Gamma_0} - \frac{2\Gamma_1\beta_1}{\Gamma_0\beta_0} + \frac{\beta_1^2}{\beta_0^2}\right)(r-1) \\
&- \left(\frac{\Gamma_2}{\Gamma_0} - \frac{\Gamma_1\beta_1}{\Gamma_0\beta_0} - \frac{\beta_2}{\beta_0} + \frac{\beta_1^2}{\beta_0^2}\right)\frac{(r^2-1)}{2}\bigg] \\
&+ \frac{\alpha_s^2(\mu_0)}{(4\pi)^2}\bigg[\frac{\Gamma_2\beta_1}{2\Gamma_0\beta_0} - \frac{\Gamma_1\beta_1^2}{\Gamma_0\beta_0^2} - \left(\frac{\beta_3}{2\beta_0} + \frac{\beta_1\beta_2}{2\beta_0^2} + \left(\frac{\Gamma_2\beta_1}{\Gamma_0\beta_0} - \frac{\Gamma_1\beta_1^2}{\Gamma_0\beta_0^2} - \frac{\beta_1\beta_2}{\beta_0^2} + \frac{\beta_1^3}{\beta_0^3}\right)\frac{(r^2-1)}{2}\right)\ln r \\
&- \left(\frac{\Gamma_1}{\Gamma_0}\left(\frac{\beta_2}{\beta_0} - \frac{\beta_1^2}{\beta_0^2}\right) - \frac{\beta_1\beta_2}{\beta_0^2} + \frac{\beta_1^3}{\beta_0^3}\right)(r-1) + \left(\frac{\Gamma_3}{\Gamma_0} - \frac{3\Gamma_2\beta_1}{2\Gamma_0\beta_0} + \frac{\Gamma_1\beta_1^2}{2\Gamma_0\beta_0^2} - \frac{\beta_3}{2\beta_0} + \frac{\beta_1\beta_2}{2\beta_0^2}\right)\frac{(r^2-1)}{2} \\
&- \left(\frac{\Gamma_3}{\Gamma_0} - \frac{\Gamma_2\beta_1}{\Gamma_0\beta_0} - \frac{\Gamma_1}{\Gamma_0}\left(\frac{\beta_2}{\beta_0} - \frac{\beta_1^2}{\beta_0^2}\right) - \frac{\beta_3}{\beta_0} + \frac{2\beta_1\beta_2}{\beta_0^2} - \frac{\beta_1^3}{\beta_0^3}\right)\frac{(r^3-1)}{3}\bigg]\bigg\} .
\end{aligned} \tag{C.3}$$

Here $r = \alpha_s(\mu)/\alpha_s(\mu_0)$ (with 4-loop running) and the expansions of Γ_C and β in terms of $\Gamma_{C,i}$ and β_i are given in Eqs. (4.182) and (4.184), respectively.

C.2 Evolution factors for the jet and soft functions

We consider generic nonlocal RG equations of the type

$$\mu\frac{\mathrm{d}}{\mathrm{d}\mu}\,U_F(t,\mu,\mu_F) = \int \mathrm{d}t'\,\gamma_F(t-t',\mu)\,U_F(t',\mu,\mu_F)\,, \tag{C.4}$$

where the convolution variable t has the mass-dimension j (i.e. $j=2$ for the jet function and $j=1$ for event shape soft functions) and $\gamma_F(t,\mu)$ involves a plus- and a δ-distribution,

$$\gamma_F(t,\mu) = -\frac{2\,\Gamma_F[\alpha_s]}{j\,\mu^j}\left[\frac{\mu^j\,\theta(t-t')}{t-t'}\right] + \gamma_F[\alpha_s]\,\delta(t-t')\,. \tag{C.5}$$

The RGE becomes multiplicative in Fourier space involving a single logarithm and a constant (see Eqs. (B.5) and (B.6)), and can be thus treated along the lines of the current evolution. The solution reads [9]

$$U_F(t,\mu,\mu_0) = e^{K(\Gamma_F,\mu,\mu_0)+\frac{1}{2}\omega(\gamma_F,\,\mu,\mu_0)}\left(iy\,\mu_0^j\,e^{\gamma_E}\right)^{\frac{1}{j}\omega(\Gamma_F,\,\mu,\mu_0)}\,. \tag{C.6}$$

Transforming this expression to momentum space gives ($\bar{t}=t/\mu_0^j$)

$$\mu_0^j\,U_F(t,\mu,\mu_0) = e^{K(\Gamma_F,\mu,\mu_0)+\frac{1}{2}\omega(\gamma_F,\,\mu,\mu_0)}\,\frac{e^{\frac{1}{j}\gamma_E\omega(\Gamma_F,\mu,\mu_0)}}{\Gamma\Big[-\frac{1}{j}\,\omega(\Gamma_F,\mu,\mu_0)\Big]}\left[\frac{\theta(\bar{t})}{\bar{t}^{\,1+\frac{1}{j}\omega(\Gamma_F,\mu,\mu_0)}}\right]_+\,, \tag{C.7}$$

where the prescription for the noninteger plus-distribution has been given in Sec. B.

C.3 PDF evolution factor for $x \to 1$

The evolution factor for the PDF in the endpoint regime can be easily derived along the lines of the previous section. In fact it has an even simpler structure due to the fact that the only μ-dependence in the anomalous dimension is encoded in the strong coupling (see e.g. Eqs. (4.32) and (4.33)) leading to the fact that the function $K(\Gamma_{\tilde{\phi}},\mu,\mu_0)$ does not appear. The solution reads in terms of the cusp and noncusp anomalous dimensions defined in Eq. (4.235)

$$U_{\tilde{\phi}}(1-z,\mu,\mu_0) = e^{\frac{1}{2}\omega(\gamma_{\tilde{\phi}},\,\mu,\mu_0)}\,\frac{e^{\gamma_E\omega(\Gamma_{\tilde{\phi}},\mu,\mu_0)}}{\Gamma\big[-\omega(\Gamma_{\tilde{\phi}},\mu,\mu_0)\big]}\left[\frac{\theta(1-z)}{(1-z)^{\,1+\omega(\Gamma_{\tilde{\phi}},\mu,\mu_0)}}\right]_+\,. \tag{C.8}$$

As discussed in Sec. (4.1) the PDF evolution factor is flavor diagonal in the endpoint region.

C.4 Coefficients of the β-function

The coefficients of the β-function as defined in Eq. (4.184) are given by [125]

$$\beta_0 = \frac{11}{3}C_A - \frac{4}{3}T_F n_f\,, \tag{C.9}$$

$$\beta_1 = \frac{34}{3}C_A^2 - \left(\frac{20}{3}C_A + 4C_F\right)T_F n_f\,, \tag{C.10}$$

$$\beta_2 = \frac{2857}{54}C_A^3 - \left(\frac{1415}{27}C_A^2 + \frac{205}{9}C_F C_A - 2C_F^2\right)T_F n_f + \left(\frac{158}{27}C_A + \frac{44}{9}C_F\right)T_F^2 n_f^2\,, \tag{C.11}$$

$$\beta_3 = \frac{149753}{6} + 3564\zeta_3 - \left(\frac{1078361}{162} + \frac{6508}{27}\zeta_3\right)n_f + \left(\frac{50065}{162} + \frac{6472}{81}\zeta_3\right)n_f^2 + \frac{1093}{729}n_f^3\,, \tag{C.12}$$

where the value for β_3 is specifically for SU(3).

C.5 Anomalous dimensions of the matrix elements

We display the explicit expressions for the anomalous dimensions of the components of the factorization theorems for DIS in the endpoint region and thrust for $\tau \to 0$. The cusp anomalous dimensions of the hard current coefficient, the hemisphere jet function, the PDF and the thrust soft function appearing in Eqs. (4.182), (4.213), (4.213), (4.235) and (5.120), respectively, are related to each other via

$$\Gamma_i^C = -\frac{\Gamma_i^J}{2} = \Gamma_i^{\tilde\phi} = \frac{\Gamma_i^S}{2} = -\Gamma_i^{\rm cusp}\,, \tag{C.13}$$

where $\Gamma_{\rm cusp} = \sum_{i\ge 0} \alpha_s^{i+1}/(4\pi)^{i+1}\,\Gamma_i^{\rm cusp}$ with the first few coefficients given by [55]

$$\begin{aligned}
\Gamma_0^{\rm cusp} =& 4C_F\,, && \text{(C.14)}\\
\Gamma_1^{\rm cusp} =& C_F C_A\left(\frac{268}{9} - \frac{4\pi^2}{3}\right) - \frac{80}{9}C_F T_F n_f\,, && \text{(C.15)}\\
\Gamma_2^{\rm cusp} =& C_A^2 C_F\left(\frac{490}{3} - \frac{536\pi^2}{27} + \frac{88}{3}\zeta_3 + \frac{44\pi^4}{45}\right) + \left[C_A C_F\left(-\frac{1672}{27} + \frac{160\pi^2}{27} - \frac{224}{27}\zeta_3\right)\right.\\
&\left. + C_F^2\left(-\frac{220}{3} + 64\zeta_3\right)\right] T_F n_f - \frac{64}{27}C_F T_F^2 n_f^2\,. && \text{(C.16)}
\end{aligned}$$

The four-loop cusp anomalous dimension, which is required at N^{3}LL is currently not known, we use the Padé-approximation $\Gamma_3^{\rm cusp} = (\Gamma_2^{\rm cusp})^2/\Gamma_1^{\rm cusp}$. The noncusp anomalous dimensions for the hard current coefficient are given by [82]

$$\begin{aligned}
\gamma_0^C =& -6C_F\,, && \text{(C.17)}\\
\gamma_1^C =& C_A C_F\left(-\frac{961}{27} - \frac{11\pi^2}{3} + 52\zeta_3\right) + C_F^2\left(-3 + 4\pi^2 - 48\zeta_3\right) + C_F T_F n_f\left(\frac{260}{27} + \frac{4\pi^2}{3}\right)\,, && \text{(C.18)}\\
\gamma_2^C =& C_A^2 C_F\left(-\frac{139345}{1458} - \frac{7163\pi^2}{243} + \frac{7052}{9}\zeta_3 - \frac{88\pi^2}{9}\zeta_3 - \frac{83\pi^4}{45} - 272\zeta_5\right) + C_A C_F^2\left(-\frac{151}{2} + \frac{410\pi^2}{9}\right.\\
&\left. - \frac{1688}{3}\zeta_3 - \frac{16\pi^2}{3}\zeta_3 + \frac{494\pi^4}{135} - 240\zeta_5\right) + C_F^3\left(-29 - 6\pi^2 - 136\zeta_3 + \frac{32\pi^2}{3}\zeta_3 - \frac{16\pi^4}{5} + 480\zeta_5\right)\\
&+ \left[C_A C_F\left(-\frac{34636}{729} + \frac{5188\pi^2}{243} - \frac{3856}{27}\zeta_3 + \frac{44\pi^4}{45}\right) + C_F^2\left(\frac{5906}{27} - \frac{52\pi^2}{9} + \frac{1024}{9}\zeta_3 - \frac{56\pi^4}{27}\right)\right] T_F n_f\\
&+ C_F T_F^2 n_f^2\left(\frac{19336}{729} - \frac{80\pi^2}{27} - \frac{64}{27}\zeta_3\right)\,. && \text{(C.19)}
\end{aligned}$$

The noncusp anomalous dimensions for the (hemisphere) jet function are given by [55, 74]

$$\begin{aligned}
\gamma_0^J =& 6C_F\,, && \text{(C.20)}\\
\gamma_1^J =& C_A C_F\left(\frac{1769}{27} + \frac{22}{9}\pi^2 - 80\zeta_3\right) + C_F^2\left(3 - 4\pi^2 + 48\zeta_3\right) + C_F T_F n_f\left(-\frac{484}{27} - \frac{8\pi^2}{9}\right)\,, && \text{(C.21)}\\
\gamma_2^J =& C_A^2 C_F\left(\frac{412907}{1458} + \frac{838\pi^2}{243} - \frac{11000}{9}\zeta_3 + \frac{176\pi^2}{9}\zeta_3 + \frac{19\pi^4}{5} + 464\zeta_5\right) + C_A C_F^2\left(\frac{151}{2} - \frac{410\pi^2}{9}\right.\\
&\left. + \frac{1688}{3}\zeta_3 + \frac{16\pi^2}{3}\zeta_3 - \frac{494\pi^4}{135} + 240\zeta_5\right) + C_F^3\left(29 + 6\pi^2 + 136\zeta_3 - \frac{32\pi^2}{3}\zeta_3 + \frac{16\pi^4}{5} - 480\zeta_5\right)\\
&+ \left[C_A C_F\left(\frac{10952}{729} - \frac{2360\pi^2}{243} + \frac{5312}{27}\zeta_3 - \frac{92\pi^4}{45}\right) + C_F^2\left(-\frac{9328}{27} + \frac{64\pi^2}{9} - \frac{416}{9}\zeta_3 + \frac{328\pi^4}{135}\right)\right] T_F n_f\\
&+ C_F T_F^2 n_f^2\left(-\frac{27656}{729} + \frac{160\pi^2}{81} + \frac{512}{27}\zeta_3\right)\,. && \text{(C.22)}
\end{aligned}$$

The noncusp anomalous dimensions of the PDF and the thrust soft function can be easily obtained from these expressions via the consistency relations in Eqs. (4.35) and (5.16), respectively, i.e. $\gamma_i^{\tilde\phi} = -2\gamma_i^C - \gamma_i^J$ and $\gamma_i^S = -2\,{\rm Re}[\gamma_i^{\tilde C}] - \gamma_i^{J_\tau} = -2\gamma_i^C - 2\gamma_i^J$.

Appendix D

Computation of the hemisphere misalignment correction

D.1 Computation of the cumulant

Here we give some details on a numerically stable computation of the phase space misalignment correction to the thrust soft function, $\hat{S}^{(n_l+1,2)}_{\tau,m,\Delta}(\ell,m)$, which does not rely on the separate determination of the contributions from the quark and gluon hemisphere prescriptions in the phase space region where the two quarks enter opposite hemispheres. We consider the cumulant

$$\hat{\mathcal{S}}^{(n_l+1,2)}_{\tau,m,\Delta}(L,m) = \int_0^L d\ell\, \hat{S}^{(n_l+1,2)}_{\tau,m,\Delta}(\ell,m)\,, \tag{D.1}$$

which can be rearranged onto a single integration domain using the relation

$$\begin{aligned}
&\int_0^L d\ell\,\theta(k^- - k^+)\,\theta(q^+ - q^-)\,\big[\delta(\ell - k^+ - q^-) - \theta(q^+ + k^+ - q^- - k^-)\,\delta(\ell - k^- - q^-)\\
&\quad - \theta(q^- + k^- - q^+ - k^+)\,\delta(\ell - k^+ - q^+)\big]\\
&= \theta(k^- - k^+)\,\theta(q^+ - q^-)\,\theta(k^+ + q^+ - L)\,\theta(k^- + q^- - L)\,\theta(L - k^+ - q^-)\,.
\end{aligned} \tag{D.2}$$

After integration over the transverse momenta the cumulant adopts the form

$$\begin{aligned}
\hat{\mathcal{S}}^{(n_l+1,2)}_{\tau,m,\Delta}(L,m) = {}& \frac{\big(\alpha_s^{(n_l+1)}\big)^2 C_F T_F}{16\pi^2} \int\limits_0^L dq^- \int\limits_0^{L-q^-} dk^+ \int\limits_{L-k^+}^{\infty} dq^+ \int\limits_{L-q^-}^{\infty} dk^-\, \theta(k^+k^- - m^2)\,\theta(q^+q^- - m^2)\\
&\times f_m(k^+,k^-,q^+,q^-,m)
\end{aligned} \tag{D.3}$$

with $f_m(k,q,m)$ given in Eq. (5.75). Note that in the massless case the on-shell constraint θ-functions can be dropped in Eq. (D.3) and the integrations yield directly a constant corresponding to Eq. (5.82). In order to unambiguously determine the integration domains in the 4-dimensional integral it is convenient to distinguish between 4 parameter regimes: $L < m$, $m < L < (1+\sqrt{5})m/2$, $(1+\sqrt{5})m/2 < L < 2m$ and $2m < L$. We illustrate the areas with different integration domains for the larger momenta, q^+ and k^-, for each regime in Fig. D.1 (a) – (d) in the plane of the smaller momenta q^-, k^+. One of the integrations in Eq. (D.3) can be performed analytically, the remaining ones can be done numerically using the Cuba library [118]. Using both deterministic as well as Monte-Carlo algorithms we obtain the same result. Differentiating with respect to L yields $\hat{S}^{(n_l+1,2)}_{\tau,m,\Delta}(\ell,m)$.

D.2 Asymptotic expansion for $\ell \gg m$

We give a short outline for the calculation of the asymptotic expansion of $\hat{S}^{(n_l+1,2)}_{\tau,m,\Delta}(\ell,m)$ for large thrust momenta. The asymptotic expansion has been performed for each area in Fig. D.1 (d) with cutoff regularization taking $m^2/L \ll \Lambda_1 \ll m \ll \Lambda_2 \ll L$, since using dimensional regularization we have not

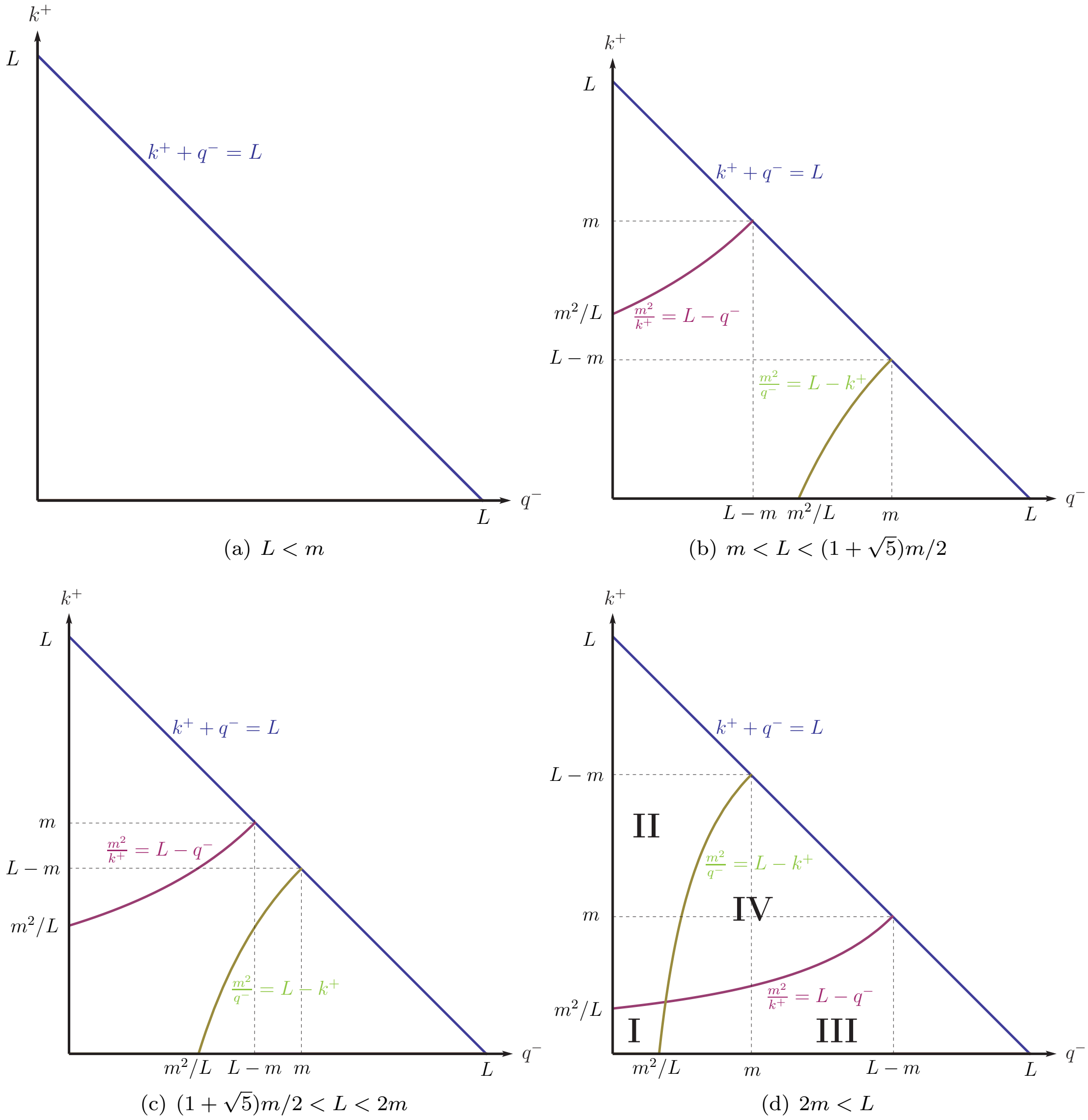

Figure D.1: The integration areas for different parameter regimes. For $L < m$ we have one single integration domain. For $m < L < (1+\sqrt{5})m/2$ and $(1+\sqrt{5})m/2 < L < 2m$ there are three domains, the regimes differ by the hierarchy between $L - m$ and m^2/L. Finally, for $L > 2m$ we have 4 areas, where the central one (IV) becomes dominating for large values of L.

been able to obtain an analytic result. The result from area I is suppressed by m^6/L^6 and thus irrelevant. For the computation of the areas II and III we obtain

$$\begin{aligned}\hat{\mathcal{S}}^{(n_l+1,2,\mathrm{II})}_{\tau,m,\Delta}(L,m) &= \hat{\mathcal{S}}^{(n_l+1,2,\mathrm{III})}_{\tau,m,\Delta}(L,m) \\ &= \frac{\left(\alpha_s^{(n_l+1)}\right)^2 C_F T_F}{16\pi^2}\left\{\frac{m^2}{L^2}\left[2\ln^2\left(\frac{m^2}{L^2}\right) + 12\ln\left(\frac{m^2}{L^2}\right) + 12 + \frac{8\pi^2}{3}\right] + \mathcal{O}\left(\frac{m^3}{L^3}\right)\right\},\end{aligned} \tag{D.4}$$

The expansions in area IV are cumbersome. We have to go to subleading orders in the m/L-expansion and consider a large number of different scaling regions with difficult integrations. Special care has to be taken of power counting breaking terms arising in the computation with the two cutoffs separating the different regions. Furthermore, cancellations in the denominator appear at the subleading order which require a special treatment for the hemisphere border region with $q^- \approx q^+$ and $k^+ \approx k^-$. The calculation for area IV eventually yields

$$\begin{aligned}\hat{\mathcal{S}}^{(n_l+1,2,\mathrm{IV})}_{\tau,m,\Delta}(L,m) = \frac{\left(\alpha_s^{(n_l+1)}\right)^2 C_F T_F}{16\pi^2}&\left\{-\frac{64}{9} + \frac{104\pi^2}{27} - \frac{64}{3}\zeta_3 - \frac{m^2}{L^2}\left[8\ln^2\left(\frac{m^2}{L^2}\right) + 56\ln\left(\frac{m^2}{L^2}\right)\right.\right. \\ &\left.\left. + \frac{296}{3} + \frac{386\pi^2}{45} + 16\pi\right] + \mathcal{O}\left(\frac{m^3}{L^3}\right)\right\}.\end{aligned} \tag{D.5}$$

Thus, the final result for the integrated soft function difference reads

$$\begin{aligned}\hat{\mathcal{S}}^{(n_l+1,2)}_{\tau,m,\Delta}(L,m) = \frac{\left(\alpha_s^{(n_l+1)}\right)^2 C_F T_F}{16\pi^2}&\left\{-\frac{64}{9} + \frac{104\pi^2}{27} - \frac{64}{3}\zeta_3 - \frac{m^2}{L^2}\left[4\ln^2\left(\frac{m^2}{L^2}\right) + 32\ln\left(\frac{m^2}{L^2}\right)\right.\right. \\ &\left.\left. + \frac{224}{3} + \frac{146\pi^2}{45} + 16\pi\right] + \mathcal{O}\left(\frac{m^3}{L^3}\right)\right\},\end{aligned} \tag{D.6}$$

which gives, after differentiation, Eq. (5.81).

Appendix E

Massive gluon radiation in thrust at $\mathcal{O}(\alpha_s)$ in full QCD

In this section we present the fixed-order calculation of the massive gluon corrections at $\mathcal{O}(\alpha_s)$ in full QCD. We also discuss the various expansions needed to identify the singular terms. Since the full theory result has nontrivial threshold contributions related to the mass scale, these expansions deserve a separate discussion.

E.1 General result

The relevant diagrams for the computation are shown in Fig. E.1. The virtual contributions yield $\tilde{F}^{(1)}_{M,\mathrm{QCD}}(Q,M)$ corresponding to the result for DIS in Eq. (3.70) apart from an analytic continuation from $Q^2 \to -Q^2$. What is left to be done, is the calculation of the real radiation diagrams for the massive gluons and the integration over the three-particle phase space. It is convenient to introduce the usual energy fraction variables,

$$x_1 = \frac{2p_0}{Q}, \quad x_2 = \frac{2p_0'}{Q}, \quad x_3 = \frac{2q_0}{Q}\,, \tag{E.1}$$

where $x_1 + x_2 + x_3 = 2$. Here p, p' and q are the quark, antiquark and massive gluon momenta. The double differential cross section in $d = 4$ dimensions reads in terms of these variables ($\hat{M} = M/Q$)

$$\frac{1}{\sigma_0}\frac{\mathrm{d}\sigma^{\mathrm{real}}}{\mathrm{d}x_1\,dx_2} = \frac{\alpha_s C_F}{2\pi}\frac{1}{(1-x_1)(1-x_2)}\left[x_1^2 - \hat{M}^2\left(\frac{1-3x_2+2x_1x_2}{1-x_1}\right) + \hat{M}^4 + (x_1 \leftrightarrow x_2)\right]. \tag{E.2}$$

The relation of the thrust variable τ to $x_{1,2,3}$ reads

$$\tau \equiv 1 - \max_{\hat{\mathbf{t}}}\frac{\sum_i |\hat{\mathbf{t}}\cdot\vec{p}_i|}{Q} = 1 - \max\left(x_1, x_2, \sqrt{x_3^2 - 4\hat{M}^2}\right). \tag{E.3}$$

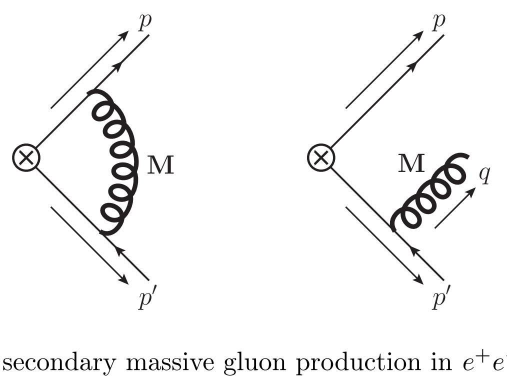

Figure E.1: Diagrams for secondary massive gluon production in e^+e^- annihilation at $\mathcal{O}(\alpha_s)$.

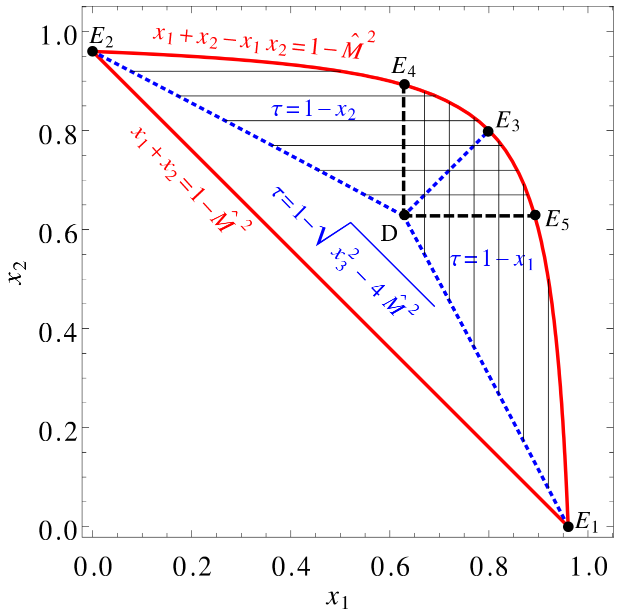

Figure E.2: The phase space for the real radiation of a massive gluon in terms of the variables x_1 and x_2 for $\hat{M} = 0.2$. The kinematic constraints yield the allowed area within the red, continuous lines. The blue dotted lines bound the areas with the same thrust relation to x_1 and x_2 and are given by $x_1 = x_2$, $2x_1(2-x_2) = (2-x_2)^2 - 4\hat{M}^2$ and $2x_2(2-x_1) = (2-x_1)^2 - 4\hat{M}^2$. D (located at $x_1 = x_2 = \sqrt{x_3^2 - 4\hat{M}^2} = 1 - \tau_{\rm max}$) is the point of maximal thrust, E_1 and E_2 have minimal thrust configurations. At E_3 the produced gluon is at rest with $\tau = \bar{\tau}$. The triangle $\mathrm{E_1DE_2}$ corresponds to $\tau = 1 - \sqrt{x_3^2 - 4\hat{M}^2}$ and generates the function $A(\tau, \hat{M})$. $B(\tau, \hat{M})$ is obtained by increasing the areas of the segments $\mathrm{E_1E_3D}$ ($\mathrm{E_3E_2D}$) to $\mathrm{E_1E_4D}$ ($\mathrm{E_5E_2D}$) and integrating with $\tau = 1 - x_1$ ($\tau = 1 - x_2$). Subtracting $\mathrm{E_5E_4D}$ with the corresponding opposite thrust prescription gives the soft function piece $C(\tau, \hat{M})$.

The resulting thrust distribution (including also the virtual contributions) displays structures associated to collinear and soft gluon radiation thresholds. It has the form

$$\frac{1}{\sigma_0}\frac{\mathrm{d}\sigma}{\mathrm{d}\tau} = \frac{\alpha_s C_F}{4\pi}\bigg\{2 f^{(1)}_{\rm QCD}(\hat{M})\,\delta(\tau) + \theta(\tau - \tau_{\rm min})\,\theta(\tau_{\rm max} - \tau)\Big(A(\tau,\hat{M}) + B(\tau,\hat{M})\Big) \\ + \theta(\tau - \bar{\tau})\,\theta(\tau_{\rm max} - \tau)\,C(\tau,\hat{M})\bigg\}, \tag{E.4}$$

where the minimal and maximal thrust values and the intermediate threshold for the real radiation contributions are given by

$$\tau_{\rm min} \equiv \hat{M}^2\,, \quad \tau_{\rm max} \equiv \frac{1}{3}\left(-1 + 2\sqrt{1 + 3\hat{M}^2}\right)\,, \quad \bar{\tau} \equiv \hat{M}\,. \tag{E.5}$$

The real corrections associated to the threshold at $\tau_{\rm min} = M^2/Q^2$ correspond to collinear radiation, and those associated to the threshold at $\bar{\tau} = M/Q$ correspond to soft radiation. As illustrated in Fig. E.2, we have distributed the contributions from the various phase space regions such that collinear and soft terms both extend to the endpoint at $\tau_{\rm max}$. This facilitates the identification of the singular terms in the SCET framework as contributions coming from the jet and the soft functions. We emphasize that this setup appears to be the only practical choice to achieve a separation of collinear and soft contributions compatible with singular terms that can be analytically defined for the whole kinematic τ-range and for

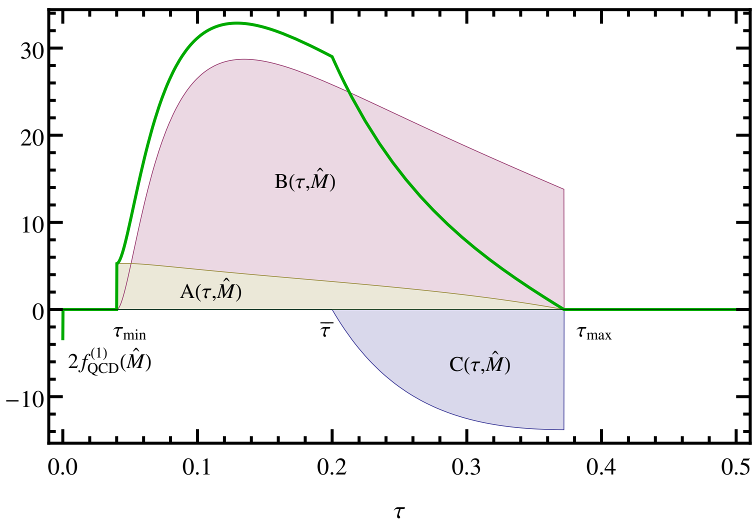

Figure E.3: The three contributions $A(\tau,\hat{M})$, $B(\tau,\hat{M})$ and $C(\tau,\hat{M})$ to the $\mathcal{O}(\alpha_s)$ full theory thrust distribution for the radiation of a massive gluon for $\hat{M}=M/Q=0.2$. The sum of all terms, given by the thick green line, is positive. The vertical green line at $\tau=0$ indicates the virtual corrections proportional to $\delta(\tau)$.

all possible values of $\hat{M}$. Note that in Eq. (E.4) we have factored out an overall loop factor and redefined

$$\mathrm{Re}\left[\tilde{F}^{(1)}_{M,\mathrm{QCD}}(Q,M)\right]=\frac{\alpha_s C_F}{4\pi}f^{(1)}_{\mathrm{QCD}}(\hat{M})\,. \tag{E.6}$$

The functions $A(\tau,\hat{M})$, $B(\tau,\hat{M})$ and $C(\tau,\hat{M})$ are obtained by integrating $\mathrm{d}\sigma^{\mathrm{real}}/dx_1\,dx_2$ in the phase-space regions as described in the caption of Fig. E.2. The analytic results read

$$\begin{aligned}
A(\tau,\hat{M}) &= \frac{4(1-\tau)}{\hat{w}^2}\ln\left(\frac{\hat{w}-\tau}{\tau}\right)\left[3-2\tau+\tau^2-2\hat{w}(1+\hat{M}^2)+2\hat{M}^4\right]\\
&\quad-\frac{(\hat{w}-2\tau)(1-\tau)}{\tau\hat{w}(\hat{w}-\tau)}\left[\hat{w}\tau(1-\tau)-\hat{M}^2\right], && \text{(E.7)}\\
B(\tau,\hat{M}) &= \frac{4}{\tau}\ln\left(\frac{\tau(\hat{w}-\tau)}{\hat{M}^2}\right)\left[2-2\tau+\tau^2+2\hat{M}^2(2-\tau)+2\hat{M}^4\right]\\
&\quad-\frac{2}{\tau^3(\hat{w}-\tau)}\Big[\tau^2\big(4-\hat{w}-\tau(5+6\hat{w})+2\tau^2(1-\hat{w})+2\tau^3\big)\\
&\quad+2\hat{M}^2\tau\big(1-2\hat{w}-\tau(6+4\hat{w})-\tau^2(5+4\hat{w})+4\tau^3\big)-\hat{M}^4\big(\hat{w}+\tau(7+4\hat{w})+12\tau^2\big)\Big], && \text{(E.8)}\\
C(\tau,\hat{M}) &= -\frac{8}{\tau^3}\ln\left(\frac{\tau}{\hat{M}}\right)\left[2-2\tau+\tau^2+2\hat{M}^2(2-\tau)+2\hat{M}^4\right]+\frac{2(\tau^2-\hat{M}^2)}{\tau^3}\left[\tau(4+\tau)+\hat{M}^2(1+4\tau)\right], && \text{(E.9)}
\end{aligned}$$

with

$$\hat{w}\equiv\sqrt{(1-\tau)^2+4\hat{M}^2}\,. \tag{E.10}$$

Our result agrees with the one given in Ref. [126]. The result for the fixed-order thrust distribution in arbitrary units is displayed for $\hat{M}=0.2$ in Fig. E.3. As a cross-check, from Eq. (E.4) we obtain the correct massless expression for $\hat{M} \to 0$ [4, 107],

$$\frac{1}{\sigma_0}\frac{\mathrm{d}\sigma^{\mathrm{real}}}{\mathrm{d}\tau} \overset{M\to 0}{\longrightarrow} \frac{\alpha_s C_F}{4\pi}\Biggl\{2\delta(\tau)\left(-1+\frac{\pi^2}{3}\right) - 6\left[\frac{\theta(\tau)}{\tau}\right]_+ - 8\left[\frac{\theta(\tau)\ln\tau}{\tau}\right]_+ \\ + \frac{2}{1-\tau}\left[6+3\tau-9\tau^2+(2-4\tau)\ln\tau+\left(\frac{4}{\tau}-6+6\tau\right)\ln(1-2\tau)\right]\Biggr\}\,, \tag{E.11}$$

valid for $0 \le \tau \le 1/3$. To obtain this result involving the plus-distributions it is required to exactly account for the analytic behavior of the collinear and soft thresholds when taking the massless limit.

E.2 Expansions

The massless fixed-order thrust distribution shown in Eq. (E.11) only depends on τ, and the expansion parameter relevant for approaching the dijet limit is simply $\lambda \sim \sqrt{\tau} \ll 1$. There is only one single threshold located at $\tau = 0$. Thus in the massless limit we can identify the fixed-order singular pieces that are being summed in the factorization theorem and that can be used for the matching calculations within SCET by simply performing an expansion in small τ. The collinear and soft contributions are not separated. In the presence of the massive gluons the collinear and soft thresholds are separated due to their different mass-dependence: collinear radiation arises for $\tau \ge \tau_{\min} = M^2/Q^2$ and soft radiation arises for $\tau \ge \bar{\tau} = M/Q$. Thus the identification of the singular terms – which shall be defined for the whole kinematic τ-range and include the full mass-dependence – needs to account for the location of the thresholds. In this subsection we discuss the required expansions for the full theory results.

The $\delta(\tau)$ term is left unexpanded since we aim at determining the full mass-dependence of the singular contributions. The term proportional to $\theta(\tau - \hat{M}^2)$ contains the collinear contributions. Here the jet invariant mass $Q\sqrt{\tau}$ and the mass M have to be considered at the same footing. Since the mass threshold is treated exactly, we expand for $\tau \sim \hat{M}^2 \ll 1$. Here only the function $B(\tau, \hat{M})$ contains singular terms as it originates from the collinear regions in the x_1-x_2 phase space where $x_1 \sim 1$ or $x_2 \sim 1$:

$$B(\tau,\hat{M}) \overset{\tau\sim\hat{M}^2}{\longrightarrow} \frac{2}{\tau^3}\left[(\hat{M}^2-\tau)(3\tau+\hat{M}^2)+4\tau^2\ln\left(\frac{\tau}{\hat{M}^2}\right)\right] + \mathcal{O}(\tau^0,\hat{M}^0)\,. \tag{E.12}$$

The function $B(\tau, \hat{M})$ and all terms in the expansion vanish at $\tau = \hat{M}^2$ giving a continuous turn-on of the singular $\mathcal{O}(\tau^{-1})$ terms (with $\tau \sim \hat{M}^2$). On the other hand, the function $A(\tau, x)$ does not contain singular $\mathcal{O}(\tau^{-1})$ terms as it stems from configurations which are neither collinear nor soft. Interestingly the function $A(\tau, \hat{M})$ is nonvanishing at $\tau = \hat{M}^2$ and responsible for the step visible in Fig. E.3. For $\tau \sim \hat{M}^2 \ll 1$ the expansion for the function $A(\tau, \hat{M})$ reads

$$A(\tau,\hat{M}) \overset{\tau\sim\hat{M}^2}{\longrightarrow} -4\,\frac{\tau+\hat{M}^2+\tau\ln\tau}{\tau} + \mathcal{O}(\tau,\hat{M}^2) \tag{E.13}$$

showing that it contributes at $\mathcal{O}(\tau^0 \sim 1)$. Although the contribution from function $A(\tau, \hat{M})$ exceeds the singular contribution from $B(\tau, \hat{M})$ numerically at $\tau \approx \hat{M}^2$, it only contains nonsingular terms which are not described in the factorization theorems. It remains to discuss the term proportional to $\theta(\tau - \hat{M})$, which contains the soft contributions. Here the soft scale $Q\tau$ and the mass M have to be considered at the same footing. Since the soft mass threshold is treated exactly we expand in $\tau \sim \hat{M} \ll 1$. For the function $C(\tau, \hat{M})$ this yields singular $\mathcal{O}(\tau^{-1})$ terms which read

$$C(\tau,\hat{M}) \overset{\tau\sim\hat{M}}{\longrightarrow} -\frac{16}{\tau}\ln\left(\frac{\tau}{\hat{M}}\right) + \mathcal{O}(\tau^0,\hat{M}^0)\,. \tag{E.14}$$

Similar to $B(\tau, \hat{M})$, the singular $\mathcal{O}(1/\tau)$ terms turn on continuously at $\tau = \hat{M}$.

Assembling all singular pieces we obtain

$$\frac{1}{\sigma_0}\,\frac{\mathrm{d}\sigma}{\mathrm{d}\tau}\bigg|_{\mathrm{FO}} = \delta(\tau) + \frac{\alpha_s C_F}{4\pi}\bigg\{2f^{(1)}_{\mathrm{QCD}}(\hat{M})\,\delta(\tau) + \theta(Q^2\tau - M^2)\bigg[\frac{2(M^2-Q^2\tau)(3Q^2\tau+M^2)}{Q^4\tau^3} + \frac{8}{\tau}\ln\!\bigg(\frac{Q^2\tau}{M^2}\bigg)\bigg] - \theta(Q\tau - M)\frac{8}{\tau}\ln\!\bigg(\frac{Q^2\tau^2}{M^2}\bigg)\bigg\}\,. \tag{E.15}$$

We emphasize that the factorization theorems for *all* EFT scenarios account for the full-mass dependence displayed in Eq. (E.15). The terms corresponding to the collinear and soft thresholds yield functions which match exactly to the EFT real radiation contributions from collinear mass modes, denoted by $J^{(1)}_{\tau,M,\mathrm{real}} = 2J^{(1)}_{M,\mathrm{real}}$ with $J^{(1)}_{M,\mathrm{real}}$ given in Eq. (4.107), and soft mass modes, denoted by $\hat{S}^{(1)}_{\tau,M,\mathrm{real}}$ given in Eq. (5.64), respectively. We note that from Eq. (E.15) the singular terms in the massless limit (first three terms on the RHS of Eq. (E.11)) can be recovered, requiring the proper combination of the terms into plus- and delta-distributions in τ.

An interesting issue we would like to mention is that the parametric precision of the expansions leading to the singular contributions in Eq. (E.15) is not uniform and depends on τ. Above the collinear threshold ($\tau > \tau_{\mathrm{min}}$) the expansion is valid up to higher order power corrections of order $\hat{M}^2$. On the other hand, above the soft threshold ($\tau > \bar{\tau}$) the expansion is valid up to higher order power corrections of order $\hat{M}$. This is an intrinsic property and also inherited to the factorization theorems we derived in the various scenarios. So, from a strict power counting point of view, for $\hat{M} \ll 1$ the soft sector would need to be treated with the first order power corrections included to reach the same parametric precision as the collinear sector. We stress, however, that this does not affect in any way the consistency of treating only the singular collinear and soft mass mode contribution in the effective theory description.

Appendix F

Secondary mass effects with primary massive quarks

In chapter 5 we have computed the secondary massive quark corrections at $\mathcal{O}(\alpha_s^2 C_F T_F)$ to the thrust distribution for the production of primary massless quarks. Here we investigate these types of corrections in the presence of primary massive quarks of the same flavor. Our presentation follows Refs. [8, 9], but specifies for the first time the treatment of massive top quark loops and provides explicit results. We discuss briefly the factorization theorem in the peak region for a primary massive top quark, which requires the matching onto an additional EFT, namely boosted Heavy Quark Effective Theory (bHQET), and present the calculation of the corresponding matching correction for secondary massive quark effects at $\mathcal{O}(\alpha_s^2 C_F T_F)$ within this factorization framework in two different ways. This computation provides a necessary ingredient for a N^{3}LL analysis of event shape distributions, which might be used for a precise extraction of a properly defined short distance top quark mass from the peak position.

F.1 Factorization for primary massive quarks

For the production of primary massive quarks the jet invariant mass of a single jet satisfies always $s \geq m^2$, so that only the scaling scenarios III ($\mu_J \gtrsim \mu_m$ and $\mu_m \gtrsim \mu_S$) and IV ($\mu_S \gtrsim \mu_m$) have to be considered in the SCET mass mode setup described in Sec. 5.3. Thus the dependence on $m \ll Q$ can be dropped in the hard matching coefficient [1] and the only difference concerning secondary mass effects at $\mathcal{O}(\alpha_s^2 C_F T_F)$ with respect to the case of primary massless quarks lies in the jet function and the current and jet function threshold corrections. [2]

Furthermore, we can have the additional regime, where the invariant masses of either of the outgoing jets are very close to the mass of the heavy quark, i.e. $(s - m^2)/m^2 \ll 1$, and where the SCET factorization theorem does not resum all large logarithms any more. This scaling holds in particular in the phenomenologically interesting peak region for top quark production, where $s - m^2 \sim Q\Lambda_{\rm QCD}$, for not too large c.m. energies at a future ILC ($Q \ll m^2/\Lambda_{\rm QCD} \sim 30$ TeV). [3] Note that this scaling can be only preserved to all orders in perturbation theory if a proper short distance mass scheme with $\delta m \lesssim Q\Lambda_{\rm QCD}/m$ is employed, which excludes e.g. the $\overline{\rm MS}$ mass (with $\delta m \sim m \gg Q\Lambda_{\rm QCD}/m$). To account for the resummation of the logarithms $\ln(\hat{s}/m) = \ln((s-m^2)/m^2)$ one has to switch to two boosted versions of HQET for the top and antitop quark. The factorization theorem for the thrust distribution

[1] In contrast to virtual secondary mass effects one cannot incorporate the full mass dependence into the hard matching coefficient of the leading order current since the primary quark mass appears as physically visible real radiation scale directly tied to the SCET expansion parameter. Terms which are suppressed by $(m/Q)^n$ appear in matching coefficients for subleading currents in SCET.

[2] In the SCET setup we are currently still missing an analytic expression for the real radiation contributions of the secondary massive quarks in the jet function. Note that also the other corrections to the jet function at $\mathcal{O}(\alpha_s^2)$ have not been given in literature.

[3] We neglect here the dependence on the top quark decay width Γ_t, which will be irrelevant for our discussion. Generally, one has $s - m^2 \sim Q\Lambda_{\rm QCD} + m\Gamma_t$ in the peak region.

with jet invariant masses close to threshold reads in bHQET [8, 9]

$$\begin{aligned}\frac{1}{\sigma_0}\frac{\mathrm{d}\sigma}{\mathrm{d}\tau} &= Q\,\left|\tilde{C}^{(n_l+1)}(Q,\mu_H)\right|^2\left|U_{\tilde{C}}^{(n_l+1)}(Q,\mu_H,\mu_m)\right|^2|C_m(Q,m,\mu_m)|^2\left|U_m^{(n_l)}(Q,m,\mu_m,\mu)\right|^2\\ &\times\int\mathrm{d}\hat{s}\int\mathrm{d}\hat{s}'\int\mathrm{d}\ell\,B_\tau^{(n_l)}(\hat{s}',\mu_B)\,U_{B_\tau}^{(n_l)}(\hat{s}-\hat{s}',\mu,\mu_B)\,S_\tau^{(n_l)}\left(Q\tau-\frac{2m^2}{Q}-\frac{m\hat{s}}{Q}-\ell,\mu_S\right)\\ &\times U_{S_\tau}^{(n_l)}(\ell,\mu,\mu_S)\end{aligned} \tag{F.1}$$

up to higher orders in the power counting parameters $\lambda_{\mathrm{SCET}} = m/Q$ and $\lambda_{\mathrm{bHQET}} = (Q^2\tau - 2m^2)/m^2$. Here the term $\tilde{C}^{(n_l+1)}(Q,\mu)$ is the same massless hard matching coefficient between the SCET and the QCD current as in Eq. (5.4). At $\mu_m \sim m$ the fluctuations of the order of the mass scale have to be integrated out resulting in a matching coefficient $C_m(Q,m,\mu_m)$ between the bHQET and the SCET current. Here we also include all (virtual) secondary mass effects into C_m, which were partially separated in terms of a matrix element of soft mass mode Wilson lines in Refs. [8, 9]. [4] The perturbative bHQET thrust jet function $B_\tau^{(n_l)}(\hat{s},\mu)$ describes the small fluctuations of the collinear top and antitop quark close to the mass shell. It is defined as a time-ordered operator matrix element in terms of boosted heavy quark fields and depends on the sum of the offshellnesses of the two jets via $\hat{s} \sim \mu_B \sim (Q^2\tau - 2m^2)/m$, see Ref. [8]. [5] The soft function in bHQET is in fact the same as the one in SCET with n_l massless flavors, which in particular does not rely on the fact whether the primary quark is massless or massive, and is thus given by Eq. (5.7). All matrix elements are evolved to a common renormalization scale μ with the RG factors $U_{\tilde{C}}^{(n_l+1)}$, $U_m^{(n_l)}$, $U_{B_\tau}^{(n_l)}$ and $U_{S_\tau}^{(n_l)}$ associated to the SCET current, the bHQET current, jet and soft functions, respectively. Here we have set $\mu < \mu_m$ implying that the final renormalization scale lies in the bHQET regime and the matching coefficient C_m arises when the evolution of the current crosses the mass scale from above. An equivalent picture where $\mu > \mu_m$ and the jet and soft functions cross the mass threshold from below will be discussed in Sec. F.3.

Due to the fact that the real radiation of an additional massive top quark pair increases the invariant mass by $\Delta s \gtrsim m^2 \gg Q\Lambda_{\mathrm{QCD}}$, secondary top quarks can only appear via virtual radiation in the peak region. They are integrated out in the matching from bHQET to SCET in the coefficient $C_m(Q,m,\mu_m)$.

F.2 Current matching with secondary massive quarks

Here we perform the computation of the matching coefficient $C_m(Q,m,\mu_m)$ at $\mathcal{O}(\alpha_s^2 C_F T_F)$. In fact we can split the calculation by first integrating out the secondary massive quark effects in the SCET current resulting in a mass mode matching factor $\mathcal{M}_{C_m}$ and then matching the remainder to bHQET with a matching coefficient $\tilde{C}_m^{(n_l)}$. In terms of renormalization conditions we thus switch from a SCET current that is renormalized in $\overline{\mathrm{MS}}$ concerning the secondary massive quark corrections to a corresponding one in the OS scheme, which is then matched to the bHQET current where secondary massive quark correction do not appear (which also corresponds to an OS description), i.e.

$$C_m(Q,m,\mu_m) = \mathcal{M}_{C_m}(Q,m,\mu_m)\,\tilde{C}_m^{(n_l)}(m,\mu_m)\,. \tag{F.2}$$

Note that this formula holds independently whether the primary and the secondary quark masses are equal. To obtain $\mathcal{M}_{C_m}^{(2)}(Q,m,\mu)$ and eventually $C_m^{(2)}(Q,m,\mu)$ we will compute the secondary massive quark corrections to the hard current in a similar way as in chapter 4. We start with the calculation of the one-loop diagrams for the radiation of a "massive gluon" with mass M and apply in a second step the dispersion relation (3.62) to account for the gluon splitting into two massive quarks with mass m. We will be able to perform the calculation in close analogy to the one for primary massless quarks explicitly described for DIS in the endpoint region in chapter 4, where the difference results in an UV and IR finite

[4] Note that our understanding of mass modes is different compared to Refs. [8, 9], where the corresponding secondary effects were not investigated systematically, and comprises in particular also collinear mass modes.

[5] Compared to Ref. [8] we have normalized the bHQET jet function with a factor m differently such that $B_\tau^{(0)}(\hat{s}) = \delta(\hat{s})$ instead of $B_\tau^{(0)}(\hat{s}) = 1/m\delta(\hat{s}) = \delta(s - m^2)$.

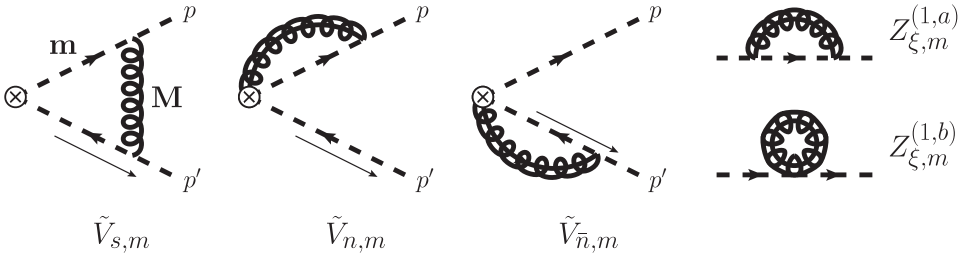

Figure F.1: Non-vanishing EFT diagrams for the computation of the hard current at $\mathcal{O}(\alpha_s)$ with primary massive quarks and secondary massive gluons with masses m and M, respectively. Soft-bin subtractions are implied for the collinear diagrams.

remainder at the level of the massive gluon that yields just a constant, nonlogarithmic correction at the level of the secondary massive quarks. This has the important consequence that the rapidity logarithms are the same for primary massless and massive quarks at $\mathcal{O}(\alpha_s^2 C_F T_F)$, which is a fact that holds to any order in perturbation theory as will be explained in Sec. F.3.

F.2.1 One-loop computation for secondary massive gluons

We compute the diagrams in Fig. F.1 using the Feynman rules in Fig. 2.3. Due to the eikonal structure we obtain for the soft diagram $\tilde{V}_{s,m}$ the same result as for primary massless quarks which is given in analogy to Eq. (4.68) by [6]

$$\tilde{V}_{s,m} = -2ig^2 C_F \tilde{\mu}^{2\epsilon} \int \frac{\mathrm{d}^d k}{(2\pi)^d} \frac{1}{[k^- + i\epsilon]} \frac{1}{[k^+ - i\epsilon]} \frac{1}{[k^2 - M^2 + i\epsilon]} \,. \tag{F.3}$$

For the n-collinear diagram we get

$$\tilde{V}_{n,m} = 2ig^2 C_F \tilde{\mu}^{2\epsilon} \int \frac{\mathrm{d}^d k}{(2\pi)^d} \frac{Q - k^-}{[k^2 - Qk^+ - \frac{m^2}{Q} k^- + i\epsilon]} \frac{1}{[k^- + i\epsilon]} \frac{1}{[k^2 - M^2 + i\epsilon]} \,. \tag{F.4}$$

We can decompose this contribution into a correction corresponding to the diagram with primary massless quarks $\tilde{V}_{n,m=0}$, which is the same as V_n given in Eq. (4.70) apart from a different pole prescription, and a UV (and IR) finite piece that accounts for contributions due to the mass of the primary quark and can be computed in 4 dimensions,

$$\tilde{V}_{n,m} = \tilde{V}_{n,m=0} + (\tilde{V}_{n,m} - \tilde{V}_{n,m=0}) \,. \tag{F.5}$$

The latter reads

$$\begin{aligned} \tilde{V}_{n,m} - \tilde{V}_{n,m=0} &= -\frac{\alpha_s C_F}{2\pi} \Gamma\left(2 - \frac{d}{2}\right) \left(\frac{\mu^2 e^{\gamma_E}}{M^2}\right)^{2-\frac{d}{2}} \int_0^1 \mathrm{d}z \, \frac{1-z}{z} \left[\left(1 - z + \frac{m^2}{M^2} z^2\right)^{\frac{d}{2}-2} - (1-z)^{\frac{d}{2}-2}\right] \\ &= \frac{\alpha_s C_F}{2\pi} \left[\ln\left(\frac{1+a}{2}\right) \ln\left(\frac{1-a}{2}\right) + \frac{1+a}{1-a} \ln\left(\frac{1+a}{2}\right) + \frac{1-a}{1+a} \ln\left(\frac{1-a}{2}\right) + 1 + \mathcal{O}(\epsilon)\right] \end{aligned} \tag{F.6}$$

with

$$a = \sqrt{1 - \frac{4m^2}{M^2}} \,. \tag{F.7}$$

[6] Note that compared to the DIS calculation only one $i\epsilon$-prescription has changed corresponding to the fact that we have an antiquark in the final state instead of a quark in the initial state.

Note that the result in Eq. (F.6) does not contain any rapidity divergences, so that rapidity logarithms arise only in the computation of $\tilde{V}_{n,m=0}$. For the soft-bin subtraction of $\tilde{V}_{n,m}$ the dependence on the primary quark mass drops out as for the soft diagram and we obtain the same result as for primary massless quarks (namely $\tilde{V}_{s,m}$ if the α-regulator in Eq. (4.66) is applied).

The $\bar{n}$-collinear diagram corresponds to switching k^- and k^+ in Eq. (F.4). We perform an analogous decomposition to Eq. (F.5),

$$\tilde{V}_{\bar{n},m} = \tilde{V}_{\bar{n},m=0} + (\tilde{V}_{\bar{n},m} - \tilde{V}_{\bar{n},m=0})\,, \tag{F.8}$$

Since all rapidity divergences are encoded in the results with primary massless quarks, no additional regulator has to be imposed for the computation of the UV (and IR) finite difference contribution, so that the corresponding integral is symmetric to the one in the n-collinear sector and yields the same result,

$$\tilde{V}_{\bar{n},m} - \tilde{V}_{\bar{n},m=0} = \tilde{V}_{n,m} - \tilde{V}_{n,m=0}\,. \tag{F.9}$$

Finally, we also have to consider the wave function corrections. The diagrams give in analogy to the computation in Ref. [9]

$$Z^{(1,a)}_{\xi,m} + Z^{(1,b)}_{\xi,m} = 2ig^2 C_F \tilde{\mu}^{2\epsilon} \frac{\not{\bar{n}}}{2} \int \frac{\mathrm{d}^d k}{(2\pi)^d} \frac{Qm^2(3-\epsilon) - (Q^2k^+ + Qp^2 + m^2 k^-)(1-\epsilon)}{Q^2[k^2 - M^2 + i\epsilon][(k+p)^2 - m^2 + i\epsilon]}\,. \tag{F.10}$$

Using $p^2 = m^2 + \Delta^2$ and decomposing the integrals into elementary one- and two-point functions we obtain

$$\begin{aligned} Z^{(1,a)}_{\xi,m} + Z^{(1,b)}_{\xi,m} =& ig^2 C_F \tilde{\mu}^{2\epsilon} \frac{\not{\bar{n}}}{2} \frac{(1-\epsilon)}{Q(m^2+\Delta^2)} \Big\{ \left[A_0(m^2) - A_0(M^2)\right]\left[2m^2 + \Delta^2\right] \\ &+ B_0(m^2+\Delta^2, M^2, m^2)\left[\frac{4m^2(m^2+\Delta^2)}{1-\epsilon} + 2m^2M^2 + M^2\Delta^2 - \Delta^4\right]\Big\}\,. \end{aligned} \tag{F.11}$$

The wave function renormalization constant $Z^{(1)}_{\xi,m}$ is defined by

$$Z^{(1,a)}_{\xi,m} + Z^{(1,b)}_{\xi,m} \xrightarrow{\Delta\to 0} i\frac{\not{\bar{n}}}{2}\frac{1}{Q}\left[2m\,\delta m^{(\mathrm{OS},1)}_M + \Delta^2 Z^{(1)}_{\xi,m} + \mathcal{O}(\Delta^4)\right]\,, \tag{F.12}$$

where $\delta m^{(\mathrm{OS},1)}_M$ is the one-loop renormalization constant for the quark mass m in the pole mass scheme for the interaction with a massive gluon (with mass M). $Z^{(1)}_{\xi,m}$ can be written in terms of the counterterm correction for primary massless quarks given in Eq. (3.82), which can be recovered from Eq. (F.11) for $m \to 0$, and a UV (and IR) finite remainder,

$$Z^{(1)}_{\xi,m} = Z^{(1)}_{\xi,m=0} + (Z^{(1)}_{\xi,m} - Z^{(1)}_{\xi,m=0})\,. \tag{F.13}$$

The mismatch contribution between massive and massless primary quarks reads in $d = 4$ dimensions

$$\begin{aligned} Z^{(1)}_{\xi,m} - Z^{(1)}_{\xi,m=0} =& \frac{\alpha_s C_F}{4\pi}\frac{3}{2a(1-a^2)^2}\left[2(1+a)^4(2-a)\ln\left(\frac{1+a}{2}\right) - 2(1-a)^4(2+a)\ln\left(\frac{1-a}{2}\right)\right. \\ &\left. + a\left(11 - 14a^2 + 3a^4\right) + \mathcal{O}(\epsilon)\right]\,. \end{aligned} \tag{F.14}$$

Thus the complete (unrenormalized) SCET result for the current at $\mathcal{O}(\alpha_s)$ reads

$$\tilde{F}^{(1)}_{M,\mathrm{SCET},m}(Q,M,m,\mu) = \tilde{F}^{(1)}_{M,\mathrm{SCET},m=0}(Q,M,\mu) + \underbrace{\tilde{F}^{(1)}_{M,\mathrm{SCET},m}(Q,M,m,\mu) - \tilde{F}^{(1)}_{M,\mathrm{SCET},m=0}(Q,M,\mu)}_{=\delta\tilde{F}^{(1)}_{M,\mathrm{SCET},m}(M,m)} \tag{F.15}$$

with $\tilde{F}^{(1)}_{M,\mathrm{SCET},m=0}$ being the corrections with primary massless quarks in d dimensions, which can be computed in close analogy to Sec. 4.3.1, [7]

$$\tilde{F}^{(1)}_{M,\mathrm{SCET},m=0}(Q,M,\mu) = \frac{\alpha_s C_F}{2\pi}\,\Gamma\!\left(2-\frac{d}{2}\right)\left(\frac{\mu^2 e^{\gamma_E}}{M^2}\right)^{2-\frac{d}{2}}\left\{H_{\frac{d}{2}-1} - (-1)^{2-\frac{d}{2}}\,\Gamma\!\left(\frac{d}{2}\right)\Gamma\!\left(1-\frac{d}{2}\right) - \frac{d^2-6d+4}{d(d-2)} + \ln\!\left(\frac{M^2}{Q^2}\right)\right\}. \tag{F.16}$$

The UV finite correction due to the mass of the primary quark is given in terms of Eqs. (F.6) and (F.14) by

$$\delta\tilde{F}^{(1)}_{M,\mathrm{SCET},m}(M,m) = 2(\tilde{V}_{n,m} - \tilde{V}_{n,m=0}) - (Z^{(1)}_{\xi,m} - Z^{(1)}_{\xi,m=0})\,. \tag{F.17}$$

F.2.2 Two-loop computation for secondary massive quarks

Following Eq. (3.62) we can obtain the $\mathcal{O}(\alpha_s^2 C_F T_F)$ secondary massive quark form factor corrections in analogy to Eq. (4.154). For the d dimensional piece we obtain the same results as computed in Sec. 4.4.1 apart from the replacements $L_Q \to L_{-Q}$ and $\ln(\hat{m}^2) \to \ln(-\hat{m}^2 + i0)$. For the convolution of the additional UV and IR finite piece $\delta\tilde{F}^{(1)}_{M,\mathrm{SCET},m}(M,m)$ we get

$$\delta\tilde{F}^{(n_l+1,2)}_{\mathrm{SCET},m} = \frac{\left(\alpha_s^{(n_l+1)}\right)^2 C_F T_F}{16\pi^2}\left\{\frac{1241}{81} - \frac{56\pi^2}{27} + \frac{16}{3}\zeta_3\right\}. \tag{F.18}$$

This allows us to compute the threshold correction $\mathcal{M}_{C_m}(Q,m,\mu_m)$ via Eq. (4.164),

$$\mathcal{M}^{(2)}_{C_m}(Q,m,\mu_m) = \mathcal{M}^{(2)}_{\tilde{C}}(Q,m,\mu_m) + \delta\tilde{F}^{(n_l+1,2)}_{\mathrm{SCET},m}\,, \tag{F.19}$$

where $\mathcal{M}^{(2)}_{\tilde{C}}$ is the matching coefficient for primary massless quarks at $\mathcal{O}(\alpha_s^2 C_F T_F)$ appearing in Eq. (5.27). Thus the only modification in the mass mode threshold correction for primary massive quarks with respect to primary massless quarks is just a constant. If we write the matching coefficient $C_m(Q,m,\mu_m)$ between bHQET and SCET in the n_l-flavor scheme for α_s, we obtain

$$C^{(n_l,2)}_{m,T_F}(Q,m,\mu_m) = \mathcal{M}^{(2)}_{C_m}(Q,m,\mu_m)\,, \tag{F.20}$$

since the coefficient $\tilde{C}^{(n_l)}_m(m,\mu_m)$ in Eq. (F.2) does not contain any information about the secondary massive flavor. For convenience we display the result also in the (n_l+1)-flavor scheme, which is given by ($L_m \equiv \ln(m^2/\mu_m^2)$, $\alpha_s^{(n_l+1)} \equiv \alpha_s^{(n_l+1)}(\mu_m)$),

$$C^{(n_l+1,2)}_{m,T_F}(Q,m,\mu_m) = \mathcal{M}^{(2)}_{C_m}(Q,m,\mu_m) + \frac{\alpha_s^{(n_l+1)} T_F}{3\pi} L_m\, C^{(n_l+1,1)}_m(m,\mu_m)\,, \tag{F.21}$$

where the one-loop matching coefficient $C^{(n_l+1,1)}_m(m,\mu_m)$ reads [9]

$$C^{(n_l+1,1)}_m(m,\mu_m) = \frac{\alpha_s^{(n_l+1)} C_F}{4\pi}\left\{L_m^2 - L_m + 4 + \frac{\pi^2}{6}\right\}. \tag{F.22}$$

Plugging in Eqs. (4.166), (F.18) and (F.22) into Eq. (F.21) we obtain at fixed order

$$C^{(n_l+1,2)}_{m,T_F}(Q,m,\mu_m) = \frac{\left(\alpha_s^{(n_l+1)}\right)^2 C_F T_F}{16\pi^2}\left\{\left(\frac{4}{3}L_m^2 + \frac{40}{9}L_m + \frac{112}{27}\right)\ln\!\left(-\frac{m^2}{Q^2}\right) + \frac{4}{9}L_m^3 - \frac{14}{9}L_m^2 + \left(\frac{274}{27} + \frac{8\pi^2}{9}\right)L_m + \frac{5107}{162} - \frac{41\pi^2}{27} - \frac{4}{9}\zeta_3\right\}. \tag{F.23}$$

[7] Note that compared to the result in Eq. (4.76) there is a slight modification due to the different pole prescriptions corresponding to the analytic continuation from a spacelike to a timelike process.

Note that the terms involving the rapidity logarithm $\ln(m^2/Q^2)$ are exactly the same as for massless primary quarks and can be dealt with along the lines of Sec. 4.4.1. As a cross-check we remark that the result in Eq. (F.23) is consistent with the difference of the RG evolution of the currents in bHQET and SCET (in analogy to Eq. (4.180)), i.e.

$$\begin{aligned}\mu\frac{\mathrm{d}}{\mathrm{d}\mu}\,C_m^{(n_l+1)}(Q,m,\mu_m)\Big|_{\alpha_s^2C_FT_F} &= -\,\Big(\gamma_{\tilde{C}}^{(n_l+1)}(Q,\mu)-\gamma_m^{(n_l)}(Q,m,\mu)\Big)\,C_m^{(n_l+1)}(Q,m,\mu_m)\Big|_{\alpha_s^2C_FT_F}\\ &= \frac{\alpha_s^{(n_l+1)}T_F}{3\pi}\,L_m\gamma_m^{(n_l+1,1)}(Q,m,\mu)-\gamma_{\tilde{C},T_F}^{(n_l+1,2)}(Q,\mu)\,.\end{aligned}\tag{F.24}$$

Here the anomalous dimension $\gamma_{\tilde{C}}^{(n_l+1)}$ at $\mathcal{O}(\alpha_s^2C_FT_F)$ related to the SCET current is given in analogy to Eq. (4.29). The one-loop anomalous dimension $\gamma_m^{(n_f,1)}$ related to the bHQET current is given by [9]

$$\gamma_m^{(n_f,1)}(Q,m,\mu)=\frac{\alpha_s^{(n_f)}C_F}{4\pi}\left\{4\ln\left(-\frac{Q^2}{m^2}\right)-4\right\}\,,\tag{F.25}$$

with the corresponding evolution equation

$$\mu\frac{\mathrm{d}}{\mathrm{d}\mu}\,U_m^{(n_f)}(Q,m,\mu_m,\mu)=\gamma_m^{(n_f)}(Q,m,\mu)\,U_m^{(n_f)}(Q,m,\mu_m,\mu)\,.\tag{F.26}$$

We note that one can perform the computation of the matching coefficient C_m without computing any SCET diagrams by exploiting the fact that the infrared structure of QCD is fully contained in the corresponding EFT description. The two-loop QCD result for the form factor was computed in Refs. [127, 128] [8] and the $\mathcal{O}(\alpha_s^2C_FT_F)$ correction can be also found in Ref. [70]. Using dimensional regularization as an IR regulator the bHQET diagrams are scaleless, such that C_m can be extracted from the expanded QCD result for $m\ll Q$ and the hard current matching between SCET and QCD. Our result in Eq. (F.23) agrees with this calculation that will be described in more detail in a future publication [13]. We note that the UV finite difference between primary massive and primary massless quarks $\delta\tilde{F}_{\mathrm{SCET},m}^{(n_l+1,2)}$ given in Eq. (F.18) can be also directly read off from the difference of Eqs. (1.74) and Eq. (1.64) in Ref. [70].

F.3 Consistency relations

Let us reconsider the bHQET factorization theorem in Eq. (F.1), where we now want to use a final renormalization scale that is above the mass scale, i.e. $\mu>\mu_m$,

$$\begin{aligned}\frac{1}{\sigma_0}\frac{\mathrm{d}\sigma}{\mathrm{d}\tau} &= Q\,m^2\,\Big|\tilde{C}^{(n_l+1)}(Q,\mu_H)\Big|^2\,\Big|U_{\tilde{C}}^{(n_l+1)}(Q,\mu_H,\mu)\Big|^2\int\mathrm{d}\hat{s}\int\mathrm{d}\hat{s}'\int\mathrm{d}\hat{s}''\int\mathrm{d}\hat{s}'''\,U_{J_\tau}^{(n_l+1)}(m\hat{s}''',\mu,\mu_m)\\ &\times C_{m,J}(m\hat{s}''-m\hat{s}''',m,\mu_m)\,U_{B_\tau}^{(n_l)}(\hat{s}'-\hat{s}'',\mu_m,\mu_B)\,B_\tau^{(n_l)}(\hat{s}-\hat{s}',\mu_B)\\ &\times\int\mathrm{d}\ell\int\mathrm{d}\ell'\int\mathrm{d}\ell''\,U_{S_\tau}^{(n_l+1)}(\ell'',\mu,\mu_m)\,C_{m,S}(\ell'-\ell'',m,\mu_m)\,U_{S_\tau}^{(n_l)}(\ell-\ell',\mu_m,\mu_S)\\ &\times S_\tau^{(n_l)}\left(Q\tau-\frac{2m^2}{Q}-\frac{m\hat{s}}{Q}-\ell,\mu_S\right)\,.\end{aligned}\tag{F.27}$$

Here $C_{m,J}(s,m,\mu)$ and $C_{m,S}(\ell,m,\mu)$ denote the matching coefficients between the jet and soft functions in bHQET and SCET,

$$J_\tau^{(n_l+1)}(m\hat{s},m,\mu)=\int\mathrm{d}\hat{s}'\,C_{m,J}(m\hat{s}-m\hat{s}',m,\mu)\,B_\tau^{(n_l)}(\hat{s}',\mu)+\mathcal{O}\left(\frac{\hat{s}}{m}\right)\,,\tag{F.28}$$

$$S_\tau^{(n_l+1)}(\ell,m,\mu)=\int\mathrm{d}\ell'\,C_{m,S}(\ell-\ell',m,\mu)\,S_\tau^{(n_l)}(\ell',\mu)+\mathcal{O}\left(\frac{\ell}{m}\right)\,.\tag{F.29}$$

[8] Note that the result in Ref. [127] is not given in the $\overline{\mathrm{MS}}$ scheme, since an additional factor $\Gamma[1+\epsilon]$ is included in the renormalization constants of the strong coupling.

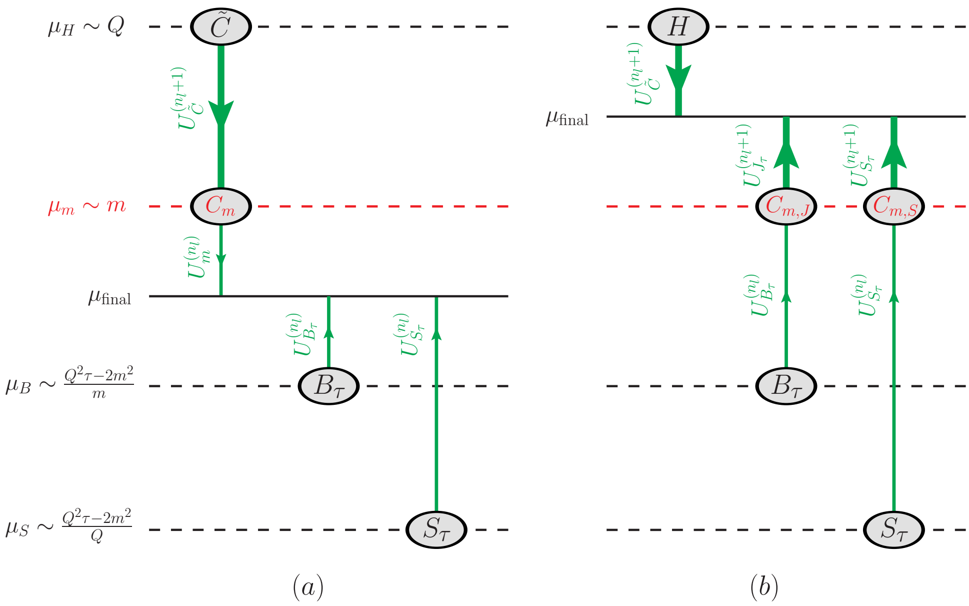

Figure F.2: Illustration of the different RG setups for the bHQET factorization setup leading to the consistency relations mentioned in the text. We display the cases where the final renormalization scale $\mu_{\rm final}$ satisfies (a) $\mu_m > \mu_{\rm final} > \mu_B$ and (b) $\mu_H > \mu_{\rm final} > \mu_m$.

Note that the matching including mass mode effects involves convolutions in contrast to the purely multiplicative form proposed in Ref. [9].

The two different ways of evolution are displayed in Fig. F.2. Since the final renormalization scale is arbitrary, both factorization theorems in Eqs. (F.1) and (F.27) are equivalent. On the one hand this implies relations between the anomalous dimensions in SCET (see Eq. (5.16)) and in bHQET (see Ref. [9]). On the other hand we also get a consistency relation for the matching coefficients C_m, $C_{m,J}$ and $C_{m,S}$,

$$|C_m(Q,m,\mu)|^2\,\delta(m\hat{s}) = \int \mathrm{d}\ell\, C_{m,J}(m\hat{s}-Q\ell,m,\mu)\, C_{m,S}(\ell,m,\mu)\,, \tag{F.30}$$

which is in the spirit of Eqs. (4.217) and (5.98).

In the following we want to check Eq. (F.30) by providing explicit expressions for the matching functions $C_{m,J}(s,m,\mu)$ and $C_{m,S}(\ell,m,\mu)$ at $\mathcal{O}(\alpha_s^2 C_F T_F)$. Due to the fact that the soft function does not contain any dependence on the primary quark mass, the corresponding matching correction contains just purely secondary mass effects and is thus the same as the threshold correction for primary massless quarks $\mathcal{M}_{S_\tau}$ given in Eq. (5.103) at fixed $\mathcal{O}(\alpha_s^2 C_F T_F)$. Thus we will only have to compute the $\mathcal{O}(\alpha_s^2 C_F T_F)$ massive quark corrections to the jet function matching correction.

We start with the calculation of the jet function for the radiation of a massive gluon given by the diagrams in Fig. F.3, where for the case of a primary massive quark also a mass counterterm on the internal fermion line has to be taken into account. Here we will perform the computation just for the distributive contributions corresponding to virtual radiation, since the real gluon radiation corrections containing the threshold $s=(m+M)^2$ for the single jet invariant mass are tedious, which especially concerns the subsequent dispersive integration, and are not required for the matching procedure. For diagram J_a we obtain

$$J_{a,m} = -\frac{2g^2C_F}{\pi(s-m^2+i\epsilon)}\tilde{\mu}^{2\epsilon}\int\frac{\mathrm{d}^dk}{(2\pi)^d}\,\frac{1}{[k^-+i\epsilon]}\,\frac{1}{[k^2-M^2+i\epsilon]}\,\frac{Q-k^-}{[s(1-k^-/Q)-Qk^++k^2-m^2+i\epsilon]}\,. \tag{F.31}$$

Figure F.3: Non-vanishing EFT diagrams for the computation of the jet function with primary massive quarks and a secondary massive gluon. The required soft-bin subtractions are implicit. Concerning $J_{a,m}$ also the right-symmetric diagram has to be taken into account.

The corresponding soft-bin subtraction reads

$$J_{a,m,0M} = -\frac{2g^2 C_F}{\pi(s-m^2+i\epsilon)}\tilde{\mu}^{2\epsilon}\int\frac{\mathrm{d}^d k}{(2\pi)^d}\,\frac{1}{[k^-+i\epsilon]}\,\frac{1}{[k^2-M^2+i\epsilon]}\,\frac{Q}{[s-Qk^--m^2+i\epsilon]}\,. \tag{F.32}$$

Notice that as in Sec. 4.3.2 we have kept the jet invariant mass s and here also the mass m in the expression of the soft-bin subtraction, although they seem at first sight formally suppressed. However, since the interaction with a mode scaling like $Q(\lambda_m,\lambda_m,\lambda_m)$ would "kick" them out from their natural scaling, their parametric scaling changes. This is indeed exactly the contribution we have to subtract to get an expression for the jet function that contains only fluctuations around the jet scale.

In analogy to the current diagrams we decompose $J_{a,m}$ into singular contributions in d dimensions for primary massless (internal) quarks with an offshellness $s-m^2$, which we denote by $J_{a,m}^{(0m)}$, and a UV-finite difference,

$$J_{a,m} = J_{a,m}^{(0m)} + (J_{a,m} - J_{a,m}^{(0m)})\,. \tag{F.33}$$

The difference correction between the proper and the modified integrand reads ($a=\sqrt{1-4m^2/M^2}$)

$$\begin{aligned}
J_{a,m} - J_{a,m}^{(0m)} =& -\frac{2i}{\pi(s-m^2+i\epsilon)}\,\frac{\alpha_s C_F}{4\pi}\,\Gamma\left(2-\frac{d}{2}\right)\left(\frac{\mu^2 e^{\gamma_E}}{M^2}\right)^{2-\frac{d}{2}}\int_0^1 dz\,\frac{1-z}{z}\\
&\times\left[\left(1-z\left(1+\frac{s-m^2}{M^2}\right)+\frac{s}{M^2}z^2\right)^{\frac{d}{2}-2}-\left(1-z\left(1+\frac{s-m^2}{M^2}\right)+\frac{s-m^2}{M^2}z^2\right)^{\frac{d}{2}-2}\right]\\
=&\,\frac{2i}{\pi(s-m^2+i\epsilon)}\,\frac{\alpha_s C_F}{4\pi}\Bigg\{\ln\left(\frac{1+a}{2}\right)\ln\left(\frac{1-a}{2}\right)+\frac{1+a}{1-a}\ln\left(\frac{1+a}{2}\right)+\frac{1-a}{1+a}\ln\left(\frac{1-a}{2}\right)\\
&+1+\mathcal{O}\left(\epsilon,(s-m^2)^0\right)\Bigg\}\,.
\end{aligned} \tag{F.34}$$

In the second equality we have expanded for $\epsilon\to 0$ and around $s=m^2$ to obtain the singular distributive corrections. This yields the same integral as in Eq. (F.6) for the hard current form factor. For $J_{a,m}^{(0m)}$ and the corresponding soft-bin subtraction $J_{a,m,0M}$ we obtain the same results as in Eqs. (4.101) and (4.102) apart from a shift in the variable $s\to s-m^2$.

In a similar way, the result for the virtual corrections in the diagrams $J_{b,m}$ and $J_{c,m}$ can be inferred from the result for the corresponding primary massless diagrams $J_{b,m}^{(0m)}$ and $J_{c,m}^{(0m)}$ which can be read off in their sum from Eq. (4.103) with $s\to s-m^2$, and a UV finite difference. The latter is related to the difference of the wave-function renormalizations in Eq. (F.14),

$$J_{b+c,m} - J_{b+c,m}^{(0m)} = -\frac{i}{\pi(s-m^2+i\epsilon)}\left[\frac{2m\,\delta m_M^{(\mathrm{OS},1)}}{s-m^2+i\epsilon}+\left(Z_{\xi,m}^{(1)}-Z_{\xi,m=0}^{(1)}\right)+\mathcal{O}\left(\epsilon,(s-m^2)^0\right)\right]\,. \tag{F.35}$$

Finally, also one insertion of the mass counterterm δm_M (in an arbitrary mass scheme) on the internal quark line has to be taken into account yielding

$$J_{\delta m} = \frac{i}{\pi(s-m^2+i\epsilon)^2}\,2m\,\delta m_M^{(1)}\,. \tag{F.36}$$

Summing up all corrections and taking the discontinuity gives for the one-loop virtual massive gluon corrections for the (single direction) jet function ($t = s - m^2$)

$$\begin{aligned} J^{(\text{bare},1)}_{M,m,\text{virt}}(t,m,M,\mu) &= \text{Disc}\Big[2(J^{(0m)}_{a,m} - J_{a,m,0M}) + J^{(0m)}_{b+c,m} + 2(J_{a,m} - J^{(0m)}_{a,m}) + (J_{b+c,m} - J^{(0m)}_{b+c,m}) + J_{\delta m}\Big] \\ &= J^{(\text{bare},1)}_{M,\text{virt}}(t,M,\mu) + \delta(t)\,\delta\tilde{F}^{(1)}_{M,\text{SCET},m}(M,m) - 2m\,\delta^{(1)}_{m,M}\,\delta'(t)\,. \end{aligned} \tag{F.37}$$

with $J^{(\text{bare},1)}_{M,\text{virt}}(t,M,\mu)$ and $\delta\tilde{F}^{(1)}_{M,\text{SCET},m}(M,m)$ given in Eqs. (4.106) and (F.17), respectively. Here $\delta_{m,M} \equiv \delta m_M - \delta m^{(\text{OS})}_M$ denotes the difference between the employed mass scheme and the OS scheme. Furthermore, we note again that since all of the plus-distributions are encoded fully in the first contribution, any arising rapidity logarithms have to agree with the case of primary massless quarks.

Performing the dispersive integral for the jet function along the lines of Eq. (4.187) we obtain for the virtual piece of the two-loop jet function ($\bar{t} = t/\mu^2$) [9]

$$\begin{aligned} \mu^2 J^{(n_l,\text{bare},2)}_{m,\text{virt}}(t,m,\mu) &= \frac{\big(\alpha_s^{(n_l)}\big)^2 C_F T_F}{(4\pi)^2}\bigg\{\delta(\bar{t})\bigg[\frac{4}{\epsilon^3} + \frac{1}{\epsilon^2}\bigg(-\frac{16}{3}L_m - \frac{2}{9}\bigg) + \frac{1}{\epsilon}\bigg(\frac{8}{3}L_m^2 - 4L_m - \frac{121}{27} + \frac{2\pi^2}{9}\bigg) \\ &\quad + \frac{76}{9}L_m^2 + \frac{466}{27}L_m + \frac{7075}{162} - \frac{37\pi^2}{27} - \frac{16}{3}\zeta_3\bigg] + \bigg[\frac{\theta(\bar{t})}{\bar{t}}\bigg]_+\bigg[-\frac{8}{3\epsilon^2} + \frac{1}{\epsilon}\bigg(\frac{16}{3}L_m + \frac{40}{9}\bigg) \\ &\quad - \frac{16}{3}L_m^2 - \frac{80}{9}L_m - \frac{224}{27} - \frac{4\pi^2}{9}\bigg]\bigg\}\,. \end{aligned} \tag{F.38}$$

The corresponding OS counterterm cancels all virtual secondary massive corrections,

$$Z^{(n_l,2)}_{J,m}(s,m,\mu) = J^{(n_l,\text{bare},2)}_{m,\text{virt}}(t,m,\mu)\,. \tag{F.39}$$

Switching to the unsubtracted dispersion relation involves the unrenormalized massive jet function at one-loop, which reads [9]

$$\begin{aligned} \mu^2 J^{(\text{bare},1)}_{m}(t,m,\mu) &= \frac{\alpha_s C_F}{4\pi}\bigg\{\delta(\bar{t})\bigg[\frac{4}{\epsilon^2} + \frac{3}{\epsilon} + 2L_m^2 + L_m + 8 - \frac{\pi^2}{3}\bigg] - 4\bigg[\frac{\theta(\bar{t})}{\bar{t}}\bigg]\bigg[\frac{1}{\epsilon} + L_m + 1\bigg] \\ &\quad + 8\bigg[\frac{\theta(\bar{t})\ln\bar{t}}{\bar{t}}\bigg]_+ + \mathcal{O}\big(\epsilon, t^0\big)\bigg\} - \frac{2m\,\delta^{(1)}_m}{\mu^2}\,\delta'(\bar{t})\,, \end{aligned} \tag{F.40}$$

with δ_m defined in analogy to the massive gluon case. Thus the corresponding contribution at $\mathcal{O}(\alpha_s^2 C_F T_F)$ needed to change from the n_l to the (n_l+1)-flavor scheme reads [10]

$$\begin{aligned} \mu^2 J^{(n_l\to n_l+1,2)}_{m}(t,m,\mu) &= -\bigg(\Pi(m^2,0) - \frac{\alpha_s T_F}{3\pi}\frac{1}{\epsilon}\bigg)\mu^2 J^{(\text{bare},1)}_m(t,m,\mu) - \frac{2m(\delta m^{(n_l+1,2)} - \delta m^{(n_l,2)})}{\mu^2}\,\delta'(\bar{t}) \\ &= \frac{\alpha_s^2 C_F T_F}{(4\pi)^2}\bigg\{\delta(\bar{t})\bigg[\frac{16}{3\epsilon^2}L_m + \frac{1}{\epsilon}\bigg(-\frac{8}{3}L_m^2 + 4L_m - \frac{4\pi^2}{9}\bigg) + \frac{32}{9}L_m^3 - \frac{2}{3}L_m^2 \\ &\quad + \frac{32}{3}L_m - \frac{\pi^2}{3} + \frac{16}{9}\zeta_3\bigg] + \bigg[\frac{\theta(\bar{t})}{\bar{t}}\bigg]_+\bigg[-\frac{16}{3\epsilon}L_m - \frac{8}{3}L_m^2 - \frac{16}{3}L_m + \frac{4\pi^2}{9}\bigg] \\ &\quad + \frac{32}{3}L_m\bigg[\frac{\theta(\bar{t})\ln\bar{t}}{\bar{t}}\bigg]_+\bigg\} - \delta'(\bar{t})\,\frac{2m}{\mu^2}\bigg[\delta m^{(n_l+1,2)} - \delta m^{(n_l,2)} + \frac{\alpha_s T_F}{3\pi}\,L_m\,\delta^{(1)}_m\bigg]\,. \end{aligned} \tag{F.41}$$

[9] Besides α_s we also employ the mass in the n_l scheme, i.e. $m = m^{(n_l)}(\mu)$ with $\delta m^{(n_l,2)}_{T_F} = \delta m^{(\text{OS},2)}_{T_F}$ for the secondary massive flavor corrections.

[10] Our conclusions do not rely on the specific expressions of $\delta m^{(n_l+1,2)}$ and $\delta m^{(n_l,2)}$, so that any appropriate (renormalon-free) mass scheme can be picked. Here it is only important that the massive quark loops are renormalized in the n_l-scheme using low momentum subtraction and in the (n_l+1)-scheme by same renormalization condition as massless quark loops.

The virtual corrections to the jet function at $\mathcal{O}(\alpha_s^2 C_F T_F)$ which are renormalized in the $\overline{\rm MS}$ scheme by the counterterm contribution in Eq. (4.19) read for the complete thrust jet function

$$\begin{aligned}\mu^2 J^{(n_l+1,2)}_{\tau,m,\rm virt}(t,m,\mu) =&\, 2\left(\mu^2 J^{(n_l,\rm bare,2)}_{m,\rm virt}(t,m,\mu) + \mu^2 J^{(n_l\to n_l+1,2)}_{m}(t,m,\mu) - \mu^2 Z^{(n_l+1,2)}_{J,T_F}(t,\mu)\right)\\ =&\, \frac{\big(\alpha_s^{(n_l+1)}\big)^2 C_F T_F}{(4\pi)^2}\bigg\{\delta(\bar t)\left[\frac{64}{9}L_m^3 + \frac{140}{9}L_m^2 + \frac{1508}{27}L_m + \frac{7075}{81} - \frac{92\pi^2}{27} - \frac{64}{9}\zeta_3\right]\\ &+\left[\frac{\theta(\bar t)}{\bar t}\right]_+\left[-16L_m^2 - \frac{256}{9}L_m - \frac{448}{27}\right] + \frac{64}{3}L_m\left[\frac{\theta(\bar t)\ln\bar t}{\bar t}\right]_+\bigg\}\\ &-\delta'(\bar t)\,\frac{4m^{(n_l+1)}}{\mu^2}\left[\delta m^{(n_l+1,2)} - \delta m^{(n_l,2)} + \frac{\alpha_s^{(n_l+1)}T_F}{3\pi}\,L_m\,\delta_m^{(1)}\right].\end{aligned} \tag{F.42}$$

We are now ready to compute the matching correction between the SCET and bHQET jet function. In analogy to Eq. (F.2) it can be computed in two steps, by first switching the scheme of the SCET jet function from $\overline{\rm MS}$ to OS (with respect to the secondary massive contributions) giving rise to the threshold correction $\mathcal{M}_{J_\tau,m}(t,m,\mu)$ and then matching it afterwards to the corresponding bHQET jet function,

$$C_{m,J}(t,m,\mu) = \mathcal{M}_{J_\tau,m}(t,m,\mu)\,\tilde C^{(n_l)}_{m,J}(m,\mu)\,. \tag{F.43}$$

The threshold correction $\mathcal{M}_{J_\tau,m}$ can be easily obtained similar to Eq. (4.195) from the results in Eqs. (F.38) and (F.42) taking into account that the strong coupling constant and mass are displayed in different schemes. [11] The decoupling relation between the masses is given by

$$m^{(n_l)}(\mu_m) = m^{(n_l+1)}(\mu_m) + \delta m^{(n_l+1,2)} - \delta m^{(n_l,2)} + \frac{\alpha_s^{(n_l+1)}T_F}{3\pi}\,L_m\,\delta_m^{(n_l+1,1)} + \mathcal{O}(\alpha_s^3)\,. \tag{F.44}$$

This yields

$$\begin{aligned}\mathcal{M}_{J_\tau,m}(t,m,\mu_m) =&\, \delta\big(t\big) + J^{(n_l+1,2)}_{\tau,m,\rm virt}(t,m,\mu) - \frac{\alpha_s T_F}{3\pi}\,L_m\,J^{(n_l+1,1)}_{\tau,m}(t,m,\mu)\\ &+\delta'\big(t\big)\,4m\left[\delta m^{(n_l+1,2)} - \delta m^{(n_l,2)} + \frac{\alpha_s^{(n_l+1)}T_F}{3\pi}\,L_m\,\delta_m^{(n_l+1,1)}\right].\end{aligned} \tag{F.45}$$

At $\mathcal{O}(\alpha_s^2 C_F T_F)$ in the fixed-order expansion one obtains

$$\begin{aligned}\mu_m^2\,\mathcal{M}^{(2)}_{J_\tau,m}(t,m,\mu_m) =&\, \frac{\alpha_s^2 C_F T_F}{(4\pi)^2}\bigg\{\delta(\bar t)\left[\frac{16}{9}L_m^3 + \frac{116}{9}L_m^2 + \left(\frac{932}{27} + \frac{8\pi^2}{9}\right)L_m + \frac{7075}{81} - \frac{92\pi^2}{27} - \frac{64}{9}\zeta_3\right]\\ &+\left[\frac{\theta(\bar t)}{\bar t}\right]_+\left[-\frac{16}{3}L_m^2 - \frac{160}{9}L_m - \frac{448}{27}\right]\bigg\}\,.\end{aligned} \tag{F.46}$$

In the n_l-scheme we have

$$C^{(n_l,2)}_{m,J,T_F}(t,m,\mu_m) = \mathcal{M}^{(2)}_{J_\tau,m}(t,m,\mu_m)\,. \tag{F.47}$$

To write the expression for $C_{m,J}$ at $\mathcal{O}(\alpha_s^2 C_F T_F)$ in the (n_l+1)-scheme we need the one-loop term of the matching factor $\tilde C_{m,J}(m,\mu)$ in Eq. (F.43). In fact $\tilde C^{(n_l)}_{m,J}$ is identical to $|\tilde C^{(n_l)}_m|^2$ with $\tilde C^{(n_l)}_m$ contributing to the current matching coefficient (see Eq. (F.2)) which follows from the fact that the soft function in bHQET agrees with the soft function in SCET in the n_l scheme and from the consistency relation in Eq. (F.30). At one-loop, where no secondary mass mode corrections enter, this has been shown by an

[11] Note that $\mathcal{M}_{J_\tau,m}$ is here defined by the inverse ratio with respect to $\mathcal{M}_J$ in Eq. (4.195).

explicit computation in Ref. [9]. Thus, using Eq. (F.22) $C_{m,J}(t,m,\mu)$ is given at $\mathcal{O}(\alpha_s^2 C_F T_F)$ in the (n_l+1)-scheme for the strong coupling by

$$\begin{aligned}\mu_m^2 C_{m,J,T_F}^{(n_l+1,2)}(t,m,\mu_m) &= \mu_m^2\, \mathcal{M}_{J_\tau,m}^{(2)}(t,m,\mu_m) + \frac{2\alpha_s^{(n_l+1)} T_F}{3\pi}\, L_m\, \tilde{C}_m^{(n_l+1,1)}(m,\mu_m)\, \delta(\bar{t}) \\ &= \frac{\big(\alpha_s^{(n_l+1)}\big)^2 C_F T_F}{(4\pi)^2} \bigg\{ \delta(\bar{t}) \bigg[\frac{40}{9} L_m^3 + \frac{92}{9} L_m^2 + \bigg(\frac{1220}{27} + \frac{4\pi^2}{3} \bigg) L_m + \frac{7075}{81} \\ &\quad - \frac{92\pi^2}{27} - \frac{64}{9}\zeta_3 \bigg] + \bigg[\frac{\theta(\bar{t})}{\bar{t}} \bigg]_+ \bigg[-\frac{16}{3} L_m^2 - \frac{160}{9} L_m - \frac{448}{27} \bigg] \bigg\}\,. \end{aligned} \tag{F.48}$$

Inserting the results for the matching coefficients between SCET and bHQET in Eqs. (F.23), (F.48) and (5.103) into Eq. (F.30) we can confirm explicitly that the consistency relation is satisfied at $\mathcal{O}(\alpha_s^2 C_F T_F)$.

Bibliography

[1] M. Aivazis, J. C. Collins, F. I. Olness, and W.-K. Tung, "Leptoproduction of heavy quarks. 2. A Unified QCD formulation of charged and neutral current processes from fixed target to collider energies," *Phys. Rev.* **D50** (1994) 3102–3118, `arXiv:hep-ph/9312319 [hep-ph]`.

[2] M. Aivazis, F. I. Olness, and W.-K. Tung, "Leptoproduction of heavy quarks. 1. General formalism and kinematics of charged current and neutral current production processes," *Phys. Rev.* **D50** (1994) 3085–3101, `arXiv:hep-ph/9312318 [hep-ph]`.

[3] F. Olness and I. Schienbein, "Heavy Quarks: Lessons Learned from HERA and Tevatron," *Nucl.Phys.Proc.Suppl.* **191** (2009) 44–53, `arXiv:0812.3371 [hep-ph]`.

[4] R. Abbate, M. Fickinger, A. H. Hoang, V. Mateu, and I. W. Stewart, "Thrust at N^3LL with Power Corrections and a Precision Global Fit for $\alpha_s(m_Z)$," *Phys. Rev.* **D83** (2011) 074021, `arXiv:1006.3080 [hep-ph]`.

[5] R. Abbate, M. Fickinger, A. H. Hoang, V. Mateu, and I. W. Stewart, "Precision Thrust Cumulant Moments at N^3LL," *Phys.Rev.* **D86** (2012) 094002, `arXiv:1204.5746 [hep-ph]`.

[6] V. S. Fadin and V. A. Khoze, "Threshold Behavior of Heavy Top Production in e+ e- Collisions," *JETP Lett.* **46** (1987) 525–529.

[7] A. Hoang, M. Beneke, K. Melnikov, T. Nagano, A. Ota, *et al.*, "Top - anti-top pair production close to threshold: Synopsis of recent NNLO results," *Eur.Phys.J.direct* **C2** (2000) 1, `arXiv:hep-ph/0001286 [hep-ph]`.

[8] S. Fleming, A. H. Hoang, S. Mantry, and I. W. Stewart, "Jets from massive unstable particles: Top-mass determination," *Phys. Rev.* **D77** (2008) 074010, `arXiv:hep-ph/0703207 [hep-ph]`.

[9] S. Fleming, A. H. Hoang, S. Mantry, and I. W. Stewart, "Top Jets in the Peak Region: Factorization Analysis with NLL Resummation," *Phys. Rev.* **D77** (2008) 114003, `arXiv:0711.2079 [hep-ph]`.

[10] S. Gritschacher, A. H. Hoang, I. Jemos, and P. Pietrulewicz, "Secondary Heavy Quark Production in Jets through Mass Modes," *Phys.Rev.* **D88** (2013) 034021, `arXiv:1302.4743 [hep-ph]`.

[11] S. Gritschacher, A. Hoang, I. Jemos, and P. Pietrulewicz, "Two loop soft function for secondary massive quarks," *Phys.Rev.* **D89** (2014) 014035, `arXiv:1309.6251 [hep-ph]`.

[12] P. Pietrulewicz, S. Gritschacher, A. H. Hoang, I. Jemos, and V. Mateu, "Variable Flavor Number Scheme for Final State Jets in Thrust," *accepted for publication in Phys.Rev.D* (2014) , `arXiv:1405.4860 [hep-ph]`.

[13] A. Hoang, A. Pathak, P. Pietrulewicz, and I. W. Stewart, "in preparation,".

[14] A. Hoang, P. Pietrulewicz, and D. Samitz, "in preparation,".

[15] A. H. Hoang, P. Pietrulewicz, and D. Samitz, "Variable Flavor Number Scheme for Final State Jets," `arXiv:1406.5885 [hep-ph]`.

[16] I. Wolfram Research, "Mathematica Version 9.0,".

[17] T. Huber and D. Maitre, "HypExp: A Mathematica package for expanding hypergeometric functions around integer-valued parameters," *Comput.Phys.Commun.* **175** (2006) 122–144, `arXiv:hep-ph/0507094 [hep-ph]`.

[18] D. Binosi, J. Collins, C. Kaufhold, and L. Theussl, "JaxoDraw: A Graphical user interface for drawing Feynman diagrams. Version 2.0 release notes," *Comput.Phys.Commun.* **180** (2009) 1709–1715, `arXiv:0811.4113 [hep-ph]`.

[19] A. Pich, "Effective field theory: Course," `arXiv:hep-ph/9806303 [hep-ph]`.

[20] A. V. Manohar and M. B. Wise, "Heavy quark physics," *Camb.Monogr.Part.Phys.Nucl. Phys.Cosmol.* **10** (2000) 1–191.

[21] C. W. Bauer, S. Fleming, and M. E. Luke, "Summing Sudakov logarithms in $B \to X_s\gamma$ in effective field theory," *Phys. Rev.* **D63** (2000) 014006, `arXiv:hep-ph/0005275 [hep-ph]`.

[22] C. W. Bauer, S. Fleming, D. Pirjol, and I. W. Stewart, "An Effective field theory for collinear and soft gluons: Heavy to light decays," *Phys. Rev.* **D63** (2001) 114020, `arXiv:hep-ph/0011336 [hep-ph]`.

[23] C. W. Bauer and I. W. Stewart, "Invariant operators in collinear effective theory," *Phys.Lett.* **B516** (2001) 134–142, `arXiv:hep-ph/0107001 [hep-ph]`.

[24] C. W. Bauer, D. Pirjol, and I. W. Stewart, "Soft collinear factorization in effective field theory," *Phys. Rev.* **D65** (2002) 054022, `arXiv:hep-ph/0109045 [hep-ph]`.

[25] I. W. Stewart, "Effective field theory: Course," *MIT OpenCourseWare 8.851* (2013) .

[26] S. Gritschacher, "Massive gluino effects in event shape distributions," *diploma thesis* (2011) .

[27] M. Beneke, A. Chapovsky, M. Diehl, and T. Feldmann, "Soft collinear effective theory and heavy to light currents beyond leading power," *Nucl.Phys.* **B643** (2002) 431–476, `arXiv:hep-ph/0206152 [hep-ph]`.

[28] M. Beneke and T. Feldmann, "Multipole expanded soft collinear effective theory with nonAbelian gauge symmetry," *Phys.Lett.* **B553** (2003) 267–276, `arXiv:hep-ph/0211358 [hep-ph]`.

[29] A. V. Manohar and I. W. Stewart, "The Zero-Bin and Mode Factorization in Quantum Field Theory," *Phys. Rev.* **D76** (2007) 074002, `arXiv:hep-ph/0605001 [hep-ph]`.

[30] C. W. Bauer, D. Pirjol, and I. W. Stewart, "On Power suppressed operators and gauge invariance in SCET," *Phys.Rev.* **D68** (2003) 034021, `arXiv:hep-ph/0303156 [hep-ph]`.

[31] A. K. Leibovich, Z. Ligeti, and M. B. Wise, "Comment on quark masses in SCET," *Phys. Lett.* **B564** (2003) 231–234, `arXiv:hep-ph/0303099 [hep-ph]`.

[32] A. V. Manohar, T. Mehen, D. Pirjol, and I. W. Stewart, "Reparameterization invariance for collinear operators," *Phys.Lett.* **B539** (2002) 59–66, `arXiv:hep-ph/0204229 [hep-ph]`.

[33] J. Chay, C. Kim, Y. G. Kim, and J.-P. Lee, "Soft Wilson lines in soft-collinear effective theory," *Phys.Rev.* **D71** (2005) 056001, `arXiv:hep-ph/0412110 [hep-ph]`.

[34] C. W. Bauer, D. Pirjol, and I. W. Stewart, "Factorization and endpoint singularities in heavy to light decays," *Phys.Rev.* **D67** (2003) 071502, `arXiv:hep-ph/0211069 [hep-ph]`.

[35] J.-Y. Chiu, A. Fuhrer, A. H. Hoang, R. Kelley, and A. V. Manohar, "Soft-Collinear Factorization and Zero-Bin Subtractions," *Phys. Rev.* **D79** (2009) 053007, `arXiv:0901.1332 [hep-ph]`.

[36] C. Marcantonini and I. W. Stewart, "Reparameterization Invariant Collinear Operators," *Phys.Rev.* **D79** (2009) 065028, `arXiv:0809.1093 [hep-ph]`.

[37] C. W. Bauer, S. Fleming, D. Pirjol, I. Z. Rothstein, and I. W. Stewart, "Hard scattering factorization from effective field theory," *Phys.Rev.* **D66** (2002) 014017, arXiv:hep-ph/0202088 [hep-ph].

[38] J.-Y. Chiu, F. Golf, R. Kelley, and A. V. Manohar, "Electroweak Corrections in High Energy Processes using Effective Field Theory," *Phys. Rev.* **D77** (2008) 053004, arXiv:0712.0396 [hep-ph].

[39] T. Becher and M. Neubert, "Drell-Yan production at small q_T, transverse parton distributions and the collinear anomaly," *Eur.Phys.J.* **C71** (2011) 1665, arXiv:1007.4005 [hep-ph].

[40] J.-Y. Chiu, A. Jain, D. Neill, and I. Z. Rothstein, "The Rapidity Renormalization Group," *Phys.Rev.Lett.* **108** (2012) 151601, arXiv:1104.0881 [hep-ph].

[41] J.-Y. Chiu, A. Jain, D. Neill, and I. Z. Rothstein, "A Formalism for the Systematic Treatment of Rapidity Logarithms in Quantum Field Theory," *JHEP* **1205** (2012) 084, arXiv:1202.0814 [hep-ph].

[42] R. K. Ellis, W. J. Stirling, and B. Webber, "QCD and collider physics," *Camb.Monogr.Part.Phys.Nucl.Phys.Cosmol.* **8** (1996) 1–435.

[43] I. Schienbein, V. A. Radescu, G. Zeller, M. E. Christy, C. Keppel, *et al.*, "A Review of Target Mass Corrections," *J.Phys.* **G35** (2008) 053101, arXiv:0709.1775 [hep-ph].

[44] R. K. Ellis, H. Georgi, M. Machacek, H. D. Politzer, and G. G. Ross, "Perturbation Theory and the Parton Model in QCD," *Nucl.Phys.* **B152** (1979) 285.

[45] J. C. Collins, D. E. Soper, and G. F. Sterman, "Factorization of Hard Processes in QCD," *Adv. Ser. Direct. High Energy Phys.* **5** (1988) 1–91, arXiv:hep-ph/0409313 [hep-ph].

[46] I. W. Stewart, F. J. Tackmann, and W. J. Waalewijn, "The Quark Beam Function at NNLL," *JHEP* **1009** (2010) 005, arXiv:1002.2213 [hep-ph].

[47] J. C. Collins and D. E. Soper, "Parton Distribution and Decay Functions," *Nucl.Phys.* **B194** (1982) 445.

[48] J. Vermaseren, A. Vogt, and S. Moch, "The Third-order QCD corrections to deep-inelastic scattering by photon exchange," *Nucl.Phys.* **B724** (2005) 3–182, arXiv:hep-ph/0504242 [hep-ph].

[49] W. A. Bardeen, A. Buras, D. Duke, and T. Muta, "Deep Inelastic Scattering Beyond the Leading Order in Asymptotically Free Gauge Theories," *Phys.Rev.* **D18** (1978) 3998.

[50] W. van Neerven and E. Zijlstra, "$\mathcal{O}(\alpha_s^2)$ contributions to the deep inelastic Wilson coefficient," *Phys.Lett.* **B272** (1991) 127–133.

[51] E. Zijlstra and W. van Neerven, "$\mathcal{O}(\alpha_s^2)$ QCD corrections to the deep inelastic proton structure functions F2 and F(L)," *Nucl.Phys.* **B383** (1992) 525–574.

[52] V. Gribov and L. Lipatov, "Deep inelastic e p scattering in perturbation theory," *Sov.J.Nucl.Phys.* **15** (1972) 438–450.

[53] G. Altarelli and G. Parisi, "Asymptotic Freedom in Parton Language," *Nucl.Phys.* **B126** (1977) 298.

[54] Y. L. Dokshitzer, "Calculation of the Structure Functions for Deep Inelastic Scattering and e+ e- Annihilation by Perturbation Theory in Quantum Chromodynamics.," *Sov.Phys.JETP* **46** (1977) 641–653.

[55] S. Moch, J. Vermaseren, and A. Vogt, "The Three loop splitting functions in QCD: The Nonsinglet case," *Nucl. Phys.* **B688** (2004) 101–134, `arXiv:hep-ph/0403192 [hep-ph]`.

[56] A. Vogt, S. Moch, and J. Vermaseren, "The Three-loop splitting functions in QCD: The Singlet case," *Nucl.Phys.* **B691** (2004) 129–181, `arXiv:hep-ph/0404111 [hep-ph]`.

[57] J. C. Collins, "Hard scattering factorization with heavy quarks: A General treatment," *Phys.Rev.* **D58** (1998) 094002, `arXiv:hep-ph/9806259 [hep-ph]`.

[58] J. C. Collins, F. Wilczek, and A. Zee, "Low-Energy Manifestations of Heavy Particles: Application to the Neutral Current," *Phys.Rev.* **D18** (1978) 242.

[59] D. Samitz, "Effective field theory approach to heavy flavor production in deep inelastic scattering," *master thesis* (2014) .

[60] M. Gluck, R. Godbole, and E. Reya, "Heavy flavor production at high-energy e p colliders," *Z.Phys.* **C38** (1988) 441.

[61] S. Kretzer and I. Schienbein, "Heavy quark initiated contributions to deep inelastic structure functions," *Phys.Rev.* **D58** (1998) 094035, `arXiv:hep-ph/9805233 [hep-ph]`.

[62] W.-K. Tung, S. Kretzer, and C. Schmidt, "Open heavy flavor production in QCD: Conceptual framework and implementation issues," *J.Phys.* **G28** (2002) 983–996, `arXiv:hep-ph/0110247 [hep-ph]`.

[63] R. Thorne and R. Roberts, "An Ordered analysis of heavy flavor production in deep inelastic scattering," *Phys.Rev.* **D57** (1998) 6871–6898, `arXiv:hep-ph/9709442 [hep-ph]`.

[64] R. Mertig, M. Bohm, and A. Denner, "FEYN CALC: Computer algebraic calculation of Feynman amplitudes," *Comput.Phys.Commun.* **64** (1991) 345–359.

[65] G. 't Hooft and M. Veltman, "Scalar One Loop Integrals," *Nucl.Phys.* **B153** (1979) 365–401.

[66] R. K. Ellis and G. Zanderighi, "Scalar one-loop integrals for QCD," *JHEP* **0802** (2008) 002, `arXiv:0712.1851 [hep-ph]`.

[67] B. A. Kniehl, M. Krawczyk, J. H. Kuhn, and R. Stuart, "Hadronic Contributions to $O(\alpha^2)$ Radiative Corrections in e^+e^- Annihilation," *Phys. Lett.* **B209** (1988) 337.

[68] A. Hoang, J. H. Kuhn, and T. Teubner, "Radiation of light fermions in heavy fermion production," *Nucl. Phys.* **B452** (1995) 173–187, `arXiv:hep-ph/9505262 [hep-ph]`.

[69] B. A. Kniehl, "Two Loop QED Vertex Correction From Virtual Heavy Fermions," *Phys.Lett.* **B237** (1990) 127.

[70] A. Hoang, "Applications of two loop calculations in the standard model and its minimal supersymmetric extension,".

[71] M. Buza, Y. Matiounine, J. Smith, R. Migneron, and W. van Neerven, "Heavy quark coefficient functions at asymptotic values $Q^2 \gg m^2$," *Nucl.Phys.* **B472** (1996) 611–658, `arXiv:hep-ph/9601302 [hep-ph]`.

[72] G. F. Sterman, "Summation of Large Corrections to Short Distance Hadronic Cross-Sections," *Nucl.Phys.* **B281** (1987) 310.

[73] A. V. Manohar, "Deep inelastic scattering as $x \to 1$ using soft collinear effective theory," *Phys.Rev.* **D68** (2003) 114019, `arXiv:hep-ph/0309176 [hep-ph]`.

[74] T. Becher, M. Neubert, and B. D. Pecjak, "Factorization and Momentum-Space Resummation in Deep-Inelastic Scattering," *JHEP* **0701** (2007) 076, `arXiv:hep-ph/0607228 [hep-ph]`.

[75] J. Chay and C. Kim, "Proper factorization theorems in high-energy scattering near the endpoint," *JHEP* **1309** (2013) 126, arXiv:1303.1637 [hep-ph].

[76] I. W. Stewart, F. J. Tackmann, and W. J. Waalewijn, "Factorization at the LHC: From PDFs to Initial State Jets," *Phys.Rev.* **D81** (2010) 094035, arXiv:0910.0467 [hep-ph].

[77] C. W. Bauer, S. P. Fleming, C. Lee, and G. F. Sterman, "Factorization of e^+e^- Event Shape Distributions with Hadronic Final States in Soft Collinear Effective Theory," *Phys. Rev.* **D78** (2008) 034027, arXiv:0801.4569 [hep-ph].

[78] S. Fleming and O. Zhang, "Rapidity Divergences and Deep Inelastic Scattering in the Endpoint Region," arXiv:1210.1508 [hep-ph].

[79] J. Chay and C. Kim, "Deep inelastic scattering near the endpoint in soft-collinear effective theory," *Phys.Rev.* **D75** (2007) 016003, arXiv:hep-ph/0511066 [hep-ph].

[80] A. Idilbi, X.-d. Ji, and F. Yuan, "Resummation of threshold logarithms in effective field theory for DIS, Drell-Yan and Higgs production," *Nucl.Phys.* **B753** (2006) 42–68, arXiv:hep-ph/0605068 [hep-ph].

[81] P.-y. Chen, A. Idilbi, and X.-d. Ji, "QCD Factorization for Deep-Inelastic Scattering At Large Bjorken $x_B \sim 1 - \mathcal{O}(\Lambda_{\mathrm{QCD}}/Q)$," *Nucl.Phys.* **B763** (2007) 183–197, arXiv:hep-ph/0607003 [hep-ph].

[82] S. Moch, J. Vermaseren, and A. Vogt, "The Quark form-factor at higher orders," *JHEP* **0508** (2005) 049, arXiv:hep-ph/0507039 [hep-ph].

[83] T. Becher and M. Neubert, "Toward a NNLO calculation of the $\bar{B} \to X_s\gamma$ decay rate with a cut on photon energy. II. Two-loop result for the jet function," *Phys. Lett.* **B637** (2006) 251–259, arXiv:hep-ph/0603140 [hep-ph].

[84] J. Ablinger, A. Behring, J. Blümlein, A. De Freitas, A. Hasselhuhn, *et al.*, "The 3-Loop Non-Singlet Heavy Flavor Contributions and Anomalous Dimensions for the Structure Function $F_2(x, Q^2)$ and Transversity," arXiv:1406.4654 [hep-ph].

[85] V. A. Smirnov, "Asymptotic expansions of two loop Feynman diagrams in the Sudakov limit," *Phys.Lett.* **B404** (1997) 101–107, arXiv:hep-ph/9703357 [hep-ph].

[86] T. Becher and G. Bell, "Analytic Regularization in Soft-Collinear Effective Theory," *Phys. Lett.* **B713** (2012) 41–46, arXiv:1112.3907 [hep-ph].

[87] A. Idilbi and T. Mehen, "On the equivalence of soft and zero-bin subtractions," *Phys. Rev.* **D75** (2007) 114017, arXiv:hep-ph/0702022 [HEP-PH].

[88] J.-Y. Chiu, F. Golf, R. Kelley, and A. V. Manohar, "Electroweak Sudakov corrections using effective field theory," *Phys. Rev. Lett.* **100** (2008) 021802, arXiv:0709.2377 [hep-ph].

[89] B. Jantzen and V. A. a. Smirnov, "The Two-loop vector form-factor in the Sudakov limit," *Eur. Phys. J.* **C47** (2006) 671–695, arXiv:hep-ph/0603133 [hep-ph].

[90] C. Lee and G. F. Sterman, "Momentum Flow Correlations from Event Shapes: Factorized Soft Gluons and Soft-Collinear Effective Theory," *Phys.Rev.* **D75** (2007) 014022, arXiv:hep-ph/0611061 [hep-ph].

[91] K. Chetyrkin, B. A. Kniehl, and M. Steinhauser, "Decoupling relations to $\mathcal{O}(\alpha_s^3)$ and their connection to low-energy theorems," *Nucl.Phys.* **B510** (1998) 61–87, arXiv:hep-ph/9708255 [hep-ph].

[92] A. H. Hoang and I. W. Stewart, "Designing gapped soft functions for jet production," *Phys.Lett.* **B660** (2008) 483–493, arXiv:0709.3519 [hep-ph].

[93] S. Weinzierl, "NNLO corrections to 3-jet observables in electron-positron annihilation," *Phys.Rev.Lett.* **101** (2008) 162001, arXiv:0807.3241 [hep-ph].

[94] S. Weinzierl, "Event shapes and jet rates in electron-positron annihilation at NNLO," *JHEP* **0906** (2009) 041, arXiv:0904.1077 [hep-ph].

[95] A. Gehrmann-De Ridder, T. Gehrmann, E. Glover, and G. Heinrich, "Second-order QCD corrections to the thrust distribution," *Phys.Rev.Lett.* **99** (2007) 132002, arXiv:0707.1285 [hep-ph].

[96] A. Gehrmann-De Ridder, T. Gehrmann, E. Glover, and G. Heinrich, "NNLO corrections to event shapes in e+ e- annihilation," *JHEP* **0712** (2007) 094, arXiv:0711.4711 [hep-ph].

[97] T. Becher and M. D. Schwartz, "A Precise determination of α_s from LEP thrust data using effective field theory," *JHEP* **0807** (2008) 034, arXiv:0803.0342 [hep-ph].

[98] Y.-T. Chien and M. D. Schwartz, "Resummation of heavy jet mass and comparison to LEP data," *JHEP* **1008** (2010) 058, arXiv:1005.1644 [hep-ph].

[99] T. Becher and G. Bell, "NNLL Resummation for Jet Broadening," *JHEP* **1211** (2012) 126, arXiv:1210.0580 [hep-ph].

[100] T. Gehrmann, G. Luisoni, and P. F. Monni, "Power corrections in the dispersive model for a determination of the strong coupling constant from the thrust distribution," *Eur.Phys.J.* **C73** (2013) 2265, arXiv:1210.6945 [hep-ph].

[101] A. H. Hoang, A. Jain, I. Scimemi, and I. W. Stewart, "R-evolution: Improving perturbative QCD," *Phys.Rev.* **D82** (2010) 011501, arXiv:0908.3189 [hep-ph].

[102] T. Gehrmann, M. Jaquier, and G. Luisoni, "Hadronization effects in event shape moments," *Eur.Phys.J.* **C67** (2010) 57–72, arXiv:0911.2422 [hep-ph].

[103] C. F. Berger, T. Kucs, and G. F. Sterman, "Event shape / energy flow correlations," *Phys.Rev.* **D68** (2003) 014012, arXiv:hep-ph/0303051 [hep-ph].

[104] E. Farhi, "A QCD Test for Jets," *Phys.Rev.Lett.* **39** (1977) 1587–1588.

[105] S. Catani, G. Turnock, and B. Webber, "Jet broadening measures in e^+e^- annihilation," *Phys.Lett.* **B295** (1992) 269–276.

[106] T. Chandramohan and L. Clavelli, "Consequences of Second Order QCD for Jet Structure in e^+e^- Annihilation," *Nucl.Phys.* **B184** (1981) 365.

[107] R. K. Ellis, D. Ross, and A. Terrano, "The Perturbative Calculation of Jet Structure in e^+e^- Annihilation," *Nucl. Phys.* **B178** (1981) 421.

[108] I. W. Stewart, F. J. Tackmann, and W. J. Waalewijn, "N-Jettiness: An Inclusive Event Shape to Veto Jets," *Phys. Rev. Lett.* **105** (2010) 092002, arXiv:1004.2489 [hep-ph].

[109] M. Dasgupta and G. P. Salam, "Event shapes in e+ e- annihilation and deep inelastic scattering," *J.Phys.* **G30** (2004) R143, arXiv:hep-ph/0312283 [hep-ph].

[110] G. P. Korchemsky and G. F. Sterman, "Power corrections to event shapes and factorization," *Nucl.Phys.* **B555** (1999) 335–351, arXiv:hep-ph/9902341 [hep-ph].

[111] M. D. Schwartz, "Resummation and NLO matching of event shapes with effective field theory," *Phys.Rev.* **D77** (2008) 014026, arXiv:0709.2709 [hep-ph].

[112] R. Kelley, M. D. Schwartz, R. M. Schabinger, and H. X. Zhu, "The two-loop hemisphere soft function," *Phys. Rev.* **D84** (2011) 045022, arXiv:1105.3676 [hep-ph].

[113] P. F. Monni, T. Gehrmann, and G. Luisoni, "Two-Loop Soft Corrections and Resummation of the Thrust Distribution in the Dijet Region," *JHEP* **1108** (2011) 010, `arXiv:1105.4560 [hep-ph]`.

[114] M. Beneke, "Renormalons," *Phys.Rept.* **317** (1999) 1–142, `arXiv:hep-ph/9807443 [hep-ph]`.

[115] A. H. Hoang and S. Kluth, "Hemisphere Soft Function at $\mathcal{O}(\alpha_s^2)$ for Dijet Production in $e^+ e^-$ Annihilation," `arXiv:0806.3852 [hep-ph]`.

[116] A. H. Hoang, A. Jain, I. Scimemi, and I. W. Stewart, "Infrared Renormalization Group Flow for Heavy Quark Masses," *Phys.Rev.Lett.* **101** (2008) 151602, `arXiv:0803.4214 [hep-ph]`.

[117] A. Hornig, C. Lee, I. W. Stewart, J. R. Walsh, and S. Zuberi, "Non-global Structure of the $O(\alpha_s^2)$ Dijet Soft Function," *JHEP* **1108** (2011) 054, `arXiv:1105.4628 [hep-ph]`.

[118] T. Hahn, "CUBA: A Library for multidimensional numerical integration," *Comput.Phys.Commun.* **168** (2005) 78–95, `arXiv:hep-ph/0404043 [hep-ph]`.

[119] "Wolfram Research, Inc., The Wolfram Functions Site, 2008-2013, http://functions.wolfram.com.".

[120] M. Beneke, V. M. Braun, and V. I. Zakharov, "Bloch-Nordsieck cancellations beyond logarithms in heavy particle decays," *Phys.Rev.Lett.* **73** (1994) 3058–3061, `arXiv:hep-ph/9405304 [hep-ph]`.

[121] A. Hoang and A. Manohar, "Charm effects in the MS-bar bottom quark mass from Upsilon mesons," *Phys.Lett.* **B483** (2000) 94–98, `arXiv:hep-ph/9911461 [hep-ph]`.

[122] A. Hoang, "Bottom quark mass from Upsilon mesons: Charm mass effects," `arXiv:hep-ph/0008102 [hep-ph]`.

[123] T. Becher and K. Melnikov, "Two-loop QED corrections to Bhabha scattering," *JHEP* **0706** (2007) 084, `arXiv:0704.3582 [hep-ph]`.

[124] A. Ferroglia, S. Marzani, B. D. Pecjak, and L. L. Yang, "Boosted top production: factorization and resummation for single-particle inclusive distributions," *JHEP* **1401** (2014) 028, `arXiv:1310.3836 [hep-ph]`.

[125] T. van Ritbergen, J. Vermaseren, and S. Larin, "The Four loop beta function in quantum chromodynamics," *Phys.Lett.* **B400** (1997) 379–384, `arXiv:hep-ph/9701390 [hep-ph]`.

[126] E. Gardi, "Perturbative and nonperturbative aspects of moments of the thrust distribution in e+ e- annihilation," *JHEP* **0004** (2000) 030, `arXiv:hep-ph/0003179 [hep-ph]`.

[127] W. Bernreuther, R. Bonciani, T. Gehrmann, R. Heinesch, T. Leineweber, *et al.*, "Two-loop QCD corrections to the heavy quark form-factors: The Vector contributions," *Nucl.Phys.* **B706** (2005) 245–324, `arXiv:hep-ph/0406046 [hep-ph]`.

[128] J. Gluza, A. Mitov, S. Moch, and T. Riemann, "The QCD form factor of heavy quarks at NNLO," *JHEP* **0907** (2009) 001, `arXiv:0905.1137 [hep-ph]`.

Curriculum vitae

Education

10/2011-	PhD studies at the University of Vienna/Austria Title: Variable Flavor Number Scheme for Final State Jets PhD advisor: Prof. Dr. Andre H. Hoang
08/2011	Master of Science at the LMU in Munich/Germany (grade: 1.02*)
09/2010-08/2011	Master thesis: Effective Field Theory for electromagnetic transitions of heavy quarkonium (grade: 1.0*) Thesis advisor: Prof. Dr. Nora Brambilla (Technische Universität München)
09/2009-02/2010	Exchange semester at Universiteit Utrecht/ Netherlands
08/2009	Bachelor of Science at the LMU in Munich/Germany (grade: 1.05*)
10/2006-07/2011	Physics studies at the Ludwig-Maximilians-Universität (LMU) in Munich/Germany
06/2005	Abitur (A-levels) at Apian-Gymnasium Ingolstadt/Germany (grade: 1.2*)
	* on a scale from 1 (best) to 5 (fail)

Teaching

Tutorials at the University of Vienna in

- Mathematical Methods for Physicists II
- Quantum Mechanics
- Electrodynamics

Published papers

[1] M. Busse, P. Pietrulewicz, H.-P. Breuer and K. Hornberger, *Stochastic simulation algorithm for the quantum linear Boltzmann equation*, Phys. Rev. E **82** (2010) 026706, arXiv:1005.0365 [quant-ph].

[2] N. Brambilla, P. Pietrulewicz and A. Vairo, *Model-independent Study of Electric Dipole Transitions in Quarkonium*, Phys. Rev. D **85** (2012) 094005, arXiv:1203.3020 [hep-ph].

[3] S. Gritschacher, A. H. Hoang, I. Jemos and P. Pietrulewicz, *Secondary Heavy Quark Production in Jets through Mass Modes*, Phys. Rev. D **88** (2013) 034021, arXiv:1302.4743 [hep-ph].

[4] S. Gritschacher, A. Hoang, I. Jemos and P. Pietrulewicz, *Two loop soft function for secondary massive quarks*, Phys. Rev. D **89** (2014) 014035 [arXiv:1309.6251 [hep-ph]].

[5] P. Pietrulewicz, S. Gritschacher, A. H. Hoang, I. Jemos and V. Mateu, *Variable Flavor Number Scheme for Final State Jets in Thrust*, arXiv:1405.4860 [hep-ph], sent to Phys. Rev. D.

Conference proceedings

[1] P. Pietrulewicz, *Electric dipole transitions of heavy quarkonium in pNRQCD*, Conf.Proc. C110613 (2011) 382, arXiv:1203.4743 [hep-ph].

[2] P. Pietrulewicz, *Electric dipole transitions in pNRQCD*, PoS ConfinementX (2012) 135, arXiv:1301.1308 [hep-ph].

[3] A. H. Hoang, P. Pietrulewicz and D. Samitz, *Variable Flavor Number Scheme for Final State Jets*, PoS DIS2014 (2014) 049, arXiv:1406.5885 [hep-ph].

Talks at conferences and invited seminar talks

04/2014	XXII. International Workshop on Deep-Inelastic Scattering and Related Subjects, Warsaw/Poland
03/2014	XIth Workshop on Soft-Collinear Effective Theory, Munich/Germany
10/2013	Theorie-Palaver (Seminar), Mainz/Germany
07/2013	ESI Programm on Jets and Quantum Fields for LHC and Future Colliders, Vienna/Austria
03/2013	Xth Workshop on Soft-Collinear Effective Theory, Durham/USA
10/2012	Quark Confinement and the Hadron Spectrum X, Munich/Germany
09/2012	44th Autumn School on High-Energy Physics, Maria Laach/Germany
02/2012	DPG-Frühjahrstagung 2012, Göttingen/Germany
10/2011	International Workshop on Heavy Quarkonium 2011, Darmstadt/Germany
06/2011	Hadron 2011, Munich/Germany